Radionuclide Parathyroid Imaging

Book and Atlas

Qaisar Hussain Siraj
Editor

Springer

Radionuclide Parathyroid Imaging

Qaisar Hussain Siraj
Editor

Radionuclide Parathyroid Imaging

Book and Atlas

Springer

Editor
Qaisar Hussain Siraj
Department of Nuclear Medicine
Farwaniya Hospital
Kuwait

ISBN 978-3-030-17350-0 ISBN 978-3-030-17351-7 (eBook)
https://doi.org/10.1007/978-3-030-17351-7

© Springer Nature Switzerland AG 2019
This work is subject to copyright. All rights are reserved by the Publisher, whether the whole or part of the material is concerned, specifically the rights of translation, reprinting, reuse of illustrations, recitation, broadcasting, reproduction on microfilms or in any other physical way, and transmission or information storage and retrieval, electronic adaptation, computer software, or by similar or dissimilar methodology now known or hereafter developed.
The use of general descriptive names, registered names, trademarks, service marks, etc. in this publication does not imply, even in the absence of a specific statement, that such names are exempt from the relevant protective laws and regulations and therefore free for general use.
The publisher, the authors, and the editors are safe to assume that the advice and information in this book are believed to be true and accurate at the date of publication. Neither the publisher nor the authors or the editors give a warranty, expressed or implied, with respect to the material contained herein or for any errors or omissions that may have been made. The publisher remains neutral with regard to jurisdictional claims in published maps and institutional affiliations.

This Springer imprint is published by the registered company Springer Nature Switzerland AG.
The registered company address is: Gewerbestrasse 11, 6330 Cham, Switzerland

Preface

The only source of knowledge is experience. (Albert Einstein)

The *Radionuclide Parathyroid Imaging: Book and Atlas* is the first dedicated comprehensive book and atlas on radionuclide parathyroid imaging. It is designed as a ready reference on the use of parathyroid scintigraphy in patients with hyperparathyroidism, both for the localisation of parathyroid pathology and as an aid to surgery. The introductory chapters (Chaps. 1–5) review the basic core knowledge on the subject including parathyroid anatomy, embryology, and histology (Chap. 1), parathyroid physiology (Chap. 2), hyperparathyroid disorders (Chap. 3), the current structural diagnostic imaging modalities (Chap. 4), and parathyroid scintigraphy (Chap. 5). Chapter 6 highlights the utility of the ^{18}F-Choline PET/CT in the localisation of hyperactive parathyroid pathology; Chap. 7 includes the atlas of cases of parathyroid scintigraphy, and Chap. 8 includes ^{18}F-Choline parathyroid PET/CT example cases.

A total of 80 case reviews are presented, covering gamma camera planar imaging, SPECT, hybrid SPECT-CT, and also PET-CT. Illustrations and figures comprising line drawings, greyscale photos depicting nuclear medicine, and CT images and dual-modality fusion colour photos are included. This compilation of illustrative clinical cases will greatly assist clinicians and imaging specialists in image interpretation in different settings. The images replicate normal conventional formats used for routine reporting and hence facilitate fast and reliable diagnosis. Each of the case reviews includes documentation of the procedure, findings, and conclusions with relevant commentary. Surgeons, physicians, endocrinologists, nephrologists, nuclear medicine physicians, and radiologists will find this book and atlas on radionuclide parathyroid imaging to be a valuable practical tool and learning aid.

This book represents my many years of experience with parathyroid scintigraphy. There is a wide range of cases included in the atlas section with many rare and a large number of previously unreported cases. The use of planar thallium/technetium subtraction scan for the diagnosis of sestamibi-negative parathyroid adenomas has not been previously reported, nor have the several cases of sestamibi-negative scan results in patients with parathyroid adenomas which were successfully imaged with thallium parathyroid SPECT/CT imaging. This defines a new role of thallium parathyroid SPECT/CT imaging in patients with primary biochemical hyperparathyroidism with sestamibi-negative scan results. Thallium SPECT/CT can also at times help in localisation of sestamibi-negative parathyroid hyperplasia though in general sestamibi parathyroid imaging is preferable in patients with secondary hyperparathyroidism.

The increasing popularity of the new surgical approach of minimally invasive parathyroid surgery technique, which has evolved in tandem with the introduction of accurate and sensitive preoperative localisation techniques and intraoperative gamma probe localisation of the overactive parathyroid lesions, has revived the need for preoperative parathyroid localisation with the hybrid SPECT/CT radionuclide techniques still leading the diagnostic first-line imaging modalities.

We present SPECT image processing and optimisation methods with special emphasis on logarithmic inverse greyscale image conversion, which expands the values of high pixels and compresses the values of low pixels thereby enhancing the modest increase in uptake in the parathyroid lesions and suppressing the background thyroid activity. This together with appropriate colour display improves the identification of the smaller hyperactive parathyroid glands, both adenomatous and hyperplastic, thereby considerably increasing the sensitivity of parathyroid scintigraphy. Retrospective and prospective application of inverse-log transformation has very significantly improved our diagnostic yield and reduced the false-negative rate to a minimum.

The hybrid functional/structural imaging further improves the identification of lesions that only show a subtle increase in the radionuclide uptake or are too small to resolve individually on scintigraphy alone. This also aids in the identification of a sestamibi-non-avid lesion for subsequent thallium-201 SPECT/CT in cases with non-oncogenic cell hyperactive parathyroid lesions.

Due to the wide availability of the current automated laboratory biochemistry procedures, the diagnosis of hyperparathyroidism is now being made at an early stage in the disease, when most patients are yet asymptomatic. Biochemical hypercalcaemia and hyperparathyroidism are diagnostic, but increasingly normal or borderline sporadic elevations in serum calcium with inappropriate PTH elevation are the only clue to what is now termed as eucalcaemic or normocalcaemic hyperparathyroidism. This coupled with widespread vitamin D deficiency, which results in an increase in the PTH in the presence of normal serum calcium, makes the diagnosis somewhat confounding. The atlas cases are interpreted in the light of comprehensive biochemical analyses, which helps elucidate the complex interplay between various factors and allows identification of the cause of primary, secondary, and tertiary hyperparathyroidism due to benign or malignant parathyroid disease.

Al Farwaniyah, Kuwait Qaisar Hussain Siraj

Acknowledgements

I am extremely indebted to Miss Aleks Rasulova from Tashkent, a gifted and extremely talented artist, for all the original anatomical drawings in Chaps. 1, 2, 4, and 5. I am grateful to her sister and my colleague Dr. Nigora Rasulova, for her painstaking efforts in tabulating the patient's clinical, radiological, biochemical, and histopathological data and her assistance in the writing of this book. I acknowledge with thanks the help and assistance of Dr. Amir Javaid from Farwaniya Hospital in proofreading of the manuscript and his contribution to the book and for the collection of radiological images of the patients. I am also grateful to my medical colleagues at the nuclear medicine department at Farwaniya Hospital (Dr. Anwar Al-Banna, Dr. Saud Alenezi, Dr. Marwa El-Bedwihy, and Dr. Mohammad Naeem) for clinical work in parathyroid scintigraphy, and the technical staff headed by our Chief Technician Reem Al-Salem for high-quality radionuclide parathyroid image acquisition and processing.

This work has encompassed the last 36 years of my clinical career starting in 1982 with thallium/technetium parathyroid imaging at the Royal Free Hospital, London, under the guidance of my teacher and mentor Dr. AJW Hilson. And later when I first introduced parathyroid imaging in Pakistan at the Nuclear Medical Centre, AFIP Rawalpindi, I was readily helped by surgeons and pathologists and I thank the trust shown to me by my many patients who made this endeavour so rewarding. This work continued in several NHS teaching hospitals in London, but a substantial volume of work was performed at the Royal Hospital Haslar and the Portsmouth Hospitals NHS Trust, and I am indebted to my surgical colleagues there for their close collaboration (particularly Dr. Martin Wise) and my technical colleagues (especially Paul Griffiths) for their efforts in producing high-quality images. There are several other colleagues, too numerous to name, who were involved in this work over the years, and I gratefully acknowledge their help. I thank Miss Smitha Diveshan and Mr. Deepak Srinivasan from Springer for their advice and assistance.

Finally, I am grateful to my family for their understanding during my preoccupation with my writing to the exclusion of other duties. A Special Grace buoyed me during writing of this book and made the long hours bearable and indeed pleasurable. This undertaking was by itself quite rewarding as new subtleties were revealed and complexities unravelled.

Dr. Qaisar Hussain Siraj

Contents

Contributors

Marko Grmek, MD, PhD Department of Nuclear Medicine, University Medical Centre Ljubljana, Ljubljana, Slovenia

Amir Javaid Department of Nuclear Medicine, Farwaniya Hospital, Kuwait

Luka Lezaic, MD, PhD Department of Nuclear Medicine, University Medical Centre Ljubljana, Ljubljana, Slovenia

Nigora Rasulova, MD, PhD Department of Nuclear Medicine, Farwaniya Hospital, Kuwait

Sonya Borisova Sergieva, MD, PhD Department of Nuclear Medicine, Sofia Cancer Center, Sofia, Bulgaria

Qaisar Hussain Siraj, MB, BS, MSc, PhD, FANMB Department of Nuclear Medicine, Farwaniya Hospital, Kuwait

Parathyroid Anatomy, Embryology and Histology

1

Nigora Rasulova and Qaisar Hussain Siraj

1.1 Introduction

1.1.1 Historical Perspective

The parathyroid gland has had a fascinating history since its serendipitous recognition in 1850 by Sir Richard Owen, the curator of the Natural History Museum, while dissecting a great Indian rhinoceros who had died in the London zoo [1]. However, the credit for the discovery of this last organ to be recognised in humans rests with Ivar Sandström, a 25-year-old Swedish medical student who first described the gland 30 years later in 1880 [2]. Sandström discovered the gland while working at the Department of Anatomy in Uppsala through his initial animal dissections in dogs, cats, rabbits, oxen and horses, which were followed by identification of the gland in human corpses. He gave the gland its present name of glandulae parathyroidea. Sandström's work however remained unnoticed for many years. He suffered from a hereditary mental illness and unfortunately had a tragic death at the age of only 37 years!

In 1891, Friedrich Daniel von Recklinghausen described a case of what was subsequently termed 'osteitis fibrosa cystica of von Recklinghausen', now recognised as one of the most severe findings in advanced parathyroid disease [3]. In 1915, Friedrich Schlaugenhaufer implicated an enlarged parathyroid gland as a possible cause of bone disease [4]. In 1929, Felix Mandl performed the first parathyroidectomy in Vienna for von Recklinghausen's disease of bone, three decades before the isolation of human parathyroid hormone [5, 6]. Fuller Albright in 1934 was the first to describe the relationship between chronic renal disease and hyperparathyroidism providing a

N. Rasulova · Q. H. Siraj (✉)
Department of Nuclear Medicine, Farwaniya Hospital, Kuwait

© Springer Nature Switzerland AG 2019

Q. Siraj (ed.), *Radionuclide Parathyroid Imaging*,
https://doi.org/10.1007/978-3-030-17351-7_1

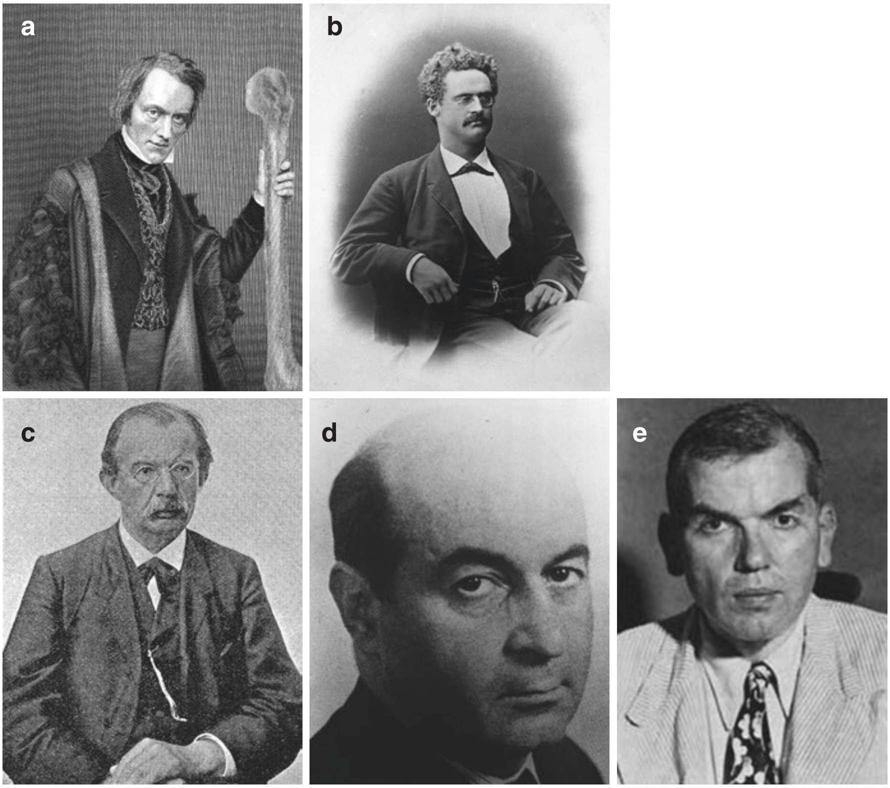

Fig. 1.1 Parathyroid hall of fame: (**a**) engraving of Sir Richard Owen; (**b**) photograph of Ivar Victor Sandström; (**c**) newspaper cutting portrait of F.D. von Recklinghausen, probably from Deutsche Medizinische Wochenschrift, 1910, page 1767 (credit: Wellcome Collection CC BY); (**d**) photograph of Felix Mandl; and (**e**) photo of Fuller Albright (http://resource.nlm.nih.gov/101422987; pre-1978 without copyright notice US public domain images)

comprehensive framework for understanding the regulation of calcium and phosphate in healthy subjects and patients with parathyroid disorders [7] (Fig. 1.1).

1.2 Morphology

The parathyroid glands (Fig. 1.2) vary significantly in size, shape, number and location. They are usually ovoid (beanlike or almond-shaped) but uncommonly can be elongated or flattened to a leaflike shape or can be multilobulated [8, 9]. The normal parathyroid gland dimension is affected by its shape with the gland size ranging from 4 to 6 mm, 2–4 mm and 0.5–2 mm, in length, width and thickness, respectively [9]. The colour of the glands is mustard yellow varying from light yellowish to reddish, depending on the vascularity, fat content and percentage of oxyphil cells within the glands [10].

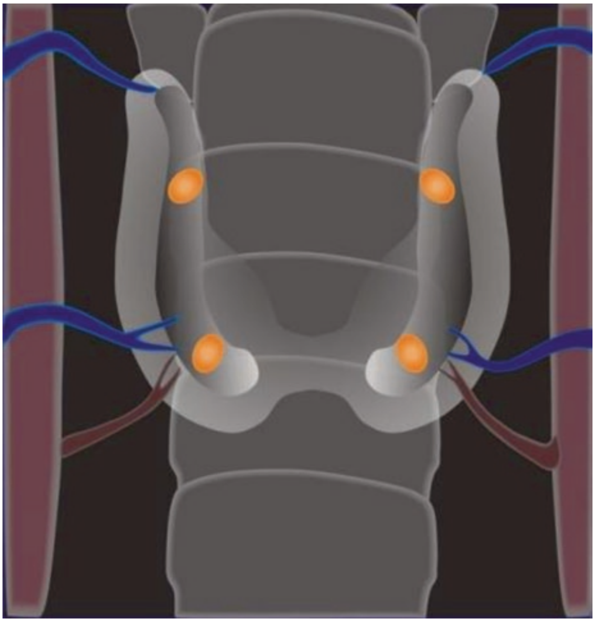

Fig. 1.2 The superior and inferior parathyroid glands. The superior glands are located on the posteromedial aspect of the thyroid at the level of the upper and middle thirds of the gland near the tracheoesophageal groove. The inferior glands are located on the posterior aspect of the lower one-third of the thyroid gland in the region below the inferior thyroid artery

The weight of the normal parathyroid glands differs in surgical specimens and cadavers with higher weights reported for surgically dissected glands. The average weight of normal parathyroid gland is 30–50 mg in cadavers with the total parathyroid weight of 120–140 mg in adults [9, 11, 12]. The mean weight of a normal gland removed during surgery is reported at 62.4 ± 31.6 mg [13]. The lower glands are slightly larger than the upper glands. The number of parathyroid glands varies from two to six, but the majority have two pairs of parathyroid glands superior and inferior, with four glands found in 80–97% of the cases, less than four in 5% and supernumerary (more than four) in 3–13% of the cases [14].

The superior glands are typically located on the posteromedial aspect of the thyroid near the tracheoesophageal groove, whereas the inferior parathyroids are more widely distributed in the region below the inferior thyroid artery (Figs. 1.3 and 1.8). The superior parathyroids are generally located more posterior and medial than the inferior parathyroids. The coronal plane of the recurrent laryngeal nerves separates the superior and inferior parathyroids anteroposteriorly, with the superior parathyroid glands located dorsally or deeper in the neck to this plane and the inferior parathyroid glands ventral or anterior to this plane [15, 16].

The superior and inferior parathyroid glands receive their blood supply from the inferior thyroid artery in 80% of cases [16]. The superior parathyroid glands are typically supplied by the paired inferior thyroid arteries that branch from the thyrocervical trunk or by an anastomotic branch between the inferior thyroid and the superior thyroid artery. The inferior parathyroid glands are also usually supplied by the inferior parathyroid arteries from the thyrocervical trunk (Fig. 1.4); however, the

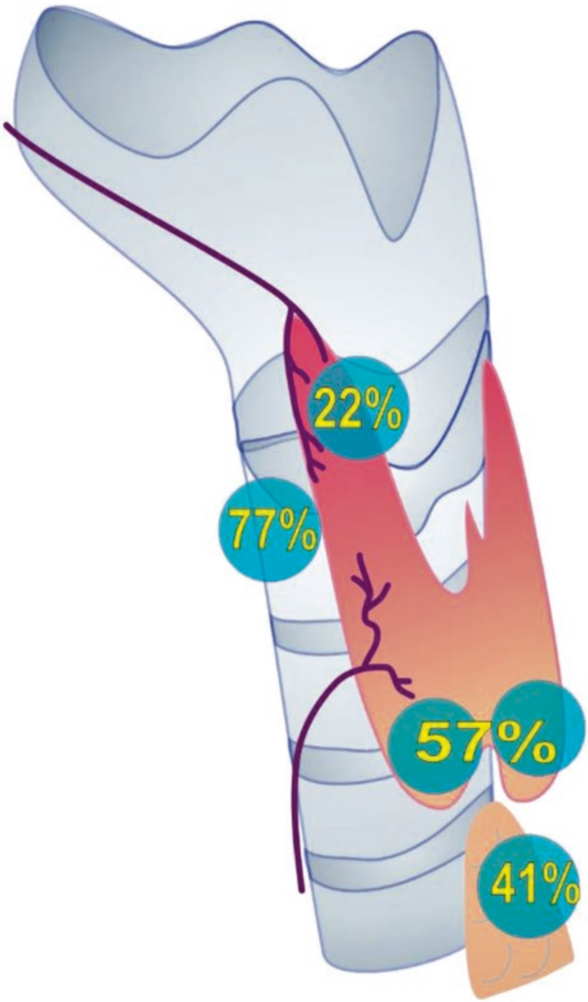

Fig. 1.3 Normal locations of the superior and inferior parathyroid glands. The superior glands are usually either posterior to the upper pole or the middle one-third of the thyroid gland but rarely can be intrathyroidal. The inferior glands are located posterior or lateral to the lower pole of the thyroid or in the thyrothymic ligament

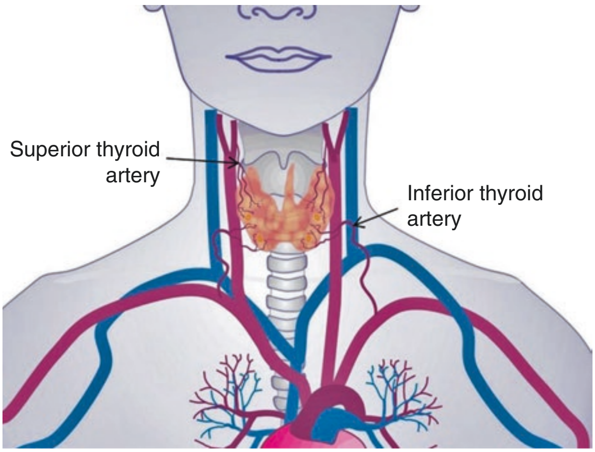

Fig. 1.4 Parathyroid gland blood supply

blood supply can also be derived from the superior thyroid arteries, the superior and inferior thyroid artery anastomosis, small branches of the laryngeal and tracheo-esophageal arteries and, occasionally, a thyroidea ima artery [17–19].

1.3 Embryology

A good knowledge of parathyroid gland embryology is crucial to correct parathyroid gland localisation and imaging interpretation. The parathyroid glands develop from the endoderm of the fourth and third pharyngeal pouches (see Fig. 1.5).

The pair of superior parathyroid glands develop from the dorsal aspect of the fourth branchial pouch and are hence also known as parathyroid IVs. They migrate downwards with the ultimobranchial bodies or the lateral thyroid lobes. Because of their short migratory pathway, the location of the superior parathyroid glands is

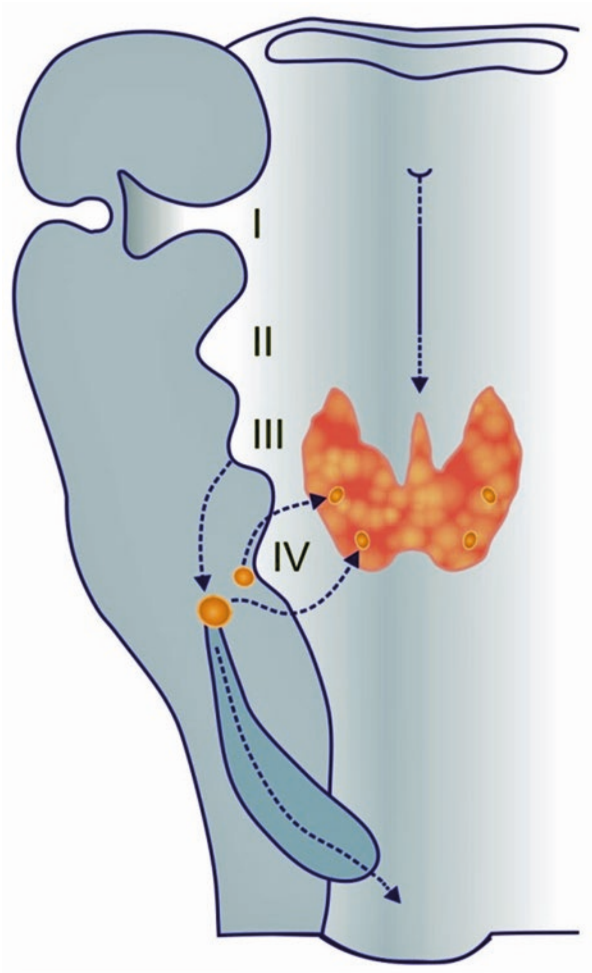

Fig. 1.5 Embryological origins of the thyroid, parathyroid and thymus glands. Arrows show the migration pathways. Pouch III develops into the inferior parathyroid gland, and the thymus and pouch IV develops into the superior parathyroid glands

relatively constant, with the glands positioned in close proximity to the posterior aspect of the middle one-third of the thyroid lobes outside the thyroid capsule at the level of the cricothyroid junction commonly about 1 cm above the intersection of the inferior thyroid artery and the recurrent laryngeal nerve [20–22].

The inferior parathyroid glands arise from the dorsal aspect of the third pharyngeal pouch (hence also known as parathyroid IIIs) with the thymus arising from its ventral part. The inferior parathyroid glands and the thymus together migrate down towards the mediastinum eventually separating, with the inferior parathyroid glands usually stopping their descent at the dorsal surface of the thyroid gland but outside of the fibrous capsule of the gland itself. The thymus continues to migrate towards the mediastinum, but in most cases, the inferior parathyroid glands become localised near the inferior poles of the thyroid, located usually at the anterolateral, posterolateral, posterior or infero-ventral aspect of the lower thyroid pole. Occasionally, they can be located at a slightly higher level near to the intersection of the inferior thyroid artery and the recurrent laryngeal nerve. Their relatively long migratory pathway and their tendency to move anteriorly during descent cause them to be much more variable in location and distribution.

Ectopic parathyroid glands occur in 15–20% of patients. The ectopic parathyroid glands can be found in variable locations along their migratory pathway (Figs. 1.6, 1.7, and 1.8). The superior glands may be ectopic, found embedded within the thyroid gland or its capsule, because of their shared embryological origin. The ectopic superior gland migration may be undescended; retropharyngeal, retrolaryngeal or retroesophageal in location, or they can lie in the posterior mediastinum [22].

Ectopic inferior glands may be found along the migratory pathway of the thymus, which descends from the angle of the mandible to the pericardium. Common ectopic locations include the carotid sheath, the thyrothymic ligament, the upper

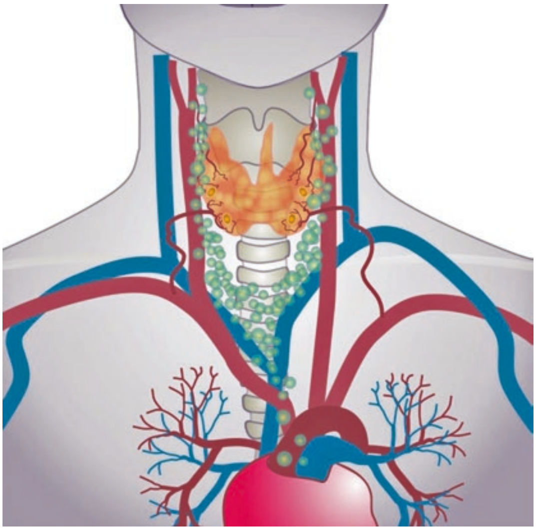

Fig. 1.6 Ectopic glands can be found along the migratory pathway of the glands from the angle of the mandible down to the pericardium

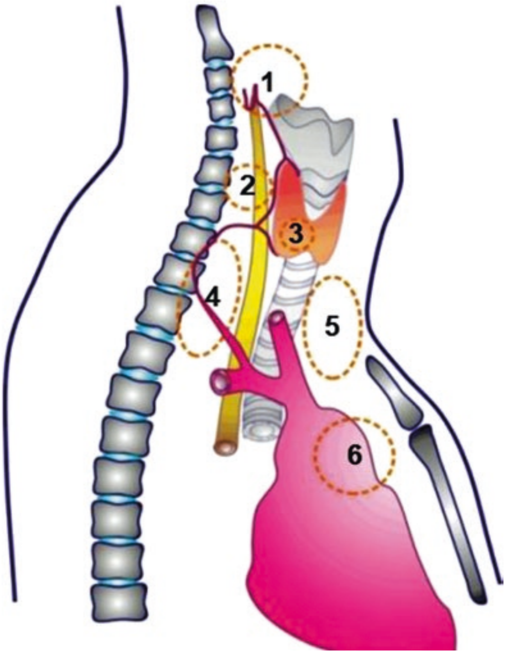

Fig. 1.7 Distribution of ectopic sites of parathyroid adenomas [23]. From top to bottom: (1) undescended, (2) retropharyngeal, (3) intrathyroidal, (4) posterior superior mediastinum, (5) anterior superior mediastinum and (6) true superior mediastinum

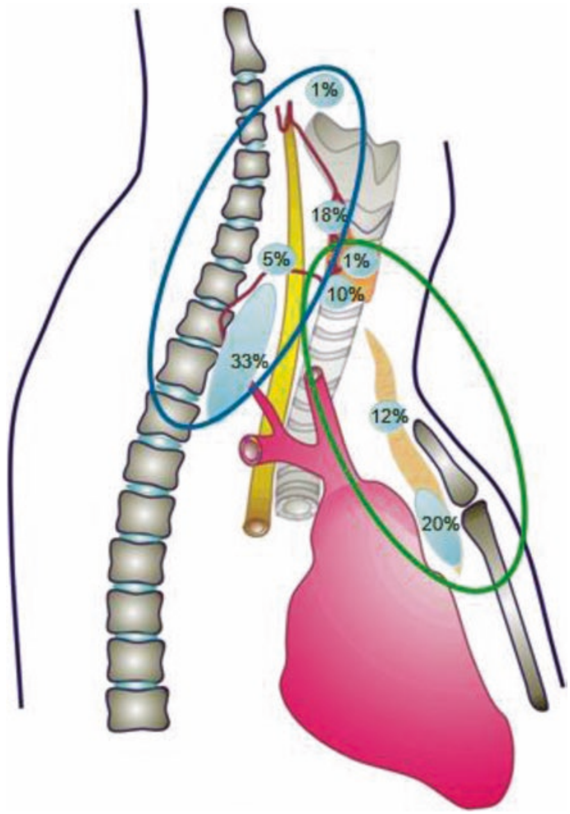

Fig. 1.8 Ectopic superior (blue oval) and inferior (green oval) parathyroid gland locations [15]. As a result of anomalous embryological descent, the limits of ectopic gland locations can range from carotid bifurcation cranially down to the region of the pericardium caudally. The ectopic glands can be located anterior to the thyroid, posterior in the tracheoesophageal groove and in the superior mediastinum. In the anterior-posterior plane, inferior glands descend anteriorly, and superior glands descend more posteriorly

mediastinum and within the thymus itself. Approximately 25% are located within the thyrothymic ligament or posterior cervical thymic horns [15]. Approximately 4–5% occur retrosternally in the anterior mediastinum in the thymus or related to the innominate vein and the ascending aorta. Only a few are located outside the thymus adjacent to the aortic arch and origin of the great vessels or even lower in position in contact with pleura or pericardium. In the event of a failed descent of the parathymus complex, the inferior parathyroid may become stranded high in the neck usually found with a segment of thymic tissue above the thyroid gland and superior to the superior parathyroid [24, 25]. Uncommonly, the gland is situated within the carotid sheath, medial to it or at the level of the mandible. The inferior parathyroid gland is truly intrathyroidal within the lower pole of the thyroid in 1–3% of people [26].

Ectopic location may also be acquired due to enlargement of a gland, with gravitational forces causing migration, or as a result of regional dynamics, such as laryngeal movement during swallowing or the influence of negative intrathoracic pressure [27]. Congenital ectopias are generally caused by anomalies in the migration of parathyroid IIIs, whereas acquired ectopias usually affect parathyroid IVs.

Supernumerary glands are present in 13% of the cases. It is essential to differentiate between the small rudimentary rests of parathyroid tissue which weigh less than 5 mg and are derived from embryological parathyroid debris and true supernumerary glands, which, on average, weigh 24 mg. True supernumerary glands only occur in 5% of random autopsy cases and occupy a location completely separate from the four normally situated glands. More than five glands are present only in 1.25% of the cases [28].

1.4 Histology

The parathyroid glands are surrounded by a thin fibrous capsule, a continuation of thyroid capsule, which extends into the parenchyma dividing the glands into multiple lobules. The stromal fat around the parathyroid glands increases gradually with age up to 30% by age 25. The percentage of fat in the glands is related to body fat percentage [29]. The parenchyma of the parathyroid glands is composed of masses of mostly chief cells with some wasserhelle (water-clear) and oxyphil cells arranged in trabeculae within a stroma composed primarily of adipose cells (Figs. 1.9 and 1.10).

In the normal adult parathyroid, there are four types of cells including (1) chief cells, (2) oxyphil (acidophilic) cells, (3) transitional cells and (4) water-clear cells. Parathyroid cells have a monophyletic origin in that they are all derived from a fundamental cell, which is the chief cell, which means that the four parathyroid gland cell types are all derived from the chief cells. Therefore, there is no functional significance to these different types of cells: they are thought to represent chief cells in varying stages of activity or variable expression of morphological characteristics of chief cells [30] (Fig. 1.10).

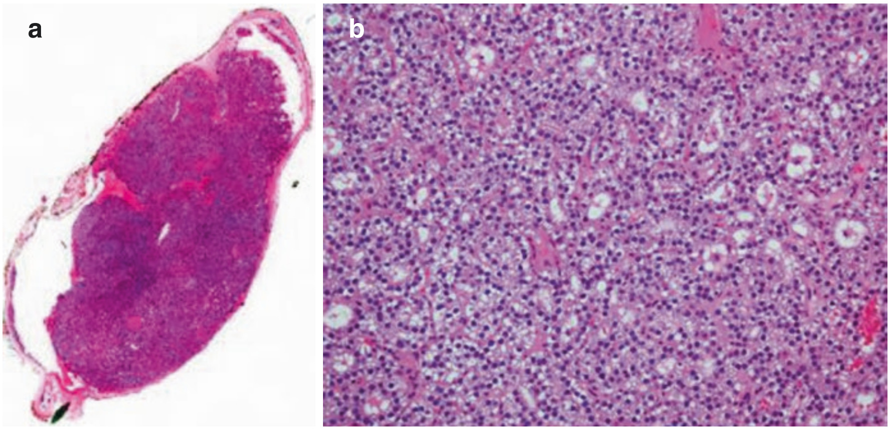

Fig. 1.9 Normal parathyroid gland: (**a**) whole parathyroid (×20 magnification); (**b**) normal parathyroid tissue (×400 magnification) showing the nests and chords of polygonal cells separated by a delicate fibroreticular stroma. A variable number of adipose tissue cells are mixed with the parathyroid tissue

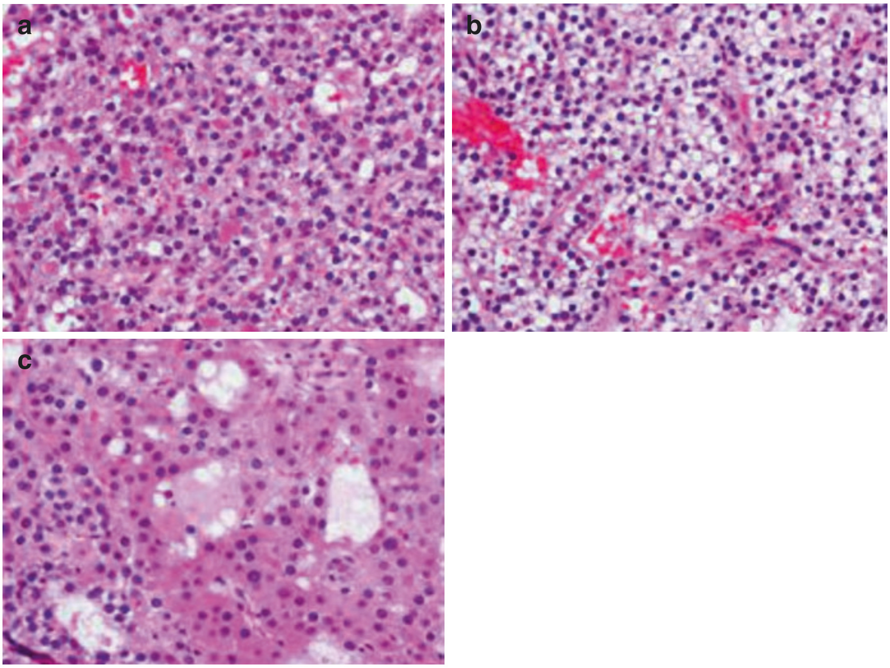

Fig. 1.10 Chief cells (**a**), water-clear cells (**b**) and oxyphil or granular cells (**c**), at ×400 magnification

Chief cells are the predominant cell type found in the adult parathyroid. They are polygonal in shape and measure about 6–8 μm in diameter with a central round nucleus. They appear dark purple on haematoxylin and eosin stain (Fig. 1.10a). The inactive chief cells are cuboidal in shape with low levels of secretory granules compared with the active chief cells. Water-clear ("wasserhelle") cells are larger with unstained cytoplasm rich in glycogen. They are inactive and appear vacuolated (Fig. 1.10b). Oxyphil cells are larger still and have deeply staining eosinophilic granular cytoplasm (Fig. 1.10c) because of the abundant mitochondria with a small dense nucleus [31, 32].

The predominant majority of cells in the parathyroid gland are the chief and oxyphil cells (Fig. 1.10). In preadolescence, the parathyroid glands are made up mainly of chief cells. The water-clear cell type is functionally more active and predominant in infancy but is also found in the adults in the presence of increased parathyroid hormone secretion. The mitochondria-rich oxyphil (acidophilic) cells can be identified after puberty and increase in numbers during adulthood. All these cell types including the transitional cells, which are cell forms between the chief and water-clear cells, are seen in both adenomatous and hyperplastic glands [33].

References

1. Owen R. On the anatomy of the Indian Rhinoceros (Rh. Unicornis, L). Trans Zool Soc Lond. 1862;4:31.
2. Sandström I. On a new gland in man and several mammals (glandulae parathyroideae). Ups Läk Förh. 1880;15:441.
3. Ellis H. Bailey and Bishop's notable names in medicine and surgery. London: HK Lewis; 1983. p. 196–8.
4. Carney A. The glandulae parathyroideae of Ivar Sandstrom. Am J Surg Pathol. 1996;20: 1123–44.
5. Mandl F. Therapeutischer versuch bei einem falle von ostitis fibrosa generalisata mittels exstirpation eines epithelkorperchen tumors. Zentrabl Chir. 1926;5:260.
6. Mandl F. Hyperparathyroidism. A review of historical developments and the present state of knowledge on the subject. Rec Adv Surg. 1947;21:374–439.
7. Albright F, Aub JC, Bauer W. Hyperparathyroidism: a common and polymorphic condition as illustrated by seventeen proved cases from one clinic. JAMA. 1934;102:1276–87.
8. Kunstman JW, Kirsch JD, Mahajan A, Udelsman R. Clinical review: parathyroid localization and implications for clinical management. J Clin Endocrinol Metab. 2013;98:902–12.
9. Akerstrom G, Grimelius L, Johansson H, Lundquist H, Pertoft H, Bergstrom R. The parenchymal cell mass in normal human parathyroid glands. Acta Pathol Microbiol Immunol Scand A. 1981;89(A):367.
10. Castleman B, Roth SI. Tumors of the parathyroid glands. 2nd series, Fascicle 14. Atlas of Tumor Pathology. Washington, DC: Armed Forces Institute of Pathology; 1978. p. 74–82.
11. Wang C. The anatomic basis of parathyroid surgery. Ann Surg. 1976;183:271–5.
12. Akerstrom G, Pertoft H, Grimelius L, Johansson H. Density determinations of human parathyroid glands by density gradients. Acta Pathol Microbiol Scand. 1979;87A:91–6.
13. Yao K, Singer FR, Roth SI, Sassoon A, Ye C, Giuliano AE. Weight of normal parathyroid glands in patients with parathyroid adenomas. J Clin Endocrinol Metab. 2004;89:3208–13.
14. Lappas D, Noussios G, Anagnostis P, Adamidou F, Chatzigeorgiou A, Shandalakis P. Location, number and morphology of parathyroid glands: results from a large anatomical series. Anat Sci Int. 2012;87:160–4.

15. Ziessman HA, O'Malley JP, Thrall JH, Fahey FH. Nuclear medicine: the requisites. 4th ed. Philadelphia, PA: Elsevier; 2014. p. 66–97.
16. Åkerström G, Malmaeus J, Bergström R. Surgical anatomy of human parathyroid glands. Surgery. 1984;95:14–21.
17. Shaha AR, Jaffe BM. Parathyroid preservation during thyroid surgery. Am J Otolaryngol. 1998;19(2):113–7.
18. Bliss RD, Gauger PC, Delbridge LW. Surgeon's approach to the thyroid gland: surgical anatomy and the importance of technique. World J Surg. 2000;24:891–7.
19. Hunt PS. A reappraisal of the surgical anatomy of the thyroid and parathyroid glands. Br J Surg. 1968;55:63–6.
20. Moore AA, Roy WA. Rapid review gross and developmental anatomy. 3rd ed. Philadelphia, PA: Mosby Elsevier; 2010.
21. Thompson NW. The techniques of initial parathyroid exploration and reoperative parathyroidectomy. In: Thompson NW, Vinik AI, editors. Endocrine surgery update. New York, NY: Grune and Stratton; 1983. p. 365–83.
22. Nilsson M, Fagman H. Mechanisms of thyroid development and dysgenesis: an analysis based on developmental stages and concurrent embryonic anatomy. Curr Top Dev Biol. 2013;106:123–70.
23. Kettle AG, O'Doherty MJ. Parathyroid imaging: how good is it and how should it be done? Semin Nucl Med. 2006;36:206–11.
24. Thompson NW, Eckhauser FE, Harness JK. The anatomy of primary hyperparathyroidism. Surgery. 1982;92(5):814–21.
25. Edis AJ, Purnell DC, van Heerden JA. The undescended' parathymus: an occasional cause of failed neck exploration for hyperparathyroidism. Ann Surg. 1979;190:64–8.
26. Fraker DL, Doppman JL, Shawker TH, et al. Undescended parathyroid adenoma: an important etiology for failed operations for primary hyperparathyroidism. World J Surg. 1990;14:342–8.
27. Wheeler MH, Williams ED, Wade JSH. The hyperfunctioning intrathyroidal parathyroid gland: a potential pitfall in parathyroid surgery. World J Surg. 1987;11:110–4.
28. Wheeler MH. Clinical anatomy, developmental aberrations and endocrinology. In: Arora A, Tolley N, Tuttle M, editors. A practical manual of thyroid and parathyroid disease. London: Wiley-Blackwell; 2010. p. 184–5.
29. Dufour DR, Wilkerson SY. The normal parathyroid revisited: percentage of stromal fat. Hum Pathol. 1982;13:717–21.
30. Emura S, Shoumura S, Utsumi M, Yamahira T, Chen H, Arakawa M, et al. Origin of the water-clear cell in the parathyroid gland of the golden hamster. Acta Anat. 1991;140:357–61.
31. Lynn J, Lewis P. Pathological spectrum of parathyroid disease. In: Arora A, Tolley N, Tuttle M, editors. A practical manual of thyroid and parathyroid disease. London: Wiley-Blackwell; 2010. p. 175–80.
32. Chen H, Senda T, Emura S, Kubo K. An update on the structure of the parathyroid gland. Open Anat J. 2013;5:1–9. https://doi.org/10.2174/1877609401305010001.
33. Bilezikian JP, Marcus R, Levine MA, Marcocci C, Silverberg SJ, Potts JT, Bilezikian JP. Basic and clinical concepts. London: Elsevier; 2014.

2 Physiology

Qaisar Hussain Siraj and Nigora Rasulova

2.1 Introduction

Calcium plays a vital role in a wide range of biologic functions, either in its ionic form or as bound complexes. It is responsible for many essential functions, including extra- and intracellular signalling, enzyme activation, cell differentiation, immune response, programmed cell death, nerve impulse transmission, and muscle contraction [1–3].

The primary role of the parathyroid gland is the regulation of calcium metabolism through secretion of the parathyroid hormone (PTH). Since the clinical problem in patients with hypercalcaemia is to distinguish patients who have hypercalcemia caused by hyperparathyroidism from that arising from other causes, it is therefore essential to understand the basics of calcium homeostasis and the physiological role of parathyroid hormone in calcium regulation.

2.2 Parathyroid Hormone

Parathyroid hormone (PTH) is a polypeptide synthesised by the parathyroid glands, through cleavage of the pre-pro-PTH (115 amino acids) to pro-PTH (90 amino acids), which is converted in the Golgi apparatus by the action of furin to the 84-amino acid mature form of PTH hormone. PTH is packaged in the secretory granules in the cell and is released by exocytosis in response to hypocalcaemia. In the absence of a stimulus for release, intraglandular metabolism of PTH occurs by complete degradation to its constituent amino acids. Hormone stores are insufficient to maintain secretion for

Q. H. Siraj (✉) · N. Rasulova
Department of Nuclear Medicine, Farwaniya Hospital, Kuwait

© Springer Nature Switzerland AG 2019
Q. Siraj (ed.), *Radionuclide Parathyroid Imaging*,
https://doi.org/10.1007/978-3-030-17351-7_2

more than a few hours, and therefore in the presence of sustained severe hypocalcaemia, additional PTH secretion depends on an increase in the number of parathyroid cells. Vitamin D metabolites modulate PTH release: there is a feedback loop between the PTH-induced increase in 1,25-dihydroxy vitamin D and vitamin D metabolite-induced decrease in PTH levels independent of any changes in calcium concentration (Fig. 2.1). In addition to calcium and vitamin D, other factors affect PTH release, including magnesium and aluminium which suppress PTH release and hyperphosphatemia and glucocorticoids which increase PTH release [4].

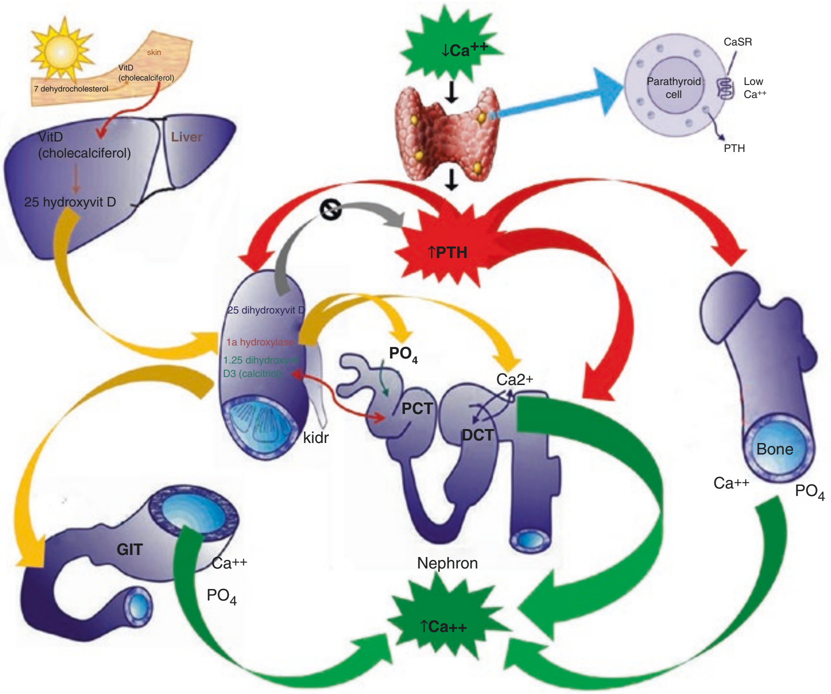

Fig. 2.1 Overview of calcium homeostasis by parathyroid hormone (red arrows) and vitamin D (yellow arrows). Hypocalcaemia activates the calcium-sensing receptors (CaSR) in the parathyroid gland causing the release of PTH into the blood. PTH stimulates bone resorption releasing Ca^{2+} (green arrows) and PO_4 into the bloodstream; it acts on the bone to increase blood calcium levels; on the GI tract to increase the activity of the enzyme in the intestines that activates vitamin D; and on the kidneys to promote direct stimulation of Ca^{2+} reabsorption from the distal convoluted tubules. PTH also stimulates the production of 1,25-dihydroxy vitamin D (calcitriol) from its precursors in the proximal convoluted tubules of the kidneys. All of these actions lead to increased plasma Ca^{2+} levels. The active form of vitamin D has a negative feedback on parathyroid glands (grey arrow)

The calcium-sensing receptor (CaSR) is a G-protein cell-surface receptor primarily expressed in the chief cells of the parathyroid gland and the renal tubules of the kidney, which senses extracellular levels of calcium ion and responds by rapid alteration of PTH secretion. Hypocalcaemia retards the rate of degradation of PTH within the parathyroid gland, making more PTH available for release, and increases cell division in the parathyroid gland possibly through the action of the CaSR [5].

PTH is essential for the maintenance of calcium homeostasis through its direct actions on the bone and kidney and indirect actions on the gastrointestinal tract. The extracellular concentration of calcium determines PTH secretion. PTH controls calcium level through four principal mechanisms including (1) direct action on the skeleton stimulating osteoblastic activity to promote calcium release from the bone; (2) facilitation of calcium absorption by the kidneys through its effects in increasing the conversion of 25-hydroxy vitamin D to 1,25-dihydroxy vitamin D; (3) increasing calcium absorption from the gastrointestinal tract; and (4) blocking reabsorption of phosphate in the proximal tubule while promoting calcium reabsorption in the ascending limb of the loop of Henle, distal tubule, and collecting tubule [6].

2.3 Calcium Physiology and Homeostasis

The human body contains approximately 1–1.2 kg of calcium with 99% of the total body calcium deposited in the skeleton as calcium-phosphate complexes, primarily as hydroxyapatite ($Ca_{10}(PO_4)_6(OH)_2$), which is responsible for much of the material properties of bone [4]. One of its most important functions as bound calcium is in skeletal mineralisation where it has a dual purpose of providing skeletal strength and providing a dynamic store for maintaining the intra- and extracellular calcium pools. Renal reabsorption of calcium is 97–98% efficient under normal conditions, leaving little room for improvement. The only other source of calcium to replace the losses due to excretion is bone resorption, which is the major protection against extracellular fluid calcium depletion. Non-bone calcium represents ~1% of total body calcium (~10 g in an adult). However, it is in constant and rapid exchange within the various calcium pools [7] (Fig. 2.2).

Serum calcium level ranges from 2.2 to 2.6 mM in healthy subjects. In serum, calcium is present in three main forms: ionised (~51%), ionic complexes (~9%) bound with anions such as citrate, and protein-bound complexes (~40%) chiefly albumin. Calcium concentration is tightly controlled in extracellular fluid and cellular compartments. The concentrations of calcium in the blood and extracellular fluid is usually maintained at 1–2 mmol/L, while the concentration of intracellular calcium at resting state is maintained at 100 nmol/L or less [8]. Calcium homeostasis or the maintenance of the body stores of calcium at equilibrium over time results from the net effects of intestinal absorption, and renal, intestinal and sweat gland

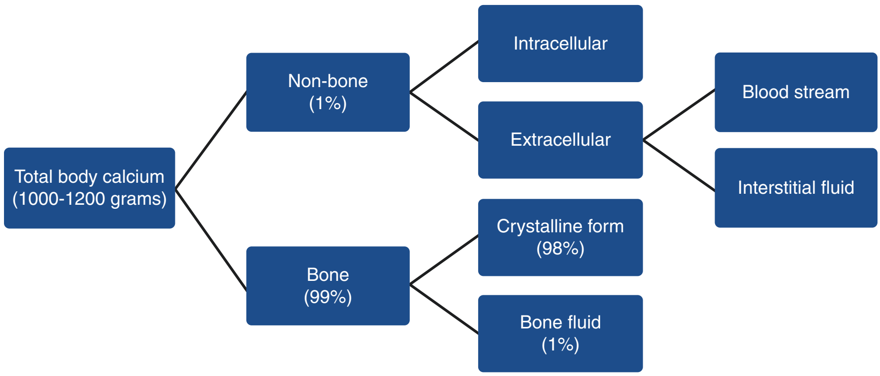

Fig. 2.2 Total body calcium distribution

Table 2.1 The hormones involved in calcium homeostasis and their site and mechanisms of action

Hormone	Bone	Kidney	Intestine
Parathyroid hormone	Stimulation of calcium and phosphate resorption	Stimulation of calcium resorption Production of 1,25-dihydroxy vitamin D Inhibition of calcium and phosphate resorption	No direct effects
Vitamin D	Stimulation of calcium transport	Inhibition of calcium resorption	Stimulation of calcium and phosphate resorption
Calcitonin	Inhibition of calcium and phosphate resorption	Inhibition of calcium and phosphate resorption	No direct effects

excretion, on bone calcium, the dominant calcium pool. The calcium levels are modulated through a delicate interplay among parathyroid hormone (PTH), calcitonin, and 1,25-dihydroxy vitamin D acting on target organs such as the bone, kidney, and the gastrointestinal (GI) tract. PTH and vitamin D are primarily responsible for calcium homeostasis. Calcitonin stimulates bone accretion through targeting bone to inhibit the osteoclasts and terminate bone resorption and inhibits the renal tubular cells to increase the urinary secretion of Ca^{2+} and PO_4. However, calcitonin plays a relatively minor physiological role since thyroidectomy has no adverse effect on bone strength or density (Table 2.1).

When the Ca^{2+} plasma level is low, the parathyroid glands release parathyroid hormone (PTH), which has three major effects: (1) direct stimulation of bone resorption releasing Ca^{2+} and PO_4; (2) direct stimulation of Ca^{2+} reabsorption from the distal convoluted tubules of the kidneys and decreasing reabsorption of phosphate; and (3) stimulating the production of 1,25-dihydroxy vitamin D (calcitriol) from its precursors. Calcitriol targets the gastrointestinal tract to reabsorb Ca^{2+} and PO_4 in the proximal tubules of the kidneys. All of these actions lead to increased plasma Ca^{2+} levels. However, the active form of vitamin D has a negative feedback on parathyroid glands (Fig. 2.1).

References

1. Wang L, Nancollas GH, Henneman ZJ. Nanosized particles in bone and dissolution insensitivity of bone mineral. Biointerphases. 2006;1:106–11.
2. Campbell AK. Calcium as an intracellular regulator. Proc Nutr Soc. 1990;49:51–6.
3. Bootman MD, Collins TJ, Peppiatt CM, Prothero LS, MacKenzie L, De Smet P, Travers M, Tovey SC, Seo JT, Berridge MJ, Ciccolini F, Lipp P. Calcium signalling—an overview. Semin Cell Dev Biol. 2001;12:3–10.
4. Hendy GN. Calcium-regulating hormones. Vitamin D and parathyroid hormone. In: Conn PM, Shlomo M, editors. Endocrinology. Basic and clinical principles. Totowa, NJ: Humana Press; 1997. p. 307–23.
5. Morrissey JJ, Cohn DV. Secretion and degradation of parathormone as a function of intracellular maturation of hormone pools. Modulation by calcium and dibutyryl cyclic AMP. J Cell Biol. 1979;83:521–8.
6. Hanley DA, Watson PH, Hodsman AB. Dempster DW. Pharmacological mechanisms of therapeutics: parathyroid hormone. In: Bilezikian J, Raisz LG, Martin TJ, editors. Principles of bone biology. 3rd ed. London: Elsevier; 2008. p. 1661–95.
7. Neer R, Berman M, Fisher L, et al. Multicompartmental analysis of calcium kinetics in normal adult males. J Clin Invest. 1967;46:1364–79.
8. Robertson WG, Marshall RW. Calcium measurements in serum and plasma—total and ionized. CRC Crit Rev Clin Lab Sci. 1979;11:271–304.

3 Hyperparathyroid Disorders

Qaisar Hussain Siraj

3.1 Introduction

Parathyroid disorders can result in either excessive production of parathyroid hormone causing hyperparathyroidism or underproduction of the hormone resulting in a hypoparathyroid state. This chapter deals with hyperparathyroid disorders, resulting from an overproduction of parathyroid hormone (PTH) with grave consequences to the patient's state of health. PTH is responsible for minute-to-minute regulation of serum calcium, and therefore parathyroid disorders, causing overproduction of PTH, profoundly affect serum calcium levels causing hypercalcaemia, which is defined as total serum calcium greater than 2 standard deviations above the normal mean, when corrected for serum albumin levels. Typically, this means a calcium level greater than 2.6 mmol/L. Hypercalcaemia as a result of hyperparathyroidism is a multisystem disease affecting the skeletal, renal, cardiovascular, gastrointestinal, and neuromuscular systems.

3.2 Symptoms and Signs of Hypercalcaemia

The historical adage 'moans, bones, groans and renal stones' have long been used to describe the symptoms of hypercalcaemia or hyperparathyroidism, but these are not specific to either diagnosis alone and represent a combination of both [1]. Table 3.1 lists the gamut of symptoms associated with hypercalcaemia due to hyperparathyroidism.

These classic symptoms have long been considered pathognomonic of the disease, but thanks to the automated laboratory biochemistry procedures, the diagnosis is now being made at an early stage in the disease, when most patients are yet

Q. H. Siraj (✉)
Department of Nuclear Medicine, Farwaniya Hospital, Kuwait

© Springer Nature Switzerland AG 2019
Q. Siraj (ed.), *Radionuclide Parathyroid Imaging*,
https://doi.org/10.1007/978-3-030-17351-7_3

Table 3.1 Symptoms and signs of hypercalcaemia

Gastrointestinal symptoms (moans):
– Abdominal pain
– Anorexia
– Nausea, vomiting
– Vomiting
– Constipation
– Peptic ulceration
– Pancreatitis (rare)
Neuromuscular (groans):
– Muscle weakness
– Fatigue
– Headache
– Depression
– Mental instability
– Lethargy
– Confusion
– Psychotic behaviour
– Stupor
– Coma
Skeletal (bones):
– Bone pain
– Arthralgia
– Osteitis fibrosa cystica (von Recklinghausen's disease of the bone)
– Osteoporosis
Renal (renal stones):
– Polyuria (nocturia)
– Polydipsia
– Nephrocalcinosis
– Nephrolithiasis
– Nephrogenic diabetes insipidus
– Renal failure
Cardiovascular:
– Arrhythmias
– Bradycardia
– Short QT interval
– Bundle branch block
– Atrioventricular block
– Hypertension (rare)
– Cardiac arrest (rare)
– Venous thrombosis
– Vascular calcification

asymptomatic. Biochemical hypercalcaemia and hyperparathyroidism are diagnostic, but increasingly, normal or borderline sporadic elevations in serum calcium with inappropriate PTH elevation are the only clue to what is now termed as eucalcaemic or normocalcaemic hyperparathyroidism [2]. This coupled with widespread vitamin D deficiency, which results in an increase in the PTH in the presence of normal serum calcium, makes the diagnosis somewhat confounding.

The severity of symptoms is related not only to the absolute calcium level but also to the rate of the rise in serum calcium levels. Patients with mild hypercalcaemia (serum calcium level <2.75 mmol/L) are mostly asymptomatic though some may report mild fatigue, vague changes in cognitive function, depression, or constipation.

Patients with moderate hypercalcaemia (serum calcium level 3.0–3.50 mmol/L) more commonly report the typical hypercalcaemic symptoms such as anorexia, nausea, abdominal pain, muscle weakness, and mental depression. Polyuria and polydipsia are common as a result of dehydration associated with a decreased urinary concentration ability secondary to hypercalcaemia. Patients with calcium levels >3.50 mmol/L may have progressive lethargy, disorientation, and even coma. Elderly or debilitated patients are more likely to be symptomatic even with mild hypercalcaemia. However, patients with chronic hypercalcaemia, despite higher serum calcium values (at around 3.75–4.0 mmol/L), are likely to have fewer symptoms compared with those showing an acute rise in the serum calcium level [3].

3.3 Causes of Hypercalcaemia

The causes of hypercalcaemia can be classified into two major categories: (1) non-PTH-related (Table 3.2) and (2) PTH-related (Table 3.3).

Table 3.2 PTH-independent causes of hypercalcaemia

Humoral hypercalcaemia of malignancy (HHM): PTHrP-mediated
Squamous carcinoma of the lung, oropharynx, nasopharynx, larynx, and oesophagus
Gynaecologic (cervical and ovarian)
Urologic (renal, transitional cell of the bladder)
Pheochromocytoma
Pancreatic islet cell tumours
T-cell lymphoma
Others
HHM: excess calcitriol (1,25-(OH)2-D3) mediated
B-cell lymphoma
Local osteolytic hypercalcaemia
Multiple myeloma
Breast carcinoma metastatic to bone
Lymphoma
Others
Medications/supplements
Vitamins A and D
Calcium-containing antacids (milk-alkali syndrome)
Thiazide diuretics
Granulomatous diseases
Sarcoidosis
Tuberculosis
Histoplasmosis
Leprosy
Endocrine
Severe thyrotoxicosis
Adrenal insufficiency
Pheochromocytoma
Other conditions
Factitious hypercalcaemia (due to increased plasma protein levels)
Acute renal failure
Immobilisation
Post rhabdomyolysis

Table 3.3 Causes of hypercalcaemia secondary to hyperparathyroidism (PTH-dependent hypercalcaemia)

Primary hyperparathyroidism (sporadic)
Tertiary hyperparathyroidism
Hereditary
Familial isolated
MEN 1
MEN 2A
MEN 4
HPT-JT
CaSR disorders
Familial hypocalciuric hypercalcaemia
Neonatal severe hyperparathyroidism
Ectopic PTH production
Lithium

Hypercalcaemia of malignancy has two forms: humoral hypercalcaemia of malignancy (HHM) and local osteolytic hypercalcaemia (LOH). The PTH-related protein (PTHrP) action accounts for the majority of HHM, whereas LOH results from the release of cytokines or other factors that activate bone resorption by osteoclasts from tumours growing in the bone. The amino terminus of the PTHrP peptide is homologous with PTH, and they share a common receptor. The metabolic effects of PTHrP are similar to those of PTH including activation of osteoclasts to resorb bone, decreasing renal calcium loss, and increasing renal phosphate clearance [4].

PTH-independent hypercalcaemia may occur due to excess production of calcitriol by granulomas, or bone resorption in severe hyperthyroidism or immobilised patients, or volume depletion in Addison's disease, or excessive intake of vitamins A and D causing bone resorption, or enhanced renal calcium reabsorption caused by thiazide diuretics.

Clinically, on the basis of the cause of hypersecretion of the PTH, hyperparathyroidism can be divided into primary, secondary, and tertiary types. Primary hyperparathyroidism (PHPT) is characterised by hypercalcaemia due to inappropriate secretion of PTH from one or more parathyroid glands in the absence of a known stimulus to parathyroid enlargement [5, 6].

Secondary hyperparathyroidism (SHPT), also known as renal osteodystrophy, is compensatory functional hyperplasia and hypertrophy of the parathyroid glands due to chronic kidney disease and is caused by hypocalcaemia or vitamin D deficiency, or both, or due to peripheral resistance to parathyroid hormone. The condition is usually associated with multiglandular parathyroid hyperplasia, although parathyroid adenomas may develop in rare instances.

The most common underlying cause of SHPT is end-stage renal failure, with vitamin D deficiency and malabsorption syndromes being less common causes. Less commonly, SHPT may be caused by calcium malabsorption, osteomalacia, vitamin D deficiency, or deranged vitamin D metabolism. It is typically associated with low or normal concentrations of serum calcium and increased PTH secretion, which represents an adaptive response, most commonly in patients with hypocalcaemia or hyperphosphataemia associated with renal failure [7]. The conversion of

25(OH)D to 1,25(OH)2D is also impaired, leading to decreased intestinal calcium absorption. In contrast to primary hyperparathyroidism, treating the underlying cause can reverse secondary hyperparathyroidism.

In PHPT, oversecretion of PTH results in impaired renal function due to hypercalcaemia caused by increased calcium absorption from the gut and calcium mobilisation from the bone. Sustained and non-treated PHPT results in renal failure with SHPT as a sequel, and hence it might be difficult to distinguish between PHPT and SHPT in the presence of renal injury.

Tertiary hyperparathyroidism refers to autonomous parathyroid hyperfunction in patients who have a history of prior secondary hyperparathyroidism in which the glandular hyperfunction and hypersecretion continue despite correction of the underlying abnormality, as in renal transplantation [8].

Familial hypocalciuric hypercalcaemia (FHH) is a genetic disorder due to calcium-sensing receptor (CaSR) mutation resulting in impaired inhibition of calcium reabsorption in the renal proximal convoluted tubule thick ascending limb of loop of Henle causing hypercalcaemia in the presence of an inappropriately normal PTH [9].

Lithium therapy can change the set point for the CaSR on the parathyroid gland so that a higher serum calcium concentration is needed to inhibit PTH secretion.

Rare cases of ectopic PTH-secreting tumours (small cell lung cancers, ovarian cancers, and papillary thyroid cancer) causing hypercalcaemia and hyperparathyroidism in the absence of a parathyroid adenoma have been reported [10, 11].

3.4 Primary Hyperparathyroidism (PHPT)

Primary hyperparathyroidism (PHPT) is an endocrine disorder that develops as a result of autonomous production and secretion of parathyroid hormone (PTH) from parathyroid gland (s). It is the most common cause of hypercalcaemia with an incidence of about 3:1000 in the general population though it is thought to be rising as a result of the introduction of automated methods for serum calcium determination. It is defined by an elevation of ionised serum calcium in the setting of an inappropriate elevation of PTH [12]. The diagnosis may extend from normocalcaemia accompanied by elevated PTH levels to hypercalcaemia accompanied by elevated or inappropriately normal PTH levels. The disorder results from abnormal hypersecretion of parathyroid hormone in the face of persistent hypercalcaemia due to a disorder of negative feedback inhibition of the parathyroid glands. PHPT is the most common cause of PTH and calcium level elevation and the third most common endocrine disorder, after diabetes and thyroid dysfunction. PHPT is either hereditary or sporadic.

3.4.1 Hereditary PHPT

Primary hyperparathyroidism (PHPT) is usually a sporadic disease, but in approximately 5–10% of cases, a familial and hereditary hyperparathyroid syndrome is diagnosed. The familial causes include familial isolated hyperparathyroidism, MEN 1, MEN 2A, MEN 4, and hyperparathyroidism-jaw tumour (HPT-JT) syndrome.

Familial isolated hyperparathyroidism is an inherited form of primary hyperparathyroidism characterised by parathyroid adenoma/hyperplasia in the absence of other associated endocrinopathies. In some cases, individuals also develop parathyroid carcinoma.

Multiple endocrine neoplasia (MEN) syndromes are a group of hereditary syndromes with an autosomal dominant hereditary pattern with a predilection to develop tumours of the endocrine organs, including the parathyroid glands. MEN syndromes are characterised by neoplasms in two or more endocrine organs. The neoplasms can be benign or malignant and secretory or non-secretory. Syndromes, in which primary hyperparathyroidism has been described, include MEN 1, MEN 2, and MEN 4 [13]. MEN 1 and MEN 2 are neoplastic syndromes which demonstrate an autosomal dominant inheritance pattern.

In MEN 1 syndrome, PHPT is the earliest and the most frequent expression with 80% occurrence, reaching 90% by the age of 35 years and almost 100% by the age of 50 years [14, 15].

Pancreatic endocrine tumours, anterior pituitary gland neoplasms and PHPT characterise MEN 1. The cause of PHPT in MEN 1 is hyperplasia of all four parathyroid glands over the lifetime of the patient, and there is an increased incidence of supernumerary glands by up to 20%, which are ectopically located [16].

MEN 2A is defined by medullary thyroid carcinoma, pheochromocytoma in about 50% of the patients, and PHPT caused by parathyroid gland hyperplasia in about 20% of patients. Clinical expression of MEN 1 and MEN 2A is different from sporadic hyperparathyroidism and is summed in Table 3.4 [17].

MEN 4 is a newly identified MEN syndrome with phenotypic overlap of both MEN 1 and MEN 2. It consists of bilateral pheochromocytomas, parathyroid adenomas, multifocal thyroid C-cell hyperplasia, paragangliomas, and endocrine pancreatic hyperplasia [18].

HPT-JT syndrome is a rare but unique autosomal dominant form of familial hyperparathyroidism syndrome, characterised by hyperparathyroidism due to multiple adenomas, and mandibular or maxillary ossifying fibromas, with a significantly increased prevalence of carcinomas and atypical adenomas, uterine tumours, and cystic and neoplastic renal lesions [19, 20].

Table 3.4 Expression of primary hyperparathyroidism by syndrome

Feature	Sporadic hyperparathyroidism	MEN 1	MEN 2A
Inheritance	None	Autosomal dominant	Autosomal dominant
Mean age of onset	55 years	25 years	>30 years
M:F ratio	1:3	1:1	1:1
Multiplicity	Single ~80% of cases	Multiple	Can be multiple
Other common tumours	None	Pancreatic tumours Pituitary tumours	Medullary thyroid cancer Pheochromocytoma

3.4.2 Sporadic PHPT

In the majority of cases (~90%), PHPT is a sporadic, non-familial, and non-syndromic disease [21]. An isolated parathyroid adenoma causes the pathologic lesions responsible for sporadic PHPT in approximately 85% of cases, 15% by diffuse parathyroid hyperplasia, 1–4% by double parathyroid adenomas, and <1% by parathyroid carcinoma [22–25]. Parathyroid adenomas are benign monoclonal tumours resulting from the neoplastic proliferation of a single abnormal cell, which autonomously produces and secretes the parathyroid hormone. This parathyroid gland disorder can occur in all age groups though it is rare in children, with a peak incidence in the sixth decade of life, with a female-to-male ratio between 2 and 3:1 [5].

3.4.3 Parathyroid Adenoma

3.4.3.1 Solitary Adenoma

Parathyroid adenoma can originate in any of the four parathyroid glands but is more common in the lower glands [26]. Grossly, adenomas are oval- or kidney-shaped, reddish brown in colour, and soft in consistency [27]. Parathyroid adenomas can vary markedly in size and weight, with the gland size ranging from <1 to >3 cm and the weight ranging from 50 mg to several grams [6]. The normal glands in patients with a parathyroid adenoma are suppressed with lower secretory activity and are smaller in size.

The tumour cells are usually arranged in nests and cords surrounded by a rich capillary network. In the majority of parathyroid adenomas, the chief cells are the dominant cell type, with varying proportions of oxyphil and transitional oxyphil cells seen scattered within the collections of chief cells [28]. Chief cell adenomas have rounded, hyperchromatic, pleomorphic nuclei, which are larger than those present in the normal parathyroid tissue. The histological diagnosis of an adenoma and hyperplasia rests on finding a rim of intervening normal or suppressed parathyroid tissue.

Oxyphil cell or oncocytic adenomas occur less frequently and are found in the sixth to seventh decades of life. They tend to be larger than the chief cell adenomas and are either non-functional or associated with minimal elevation of serum calcium levels [29].

Water-clear cell parathyroid adenoma as a cause of PHPT is extremely rare with only few reported cases to date [30, 31]. These adenomas consist of nests and acini of water-clear cells containing abundant foamy, granular cytoplasm, and mild nuclear pleomorphism.

3.4.3.2 Double or Multiple Adenomas

Parathyroid adenomas are most commonly a single-gland disease, but rarely double-gland or multigland parathyroid adenomas have been reported [32]. ‘Double’ or ‘multiple’ adenomas in some cases might well represent asymmetric or asynchronous multigland hyperplasia [33]. Patients with double or multiple adenomas are understandably relatively more symptomatic with higher PTH and serum alkaline phosphatase levels than those with solitary parathyroid adenomas or hyperplasia.

3.4.3.3 Microadenoma

Very rarely, tiny parathyroid adenomas can develop in parathyroid glands that are normal in size (6–7 mm) and weight (50–60 mg) [34]. Typical parathyroid adenomas are surrounded by a fibrous capsule; however, microadenomas (weighing <10 mg) are usually non-encapsulated [35].

3.4.3.4 Lipoadenomas

Lipoadenomas or parathyroid hamartomas are quite rare with an equal sexual predilection and occur beyond the fourth decade of life [36]. They consist of nests and cords of chief cells with a few intimately mixed oxyphil cells with a variable amount of mature adipose tissue and fibrous stroma. These may or may not be functional [33]. The high-fat content and relatively lower function make them difficult to diagnose on scintigraphy [36].

3.4.3.5 Cystic Adenoma (Functional Parathyroid Cyst)

Parathyroid adenomas with central necrosis or cystic degeneration are known as functional parathyroid cysts as opposed to the asymptomatic true parathyroid cysts which are embryonic vestiges or enlarged colloid microcysts within the parathyroids. They represent <9% of all adenomas and are frequently associated with PHPT [37, 38].

3.4.4 Parathyroid Hyperplasia

Parathyroid hyperplasia usually affects 10–15% of cases with sporadic PHPT. The multigland enlargement may be diffuse, asymmetric, or asynchronous. There are two major histological types of hyperplasia with the predominant majority of hyperplasia representing chief cell proliferation, although, very rarely, the water-clear cell hyperplasia can be encountered.

3.4.4.1 Chief Cell Hyperplasia

Chief cell hyperplasia, also known as nodular hyperplasia due to the range of cell types found, can occur in either primary or secondary hyperparathyroidism. Chief cell hyperplasia is commonly seen in PHPT associated with MEN 1 and MEN 2A syndromes. The hyperplastic glands are rounded and grossly lobulated, grey or brown in colour, and vary in weight from 50 mg to over 10 g. In chief cell hyperplasia associated with secondary hyperparathyroidism, the glands are hard, nodular, and firm, with the nodules macroscopically resembling multinodular thyroid disease [39]. Hyperplastic glands in patients with tertiary hyperparathyroidism are even larger in size and show more asymmetric enlargement and parenchymal nodularity.

3.4.4.2 Water-Clear Cell Hyperplasia

Water-clear cell hyperplasia is a very rare condition with marked enlargement of all four glands, which are lobulated, chocolate brown in colour, and translucent. The upper glands, however, can be 5–10 times larger than the lower pair of glands. The water-clear cell hyperplastic glands commonly contain large cysts with haemorrhagic areas. Histologically, the gland contains large (20 μm) water-clear cells with peripherally located nuclei [35, 39].

3.4.5 Parathyroid Carcinoma

Parathyroid carcinoma is very rare accounting for <1% to 5% of cases of sporadic PHPT [40, 41] with a challenging histological diagnosis. The World Health Organization histopathological criteria for parathyroid carcinoma diagnosis include unequivocal presence of vascular invasion in the capsule or adjacent tissues, perineural space invasion, capsular invasion with extension to adjacent tissues, and/or presence of metastases [42, 43].

Cancerous parathyroid glands generally weigh more than 1 g in weight, with the tumour appearing as a lobulated, firm, and encapsulated mass, which is generally larger than an adenoma in size [44]. Clinical and biochemical manifestations of parathyroid cancer are those of severe PHPT. The mean age at presentation is 50 years with equal preponderance between the two sexes [45, 46]. It is a slow-growing but eventually fatal cancer with 5-year survival ranging from 50% to 86% [46, 47]. Survival depends on the timely diagnosis, the pathological nature of the disease, and the surgical technique, but the primary determinant of survival is the uncontrollable hypercalcaemia and its fatal consequences [48].

References

1. Cox J, Stearns M. Symptoms, differential diagnosis and management. In: Arora A, Tolley N, Tuttle M, editors. A practical manual of thyroid and parathyroid disease. London: Wiley-Blackwell; 2010. p. 184–5.
2. Licata AA, Lerma EV, editors. Diseases of the parathyroid glands. Berlin: Springer Science+Business Media; 2012.
3. Holt EH. Diagnosis and treatment of the patient with abnormal calcium. In: Licata AA, Lerma EV, editors. Diseases of the parathyroid glands. Berlin: Springer Science+Business Media; 2012. https://doi.org/10.1007/978-1-4419-5550-0_3.
4. Dunbar ME, Wysolmerski JJ, Broadus AE. Parathyroid hormone-related protein: from hypercalcemia of malignancy to developmental regulatory molecule. Am J Med Sci. 1996;312:287.
5. DeLellis RA, Mazzaglia P, Mangray S. Primary hyperparathyroidism: a current perspective. Arch Pathol Lab Med. 2008;132:1251–62.
6. Carlson D. Parathyroid pathology: hyperparathyroidism and parathyroid tumors. Arch Pathol Lab Med. 2010;134:1639–44.
7. Rodriguez M, Canalejo A, Garfia B, Aguilera E, Almaden Y. Pathogenesis of refractory secondary hyperparathyroidism. Kidney Int. 2002;80:155–60.

8. Rivkees SA, el-Hajj-Fuleihan G, Brown EM, Crawford JD. Tertiary hyperparathyroidism during high phosphate therapy of familial hypophosphatemic rickets. J Clin Endocrinol Metab. 1992;75:1514–8.
9. Burski K, Torjussen B, Paulsen AQ, Boman H, Bollerslev J. Parathyroid adenoma in a subject with familial hypocalciuric hypercalcemia: coincidence or causality? J Clin Endocrinol Metab. 2002;87(3):1015–6.
10. Yoshimoto K, Yamasaki R, Sakai H, Tezuka U, Takahashi M, Iizuka M, Sekiya T, Saito S. Ectopic production of parathyroid hormone by small cell lung cancer in a patient with hypercalcemia. J Clin Endocrinol Metab. 1989;68(5):976–81.
11. Nussbaum SR, Gaz RD, Arnold A. Hypercalcemia and ectopic secretion of parathyroid hormone by an ovarian carcinoma with rearrangement of the gene for parathyroid hormone. N Engl J Med. 1990;323(19):1324–8.
12. Thompson NW, Eckhauser FE, Harness JK. The anatomy of primary hyperparathyroidism. Surgery. 1982;92:814–21.
13. Marx SJ. Molecular genetics of multiple endocrine neoplasia types 1 and 2. Nat Rev Cancer. 2005;5(5):367–75.
14. Tonelli F, Marcucci T, Giudici F, Falchetti A, Brandi ML. Surgical approach in hereditary hyperparathyroidism. Endocr J. 2009;56(7):827–41.
15. Brandi ML, Gagel RF, Angeli A, Bilezikian JP, Beck-Peccoz P, Bordi C, Conte-Devolx B, Falchetti A, Gheri RG, Libroia A, Lips CJ, Lombardi G, Mannelli M, Pacini F, Ponder BA, Raue F, Skogseid B, Tamburrano G, Thakker RV, Thompson NW, Tomassetti P, Tonelli F, Wells SA Jr, Marx SJ. Guidelines for diagnosis and therapy of MEN type 1 and type 2. J Clin Endocrinol Metab. 2001;86(12):5658–71.
16. Lambert LA, Shapiro SE, Lee JE, Perrier ND, Truong M, Wallace MJ, Hoff AO, Gagel RF, Evans DB. Surgical treatment of hyperparathyroidism in patients with multiple endocrine neoplasia type 1. Arch Surg. 2005;140(4):374–82.
17. Zaidi SS, Lakhani VT, Broome JT. Hyperparathyroidism in multiple endocrine neoplasia. In: Licata AA, Lerma EV, editors. Diseases of the parathyroid glands. Berlin: Springer Science+Business Media, LLC; 2012. https://doi.org/10.1007/978-1-4419-5550-0_11.
18. Benson L, Ljunghall S, Akerstrom G, Oberg K. Hyperparathyroidism presenting as the first lesion in multiple endocrine neoplasia type 1. Am J Med. 1987;82(4):731–7.
19. Masi G, Barzon L, Iacobone M, Viel G, Porzionato A, Macchi V, De Caro R, Favia G, Palù G. Clinical, genetic, and histopathologic investigation of CDC73-related familial hyperparathyroidism. Endocr Relat Cancer. 2008;15:1115–26.
20. Iacobone M, Masi G, Barzon L, Porzionato A, Macchi V, Ciarleglio FA, Palù G, De Caro R, Viel G, Favia G. Hyperparathyroidism-jaw tumor syndrome: a report of three large kindred. Langenbecks Arch Surg. 2009;394:817–25.
21. Thakker RV. Genetics of parathyroid tumours. J Intern Med. 2016;280(6):574–83.
22. Massaro A, Cittadin S, Rampin L, et al. Accurate planning of minimally invasive surgery of parathyroid adenomas by means of [(99m)Tc]MIBI SPECT. Minerva Endocrinol. 2007;32:9–16.
23. Pelizzo MR, Piotto A, Bergamasco A, Rubello D. Parathyroid carcinoma. Therapeutic strategies derived from 20 years of experience. Minerva Endocrinol. 2001;26:23–9.
24. Lumachi F, Zucchetta P, Marzola MC, et al. Advantages of combined technetium-99m-sestamibi scintigraphy and high-resolution ultrasonography in parathyroid localization. Eur J Endocrinol. 2000;26:755–60.
25. Udelsman R. Primary hyperparathyroidism. In: Cameron JL, editor. Current surgical therapy. St. Louis, MO: Mosby; 2001. p. 662–7.
26. Grimelius L, Akerstrom G, Johansson H, Bergstrom R. Anatomy and histopathology of human parathyroid glands. Pathol Annu. 1981;16:1–24.
27. Summers GW. Parathyroid update: a review of 220 cases. Ear Nose Throat J. 1996;75:434–9.
28. Grimelius L, Johansson H. Pathology of parathyroid tumors. Semin Surg Oncol. 1997;13:142–54.

29. Giorgadze T, Stratton B, Baloch ZW, Livolsi VA. Oncocytic parathyroid adenoma: problem in cytological diagnosis. Diagn Cytopathol. 2004;31:276–80.
30. Bégueret H, Belleannée G, Dubrez J, Trouette H, Parrens M, Velly JF, de Mascarel A. Clear cell adenoma of the parathyroid gland: a rare and misleading lesion. Ann Pathol. 1999;19(4):316–9.
31. Prasad KK, Agarwal G, Krishnani N. Water-clear cell adenoma of the parathyroid gland: a rare entity. Indian J Pathol Microbiol. 2004;47(1):39–40.
32. Harkness JK, Ramsburg SR, Nishiyamarh RH, et al. Multiple adenomas of the parathyroids: do they exist? Arch Surg. 1979;114:468–74.
33. van der Walt J. Pathology of the parathyroid glands. Diagn Histopathol. 2012;18:221–33.
34. Liechly RD, Teter A, Suba EJ. The tiny parathyroid adenoma. Surgery. 1986;100:1048.
35. Mizamtsidi M, Nastos C, Mastorakos G, Dina R, Vassiliou I, Gazouli M, Palazzo F. Diagnosis, management, histology and genetics of sporadic primary hyperparathyroidism: old knowledge with new tricks. Endoc Connect. 2018;7(2):R56–68.
36. Turner WJD, Baergen RN, Pellitteri PK, Orloff LA. Parathyroid lipoadenoma: case report and review of the literature. Otolaryngol Head Neck Surg. 1996;114:313–6.
37. Rogers LA, Fetter BF, Peete WPJ. Parathyroid cyst and cystic degeneration of parathyroid adenoma. Arch Pathol. 1969;88:476–9.
38. Johnson NA, Yip L, Tublin ME. Cystic parathyroid adenoma: sonographic features and correlation with 99mTc-sestamibi SPECT findings. AJR Am J Roentgenol. 2010;195(6):1385–90. https://doi.org/10.2214/AJR.10.4472.
39. Lynn J, Lewis P. Pathological spectrum of parathyroid disease. In: Arora A, Tolley NS, Tuttle RM, editors. A practical manual of thyroid and parathyroid disease. Chichester: Wiley-Blackwell; 2010. p. 164–73.
40. Schantz A, Castleman B. Parathyroid carcinoma. A study of 70 cases. Cancer. 1973;31(3):600–5.
41. Koea JB, Shaw JH. Parathyroid cancer: biology and management. Surg Oncol. 1999;8:155–65.
42. DeLellis RA. World health organisation classification of tumours. Pathology and genetics of tumours of endocrine organs. Lyon: AIRC; 2006.
43. Kruijff S, Sidhu SB, Sywak MS, Gill AJ, Delbridge LW. Negative parafibromin staining predicts malignant behavior in atypical parathyroid adenomas. Ann Surg Oncol. 2014;21:426–33.
44. Lack CA, Rarber JL, Rubin E. The endocrine system. In: Rubin E, Farber JL, editors. Pathology. 3rd ed. Philadelphia, PA: Lippincott-Raven; 1999. p. 1179–83.
45. Shane E. Clinical review 122: parathyroid carcinoma. J Clin Endocrinol Metab. 2001;86:485–93.
46. Hundahl SA, Fleming ID, Fremgen AM, et al. Two hundred eighty-six cases of parathyroid carcinoma treated in the U.S. between 1985–1995: a National Cancer Data Base Report. The American College of Surgeons Commission on Cancer and the American Cancer Society. Cancer. 1999;86:538–44.
47. Sandelin K, Auer G, Bondeson L, et al. Prognostic factors in parathyroid cancer: a review of 95 cases. World J Surg. 1992;16:724–31.
48. Kebebew E. Parathyroid carcinoma. Curr Treat Options Oncol. 2001;2:347–54.

4 Diagnostic Imaging: Structural Modalities

Amir Javaid and Qaisar Hussain Siraj

4.1 Introduction

Primary hyperparathyroidism has evolved from a historically advanced disease at the time of diagnosis, typified by the adage "bones, moans, stones, and groans" to a mostly asymptomatic disorder, particularly in the developed world [1–3]. This advance is due to the early laboratory diagnosis and timely surgery, which remains the mainstay of curative treatment even though the majority of asymptomatic patients have stable disease [4].

The introduction of the minimally invasive technique in the mid-1990s produced a dramatic change in parathyroid surgical approach, with the result that now, limited parathyroid exploration surgery is being more frequently undertaken as compared with the traditional bilateral neck exploration. The minimally invasive parathyroid surgical technique has evolved in tandem with the introduction of accurate and sensitive preoperative localisation techniques and intraoperative parathyroid monitoring through the development of rapid intraoperative parathyroid hormone (ioPTH) level assay and intraoperative gamma probe localisation of the overactive parathyroid lesions.

This new surgical approach has changed the algorithm and revived the need for preoperative parathyroid localisation, which was previously considered practically only useful for the detection of ectopic parathyroid pathology: it was said that the best localisation test that can be performed is to localise a good parathyroid surgeon [5].

The role of noninvasive preoperative localisation has now become crucial to a successful surgical outcome. Imaging for parathyroid localisation is performed in patients with biochemically confirmed sporadic primary hyperparathyroidism to

A. Javaid · Q. H. Siraj (✉)
Department of Nuclear Medicine, Farwaniya Hospital, Kuwait

© Springer Nature Switzerland AG 2019

Q. Siraj (ed.), *Radionuclide Parathyroid Imaging*,
https://doi.org/10.1007/978-3-030-17351-7_4

identify patients who are candidates for a minimally invasive approach. Imaging is also valuable in patients with recurrent or persistent disease.

The older noninvasive imaging studies such as barium swallow, thermography, non-contrast enhanced computerised tomography (NECT), and selenomethionine-75 scintigraphy had a poor diagnostic yield and had long been abandoned. Current noninvasive preoperative parathyroid localisation techniques include radionuclide scintigraphy, ultrasound, magnetic resonance imaging (MRI), and contrast-enhanced computed tomography (CECT). The invasive localisation techniques of selective venous sampling and arteriography have a good diagnostic yield but are technically cumbersome, time-consuming, and costly and may involve a degree of risk. This chapter shall focus on the invasive and the noninvasive correlative structural imaging modalities, with the scintigraphic imaging covered in detail in Chap. 5.

4.2 Ultrasonography

Ultrasonography is the most commonly employed structural imaging modality for preoperative localisation of parathyroid gland pathology. The advantages of this modality are manifold including a lack of radiation exposure, speed, cost, convenience, and widespread availability. A further advantage is its ability to screen for concomitant thyroid gland pathology.

Normal-sized parathyroid glands are usually not visualised with ultrasound. Parathyroid adenomas are larger and can be demonstrated with the use of high-frequency transducers (12 or 15 MHz). The ultrasound field should cover the neck and the surrounding ectopic parathyroid region, from the carotid bifurcation superiorly to the sternal notch inferiorly and the carotid artery/internal jugular vein laterally [6, 7].

On greyscale images, parathyroid adenomas appear as discrete, oval, or round-shaped anechoic or hypoechoic masses (Fig. 4.1). They are located posterior to the thyroid gland, anterior to the longus colli muscles, and usually, medial to the common carotid artery. An echogenic line separating the thyroid gland from the enlarged parathyroid gland can usually be seen [8]. Cystic changes and lobulations may be seen in larger adenomas with increased echogenicity at times due to fatty deposition and occasionally calcifications [9].

Colour Doppler ultrasound has been used for localising enlarged parathyroid glands and differentiating these from other cervical structures including lymph nodes, which have a different vascular supply pattern. Parathyroid adenomas tend to be hypervascular lesions especially when the adenoma is larger than 1 cm in size. The sensitivity of ultrasound for detecting parathyroid adenomas has been reported from 55% to 83%; it is especially low in the mediastinum, owing to a poor or absent acoustic window. The specificity of ultrasound ranges from 40% to 98%. The success rate of ultrasound for the detection of parathyroid lesions is operator-dependent and hence variable depending on the sonographer's skill and experience and their knowledge of cervical anatomy. Despite these factors, ultrasound appears to be a practical first-line structural imaging modality for the preoperative localisation of parathyroid adenomas [10].

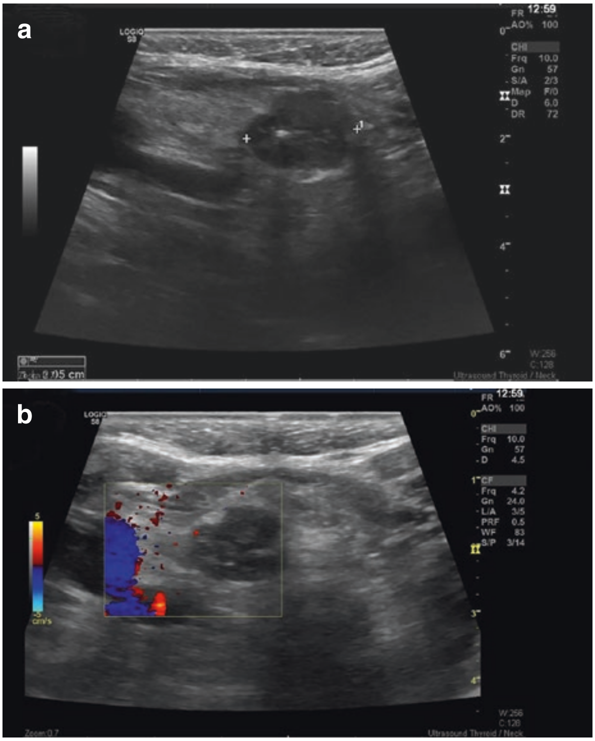

Fig. 4.1 (**a**) Ultrasonography of a right lower parathyroid adenoma showing a well-defined hypoechoic lesion at the lower pole of the right thyroid lobe measuring about 2 × 1.5 cm, showing a tiny calcified focus. (**b**) No abnormal vascularity is seen on colour Doppler imaging

False-positive findings are seen in cases of thyroid nodules and enlarged lymph nodes in the neck. Sometimes peri-thyroid veins are mistaken for enlarged parathyroid glands. False-negative studies are frequent in cases of small parathyroid glands, ectopic glands, scarring after previous surgery, concomitant goitre or thyroid disease, or body habitus. Where an intrathyroidal parathyroid adenoma is suspected, fine needle aspiration biopsy is required to confidently differentiate between a parathyroid adenoma and a thyroid nodule [7].

4.3 Computed Tomography (CT)

Non-contrast-enhanced CT is not employed by itself for the diagnosis of parathyroid lesions but has now become integral to hybrid radionuclide imaging with single-photon emission computed tomography (SPECT) and positron emission tomography (PET). As an integral component of the SPECT/CT and PET/CT hybrid systems, its function is both attenuation correction and image registration, and, in this context, it can provide invaluable additional structural information increasing the diagnostic yield of the multimodality radionuclide imaging. Density measurements and anatomical location can identify parathyroid lesions. In general, parathyroid adenomas are well defined and have attenuation measurements lower than 80 Hounsfield units (HU), compared with the normal thyroid tissue with a density higher than 80 HU due to its high iodine content [11]. However, it is more challenging to separate parathyroid adenomas from the surrounding muscles and lymph nodes with similar tissue density.

Conventional multidetector thin-slice contrast-enhanced spiral CT imaging for parathyroid localisation involves imaging from the base of the skull down to 2 cm below the carina after intravenous iodinated contrast injection. Parathyroid lesions show intense enhancement (>130 HU), with a lower enhancement seen in the lymph nodes and the adjacent skeletal muscles [12].

Recent improvements in CT technology coupled with improved imaging algorithms have improved the sensitivity of contrast-enhanced CT, which reportedly ranges from 46% to 87%, which however is still lower than the current first-line radionuclide and ultrasound imaging techniques [13].

In the past decade, multiphase (three- or four-phase) “four-dimensional” computed tomography (4D-CT) has emerged as an improved CT technique, which is increasingly being propagated as the primary structural imaging technique for adenoma localisation. The four-phase method involves acquiring the scan in four imaging phases to include (1) an initial non-contrast phase, followed by (2) post-contrast arterial phase at 30 s and delayed phases at (3) 60-s and (4) 90-s. The multiphase acquisition allows temporal data acquisition for respiratory motion correction that affects contrast attenuation over time. At least the first three of the four phases are required because only 20% of parathyroid lesions have higher attenuation than thyroid on the arterial phase and 22% of adenomas have a similar enhancement to the thyroid on both the arterial and delayed phases and could be missed without the non-contrast and the delayed imaging [14, 15].

The 4D-CT provides both functional and in-depth anatomic information. The first non-contrast image helps distinguish adenomas from the iodine-rich dense thyroid gland but has a similar attenuation as that of the surrounding muscles. The early and delayed post-contrast imaging highlights the hypervascular nature of adenomas during the arterial phase and their characteristic early washout [16]. A hypervascular soft tissue mass near the expected location of the parathyroid gland with variable contrast enhancement and rapid washout is considered to be a parathyroid adenoma (Figs. 4.2 and 4.3). 4D-CT is sensitive for small adenomas that may elude other imaging techniques. Also, ectopic glands may be seen, most commonly within the mediastinum area.

The sensitivity of 4D-CT for parathyroid lesion localisation has been reported as high as 88% to 91% [15, 17]. Most modern multiphase 4D-CT techniques report a higher than 90% sensitivity and specificity. However, the diagnosis of multigland adenomatous disease is challenging despite the contemporary CT techniques. A recent study of 4D-CT in multigland adenomas reported a lower sensitivity at 44.9% [17]. 4D-CT may be falsely negative in the presence of ectopic or small-sized parathyroid adenomas. Technical artefacts on CT such as streak artefacts due to beam hardening and Compton scatter caused by metallic objects and bone may occasionally affect image quality to the point where lesions may be missed. Prior neck

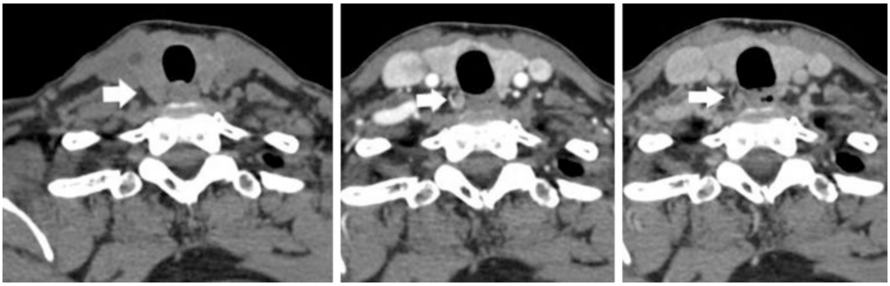

Fig. 4.2 Axial non-contrast (left), early arterial phase post-contrast (middle), and delayed venous phase post-contrast (right) images show a hypoattenuated hypodense nodule at the posterior aspect of the right thyroid lobe with avid early contrast enhancement followed by washout (images courtesy Dr. T Sudarshan, Ninewells Hospital and Medical School, Dundee, UK)

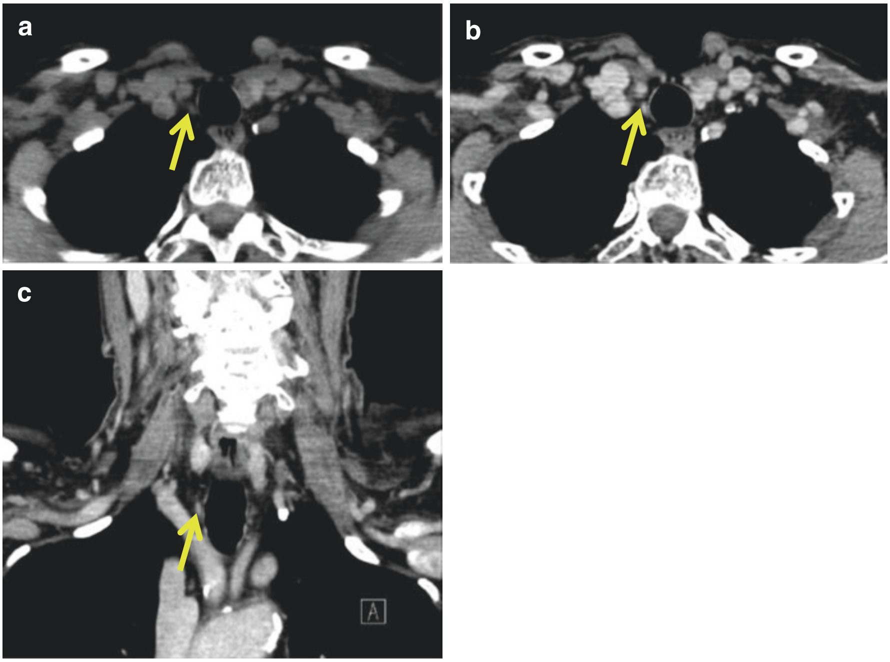

Fig. 4.3 A 62-year-old woman with small right parathyroid adenoma. Non-enhanced phase axial image (**a**) shows an 8 × 3 × 3 mm low-density soft tissue lesion overlying the right side of the trachea, just medial to the right common carotid artery, with the post-contrast axial (**b**) and coronal (**c**) images showing enhancement within the soft tissue (images courtesy Drs. S. Voo & J. Bomanji, UCLH, London)

surgery can also distort the anatomy resulting in a false-negative CT scan result. However, the main drawback of 4D-CT is the high radiation dose to the patient. Even with the use of dose reduction techniques, the 4D-CT still delivers a significant radiation dose [18, 19].

4.4 Magnetic Resonance Imaging (MRI)

Normal parathyroid glands are usually not seen on MR images though occasionally a soft tissue density focus in the expected location of a parathyroid gland can be identified. Parathyroid adenomas can be recognised on MRI as they may demonstrate characteristically low-intermediate signal intensity on T1-weighted MR pulse sequences and high signal intensity on T2-weighted images [20]. However, as many as 30% of the adenomas do not have typical MRI signal intensity characteristics. Atypical MRI patterns include (1) high signal intensity on T1-weighted images and low-to-medium signal intensity on T2-weighted images, (2) low signal intensity on both T1- and T2-weighted images, and (3) high signal intensity on both T1- and T2-weighted images [21]. Low signal intensity on T1- and T2-weighted images both may be associated with degenerative cellular changes, old haemorrhage with hemosiderin-laden macrophages, and fibrosis in the abnormal parathyroid gland. High signal intensity on both T1- and T2-weighted images indicates acute haemorrhage without significant degenerative or fibrotic changes [22].

False-positive findings are due to enlarged lymph nodes, thyroid nodules (solid and cystic), enlarged cervical ganglia, and other neck masses. Enlarged lymph nodes have a signal intensity similar to that of abnormal parathyroid glands.

False-negative findings are mostly associated with small parathyroid glands. The mean volume for the detection of abnormal glands has been reported at 3.5 cm^3, whereas the mean volume for missed adenomatous glands is 1.4 cm^3. Other reported false-negative findings result from anatomic distortion due to prior surgery, ectopic glands, metallic artefacts, and patient motion [21].

Parathyroid adenomas frequently show avid gadolinium enhancement on T1-weighted images (Fig. 4.4), and consequently it is possible to perform dynamic or early uptake and late washout phase 4D-MRI like 4D-CT (Figs. 4.2 and 4.3). However, in patients with moderate to end-stage renal disease with secondary or tertiary hyperparathyroidism, the development of nephrogenic systemic fibrosis is a significant risk associated with gadolinium-based MRI contrast agent [23].

MRI has the inherent advantage of a lack of radiation exposure. However, the sensitivity of MRI is significantly lower than CT (~70%), but it has a higher sensitivity (>80%) in locating ectopic mediastinal glands [24]. Its use can be justified in the context of ectopic adenomas and when radionuclide imaging and ultrasound are equivocal or discordant.

4.5 Angiography

Digital subtraction angiography (DSA) or conventional arteriography can be used to localise a parathyroid adenoma. Parathyroid adenomas are hypervascular compared with normal thyroid and normal parathyroid tissue and show a characteristic “blush” on digital subtraction angiography. Arteriography of both thyrocervical trunks, both internal mammary arteries, and both common carotid arteries is recommended [25]. Because of its associated risk, this highly invasive technique is rarely used today.

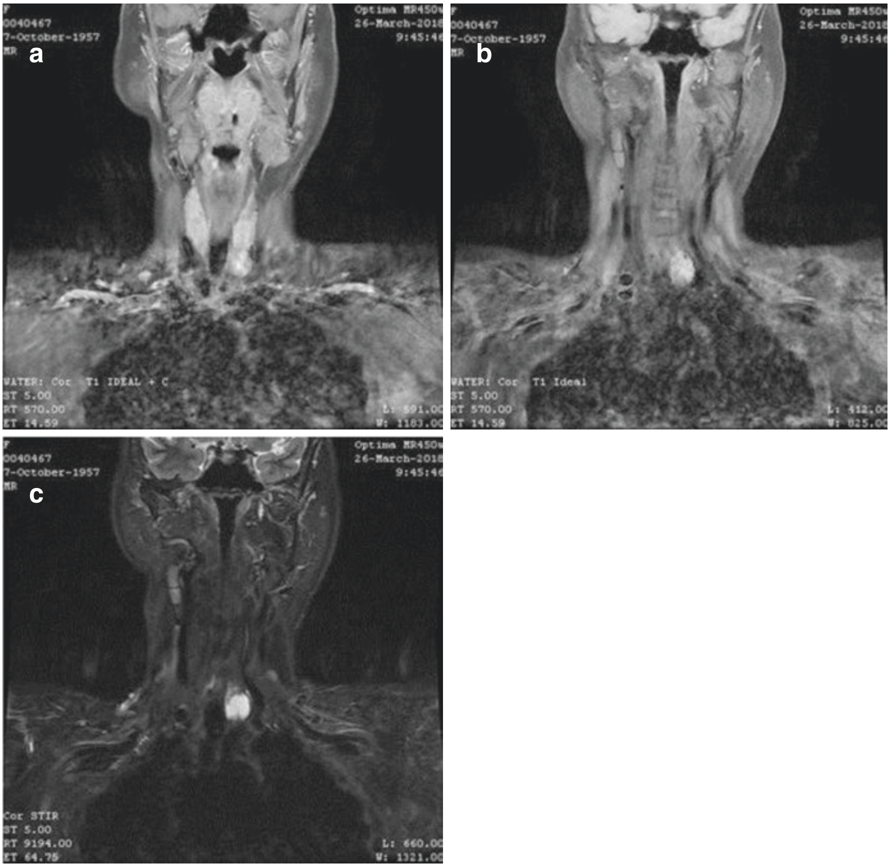

Fig. 4.4 MRI showing avid gadolinium enhancement (**a**–**c**) on T1-weighted images in a left lower parathyroid adenoma

Stroke and spinal cord injury are the two significant risks of parathyroid arteriography. The sensitivity of DSA has been reported at 49% [25] and the false-positive rate at approximately 9% [26].

4.6 Selective Venous Sampling

Selective venous sampling for parathyroid hormone (PTH) allows estimation of the general location of a parathyroid adenoma. The technique involves obtaining blood samples from multiple sites proximal and distal to the potential location of a parathyroid adenoma. PTH gradients are measured by comparing PTH levels from the sampled vein with a peripheral venous sample (Fig. 4.5). A parathyroid arteriogram, however, needs to be performed first to identify the variable parathyroid venous pathway [25].

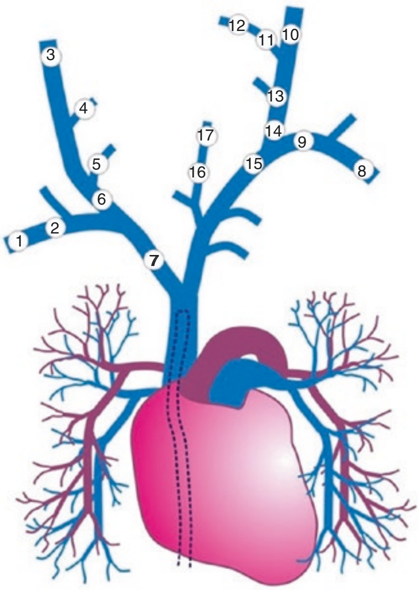

No.	PTH (pmol)	Vein site
1	18.26	Right axillary
2	17.16	Right subclavian
3	20.46	High right internal jugular
4	19.91	Right superior thyroid
5	18.70	Right middle thyroid
6	21.67	Right lower internal jugular
7	17.82	Right brachiocephalic
8	15.62	Left axillary
9	12.32	Left subclavian
10	13.55	High left internal jugular
11	395	Left superior thyroid
12	645	Left superior thyroid
13	95	Left internal jugular (mid thyroid level)
14	130	Left internal jugular (low level)
15	12.84	Left brachiocephalic
16	20.05	Left inferior thyroid (higher level)
17	17.64	Left inferior thyroid vein (lower level)

Fig. 4.5 PTH levels sampled from various selected venous sites show the highest values from the sample obtained from left superior thyroid vein indicating that the left upper parathyroid adenoma is responsible for PTH hypersecretion [27]

The interventional and complex nature of this invasive technique, its cost, and associated radiation exposure limit its utilisation. It is an operator-dependent and technically cumbersome technique with a variable success rate. The use of the method is limited to revision surgeries where preoperative imaging modalities are either negative or equivocal. The success rate of the technique in identifying the location of a parathyroid adenoma in such cases is reported from 70% to 80% [25, 27].

4.7 Conclusion

A range of imaging modalities and a variety of techniques are available for the pre-operative localisation of parathyroid pathology in patients with hyperparathyroidism. The diagnostic imaging algorithms vary between institutions based on local availability, expertise and experience in parathyroid imaging, and clinician's preferences. Parathyroid scintigraphy and ultrasonography are usually the first-line imaging modalities, whereas MRI and contrast-enhanced CT play a corroborative and problem-solving role when the results of the initial imaging studies are negative, equivocal, or incongruous.

References

1. Albright F, Reifenstein EC Jr. The parathyroid glands and metabolic bone disease. Baltimore, MD: Williams & Wilkins; 1948.
2. Mundy GR, Cove DH, Fisken R. Primary hyperparathyroidism: changes in the pattern of clinical presentation. Lancet. 1980;1:1317–20.
3. Bilezikian JP, Silverberg SJ, Gartenberg F, et al. Clinical presentation of primary hyperparathyroidism. In: Bilezikian JP, editor. The parathyroids: basic and clinical concepts. New York, NY: Raven Press; 1994. p. 457–70.
4. Coe FL, Favus MJ. Does mild, asymptomatic hyperparathyroidism require surgery? N Engl J Med. 1980;302:224–5.
5. Coakley AJ, Wells CP. Parathyroid. In: Maisey MN, Britton KE, Collier BD, Siraj QH, editors. Clinical nuclear medicine. Cambridge, MA: Chapman & Hall; 1998. p. 381–7.
6. Leupe PK, Delaere PR, Vander Poorten VL, Debruyne F. Pre-operative imaging in primary hyperparathyroidism with ultrasonography and sestamibi scintigraphy. B-ENT. 2011;7(3):173–80.
7. Gooding GA. Sonography of the thyroid and parathyroid. Radiol Clin North Am. 1993;31(5):967–89.
8. Hopkins CR, Reading CC. Thyroid and parathyroid imaging. Semin Ultrasound CT MR. 1995;16(4):279–95.
9. Johnson NA, Yip L, Tublin ME. Cystic parathyroid adenoma: sonographic features and correlation with 99mTc-sestamibi SPECT findings. AJR Am J Roentgenol. 2010;195(6):1385–90.
10. Chazen JL. Parathyroid adenoma imaging. 2018. https://emedicine.medscape.com/article/384024-overview#a4. Accessed on 14 Mar 2018.
11. Reading CC, Gorman CA. Thyroid imaging techniques. Clin Lab Med. 1993;13:711–24.
12. Ernst O. Hyperparathyroidism: CT and MR findings. J Radiol. 2009;90:409–12.
13. Gotway MB, Higgins CB. MR imaging of the thyroid and parathyroid glands. Magn Reson Imaging Clin N Am. 2000;8:163–82.
14. Bahl M, Sepahdari AR, Sosa JA, Hoang JK. Parathyroid adenomas and hyperplasia on four-dimensional CT Scans: three patterns of enhancement relative to the thyroid gland justify a three-phase protocol. Radiology. 2015;277(2):454–62.
15. Rodgers SE, Hunter GJ, Hamberg LM, et al. Improved preoperative planning for directed parathyroidectomy with 4-dimensional computed tomography. Surgery. 2006;140(6):932–40.
16. Beland MD, Mayo-Smith WW, Grand DJ, Machan JT, Monchik JM. Dynamic MDCT for localisation of occult parathyroid adenomas in 26 patients with primary hyperparathyroidism. AJR Am J Roentgenol. 2011;196(1):61–5.
17. Chazen JL, Gupta A, Dunning A, Phillips CD. Diagnostic accuracy of 4D-CT for parathyroid adenomas and hyperplasia. Am J Neuroradiol. 2012;33(3):429–33.
18. Welling RD, Olson JA Jr, Kranz PG, et al. Bilateral retropharyngeal parathyroid hyperplasia detected with 4D multidetector row CT. AJNR Am J Neuroradiol. 2010;32:E80–2.
19. Russell MT, Fink JR, Rebeles F, et al. Balancing radiation dose and image quality: clinical applications of neck volume CT. AJNR Am J Neuroradiol. 2008;29:727–31.
20. Kabala JE. Computed tomography and magnetic resonance imaging in diseases of the thyroid and parathyroid. Eur J Radiol. 2008;66:480–92.
21. Auffermann W, Guis M, Tavares NJ, Clark OH, Higgins CB. MR signal intensity of parathyroid adenomas: correlation with histopathology. AJR Am J Roentgenol. 1989;153(4):873–6.
22. Neumann DR, Shin JJ. Imaging in parathyroid diseases. In: Licata AA, Lerma EV, editors. Diseases of the parathyroid glands. Berlin: Springer Science & Business Media, LLC; 2012. p. 343–62.

23. Chen AY, Zirwas MJ, Hefferman MP. Nephrogenic systemic fibrosis: a review. J Drugs Dermatol. 2010;9:829–34.
24. Stevens SK, Chang JM, Clark OH, Chang PJ, Higgins CB. Detection of abnormal parathyroid glands in postoperative patients with recurrent hyperparathyroidism: sensitivity of MR imaging. AJR Am J Roentgenol. 1993;160(3):607–12.
25. Miller DL. Endocrine angiography and venous sampling. Radiol Clin North Am. 1993;31(5):1051–67.
26. Jaskowiak N, Norton JA, Alexander HR, et al. A prospective trial evaluating a standard approach to reoperation for missed parathyroid adenoma. Ann Surg. 1996;224:308–20.
27. Stack BC, Randolph G. Investigations. In: Arora A, Tolley NS, Tuttle RM, editors. A practical manual of thyroid and parathyroid disease. Oxford: Wiley Blackwell; 2010. p. 164–74.

Parathyroid Scintigraphy

5

Qaisar Hussain Siraj, Sonya Borisova Sergieva, and Amir Javaid

5.1 Introduction

Over the years, a variety of radiotracers have been employed for imaging the parathyroid glands. Parathyroid scintigraphy dates back to the early 1960s when ^{57}Co-cyanocobalamine and ^{75}Se-selenomethionine were first used for the detection of parathyroid adenomas [1, 2]. However, these tracers showed suboptimal uptake, resulting in poor image quality and a high radiation dose to the patient. The specific activity of ^{57}Co-B_{12} in the parathyroid tissues was deemed much too low for it to be considered a practical agent for visualising hyperfunctioning parathyroid adenomas in humans [3, 4]. However, selenomethionine, an amino acid analogue of methionine with its sulphur atom replaced by selenium, proved more successful. Parathyroid scintigraphy with ^{75}Se-selenomethionine, however, had suboptimal imaging characteristics and showed a low sensitivity and specificity, especially in small tumours displaying little hormonal activity [4].

In 1979, thallium-201, a new radiotracer for parathyroid imaging, was discovered incidentally when Fukuda and colleagues reported accumulation of ^{201}Tl-chloride in abnormal parathyroid glands [5]. Ferlin *et al.* in the early 1980s introduced the dual-tracer sequential subtraction parathyroid scintigraphy [6]. Since ^{201}Tl-chloride accumulates both in the thyroid and parathyroid tissues, whereas the

Q. H. Siraj (✉) · A. Javaid
Department of Nuclear Medicine, Farwaniya Hospital, Kuwait

S. B. Sergieva
Department of Nuclear Medicine, Sofia Cancer Center, Sofia, Bulgaria

© Springer Nature Switzerland AG 2019

Q. Siraj (ed.), *Radionuclide Parathyroid Imaging*,
https://doi.org/10.1007/978-3-030-17351-7_5

functioning thyroid parenchyma concentrates ^{99m}Tc-pertechnetate and ^{123}I-sodium iodide, the dual-tracer (^{201}Tl/^{99m}Tc or ^{201}Tl/^{123}I) sequential subtraction parathyroid scintigraphy could, therefore, localise a parathyroid adenoma.

In 1989, Coakley and colleagues first recommended the use of ^{99m}Tc-sestamibi, a radiopharmaceutical used for myocardial perfusion and as a non-specific tumour imaging agent for parathyroid imaging as it was seen to concentrate in hyperactive parathyroid lesions [7]. This lipophilic cationic agent was subsequently introduced into clinical practice in the early 1990s for parathyroid imaging. ^{99m}Tc-sestamibi localises both in the parathyroid gland and functioning thyroid tissue and usually washes out of normal thyroid tissue more rapidly than out of the abnormal parathyroid tissue. Double-phase scanning is a widely used method for the preoperative detection of abnormal parathyroid glands. The imaging data reflects washout difference between the early and late phases, mainly retention of tracer in parathyroid glands with a progressive decrease in activity from the normal thyroid gland [8, 9].

In 1995, another lipophilic cationic radiopharmaceutical, ^{99m}Tc-tetrofosmin, was proposed as an alternative to ^{99m}Tc-sestamibi [10]. The mechanism of its intracellular incorporation and retention in the thyroid and parathyroid adenoma is different compared to ^{99m}Tc-sestamibi [11, 12]. ^{99m}Tc-tetrofosmin accumulates mainly in the cytosol and has a slower washout from the thyroid tissue. Hence, ^{99m}Tc-tetrofosmin dual-phase imaging is not recommended due to its rapid washout from parathyroid adenomas. This tracer can, however, be used for parathyroid scintigraphy as part of a dual-radionuclide subtraction protocol [8, 9].

The biodistribution of the technetium-labelled parathyroid imaging agents depends on blood flow and functional status of the parathyroid cells mostly accumulating within the mitochondria [7]. These technetium-labelled agents are either used alone or as a part of dual-isotope image subtraction with ^{99m}Tc-pertechnetate or iodine-123 with different acquisition techniques. SNM- and EANM-approved procedure guidelines for parathyroid scintigraphy were published in 2009 and 2012 [11, 13].

The addition of single-photon emission computed tomography (SPECT) imaging without or with low-dose CT (SPECT/CT) allowed precise localisation of enlarged parathyroid glands in ectopic locations. SPECT/CT was found useful for differentiating functionally active thyroid nodules from parathyroid adenomas. This imaging technique is particularly applicable in patients who have previously undergone total or near-total thyroidectomy or in cases with multinodular goitres [8, 9, 11, 13]. The two-phase ^{99m}Tc-sestamibi scan is currently the most commonly performed procedure for parathyroid adenoma localisation. With the recent boom in PET/CT technology, new PET radiotracers are now available for parathyroid imaging with variable results. ^{18}F-Fluorodeoxyglucose, ^{18}F-fluorocholine and ^{11}C-methionine are the notable PET tracers for parathyroid imaging. These shall be discussed in Chap. 6.

5.2 Single-Photon Emitting Radiotracers for Thyroid and Parathyroid Imaging

5.2.1 ^{123}Iodine-Sodium Iodide

Iodine-123 is a cyclotron-produced radiopharmaceutical with suitable radiation characteristics for gamma camera imaging including a short half-life of 13.2 h and ɣ-ray photon energy of 159 keV energy photons which are well-suited for imaging. Iodine-123 is trapped as well as organified by the functioning thyroid tissue. It has been used as a thyroid imaging agent in subtraction studies with ^{99m}Tc-sestamibi. The major drawback of ^{123}I is its expense, geographically limited availability as well as the longer duration of the procedure.

Like stable iodine (^{127}I), radioactive isotopes of iodine such as ^{123}I or ^{131}I are actively concentrated or trapped by the thyroid gland and are therefore useful for evaluating thyroid gland function. Iodide ions are transported into thyroid cells via the Na^+/I^- symporter where they are organified, i.e. incorporated into tyrosine residues of thyroglobulin [14].

^{123}I delivers a low-radiation-absorbed dose since it does not emit beta particles. The administered radioactivity, given orally, ranges from 7.5 to 22 MBq. The reference diagnostic dose for ^{123}I is 20 MBq which delivers an effective dose of 0.04 mSv with the dose to the uterus at 0.3 mGy [12].

5.2.2 ^{99m}Tc-Pertechnetate

^{99m}Tc-pertechnetate is the most popular radionuclide for gamma camera imaging accounting for about 80% of radiopharmaceuticals used in nuclear medicine. It is a generator-produced radiopharmaceutical with almost ideal physical and radiation characteristics. ^{99m}Tc is readily available as sodium pertechnetate in a sterile, pyrogen-free and carrier-free state from ^{99}Mo/^{99m}Tc generators. Its physical half-life of 6 h and absence of particulate emissions result in a low-radiation dose to the patient, and its monochromatic gamma energy and 140 keV photopeak (89% abundance) is suitably collimated to provide high-resolution images [14]

When administered intravenously, pertechnetate normally localises in the salivary glands, thyroid, choroid plexus, gastric mucosa and genitourinary tract. ^{99m}Tc-pertechnetate is taken up by the thyroid gland by a trapping mechanism. ^{99m}Tc-pertechnetate (TcO_4^-) has an ionic radius and negative charge comparable to the iodide ions and therefore is also transported like iodide into the thyroid cells via the Na^+/I^- symporter. Following intravenous administration, ^{99m}Tc-pertechnetate is trapped by the thyroid by the same mechanism as iodine but is neither organified nor incorporated into thyroid hormone or stored in the thyroid gland. Thus it is not retained in the thyroid, and imaging must be performed early, usually at peak uptake, 20–30 min after injection.

The diagnostic reference dose of ^{99m}Tc-pertechnetate for thyroid imaging is 80 MBq, but when utilising with thallium, the administered activity is usually 75–150 MBq. ^{99m}Tc-pertechnetate in a standard 80 MBq dose delivers a low radiation absorbed dose to the thyroid gland with an effective dose of 1 mSv, and with the dose to the uterus of only 0.5 mGy [5].

5.2.3 Thallium-201

Thallium-201 was the first radiopharmaceutical to become clinically popular for parathyroid imaging. It is a cyclotron-produced radionuclide supplied in the form of thallous chloride in isotonic saline solution for intravenous administration. It has a physical half-life of 73 h and decays by electron capture to stable mercury-201. The photons available for imaging are characteristic x-rays ranging in energy from 69 to 83 keV (95% abundant) and gamma rays of 167 keV (10%) and 135 keV (3%). For gamma camera imaging, a 20–30% window is centred at 69–83 keV and a 20% window at 167 keV.

Thallium-201 thallous chloride is taken up by abnormal parathyroid tissue and thyroid tissue in proportion to blood flow. Although thallium is not a chemical analogue of potassium, it is, however, a transition metal and the ionic radius of the thallous ion (Tl^+) is similar to K^+ and fits in the Na^+/K^+ pump. The mechanism of ^{201}Tl-chloride incorporation in the cytosol is related to the potassium and calcium channels and is mediated by the Na^+/K^+-ATPase and the Na-K-Cl cotransporter [12]. Thallium-201 uptake by the abnormal parathyroid glands is related to the perfusion and cellular density of the lesions. The usually administered activity of ^{201}Tl is 80 MBq intravenously, which results in 14 mSv effective dose with 4 mGy dose to the uterus [15, 16].

5.2.4 ^{99m}Tc-Sestamibi (Cardiolite)

^{99m}Tc-sestamibi (brand name Cardiolite) is a lipophilic cationic isonitrile that forms a complex with ^{99m}Tc after reduction with stannous ions. Sestamibi is methoxyisobutylisonitrile (MIBI) supplied in a lyophilised kit with labelling carried out by adding $^{99m}TcO_4^-$ to the kit vial and heating the mixture in a boiling water bath for 10 min. The labelling efficiency is greater than 90%. The kit is stored at room temperature and can be used for 6 h after reconstitution. ^{99m}Tc-sestamibi is used primarily for assessment of myocardial perfusion and in patients with hyperparathyroidism.

The uptake of MIBI depends upon the perfusion and the functional status of the gland. MIBI crosses the cell membrane by passive diffusion, and once inside the cell, it is bound to the mitochondria. The washout time from the parathyroid tissue is longer than that from the thyroid gland. The large number of mitochondria in oxyphil cells in adenomatous and hyperplastic parathyroid glands is thought to be responsible for its avid uptake and slow release. ^{99m}Tc-sestamibi clears from the thyroid with a half-life of ~30 min but is usually retained by abnormal parathyroid glands.

The radiopharmaceutical enters into a cell under the influence of an electric gradient. After intravenous administration, ^{99m}Tc-sestamibi rapidly leaves the blood pool, and within 3–5 m the blood levels fall to 2% of the dose administered. In the cells, 90% of the isotope is fixed on the membranes of the cellular mitochondria [7]. The degree of retention of ^{99m}Tc-sestamibi within the cells depends on the mitochondrial cells' metabolism and their transmembrane potential.

The average adult dose is 740 MBq (range 740–1100 MBq) [11, 13]. The recommended adult diagnostic reference dose level is 900 MBq, which is associated with an effective dose of 8 mSv, and the dose to the uterus is 7 mGy [15].

5.2.5 ^{99m}Tc-Tetrofosmin

^{99m}Tetrofosmin (brand name Myoview) is a lipophilic cationic complex supplied in kit form for myocardial and parathyroid imaging. It is a lipophilic technetium phosphine dioxo cation that is formulated into a freeze-dried kit containing tetrofosmin and stannous chloride. Labelling is carried out by adding $^{99m}TcO_4^-$ to the kit vial and incubating for 15 min at room temperature. The labelling yield should exceed 90%. The kit is stored at room temperature before and after reconstitution and can be used for 8 h after formulation.

^{99m}Tc-tetrofosmin and ^{99m}Tc-sestamibi both cross the cell membranes by lipophilic diffusion and then are retained by electrostatic binding to negative electrical charges on the mitochondrial membranes. While ^{99m}Tc-sestamibi uptake depends primarily on mitochondrial potential, the uptake mechanism of ^{99m}Tc-tetrofosmin depends on both the cell membrane potential and the mitochondrial potential [16]. ^{99m}Tc-tetrofosmin has a slower washout from the thyroid tissue compared with ^{99m}Tc-sestamibi resulting in lower adenoma-to-thyroid background ratios, and therefore ^{99m}Tc-sestamibi is the current radiopharmaceutical of choice.

The average adult dose is 740 MBq (range 740–1100 MBq), which is similar to that of ^{99m}Tc-sestamibi [10, 13]. The recommended adult diagnostic reference dose level is 900 MBq, which is associated with an effective dose of 7 mSv, and the dose to the uterus is 7 mGy [15].

5.3 Imaging Protocols

The SNM- and EANM-approved procedure guidelines for parathyroid scintigraphy were published in 2009 and 2012 [11, 13]. Parathyroid scan timings and protocols vary and are specific to an institution based on local experience and preferences. In our institute we perform a planar ^{99m}Tc-pertechnetate thyroid scan at 15 min postinjection followed by early and late planar ^{99m}Tc-sestamibi scans at 10 and 180 min,

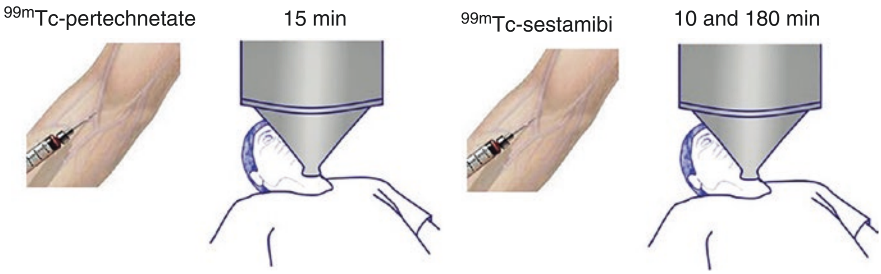

Fig. 5.1 ^{99m}Tc-pertechnetate is injected, and 15 min later a planar pinhole image of the thyroid gland is acquired for 10 min. ^{99m}Tc-sestamibi is next injected with a 10-min duration image acquired at 10 min postinjection followed by a late planar sestamibi image at 3 h

followed by an unzoomed planar scan of the neck and chest at 3 h (Fig. 5.1), with a SPECT/CT performed in the interim at 120 min postinjection.

5.3.1 Dual-Tracer Subtraction Technique

Although thyroid-specific radiotracers have long been employed for thyroid imaging, to date, there is no parathyroid-specific radiotracer for gamma camera imaging of the parathyroid gland alone as the radiopharmaceuticals available for parathyroid imaging localise in both the thyroid and the parathyroid glands. This, therefore, entails subtracting the ^{99m}Tc-pertechnetate or ^{123}I-sodium iodide thyroid image from the combined thyroid-parathyroid scan image. ^{99m}Tc-pertechnetate thyroid imaging is usually preferred due to its widespread availability and significantly lower overall radiation dose compared to iodine-123.

Thallium-201 accumulation in the tissues is dependent on perfusion and cellular density of organ [17]. Since both the thyroid and parathyroid glands have a high cellular density, thallium-201 accumulates in both of these glands. ^{201}Tl/^{99m}TcO$_4^-$ subtraction techniques are employed to exploit the difference in the biological behaviour and tissue distribution of the two tracers, i.e. the thyroid-specific ^{99m}TcO$_4^-$ uptake and more diffuse perfusion-dependent distribution of ^{201}TI [17].

A variety of techniques and methodological variations have been employed for subtraction scanning including static and dynamic imaging. Technetium-99m is injected first, and imaging is performed 15–20 min later in the 140-keV technetium window. Next, an image is acquired in the 80-keV thallium window for scatter correction of ^{99m}Tc gamma rays into the ^{20I}Tl x-ray emission window. Thallium-201 is then injected, and scanning is performed 10 min later. Thallium image is normalised to the technetium image by ensuring that the thyroid-to-background region counts are proportionate on both scans and the technetium image is then subtracted from the thallium image. See Fig. 5.2.

Fig. 5.2 The ^{99m}Tc-pertechnetate or ^{123}I-sodium iodide thyroid scan image is subtracted from the ^{201}Tl-thallous chloride or ^{99m}Tc-sestamibi or ^{99m}Tc-tetrofosmin combined thyroid-parathyroid scan image to obtain the parathyroid subtraction scan image

5.3.2 Dual-Phase Subtraction Imaging

The combined thyroid and parathyroid imaging protocol is similar to that used for the binuclide ^{201}Tl/^{99m}Tc-pertechnetate subtraction imaging. The imaging can be dual nuclide using ^{123}I and ^{99m}Tc-pertechnetate for the thyroid or mononuclide using ^{99m}Tc-pertechnetate and ^{99m}Tc-sestamibi. The pertechnetate or ^{123}I-sodium iodide thyroid image is subtracted from the combined thyroid-parathyroid scan image. ^{99m}Tc-pertechnetate thyroid imaging is usually preferred due to its widespread availability and significantly lower radiation dose compared to iodine-123. In the mononuclide dual-phase technique, the ^{99m}Tc-pertechnetate thyroid scan is first performed with a low (50 MBq) or standard (75 MBq) dose followed by imaging at 15–20 min. Next ^{99m}Tc-MIBI is injected in a much higher dose (~800 MBq) – 10–12 times the pertechnetate dose, and early planar imaging performed after 10–15 min followed by late planar imaging at 2–3 h (dual-phase imaging). A high-count image of the neck and chest is also obtained. Pinhole collimation is preferable to the parallel-hole if SPECT or SPECT/CT isn't a part of the scan protocol. A side-by-side comparison of the pertechnetate and MIBI scans is visually performed, and the thyroid image is digitally subtracted from the early MIBI scan image to get a subtraction image as that obtained by the ^{201}Tl/^{99m}TcO$_4^-$ subtraction technique. This mononuclide technique is now widely accepted. ^{99m}Tc-tetrofosmin can be substituted for ^{99m}Tc-MIBI in which case only an early planar scan is performed for visual comparison and digital subtraction. Dual-phase imaging with ^{99m}Tc-tetrofosmin isn't useful because of rapid washout from the parathyroid tissue.

5.3.3 SPECT or SPECT/CT Protocols

SPECT and SPECT/CT allow precise anatomic localisation and in our experience increases the sensitivity, specificity and accuracy of detecting both ectopic and eutopic enlarged parathyroid glands, particularly in cases of parathyroid hyperplasia or small parathyroid adenomas. However, in general, the SPECT and SPECT/CT imaging does not obviate the need for planar imaging but rather supplements planar scans and provides a template for interpreting the SPECT images as well as a fallback when the SPECT images are technically poor due to patient movement or fail due to equipment malfunction. Anterior planar images with appropriate magnification are acquired for 10-min duration each, using a 256 × 256 matrix (16 bit). The thyroid gland is centred in the field-of-view, which extends from the parotid or angle of the jaw to the same distance inferiorly, but the delayed planar MIBI scan and SPECT/CT image should extend all the way from the angle of the jaw to the base of the heart without any magnification. Pinhole collimator provides optimum quality planar images, but for the delayed image, parallel-hole collimation is necessary and also for SPECT, and most, therefore, opt for imaging using a high-resolution low-energy parallel-hole collimator. SPECT data is acquired in the 128 × 128 (16-bit) matrix, over 360° of rotation, using an elliptic body-contoured orbit, in a stop-and-shoot or continuous mode with a minimum of 64 (but optimally 128) projections at 25 s per projection (3–6° angle), depending on the sensitivity of the detector and the local clinical preferences and protocols. The SPECT acquisition time, in general, is about 26 min for a dual-head camera high-quality SPECT and 13 min for the standard-quality SPECT. The images are attenuation corrected and reconstructed, and the post-processing filter is applied.

SPECT/CT can be performed immediately after the planar imaging, at the early, the delayed or both time points, but because of the additional radiation associated with the CT component, the CT should be performed at one time point only, preferably before or after the delayed planar image, which reportedly has the highest accuracy [18, 19].

In our institute, we perform ^{99m}Tc-pertechnetate planar thyroid scan at 15–25 min followed by an early ^{99m}Tc-MIBI planar scan from 10–20 min postinjection, a single SPECT/CT scan at 120 min, a late planar scan at 3 h and lastly an unzoomed planar image from the jaw to the base of the heart. We obtain a full biochemical profile of the patient before deciding on the scan protocol. For patients with renal failure suspected of parathyroid hyperplasia, we advise a 128-projection SPECT, and for patients with primary hyperparathyroidism, we opt for a 64-projection SPECT scan. The planar pertechnetate and MIBI scan images are interpreted side by side, and the pertechnetate thyroid image is subtracted from the early planar MIBI image. The SPECT/CT images are processed and displayed in the coronal, sagittal and transaxial planes. Recently, we have added grey-level inverse logarithmic scale image transformation and image enhancement to the standard linear SPECT image display with marked improvement in the scan accuracy, interpretation and diagnostic yield of parathyroid scintigraphy (see below).

5.3.4 Image Processing and Optimisation

5.3.4.1 Negative Image Transformation

Negative image transformation produces the equivalent of a photographic negative. It is the most basic and simple operation in digital image processing. To compute the negative of an image, the grey pixel values are inverted so that the resultant

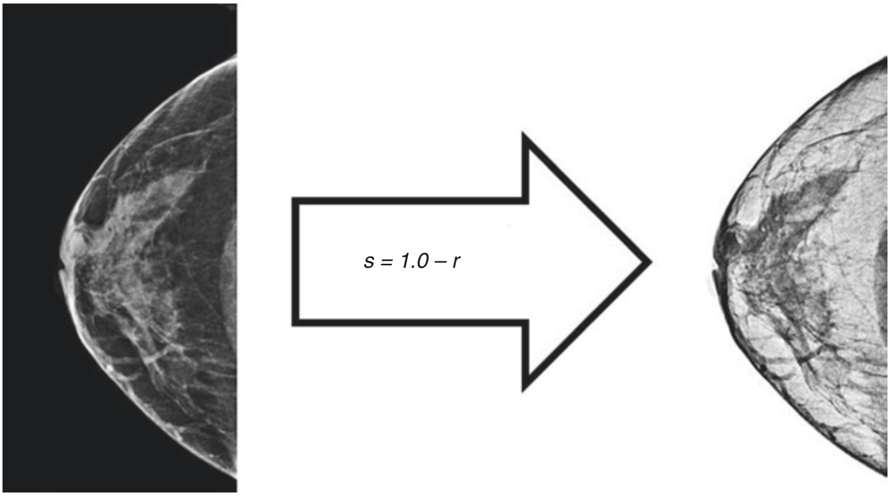

Fig. 5.3 Negative transformation of a mammogram demonstrating better detail and much clearer tissue compared with the positive image. Every input pixel value *s* from the original image is subtracted from the maximum pixel value 1.0 to get the output pixel value *r*

image becomes negative of the original image [20, 21]. Negative images are useful for enhancing white or grey detail embedded in dark regions of an image particularly when the image has predominantly dark regions (Fig. 5.3).

5.3.4.2 Inverse Logarithmic Greyscale Transformation

In mathematics, the logarithm of a number is defined as the power that is raised to a fixed value called base (b). The logarithm is the inverse function to exponentiation, where the logarithm of a given number x is the exponent to which another fixed number, the base b, must be raised, to produce that number x. An inverse logarithm is the inverse or opposite of a logarithm function and is also known as antilogarithm or antilog. Figure 5.4 shows the relationship graphically.

Logarithmic or log transformations enable compression/expansion of intensity levels and map a narrow range of low-intensity values in the input to a wider range in the output image and the opposite with the higher values, thereby reducing wide-ranging quantities to tiny scopes. When inverse log transformation is applied to a linear scale image, the values of high pixels are expanded, and those of the lower-level pixels (darker on greyscale and lighter on inverse greyscale images) are compressed [21].

Inverse log transformation together with appropriate image contrast enhancement improves the details in the image with better delineation of lesions through suppression of background activity and enhancement of lesions with higher uptake, which are otherwise difficult to detect on the linear scale images. We have found this to be invaluable for the detection of parathyroid lesions since the background thyroid activity is suppressed and the modestly increased uptake in

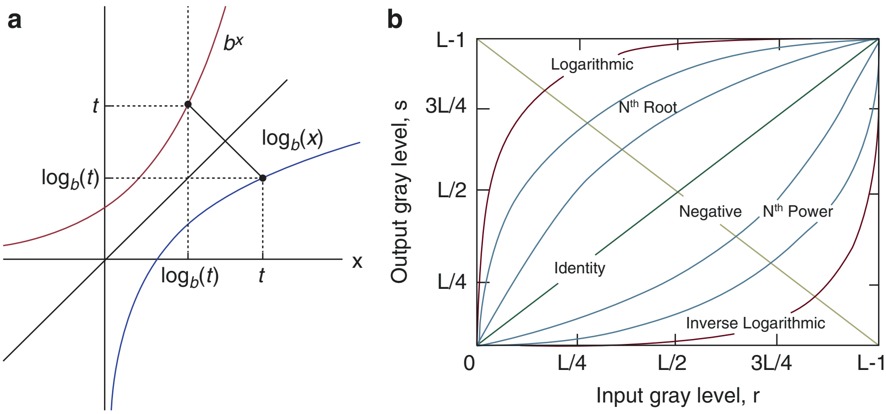

Fig. 5.4 (**a**) The blue line shows the graph of the logarithm function $\log_b(x)$ which is obtained by reflecting at the black diagonal line ($x = y$); the red line shows inverse log graph of the function bx. (**b**) Some basic grey-level intensity transformation functions [21]

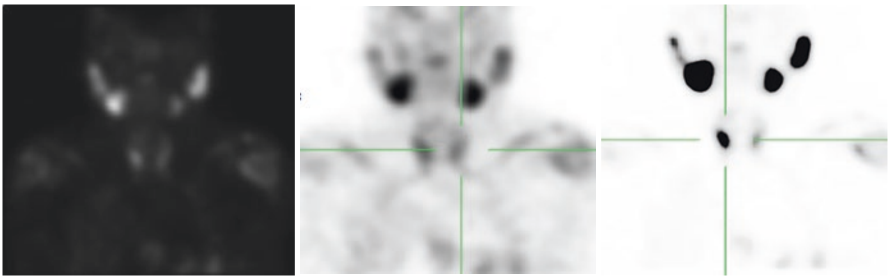

Fig. 5.5 Identical SPECT images in linear greyscale (left), inverse linear greyscale (middle) and inverse logarithmic scale (right). The logarithmic greyscale conversion expands the values of high pixels and compresses the values of low pixels thereby enhancing the modest increase in uptake in the parathyroid lesions and suppressing the background thyroid activity

small parathyroid lesions, especially hyperplastic parathyroid glands, is enhanced. Figure 5.5 shows SPECT image comparison with and without inverse log transformation.

5.3.4.3 Colour Scale Hybrid Image Display

An appropriate colour scale is chosen to optimally display the lesion on the SPECT/CT fusion images. We prefer a three-colour scale such as blue-black-red, where the lower extra-thyroidal background is coloured light blue, the intermediate level background activity in the thyroid dark grey and the parathyroid lesion in red (Fig. 5.6). The intensity and contrast are adjusted to ensure that the colours exactly correspond to these tissues. Retrospective and prospective application of inverse log transformation have very significantly improved our diagnostic yield and reduced the false-negative rate to a minimum.

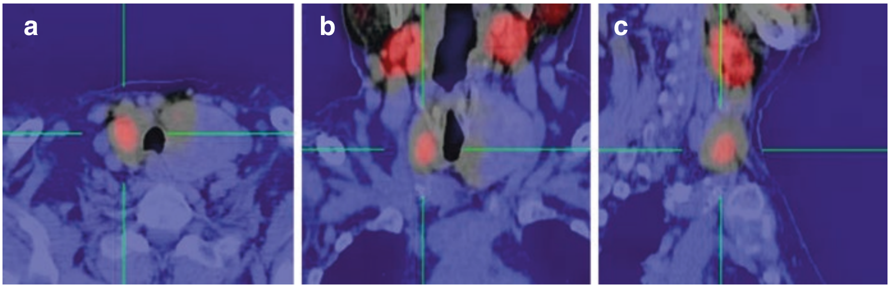

Fig. 5.6 The blue-black-red colour scale showing the right lower parathyroid gland hyperplasia on a dark grey thyroid background in the transverse (**a**), coronal (**b**) and sagittal (**c**) axes

5.4 Clinical Aspects

The availability of technetium-labelled agents including ^{99m}Tc-sestamibi and ^{99m}Tc-tetrofosmin, with their excellent imaging quality and low radiation dose to the patient, was pivotal in the wide clinical acceptance of parathyroid scintigraphy as a reliable diagnostic tool in patients with hyperparathyroidism. However, the uptake and retention of technetium-labelled parathyroid imaging agents are significantly influenced by clinical, biological and technical factors, with resultant false-positive and false-negative scan results affecting the sensitivity, specificity and diagnostic accuracy of parathyroid scintigraphy.

5.4.1 Sensitivity and Specificity

The dual-tracer (^{99m}Tc-sestamibi/^{99m}Tc or ^{99m}Tc-sestamibi/^{123}I) sequential subtraction parathyroid scintigraphy can reportedly localise abnormal parathyroid adenoma in 79% of the cases with a positive predictive value of 91% [9]. In a review of the literature, based on 14 studies, with a total of 317 patients with primary hyperparathyroidism, who had been operated upon, Hauty *et al*. found a sensitivity of 82% for the detection of parathyroid adenomas, with a diagnostic accuracy of 78% and a positive predictive value of 94% [22]. The sensitivity of sestamibi planar studies ranges from 54% to 96%, with the specificity ranging from 83% to 99% [10, 23–32]. The availability of SPECT and later SPECT/CT has helped increase the sensitivity and accuracy for the detection of eutopic and ectopic parathyroid lesions. Lavely *et al*. in their comprehensive study of dual-phase ^{99m}Tc-sestamibi planar imaging with SPECT/CT reported a sensitivity of ~73%, specificity of ~99%, accuracy at ~86%, a positive predictive value from 86% to 91% and a negative predictive value at ~98% [19]. A meta-analysis of 24 studies demonstrated the superior sensitivity of SPECT/CT compared to SPECT and planar techniques [33]. There is a wide range of sensitivities reported in different studies, which may be attributable to inter-institutional variations in imaging techniques and methodology.

The sensitivity of parathyroid scintigraphy is very significantly affected by patient-related biochemical and biological factors (Tables 5.1 and 5.4). Scintigraphy has a higher sensitivity for detecting large-sized adenomas and single-gland disease [38–40]. Higher parathyroid hormone and calcium levels and vitamin D levels generally increase the sensitivity of scintigraphy [34, 35, 39]. Thyroid suppression is also associated with increased sensitivity for detecting adenomas [41].

5.4.2 False-Positive and False-Negative Scans

The sensitivity and specificity of the sestamibi parathyroid scintigraphy are affected by the various technical and biological factors resulting in both false-negative and false-positive scans. False-positive results may be obtained in thyroid adenomas that show ^{99m}Tc-sestamibi uptake. Other causes of false-positive results are thyroid carcinoma and inflammatory thyroid disease (such as chronic lymphocytic thyroiditis and inflammatory or malignant cervical lymphadenopathy). Table 5.2 lists eutopic and ectopic causes of false-positive parathyroid scans [42–47]. The scintigraphic sensitivity is reportedly lower with the use of calcium channel blockers, high P-glycoprotein levels and multidrug resistance proteins. Table 5.3 lists the various factors that may result in a false-negative ^{99m}Tc-sestamibi parathyroid scan [36, 43, 48–51].

Table 5.1 Biochemical factors affecting the probability of a positive or a negative parathyroid scan result [34–37]

Factor	Positive scan	Negative scan
Calcium level	>11.3 mg/dL	<11.3 mg/dL
PTH level	>160 pg/mL	<160
25-Hydroxy vitamin D	<25 ng/dL	>25 ng/dL
Calcium channel blocker	No	Yes

Table 5.2 Causes of false-positive parathyroid scan

Thyroid
Thyroid adenomas
Thyroid carcinoma
Metastatic thyroid carcinoma
Inflammatory thyroid disease
Hypofunctional thyroid nodules
Hyperfunctional thyroid nodules
Colloid thyroid nodules
Brown adipose tissue
Sarcoidosis
Cervical lymph nodes
Inflammatory cervical lymph nodes
Malignant cervical lymph nodes

Table 5.3 Causes of false-negative ^{99m}Tc-sestamibi parathyroid scan

Small parathyroid gland size
Location
Cellular functional status
Water-clear cell predominance
Diffuse hyperplasia
High P-glycoprotein levels
Multidrug resistance protein expression
Haemorrhage
Necrosis
Cysts
Large thyroid (>35 gm)
Multigland parathyroid disease

5.4.3 Factors Affecting Uptake

There is a positive correlation between the scintigraphic detection of hyperactive parathyroid glands and tumour size, the oxyphil cell content of the parathyroid lesions, the presence of nodular hyperplasia, accelerated cell metabolism and the proliferative activity of the gland or active phase of the cell cycle. Sestamibi concentration in inner mitochondrial cell membranes correlates directly with the respiration rate of the metabolically active parathyroid cell, in proportion to the amount of adenosine triphosphate (ATP) production. There is a greater likelihood of a positive scan result and the volume of an adenoma [52]. Adenomas with a mean weight greater than 1434 ± 403 mg are more likely to be associated with a positive scan result, and there is a higher likelihood of a negative result with adenomas less than 480 ± 156 mg in weight [37]. However, false-negative results have been reported with large adenomas, while some very small adenomas have been detected [49]. A large clinicopathological review of patients with false-negative sestamibi scans showed that sestamibi uptake correlates with parathyroid oxyphil cell content, and false-negative scans are more likely when parathyroid glands contain predominantly clear cells [53]. Table 5.4 lists the factors that affect accumulation and retention of ^{99m}Tc-sestamibi and ^{99m}Tc-tetrofosmin in hyperfunctioning parathyroid tissue [34–37, 39, 42, 51, 54, 55].

5.4.4 Thallium Parathyroid Scintigraphy: Current Role

The dual-tracer (^{201}Tl/^{99m}Tc or ^{201}Tl/^{123}I) sequential subtraction parathyroid scintigraphy can localise parathyroid adenomas with high sensitivity (93%) and a reasonable specificity (73%) for the reliable imaging of enlarged parathyroid glands. The disadvantages of this planar technique were an inability to detect tumour tissue less than 300 mg in size and a high tracer uptake in coexisting nodular goitre [56]. Although the thallium-201 uptake is higher in the parathyroid tissue than that of sestamibi, sestamibi however, shows a higher concentration in the parathyroid tissue compared with the thyroid tissue, resulting in a higher target-to-background ratio [25]. Also, thallium-201 is not considered as an ideal tracer, owing to its physical properties of

Table 5.4 Factors that affect accumulation and retention of ^{99m}Tc-sestamibi and ^{99m}Tc-tetrofosmin in hyperfunctioning parathyroid tissue

Size of hyperfunctioning parathyroid glands
Perfusion
Chief cell content
Oxyphil cell content
Water-clear cell content
Nodular or diffuse hyperplasia
Metabolic activity
Secretory activity
Cell membrane potentials
Mitochondrial membrane potentials and volumes
Phase of the cell cycle (proliferative activity)
P-gp/MRP1 expression
Angiogenesis, lymphangiogenesis
Parathyroid haemorrhage/necrosis
Calcium-sensing receptor expression

low photon energy and a relatively long half-life. The technetium-labelled radiopharmaceuticals for parathyroid imaging replaced thallium-201 parathyroid scintigraphy. However, the sestamibi parathyroid scan is influenced by a large number of biological factors that may lower the sensitivity for the detection of parathyroid adenomas and hyperplasia with false-negative scan results (Table 5.3). The classical planar thallium-201/technetium-99m subtraction scan was abandoned in favour of planar sestamibi imaging due to the better physical characteristics of technetium and due to dual-phase imaging with sestamibi with the parathyroid lesions showing retention of tracer compared with the thyroid gland.

Oxyphil cell content is a statistically significant variable for discriminating between sestamibi-positive and sestamibi-negative adenomas. Adenomas with oxyphil-rich cells are more likely to be positive on a ^{99m}Tc-sestamibi scan compared with predominantly clear cell or chief cell adenomas [57–59]. Sestamibi uptake is more closely related to the cell cycle than to gland size [53] as well and the mitochondrial content of the parathyroid lesions [39, 54]. However, some authors have found that no relationship exists between oxyphil predominance and the sestamibi scan result [39, 60]. Parathyroid hormone expression is reported to be highest in adenomas with a predominance of chief cells with less intense expression of PTH seen in oxyphil cells. There is a trend towards increased expression of PTH in tumours with false-negative results and reduced oncocytic cell content [61]. This disparity between parathyroid hormone expression and histological composition of the parathyroid adenomas can explain the false-negative sestamibi scan results.

The most commonly quoted factor held responsible for a false-negative sestamibi parathyroid scan is the P-glycoprotein (P-gp) or multidrug resistance-associated protein 1 (MRP1) expression [49, 56]. P-gp and MRP1 are transmembrane lipoproteins that enhance the efflux of sestamibi out of parathyroid cells. However, later research has been inconclusive in this regard with some studies showing a strong correlation between P-gp and MRP1 expression and false-negative results of MIBI scans [48, 51, 56], while others have found no correlation between P-gp and MRP1 expression and the true-positive and false-negative parathyroid scans [61, 62]. We have documented large-sized sestamibi-negative parathyroid adenomas without any P-gp expression, which were strikingly positive on thallium subtraction scintigraphy (see cases 7.8, 7.10, and 7.11). It has been reported that parathyroid adenomas that express either P-gp or the MRP1 failed to accumulate sestamibi, but in these cases, there was no expression of these proteins seen.

The chief cells are responsible for parathyroid hormone production, whereas the oxyphil cells are mainly involved in the proliferative activity. Mitochondria-rich oxyphil cells account for sestamibi uptake in parathyroid lesions. Therefore, it appears that sestamibi only indirectly images hyperactive parathyroid glands, and in this regard, a perfusion imaging agent such as thallium-201 may prove more effective when the sestamibi scan result is false-negative. Fewer oxyphil cells and hence fewer mitochondria may explain both lower uptake and rapid washout of sestamibi from some parathyroid adenomatous lesions, and it is logical to assume that parathyroid adenomas composed mostly of chief or water-clear cells would appear false-negative on a ^{99m}Tc-sestamibi parathyroid scan. It has been reported that an adenoma with an oxyphil cell content >20% and adenoma weight >600 mg is associated with an increased rate of obtaining a positive sestamibi scan result by four- and tenfold, respectively [37].

Since the mechanism of thallium uptake by the parathyroid glands is not affected by oxyphil cell content, it is apparent that some of the factors that influence sestamibi parathyroid imaging may not affect thallium uptake by the parathyroid [63]. We have found it worthwhile to repeat a sestamibi-negative scan with thallium-201 and have identified fair-sized parathyroid adenomas with thallium scans on several occasions (see cases 7.8, 7.10–7.13, 7.44, 7.45) as well as sestamibi-negative thallium-positive hyperplastic parathyroid glands (cases 7.71 and 7.72).

One of the disadvantages associated with thallium parathyroid imaging was the fact that only planar subtraction scanning was performed. The thallium/pertechnetate subtraction scintigraphy was the only available parathyroid imaging modality in the 1980s, but with the introduction of dual-phase sestamibi imaging in the 1990s, planar thallium subtraction scintigraphy was abandoned due to the better physical characteristics and the better imaging properties of technetium-labelled agents, in particular, the dual-phase planar ^{99m}Tc-sestamibi scintigraphy with retention of the radiotracer in most hyperactive parathyroid lesions. This, however, preceded SPECT imaging which could have improved the diagnostic yield of thallium scintigraphy. Thallium-201 uptake by the abnormal parathyroid glands is related to the perfusion and cellular density of the lesions. Further, due to its biological retention characteristic which is not dependent on oxyphil cell concentration, thallium SPECT scintigraphy can either have a superior or similar diagnostic yield as that of the sestamibi SPECT scan depending on cellular composition of the parathyroid lesion.

Thallium SPECT/CT has shown similar uptake in parathyroid adenomas when compared with ^{99m}Tc-sestamibi SPECT/CT as shown in cases 7.21 and 7.70. In other sestamibi-negative cases, the parathyroid adenomas were successfully detected by thallium-201 SPECT/CT (see above). The improved detection of parathyroid adenomas by thallium-201 SPECT or SPECT/CT may be attributable to the known higher concentration of thallium-201 per gram tissue compared to that of sestamibi. SPECT imaging, however, removes the background activity, and hence equivalent quality images can, therefore, be obtained with thallium SPECT depending on the cellular composition of the hyperactive parathyroid glands. It appears that SPECT thallium scintigraphy has a useful and crucially important role in sestamibi-negative parathyroid scans in patients with primary hyperparathyroidism.

The detectability of small hyperactive parathyroid lesions is improved when the thyroid gland is suppressed pathologically, iatrogenically or on purpose to improve the yield of parathyroid scintigraphy [41, 64]. On occasion, it is helpful to repeat the scan after a few months when there is a further rise in PTH level as this may be associated with an increase in biological activity of the parathyroid cells, and a previously negative scan can later become positive. A proposed schema for parathyroid scintigraphic diagnosis in hyperparathyroidism is outlined in Fig. 5.7.

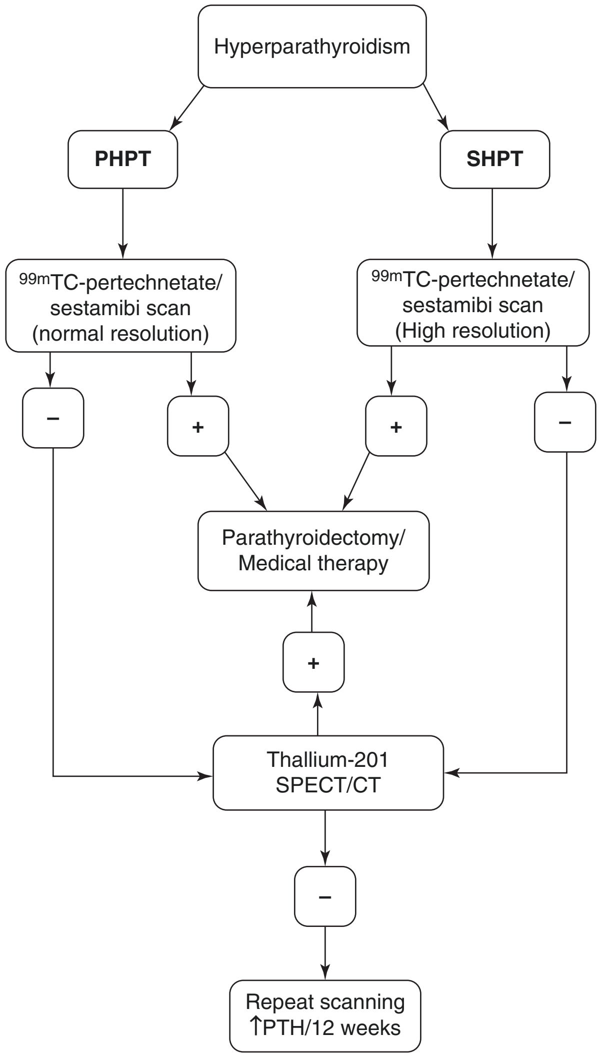

Fig. 5.7 A suggested schema for parathyroid scintigraphic diagnosis in hyperparathyroidism

References

1. Sisson JC, Beierwalters WH. Radiocyanocobalamine (Co57B12) concentration in the parathyroid glands. J Nucl Med. 1962;3:160–6.
2. Potchen EJ, Adelstein SJ, Delay JB. Radioisotopic localization of the overactive human parathyroid. Am J Roentgenol Radium Ther Nucl Med. 1965;93:955–61.
3. DiGiulio W, Beierwaltes WH. Parathyroid scanning with selenium-75 labelled methionine. J Nucl Med. 1964;5:417–27.
4. Di Giulio W, Morales J. An evaluation of parathyroid scanning using selenium-75-methionine. J Nucl Med. 1966;7:380–4.
5. Fukunaga M, Fujita T, Yonekura Y, Dokoh S, Yamamoto I, Morita R, Torizuka K. Visualization of parathyroid tumor with ^{201}Tl-chloride. Kaku Igaku. 1979;16(3):327–31.
6. Ferlin G, Borsato N, Camerani M, Conte N, Zotti D. New perspectives in localizing enlarged parathyroids by technetium-thallium subtraction scan. J Nucl Med. 1983;24:438–41.
7. Coakley AJ, Kettle AG, Wells CP, O'Doherty MJ, Collins REC. ^{99m}Tc-Sestamibi – a new agent for parapthyroid imaging. Nucl Med Commun. 1989;10(11):791–4.
8. Mariani G, Gulec SA, Rubello D, Boni G, Puccini M, Pelizzo MR, et al. Preoperative localization and radioguided parathyroid surgery. J Nucl Med. 2003;44:1443–58.
9. Khan AA, Hanley DA, Rizzoli R, Bollerslev J, et al. Primary hyperparathyroidism: review and recommendations on evaluation, diagnosis, and management. A Canadian and international consensus. Osteoporos Int. 2017;28(1):1–19.
10. Ishibashi M, Nishida H, Kumabe T, Morita S, Matoba F, Nomura G, et al. Tc-99 m tetrofosmin. A new diagnostic tracer for parathyroid imaging. Clin Nucl Med. 1995;20:902–5.
11. Greenspan BS, Dillehay G, Intenzo C, Lavely WC, O'Doherty M, Palestro CJ, et al. SNM practice guideline for parathyroid scintigraphy. J Nucl Med Technol. 2012;40(2):1–8.
12. Zolle I. Technetium-99m pharmaceuticals. Preparation and quality control in nuclear medicine. Berlin: Springer; 2007. p. 237.
13. Hindié E, Ugur O, Fuster D, O'Doherty M, Grassetto G, Ureña P, et al. 2009 EANM parathyroid guidelines. Eur J Nucl Med Mol Imaging. 2009;36:1201–16.
14. Saha GB. Characteristics of specific radiopharmaceuticals. In: Fundamentals of nuclear pharmacy. 6th ed. New York, NY: Springer; 2010. p. 126.
15. Administration of Radioactive Substances Advisory Committee. Notes for guidance on the clinical administration of radiopharmaceuticals and use of sealed radioactive sources. Oxon: ARSAC; 2018.
16. Arbab AS, Koizumi K, Toyama K, Arki T. Uptake of technetium-99 m tetrofosmin, technetium-99 m MIBI and thallium-201 in tumor cell lines. J Nucl Med. 1996;37:551–6.
17. Basarab RM, Manni A, Harrison TS. Dual isotope subtraction parathyroid scintigraphy in the preoperative evaluation of suspected hyperparathyroidism. Clin Nucl Med. 1985;10:300–14.
18. Tutty L. EANM parathyroid scintigraphy: a technologist's guide. Kuchl: Die Druckerei Christian Schцnleitner; 2005. p. 13–7.
19. Lavely WC, Goetze S, Friedman KP, et al. Comparison of SPECT/CT, SPECT, and planar imaging with single- and dual-phase 99mTc-sestamibi parathyroid scintigraphy. J Nucl Med. 2007;48:1084–9.
20. Maini R, Aggarwal H. J Comput. 2010;2(3):8–13.
21. Gonzalez RC, Woods RE. Digital image processing. 3rd ed. Upper Saddle River, NJ: Pearson Education; 2008.
22. Hauty M, Swartz K, McClung M, Lowe DK. Technetium-thallium scintiscanning for localization of parathyroid adenomas and hyperplasia. A reappraisal. Am J Surg. 1987;153:479–86.
23. O'Doherty MJ, Kettle AG, Wells R, Collins RE, Coakley AJ. Parathyroid imaging with technetium-99 m-sestamibi: preoperative localization and tissue uptake studies. J Nucl Med. 1992;33:313–8.

24. Geatti O, Shapiro P, Orsolon PG, Proto G, Guerra UP, Antonucci F, et al. Localization of parathyroid enlargement: experience with technetium-99m MIBI and thallium-201 scintigraphy, ultrasonography and computerized tomography. Eur J Nucl Med. 1994;21:17–22.
25. Wei JP, Burke GJ, Mansberger AR. Preoperative imaging of abnormal thyroid glands in patients with hyperparathyroid disease using combination Tc-99 m pertechnetate and Tc-99 m sestamibi radionuclide scans. Ann Surg. 1994;5:568–72. Discussion 572–3.
26. McBiles M, Lambert AT, Cote MG, Kim SY. Sestamibi parathyroid imaging. Semin Nucl Med. 1995;25:221–34.
27. Osmanagaoglu K, Schelstraete K, Lippens M, Obrie E, De Feyter I, et al. Visualization of a parathyroid adenoma with Tc-99m MIBI in a case with iodine saturation and impaired thallium uptake. Clin Nucl Med. 1993;18:214–6.
28. Taillefer R, Boucher Y, Potvin C, Lambert R. Detection and localization of parathyroid adenomas in patients with hyperparathyroidism using a single radionuclide imaging procedure with technetium-99m sestamibi (double-phase study). J Nucl Med. 1992;33:1801–7.
29. Altieri P, Loi G, Nicolosi A, Tomas MB, Afriyie MO, Attie JN, Palestro CJ. Single late phase sestamibi subtraction scintigraphy for parathyroid lesion localization. Eur J Nucl Med. 1996;23:1169.
30. Benard F, Lefebvre B, Benvan F, Langlois MF, Bisson G. Rapid washout of technetium-99m MIBI from a large parathyroid adenoma. J Nucl Med. 1995;36:241–3.
31. Piga M, Bolasco R, Satta L, Altieri P, Loi G, Nicolosi A, et al. Double phase parathyroid technetium-99m-MIBI scintigraphy to identify functional autonomy in secondary hyperparathyroidism. J Nucl Med. 1996;37:565–9.
32. Palestro CJ, Tomas MB, Buija TA, GC T. Sestamibi parathyroid scintigraphy: a prospective study in 100 patients. J Nucl Med. 1995;36:202.
33. Wong KK, Fig LM, Gross MD, Dwamena BA. Parathyroid adenoma localization with ^{99m}Tc-sestamibi SPECT/CT: a meta-analysis. Nucl Med Commun. 2015;36(4):363–75.
34. Kandil E, Tufaro AP, Carson KA, Lin F, Somervell H, Farrag T, Dackiw A, Zeiger M, Tufano RP. Correlation of plasma 25-hydroxyvitamin D levels with severity of primary hyperparathyroidism and likelihood of parathyroid adenoma localization on sestamibi scan. Arch Otolaryngol Head Neck Surg. 2008;134(10):1071–5.
35. Parikshak M, Castillo ED, Conrad MF, et al. Impact of hypercalcemia and parathyroid hormone level on the sensitivity of preoperative sestamibi scanning for primary hyperparathyroidism. Am Surg. 2003;69(5):393–8.
36. Friedman K, Somervell H, Patel P, et al. Effect of calcium channel blockers on the sensitivity of preoperative ^{99m}Tc-MIBI SPECT for hyperparathyroidism. Surgery. 2004;136(6):1199–204.
37. Erbil Y, Kapran Y, Issever H, Barbaros U, Adalet I, Dizdaroglu F, et al. The positive effect of adenoma weight and oxyphil cell content on preoperative localization with 99mTc-sestamibi scanning for primary hyperparathyroidism. Am J Surg. 2008;195(1):34–9.
38. Bergson EJ, Sznyter LA, Dubner S, et al. Sestamibi scans and intraoperative parathyroid hormone measurement in the treatment of primary hyperparathyroidism. Arch Otolaryngol Head Neck Surg. 2004;130(1):87–91.
39. Bhatnagar A, Vezza PR, Bryan JA, et al. Technetium-99m-sestamibi parathyroid scintigraphy: effect of P-glycoprotein, histology and tumor size on detectability. J Nucl Med. 1998;39(9):1617–20.
40. Katz SC, Wang GJ, Kramer EL, et al. Limitations of technetium-99m sestamibi scintigraphic localization for primary hyperparathyroidism associated with multiglandular disease. Am Surg. 2003;69(2):170–5.
41. Royal RE, Delpassand ES, Shapiro SE, et al. Improving the yield of preoperative parathyroid localization: technetium Tc 99m-sestamibi imaging after thyroid suppression. Surgery. 2002;132(6):968–74.

42. Perez-Monte JE, Brown ML, Shah AN, et al. Parathyroid adenomas: accurate detection and localization with Tc-99m sestamibi SPECT. Radiology. 1996;201(1):85–91.
43. Chien D, Jacene H. Imaging of parathyroid glands. Otolaryngol Clin North Am. 2010;43:399–415.
44. McHenry CR, Lee K, Saadey J, et al. Parathyroid localization with technetium-99m-sestamibi: a prospective evaluation. J Am Coll Surg. 1996;183:25–30.
45. Lee VS, Spritzer CE, Coleman RE, Wilkinson RH Jr, Coogan AC, Leight GS Jr. Hyperparathyroidism in high risk surgical patients: evaluation with double-phase technetium-99m sestamibi imaging. Radiology. 1995;197:627–33.
46. Mudun A, Kocak M, Unal S, Cantez S. Tc-99mMIBI accumulation in remnant thymus: a cause of false-positive interpretation in parathyroid imaging. Clin Nucl Med. 1995;20:379–80. 102.
47. Desai S, Yuille DL. Visualization of a recurrent carcinoid tumor and an occult distant metastasis by technetium-99m-sestamibi. J Nucl Med. 1993;4:1748–50.
48. Gupta Y, Ahmed R, Happerfield L, et al. P-glycoprotein expression is associated with sestamibi washout in primary hyperparathyroidism. Br J Surg. 2007;94(12):1491–5.
49. Pons F, Torregrosa JV, Fuster D. Biological factors influencing parathyroid localization. Nucl Med Commun. 2003;24(2):121–4.
50. Yamaguchi S, Yachiku S, Hashimoto H, et al. Relation between technetium 99m methoxyisobutylisonitrile accumulation and multidrug resistance protein in the parathyroid glands. World J Surg. 2002;26(1):29–34.
51. Sun SS, Shiau YC, Lin CC, et al. Correlation between P-glycoprotein (P-gp) expression in parathyroid and Tc-99m MIBI parathyroid image findings. Nucl Med Biol. 2001;28:929–33.
52. Berber E, Parikh RT, Ballem N, Garner CN, Milas M, Siperstein AE. Factors contributing to negative parathyroid localization: an analysis of 1000 patients. Surgery. 2008;144:74–9.
53. Westreich RW, Brandwein M, Mechanick JI, Bergman DA, Urken ML. Preoperative parathyroid localization: correlating false-negative technetium-99m sestamibi scans with parathyroid disease. Laryngoscope. 2003;13(3):567–72.
54. Hetrakul N, Civelek AC, Stagg CA, et al. In-vitro accumulation of technetium 99m sestamibi in human parathyroid mitochondria. Surgery. 2001;130:1011–8.
55. Kannan S, Milas M, Neumann D, Parikh RT, Siperstein A, Licata A. Parathyroid nuclear scan. A focused review on the technical and biological factors affecting its outcome. Clin Case Min Bone Metab. 2014;11(1):25–30.
56. Kao A, Shiau Y-C, Tsai S-C, Wang J-J, Ho S-T. Technetium-99m methoxyisobutylisonitrile imaging for parathyroid adenoma: relationship to P-glycoprotein or multidrug resistance-related protein expression. Eur J Nucl Med. 2002;29:1012–5.
57. Sandrock D, Merino M, Norton J, Neumann R. Ultrastructural histology correlates with results of thallium-201/technetium-99m parathyroid subtraction scintigraphy. J Nucl Med. 1993;34:24–9.
58. Melloul M, Paz A, Koren R, Cytron S, Feinmesser R, Gal R. 99mTc-MIBI scintigraphy of parathyroid adenomas and its relation to tumour size and oxyphil cell abundance. Eur J Nucl Med. 2001;28:209–13.
59. Carpentier A, Jeanotte S, Verreault J, et al. Preoperative localization of parathyroid lesions in hyperparathyroidism: relationship between technetium–99-MIBI uptake and oxyphil cell content. J Nucl Med. 1998;39:1441–4.
60. Pinero A, Rodriguez JM, Ortiz S, et al. Relation of biochemical, cytologic, and morphologic parameters to the result of gammagraphy with technetium 99m sestamibi in primary hyperparathyroidism. Otolaryngol Head Neck Surg. 2000;122:851–5.
61. Mehta NY, Ruda JM, Kapadia S, Boyer PJ, Hollenbeak CS, StackJr BC. Relationship of technetium Tc99m sestamibi scans to histopathological features of hyperfunctioning parathyroid tissue. Arch Otolaryngol Head Neck Surg. 2005;131:493–8.

62. Seki K, Hashimoto K, Hisada T, Maeda M, Satoh T, Uehara Y, et al. A patient with classic severe primary hyperparathyroidism in whom both Tc-99m MIBI scintigraphy and FDG-PET failed to detect the parathyroid tumor. Intern Med. 2004;43:816–23.
63. Mori K, Yamaguchi T, Maeda M. Mechanism of ^{201}Thallium-chloride uptake in tumor cells and its relationship to potassium channels. Neurol Res. 2016;20(1):19–22.
64. Gomez-Ramırez J, Posada M, Rodrıguez A, Bravo JM, Domınguez L, Martın-Perez ME, Larranaga E. Thyroid suppression in patients with primary hyperparathyroidism: does It improve the pre-surgical scintigraphy localisation? Cir Esp. 2011;89:595–8.

Parathyroid PET

6

Luka Lezaic and Marko Grmek

6.1 Introduction

Positron emission tomography (PET) is a molecular imaging technique with several advantages over the conventional single-photon radionuclide imaging approach, whether planar or tomographic (single-photon emission computed tomography, SPECT). PET has a higher sensitivity and spatial resolution compared with the single-photon technique. The radionuclides used for PET emit positrons that are quickly annihilated by collision with an electron. The typical path of a positron in tissue equals up to several millimetres. Two high-energy (511 keV) photons are emitted at an angle of 180° as the result of the annihilation. In contrast to the usual two detectors on SPECT gamma cameras, PET cameras have a ring of detectors, which identify two simultaneous activations in an extremely short time window as an annihilation event occurring on the axis between the two detectors. In the last decade, widespread adoption of hybrid PET imaging, where anatomical (computed tomography, CT) imaging is added to molecular imaging (positron emission tomography, PET), has allowed the accurate anatomical localisation of functionally detected changes by the PET/CT cameras.

Because of its technical characteristics, PET/CT theoretically enables localisation of smaller lesions. Several PET tracers have been studied in the detection of hyperfunctioning parathyroid glands. PET tracers that have been employed for parathyroid imaging include ^{18}F-fluorodeoxyglucose, ^{11}C-methionine, ^{11}C-choline and ^{18}F-fluorocholine. Other less frequently used PET tracers such as amine neurotransmitter analogue ^{18}F-DOPA [1] and amino acid analogue ^{18}F-FET [2] did not prove to be clinically useful and haven't found a place in parathyroid gland imaging.

L. Lezaic (✉) · M. Grmek
Department of Nuclear Medicine, University Medical Centre Ljubljana, Ljubljana, Slovenia
e-mail: luka.lezaic@kclj.si; marko.grmek@kclj.si

© Springer Nature Switzerland AG 2019
Q. Siraj (ed.), *Radionuclide Parathyroid Imaging*,
https://doi.org/10.1007/978-3-030-17351-7_6

6.2 ^{18}F-Fluorodeoxyglucose (^{18}F-FDG)

^{18}F-fluorodeoxyglucose (^{18}F-FDG), the most widely used PET tracer, reflects glucose uptake in various tissues. In comparison to other metabolic substrates, glucose is preferentially taken up and metabolised as an energy source in malignant tissues through anaerobic glycolysis (the Warburg effect). However, the uptake and utilisation of glucose is less extensive in well-differentiated and benign neoplasms. Nevertheless, parathyroid imaging has been attempted with ^{18}F-FDG, with conflicting results reporting either very high or very low sensitivity in a small number of patients studied [3–6].

6.3 ^{11}C-Methionine

Carbon-11-labelled methionine (^{11}C-methionine), an amino acid analogue, has been extensively studied for parathyroid gland imaging. Its use in recent years is a revival of an old PET tracer, selenium-75-labelled methionine (^{75}Se-selenomethionine), first reported for parathyroid gland imaging in 1964 [7]. The uptake of the tracer is thought to reflect the proliferative activity of the target tissue. Although ^{11}C-labelling requires an on-site cyclotron for radionuclide production which limits the availability of the tracer, a number of studies have been performed, mostly in the hybrid PET/CT imaging era. Overall, the diagnostic performance has been found to be superior in comparison to conventional imaging [8–15]. However, in the setting of multiple hyperfunctioning parathyroid glands, both adenomatous or hyperplastic, where conventional imaging typically fails to detect all offending sites, diagnostic performance was not found to be clearly superior. A recent systemic review and meta-analysis reported a pooled sensitivity of 77% and PPV of 98% [16]. Currently, the suggested use of ^{11}C-methionine PET/CT is limited to negative findings of conventional imaging methods.

6.4 Choline PET

Recently, studies are slowly accumulating that are establishing choline as the most promising PET tracer investigated, either in the form of carbon-11 (^{11}C)-choline or fluorine 18 (^{18}F)-fluorocholine, the latter being more extensively studied due to its wider availability (no need for on-site cyclotron). Biochemically, increased choline uptake in hyperfunctioning parathyroid tissue may be linked to upregulation of phospholipid-dependent choline kinase related to PTH secretion [17]; alternatively, it may reflect cell membrane synthesis and therefore proliferative activity and increased uptake in mitochondria (abundant in oxyphil-rich cells) due to the positive charge of the tracer. Imaging technique with ^{18}F-fluorocholine involves injected activities from 100 MBq to 2.5 MBq/kg and imaging of the neck and mediastinum after 60 minutes with optional early imaging 5 minutes after tracer injection [18].

Several small preliminary studies reported a very good diagnostic performance of ^{11}C-choline and ^{18}F-fluorocholine for hyperfunctioning parathyroid gland localisation. In comparison to conventional scintigraphic imaging, the superior performance of choline PET/CT was demonstrated with reported sensitivities ranging from 94% to 100% [19–24]. Whilst the studies showed improved detection of solitary adenomas, the significant advantage was the detection of multiple and/or typically smaller lesions, likely owing to the superior spatial resolution of PET over conventional scintigraphic imaging methods. Also, the radiation dose to the patient may be significantly lower in comparison to conventional imaging approaches [25].

6.5 Clinical Context

In the clinical context, PET imaging was in most instances performed in patients with primary hyperparathyroidism. In secondary and tertiary hyperparathyroidism, the role of nuclear medicine imaging in the management of these patients remains to be clearly defined. The potential role of localising techniques in patients referred for parathyroidectomy is the prevention of surgical failure, particularly due to ectopic and supernumerary parathyroid glands [26]. In a few reports available, PET with both ^{11}C-methionine and ^{18}F-fluorocholine was found to be superior to conventional parathyroid scintigraphy [15, 21, 27]. In patients with recurrent or persistent primary and secondary hyperparathyroidism after surgery, localising techniques before reoperation are mandatory, in particular, nuclear medicine imaging modalities [26, 28, 29]. Whilst several studies have reported successful localisation of hyperfunctioning parathyroid glands using ^{11}C-methionine [9, 30] and ^{18}F-fluorocholine [22, 24], the evidence in support of its use in recurrent or persistent disease is currently limited. As recurrent or persistent disease is more frequent in cases of multiple hyperfunctioning glands [31], the use of PET tracers, in particular, ^{11}C/^{18}F-choline, may potentially reduce the need for reoperation if performed before the first operation.

Diagnostic performance of several evaluated PET tracers including ^{11}C-methionine, ^{11}C-choline and ^{18}F-fluorocholine is superior to conventional scintigraphic methods and is currently used in cases with negative or discordant conventional imaging.

References

1. Lange-Nolde A, Zajic T, Slawik M, Brink I, Reincke M, Moser E, et al. PET with ^{18}F-DOPA in the imaging of parathyroid adenoma in patients with primary hyperparathyroidism. A pilot study. Nuklearmedizin. 2006;45:193–6.
2. Krakauer M, Kjaer A, Bennedbæk FN. (18)F-FET-PET in primary hyperparathyroidism: a pilot study. Diagnostics (Basel). 2016;6(3):30.
3. Neumann DR, Esselstyn CB Jr, MacIntyre WJ, Chen EQ, Go RT, Kohse LM, et al. Primary hyperparathyroidism: preoperative parathyroid imaging with regional body FDG PET. Radiology. 1994;192:509–12.

4. Neumann DR, Esselstyn CB, Maclntyre WJ, Go RT, Obuchowski NA, Chen EQ, et al. Comparison of FDG-PET and sestamibi-SPECT in primary hyperparathyroidism. J Nucl Med. 1996;37:1809–15.
5. Sisson JC, Thompson NW, Ackerman RJ, Wahl RL. Use of 2-[F-18]- fluoro-2-deoxy-D-glucose PET to locate parathyroid adenomas in primary hyperparathyroidism. Radiology. 1994;192:280.
6. Melon P, Luxen A, Hamoir E, Meurisse M. Fluorine-18- fluorodeoxyglucose positron emission tomography for preoperative parathyroid imaging in primary hyperparathyroidism. Eur J Nucl Med. 1995;22:556–8.
7. Haynie TP, Otte WK, Wright JC. Visualization of a hyperfunctioning parathyroid adenoma using se75 selenomethionine and the photoscanner. J Nucl Med. 1964;5:710–4.
8. Hayakawa N, Nakamoto Y, Kurihara K, Yasoda A, Kanamoto N, Miura M, Inagaki N, Togashi K. A comparison between ^{11}C-methionine PET/CT and MIBI SPECT/CT for localization of parathyroid adenomas/hyperplasia. Nucl Med Commun. 2015;36(1):53–9.
9. Chicklore S, Schulte KM, Talat N, Hubbard JG, O'Doherty M, Cook GJ. ^{18}F-FDG PET rarely provides additional information to ^{11}C-methionine PET imaging in hyperparathyroidism. Clin Nucl Med. 2014;39(3):237–42.
10. Martínez-Rodríguez I, Martínez-Amador N, de Arcocha-Torres M, Quirce R, Ortega-Nava F, Ibáñez-Bravo S, Lavado-Pérez C, Bravo-Ferrer Z, Carril JM. Comparison of ^{99m}Tc-sestamibi and ^{11}C-methionine PET/CT in the localization of parathyroid adenomas in primary hyperparathyroidism. Rev Esp Med Nucl Imagen Mol. 2014;33(2):93–8.
11. Chun IK, Cheon GJ, Paeng JC, Kang KW, Chung JK, Lee DS. Detection and characterization of parathyroid adenoma/hyperplasia for preoperative localization: comparison between (11)C-methionine PET/CT and (99m)Tc-sestamibi scintigraphy. Nucl Med Mol Imaging. 2013;47(3):166–72.
12. Schalin-Jäntti C, Ryhänen E, Heiskanen I, Seppänen M, Arola J, Schildt J, Väisänen M, Nelimarkka L, Lisinen I, Aalto V, Nuutila P, Välimäki MJ. Planar scintigraphy with ^{123}I/^{99m}Tc-sestamibi, ^{99m}Tc-sestamibi SPECT/CT, ^{11}C-methionine PET/CT, or selective venous sampling before reoperation of primary hyperparathyroidism? J Nucl Med. 2013;54(5):739–47.
13. Herrmann K, Takei T, Kanegae K, Shiga T, Buck AK, Altomonte J, Schwaiger M, Schuster T, Nishijima K, Kuge Y, Tamaki N. Clinical value and limitations of [11C]-methionine PET for detection and localization of suspected parathyroid adenomas. Mol Imaging Biol. 2009;11(5):356–63.
14. Tang BN, Moreno-Reyes R, Blocklet D, Corvilain B, Cappello M, Delpierre I, Devuyst F, Van Simaeys G, Goldman S. Accurate pre-operative localization of pathological parathyroid glands using 11C-methionine PET/CT. Contrast Media Mol Imaging. 2008;3(4):157–63.
15. Otto D, Boerner AR, Hofmann M, Brunkhorst T, Meyer GJ, Petrich T, Scheumann GF, Knapp WH. Pre-operative localisation of hyperfunctional parathyroid tissue with ^{11}C-methionine PET. Eur J Nucl Med Mol Imaging. 2004;31(10):1405–12.
16. Kluijfhout WP, Pasternak JD, Drake FT, Beninato T, Gosnell JE, Shen WT, Duh QY, Allen IE, Vriens MR, de Keizer B, Pampaloni MH, Suh I. Use of PET tracers for parathyroid localization: a systematic review and meta-analysis. Langenbecks Arch Surg. 2016;401(7):925–35.
17. Ishizuka T, Kajita K, Kamikubo K, Komaki T, Miura K, Nagao S, et al. Phospholipid/Ca2+-dependent protein kinase activity in human parathyroid adenoma. Endocrinol Jpn. 1987;34:965–8.
18. Rep S, Lezaic L, Kocjan T, Pfeifer M, Sever JM, Simoncic U, et al. Optimal scan time for evaluation of parathyroid adenoma with [18F]-fluorocholine PET/CT. Radiol Oncol. 2015;49(4):327–33.
19. Lezaic L, Rep S, Sever MJ, et al. ^{18}F-Fluorocholine PET/CT for localization of hyperfunctioning parathyroid tissue in primary hyperparathyroidism: a pilot study. Eur J Nucl Med Mol Imaging. 2014;41:2083–9.
20. Orevi M, Freedman N, Mishani E, Bocher M, Jacobson O, Krausz Y. Localization of parathyroid adenoma by ^{11}C-choline PET/CT: preliminary results. Clin Nucl Med. 2014;39(12):1033–8.

21. Michaud L, Balogova S, Burgess A, Ohnona J, Huchet V, Kerrou K, Lefèvre M, Tassart M, Montravers F, Périé S, Talbot JN. A Pilot Comparison of ^{18}F-fluorocholine PET/CT, ultrasonography and ^{123}I/9^{9m}Tc-sestaMIBI dual-phase dual-isotope scintigraphy in the preoperative localization of hyperfunctioning parathyroid glands in primary or secondary hyperparathyroidism: influence of thyroid anomalies. Medicine (Baltimore). 2015;94(41):e1701.
22. Kluijfhout WP, Vorselaars WM, van den Berk SA, Vriens MR, Borel Rinkes IH, Valk GD, van Dalen T, de Klerk JM, de Keizer B. Fluorine-18 fluorocholine PET-CT localizes hyperparathyroidism in patients with inconclusive conventional imaging: a multicenter study from the Netherlands. Nucl Med Commun. 2016;37(12):1246–52.
23. Thanseer N, Bhadada SK, Sood A, Mittal BR, Behera A, Gorla AKR, Kalathoorakathu RR, Singh P, Dahiya D, Saikia UN, Rao SD. Comparative effectiveness of ultrasonography, ^{99m}Tc-sestamibi, and ^{18}F-fluorocholine PET/CT in detecting parathyroid adenomas in patients with primary hyperparathyroidism. Clin Nucl Med. 2017;42(12):e491–7.
24. Quak E, Blanchard D, Houdu B, Le Roux Y, Ciappuccini R, Lireux B, de Raucourt D, Grellard JM, Licaj I, Bardet S, Reznik Y, Clarisse B, Aide N. F18-choline PET/CT guided surgery in primary hyperparathyroidism when ultrasound and MIBI SPECT/CT are negative or inconclusive: the APACH1 study. Eur J Nucl Med Mol Imaging. 2018;45(4):658–66.
25. Rep S, Hocevar M, Vaupotic J, Zdesar U, Zaletel K, Lezaic L. ^{18}F-choline PET/CT for parathyroid scintigraphy: significantly lower radiation exposure of patients in comparison to conventional nuclear medicine imaging approaches. J Radiol Prot. 2018;38(1):343–56.
26. Taïeb D, Ureña-Torres P, Zanotti-Fregonara P, Rubello D, Ferretti A, Henter I, Henry JF, Schiavi F, Opocher G, Blickman JG, Colletti PM, Hindié E. Parathyroid scintigraphy in renal hyperparathyroidism: the added diagnostic value of SPECT and SPECT/CT. Clin Nucl Med. 2013;38(8):630–5.
27. Rubello D, Fanti S, Nanni C, Farsad M, Castellucci P, Boschi S, Franchi R, Mariani G, Fig LM, Gross MD. 11C-methionine PET/CT in 99mTc-sestamibi-negative hyperparathyroidism in patients with renal failure on chronic haemodialysis. Eur J Nucl Med Mol Imaging. 2006;33(4):453–9.
28. Hessman O, Stålberg P, Sundin A, Garske U, Rudberg C, Eriksson LG, Hellman P, Akerström G. High success rate of parathyroid reoperation may be achieved with improved localization diagnosis. World J Surg. 2008;32(5):774–81.
29. Guerin C, Paladino NC, Lowery A, Castinetti F, Taieb D, Sebag F. Persistent and recurrent hyperparathyroidism. Updates Surg. 2017;69(2):161–9.
30. Cook GJ, Wong JC, Smellie WJ, Young AE, Maisey MN, Fogelman I. [11C]Methionine positron emission tomography for patients with persistent or recurrent hyperparathyroidism after surgery. Eur J Endocrinol. 1998;139(2):195–7.
31. Alhefdhi A, Schneider DF, Sippel R, Chen H. Recurrent and persistence primary hyperparathyroidism occurs more frequently in patients with double adenomas. J Surg Res. 2014;190(1):198–202.

7 Nuclear Medicine Cases

Qaisar Hussain Siraj

7.1 Case 7.1. Palpable Neck Nodule (Parathyroid Adenoma)

7.1.1 Background

A 23-year-old girl with hyperparathyroidism was referred for parathyroid scintigraphy in 1986 following a previously failed parathyroidectomy. The patient had raised serum calcium and parathormone. On examination, there was a palpable nodule in the left lobe of the thyroid.

7.1.2 Procedure

The patient was injected with 37 MBq of ^{99m}Tc-pertechnetate and a thyroid scan performed after 20 min. Next, 75 MBq of ^{201}Tl-thallous chloride was injected without moving the patient and a planar scan performed in the thallium energy window. ^{201}Tl/^{99m}Tc subtraction scan image was obtained by subtracting the pertechnetate scan image from the thallium image after scatter correction.

7.1.3 Findings

The ^{99m}Tc-pertechnetate thyroid scan showed a normal-sized image of the gland with uniform uptake. The thallium-201 (^{201}Tl) scan showed a long oval-shaped nodule occupying most of the left lobe of the thyroid. The ^{201}Tl/^{99m}Tc subtraction scan showed a large oblong residual focal lesion extending upwards from the middle one-third of the left lobe of the thyroid (Fig. 7.1).

Q. H. Siraj (✉)
Department of Nuclear Medicine, Farwaniya Hospital, Kuwait

© Springer Nature Switzerland AG 2019
Q. Siraj (ed.), *Radionuclide Parathyroid Imaging*,
https://doi.org/10.1007/978-3-030-17351-7_7

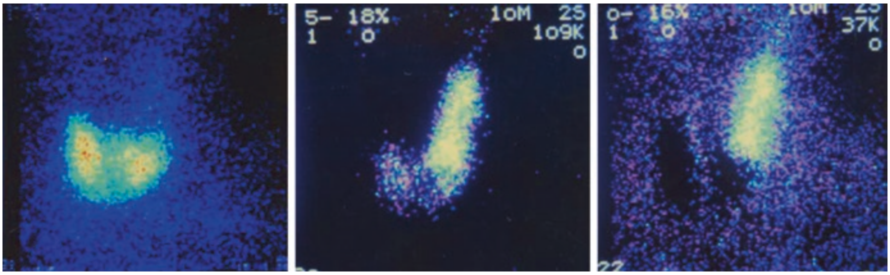

Fig. 7.1 ^{99m}Tc-pertechnetate thyroid scan (left), thallium-201 scan (middle) and ^{201}Tl/^{99m}Tc subtraction scan (right)

7.1.4 Conclusion

Findings consistent with a solitary large left upper parathyroid adenoma. The patient underwent surgery and a large adenoma was removed from the site. The patient's symptoms rapidly improved and a follow-up scan 3 months later was normal.

7.1.5 Comments and Teaching Points

- A parathyroid mass lesion may be palpable or even visible as seen in this case and may mimic a thyroid nodule.
- Clinically, however, a palpable benign parathyroid adenoma is very rare, as only 2% of benign primary hyperparathyroidism cases have an enlarged, palpable parathyroid gland [1].
- Palpable parathyroid adenomas are presumed parathyroid carcinomas unless proven otherwise [2–4], but as seen in this case, a palpable parathyroid adenoma does not always have a malignant nature.
- A large palpable parathyroid adenoma can mimic a thyroid nodule on clinical examination, and parathyroid scintigraphy is a very useful investigative tool for discriminating between a thyroid and a parathyroid adenoma.

7.2 Case 7.2. Water-Clear Cell Parathyroid Adenoma + Thyroid Adenoma

7.2.1 Background

A 40-year-old man presented in 1990 with 5 years history of renal stones with raised 24-h urinary calcium at 372 mg (normal range 50–300 mg), serum calcium at 11.6 mg/dL (normal range 9–11 mg/dL), phosphorus at 5.5 mg/dL (normal 2.5–4.5 mg/dL), raised serum alkaline phosphatase at 757 units/L (normal range

57–220 units/L) and serum PTH at 5 ng/mL (normal range 0.40–1.0 ng/mL). Skeletal x-rays revealed multiple areas of bone rarefaction. Thyroid ultrasound showed two nodules behind the right lobe of the thyroid gland suspected to be parathyroid adenomas.

7.2.2 Procedure

The patient was injected with 37 MBq of ^{99m}Tc-pertechnetate, and a thyroid scan was acquired for 10 min at 20 min postinjection. Next, 75 MBq of ^{201}Tl-thallous chloride was injected without moving the patient and a 10-min duration planar scan performed in the thallium energy window. ^{201}Tl/^{99m}Tc subtraction scan image was obtained by subtracting the pertechnetate scan image from the thallium image after scatter correction.

7.2.3 Findings

The ^{99m}Tc-pertechnetate thyroid scan showed a rounded “hot” nodule in the lower part of the right lobe of the thyroid gland with partial suppression of uptake in the remainder of the gland. The thallium-201 scan showed an additional large focus of increased uptake in the upper part of the right lobe of the thyroid without increased uptake seen in the “hot” thyroid nodule. The ^{201}Tl/^{99m}Tc subtraction scan showed a focus of intense residual uptake in the upper part of the right lobe of the thyroid (Fig. 7.2).

7.2.4 Conclusion

Findings consistent with a large thyroid adenoma in the right lower lobe together with a large parathyroid adenoma at the upper pole of the right thyroid lobe. The adenoma was surgically removed. Histopathology of the lesion showed sheets of

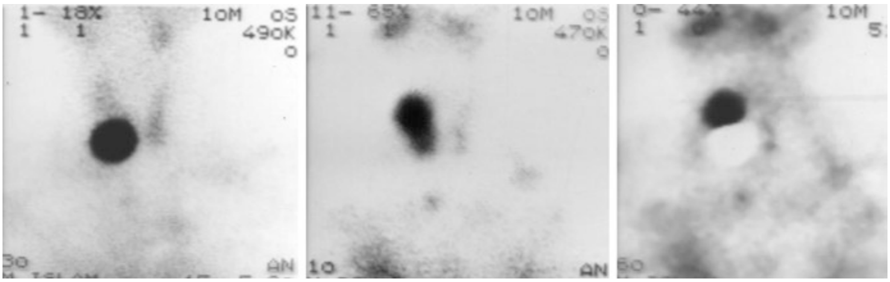

Fig. 7.2 ^{99m}Tc-pertechnetate thyroid scan (left), thallium-201 scan (middle) and ^{201}Tl/^{99m}Tc subtraction scan (right)

monomorphic cells mostly water-clear cells, but chief and oxyphil cells were also seen. The tumour was seen to be separated into lobules. The diagnosis was established as a rare water-clear cell parathyroid adenoma.

7.2.5 Comments and Teaching Points

- This is the first reported case of coexisting autonomous thyroid adenoma and a water-clear cell parathyroid adenoma in the same lobe of the thyroid gland.
- Water-clear cell adenoma is extremely rare with only six cases being previously reported [1, 5] at the time of this scan. We report two new cases of water-clear cell adenomas in this book (cases 7.2 and 7.68).
- It has been hypothesised that due to the large size of the adenoma compared with the biochemical and clinical features, water-clear cell adenomas have a “low endocrinological activity” and that calcium does not elevate until the adenoma has reached a considerable size [6]. This hypothesis is substantiated in this case, where, despite the high PTH level, serum calcium was not overtly elevated and the patient was relatively asymptomatic.

7.3 Case 7.3. Ectopic Supernumerary Left Upper Parathyroid Gland Hyperplasia

7.3.1 Background

A 28-year-old female on haemodialysis had four-gland parathyroidectomy, but the PTH levels were persistently elevated post surgery. The patient was referred for parathyroid scintigraphy to locate a possible ectopic parathyroid adenoma.

7.3.2 Procedure

The patient was injected with 54 MBq of ^{99m}Tc-pertechnetate, and a thyroid scan was acquired for 10 min at 20 min postinjection. Next, 300 MBq of ^{99m}Tc-sestamibi was injected without moving the patient and a 10-min duration planar scan performed. ^{99m}Tc-sestamibi SPECT scan was performed at 2 h followed by a late planar ^{99m}Tc-sestamibi scan at 3 h.

7.3.3 Findings

The ^{99m}Tc-pertechnetate thyroid scan was normal with uniform symmetrical uptake in both thyroid lobes. The early and late planar and SPECT ^{99m}Tc-sestamibi scans showed a clear-cut focus of increased activity superior and lateral to the upper pole of the left lobe of the thyroid (Fig. 7.3).

Fig. 7.3 Top row: ^{99m}Tc-pertechnetate thyroid scan (left), early planar ^{99m}Tc-sestamibi scan (middle) and late planar ^{99m}Tc-sestamibi scan (right). Bottom row: SPECT ^{99m}Tc-sestamibi scan in the coronal axis

7.3.4 Conclusion

Findings consistent with an ectopic supernumerary left upper hyperplastic parathyroid gland.

7.3.5 Comments and Teaching Points

- The supernumerary adenoma upper adenoma could have been confused with a submandibular gland by mistake.
- Asymmetric activity in the submandibular glands can be mistaken for an ectopic superior parathyroid adenoma.
- Supernumerary parathyroid glands are a major cause of persistent and recurrent hyperparathyroidism, and this case underscores the importance of preoperative localisation to improve the surgical results in patients with persistent or recurrent HPT.
- Supernumerary parathyroid glands arise from the rests of the normal parathyroid tissue when the pharyngeal pouches separate from the pharynx. The continuous growth stimulation in both primary and secondary parathyroid hyperplasia may stimulate the rudiments of parathyroid glands to grow, and many of them may thus appear as proper supernumerary glands [7, 8].

7.4 Case 7.4. Right Upper Parathyroid Adenoma + Ectopic Mediastinal Parathyroid Adenoma

7.4.1 Background

A 51-year-old female with primary biochemical hyperparathyroidism was referred for parathyroid scintigraphy for preoperative localisation.

7.4.2 Procedure

The patient was injected with 54 MBq of ^{99m}Tc-pertechnetate, and a thyroid scan was acquired for 10 min at 20 min postinjection. Next, 889 MBq of ^{99m}Tc-sestamibi was injected without moving the patient and a 10-min duration planar scan performed. ^{99m}Tc-sestamibi SPECT scan was performed at 2 h followed by a late planar ^{99m}Tc-sestamibi scan at 3 h.

7.4.3 Findings

The ^{99m}Tc-pertechnetate thyroid scan showed a normal-sized left lobe and an enlarged right lobe with homogenous distribution of activity within the gland. The early and late planar ^{99m}Tc-sestamibi scans showed a large focus of uptake in the region of the middle one-third of the right thyroid lobe, which was seen to be posteriorly located on the SPECT scan. The planar and the SPECT scans additionally showed a small focus of uptake in the anterior mediastinum (Figs. 7.4 and 7.5).

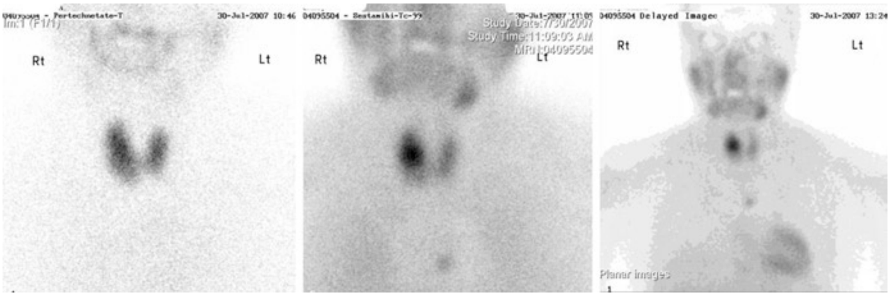

Fig. 7.4 ^{99m}Tc-pertechnetate thyroid scan (left), early planar ^{99m}Tc-sestamibi scan (middle) and late planar ^{99m}Tc-sestamibi scan (right)

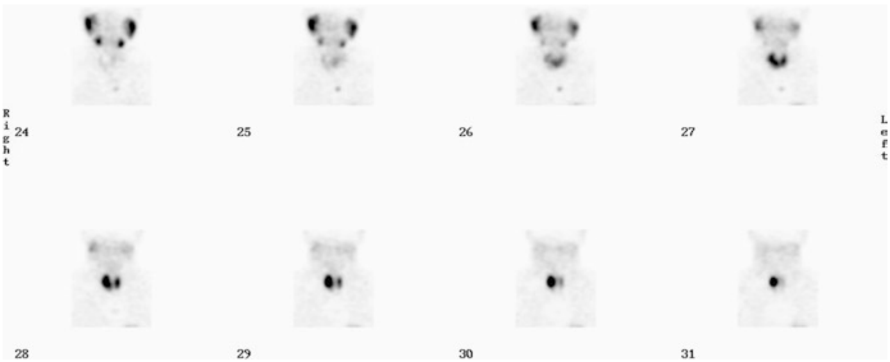

Fig. 7.5 ^{99m}Tc-sestamibi SPECT scan images in the coronal plane showing a focus of uptake in the anterior mediastinum (top row) together with focal uptake posterior to the middle one-third of the right thyroid lobe

7.4.4 Conclusion

The scan findings are consistent with a right upper parathyroid adenoma with a concomitant ectopic parathyroid adenoma in the anterior mediastinum.

7.4.5 Comments and Teaching Points

- Double parathyroid adenomas have been reported to occur in 1.7–9% of patients with primary hyperparathyroidism [9]. In 70 consecutive cases in our department with primary hyperparathyroidism due to parathyroid adenomas, we encountered 26 cases with double adenomas (8.6%).
- Some have debated whether double parathyroid adenomas are a discrete entity or represent hyperplasia with parathyroid glands of varying sizes, but it is now established that double adenomas are a discrete entity [9–11].
- Ectopic parathyroid adenomas can be overlooked at imaging performed with a field of view limited to the neck.

7.5 Case 7.5. Ectopic Right Superior Parathyroid Adenoma

7.5.1 Background

A 66-year-old male had previous parathyroid surgery with left upper and lower parathyroid glands removed. The patient again became symptomatic with raised serum parathormone and elevated serum calcium levels.

7.5.2 Procedure

The patient was injected with 44 MBq of ^{99m}Tc-pertechnetate, and a thyroid scan was acquired for 10 min at 20 min postinjection. Next, 850 MBq of ^{99m}Tc-sestamibi was injected without moving the patient and a 10-min duration planar scan performed. ^{99m}Tc-sestamibi SPECT scan was performed at 2 h followed by a late planar ^{99m}Tc-sestamibi scan at 3 h.

7.5.3 Findings

The pertechnetate thyroid scan showed a small hot nodule at the lower pole of the left lobe of the thyroid adjacent to the isthmus. The early and late planar parathyroid ^{99m}Tc-sestamibi images showed a large focus of intense increased activity in the midline at the level of upper poles of the thyroid lobes. There was significant focal uptake seen here on the probability map image. This lesion was clearly seen on the

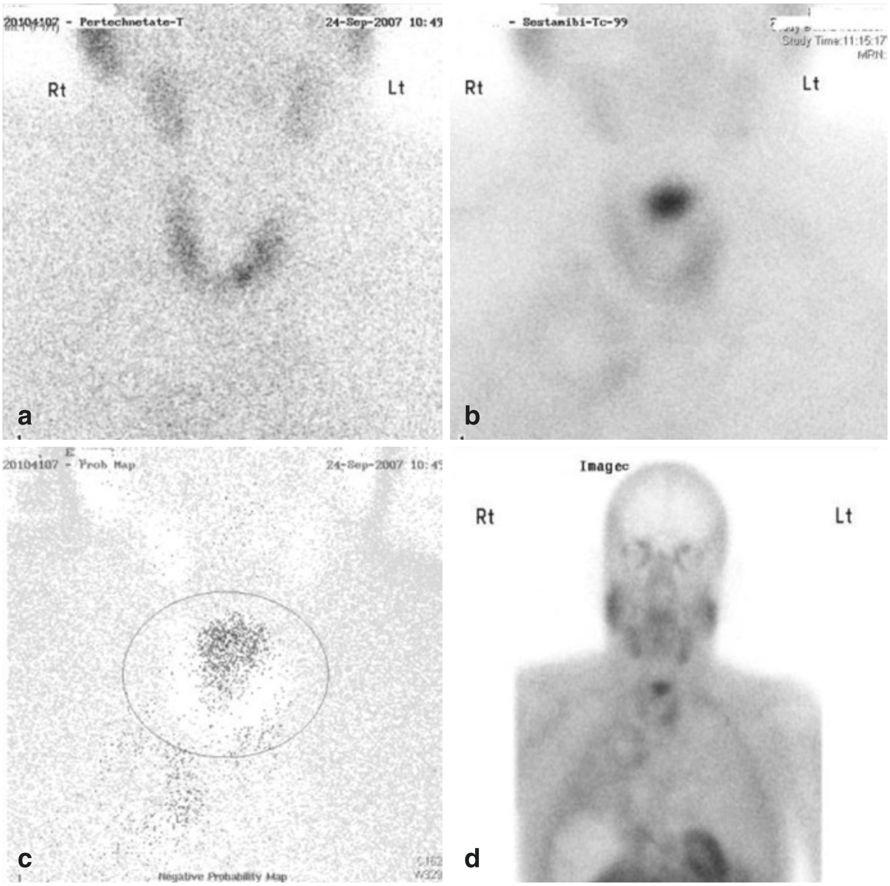

Fig. 7.6 ^{99m}Tc-pertechnetate thyroid scan (**a**), early planar ^{99m}Tc-sestamibi scan (**b**), significant difference image (**c**) and late planar ^{99m}Tc-sestamibi scan (**d**)

SPECT scan images and was posteriorly located. A review of the previous parathyroid scan showed no evidence of activity at this site (Figs. 7.6 and 7.7).

7.5.4 Conclusion

Findings consistent with an ectopic right superior parathyroid adenoma.

7.5.5 Comments and Teaching Points

- Superior parathyroid glands embryologically develop from the fourth branchial pouches and have a shorter migration path and are hence more rarely ectopic than inferior glands.

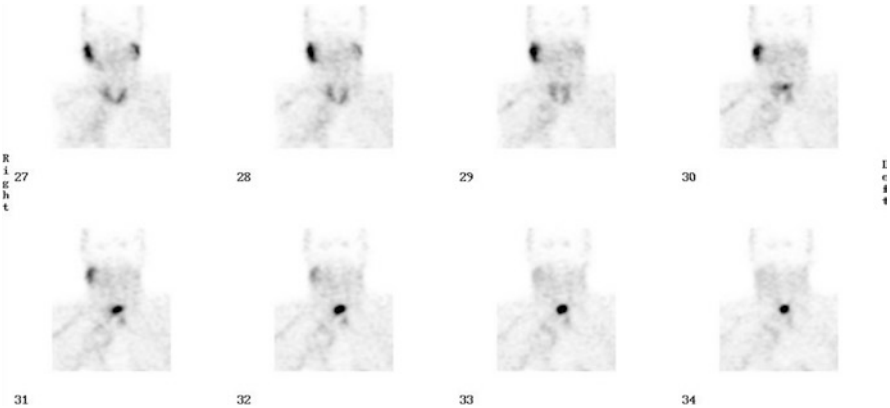

Fig. 7.7 ^{99m}Tc-sestamibi SPECT scan images in the coronal plane showing a posteriorly located mid-line focus of uptake at the level of the upper poles of the thyroid

- Superior parathyroid glands can be located as high as the level of the thyroid cartilage or even higher at the level of the hyoid bone.
- Superior parathyroids are found in their normal position in about 80% of individuals.

7.6 Case 7.6. Left Lower Parathyroid Adenoma

7.6.1 Background

A 77-year-old lady with raised serum calcium and high serum PTH, and symptoms were consistent with primary hyperparathyroidism. Ultrasound of the neck was negative for a parathyroid adenoma.

7.6.2 Procedure

The patient was injected with 58 MBq of ^{99m}Tc-pertechnetate, and a thyroid scan was acquired for 10 min at 20 min postinjection. Next, 800 MBq of ^{99m}Tc-sestamibi was injected without moving the patient and a 10-min duration planar scan performed. ^{99m}Tc-sestamibi SPECT scan was performed at 2 h followed by a late planar ^{99m}Tc-sestamibi scan at 3 h.

7.6.3 Findings

The pertechnetate thyroid scan showed a normal-sized thyroid gland with homogenous and symmetrical uptake. The early planar ^{99m}Tc-sestamibi scan showed a focus of uptake adjacent to the lower pole of the left lobe of the thyroid. The delayed ^{99m}Tc-sestamibi planar scan showed focal retention of activity at this site. The significant difference and the probability map images show statistically significant uptake at this site. The SPECT scan showed a posteriorly located focus of activity below the lower pole of the left lobe of the thyroid (Figs. 7.8 and 7.9).

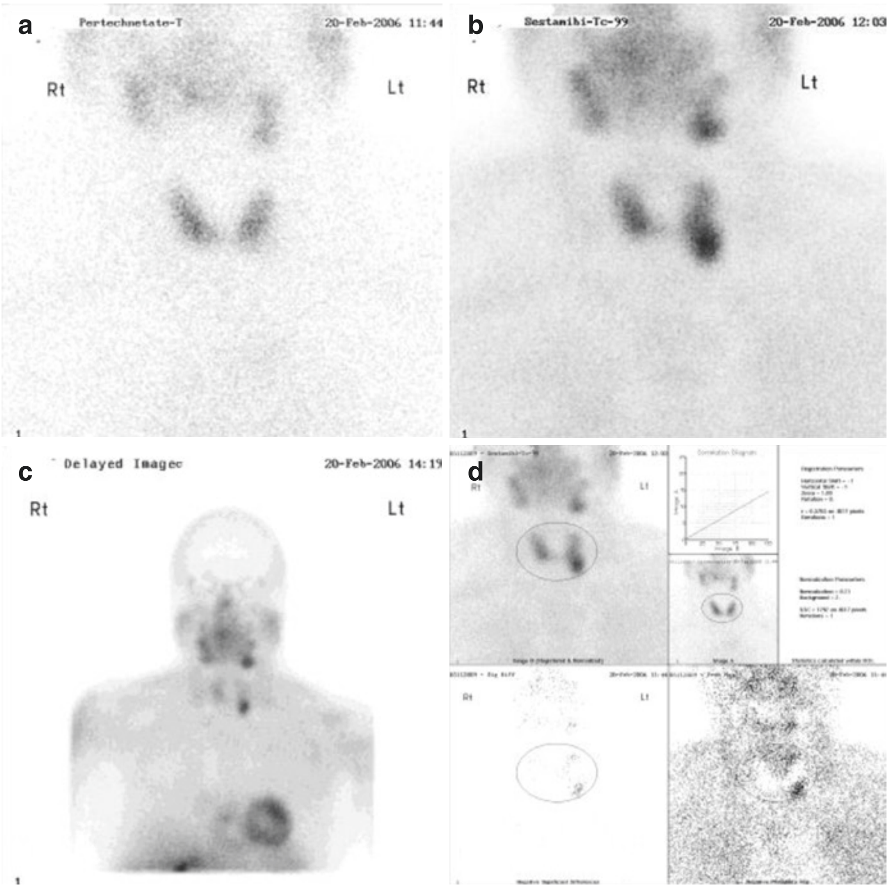

Fig. 7.8 ^{99m}Tc-pertechnetate thyroid scan (**a**), early planar ^{99m}Tc-sestamibi scan (**b**), late planar ^{99m}Tc-sestamibi scan (**c**) and the significant difference and probability map images (**d**)

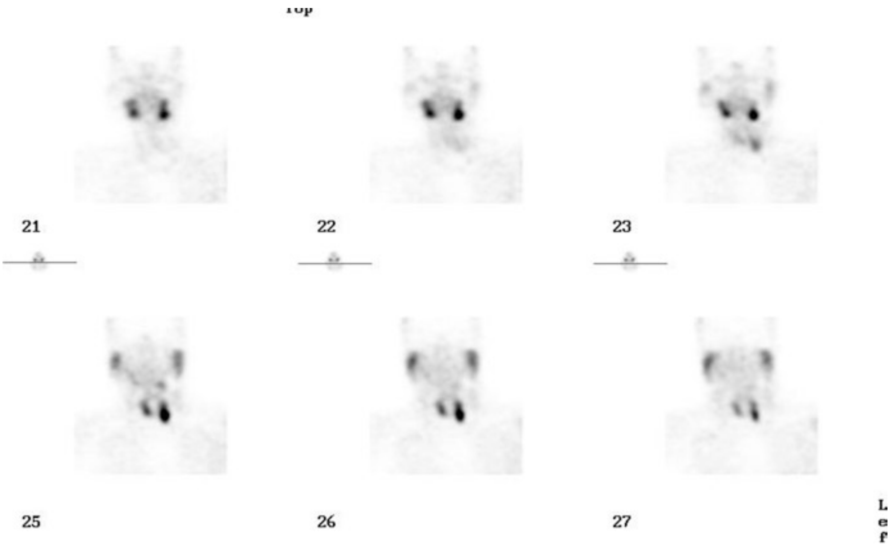

Fig. 7.9 ^{99m}Tc-sestamibi SPECT scan images in the coronal plane showing a posteriorly located focus of activity at the lower pole of the left lobe of the thyroid

7.6.4 Conclusion

Findings consistent with a left lower parathyroid adenoma.

7.6.5 Comments and Teaching Points

- The inferior parathyroid gland is more variable in position than the superior parathyroid glands because of their more complex migration process.

7.7 Case 7.7. Right Lower Parathyroid Adenoma

7.7.1 Background

A 51-year-old female with primary biochemical hyperparathyroidism referred for parathyroid scintigraphy for preoperative localisation.

7.7.2 Procedure

The patient was injected with 56 MBq of ^{99m}Tc-pertechnetate, and a thyroid scan was acquired for 10 min at 20 min postinjection. Next, 800 MBq of ^{99m}Tc-sestamibi was injected without moving the patient and a 10-min duration planar scan performed.

^{99m}Tc-sestamibi SPECT scan was performed at 2 h followed by a late planar ^{99m}Tc-sestamibi scan at 3 h.

7.7.3 Findings

The ^{99m}Tc-pertechnetate thyroid scan showed a normal-sized left lobe and a relatively enlarged right lobe with somewhat non-homogenous distribution of activity within the gland. The early and late planar ^{99m}Tc-sestamibi scan showed a large focus of intense increased uptake extending downwards from the lower pole of the right lobe of the thyroid with the washout image showing focal retention of activity here. The significant difference image showed a residual focus of uptake at the right lower poles (Figs. 7.10 and 7.11).

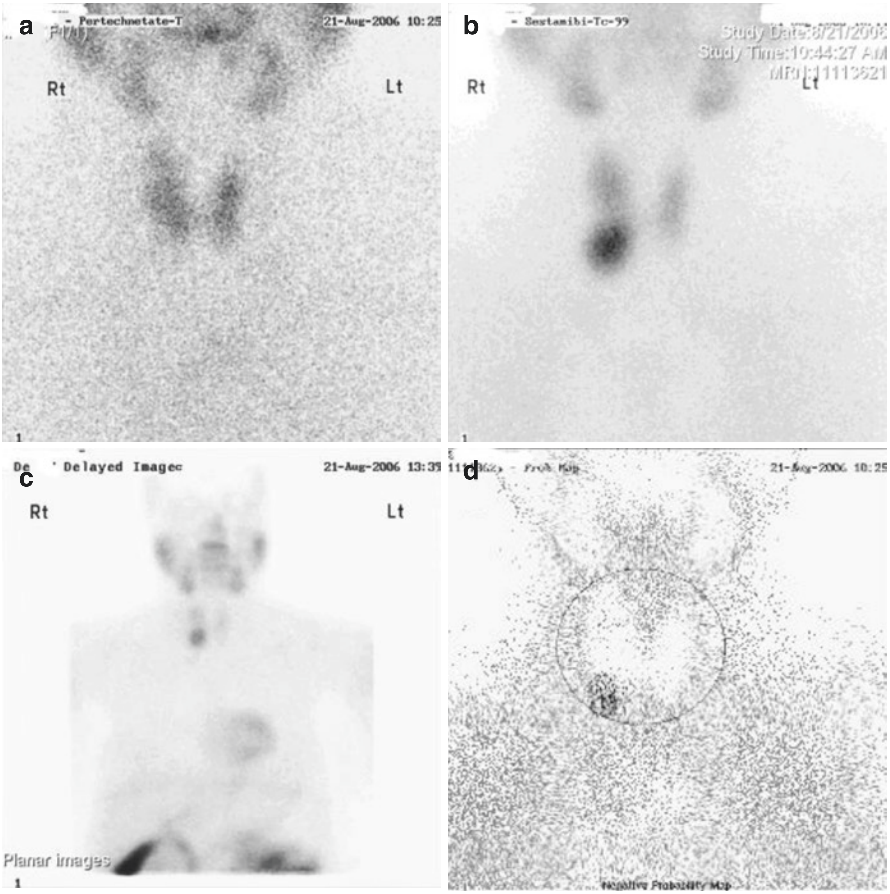

Fig. 7.10 ^{99m}Tc-pertechnetate thyroid scan (**a**), early planar ^{99m}Tc-sestamibi scan (**b**), late planar ^{99m}Tc-sestamibi scan (**c**) and significant difference image (**d**)

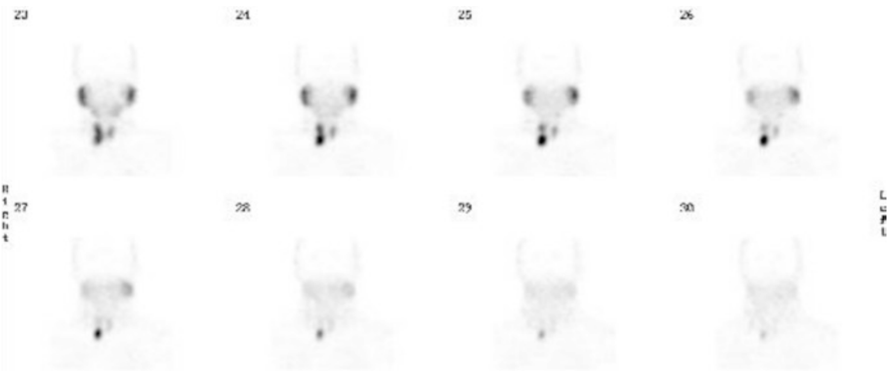

Fig. 7.11 ^{99m}Tc-sestamibi SPECT scan images in the coronal plane showing a posteriorly located focus of uptake abutting the right lower pole of the thyroid

7.7.4 Conclusion

Scan findings are consistent with a right lower parathyroid adenoma as the cause of primary hyperparathyroidism.

7.8 Case 7.8. Failed Thallium/Technetium Subtraction Scan. Single Adenoma on Dual-Phase Planar Sestamibi Scan with Tertiary Hyperparathyroidism

7.8.1 Background

A 61-year-old hypertensive female with hypothyroidism, chronic renal failure, hypercalcaemia and markedly raised serum parathyroid hormone was referred to the nuclear medicine department in 1993 for a parathyroid scan. The patient had a subtotal left lateral thyroid lobectomy performed for removal of a thyroid nodule 20 years ago when histology revealed secondary to Hashimoto's disease. At the time of the study, the patient was euthyroid on 100 µg thyroxine daily. Serum PTH was high at 600 pmol/L (normal 1.3–9.3), and serum calcium was high at 2.80 mmol/L (normal 2.2–2.6).

7.8.2 Procedure

For the thallium/technetium subtraction scan, the patient was injected with 75 MBq of ^{99m}Tc-pertechnetate, and a thyroid scan was acquired for 10 min at 20 min postinjection. Next, 80 MBq of ^{201}Tl-thallous chloride was injected without moving the patient and a 10-min duration planar scan performed after 10 min. For the dual-phase ^{99m}Tc-sestamibi scan, a planar ^{99m}Tc-sestamibi scan was performed 10 min after injection of 200 MBq of ^{99m}Tc-sestamibi with a delayed planar scan performed at 3.5 h postinjection.

7.8.3 Findings

The pertechnetate thyroid scan showed normal salivary gland uptake with non-visualisation of the thyroid (Fig. 7.12a). The lack of uptake by the thyroid was attributed both to the primary pathology and suppression of uptake by thyroxine. The thallium-201 scan (Fig. 7.12b) showed uniform uptake in both lobes of the gland with asymmetry of the right lower lobe which appeared likely to be clinically relevant; however, due to lack of pertechnetate uptake, it was not possible to perform a subtraction scan, and the study was hence considered non-diagnostic, and a ^{99m}Tc-sestamibi dual-phase planar scan (Fig. 7.13) was advised and performed. The early planar sestamibi scan showed homogenous uptake in the thyroid gland with a downward extension of the right lower pole with the 3.5-h delayed sestamibi scan showing focal retention of radiotracer in a lesion at the lower pole of the right lobe of the thyroid with partial washout of activity from the thyroid gland. A thyroid ultrasound examination of the neck subsequently revealed a well-defined 2-cm diameter hypoechogenic lesion posterior to the inferior pole (Fig. 7.14).

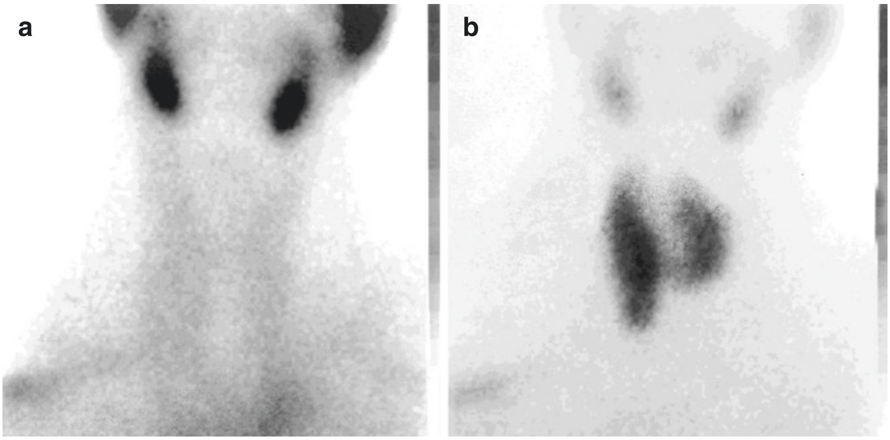

Fig. 7.12 Tc-99m pertechnetate (**a**) and thallium-201 (**b**) scans. There is non-visualization of the thyroid gland on the pertechnetate scan. The thallium scan shows uniform uptake in the thyroid but asymmetry of the two lobes of the gland

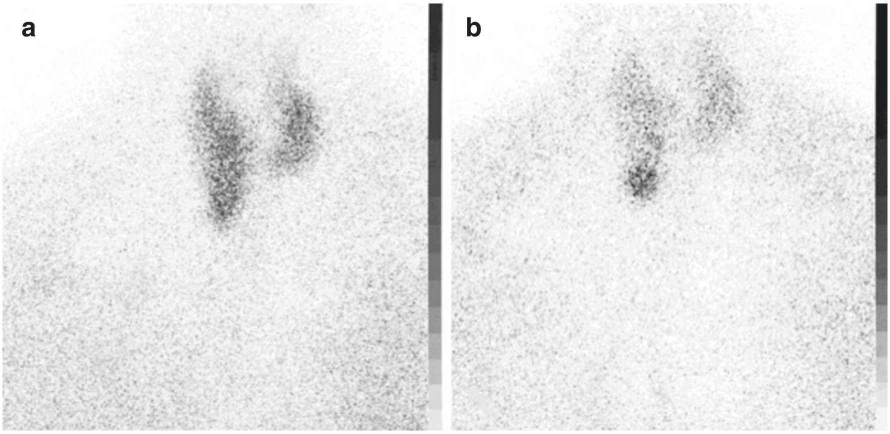

Fig. 7.13 Early planar ^{99m}Tc-sestamibi scan at 10 min (**a**) showing apparent downwards extension of the right lower pole, which region on the late planar ^{99m}Tc-sestamibi scan at 3.5 h (**b**) shows focal retention of the radiotracer with partial washout of activity from the thyroid gland

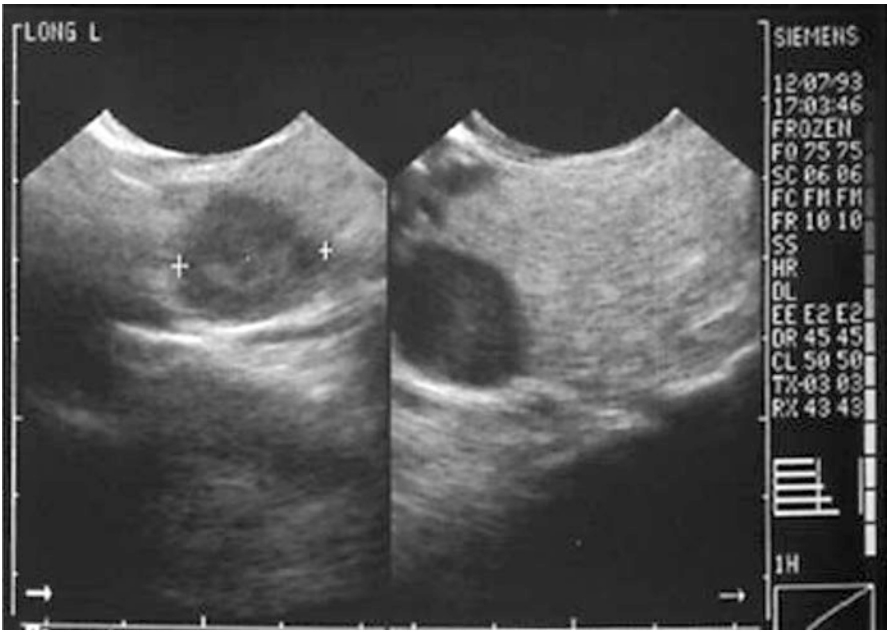

Fig. 7.14 Ultrasound scan showing a well-defined 2 cm diameter hypoechoic lesion posterior to the inferior pole of the right lobe of the thyroid. A parathyroid gland with nodular hyperplasia was later surgically removed from this site

7.8.4 Conclusion

Findings consistent with an adenomatous right lower parathyroid gland associated with tertiary hyperparathyroidism. The lesion was surgically resected with histopathology confirming an adenomatous parathyroid gland.

7.8.5 Comments and Teaching Points

- This is an early case of localisation of an adenomatous parathyroid by ^{99m}Tc-sestamibi following a failed ^{201}Tl/^{99m}Tc subtraction scan demonstrating the emerging role of dual-phase ^{99m}Tc-sestamibi parathyroid scanning.
- The value of double-phase ^{99m}Tc-sestamibi imaging in the localisation of parathyroid adenomas based on the differential washout of the tracer from the thyroid gland with time and focal retention of activity in the parathyroid adenomas has been well established [12].
- The dual-phase ^{99m}Tc-sestamibi imaging has been reported to be diagnostic in cases of iodine saturation due to amiodarone therapy producing impaired thallium-201 and ^{99m}Tc-pertechnetate uptake [13].

7.9 Case 7.9. Left Intrathyroidal Parathyroid Adenoma

7.9.1 Background

A 73-year-old female with hypercalcaemia and raised serum parathyroid hormone was referred for parathyroid scintigraphy in 2006.

7.9.2 Procedure

The patient was injected with 53 MBq of ^{99m}Tc-pertechnetate, and a thyroid scan was acquired at 20 min postinjection. Next, 828 MBq of ^{99m}Tc-sestamibi was injected and a planar scan performed after 10 min. ^{99m}Tc-sestamibi SPECT scan was performed at 2 h followed by a late planar ^{99m}Tc-sestamibi scan at 3 h.

7.9.3 Findings

The ^{99m}Tc-pertechnetate thyroid scan showed reduced uptake in the left lobe of the thyroid and normal uptake in the right lobe. The early planar ^{99m}Tc-sestamibi scan showed focally increased uptake in the upper part of the left lobe on the gland, with the late planar ^{99m}Tc-sestamibi scan showing focal retention of tracer in the left upper thyroid lobe region (Fig. 7.15). The ^{99m}Tc-sestamibi SPECT scan (Fig. 7.16)

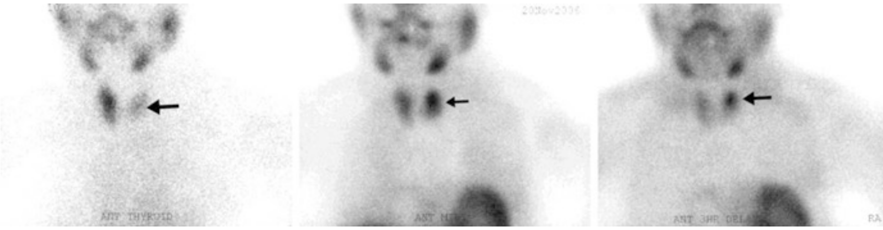

Fig. 7.15 ^{99m}Tc-pertechnetate thyroid scan (left), early planar ^{99m}Tc-sestamibi scan (middle), and late planar ^{99m}Tc-sestamibi scan (right) with the arrow pointing to the focus of decreased uptake in the left lobe on the pertechnetate thyroid scan and corresponding focal increased uptake in the early and late planar ^{99m}Tc-sestamibi scans

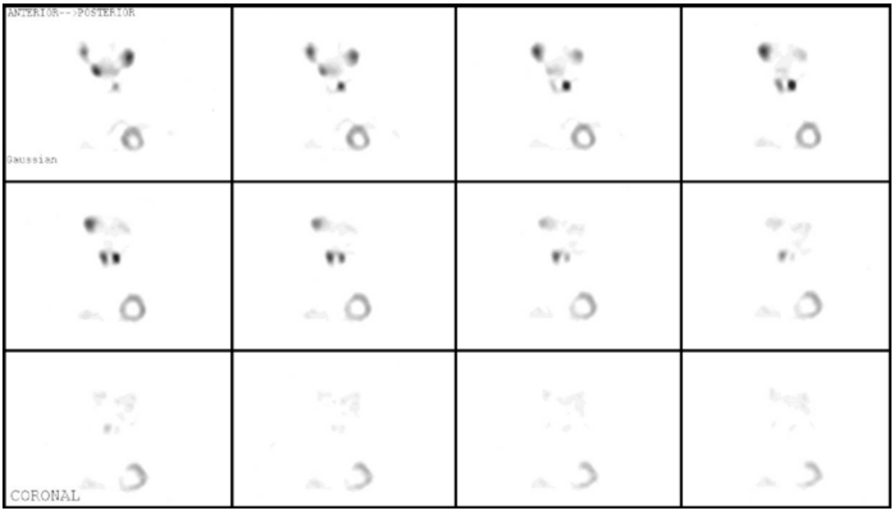

Fig. 7.16 ^{99m}Tc-sestamibi SPECT scan images in the coronal axis show an anteriorly located nodule in the upper part of the left thyroid lobe

showed an anteriorly located focus of activity in the upper part of the left thyroid lobe suggestive of an intrathyroidal parathyroid adenoma.

7.9.4 Conclusion

Findings consistent with an intrathyroidal left upper parathyroid adenoma. The patient underwent surgery, but a parathyroid adenoma could not be identified, and given the nuclear medicine report of a suspected intrathyroidal parathyroid adenoma, left hemithyroidectomy was undertaken, and histopathology revealed a fair-sized left intrathyroidal parathyroid adenoma.

7.9.5 Comments and Teaching Points

- Intrathyroidal parathyroid adenoma location is considered “major ectopy” with the other two major ectopic sites being the mediastinum or high in the neck, either within or lateral to the cervical neurovascular bundle.
- The majority of apparently intrathyroidal superior parathyroid glands are not truly intrathyroidal but hidden in a cleft or an indentation of normal or nodular thyroid tissue [14].

7.10 Case 7.10. Sestamibi-negative, Thallium-positive Right Parathyroid Adenoma

7.10.1 Background

A 51-year-old female had liver resection surgery for colorectal cancer metastases. During her postoperative recovery period, the patient developed psychotic symptoms, and at that stage, her calcium level was found to be significantly raised. Subsequently, her parathyroid hormone level also rose. An ultrasound scan showed small lesions within the thyroid with a possible 1 cm lesion posterior to the right lobe of the thyroid. CT scan also showed a low-density cystic area which was reported as unlikely to represent a parathyroid adenoma. Her serum PTH was 18.4 pmol/L (normal 0.5–6.4), corrected calcium 2.88 mmol/L (normal 2.12–2.62), phosphate 0.73 mmol/L (normal 0.80–1.40), alkaline phosphate 471 IU/L (normal 35–110), urea 2.7 mmol/L (normal range 2.6–6.0) and creatinine 94 μmol/L (normal range 62–124).

7.10.2 Procedure

The patient was injected with 50 MBq of ^{99m}Tc-pertechnetate, and a thyroid scan acquired at 20 min postinjection. Next, 800 MBq of ^{99m}Tc-sestamibi was injected without moving the patient and a planar scan performed after 10 min followed by a late planar ^{99m}Tc-sestamibi scan at 3 h.

For the thallium/technetium subtraction scan, the patient was injected with 54 MBq of ^{99m}Tc-pertechnetate, and a thyroid scan was acquired after 20 min. Next, 72 MBq of ^{201}Tl-thallous chloride was injected without moving the patient and a 10-min duration planar scan performed after 10 min.

7.10.3 Findings

The pertechnetate thyroid scan and the ^{99m}Tc-sestamibi early and late planar showed a larger right lobe and a smaller left lobe with uniform uptake in the gland, with the

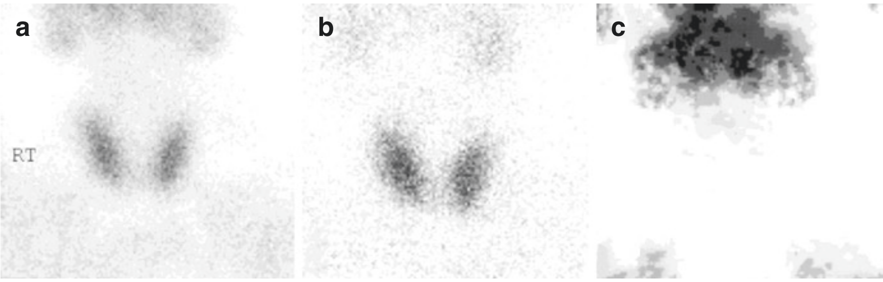

Fig. 7.17 Early planar ^{99m}Tc-sestamibi scan (**a**), ^{99m}Tc-pertechnetate thyroid scan (**b**) and ^{99m}Tc-sestamibi/^{99m}Tc-pertechnetate subtraction scan image (**c**)

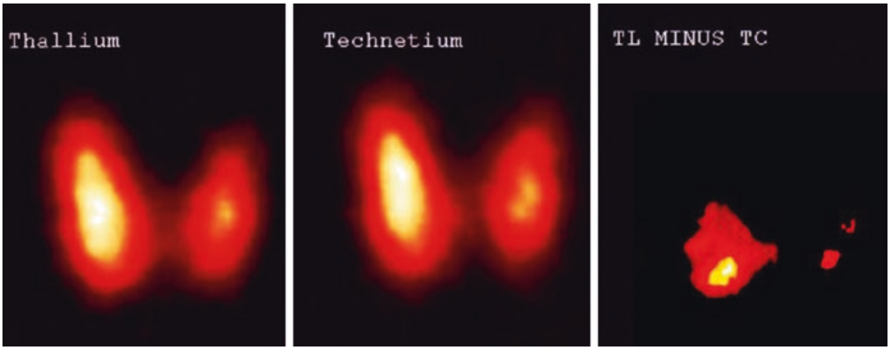

Fig. 7.18 Thallium-201 scan (left), Tc-99m pertechnetate scan (middle) and ^{201}Tl/^{99m}Tc subtraction scan (right). The technetium and the thallium scans show symmetrical uniform uptake in the two lobes of the thyroid with a larger right and a smaller left lobe. The ^{201}Tl/^{99m}Tc subtraction scan shows a fair sized residual focus of activity in the lower part of the right thyroid lobe region

^{99m}Tc-sestamibi/^{99m}Tc-pertechnetate subtraction scans showing no residual focus of activity in the thyroid bed (Fig. 7.17). The ^{201}Tl/^{99m}Tc subtraction scan, however, showed a large residual focus of activity in the right thyroid bed.

7.10.4 Conclusion

The scan findings were consistent with a sestamibi-negative but thallium-positive right thyroid adenoma as the cause of primary hyperparathyroidism. At surgery, the right thyroid lobe was dissected, and a 0.8 g encapsulated right upper parathyroid adenoma removed (Fig. 7.18). The tissue was sent for p-glycoprotein staining, but the result was negative for p-glycoprotein expression excluding this as a factor underlying the false-negative ^{99m}Tc-sestamibi scan. Histopathology of the lesion showed an encapsulated parathyroid adenoma (Fig. 7.19).

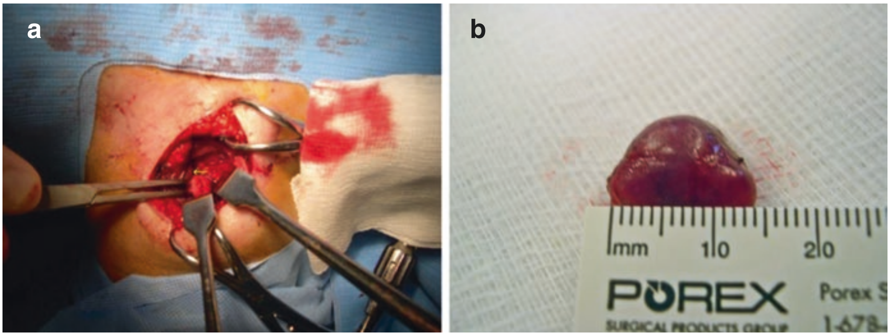

Fig. 7.19 At surgery, a collar incision was made and the right thyroid lobe dissected (**a**) with a 0.8 g encapsulated right upper parathyroid adenoma (**b**) measuring 14 mm in diameter removed

7.10.5 Comments and Teaching Points

- This is a case of a false-negative ^{99m}Tc-sestamibi scan where the adenoma was correctly identified by a ^{201}Tl/^{99m}Tc subtraction scan.
- The combination of two functional modalities together with structural imaging can potentially provide a substantial increase in sensitivity and specificity for the detection of adenomatous/hyperplastic parathyroids.
- P-glycoprotein (P-gp) membrane expression has been associated with false-negative sestamibi scan results [15, 16]. However, others have found no relationship between the sensitivity of dual-phase ^{99m}Tc-sestamibi imaging and P-gp and MRP1 expressions in resected parathyroid [17, 18]. In this case, we did not find P-gp expression in the sestamibi-negative thallium-positive adenoma.
- Thallium and sestamibi uptake mechanisms differ with former being dependent on Na^+/K^+ pump, and the latter on mitochondrial uptake, which may like to explain the discrepancy between thallium and sestamibi parathyroid imaging results.

7.11 Case 7.11. Sestamibi-Negative and Thallium-Positive Left Parathyroid Adenoma

7.11.1 Background

A 58-year-old female with raised serum calcium and parathyroid hormone with renal stones was referred for parathyroid scintigraphy. Ultrasound of the neck showed a multinodular goitre with no parathyroid masses seen.

7.11.2 Procedures

The patient was injected with 55 MBq of ^{99m}Tc-pertechnetate, and a thyroid scan was acquired at 20 min postinjection. Next, 850 MBq of ^{99m}Tc-sestamibi was injected and a planar scan performed after 10 min. ^{99m}Tc-sestamibi SPECT scan was performed at 2 h followed by a late planar ^{99m}Tc-sestamibi scan at 3 h.

For the thallium/technetium subtraction scan, the patient was injected with 70 MBq of ^{99m}Tc-pertechnetate, and a thyroid scan was acquired after 20 min. Next, 75 MBq of ^{201}Tl-thallous chloride was injected without moving the patient and a 10-min duration planar scan performed after 10 min.

7.11.3 Findings

The ^{99m}Tc-pertechnetate thyroid scan and the ^{99m}Tc-sestamibi early and late planar scan images showed a relatively prominent left lobe of the thyroid gland with a similar distribution of activity in the two lobes (Fig. 7.20), but unfortunately, due to patient movement, the image subtraction failed. However, the ^{99m}Tc-sestamibi SPECT scan (Fig. 7.21) did not show any significant abnormality to suggest the presence of a parathyroid adenoma.

A ^{201}Tl/^{99m}Tc subtraction scan was subsequently performed which showed a clear-cut focus of residual activity in the region of the left lobe of the thyroid consistent with a parathyroid adenoma (Fig. 7.22).

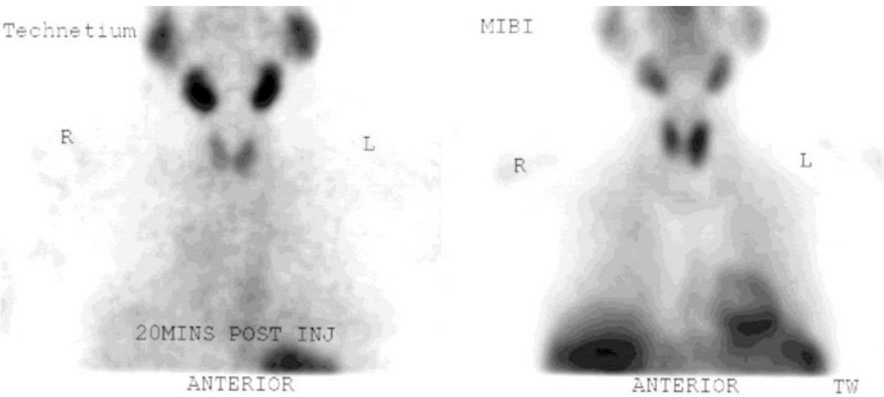

Fig. 7.20 Early Planar ^{99m}Tc-pertechnetate thyroid scan (left) and the ^{99m}Tc-sestamibi scan (right)

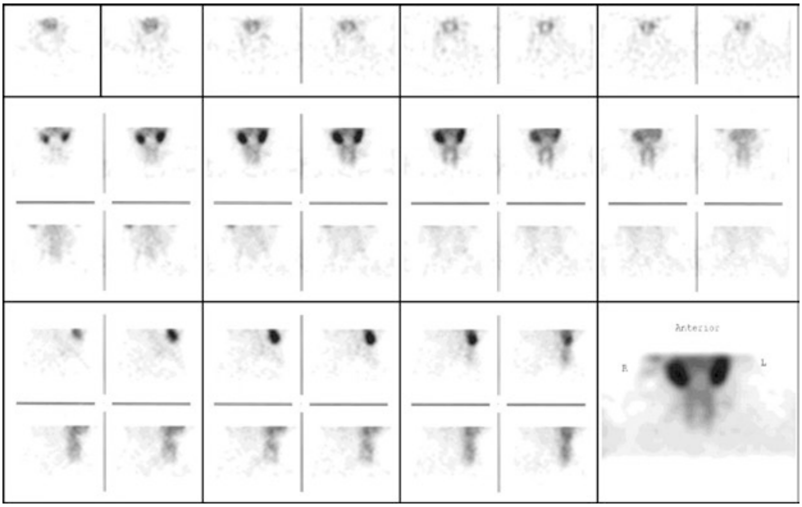

Fig. 7.21 ^{99m}Tc-sestamibi SPECT scan in transaxial (top row), coronal (2nd and 3rd rows) and sagittal (last 2 rows) axes showing no evidence of a parathyroid adenoma

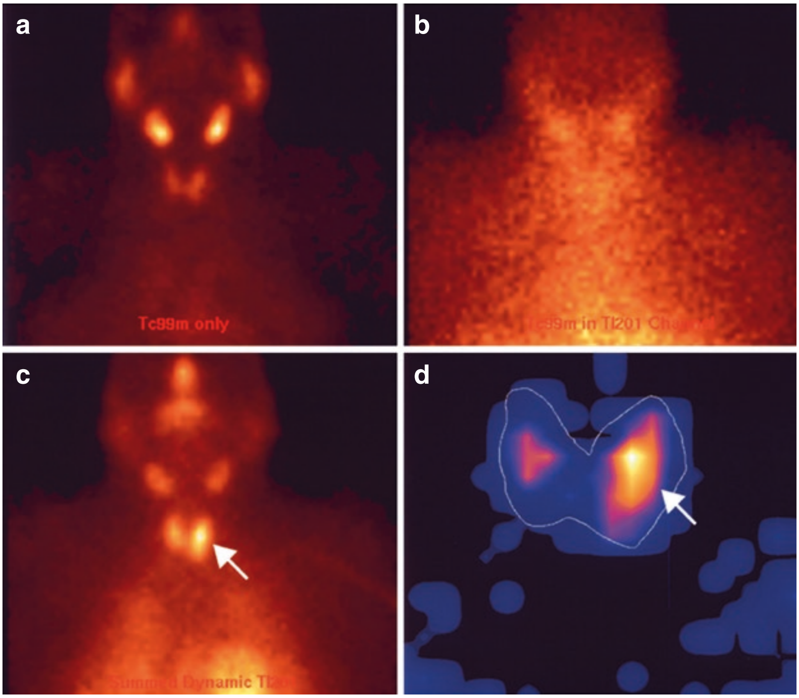

Fig. 7.22 ^{99m}Tc-pertechnetate scan (**a**), technetium scatter in thallium window, (**b**) thallium-201 scan (**c**) and ^{201}Tl/^{99m}Tc subtraction scan (**d**). The pertechnetate thyroid scan shows normal uptake in both thyroid lobes with the thallium scan showing increased focal uptake in the left thyroid lobe and the subtraction scan showing a clear-cut large residual focus of activity in the left thyroid bed (arrows) consistent with a fair-sized parathyroid adenoma

7.11.4 Conclusion

Findings consistent with a sestamibi-negative but thallium-positive left thyroid adenoma as the cause of primary hyperparathyroidism. At surgery, a left parathyroid adenoma was dissected out and confirmed on histopathology.

7.11.5 Comments and Teaching Points

- This is a case of a false-negative ^{99m}Tc-sestamibi scan where the adenoma was correctly identified by a ^{201}Tl/^{99m}Tc subtraction scan.
- In this case, as in the previous case, we did not find P-gp expression in the sestamibi-negative thallium-positive adenoma.
- The combination of two functional modalities together with structural imaging can potentially provide a substantial increase in sensitivity and specificity for the detection of adenomatous/hyperplastic parathyroids.

7.12 Case 7.12. Sestamibi-Negative, Thallium-Positive Double Parathyroid Adenomas

7.12.1 Background

An 80-year-old female with hypercalcaemia and raised serum parathyroid hormone was referred for parathyroid scintigraphy in 2003. Ultrasound of the neck was normal.

7.12.2 Procedures

The patient was injected with 52 MBq of ^{99m}Tc-pertechnetate, and a thyroid scan was acquired after 20 min. Next, 840 MBq of ^{99m}Tc-sestamibi was injected and scanning performed after 10 min. ^{99m}Tc-sestamibi SPECT scan was performed at 2 h followed by a late planar ^{99m}Tc-sestamibi scan at 3 h.

For the thallium/technetium subtraction scan, the patient was injected with 74 MBq of ^{99m}Tc-pertechnetate, and a thyroid scan was acquired at 20 min postinjection. Next, 76 MBq of ^{201}Tl-thallous chloride was injected without moving the patient and a 10-min duration scan performed after 10 min.

7.12.3 Findings

The ^{99m}Tc-pertechnetate thyroid scan (Fig. 7.23a) and the ^{99m}Tc-sestamibi early (Fig. 7.23b) and late (Fig. 7.23c) planar scan images show normal uptake in both lobes of the thyroid gland.

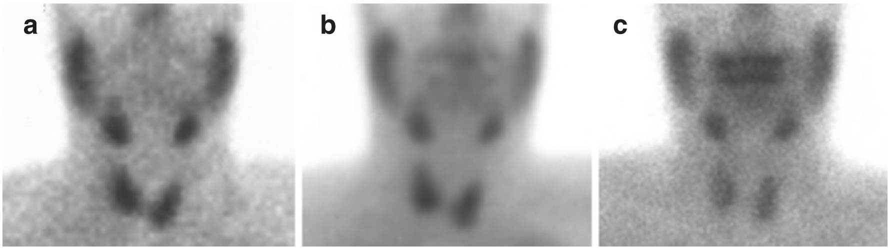

Fig. 7.23 ^{99m}Tc-pertechnetate thyroid scan (**a**), early planar ^{99m}Tc-sestamibi scan (**b**) and late planar ^{99m}Tc-sestamibi scan (**c**)

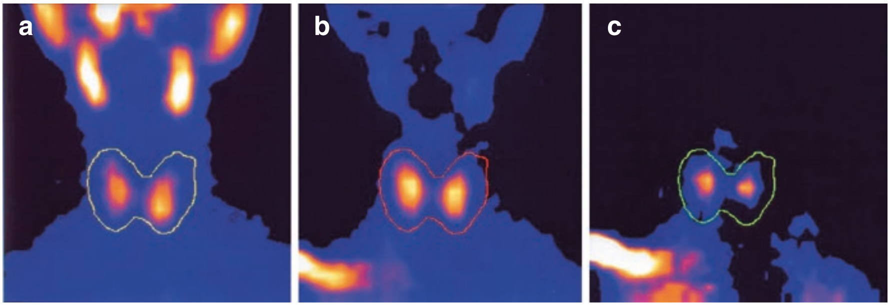

Fig. 7.24 ^{99m}Tc-pertechnetate scan (**a**), thallium-201 scan (**b**) and ^{201}Tl/^{99m}Tc subtraction scan (**c**) showing large residual foci of uptake in both lobes of the thyroid consistent with bilateral parathyroid adenomas

A ^{201}Tl/^{99m}Tc subtraction scan was subsequently performed which showed large residual foci of uptake in both lobes of the thyroid consistent with bilateral parathyroid adenomas (Fig. 7.24).

7.12.4 Conclusion

Findings consistent with double sestamibi-negative but thallium-positive parathyroid adenomas as the cause of primary hyperparathyroidism. The patient subsequently underwent surgery with excision of parathyroid adenomas from both thyroid lobes.

7.12.5 Comments and Teaching Points

- This is a novel case of a false-negative ^{99m}Tc-sestamibi scan in a patient with double parathyroid adenomas, where the two adenomas were correctly identified by a ^{201}Tl/^{99m}Tc subtraction scan.

- Subtraction scintigraphy is reported to be superior to dual-phase scintigraphy for identification of single- or multiple-gland disease [19].
- Sestamibi parathyroid uptake is dependent on the cellular density of the mitochondria-rich oxyphil cells only; however, biologically, thallium is superior to for the detection of parathyroid adenomas since its uptake depends not only on vascularity and perfusion of the parathyroid adenomas but the tracer is taken up by both the oncogenic and non-oncogenic parathyroid cells.

7.13 Case 7.13. Sestamibi-Negative, Weakly Thallium Positive Left Lower Parathyroid Adenoma

7.13.1 Background

A 34-year-old male with hypercalcaemia and raised serum parathyroid hormone was referred for parathyroid scintigraphy in 2006. The patient was admitted with nausea, reduced appetite, lethargy, generalised arthralgia, polydipsia and a change in his mood. There were no bone pains, nocturia or kidney stones. His bone density scan was normal, and ultrasound of the neck was normal too with no parathyroid gland identified.

His PTH was mildly elevated at 8.4 pmol/L (normal 0–6.4), corrected calcium 2.89 mmol/L (normal 2.2–2.6), phosphate low at 0.74 mmol/L (normal 0.84–1.45), urea 5.3 mmol/L (normal range 3.2–7.1) and creatinine 113 μmol/L (normal range 71–133).

7.13.2 Procedures

The patient was injected with 74 MBq of ^{99m}Tc-pertechnetate, and a thyroid scan was acquired after 20 min. Next, 700 MBq of ^{99m}Tc-sestamibi was injected and planar imaging performed after 10 min and 2.5 h. This was followed by 76 MBq intravenous injection of ^{201}Tl-thallous chloride with planar imaging performed after 10 min.

7.13.3 Findings

The dual-phase ^{99m}Tc-sestamibi early and late planar scan images showed normal uptake in both lobes of the thyroid gland with no evidence of an ectopic focus of uptake seen (Fig. 7.25).

The ^{201}Tl planar and the ^{201}Tl/^{99m}Tc subtraction scan showed a focus of abutting the left lower pole of the thyroid gland suggestive of a left lower parathyroid adenoma (Fig. 7.26).

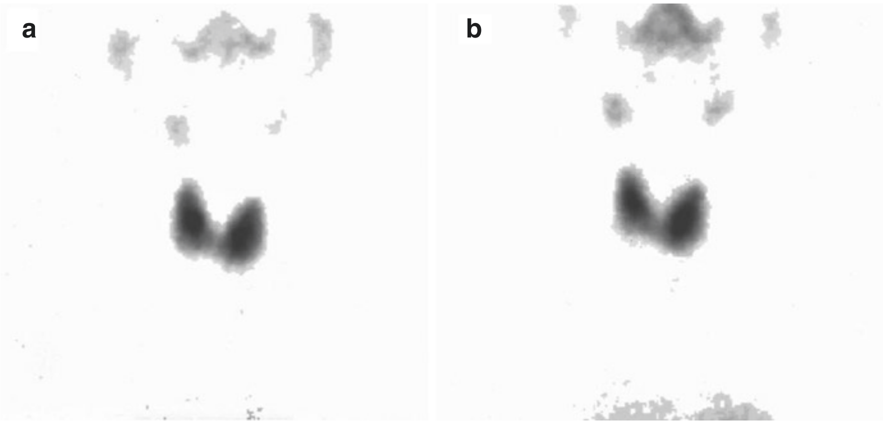

Fig. 7.25 Early (**a**) and late (**b**) planar ^{99m}Tc-sestamibi scans showing normal uptake in the thyroid bed and mediastinum

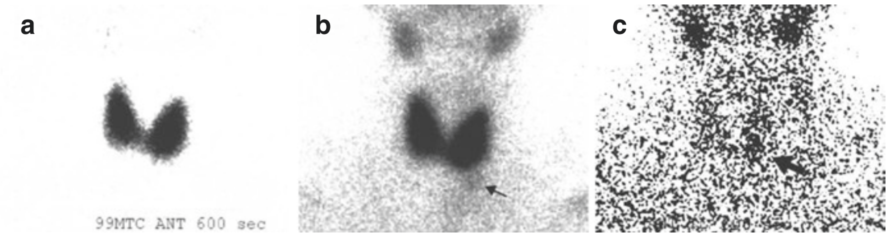

Fig. 7.26 ^{99m}Tc-pertechnetate scan (**a**), thallium-201 scan (**b**) and ^{201}Tl/^{99m}Tc subtraction scan (**c**) showing a faint focus of uptake adjacent to the lower pole of the left lobe of the thyroid (arrows)

7.13.4 Conclusion

Findings consistent with a left lower sestamibi-negative but thallium-positive parathyroid adenoma as the cause of primary hyperparathyroidism.

The patient subsequently underwent parathyroid surgery, with excision of two normal parathyroid glands including the upper left and right parathyroid glands and an enlarged adenomatous left lower parathyroid gland, with the right lower parathyroid gland left intact in place. Post parathyroidectomy his calcium fell from 2.8 to 2.26 mmol/L, and phosphate normalised from 0.74 to 0.86 (normal 0.81–1.45).

7.13.5 Comments and Teaching Points

- Symptoms attributable to PHPT include fatigue, exhaustion, weakness, polydipsia, polyuria, nocturia, constipation, bone pain, back pain, joint pain, depression, memory loss, loss of appetite, nausea, heartburn and pruritus. The patient experienced some of these symptoms including nausea, reduced appetite, lethargy,

generalised arthralgia, polydipsia and a change in his mood. These are the digestive, neurological, renal and musculoskeletal manifestation of PHPT.
- This is another case of a false-negative ^{99m}Tc-sestamibi scan with a true-positive thallium-201 scan for a parathyroid adenoma,

7.14 Case 7.14. Intact Parathyroid Hormone-Secreting Bone Metastasis from Breast Cancer

7.14.1 Background

A 50-year-old female was referred with hypercalcaemia and primary hyperparathyroidism in 2005. Her serum calcium was high at 3.30 mmol/L (normal 2.15–2.60), PTH high at 30 pmol/L (normal 0–6.4), PTHrp <0.7 pg/mL (normal <1.8), phosphate decreased at 0.42 mmol/L (normal 0.84–1.45), normal vitamin D at 21.5 nmol/L (normal 6–40) and high alkaline phosphatase at 259 IU/L (30–95). The inflammatory markers were normal. She had been diagnosed 3 years ago with carcinoma breast and had undergone surgery, chemotherapy and radiotherapy. Regular follow-up had not shown any recurrence. Ultrasound neck did not show parathyroid lump or adenoma.

7.14.2 Procedure

The patient was injected with 55 MBq of ^{99m}Tc-pertechnetate, and a thyroid scan was acquired for 10 min after 20 min postinjection. Next, 813 MBq of ^{99m}Tc-sestamibi was injected without moving the patient and a 10-min duration planar scan performed, followed by a late planar ^{99m}Tc-sestamibi scan at 3 h (Fig. 7.27).

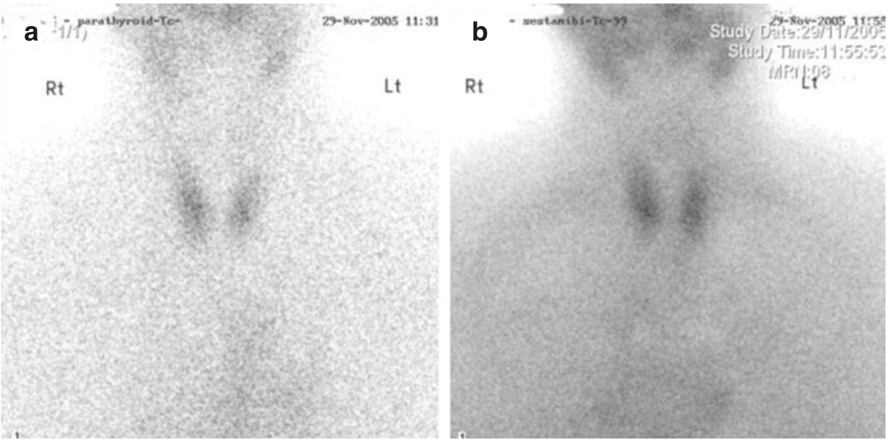

Fig. 7.27 ^{99m}Tc-pertechnetate thyroid scan (**a**), early planar ^{99m}Tc-sestamibi scan (**b**), the 3-h late planar ^{99m}Tc-sestamibi unzoomed neck and chest image (**c**) and ^{99m}Tc-sestamibi/^{99m}Tc-pertechnetate subtraction image (**d**)

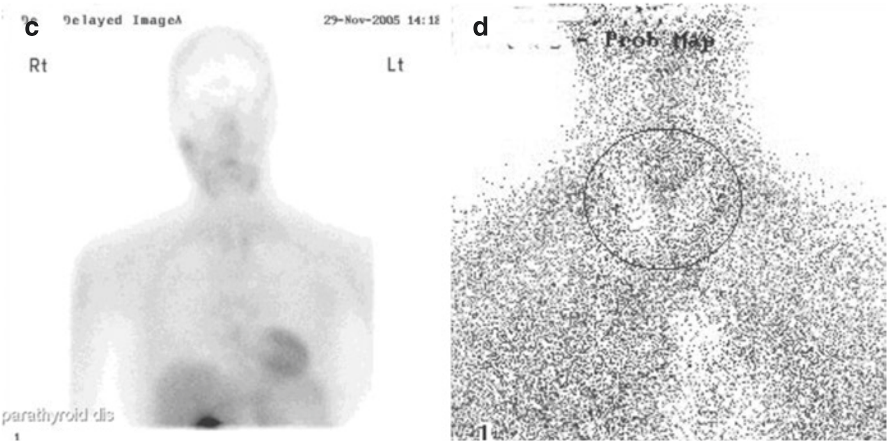

Fig. 7.27 (continued)

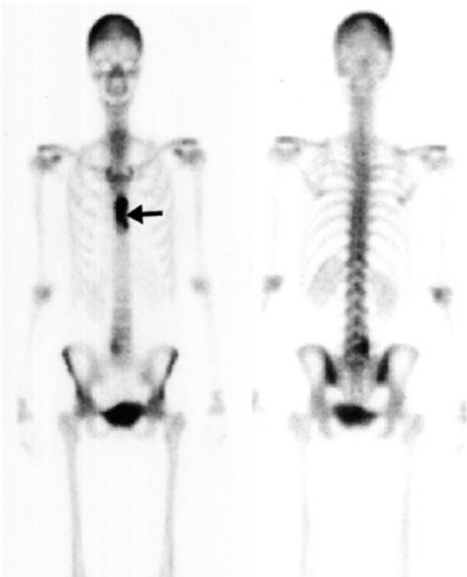

Fig. 7.28 ^{99m}Tc-methylene diphosphonate whole-body bone scan showing a metastatic deposit in the sternum (arrow) corresponding to the site of increased uptake seen on the ^{99m}Tc-sestamibi SPECT scan and some degenerative changes are seen in the right side of the lower lumbar spine

7.14.3 Findings

The pertechnetate scan of the thyroid was normal, and there was no focus of activity seen in the thyroid bed on the early as well as the late washout planar ^{99m}Tc-sestamibi scans to suggest the presence of an adenoma. The tomographic images were also essentially normal.

Serum calcium stayed elevated between 3.4 and 3.9 in spite of fluids, pamidronate infusion and frusemide. Parathyroidectomy of the right upper, lower and left lower parathyroid glands was undertaken, but no adenoma was found. No other PTH tissue noted after extensive neck exploration (Fig. 7.28).

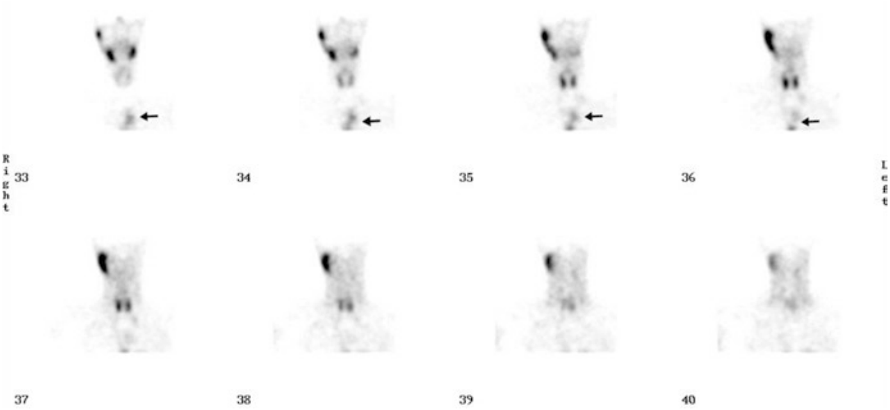

Fig. 7.29 ^{99m}Tc-sestamibi coronal SPECT scan images showing normal uptake in the thyroid bed with increased focal uptake at the edge of the images in the sternum (arrow)

Liver function subsequently deranged and an ultrasound abdomen showed a 2.5 cm lesion near the portal vein which was confirmed on CT scan. A whole-body bone scan (Fig. 7.28) was performed which showed increased uptake in the sternum suggesting of sternal metastasis. Subsequent clinical examination showed a sternal mass. A repeat ^{99m}Tc-sestamibi SPECT scan showed increased activity in the sternal lesion (Fig. 7.29). Biopsy of the sternal lesion showed a metastatic breast lesion. Calcium stayed elevated (3.75). The patient was transferred to oncology and started on chemotherapy and steroids. Calcium stayed resistant to treatment (3.78), and she was started on cinacalcet 30 mg. Further assessment post-chemotherapy showed her sternal mass to have resolved.

The patient was later admitted to hospital with tetany (Ca 1.73), Cinacalcet was stopped, and she was started on calcichew D3 tablets.

7.14.4 Conclusion

Findings consistent with a rare case of possibly true PTH-secreting breast metastasis. This patient's calcium settled as soon as her recurrence was treated.

7.14.5 Comments and Teaching Points

- This is a rare case of true PTH-secreting breast metastasis. Non-parathyroid cancers only rarely cause hypercalcaemia through ectopic expression of PTH.
- Literature review suggests the presence of a few cases of carcinoma secreting true intact PTH [20–22].
- It is important to be aware of this condition to avoid unnecessary parathyroidectomy.

7.15 Case 7.15. Large Right Parathyroid Adenoma and a Small Ectopic Left Lower Adenoma

7.15.1 Background

A 73-year-old lady with chronic renal failure and raised PTH was referred for parathyroid scintigraphy. Her serum parathormone level was 243.7 pmol/L (normal 1.3–9.3), corrected calcium 2.64 mmol/L (normal 2.2–2.6), alkaline phosphate 268 IU/L (normal 53–141), urea 6.0 mmol/L (normal range 2.9–7.5) and creatinine 148 µmol/L (normal range 53–106).

7.15.2 Procedure

The patient was injected with 42 MBq of ^{99m}Tc-pertechnetate, and a thyroid scan was acquired for 10 min at 20 min postinjection. Next, 800 MBq of ^{99m}Tc-sestamibi was injected without moving the patient and a 10-min duration planar scan performed. ^{99m}Tc-sestamibi SPECT scan was performed at 2 h followed by a late planar ^{99m}Tc-sestamibi scan at 3 h.

7.15.3 Findings

The pertechnetate thyroid scan (Fig. 7.30a) showed a "hot" nodule in the upper right lobe with suppression of uptake in the remainder of the gland. The early

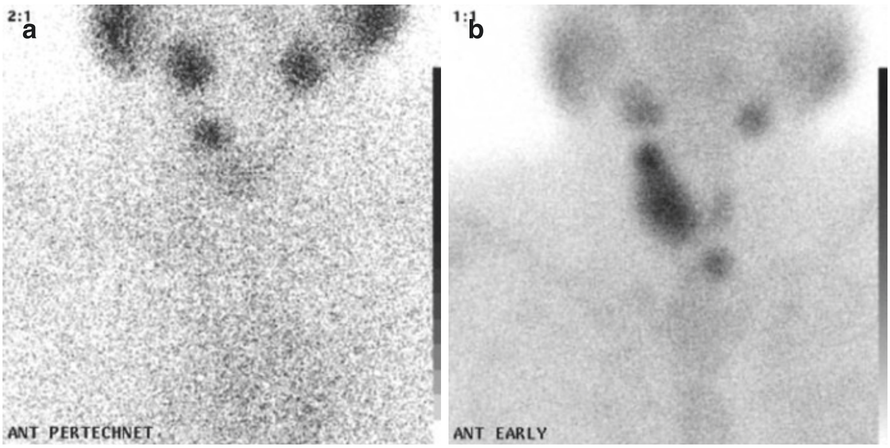

Fig. 7.30 ^{99m}Tc-pertechnetate thyroid scan (**a**), early planar ^{99m}Tc-sestamibi scan (**b**), late planar ^{99m}Tc-sestamibi scan (**c**) and the 3-h unzoomed neck and chest image (**d**)

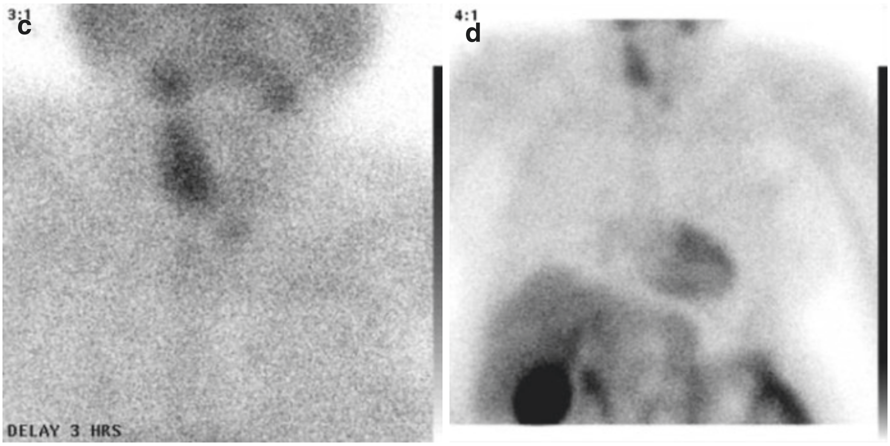

Fig. 7.30 (continued)

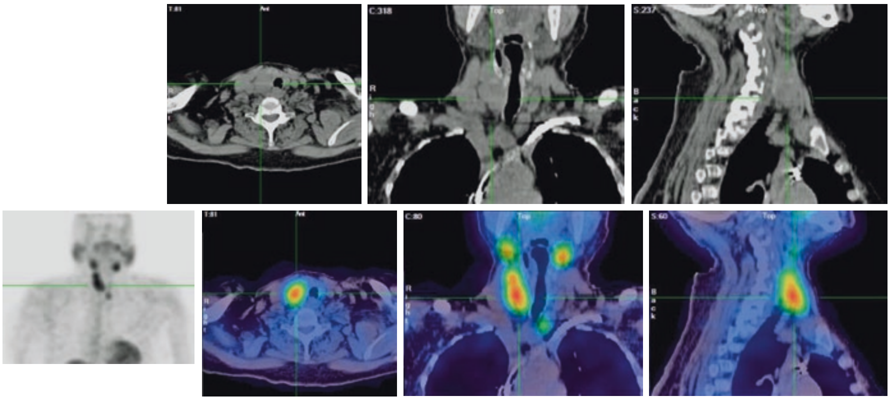

Fig. 7.31 ^{99m}Tc-sestamibi SPECT/CT scan images in the transaxial (left), coronal (middle) and sagittal (right) planes showing a large parathyroid adenoma on the right and a small left lower adenomatous/hyperplastic ectopic parathyroid gland

planar ^{99m}Tc-sestamibi scan (Fig. 7.30b) image showed uptake in the nodule in the right upper pole together with uptake in a large oval nodule occupying the right thyroid bed as well as in a small nodule below the lower pole of the left lobe. The late planar ^{99m}Tc-sestamibi scan (Fig. 7.30c) showed washout of activity from the right upper pole thyroid nodule as well as the left lobe of the thyroid with retention of uptake in the large nodule in the right lobe as well as nodule below the left lower pole of the thyroid. The SPECT/CT (Fig. 7.31) showed a large oval-shaped focus of uptake located on the right side of the trachea with a small rounded focus of uptake seen retrosternally anterolateral to the trachea at the level of the left sterno-clavicular joint.

7.15.4 Conclusion

Findings consistent with a large parathyroid adenoma on the right with a small left lower ectopic adenomatous or hyperplastic parathyroid gland in a patient with secondary hyperparathyroidism transitioning into tertiary hyperparathyroidism.

7.15.5 Comments and Teaching Points

- Tertiary hyperparathyroidism is a state of parathyroid hormone (PTH) excess occurring during PTH secretion due to secondary hyperparathyroidism transition from compensatory to autonomous evidenced by a rise in serum calcium to above the upper range of normal level.

7.16 Case 7.16. Left Upper Parathyroid Adenoma

7.16.1 Background

A 64-year-old female was referred with increased serum PTH at 30.30 pmol/L (normal 1.3–9.3) and raised serum calcium at 2.77 mmol/L (normal 2.2–2.6). Serum phosphorus was 1.10 mmol/L (normal 0.84–1.45), creatinine 131 µmol/L (normal 53–106) and urea 4.8 mmol/L (normal 2.5–6.4). The patient had undergone partial thyroidectomy 34 years ago. Ultrasound showed multiple scattered isoechoic and hypoechoic nodules in both thyroid lobes without any evidence of a parathyroid lesion seen (Fig. 7.32).

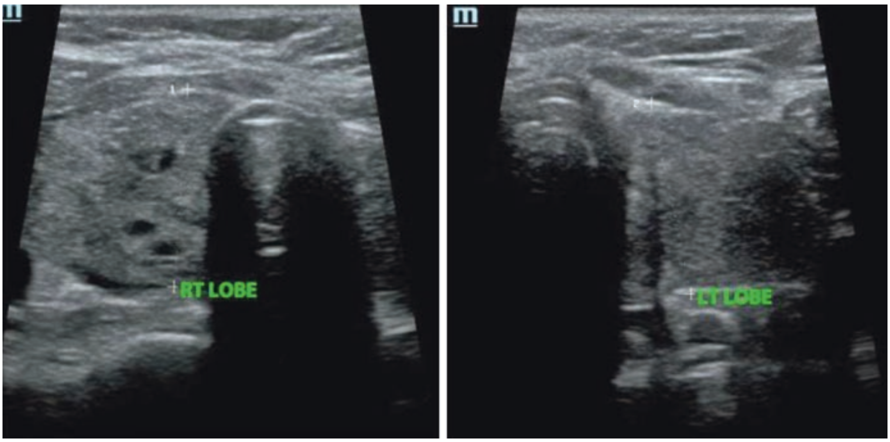

Fig. 7.32 Ultrasound showing multiple iso- and hypo-echoic nodules in both thyroid lobes without evidence of a parathyroid lesion seen

7.16.2 Procedure

The patient was injected with 59 MBq of ^{99m}Tc-pertechnetate, and a thyroid scan was acquired for 10 min at 20 min postinjection. Next, 747 MBq of ^{99m}Tc-sestamibi was injected without moving the patient and a 10-min duration planar scan performed. ^{99m}Tc-sestamibi SPECT scan was performed at 2 h followed by a late planar ^{99m}Tc-sestamibi scan at 3 h.

7.16.3 Findings

The pertechnetate thyroid scan showed a normal-sized image of the thyroid with homogenous distribution of activity in the gland (Fig. 7.33a). The early planar

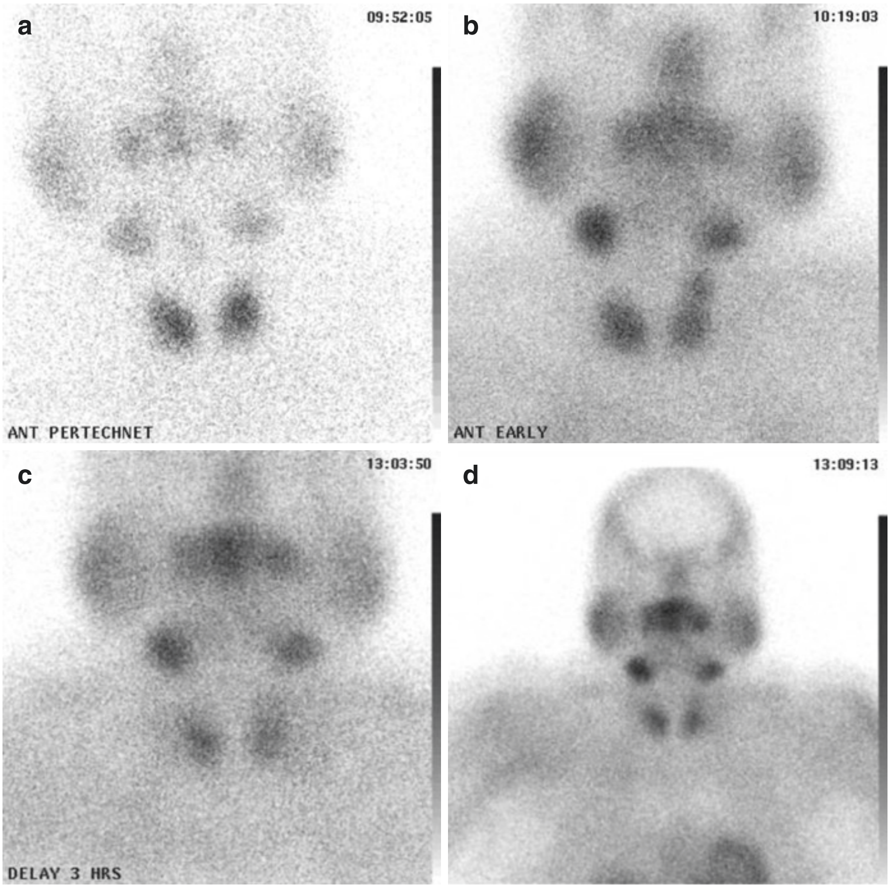

Fig. 7.33 ^{99m}Tc-pertechnetate thyroid scan (**a**), early planar ^{99m}Tc-sestamibi scan (**b**), late planar ^{99m}Tc-sestamibi scan (**c**) and the 3-h unzoomed neck and chest image (**d**)

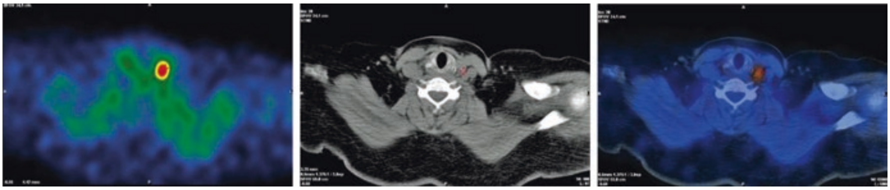

Fig. 7.34 ^{99m}Tc-sestamibi SPECT/CT scan images in the transaxial plane with SPECT (left), CT (middle) and fused SPECT & CT (right) showing the left upper parathyroid adenoma measuring 10 × 6 mm

^{99m}Tc-sestamibi scan showed a focus of uptake above the left upper pole which showed mild retention on the late planar ^{99m}Tc-sestamibi washout scan images (Fig. 7.33b–d). The SPECT/CT (Fig. 7.34) scan showed a posteriorly located lesion measuring 10 × 6 mm in size.

7.16.4 Conclusion

Findings consistent with a left upper parathyroid adenoma.

7.16.5 Comments and Teaching Points

- Normal upper parathyroid glands are in most cases located posterior to the middle upper third of the thyroid lobe. Superior parathyroids are found in their normal position in about 80% of individuals [23–25].

7.17 Case 7.17. Left Lower Parathyroid Adenoma

7.17.1 Background

A 54-year-old female was referred with hypercalcaemia and hyperparathyroidism with an intrathyroidal adenoma suspected on the MRI. Serum PTH and serum calcium were high at 10.3 pmol/L (normal 1.3–9.3) and 2.8 mmol/L (normal 2.2–2.6), respectively, with normal serum urea at 2.9 mmol/L (normal 2.5–6.4), creatinine at 48 μmol/L (normal 74–115) and alkaline phosphatase 39 IU/L (normal 42–98).

7.17.2 Procedure

The patient was injected with 79 MBq of ^{99m}Tc-pertechnetate, and a thyroid scan was acquired for 10 min at 20 min postinjection. Next, 821 MBq of ^{99m}Tc-sestamibi was injected without moving the patient and a 10-min duration planar scan acquired. ^{99m}Tc-sestamibi SPECT scan was performed at 2 h followed by a late planar ^{99m}Tc-sestamibi scan at 3 h.

7.17.3 Findings

The pertechnetate thyroid scan showed a mildly enlarged image of the thyroid with a prominent left lower pole but essentially uniform distribution of activity. The early planar ^{99m}Tc-sestamibi scan showed a pattern of uptake essentially similar to that seen on the pertechnetate thyroid scan but with faint focal increased uptake at the lower pole of the left lobe of the thyroid. However, there was marked focal retention of tracer in a left lower pole lesion on the delayed late planar ^{99m}Tc-sestamibi washout scan images. The ^{99m}Tc-sestamibi/^{99m}Tc-pertechnetate subtraction image showed a residual focus of activity at the left lower pole of the thyroid (not shown). The SPECT/CT scan showed an oval-shaped hypodense lesion at the left lower pole of the thyroid measuring 20 × 15 mm in size located lateral to the trachea (Figs. 7.35 and 7.36).

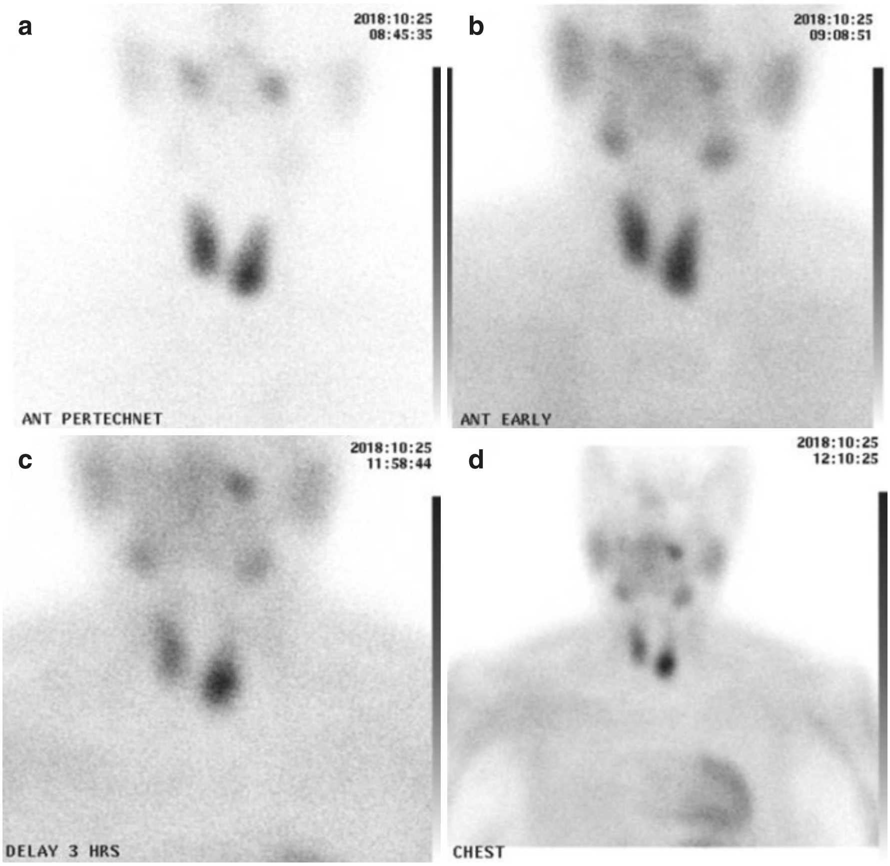

Fig. 7.35 ^{99m}Tc-pertechnetate thyroid scan (**a**), early planar ^{99m}Tc-sestamibi scan (**b**), late planar ^{99m}Tc-sestamibi scan (**c**) and the 3-h unzoomed neck and chest image (**d**)

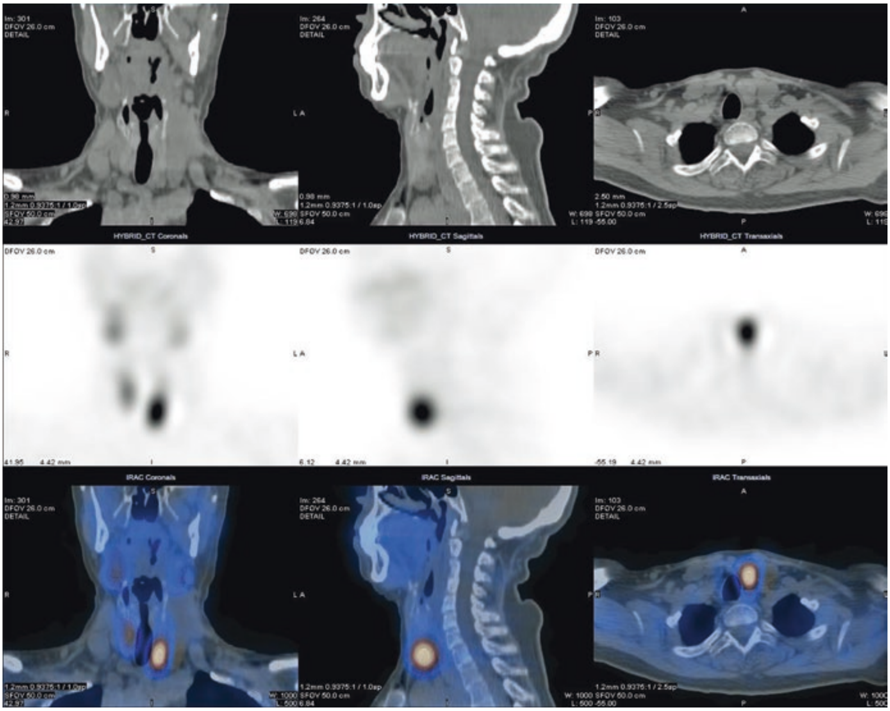

Fig. 7.36 ^{99m}Tc-sestamibi SPECT/CT scan images with CT (top row), SPECT (middle row) and fused SPECT & CT (bottom row) showing the left lower parathyroid adenoma measuring 20 × 15 mm

7.17.4 Conclusion

Findings consistent with primary hyperparathyroidism due to a left lower parathyroid adenoma.

7.17.5 Comments and Teaching Points

- In approximately 50% of surgeries, the lower parathyroid glands can be found within a 2-cm radius posteriorly or laterally to the lower pole of the thyroid lobe [26].

7.18 Case 7.18. Pertechnetate- and Sestamibi-Avid Right Lower Intrathyroidal Parathyroid Adenoma

7.18.1 Background

A 59-year-old female was referred with primary hyperparathyroidism. Ultrasound neck showed thyroid nodules in both the lobes. There was no history of renal disease. Serum PTH was 107.5 pg/mL (normal 5–65), serum calcium 2.83 mmol/L (normal 2.09–2.54), urea 3.4 mmol/L (normal 2.5–6.4) and creatinine 44 μmol/L (74–115).

7.18.2 Procedure

The patient was injected with 68 MBq of ^{99m}Tc-pertechnetate, and a thyroid scan acquired for 10 min at 20 min postinjection. Next, 775 MBq of ^{99m}Tc-sestamibi was injected without moving the patient and a 10-min duration planar scan acquired. ^{99m}Tc-sestamibi SPECT/CT scan was performed at 2 h followed by a late planar ^{99m}Tc-sestamibi scan at 3 h.

7.18.3 Findings

The pertechnetate thyroid scan showed a normal-sized left lobe and a relatively enlarged right lobe with focal increased uptake in its lower pole suggestive of a "hot" thyroid nodule.

The early planar ^{99m}Tc-sestamibi scan showed a focus of increased activity at the lower pole of the right thyroid lobe with retention of activity seen here on the delayed images. The SPECT/CT scan showed a single rounded lesion measuring 18.6 × 12 mm in the lower pole of the right lobe of the thyroid embedded in the thyroid tissue (Figs. 7.37 and 7.38).

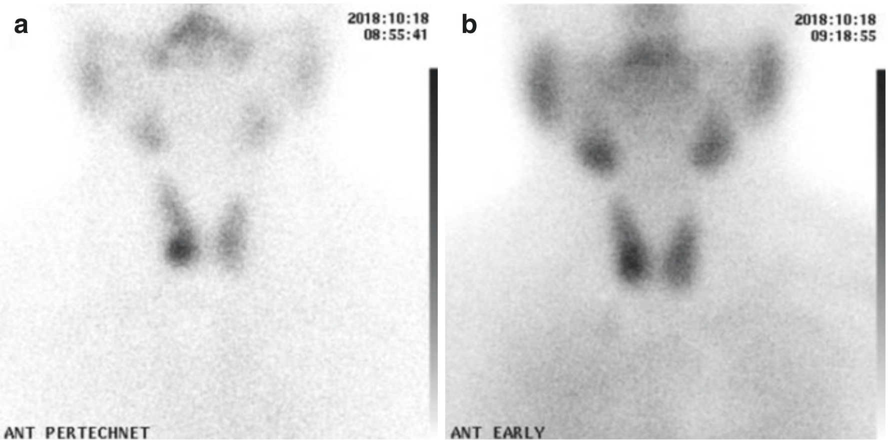

Fig. 7.37 ^{99m}Tc-pertechnetate thyroid scan (**a**), early planar ^{99m}Tc-sestamibi scan (**b**), late planar ^{99m}Tc-sestamibi scan (**c**) and the 3-h unzoomed neck and chest image (**d**)

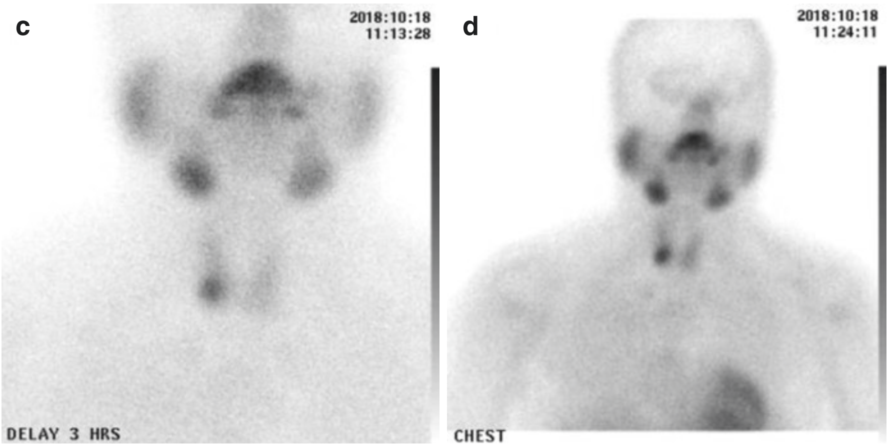

Fig. 7.37 (continued)

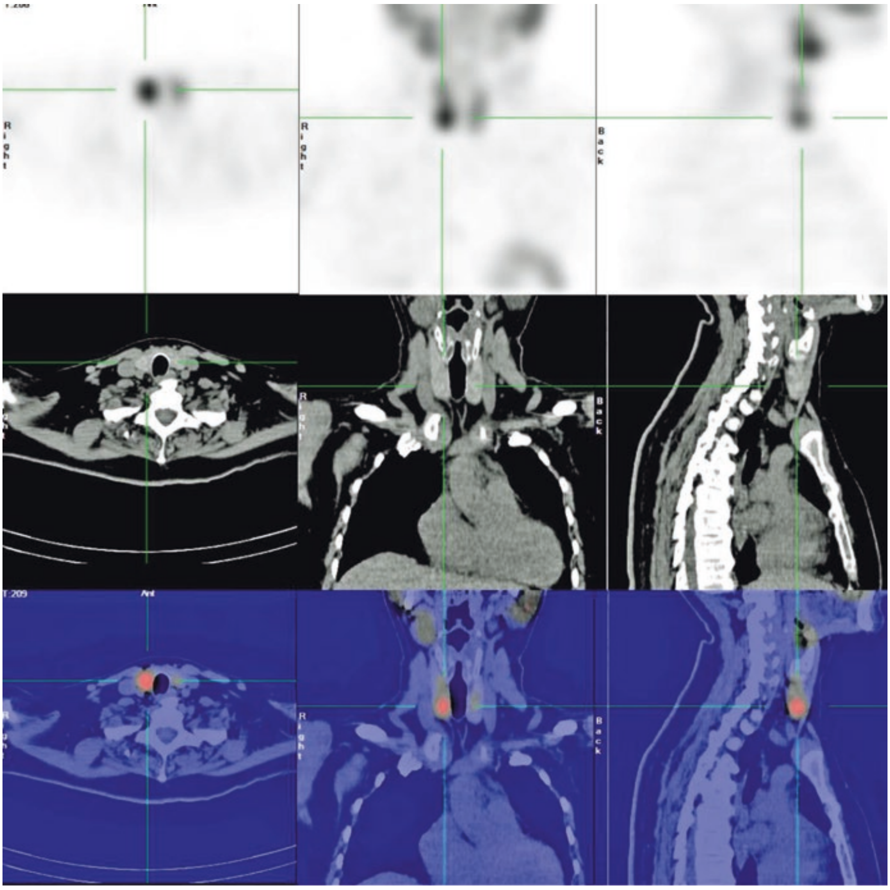

Fig. 7.38 ^{99m}Tc-sestamibi SPECT/CT scan images with CT (top row) and fused SPECT & CT (bottom row) showing the right lower parathyroid adenoma measuring 18.6 × 12 mm

7.18.4 Conclusion

Findings consistent with primary hyperparathyroidism due to a pertechnetate- and sestamibi-avid right inferior intrathyroidal parathyroid adenoma.

7.18.5 Comments and Teaching Points

- The inferior parathyroid gland is truly intrathyroidal within the lower pole of thyroid in 1–3% of individuals [27].
- The incidence of intrathyroidal parathyroid tissue is uncommon at approximately 2% [28].

7.19 Case 7.19. Multinodular Goitre with Left Lower Parathyroid Adenoma

7.19.1 Background

A 78-year-old female was referred with primary hyperparathyroidism complaining of generalised bone pains, leg swelling and raised PTH level. There was no history of renal disease. Serum PTH was 163 pmol/L (normal 1.3–9.3), serum calcium 2.62 mmol/L (normal 2.2–2.6), phosphorus 2.24 mmol/L (normal 0.84–1.45), urea 10.7 mmol/L (normal 2.5–6.4), creatinine 89 μmol/L (74–115) and albumin 33 g/L (normal 35–48). Ultrasound neck showed thyroid nodules in both the lobes with no parathyroid lesion detected.

7.19.2 Procedure

The patient was injected with 81 MBq of ^{99m}Tc-pertechnetate, and a thyroid scan acquired for 10 min at 20 min postinjection. Next, 790 MBq of ^{99m}Tc-sestamibi was injected without moving the patient and a 10-min duration planar scan acquired. ^{99m}Tc-sestamibi SPECT/CT scan was performed at 2 h followed by a late planar ^{99m}Tc-sestamibi scan at 3 h.

7.19.3 Findings

The pertechnetate thyroid scan showed an enlarged image of the gland with multiple warm nodules seen in the right lobe and in the upper and lower left lobe. The early planar ^{99m}Tc-sestamibi scan showed uptake in the thyroid nodules seen on the pertechnetate scan together with an additional focus of uptake seen below the lower pole of the left lobe of the thyroid. The planar ^{99m}Tc-sestamibi scan and the washout image showed retention of uptake in the thyroid nodules as well as in the lesion below the left lower pole. The ^{99m}Tc-sestamibi/^{99m}Tc-pertechnetate subtraction image showed only a solitary focus of activity abutting the lower pole of the left thyroid lobe. The SPECT/CT scan showed a rounded focus of increased uptake below the left lower pole of the thyroid measuring 9 mm in diameter (Figs. 7.39 and 7.40).

7.19.4 Conclusion

Findings of a multinodular goitre with a left lower parathyroid adenoma as the cause of primary hyperparathyroidism.

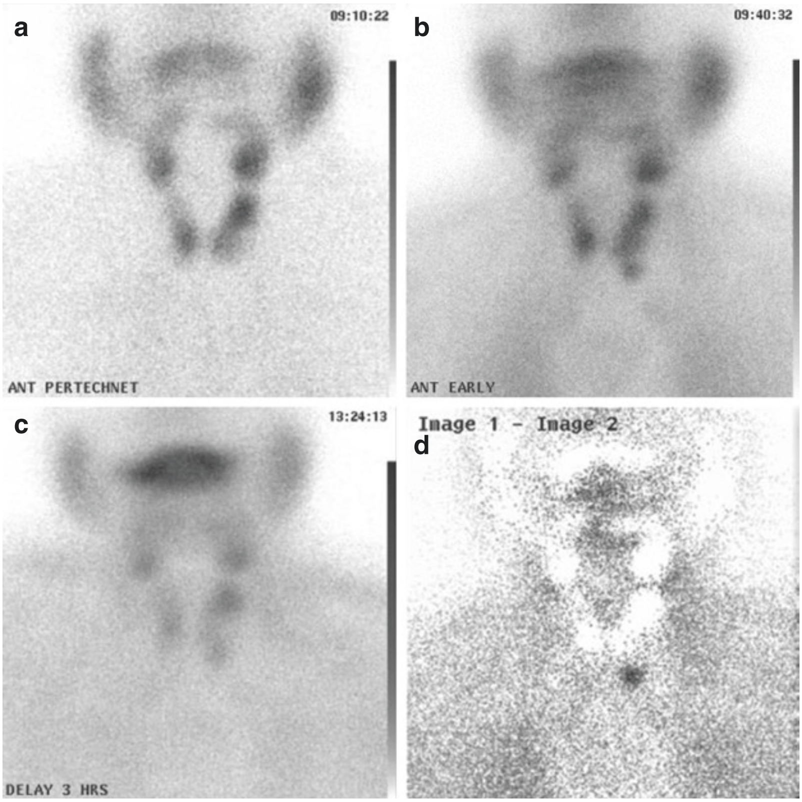

Fig. 7.39 ^{99m}Tc-pertechnetate thyroid scan (**a**), early planar ^{99m}Tc-sestamibi scan (**b**), late planar ^{99m}Tc-sestamibi scan (**c**) and the ^{99m}Tc-pertechnetate/^{99m}Tc-sestamibi subtraction image (**d**) showing multiple pertechnetate and set

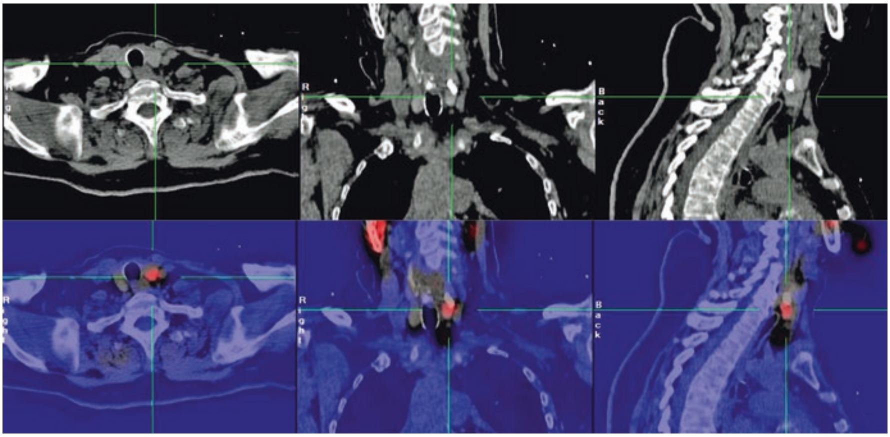

Fig. 7.40 ^{99m}Tc-sestamibi SPECT/CT scan images with CT (top row) and fused SPECT & CT (bottom row) showing the right lower parathyroid adenoma measuring 9 mm. There are also multiple calcified and non-calcified thyroid nodules seen

7.19.5 Comments and Teaching Points

- The subtraction image was very useful in this case as all the sestamibi-avid thyroid nodules were subtracted out except for the parathyroid adenoma. However, the location of the parathyroid adenoma below the lower pole separate from the thyroid gland makes it easier to identify.
- In patients with multinodular goitre and PHPT, the sensitivity of parathyroid scintigraphy declines in proportion with the thyroid volume and hormonal activity [29].

7.20 Case 7.20. Left Lower Parathyroid Gland Cancer with Brown Tumours

7.20.1 Background

A 60-year-old male presented with bone aches, pathological fracture of the left femur and multiple osteolytic bone lesions with soft-tissue component diagnosed after biopsy of one of the involved ribs as a “giant cell tumour”. Biochemical testing revealed serum calcium at 2.70 mmol/L (normal range 2.12–2.62 mmol/L), alkaline phosphatase at 870 IU/L (normal range 20–130 IU/L) and serum parathyroid hormone raised at 741 pg/mL (normal range 10–70 pg/mL). The patient’s symptoms and laboratory findings were suspicious for hyperparathyroidism and brown bone tumours. The patient was referred for parathyroid and skeletal scintigraphy.

7.20.2 Procedures

Whole-body bone scintigraphy with ^{99m}Tc-methylene diphosphonate and target SPECT/CT of the thorax and pelvic regions were performed. Dual tracer ^{99m}Tc-sestamibi/^{99m}Tc-pertechnetate subtraction scintigraphy with subsequent SPECT/CT imaging of the neck and upper thoracic area was also carried out.

7.20.3 Findings

The whole-body bone scan (Fig. 7.41a) showed multiple skeletal lesions with intense tracer uptake in the skull, mandible, upper and lower extremities, pelvis, scapulae and clavicles. The CT component of the bone SPECT/CT images (Fig. 7.41b) revealed soft-tissue masses in the medullar shafts of long bones, orthopaedic surgical stabilisation of the left femur due to pathological fracture and multiple circumscribed expansile lytic lesions elevating the periosteum but contained within a thin shell of cortical bone. These lesions were seen to correspond to the "hot" spots on the bone scan (Fig. 7.42).

The ^{99m}Tc-pertechnetate thyroid scan (Fig. 7.43b) showed normal uptake in the thyroid gland. The ^{99m}Tc-sestamibi planar scan showed an oval-shaped "hot" nodule at the lower part of the left lobe of the thyroid, which persisted on the

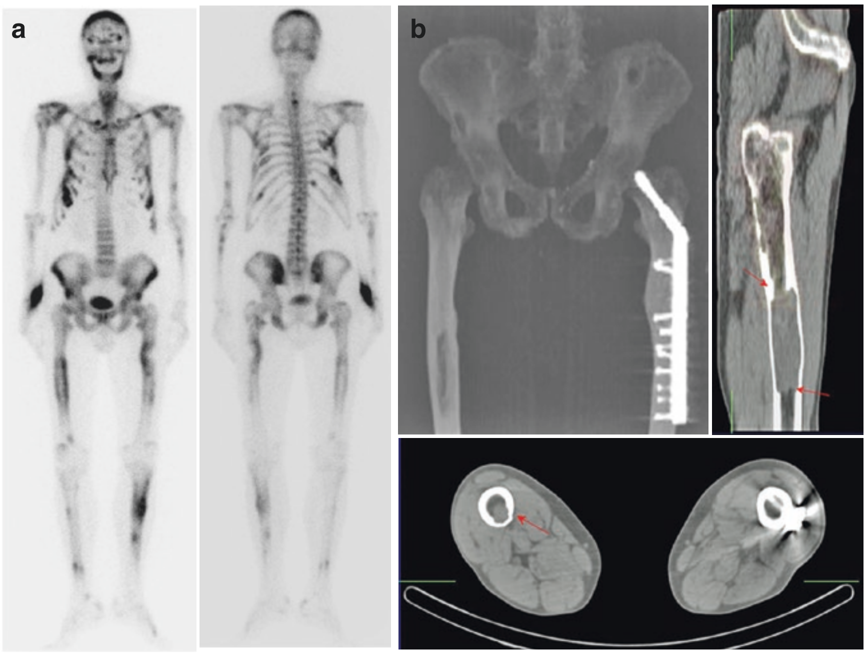

Fig. 7.41 (**a**) Whole-body bone scan showing multiple skeletal lesions with intensive tracer uptake. (**b**) SPECT-CT images showing orthopaedic stabilisation of the left femoral pathological fracture (1) and soft-tissue masses in the medulla of the shafts of long bones

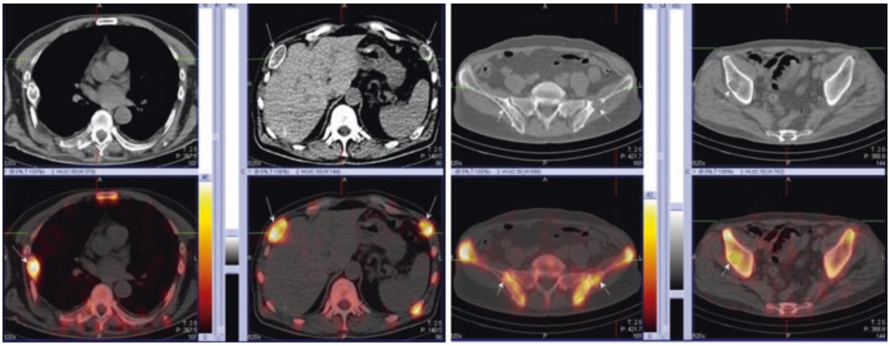

Fig. 7.42 Bone SPECT/CT images showing multiple circumscribed lytic expansile lesions with increased uptake

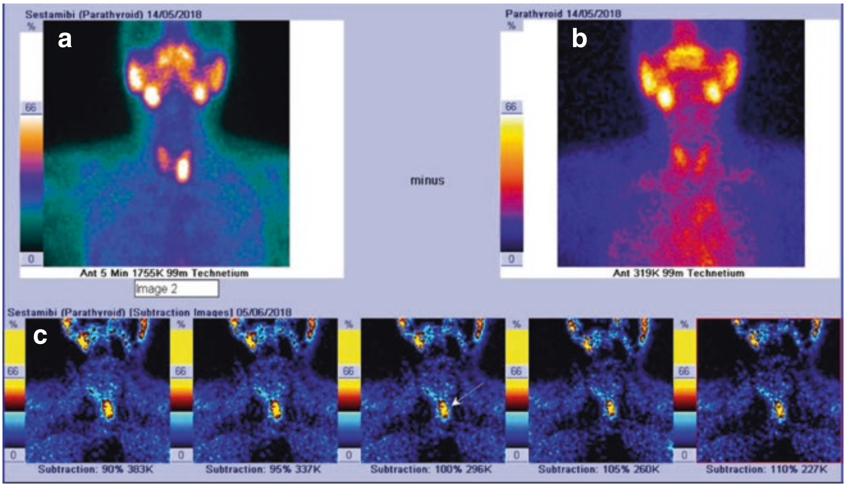

Fig. 7.43 Planar ^{99m}Tc-sestamibi scan (**a**), ^{99m}Tc-pertechnetate thyroid scan (**b**) and ^{99m}Tc-sestamibi/^{99m}Tc-pertechnetate subtraction scan (**c**)

^{99m}Tc-sestamibi/^{99m}Tc-pertechnetate subtraction scan. The SPECT/CT study (Fig. 7.44) showed an enlarged left parathyroid gland with the axial size of 27.9 mm, located paratracheally at the lower posterior aspect of thyroid lobe.

Histopathology of the specimen revealed a nodular and hypercellular tumour with evidence of capsular invasion and with appearances consistent of parathyroid adenocarcinoma (Fig. 7.44).

7.20.4 Conclusion

Findings consistent with parathyroid carcinoma mimicking a parathyroid adenoma.

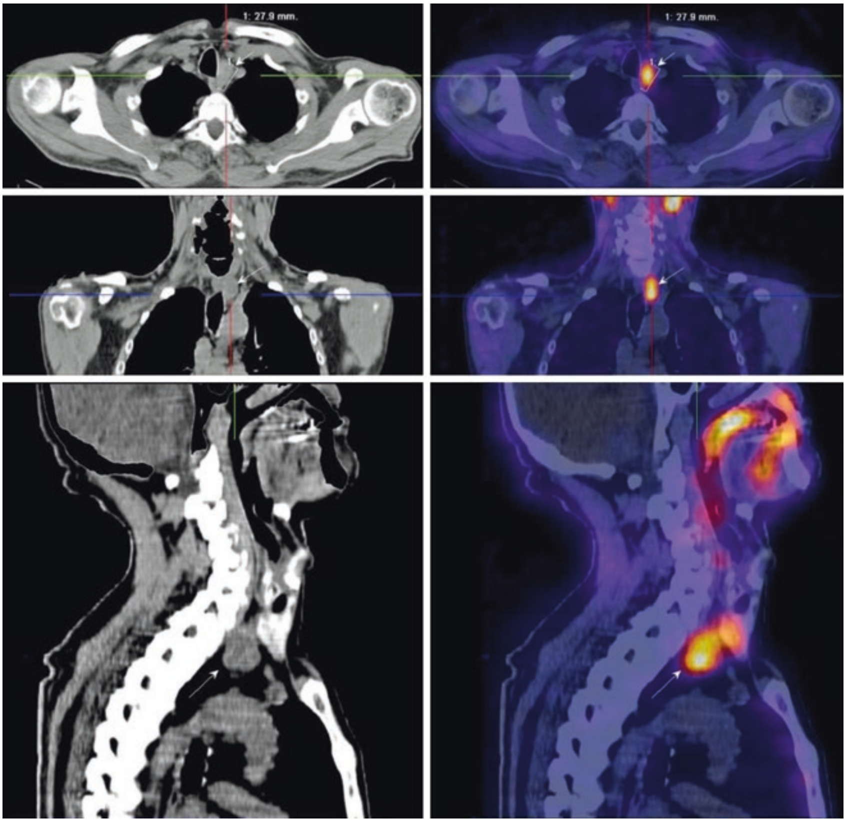

Fig. 7.44 SPECT/CT images with CT (left) and fused ^{99m}Tc-sestamibi SPECT/CT images (right) showing the left lower parathyroid lesion measuring 18.6 × 12 mm

7.20.5 Comments and Teaching Points

- Parathyroid carcinoma accounts for <2% of primary hyperparathyroidism. It is an indolent tumour with frequent recurrences (~50%) and metastases and ~50% 10-year survival with up to 15% mortality at 5 years [30].
- Parathyroid cancer may develop in any of the parathyroid glands, but as seen here and in case 7.69, it is slightly more common in the lower parathyroid glands.
- As seen in this case, extremely high blood PTH and Ca^{2+} are also typical for parathyroid cancer. The excessively high serum calcium levels are associated with nephrolithiasis, renal insufficiency and "brown tumours" in the bones [30].
- Concurrent bone disease with bone pains is more common in patients with carcinoma than adenoma as seen in this case.
- Unlike parathyroid adenomas which show a marked female predominance, parathyroid carcinoma has an equal sex distribution.

7.21 Case 7.21. Parathyroid Adenoma Positive on Both Sestamibi and Thallium Scans

7.21.1 Background

A 62-year-old hypertensive male with neurofibromatosis and thrombocytosis was admitted with high calcium and PTH levels. Biochemical analysis showed serum PTH at 28.80 pmol/L (normal 1.3–9.3), corrected serum calcium 2.74 mmol/L (normal 2.2–2.6), phosphorus 0.89 mmol/L (normal 0.84–1.45), magnesium 0.67 mmol/L (normal 0.73–1.06), alkaline phosphatase 76 IU/L (normal 42–98), serum urea 7.2 mmol/L (normal 2.9–7.5) and creatinine 103 μmol/L (normal 71–115). Thyroid US showed a multinodular thyroid with multiple variable-sized hypoechoic foci seen scattered in both thyroid lobes with areas of cystic degeneration and calcification (Fig. 7.45).

7.21.2 Procedures

The patient was injected with 50 MBq of ^{99m}Tc-pertechnetate, and a thyroid scan was acquired for 5 min after 20 min. Next, 890 MBq of ^{99m}Tc-sestamibi was injected without moving the patient, and a 5-min duration planar scan was acquired 10 min later. ^{99m}Tc-sestamibi SPECT scan was performed at 2 h followed by zoomed and unzoomed late planar ^{99m}Tc-sestamibi scans at 3 h. The next day, the patient was injected with 75 MBq of ^{201}Tl-thallous chloride and planar imaging of the neck performed followed by a SPECT/CT of the neck.

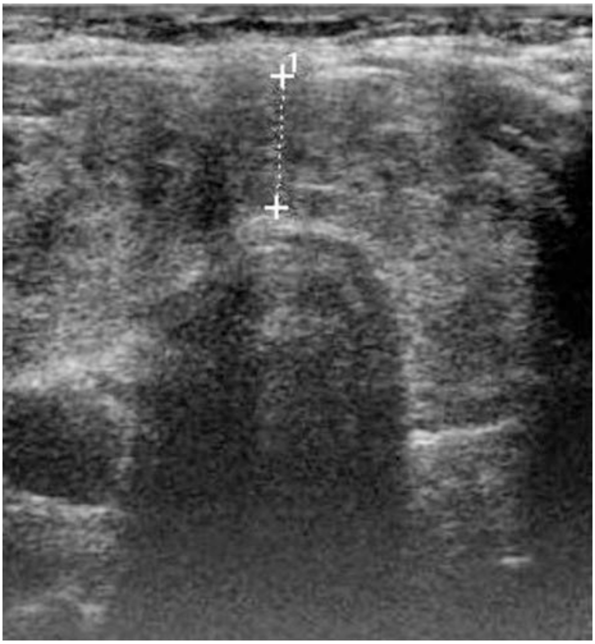

Fig. 7.45 Thyroid ultrasound showing multiple variable sized hypoechoic foci scattered in both thyroid lobes with areas of cystic degeneration and calcification, with no evidence of a parathyroid adenoma seen

7.21.3 Findings

The pertechnetate thyroid scan showed a larger right lobe and a smaller left lobe with fairly uniform uptake in the gland. The early planar ^{99m}Tc-sestamibi scan showed a focus of mildly increased uptake in the region of the lower pole of the right thyroid lobe, with the delayed washout images showing relative focal retention of the tracer here (Fig. 7.46). The ^{99m}Tc-sestamibi/^{99m}Tc-pertechnetate subtraction scan showed residual focal activity in the lower part of the right thyroid lobe region (Fig. 7.47).

The ^{99m}Tc-sestamibi SPECT/CT scan (Fig. 7.48) showed a clear-cut focus of intense increased uptake at the posterior aspect of the right lower lobe consistent with a right lower parathyroid adenoma.

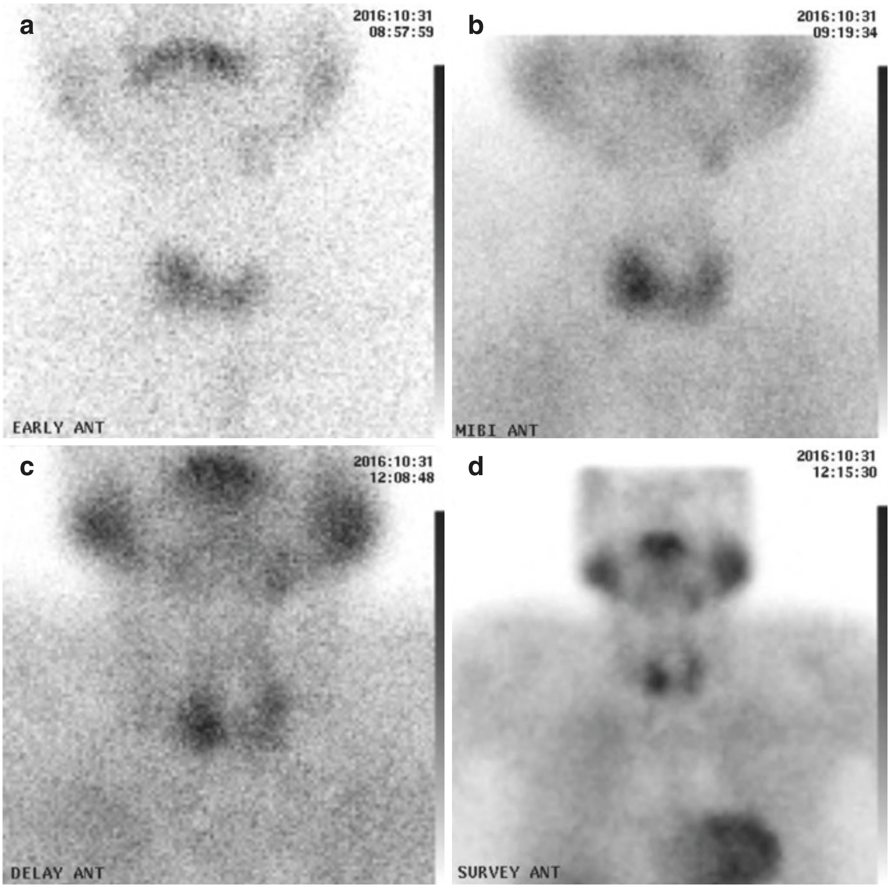

Fig. 7.46 ^{99m}Tc-pertechnetate thyroid scan (**a**), early planar ^{99m}Tc-sestamibi scan (**b**), late planar ^{99m}Tc-sestamibi scan (**c**) and the 3-h unzoomed neck and chest image (**d**)

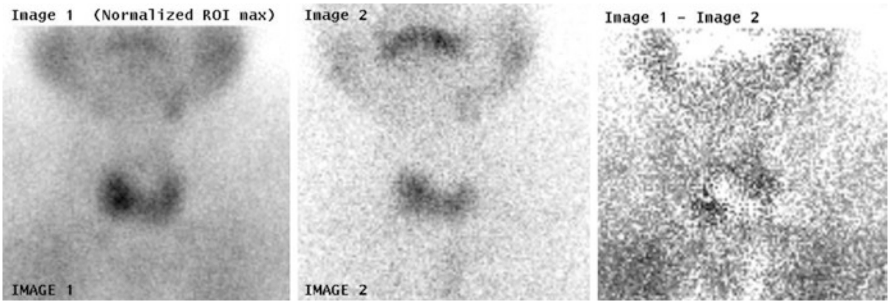

Fig. 7.47 The early planar ^{99m}Tc-sestamibi scan (left), the ^{99m}Tc-pertechnetate thyroid scan (middle) and the ^{99m}Tc-sestamibi/^{99m}Tc-pertechnetate subtraction scan (right) showing focal activity in the lower part of the right thyroid lobe region

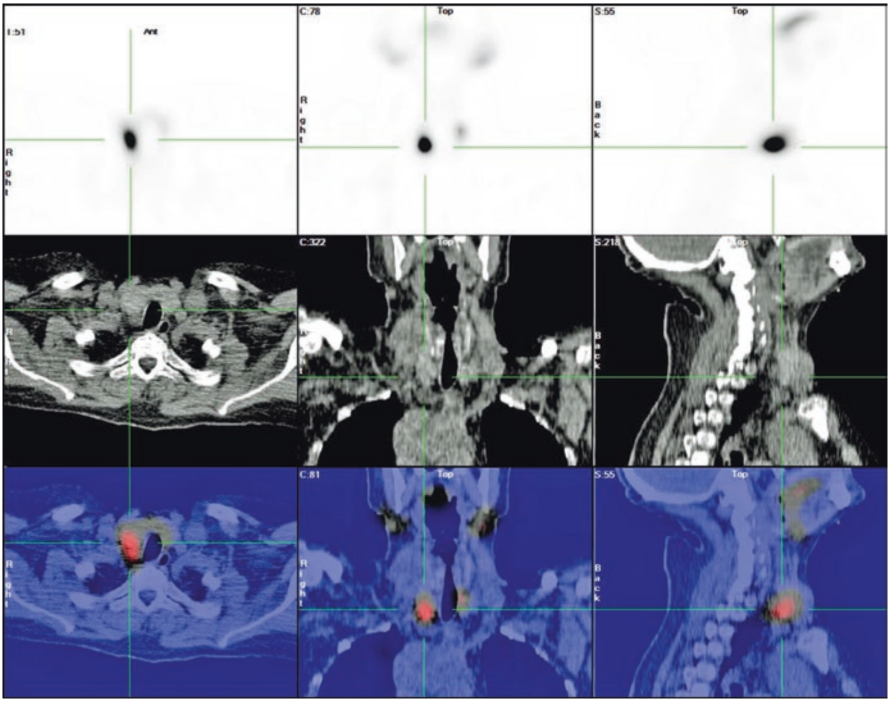

Fig. 7.48 ^{99m}Tc-sestamibi SPECT scan images using inverse logarithmic scale display (top row), CT scan images (middle row), and fused SPECT/CT images (bottom row) in the transverse (left column), coronal (middle column) and sagittal (right column) showing the right lower parathyroid adenoma

The planar ^{201}Tl scan showed a relatively prominent right lobe but wasn't significantly different from the ^{99m}Tc-pertechnetate thyroid scan, and although it showed a pattern of uptake similar to that seen on the early planar ^{99m}Tc-sestamibi scan, the

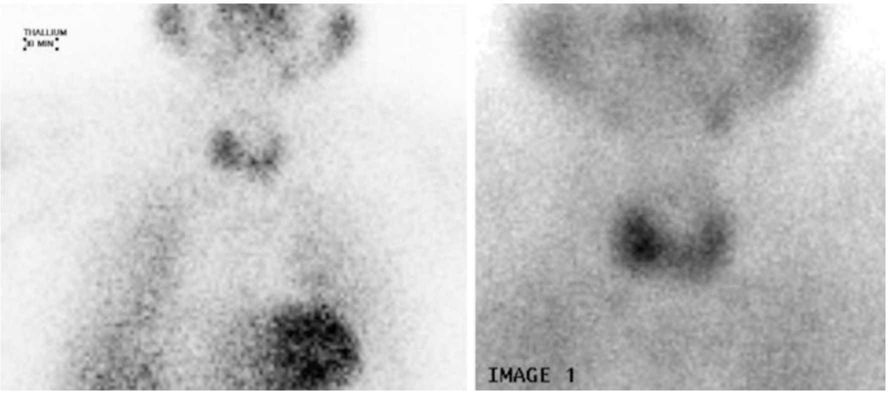

Fig. 7.49 Planar thallium-201 scan image (left) compared with the early planar ^{99m}Tc-sestamibi scan (right). Note the better imaging characteristics of the planar ^{99m}Tc-sestamibi scan compared with the ^{201}Tl planar scan

image quality was seen to be relatively poor (Fig. 7.49) and by itself not diagnostic. The ^{201}Tl SPECT/CT, however, showed a clear-cut right lower parathyroid adenoma with the image quality diagnostically similar to that obtained with ^{99m}Tc-sestamibi SPECT/CT scan (Figs. 7.49 and 7.50).

7.21.4 Conclusion

Findings consistent with primary hyperparathyroidism due to a right parathyroid gland adenoma equally avid for thallium and sestamibi.

7.21.5 Comments and Teaching Points

- Thallium-201 localises in both the thyroid and parathyroid glands, and hence the planar thallium-201 scan by itself is not diagnostic and should always be performed as a part of the ^{201}Tl/^{99m}Tc subtraction scan.
- Dual-phase planar sestamibi images are superior to the thallium/pertechnetate subtraction scan and, in conjunction with a thyroid scan either with ^{123}I sodium iodine or ^{99m}Tc-pertechnetate, also allow for subtraction imaging.
- The thallium-201 and ^{99m}Tc-sestamibi SPECT/CT scans provide an equivalent diagnosis for parathyroid adenoma as seen in this case.
- The concentration of thallium-201 per gramme tissue in the parathyroid glands is higher than that of ^{99m}Tc-sestamibi, but the background activity in the thyroid gland is also higher and therefore affords no advantage over the dual-phase sestamibi planar scan.
- SPECT methodology effectively removes the higher background thyroid activity on the thallium scan, as seen in this case, and therefore due to its equally higher concentration in the parathyroid tissue, thallium SPECT allows a diagnostically similar quality of scan as that obtained with sestamibi SPECT.

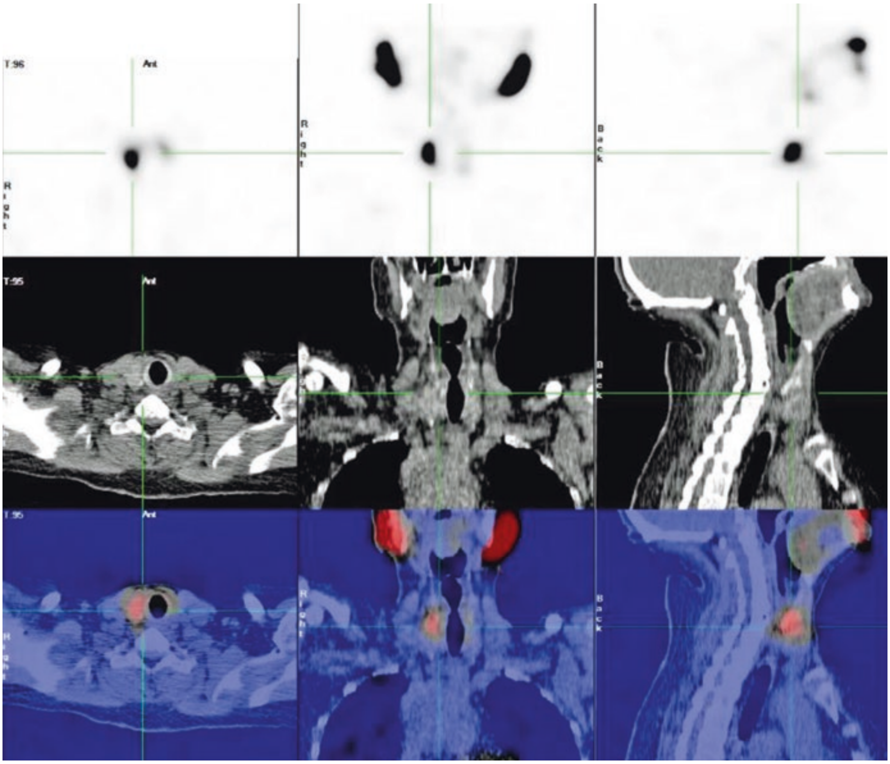

Fig. 7.50 ^{201}Tl SPECT scan images using inverse logarithmic greyscale display (top row), CT scan images (middle row) and fused SPECT/CT images (bottom row) in the transverse (left column), coronal (middle column) and sagittal (right column) showing the right lower parathyroid adenoma (crosshair). Note the quality of the ^{201}Tl SPECT/CT scan is equivalent to the ^{99m}Tc-sestamibi SPECT/CT scan

7.22 Case 7.22. Two-Gland Parathyroid Hyperplasia

7.22.1 Background

A 63-year-old female with diabetes mellitus, hypertension and end-stage renal disease (on regular haemodialysis) was found to have biochemical hyperparathyroidism on her prerenal transplantation workup. Serum PTH was 76.9 pmol/L (normal 1.3–9.3), calcium 2.05 mmol/L (normal 2.2–2.6), phosphorus 1.47 mmol/L (normal 0.84–1.45), urea 14.3 mmol/L (2.5–6.4), creatinine 553 μmol/L (74–115) and alkaline phosphate 65 IU/L (normal 42–98).

7.22.2 Procedure

The patient was injected with 91 MBq of ^{99m}Tc-pertechnetate, and a thyroid scan was acquired for 10 min 15 min postinjection. Next, 805 MBq of ^{99m}Tc-sestamibi was injected without moving the patient and a 10-min duration planar scan performed after 10 min. ^{99m}Tc-sestamibi SPECT/CT scan was acquired at 2 h followed by a late planar ^{99m}Tc-sestamibi scan at 3 h.

7.22.3 Findings

The pertechnetate thyroid scan showed a normal-sized image of the thyroid with homogenous distribution of activity in the gland. The early planar ^{99m}Tc-sestamibi scan showed a pattern of uptake in the left lobe, which was similar to that seen on the pertechnetate scan, but the lower pole of the right lobe appeared to extend further downwards as compared to the pertechnetate scan. There was no focal retention seen here however on the washout image. The SPECT/CT scan with inverse greyscale image display showed a focus of uptake in the mid part of the thyroid bed on the right (arrow), with a similar focus of uptake seen in the left thyroid lobe somewhat lower in position. A calcified lesion (arrowheads) without any uptake was seen located just below the isthmus in the jugular notch adjacent to the brachiocephalic trunk (Figs. 7.51 and 7.52).

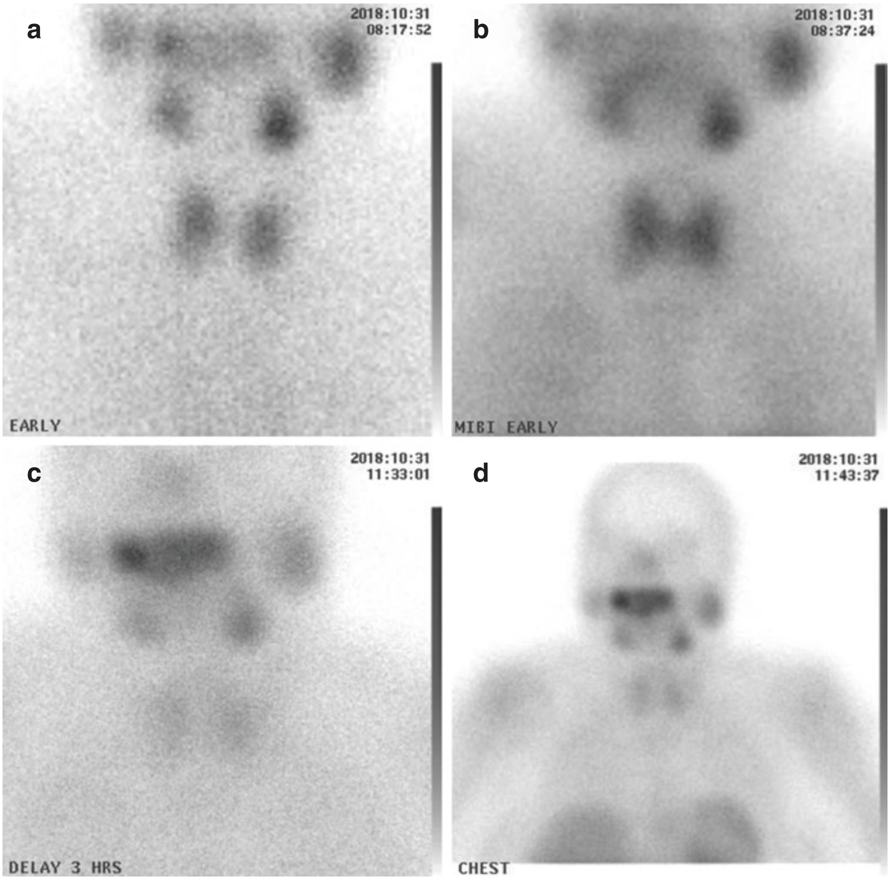

Fig. 7.51 ^{99m}Tc-pertechnetate thyroid scan (**a**), early planar ^{99m}Tc-sestamibi scan (**b**), late planar ^{99m}Tc-sestamibi scan (**c**) and the unzoomed late ^{99m}Tc-sestamibi neck and chest scan (**d**) showing no definite evidence of a hyperactive parathyroid lesion. Note the asymmetrical uptake in the submandibular glands

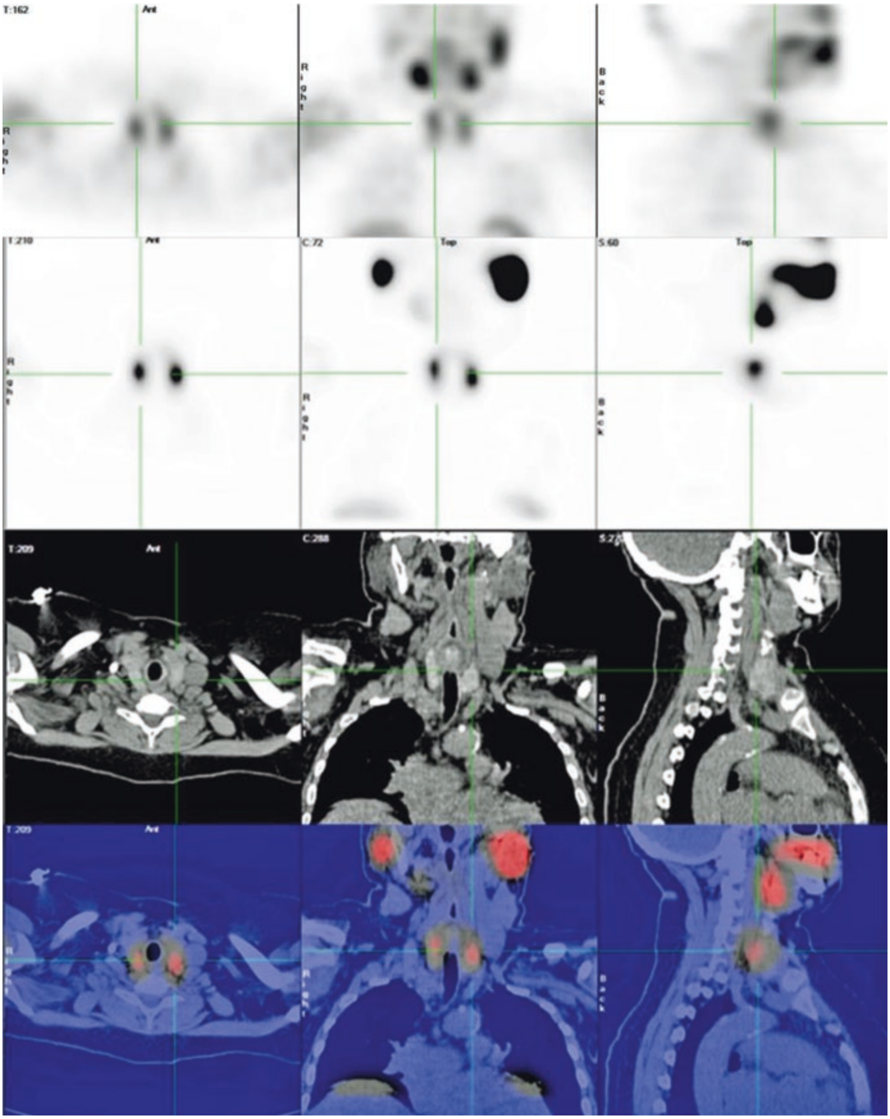

Fig. 7.52 ^{99m}Tc-sestamibi SPECT scan images using the inverse linear display (top row), inverse logarithmic scale display (second row), CT scan images (third row) and fused SPECT/CT images (bottom row) in the transverse (left column), coronal (middle column) and sagittal (right column) showing bilateral hyperplastic parathyroid glands. Note the better lesion detection with the inverse logarithmic display

7.22.4 Conclusion

Findings consistent with two-gland parathyroid hyperplasia associated with secondary hyperparathyroidism.

7.22.5 Comments and Teaching Points

- Parathyroid hyperplasia often develops in patients with longstanding renal failure who are on chronic haemodialysis, as a consequence of hyperphosphataemia and hypocalcaemia, leading to the SHPT as seen in this case.
- The planar sestamibi scan images can frequently be negative in the presence of small hyperplastic parathyroid glands which can, however, be detected on the tomographic images as in this case.
- The combination of inverse logarithmic greyscale for SPECT display and red-black-blue colour scale for the fused SPECT/CT image display, provides optimum detection of even small parathyroid lesions which can be missed on a standard linear scale SPECT/CT scan as seen in this case.

7.23 Case 7.23. Three-Gland Parathyroid Hyperplasia

7.23.1 Background

A 57-year-old female with raised serum PTH and borderline high serum calcium. Serum PTH was 13.3 pmol/L (normal 1.3–9.3), calcium (adjusted) at 2.62 mmol/L (normal 2.2–2.6), phosphorus 1.18 mmol/L (normal 0.84–1.45), urea 3.0 mmol/L (2.5–6.4), creatinine 61 µmol/L (74–115) and alkaline phosphate 70 IU/L (normal 42–98).

7.23.2 Procedure

The patient was injected with 82 MBq of ^{99m}Tc-pertechnetate, and a thyroid scan was acquired for 10 min at 15 min postinjection. Next, 790 MBq of ^{99m}Tc-sestamibi was injected without moving the patient and a 10-min duration planar scan performed after 10 min. ^{99m}Tc-sestamibi SPECT/CT scan was performed at 2 h followed by a late planar ^{99m}Tc-sestamibi scan at 3 h.

7.23.3 Findings

The pertechnetate thyroid scan showed a normal-sized image of the thyroid with homogenous distribution of activity in the gland. A pyramidal lobe was seen to be arising from the medial aspect of the right upper lobe (Fig. 7.53a). The early planar ^{99m}Tc-sestamibi scan showed a pattern of uptake similar to that seen in the thyroid scan with the delayed washout sestamibi images showing no abnormality (Fig. 7.53b, c). The ^{99m}Tc-sestamibi/^{99m}Tc-pertechnetate subtraction image (Fig. 7.53d) showed faint focal uptake at the right lobe.

The SPECT/CT scan with greyscale and colour scale thresholding showed a fair-sized oval focus in the mid part of the right thyroid bed together with two smaller foci of uptake at the left upper and lower poles (Fig. 7.54).

7.23.4 Conclusion

Findings consistent with primary hyperparathyroidism due to three-gland parathyroid hyperplasia.

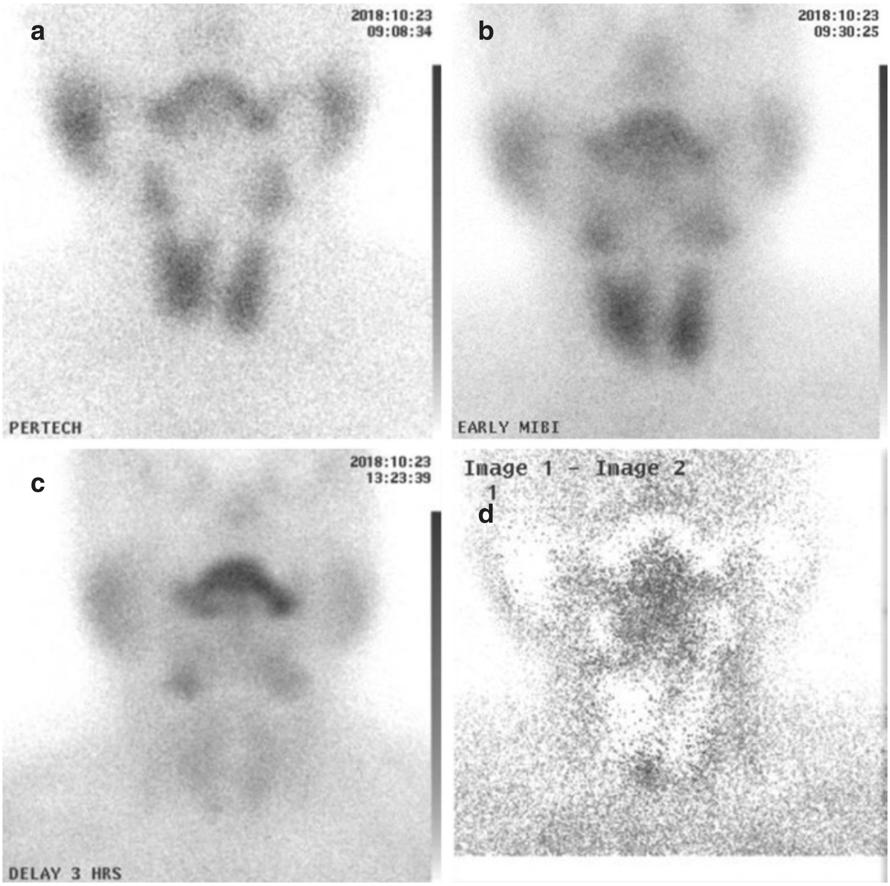

Fig. 7.53 ^{99m}Tc-pertechnetate thyroid scan (**a**), early planar ^{99m}Tc-sestamibi scan (**b**), late planar ^{99m}Tc-sestamibi scan (**c**) and ^{99m}Tc-sestamibi/^{99m}Tc-pertechnetate subtraction scan (**d**) images showing a small right lower hyperplastic parathyroid gland

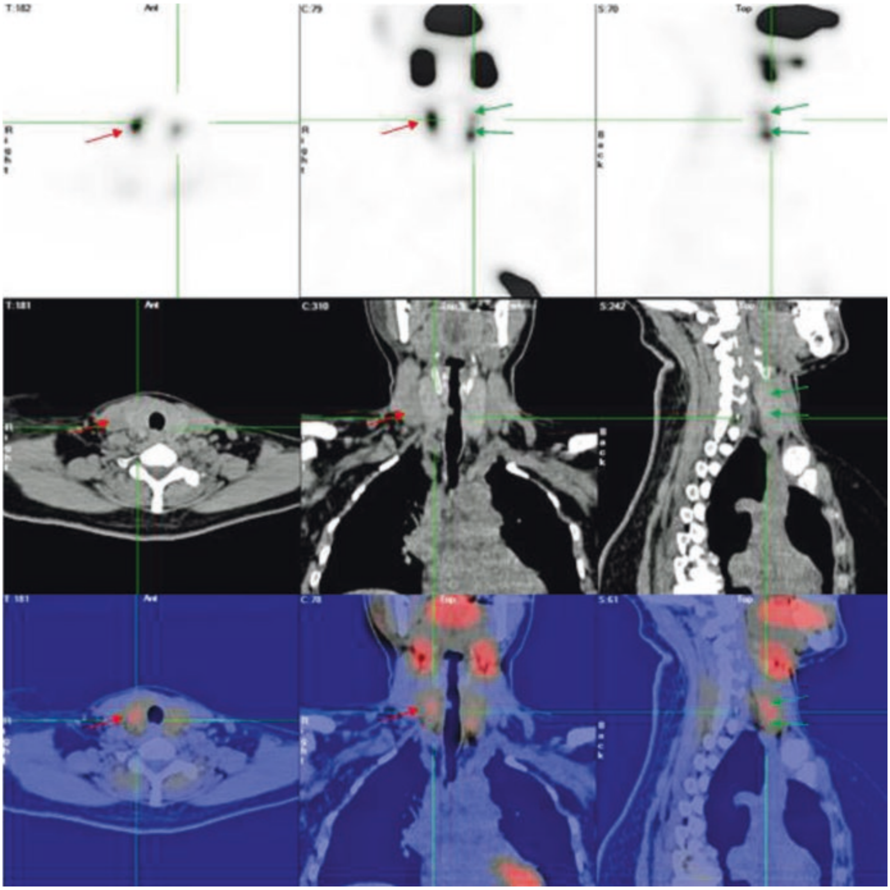

Fig. 7.54 ^{99m}Tc-sestamibi SPECT scan images using the inverse logarithmic scale display (top row), CT scan images (middle row) and fused SPECT/CT images (bottom row) in the transverse (left column), coronal (middle column) and sagittal (right column) showing a large hyperplastic parathyroid gland in the right lobe (red arrow) and left upper and lower parathyroid gland hyperplasia (green arrows)

7.23.5 Comments and Teaching Points

- In this patient without renal failure the cause of primary hyperparathyroidism is multiglandular parathyroid hyperplasia.
- Planar ^{99m}Tc-sestamibi scan images can frequently be negative in the presence of small hyperplastic parathyroid glands which can, however, be detected on the tomographic images.

- The pathologic lesions responsible for sporadic PHPT in approximately 85% of cases are an isolated parathyroid adenoma, and only 15% of PHPT cases are due to parathyroid hyperplasia.

7.24 Case 7.24. Single Left Lower Parathyroid Adenoma

7.24.1 Background

A 48-year-old female with known hypothyroidism was admitted in 2017 when her routine blood tests revealed persistent hypercalcaemia and raised serum PTH levels. Serum PTH was 15.1 pmol/L (normal 1.3–9.3), corrected calcium 2.85 mmol/L (normal 2.2–2.6), phosphorus 0.77 mmol/L (normal 0.84–1.45), magnesium 0.75 mmol/L (normal 0.77–1.03), alkaline phosphate 59 IU/L (normal 42–98), urea 2.7 mmol/L (2.5–6.4) and creatinine 63 μmol/L (74–115).

7.24.2 Procedure

The patient was injected with 60 MBq of ^{99m}Tc-pertechnetate, and a thyroid scan was acquired for 10 min at 15 min postinjection. Next, 808 MBq of ^{99m}Tc-sestamibi was injected without moving the patient and a 10-min duration planar scan performed after 10 min. ^{99m}Tc-sestamibi SPECT/CT scan was performed at 2 h followed by a late planar ^{99m}Tc-sestamibi scan at 3 h.

7.24.3 Findings

The pertechnetate thyroid scan (Fig. 7.55a) showed a normal-sized image of the thyroid with homogenous distribution of activity in the gland. The early planar ^{99m}Tc-sestamibi scan (Fig. 7.55b) showed an elliptical focus of increased uptake extending downwards from the lower pole of the left lobe of the thyroid with delayed washout sestamibi image (Fig. 7.55c) showing focal retention of tracer here with washout of activity from the thyroid gland. The ^{99m}Tc-sestamibi/^{99m}Tc-pertechnetate subtraction image (Fig. 7.55d) showed a residual focus of intense uptake abutting the lower left pole of the thyroid.

The SPECT/CT scan with greyscale and colour scale thresholding showed an oval focus of activity posterior to the lower pole of the left lobe of the thyroid with the CT component of the SPECT/CT showing a hypodense lesion located posterior to the thyroid lateral to the trachea measuring 22.4 × 16 × 5 mm in size (Fig. 7.56).

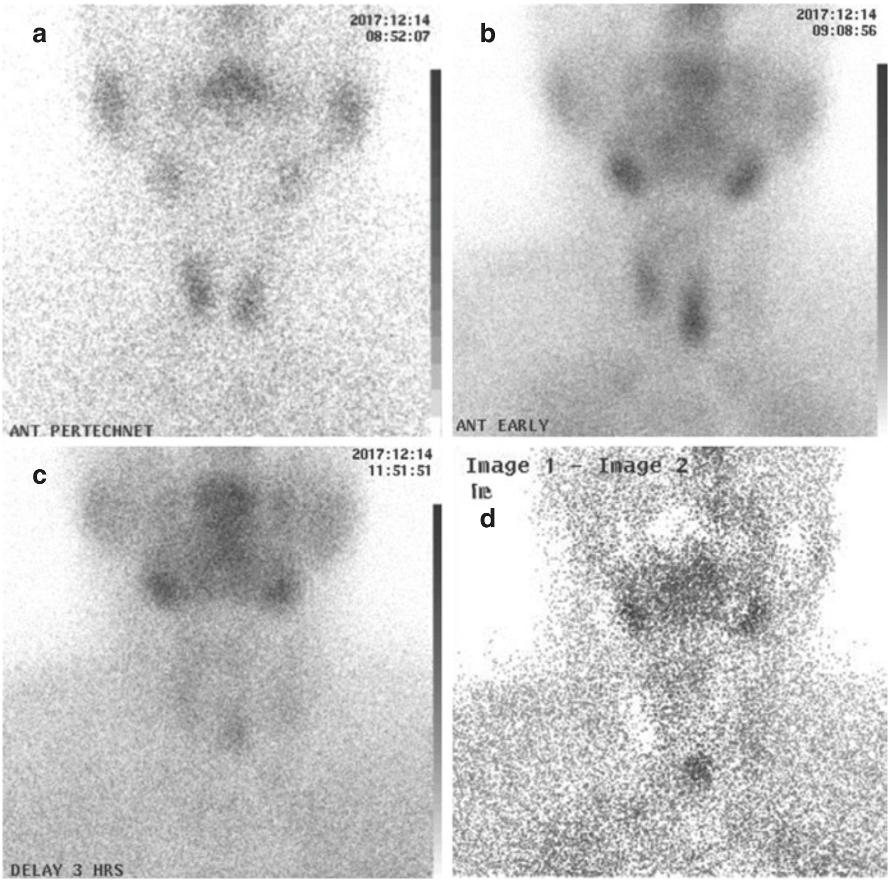

Fig. 7.55 ^{99m}Tc-pertechnetate thyroid scan (**a**), early planar ^{99m}Tc-sestamibi scan (**b**), late planar ^{99m}Tc-sestamibi scan (**c**) and ^{99m}Tc-sestamibi/^{99m}Tc-pertechnetate subtraction scan (**d**) images showing a left lower parathyroid adenoma

7.24.4 Conclusion

Findings consistent with primary hyperparathyroidism due to a single left lower parathyroid adenoma. At surgery, a tan elongated nodular lesion was removed which was confirmed as a parathyroid adenoma on frozen section histopathology.

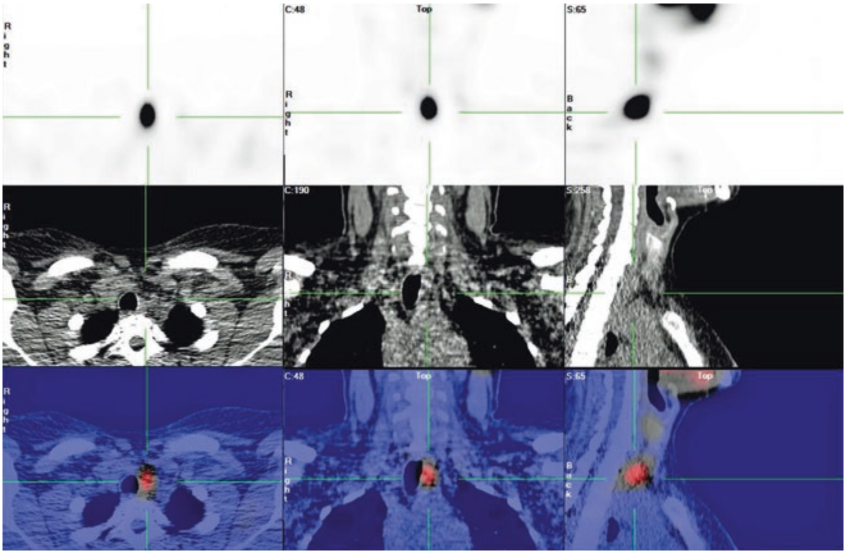

Fig. 7.56 ^{99m}Tc-sestamibi SPECT scan images using the inverse logarithmic scale display (top row), CT scan images (middle row), and fused SPECT/CT images (bottom row) in the transaxial (left column), coronal (middle column) and sagittal (right column) planes, showing a parathyroid adenoma at the lower pole of the left lobe of the thyroid

7.25 Case 7.25. Single Ectopic Retrosternal Parathyroid Adenoma

7.25.1 Background

A 43-year-old female with bilateral renal stones and hyperparathyroidism was being planned for nephrolithotomy. Her serum PTH was 40.80 pmol/L (normal 1.3–9.3), corrected calcium 2.89 mmol/L (normal 2.2–2.6), phosphorus 0.81 mmol/L (normal 0.84–1.45), magnesium 0.69 mmol/L (normal 0.77–1.03), alkaline phosphate 95 IU/L (normal 42–98), urea 3.4 mmol/L (2.5–6.4) and creatinine 51 μmol/L (74–115).

7.25.2 Procedure

The patient was injected with 59 MBq of ^{99m}Tc-pertechnetate, and a thyroid scan acquired for 5-min at 20 min postinjection. Next, 808 MBq of ^{99m}Tc-sestamibi was injected without moving the patient and a 10-min duration planar scan performed after 10 min. ^{99m}Tc-sestamibi SPECT/CT scan was performed at 2 h followed by a late planar ^{99m}Tc-sestamibi scan at 3 h.

7.25.3 Findings

The pertechnetate thyroid scan (Fig. 7.57a) showed a normal-sized image of the thyroid with homogenous distribution of activity in the gland. The early planar ^{99m}Tc-sestamibi scan (Fig. 7.57b) showed a pattern of uptake similar to that seen on the pertechnetate thyroid scan with the delayed washout sestamibi image (Fig. 7.57c) showing no focal retention of tracer in the thyroid bed. The unzoomed delayed ^{99m}Tc-sestamibi scan image (Fig. 7.57d) showed a focus of uptake in the mediastinum. The SPECT/CT scan showed a rounded focus of activity in the anterior mediastinum located behind the manubriosternal joint measuring 11 mm in diameter (Fig. 7.58).

7.25.4 Conclusion

Findings of a retrosternal ^{99m}Tc-sestamibi-avid lesion consistent with an ectopic parathyroid adenoma as the underlying cause of primary hyperparathyroidism. The

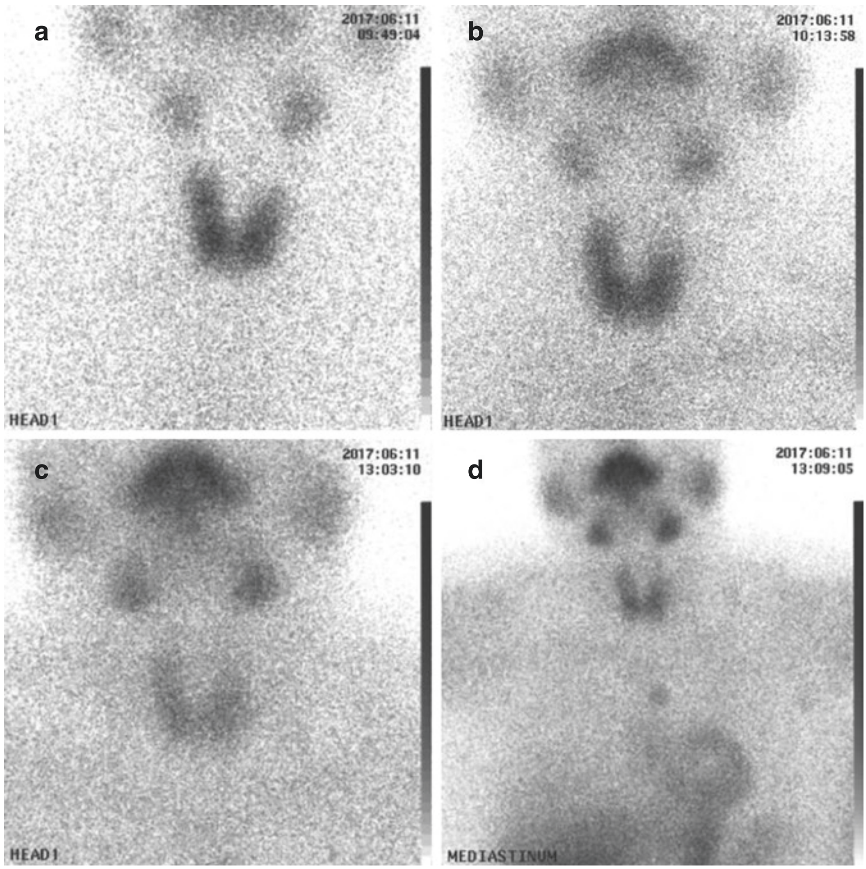

Fig. 7.57 ^{99m}Tc-pertechnetate thyroid scan (**a**), early planar ^{99m}Tc-sestamibi scan (**b**), late planar ^{99m}Tc-sestamibi scan (**c**) and unzoomed ^{99m}Tc-sestamibi delayed image of the neck and chest (**d**) with the last image showing an ectopic mediastinal parathyroid adenoma

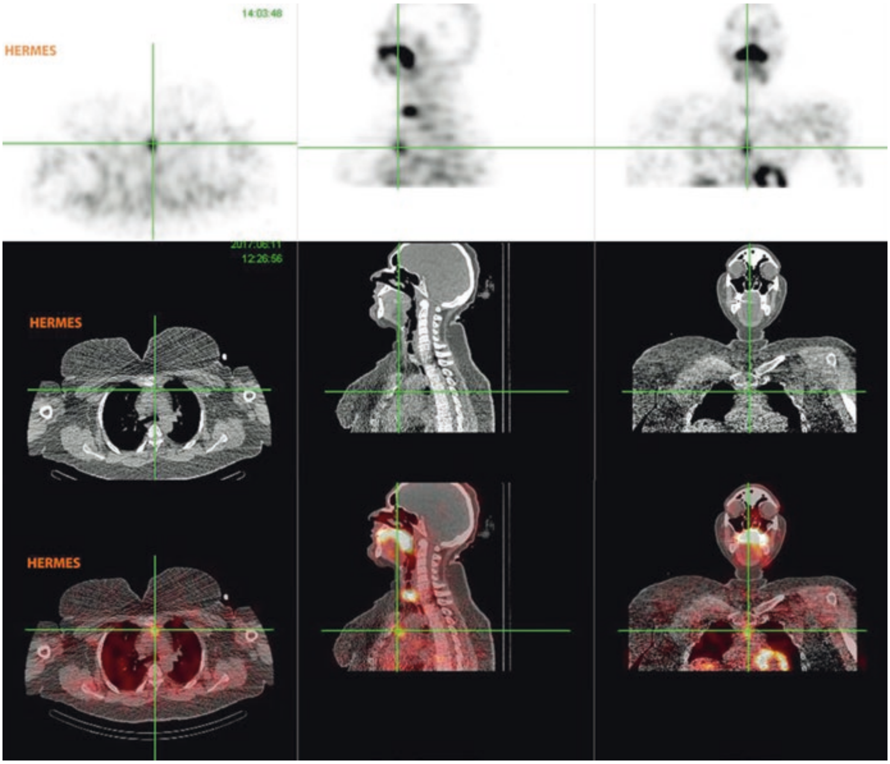

Fig. 7.58 ^{99m}Tc-sestamibi SPECT scan images (top row), CT scan images (middle row) and fused SPECT/CT images (bottom row) in the transaxial (left column), sagittal (middle column) and coronal (right column) planes, showing a parathyroid adenoma (crosshair) in the anterior mediastinum behind the manubriosternal joint

lesion was surgically resected 5 months later with serum PTH levels and serum calcium levels returning back to normal postoperatively at 3.8 pmol/L) and 2.41 mmol/L respectively.

7.26 Case 7.26. Double Ectopic Parathyroid Adenomas (Left Intrathyroidal + Ectopic Right Lower)

7.26.1 Background

A 58-year-old female with a diagnosis of incidental hypercalcaemia was referred for a parathyroid scan. Her serum PTH was normal at 4.8 pmol/L (normal 1.3–9.3), corrected calcium high at 2.97 mmol/L (normal 2.2–2.6), normal phosphorus at 1.16 mmol/L (normal 0.84–1.45), magnesium low at 0.53 mmol/L (normal 0.77–1.03), alkaline phosphate low at 37 IU/L (normal 42–98), urea normal at 3.4 mmol/L (normal range 2.5–6.4) and creatinine normal at 63 μmol (normal range 53–97). The patient was suspected of primary hyperparathyroidism on the basis of hypercalcaemia in the presence of an inappropriately normal serum PTH. Ultrasound showed a normal thyroid gland with a well-defined hypoechoic lesion inferior to the right thyroid lobe measuring 1.2 × 1.0 cm.

7.26.2 Procedure

The patient was injected with 37 MBq of ^{99m}Tc-pertechnetate, and a thyroid scan was acquired for 5 min at 20 min postinjection. Next, 812 MBq of ^{99m}Tc-sestamibi was injected without moving the patient and a 10-min duration planar scan performed after 10 min. ^{99m}Tc-sestamibi SPECT/CT scan was performed at 2 h followed by a late planar ^{99m}Tc-sestamibi scan at 3 h.

7.26.3 Findings

The pertechnetate thyroid scan showed a normal-sized image of the thyroid with homogenous distribution of activity in the gland (Fig. 7.59a). The early planar

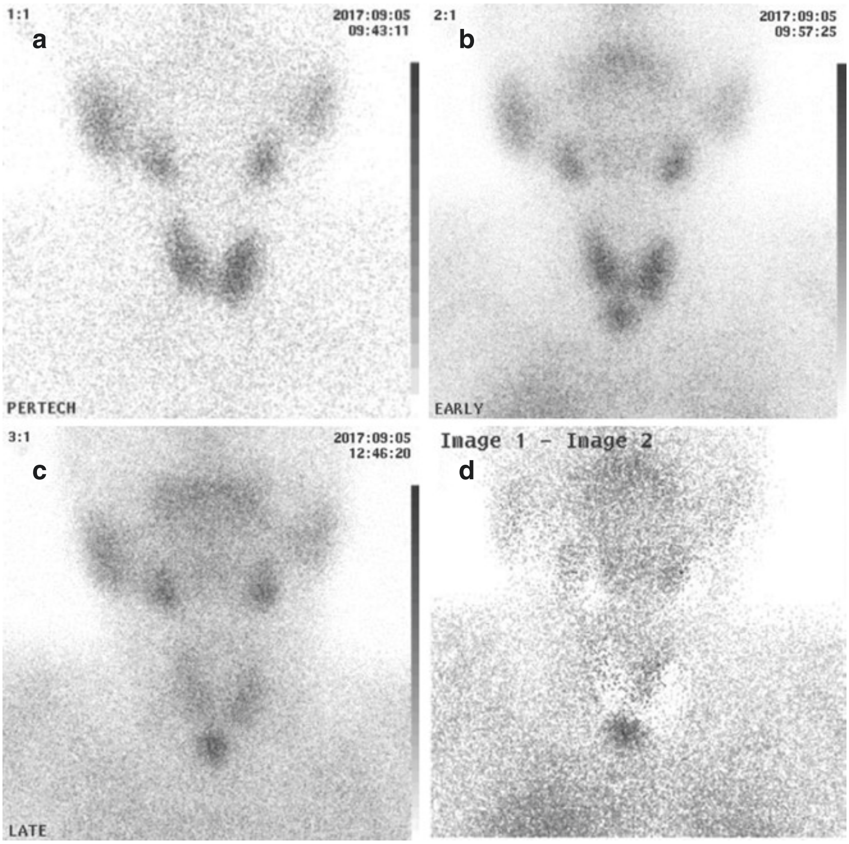

Fig. 7.59 ^{99m}Tc-pertechnetate thyroid scan (**a**), early planar ^{99m}Tc-sestamibi scan (**b**), late planar ^{99m}Tc-sestamibi scan (**c**) and ^{99m}Tc-sestamibi/^{99m}Tc-pertechnetate subtraction image (**d**) showing an ectopic parathyroid adenoma

^{99m}Tc-sestamibi scan showed a pattern of uptake in the thyroid gland itself which is similar to that seen on the pertechnetate thyroid scan but with a rounded focus of uptake below the isthmus, with the delayed washout sestamibi images showing focal retention of tracer in this lesion (Fig. 7.59b, c). The ^{99m}Tc-sestamibi/^{99m}Tc-pertechnetate subtraction image showed only the ectopic focus of activity without any residual lesion seen in the thyroid bed (Fig. 7.59d).

The SPECT/CT scan, however, showed the ectopic parathyroid adenoma below the right lower pole of the thyroid together with a focus of increased activity in the lower part of the left lobe of the thyroid, which was consistent with a partly intrathyroidal parathyroid adenoma (Fig. 7.60).

7.26.4 Conclusion

Findings consistent with double ectopic parathyroid adenomas (an ectopic right lower with an ectopic left intrathyroidal) as the cause of primary hyperparathyroidism.

The lesions were surgically resected with right lower parathyroid seen as a well-circumscribed grey-brown lesion 2.8 g in weight measuring 2.0 × 1.70 × 1.30 cm with histopathology showing an encapsulated lesion composed exclusively of uniform cellular proliferation of oxyphil cells and focal calcification within the lesion,

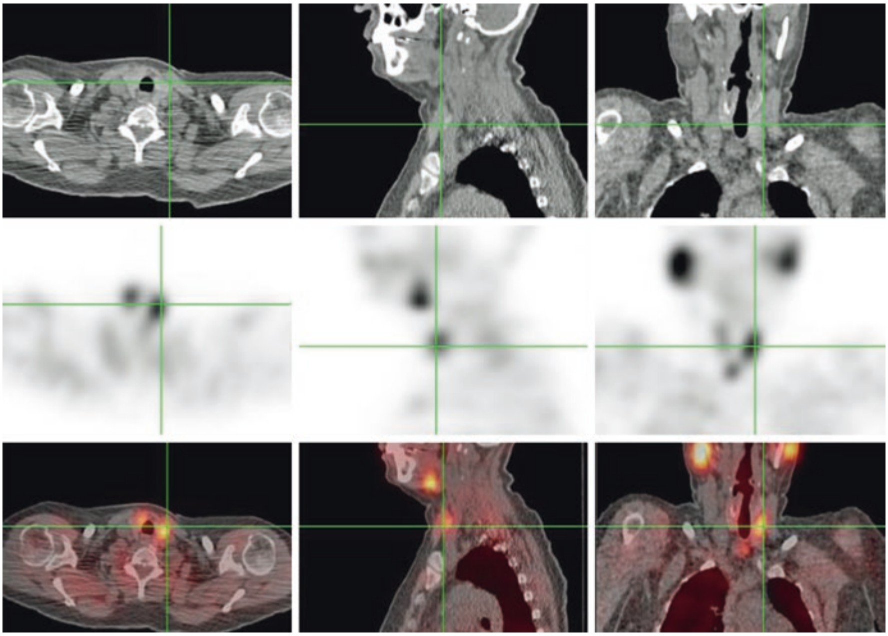

Fig. 7.60 ^{99m}Tc-sestamibi SPECT scan images (top row), CT scan images (middle row), and fused SPECT/CT images (bottom row) in the transaxial (left column), coronal (middle column) and sagittal (right column) planes, showing an intrathyroidal parathyroid adenoma (crosshair) in the left lower pole of the thyroid with an ectopic adenoma below the right thyroid lobe measuring 18.7 × 16.7 × 17.0 mm in size

and a rim of uninvolved parathyroid tissue was also seen. Left lobectomy was performed, and the histopathology identified an intrathyroidal left lower parathyroid adenoma.

The serum PTH levels fell from a preoperative value of 4.8 to <2.1 pmol/L (normal 1.3–9.3), and serum calcium level normalised to 2.39 mmol/L.

7.26.5 Comments and Teaching Points

- This is a unique (previously unreported) case of a double ectopic parathyroid adenoma (including an ectopic right lower with an ectopic left intrathyroidal) as the cause of primary hyperparathyroidism.
- Double adenomas are usually associated with relatively higher levels of serum PTH and calcium compared with single adenomas in general, but in this particular case, the PTH was quite normal.
- The patient's thyroid US showed only the ectopic right lower parathyroid gland adenoma but missed the second left lower parathyroid adenoma.
- The ectopic parathyroid adenoma could be easily diagnosed on the planar ^{99m}Tc-sestamibi scans, but the left lower intrathyroidal adenoma could only be diagnosed on the SPECT/CT scan, which shows the additional value of SPECT/CT imaging in the diagnosis of lesions in the thyroid bed particularly when the lesions are not very hyperactive in the early stage and do not show significant differential retention and are surrounded by normal thyroid tissue.
- Hypercalcaemia is said to be PTH-mediated if serum calcium is elevated and the PTH level is high or inappropriately normal as in this case.
- A high PTH level associated with a high level of calcium usually defines primary hyperparathyroidism, but a normal or subnormal PTH level with hypercalcaemia (>2.6 mmol/L) can also be regarded as primary hyperparathyroidism as, under normal conditions, hypercalcaemia physiologically suppresses the PTH production. Approximately 10% of patients with primary hyperparathyroidism will have elevated calcium levels with relatively normal PTH levels [31].
- As seen in this patient, intrathyroidal location of a parathyroid adenoma not only causes special diagnostic difficulties because the capsule of the gland is very thin and hard to distinguish on surgery and the surgeons often resort to thyroid lobectomy as in this case.

7.27 Case 7.27. A Case of Sagliker Syndrome

7.27.1 Background

A 21-year-old male with multiple medical problems was referred for skeletal and parathyroid scintigraphy. The patient suffered from hypertension, growth and mental retardation, reduced vision in the left eye with blindness of the right eye, and was on haemodialysis for stage IV chronic kidney disease and had an 8-month history of a large mandibular swelling (Fig. 7.61). The patient was osteoporotic (Fig. 7.62) and had been unable to walk due to leg pain for the last 8 months. He suffered from normocytic normochromic anaemia. His echocardiogram showed mild concentric left ventricular hypertrophy and mitral regurgitation. It was thought that the patient was suffering from an undiagnosed congenital syndrome given the fact that his two siblings, a brother and sister, suffered from similar problems.

The patient's urea was high at 16.8 mmol/L (normal range 2.5–6.4) with creatinine also high at 448 µmol/L (normal range 53–97). Serum PTH levels were high at 128.5 pmol/L (normal 1.3–9.3), corrected calcium low at 1.98 mmol/L (normal 2.2–2.6), normal phosphorus at 0.97 mmol/L (normal 0.84–1.45), normal magnesium at 0.90 mmol/L (normal 0.77–1.03), alkaline phosphate high at 783 IU/L (normal 53–128) and total vitamin D level low at 36 nmol/L (vitamin D deficient <50 nmol/L).

Fig. 7.61 21-year-old male with growth and mental retardation with reduced vision in the left eye and blindness in the right eye (insert) with an uglifying facial deformity

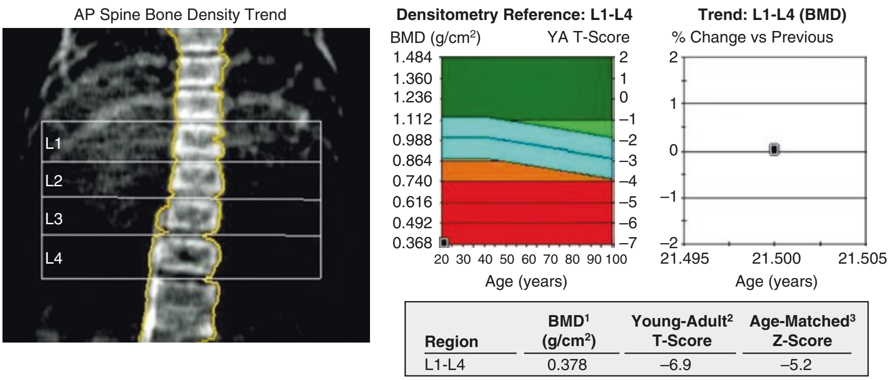

Fig. 7.62 Bone densitometry showing low *t*- and *z*-scores for the patient at −6.9 and −5.2, respectively, consistent with severe osteoporosis. Note the rugger-jersey sign appearances of the lumbar spine

7.27.2 Procedures

For parathyroid scintigraphy, the patient was first injected with 54 MBq of ^{99m}Tc-pertechnetate and a thyroid scan acquired for 5 min at 20 min postinjection. Next, 794 MBq of ^{99m}Tc-sestamibi was injected without moving the patient and a 5-min duration planar scan performed after 10 min. ^{99m}Tc-sestamibi SPECT/CT scan was performed at 2 h followed by a late planar ^{99m}Tc-sestamibi scan at 3 h.

Bone scintigraphy was undertaken 10 days later. The patient was injected with 769 MBq ^{99m}Tc-methylene diphosphonate, and a whole-body blood pool scan was acquired followed by whole-body imaging at 3-h postinjection. Bone SPECT/CT scan was additionally performed.

7.27.3 Findings (Parathyroid Scintigraphy)

The pertechnetate thyroid scan (Fig. 7.63a) showed a normal-sized image of the thyroid with homogenous distribution of activity in the gland. The early planar ^{99m}Tc-sestamibi scan (Fig. 7.63b) showed a similar pattern of uptake as seen on the pertechnetate thyroid scan, with the delayed sestamibi scan (Fig. 7.63c) showing washout of tracer from the thyroid gland with no retention of tracer seen. The ^{99m}Tc-sestamibi/^{99m}Tc-pertechnetate subtraction image (Fig. 7.63d) showed no residual lesion in the thyroid bed. SPECT/CT scan (Fig. 7.64) showed focal increased tracer uptake in the right lower lobe consistent with a large hyperplastic right inferior parathyroid gland, which was seen to measure 19 × 10.2 × 8.8 mm in size on the low-dose CT component.

The early planar ^{99m}Tc-sestamibi scan showed intense increased tracer uptake in a large mandibular mass, which partially washed out on the delayed sestamibi scan (Fig. 7.63b, c). The SPECT/CT showed a large expansile soft-tissue mass lesion showing thin internal septations with the destruction of the mandible anteriorly. Another similar lesion was seen at the upper alveolar margin (Fig. 7.64). There was an increase in the diploic space in the skull with diffusely increased tracer uptake (Fig. 7.65).

7.27.4 Findings (Skeletal Scintigraphy)

The whole-body bone scan showed a high bone/soft-tissue ratio with generalised poor definition of the bone structure and poor visualisation of the kidneys with relatively increased uptake in the long bones. These findings were consistent with metabolic bone disease together with generalised osteopenia (Fig. 7.66). There was increased uptake in the growth plates in the shoulders, hips and knees on the planar and the SPECT bone scans. There was a ricketic-looking skeletal deformity in terms of pigeon chest, rosary beads of the ribs and bowing of the femora and the tibiae. There was focal increased uptake in the right seventh rib posterolaterally seen corresponding to a callus on the CT, with a horizontal sclerotic band of

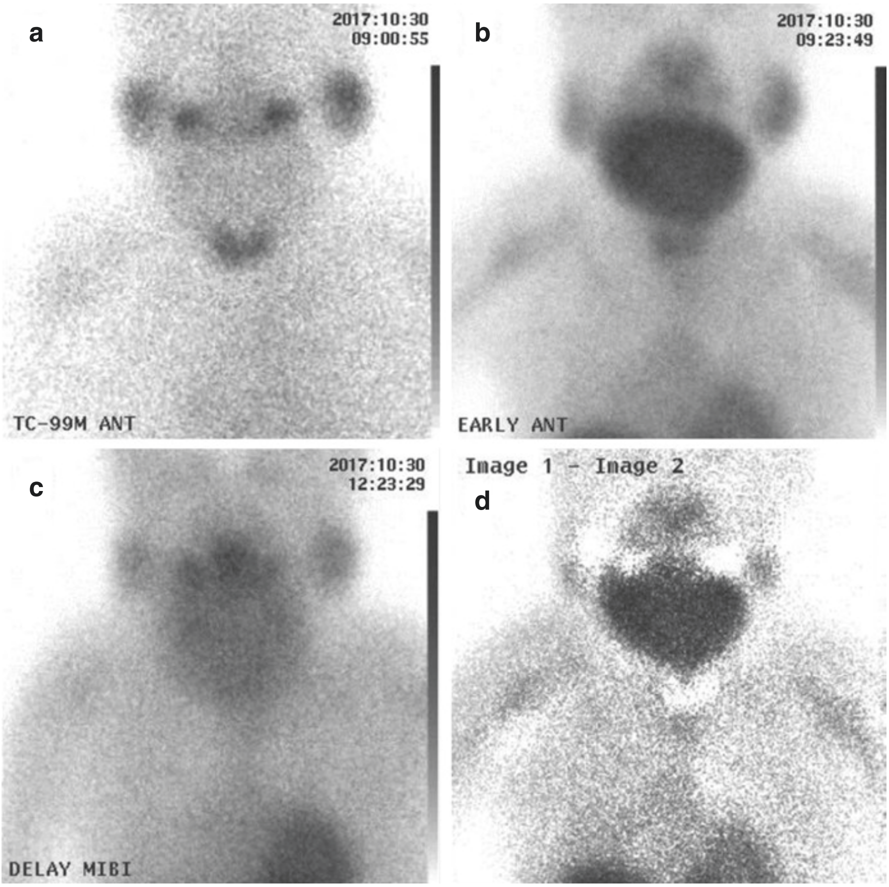

Fig. 7.63 ^{99m}Tc-pertechnetate thyroid scan (**a**), early planar ^{99m}Tc-sestamibi scan (**b**), late planar ^{99m}Tc-sestamibi scan (**c**) and ^{99m}Tc-sestamibi/^{99m}Tc-pertechnetate subtraction image (**d**)

increased activity seen traversing the upper sacrum. The rib and the sacral lesions were consistent with osteoporotic fractures. The early blood pool and the delayed osseous phase images showed increased activity in the calvarium involving the frontal and the parietal bones, which on the CT component of the SPECT/CT was seen to correspond to the expansion of the diploic space (Fig. 7.67).

The large mandibular mass deformity showed irregular increased uptake corresponding to a large unilocular cystic lesion on the CT. There was another similar smaller cystic lesion seen involving the anterior part of the hard palate with increased blood pool and bone uptake. The soft-tissue density lesions showed heterogeneous texture with some calcified material. There was a large photon-deficient lesion in the left upper acetabular roof. These lesions were suggestive of brown tumours. CT component also showed rugger-jersey sign in the spine (sclerotic-lucent-sclerotic appearance) (Figs. 7.67 and 7.68) which is considered almost diagnostic of the osteosclerosis associated with secondary hyperparathyroidism of chronic renal failure.

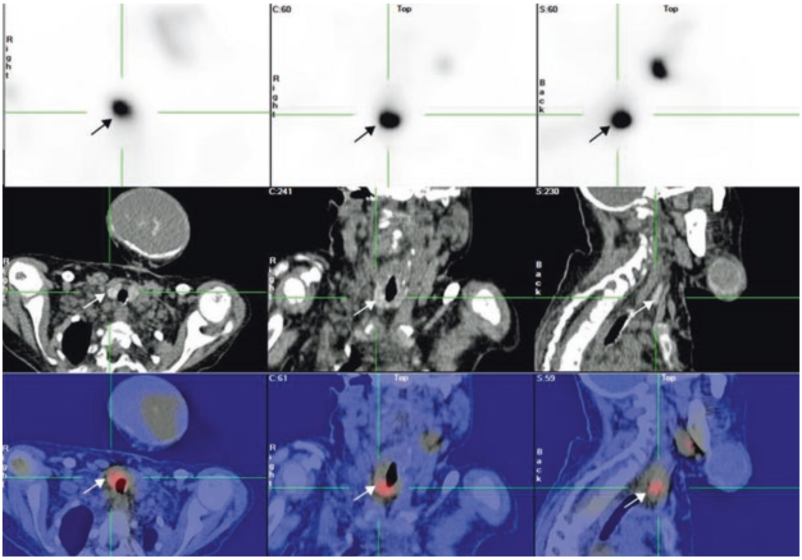

Fig. 7.64 ^{99m}Tc-sestamibi SPECT scan images (top row), CT scan images (middle row) and fused SPECT/CT images (bottom row) in the transaxial (left column), coronal (middle column) and sagittal (right column) planes, showing right lower parathyroid hyperplasia

Fig. 7.65 The low-dose CT component of the SPECT/CT scan images in the transaxial (top row), coronal (middle row) and sagittal (bottom row) axes showing an oblong lesion (arrows) behind the lower part of the right lower lobe measuring 19 × 10.2 × 8.8 mm in size

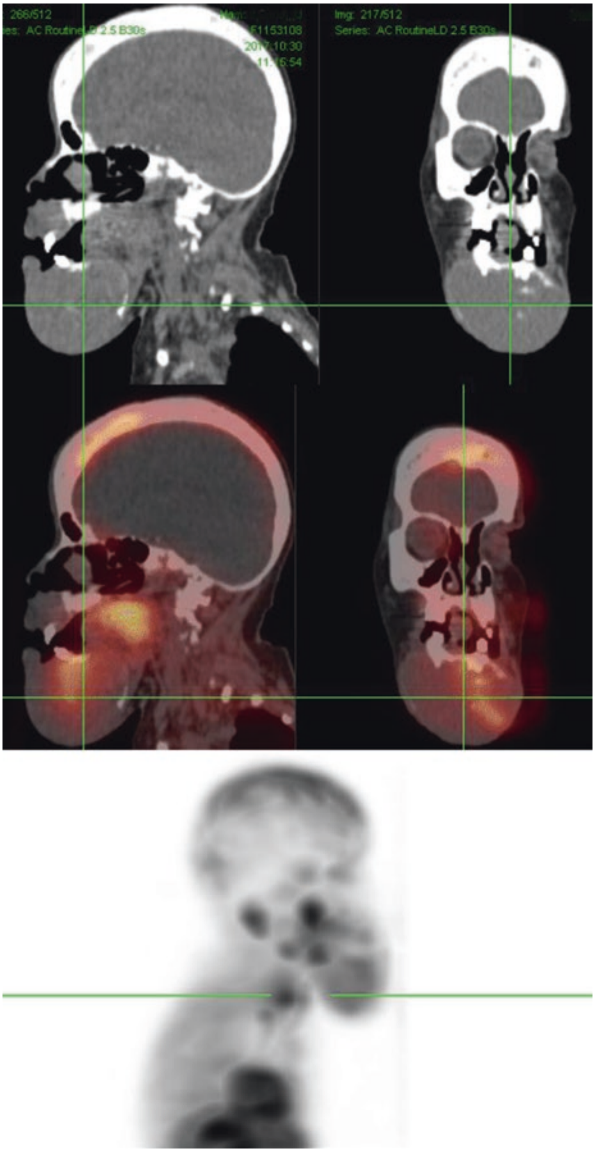

Fig. 7.66 Fused SPECT/CT scan images (top) and MIP image (bottom) showing the sestamibi uptake in the skull, the mandible and the alveolar masses

7.27.5 Conclusion

Findings consistent with right lower parathyroid hyperplasia, associated with long standing secondary hyperparathyroidism. The bone and parathyroid scans showed multiple brown tumours due to osteitis fibrosa cystica. The clinical and imaging findings of the patient are consistent with Sagliker syndrome.

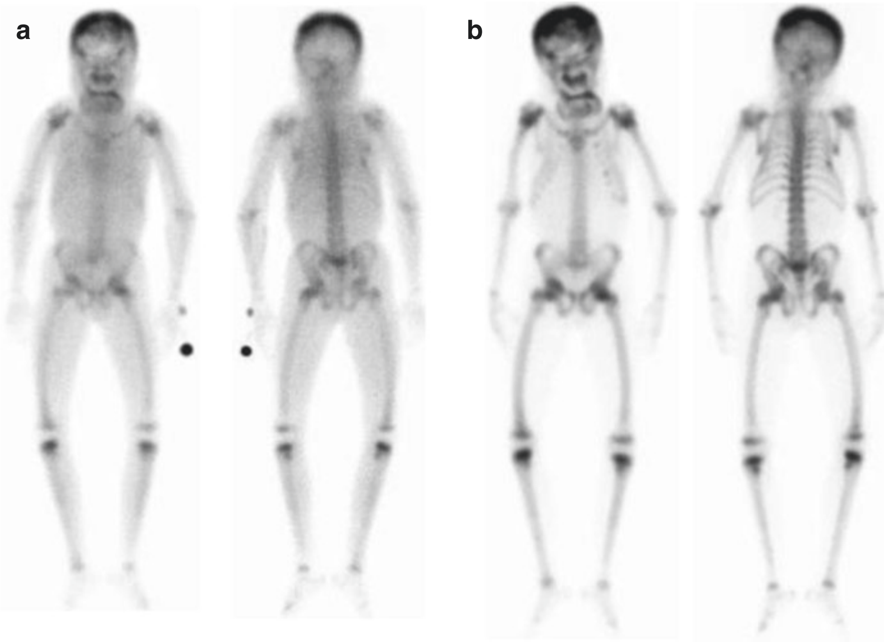

Fig. 7.67 ^{99m}Tc-methylene diphosphonate whole-body bone scan with blood pool images (**a**) and delayed bone scan images (**b**) in the anterior and posterior projections

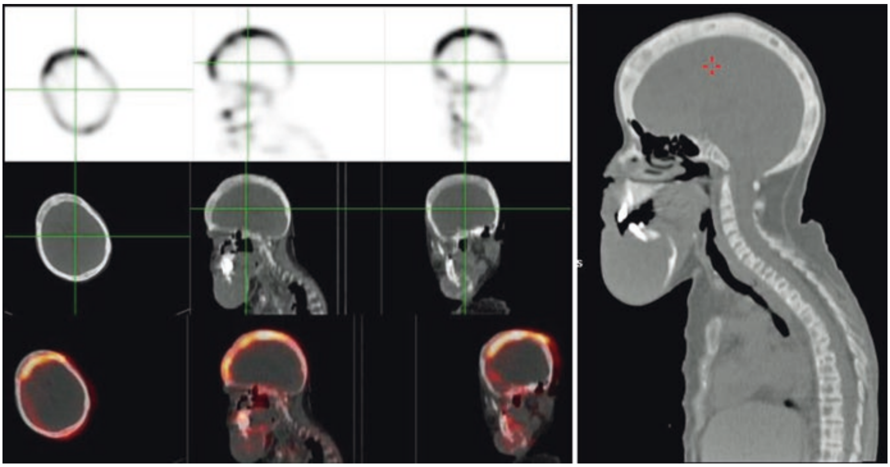

Fig. 7.68 ^{99m}Tc-methylene diphosphonate SPECT/CT scan (left panel) showing the mandibular deformity and the sagittal CT image (right panel) showing rugger-jersey sign

7.27.6 Comments and Teaching Points

- Sagliker syndrome is a rare disease associated with untreated secondary hyperparathyroidism. The features of the syndrome include metabolic bone disease with skeletal osteopenia and multiple associated fractures, a severe and advanced form of renal osteodystrophy and skeletal abnormalities and deformities. Sagliker syndrome is assumed to result from insufficient treatment of SHPT in early stages of chronic renal failure [32].
- This patient had radiologic evidence of both osteomalacia due to vitamin D deficiency and secondary hyperparathyroidism due to renal failure. Parathyroid hyperplasia develops in such cases which is initially reversible by vitamin D treatment, but if long standing, one or more adenomas may develop as is likely in this case, and parathyroid surgery may be necessary. The findings in these cases are also similar to that seen in the renal osteodystrophy.
- Rugger-jersey spine describes the prominent sub-endplate densities at multiple contiguous vertebral levels to produce an alternating sclerotic-lucent-sclerotic appearance. This mimics the horizontal stripes of a rugby jersey.
- The rugger-jersey spine sign is said to be almost diagnostic of the osteosclerosis associated with secondary hyperparathyroidism of chronic renal failure. In response to increased bone resorption due to excess PTH secretion and subsequent loss of bone mass, osteoblasts form an increased amount of osteoid that does not contain hydroxyapatite but does appear opaque on radiographs forming vertebral body superior and inferior endplate sclerotic bands that represent accumulations of excess osteoid and appear opaque because of their increased volume when compared to normal bone [33].

7.28 Case 7.28. Synchronous Parathyroid Adenoma and Papillary Thyroid Carcinoma

7.28.1 Background

A 61-year-old male presented with hypercalcaemia and hyperparathyroidism with his serum PTH high at 19.3 pmol/L (normal 1.3–9.3) and corrected calcium high at 2.84 mmol/L (normal 2.2–2.6), but serum phosphorus, magnesium, alkaline phosphate, urea and creatinine were all normal.

7.28.2 Procedure

The patient was injected with 57 MBq of ^{99m}Tc-pertechnetate, and a thyroid scan was acquired for 5 min after 20 min. Next, 747 MBq of ^{99m}Tc-sestamibi was injected without moving the patient and a 10-min duration planar scan performed after 10 min. ^{99m}Tc-sestamibi SPECT/CT scan was performed at 2 h followed by a late planar ^{99m}Tc-sestamibi scan at 3 h.

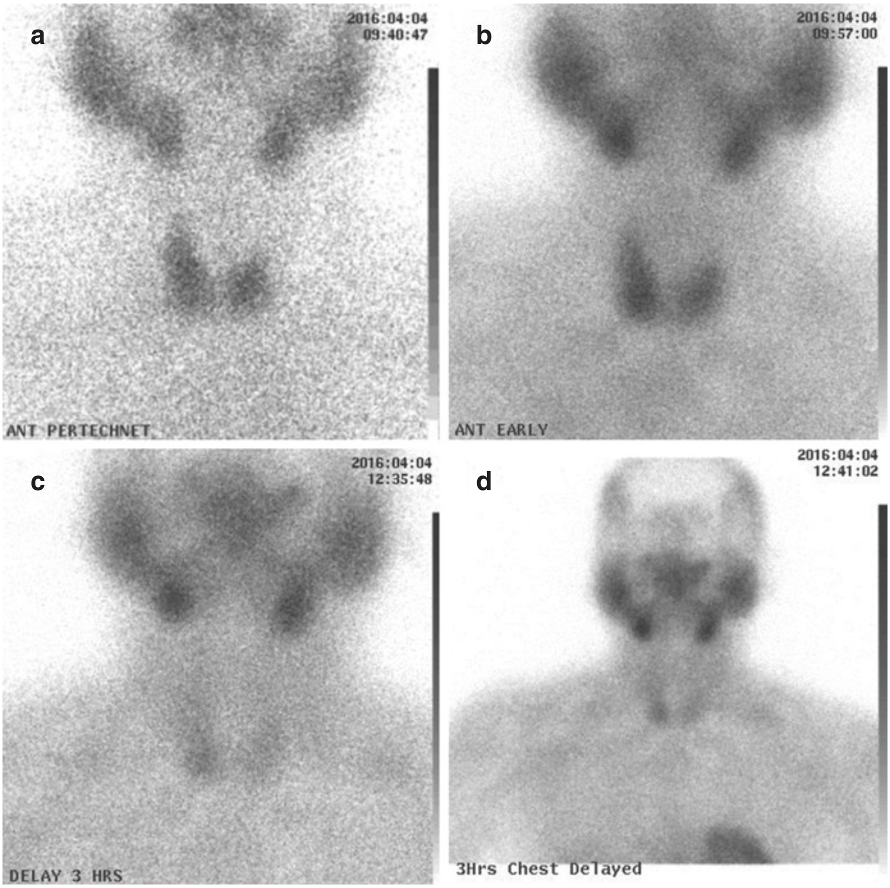

Fig. 7.69 ^{99m}Tc-pertechnetate thyroid scan (**a**), early planar ^{99m}Tc-sestamibi scan (**b**), late planar ^{99m}Tc-sestamibi scan (**c**) and the late ^{99m}Tc-sestamibi unzoomed neck and chest image (**d**)

7.28.3 Findings

The pertechnetate thyroid scan showed a normal-sized image left lobe and a larger right lobe with homogenous distribution of activity in the gland (Fig. 7.69a). The early planar ^{99m}Tc-sestamibi scan showed a pattern of uptake in the thyroid gland, which was similar to that seen on the pertechnetate thyroid scan albeit with faint increased uptake at the right lower pole, with the delayed washout sestamibi images showing focal retention of tracer at the lower pole of the right thyroid lobe (Fig. 7.69b–d). The SPECT/CT scan showed a clear-cut focus of uptake at the posterior aspect of the lower pole of the right lobe in the tracheo-oesophageal groove measuring 22.3 × 13.0 mm in size (Fig. 7.70).

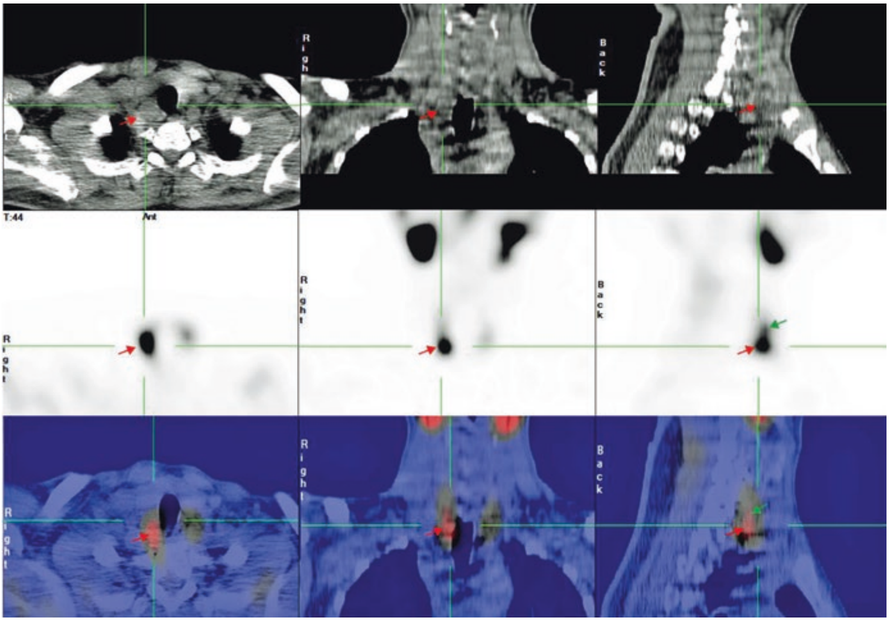

Fig. 7.70 CT scan images (top row), ^{99m}Tc-sestamibi SPECT scan images (middle row) and fused SPECT/CT images (bottom row) in the transaxial (left column), coronal (middle column) and sagittal (right column) planes, showing a focal lesion (red arrows) with increased uptake at the posterior aspect of the lower pole of the right lobe in the tracheo-oesophageal groove. Retrospective image review shows faint contiguous uptake anterosuperiorly (green arrows) which corresponded with an adjacent hypodense thyroid nodule that later proved to be a papillary thyroid carcinoma

7.28.4 Conclusion

Findings consistent with a right lower parathyroid adenoma as the cause of PHPT.

The patient was operated 2 months later with right lower parathyroidectomy attempted, but the histopathology of the specimen showed mostly thyroid tissue with only a bit of parathyroid tissue. The serum calcium remained high at 3.0 mmol/L, and the serum PTH elevated at 18.8 pmol/L.

The patient was reoperated 6 months later and a lesion removed from the right lower pole of the thyroid which proved to be a 1.5-cm diameter thyroid nodule proven as papillary thyroid carcinoma on histopathology. Another nodule posterior to the right lower pole of the thyroid was also resected and proved to be an enlarged encapsulated parathyroid adenoma. The serum calcium and PTH normalised postsurgery.

A review of the SPECT/CT scan images showed a hypodense lesion in the lower pole of the right thyroid lobe with moderately increased uptake adjacent to the parathyroid adenoma and difficult to differentiate from the high uptake in the adenoma on the SPECT scan (Figs. 7.70 and 7.71).

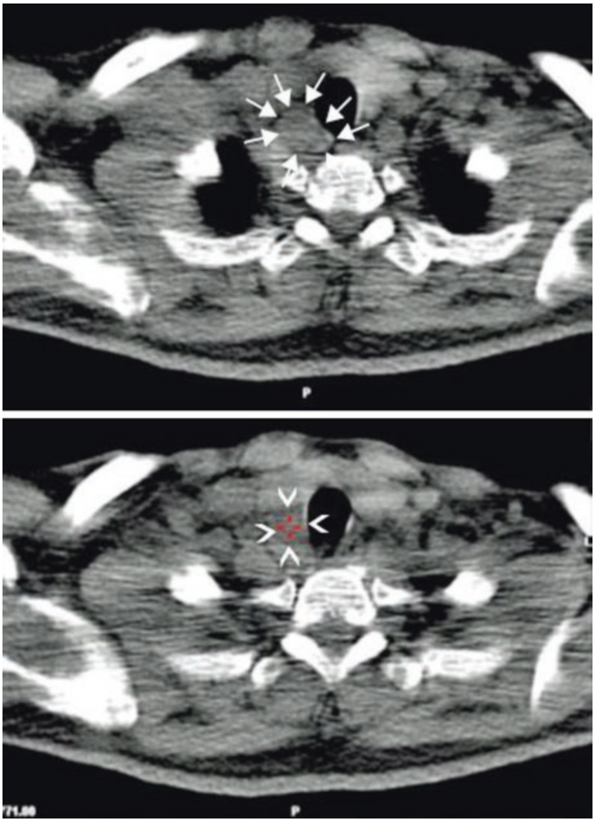

Fig. 7.71 Transaxial CT scan image on the top showing the parathyroid adenoma (arrows) and on the bottom the adjacent hypodense thyroid nodule anterior to the adenoma (chevrons) which proved to be a papillary thyroid carcinoma

7.28.5 Comments and Teaching Points

- The coincidental appearance of hyperparathyroidism and thyroid cancer is not often considered because of its low incidence but has been reported [34].
- The incidence of thyroid cancer in patients with parathyroid adenoma is ~2% [35] and thyroid nodules should, therefore, be investigated prior to surgery on the parathyroids.
- This case illustrates the need for clinical awareness of concomitant hyperparathyroidism and thyroid cancer.

7.29 Case 7.29. Left Lower Parathyroid Adenoma + Sestamibi-Avid Thyroid Adenoma (Papillary Thyroid Carcinoma)

7.29.1 Background

A 30-year-old female presented with primary hyperparathyroidism, hypercalcaemia and hypophosphataemia, with serum PTH at 17.2 pmol/L (normal 1.3–9.3), corrected calcium high at 2.7 mmol/L (normal 2.2–2.6), low phosphorus at 0.63 mmol/L (normal 0.84–1.45), magnesium at 0.90 mmol/L (normal 0.77–1.03), urea low at 1.7 mmol/L (normal range 2.5–6.4) and creatinine also low at 43 µmol/L (normal range 53–97).

7.29.2 Procedure

The patient was injected with 58 MBq of ^{99m}Tc-pertechnetate, and a thyroid scan acquired for 5 min at 20 min postinjection. Next, 780 MBq of ^{99m}Tc-sestamibi was injected without moving the patient and a 10-min duration planar scan performed after 10 min. ^{99m}Tc-sestamibi SPECT scan was performed at 2 h followed by a late planar ^{99m}Tc-sestamibi scan at 3 h.

7.29.3 Findings

The pertechnetate thyroid scan showed a normal-sized image left lobe and a slightly larger right lobe with mild relative increased uptake (Fig. 7.72a). The early planar ^{99m}Tc-sestamibi scan showed a pattern of uptake in the thyroid gland, which was similar to that seen on the pertechnetate thyroid scan, but with a focus of intense increased uptake below the lower pole of the left lobe of the thyroid, with the delayed washout sestamibi images showing focal retention of tracer in the nodule below the lower pole of the left thyroid lobe (Fig. 7.72b–d). The SPECT scan showed a clear-cut posteriorly located focus of intense uptake abutting the lower pole of the left thyroid lobe (Fig. 7.73).

7.29.4 Conclusion

Findings consistent with a left lower parathyroid adenoma as the cause of PHPT together with sestamibi-avid thyroid adenoma.

The lesion below the lower pole of the left thyroid lobe was surgically excised with histopathology confirming a parathyroid adenoma. US-guided fine-needle aspiration cytology of the right thyroid nodule was consistent with papillary thyroid carcinoma. Postoperatively the serum calcium normalised to 2.4 mmol/L, and the serum PTH fell from 17.2 to normal at 4.16 pmol/L.

7.29.5 Comments and Teaching Points

- The right lobe thyroid nodule was both pertechnetate- and sestamibi-avid but couldn't be discerned on the planar pertechnetate scan though it clearly showed increased uptake on the SPECT scan.
- "Hot" thyroid nodules on thyroid scintigraphy are generally benign with a low incidence of thyroid cancer at 1–6%.

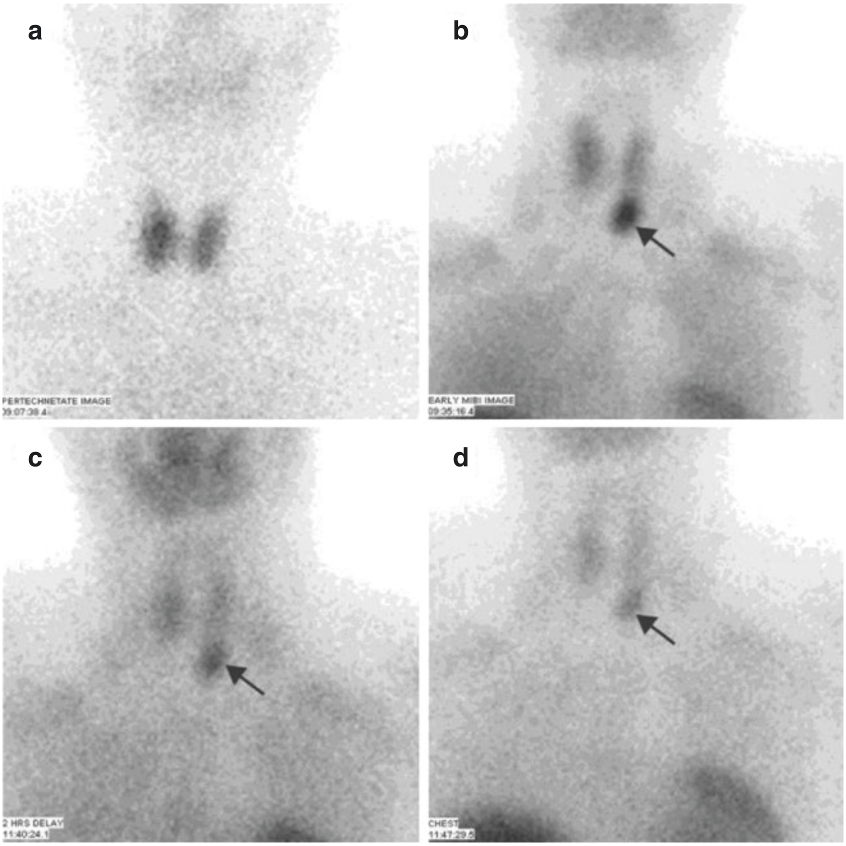

Fig. 7.72 ^{99m}Tc-pertechnetate thyroid scan (**a**), early planar ^{99m}Tc-sestamibi scan (**b**), late planar ^{99m}Tc-sestamibi scan (**c**) and the late ^{99m}Tc-sestamibi unzoomed neck and chest image (**d**) showing a sestamibi-avid nodule below the lower pole of the left lobe of the thyroid

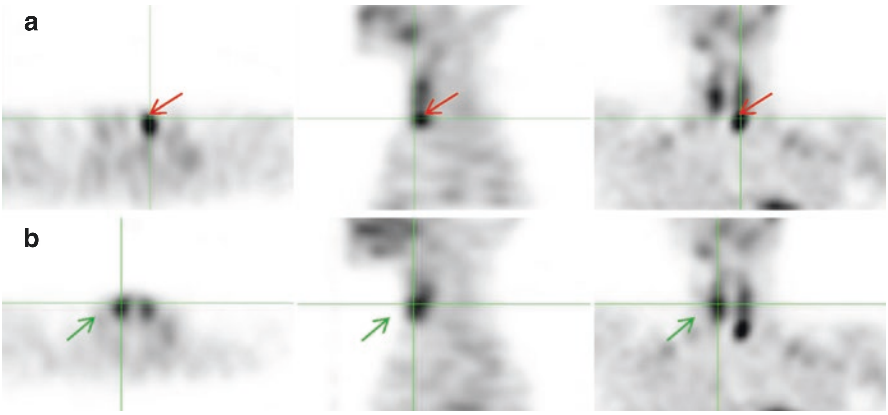

Fig. 7.73 ^{99m}Tc-sestamibi SPECT scan image showing (**a**) the left inferior parathyroid adenoma (**b**) and an anteriorly located thyroid nodule in the lower right thyroid lobe with increased sestamibi uptake

- The majority of sestamibi-avid thyroid nodules are benign, but a small proportion of such nodules have been associated with thyroid cancer.
- High sestamibi uptake considerably increases the probability of differentiated thyroid cancer and facilitates immediate surgical removal, while decreased uptake actually excludes it [36, 37].

7.30 Case 7.30. ^{18}F-FDG and ^{99m}Tc-Sestamibi Positive Parathyroid Adenoma Without Hyperparathyroidism

7.30.1 Background

A 60-year-old female with a right-sided sub-pleural nodule was referred for an ^{18}F-FDG-PET scan. She had a whole-body bone scan 2 years ago for investigation of back pain, which showed early osteoporotic fracture at level D7, severe degenerative changes, protrusions at level L5–S1 and facet joint arthropathy at level L4–L5 (Fig. 7.74). In the light of the results of the ^{18}F-FDG-PET scan (see below), parathyroid scintigraphy and biochemistry were advised.

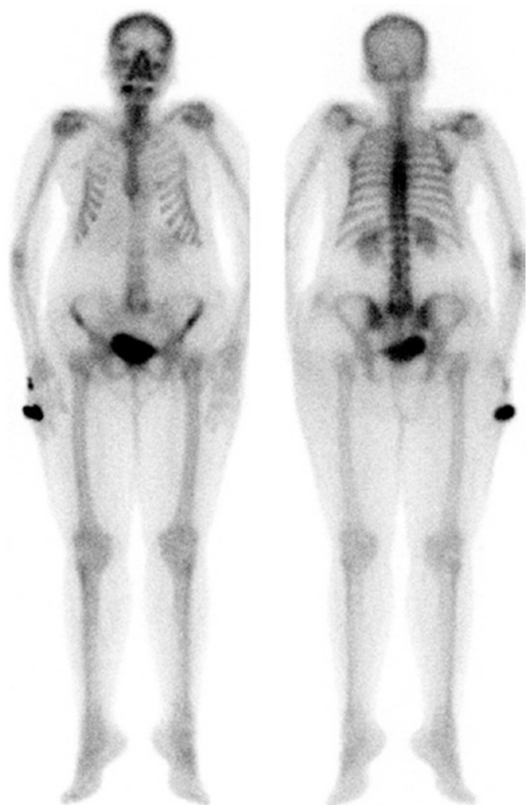

Fig. 7.74 ^{99m}Tc-methylene diphosphonate whole-body bone scan in the anterior (left) and posterior (right) projections

Biochemical laboratory tests were normal for parathyroid disease with a serum PTH of 5.4 pmol/L (normal 1.3–9.3), calcium at 2.27 mmol/L (normal 2.2–2.6), phosphorus 1.46 mmol/L (normal 0.84–1.45), serum alkaline phosphate 46 IU/L (normal 42–98), urea 5.0 mmol/L (normal 2.5–6.4) and creatinine 63 μmol/L (normal 53–97).

7.30.2 Procedures

The patient received an intravenous injection of 310 MBq of ^{18}F-FDG. After an initial uptake phase of approximately 60 min, a CT scan without oral or IV contrast without breath holding at low mA level was acquired for attenuation correction and localisation purposes only. Arms were held up. Subsequently, PET images from the vertex to mid-thigh were obtained. CT, PET and fused images were reconstructed in transaxial, coronal and sagittal projections and interpreted from a workstation.

For parathyroid scintigraphy, the patient was injected with 75 MBq of ^{99m}Tc-pertechnetate, and a thyroid scan was acquired for 10 min at 20 min postinjection. Next, 740 MBq of ^{99m}Tc-sestamibi was injected without moving the patient and a 10-min duration planar scan performed after 10 min. ^{99m}Tc-sestamibi SPECT/CT scan was performed at 2 h followed by late planar ^{99m}Tc-sestamibi scans at 3 h.

7.30.3 Findings

The FDG-PET scan showed a rounded soft-tissue density FDG-avid mass measuring 16.3 × 15 × 13.6 mm, located behind the lower pole of the left thyroid gland with SUV_{max} at 9.19 (Fig. 7.75). This hypermetabolic lesion was suggestive of a left lower parathyroid adenoma.

The pertechnetate thyroid scan showed a larger right lobe, and a normal-sized image left lobe with homogenous distribution of activity in the gland but with a “cold” lesion in the inferolateral aspect of the left lower lobe (Fig. 7.76a), with mild focal increased uptake in the lesion on the early planar ^{99m}Tc-sestamibi scan (Fig. 7.76b) and a degree of retention of tracer in the lesion on the washout images (Fig. 7.76c, d). The SPECT/CT scan showed a clear-cut focus of uptake at the posterior aspect of the lower pole of the left lobe of the thyroid (Fig. 7.77).

7.30.4 Conclusion

1. Findings consistent with incidental detection of a left lower parathyroid adenoma on an ^{18}F-FDG-PET scan confirmed on a ^{99m}Tc-sestamibi dual-phase scan without evidence of biochemical hyperparathyroidism.

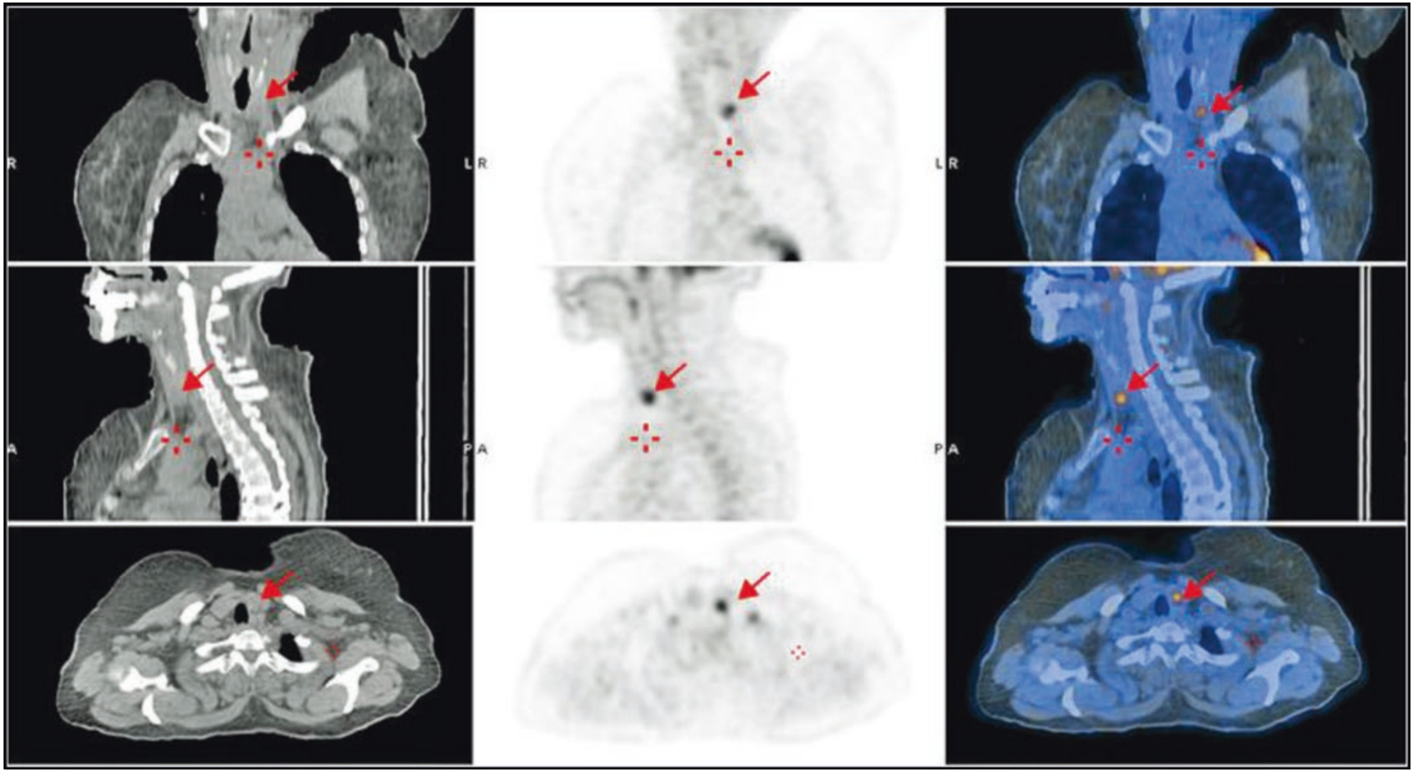

Fig. 7.75 ^{18}F-FDG-PET/CT scan with CT images (left column), PET images (middle column) and fused PET/CT images (right column) in the coronal (top row), sagittal (middle row) and transaxial (bottom row) planes, showing a metabolically active lesion at the posterior aspect of the lower pole of the left thyroid lobe (arrow) measuring 16.3 × 15 × 13.6 mm in size

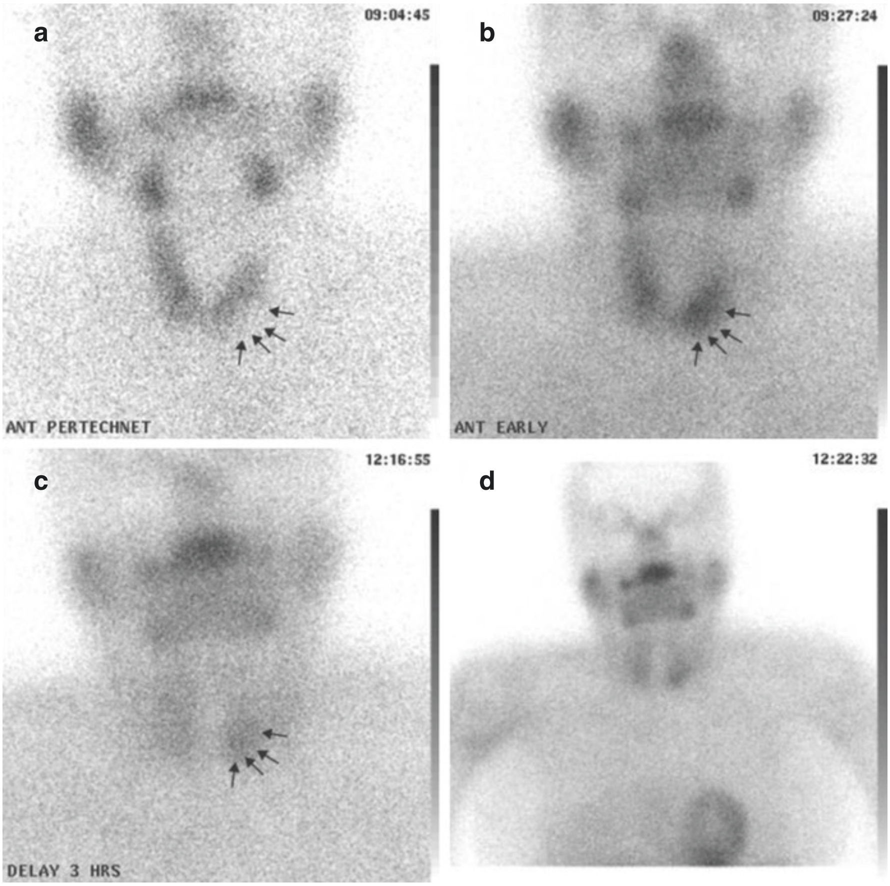

Fig. 7.76 ^{99m}Tc-pertechnetate thyroid scan (**a**), early planar ^{99m}Tc-sestamibi scan (**b**), late planar ^{99m}Tc-sestamibi scan (**c**) and the late ^{99m}Tc-sestamibi unzoomed neck and chest image (**d**). The arrows point to a "cold" lesion on the pertechnetate scan with mild focal increased uptake in the lesion on the early sestamibi scan and retention of tracer in the lesion on the washout images

7.30.5 Comments and Teaching Points

- This is the first reported case of a parathyroid adenoma with normal parathyroid function documented both on sestamibi SPECT and ^{18}F-fluorodeoxyglucose PET scans.
- Almost all parathyroid adenomas reportedly are functional and associated with the biochemical manifestation of hyperparathyroidism (increased level of serum PTH and/or calcium), with only a single report of a parathyroid adenoma without hyperparathyroidism diagnosed on a ^{99m}Tc-sestamibi scan [38].
- However, since parathyroid imaging is not undertaken in patients without biochemical hyperparathyroidism or hypercalcaemia, it is plausible that some patients may harbour undetected adenomatous parathyroid glands. This has

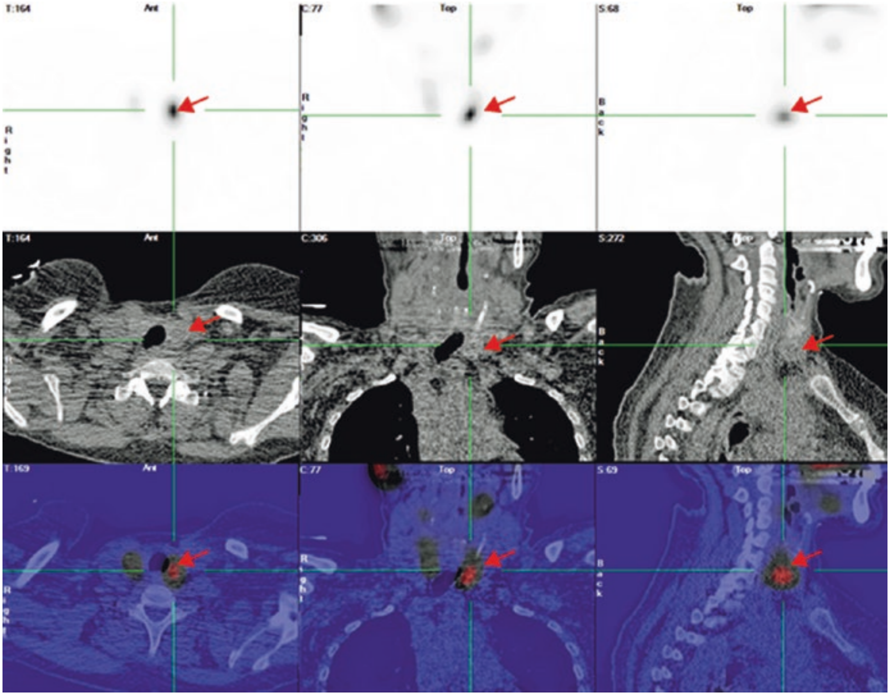

Fig. 7.77 ^{99m}Tc-sestamibi SPECT scan images (top row), CT scan images (middle row) and fused SPECT/CT images (bottom row) in the transaxial (left column), coronal (middle column) and sagittal (right column) planes, showing a left lower parathyroid adenoma

indeed been substantiated through histopathological examination of parathyroid glands during surgery. Histopathologically adenomatous and hyperplastic changes have been noted in 2.4% and 7% of parathyroid glands on dissection in 422 subjects without advanced renal disease and without biochemical hyperparathyroidism or hypercalcaemia, which indicates that early stage of histologic PHPT (hyperplasia or adenoma) may have normal or only mild abnormalities in calcium biomarkers [39].

- There would be two possible reasons for having a non-functioning parathyroid adenoma: either a low level of PTH production or inhibition of the release of the hormone into the bloodstream [38].
- It is presumed that in this patient iatrogenic factors (i.e. calcium and denosumab prescription) may have been responsible for normal serum PTH and Ca^{2+} because calcium intake will reduce the PTH and denosumab (Prolia), a human IgG2 monoclonal antibody used for the treatment of osteoporosis, which causes suppression of osteoclastic activity, can cause significant hypocalcaemia resulting in further reduction of calcium. Denosumab treatment also results in stimulation of parathyroid gland [40]. It is likely that the iatrogenic hypocalcaemia, masked by calcium prescription, is the underlying cause of the adenomatous parathyroid gland detected in this patient.

7.31 Case 7.31. ^{99m}Tc-Pertechnetate-Avid and ^{99m}Tc-Sestamibi-Avid Bilateral Parathyroid Gland Hyperplasia

7.31.1 Background

A 63-year-old female with end-stage renal disease (on dialysis) with hyperparathyroidism was referred for a parathyroid scan. Her serum PTH was very high at 141.6 pmol/L (normal 1.3–9.3), corrected calcium normal at 2.44 mmol/L (normal 2.2–2.6), phosphorus high at 1.63 mmol/L (normal 0.84–1.45), alkaline phosphate high at 210 IU/L (normal 42–98), urea high at 18.2 mmol/L (normal range 2.5–6.4) and creatinine also high at 670 µmol/L (normal range 53–97). The patient's thyroid function tests showed a persistent elevation of serum TSH at 38.43 µIU/mL (normal 0.38–5.33) with a low normal free T4 at 9.52 pmol/L (7.86–15.96).

7.31.2 Procedure

The patient was injected with 94 MBq of ^{99m}Tc-pertechnetate, and a thyroid scan was acquired for 10 min at 15 min postinjection. Next, 773 MBq of ^{99m}Tc-sestamibi was injected without moving the patient and a 10-min duration planar scan performed after 10 min. ^{99m}Tc-sestamibi SPECT/CT scan was performed at 2 h followed by a late planar ^{99m}Tc-sestamibi scan at 3 h.

7.31.3 Findings

The pertechnetate thyroid scan showed a "hot" nodule in the upper part of the right lobe of the thyroid with another "hot" nodule seen in the left lower lobe region, with these two nodules apparently suppressing uptake in the intervening normal thyroid tissue (Fig. 7.78a). The early planar ^{99m}Tc-sestamibi scan showed a pattern of uptake similar to that seen in the thyroid albeit with faint uptake in the thyroid bed (Fig. 7.78b), with the delayed washout sestamibi images showing focal retention of tracer in these lesions (Fig. 7.78c). On the ^{99m}Tc-sestamibi/^{99m}Tc-pertechnetate subtraction image, these two pertechnetate- and sestamibi-avid lesions were subtracted out (Fig. 7.78d).

The SPECT/CT scan (Fig. 7.79) showed a focus of increased uptake behind the upper part of the right lobe of the thyroid measuring 9 × 7.4 × 6.6 mm in size, with another focus of uptake located behind the left lower pole of the thyroid measuring 11 × 8.9 × 7.7 mm in size.

7.31.4 Conclusion

Findings consistent with two pertechnetate- and sestamibi-avid hyperplastic parathyroid glands associated with secondary hyperparathyroidism together with a degree of chronic thyroiditis.

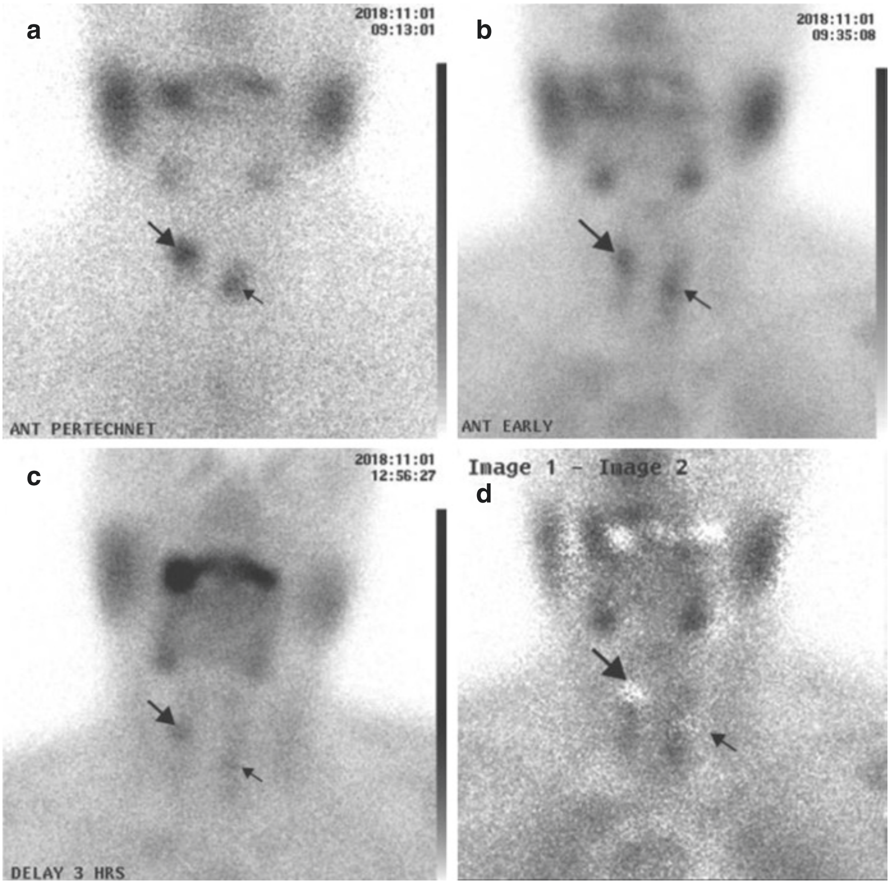

Fig. 7.78 ^{99m}Tc-pertechnetate thyroid scan (**a**), early planar ^{99m}Tc-sestamibi scan (**b**), late planar ^{99m}Tc-sestamibi scan (**c**) and ^{99m}Tc-sestamibi/^{99m}Tc-pertechnetate subtraction scan image (**d**). The large arrow points to the "hot" nodule in the right thyroid lobe and the small arrow to the "hot" nodule in the left thyroid lobe

7.31.5 Comments and Teaching Points

- This is an unusual case of two-gland parathyroid hyperplasia with the hyperplastic parathyroid glands showing both increased pertechnetate and sestamibi uptake with the result that these two glands mimic a thyroid gland with multiple autonomous nodules suggestive of Plummer's disease. This patient's thyroid function tests showed a low normal serum free T4 and a persistently high TSH suggestive of compensated hypothyroidism due to chronic thyroiditis.
- Single parathyroid adenomas showing uptake of both pertechnetate and sestamibi have been previously reported [41], but this appears to be the first case of two-gland parathyroid hyperplasia with both showing pertechnetate and sestamibi avidity.

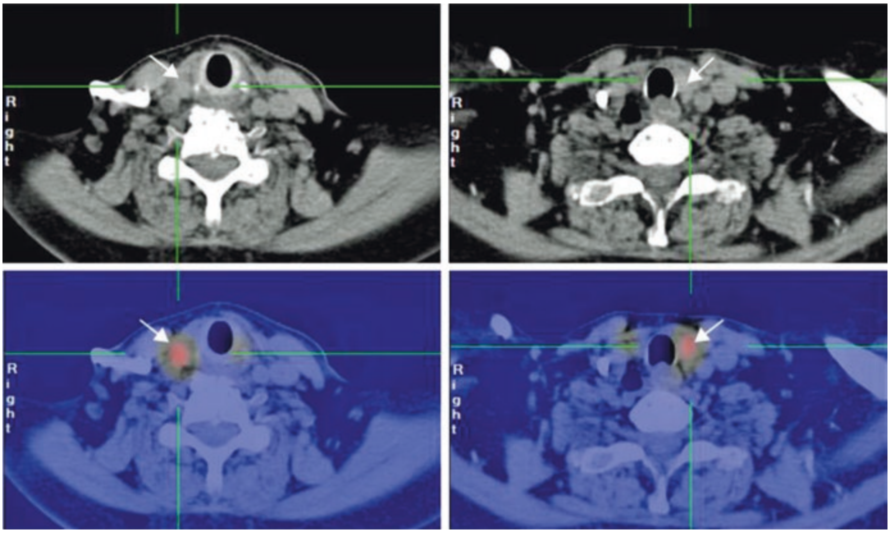

Fig. 7.79 Transaxial CT scan images (upper row) and fused ^{99m}Tc-sestamibi SPECT/CT images (lower row) showing the right and the left hyperplastic parathyroid glands

- The rare cases of pertechnetate-avid parathyroid adenomas have been attributed to hypervascularity [42]. Not all parathyroid lesions retain sestamibi and not all thyroid tissue washes out quickly, and subtraction imaging is helpful in instances [43], but as the two pertechnetate- and sestamibi-avid lesions were subtracted out, the subtraction scan was unhelpful in this case. SPECT/CT is however useful in differentiating the thyroid from the parathyroid lesions through precise anatomical localisation.
- Pertechnetate-avid hyperplastic parathyroid glands though rare should add to the differential diagnosis of single or multiple hyperfunctional autonomous thyroid nodules seen on a pertechnetate thyroid scan.

7.32 Case 7.32. Four-Gland Parathyroid Hyperplasia with Incidental Dextrocardia

7.32.1 Background

A 68-year-old female with end-stage renal disease on dialysis developed biochemical hyperparathyroidism and hyperphosphataemia. Her serum parathormone level was 82.9 pmol/L (normal 1.3–9.3), corrected calcium 2.35 mmol/L (normal 2.2–2.6), phosphorus 1.60 mmol/L (normal 0.84–1.45), alkaline phosphate 283 IU/L (normal 42–98), urea 13.0 mmol/L (normal range 2.5–6.4) and creatinine 469 μmol/L (normal range 53–106).

7.32.2 Procedure

The patient was injected with 67 MBq of ^{99m}Tc-pertechnetate, and a thyroid scan was acquired for 5 min at 20 min postinjection. Next, 748 MBq of ^{99m}Tc-sestamibi was injected without moving the patient and a planar scan performed after 10 min. ^{99m}Tc-sestamibi SPECT/CT scan was performed at 2 h followed by a late planar ^{99m}Tc-sestamibi scan at 3 h.

7.32.3 Findings

The pertechnetate thyroid scan showed a normal-sized image of the thyroid with homogenous distribution of activity in the gland (Fig. 7.80a). The early planar ^{99m}Tc-sestamibi scan (Fig. 7.80b) showed a pattern of uptake similar to that seen on

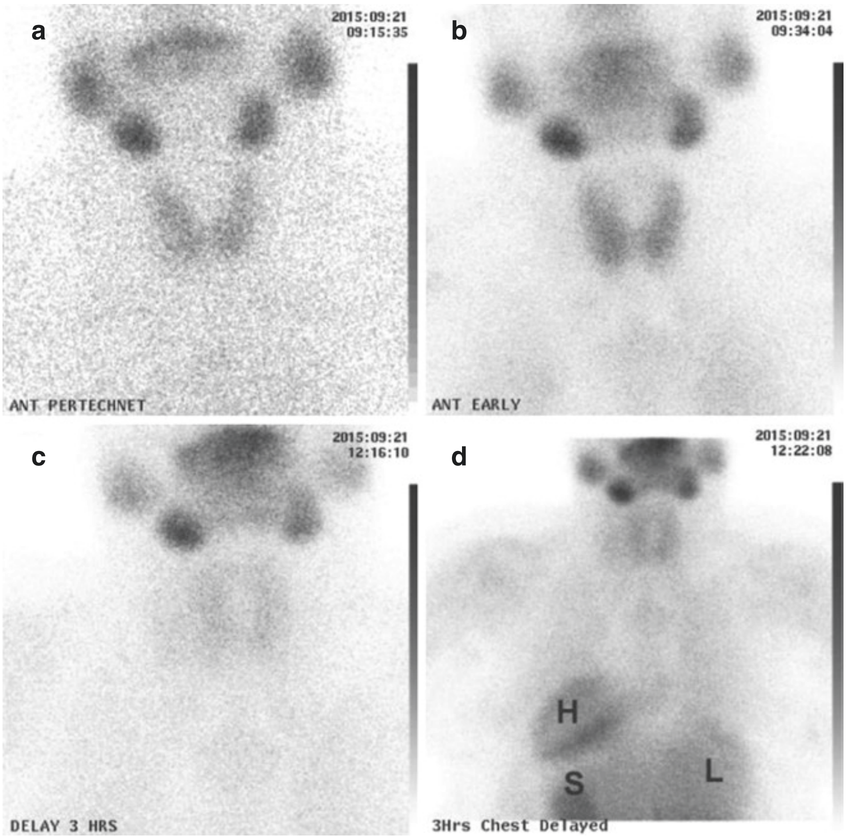

Fig. 7.80 ^{99m}Tc-pertechnetate thyroid scan (**a**), early planar ^{99m}Tc-sestamibi scan (**b**), late planar ^{99m}Tc-sestamibi scan (**c**) and the late unzoomed neck and chest image (**d**). There is homogenous tracer uptake in the thyroid seen on the pertechnetate thyroid scan with fairly uniform uptake in the thyroid on the early ^{99m}Tc-sestamibi image with washout of activity from the thyroid bed on the delayed scan. The unzoomed delayed chest image (**d**) shows situs inversus with transposition of the heart (H), spleen (S) and liver (L)

the pertechnetate thyroid scan with washout of activity from the thyroid bed on the delayed scan (Fig. 7.80c). The unzoomed delayed chest image (Fig. 7.80d) showed dextrocardia with *situs inversus* (transposition of the heart, spleen and liver). The SPECT/CT scan (Fig. 7.81) showed foci of uptake corresponding to the bilateral upper and lower enlarged parathyroid glands (Figs. 7.82 and 7.83).

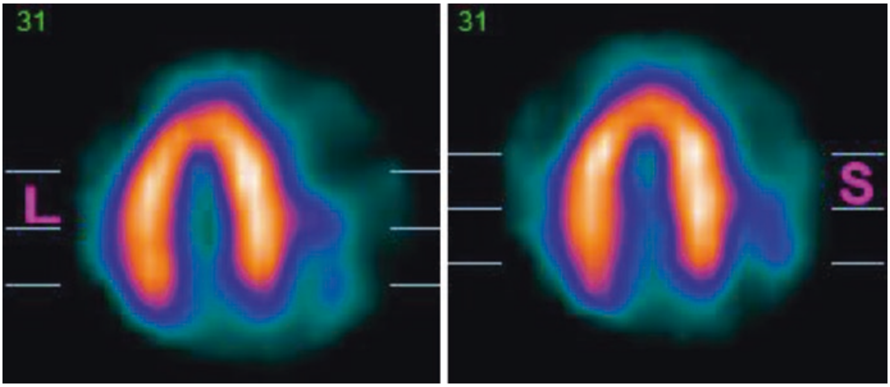

Fig. 7.81 ^{99m}Tc-sestamibi cardiac SPECT scan in the horizontal long axis showing a reversal of septal (S) and lateral wall (L) positions in this patient with dextrocardia. There is normal myocardial perfusion seen

Fig. 7.82 Coronal fused SPECT/CT images showing bilateral hyperplastic upper (**a**) and lower (**b**) parathyroid glands

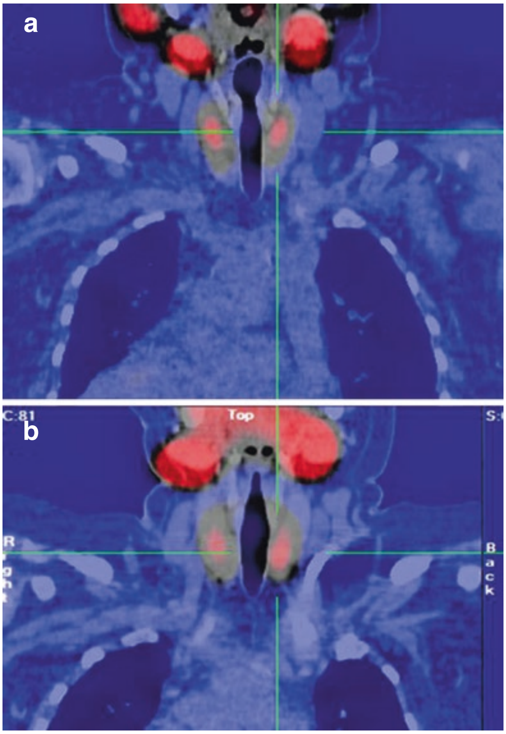

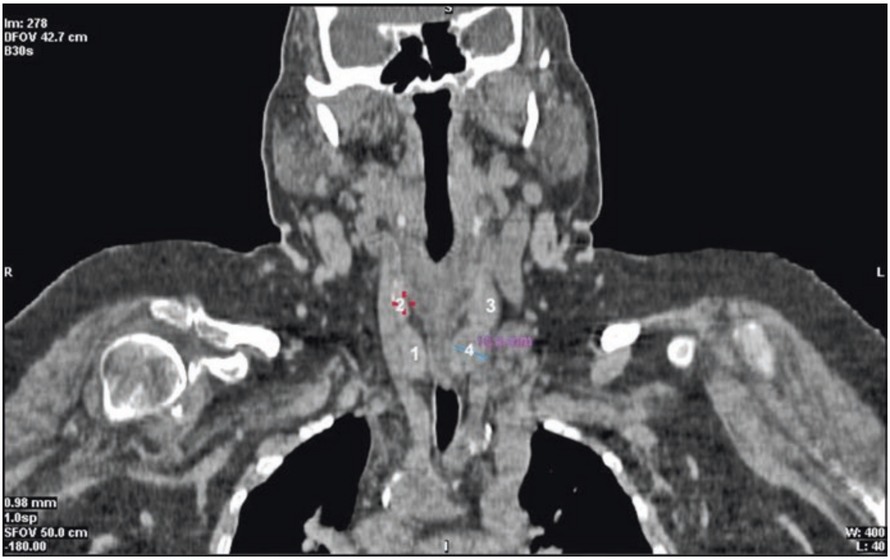

Fig. 7.83 CT component of the SPECT/CT scan showing (1) the right lower parathyroid gland measuring 24.3 × 16.5 × 11.7 mm in size, (2) the right upper gland measuring 20.4 × 10 × 10.7 mm, (3) the left upper gland measuring 23.9 × 7.8 × 7.2 mm and (4) the right lower gland measuring 24.3 × 16.5 × 11.7 mm in size

7.32.4 Conclusion

Findings consistent with four-gland parathyroid hyperplasia associated with secondary hyperparathyroidism. A note is made of incidental *situs inversus* and dextrocardia.

7.32.5 Comments and Teaching Points

- In this patient with fairly large-sized hyperplastic parathyroid glands, the planar imaging was at best equivocal, but all four glands were clearly seen on both the SPECT and the CT components of the SPECT/CT scan.
- As GFR levels fall, calcium reabsorption is impaired, resulting in hypocalcaemia and increased PTH secretion.
- Rising phosphate levels increase PTH levels both directly and indirectly by leading to worsening hypocalcaemia.
- Cardiac disease or abnormalities can frequently be seen on the sestamibi scans as in this case which shows dextrocardia and *situs inversus*.

7.33 Case 7.33. Parathyroid Adenoma + Sestamibi-Avid Thyroid Nodule (Hurthle Cell Carcinoma)

7.33.1 Background

A 77-year-old female presented with generalised body aches and pains with high serum PTH levels. The patient had a history of previous thyroidectomy. Serum PTH was 17.46 pmol/L (normal 1.3–9.3), corrected calcium 2.89 mmol/L (normal 2.2–2.6), phosphorus 1.04 mmol/L (normal 0.84–1.45), magnesium 0.82 mmol/L (normal 0.77–1.03), urea 5.9 mmol/L (normal range 2.5–6.4) and creatinine 81 μmol/L (normal range 53–97).

7.33.2 Procedure

The patient was injected with 60 MBq of ^{99m}Tc-pertechnetate, and a thyroid scan was acquired for 5 min at 20 min postinjection. Next, 831 MBq of ^{99m}Tc-sestamibi was injected without moving the patient and a 10-min duration planar scan performed after 10 min. ^{99m}Tc-sestamibi SPECT/CT scan was performed at 2 h followed by a late planar ^{99m}Tc-sestamibi scan at 3 h.

7.33.3 Findings

The pertechnetate thyroid scan showed no activity in the thyroid bed (Fig. 7.84a) due to the patient on thyroid hormone replacement therapy following previous partial thyroidectomy. The early planar ^{99m}Tc-sestamibi scan showed a large oblong lesion with increased uptake in the region of the left lobe with the delayed sestamibi images showing minimal washout of the tracer (Fig. 7.84b–d). The CT component

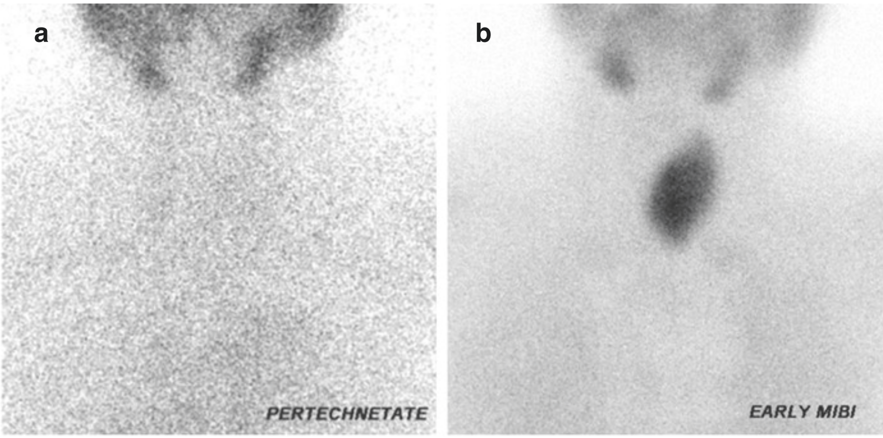

Fig. 7.84 ^{99m}Tc-pertechnetate thyroid scan (**a**), early planar ^{99m}Tc-sestamibi scan (**b**), late planar ^{99m}Tc-sestamibi scan (**c**) and the late ^{99m}Tc-sestamibi unzoomed neck and chest image (**d**)

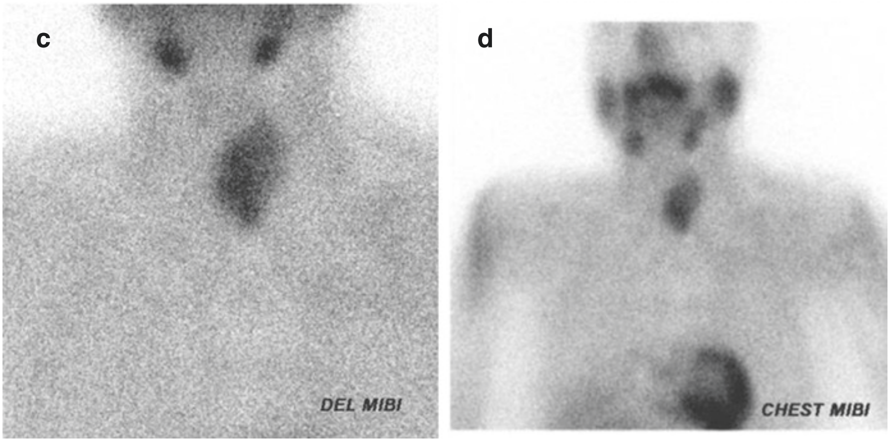

Fig. 7.84 (continued)

of the SPECT/CT scan showed a large anteriorly located nodule measuring 52.5 × 26.8 × 26.1 mm in size in the residual left thyroid lobe causing tracheal deviation to the right (Fig. 7.85). Also, there was a small focus of increased uptake inferior to the lower pole of the left thyroid lobe located just anterior to the vertebral body on the left side of the oesophagus measuring 15 × 10.4 × 8.6 mm in size (Fig. 7.86).

7.33.4 Conclusion

Findings consistent with a small left lower parathyroid adenoma as the cause of PHPT together with sestamibi-avid thyroid adenoma seen only on the SPECT scan. Fine-needle aspiration cytology of the thyroid nodule revealed Hurthle cell carcinoma.

7.33.5 Comments and Teaching Points

- This is a rare case of concomitant Hurthle cell cancer and a parathyroid adenoma.
- Hurthle cell (HC) or oxyphil cell adenoma or carcinoma is an oncogenic neoplasm rich in mitochondria which explains the uptake of ^{99m}Tc-sestamibi in these lesions.
- The term oncocytic metaplasia (OM) indicates the presence of a variable (~75%) number of HC, often mixed with follicular monomorphic and intermediate cells, in benign or malignant thyroid lesions. OM is non-neoplastic hyperplasia of HC and appears to be particularly frequent in Hashimoto's thyroiditis and nontoxic goitre [44–46].

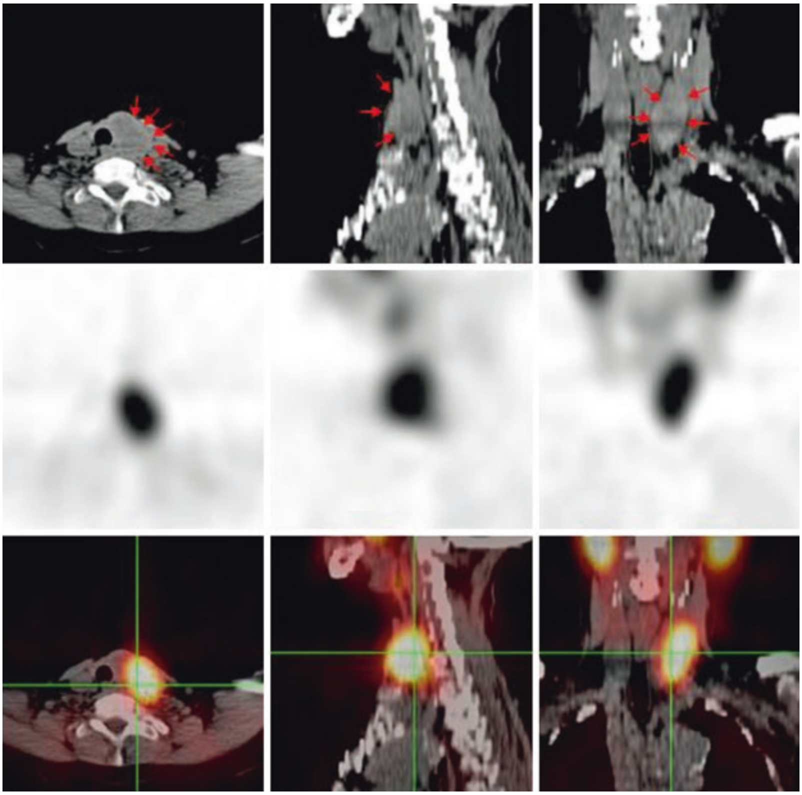

Fig. 7.85 SPECT/CT scan images with CT (top row), SPECT scan images (middle row) and fused SPECT/CT images (bottom row) in the transaxial (left column), sagittal (middle column) and coronal (right column) planes, showing a large ^{99m}Tc-sestamibi-avid left thyroid bed mass measuring 52.5 × 26.8 × 26.1 mm in size

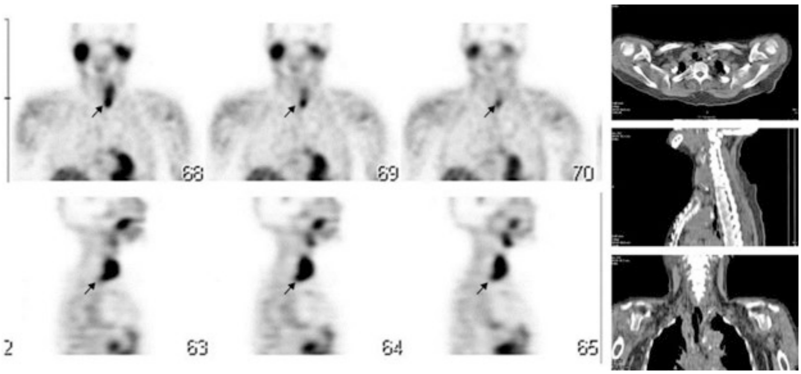

Fig. 7.86 SPECT/CT scan images with SPECT (left panel) in the coronal (top row) and sagittal (bottom row) and CT images (right panel) in the transverse (top), sagittal (middle) and coronal (bottom) planes showing a posteriorly located focus of the uptake at the left thyroid lobe separate from the ^{99m}Tc-sestamibi-avid left thyroid lobe mass (arrows) consistent with a small left lower parathyroid adenoma

- Classically, HC tumours are considered a variant of follicular neoplasms and may be classified as carcinomas or adenomas, based primarily on the architectural features of capsular or vascular invasion.
- High sestamibi uptake considerably increases the probability of differentiated thyroid cancer and facilitates immediate surgical removal, while decreased uptake actually excludes it [36].
- Most HC tumours are sestamibi-positive, but this scan is not sufficiently specific to differentiate true HC neoplasias from other thyroid lesions showing HC at fine-needle aspiration cytology, although a sestamibi-negative scan strongly supports the absence of true HC tumours [47].

7.34 Case 7.34. Single Parathyroid Adenoma Associated with Transient Renal Failure

7.34.1 Background

A 51-year-old male presented with hyperparathyroidism without renal failure. His serum PTH was 169.9 pmol/L (normal 1.3–9.3), corrected calcium 4.29 mmol/L (normal 2.2–2.6), phosphorus 0.86 mmol/L (normal 0.84–1.45), magnesium 0.64 mmol/L (normal 0.73–1.06), urea 3.7 mmol/L (normal range 2.5–6.4) and creatinine 105 μmol/L (normal range 53–97).

7.34.2 Procedure

The patient was injected with 69 MBq of ^{99m}Tc-pertechnetate, and a thyroid scan was acquired for 5 min at 15 min postinjection. Next, 773 MBq of ^{99m}Tc-sestamibi was injected without moving the patient and a 5-min duration planar scan performed after 10 min. ^{99m}Tc-sestamibi SPECT/CT scan was performed at 2 h followed by a late planar ^{99m}Tc-sestamibi scan at 3 h.

7.34.3 Findings

The pertechnetate thyroid scan (Fig. 7.87a) showed a normal-sized image of the thyroid with a relatively larger right lobe and homogenous distribution of activity in the gland. The early planar ^{99m}Tc-sestamibi scan (Fig. 7.87b) showed a pattern of uptake similar to that seen on the pertechnetate thyroid scan. The delayed washout sestamibi images (Fig. 7.87c, d) showed focal retention of tracer in lower right thyroid lobe region.

The ^{99m}Tc-sestamibi SPECT/CT scan showed a clear-cut focus of increased uptake in a well-defined nodule behind the lower pole of the right thyroid lobe, which was seen to measure 31 × 15.2 × 11.4 mm in size on the CT component (Fig. 7.88).

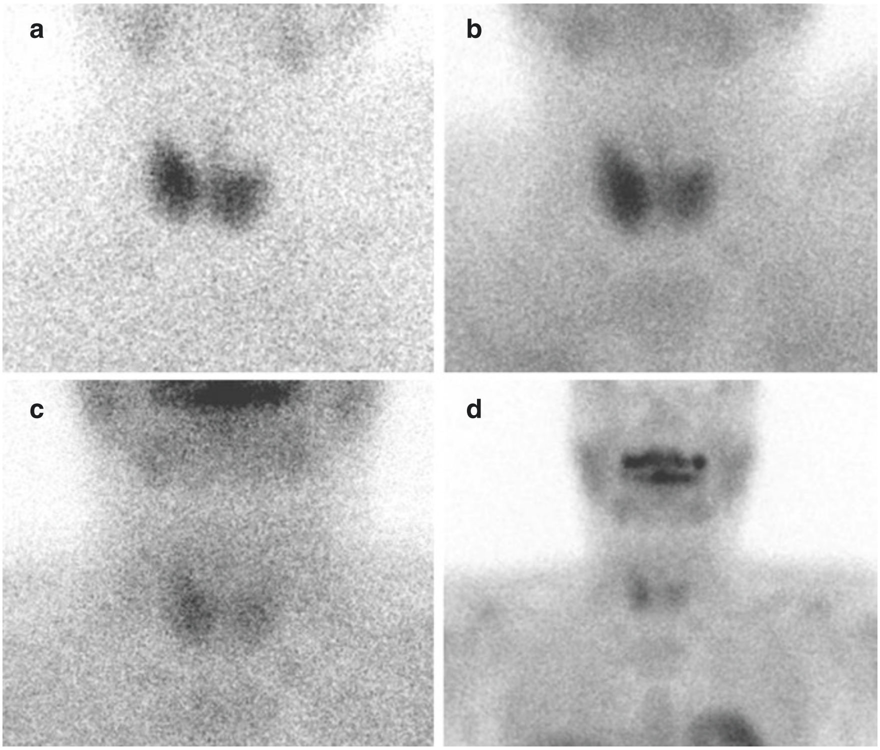

Fig. 7.87 ^{99m}Tc-pertechnetate thyroid scan (**a**), early planar ^{99m}Tc-sestamibi scan (**b**), late planar ^{99m}Tc-sestamibi scan (**c**) and unzoomed late ^{99m}Tc-sestamibi planar neck and chest scan (**d**)

7.34.4 Conclusion

Findings consistent with a right inferior parathyroid adenoma as the cause of primary hyperparathyroidism.

The patient underwent surgery, and a 3 × 2 × 1 cm nodule weighing 3.56 g was removed. The histopathology of the enlarged cellular gland was consistent with a parathyroid adenoma.

Postsurgery, PTH level fell from 169.9 to normal at 3.04 pmol/L (normal 1.3–9.3), and corrected calcium also normalised from 4.29 to 2.45 mmol/L (normal 2.2–2.6). The patient, however, had a transitory renal mild renal failure before the operation with the serum creatinine values rising above normal at 132 μmol/L (normal range 53–97) and subsequently normalising.

7.34.5 Comments and Teaching Points

- Primary hyperparathyroidism is in general not associated with renal failure in the early stages but over time disease progression secondarily leads to renal damage as seen in this case. Sustained renal damage results in secondary hyper-

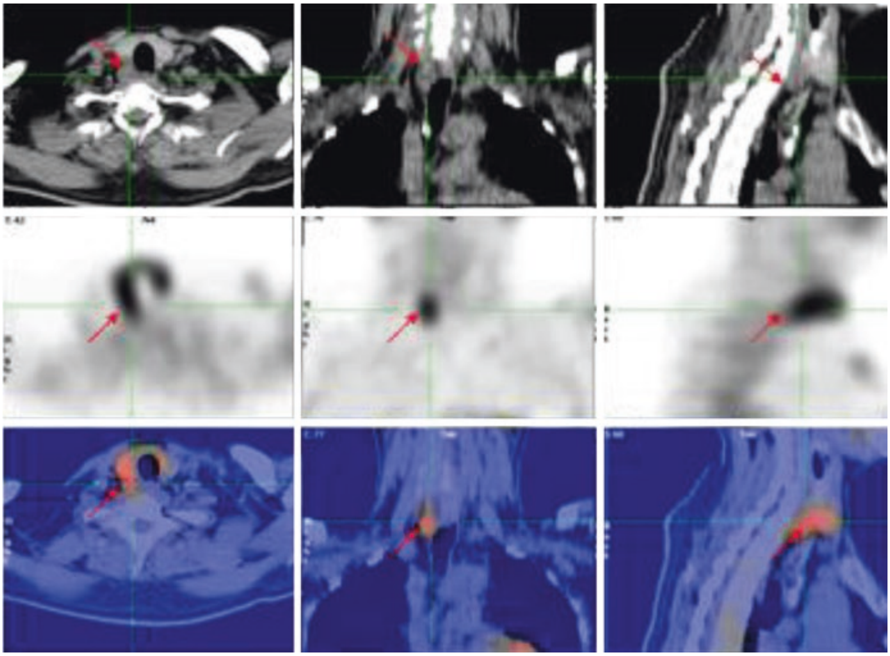

Fig. 7.88 ^{99m}Tc-sestamibi SPECT/CT scan images with CT images (top row), SPECT scan images (middle row) and fused SPECT/CT images (bottom row) in the transaxial (left column), coronal (middle column) and sagittal (right column) planes, showing a right lower parathyroid adenoma (arrows) measuring 18.7 × 16.7 × 17.0 mm in size

parathyroidism, and it becomes difficult to distinguish between the two entities.

- When hyperparathyroidism was first described more than 50 years ago, most patients presented with late-stage complications of prolonged and severe hypercalcaemia, such as abnormalities of the bone (osteitis fibrosa cystica) or kidneys including nephrocalcinosis and renal failure, but current routine laboratory detection of hyperparathyroidism often precedes the development of symptoms [48, 49].

7.35 Case 7.35. Bilateral Upper Parathyroid Gland Hyperplasia

7.35.1 Background

A 32-year-old male with end-stage renal disease on dialysis presented with hyperparathyroidism. The patient had diabetes mellitus, hypertension and bilateral eye blindness. Serum PTH was 134 pmol/L (normal 1.3–9.3), corrected calcium 1.98 mmol/L (normal 2.2–2.6), phosphorus 2.56 mmol/L (normal 0.84–1.45), alkaline phosphatase 146 IU/L (normal 42–98), magnesium 0.83 mmol/L (normal

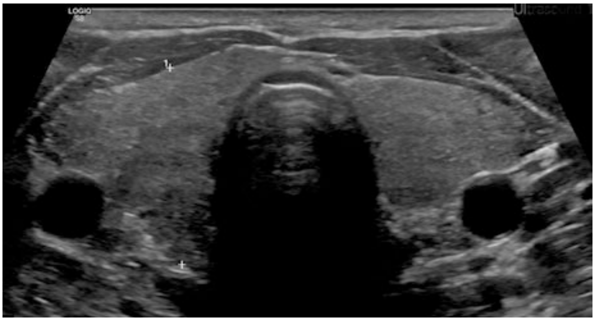

Fig. 7.89 Thyroid ultrasound showing a mildly enlarged thyroid gland with multiple isoechoic nodules in both thyroid lobes

0.73–1.06), urea 19 mmol/L (normal range 2.5–6.4) and creatinine 1031 μmol/L (normal range 53–97). Ultrasound of the neck (Fig. 7.89) showed a mildly enlarged thyroid gland with multiple isoechoic nodules in both thyroid lobes with no abnormal vascularity seen on the Doppler image. His bone mineral density measurements were consistent with osteoporosis.

7.35.2 Procedure

The patient was injected with 70 MBq of ^{99m}Tc-pertechnetate, and a thyroid scan was acquired for 10 min at 15 min postinjection. Next, 859 MBq of ^{99m}Tc-sestamibi was injected without moving the patient and a 10-min duration planar scan performed after 10 min. ^{99m}Tc-sestamibi SPECT/CT scan was performed at 2 h followed by a late planar ^{99m}Tc-sestamibi scan at 3 h.

7.35.3 Findings

The pertechnetate thyroid scan showed a mildly enlarged thyroid with homogenous distribution of activity in the gland (Fig. 7.90a). The early planar ^{99m}Tc-sestamibi scan showed diffuse uptake in the thyroid with relatively more prominent uptake in the right thyroid lobe, with no focal retention noted in the thyroid bed on the delayed washout images (Fig. 7.90b, c). The ^{99m}Tc-sestamibi/^{99m}Tc-pertechnetate subtraction scan images showed a residual focus of activity in the lower right thyroid lobe region (Fig. 7.90d).

The ^{99m}Tc-sestamibi SPECT/CT scan with colour and greyscale optimisation showed a large focus of uptake in the mid right lobe region adjacent to the trachea measuring 22 × 13 × 12 mm in size. A smaller lesion measuring 24 × 14 × 14 mm was seen behind the middle one-third of the left thyroid lobe (Fig. 7.91).

7.35.4 Conclusion

Findings consistent with parathyroid gland hyperplasia involving the upper two parathyroid glands as a consequence of secondary hyperparathyroidism.

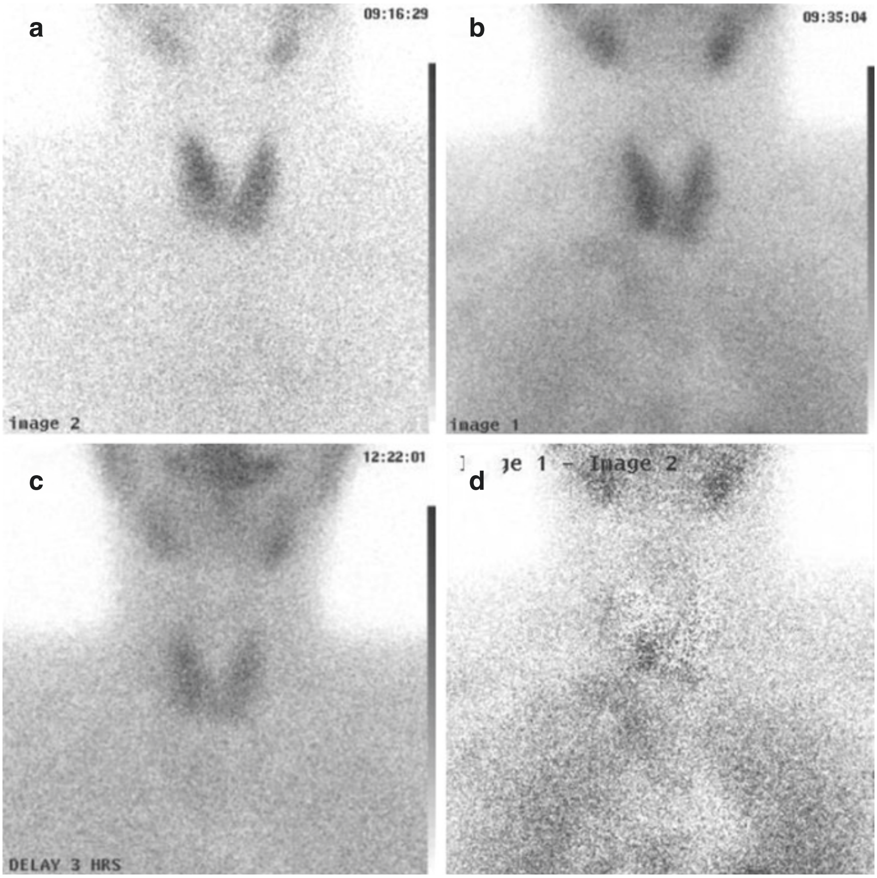

Fig. 7.90 ^{99m}Tc-pertechnetate thyroid scan (**a**), early planar ^{99m}Tc-sestamibi scan (**b**), late planar ^{99m}Tc-sestamibi scan (**c**) and ^{99m}Tc-sestamibi/^{99m}Tc-pertechnetate subtraction scan images (**d**)

7.35.5 Comments and Teaching Points

- Both parathyroid glands were undetectable on planar sestamibi two-phase imaging. However, the ^{99m}Tc-sestamibi/^{99m}Tc-pertechnetate subtraction scan still helped in identifying the larger right hyperplastic parathyroid gland. It appears that adding image subtraction to the image processing algorithm can be helpful. Subtraction scintigraphy is reportedly superior to dual-phase scintigraphy for identification of single- or multiple-gland disease [19].

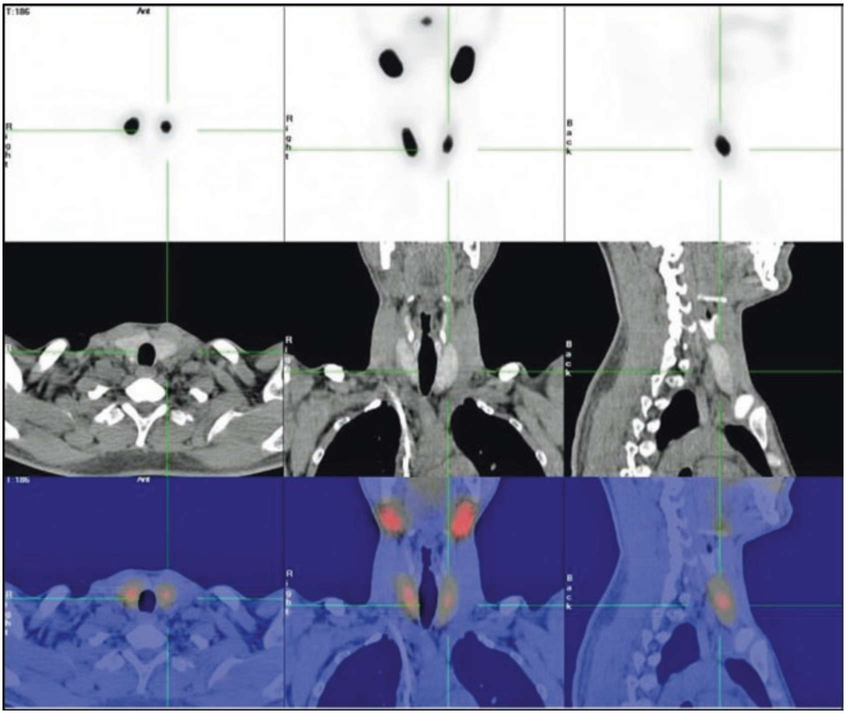

Fig. 7.91 ^{99m}Tc-sestamibi SPECT/CT scan images with SPECT scan images (top row), CT images (middle row) and fused SPECT/CT images (bottom row) in the transaxial (left column), coronal (middle column) and sagittal (right column) planes, showing a larger right and a smaller left parathyroid gland hyperplasia

7.36 Case 7.36. Concomitant Multinodular Goitre and Parathyroid Adenoma

7.36.1 Background

A 60-year-old female attended the endocrine outpatient clinic with a neck swelling. Laboratory tests revealed high serum PTH and calcium levels. Serum PTH was 15.40 pmol/L (normal 1.3–9.3), corrected calcium 2.75 mmol/L (normal 2.2–2.6), phosphorus 1.08 mmol/L (normal 0.84–1.45), alkaline phosphatase 71 IU/L (normal 42–98), magnesium 0.88 mmol/L (normal 0.73–1.06), urea 2.8 mmol/L (normal range 2.5–6.4) and creatinine 52 µmol/L (normal range 53–97). Serum TSH was 0.86 µIU/mL (normal 0.27–4.2) and free T4 13.83 pmol/L (normal 7.86–14.4).

7.36.2 Procedure

The patient was injected with 50 MBq of ^{99m}Tc-pertechnetate, and a thyroid scan was acquired for 5 min at 20 min postinjection. Next, 823 MBq of ^{99m}Tc-sestamibi

was injected without moving the patient and a 10-min duration planar scan performed after 10 min. ^{99m}Tc-sestamibi SPECT/CT scan was performed at 2 h followed by a late planar ^{99m}Tc-sestamibi scan at 3 h.

7.36.3 Findings

The pertechnetate thyroid scan (Fig. 7.92a) showed a markedly enlarged left thyroid lobe with reduced heterogeneous tracer distribution consistent with a multinodular gland. The early planar ^{99m}Tc-sestamibi scan (Fig. 7.92b) showed a multinodular thyroid with a small nodule at the lower edge of the left thyroid lobe with slightly increased uptake. No focal retention was noted in the nodule on the delayed washout images, however (Fig. 7.92c). The ^{99m}Tc-sestamibi/^{99m}Tc-pertechnetate subtraction

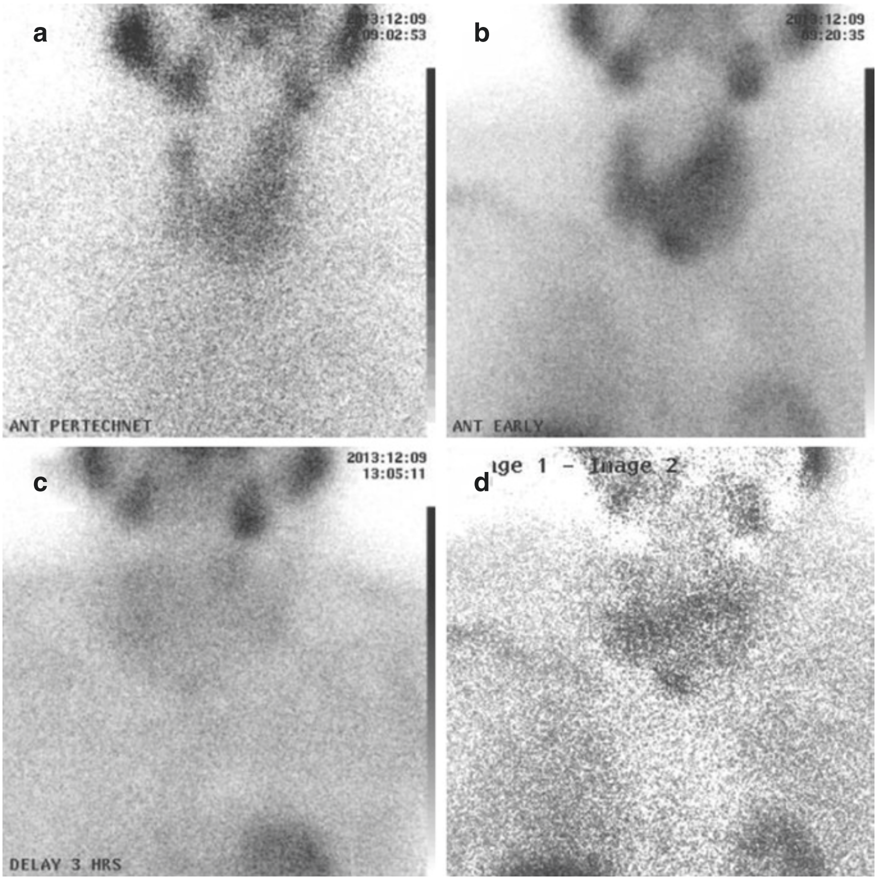

Fig. 7.92 ^{99m}Tc-pertechnetate thyroid scan (**a**), early planar ^{99m}Tc-sestamibi scan (**b**), late planar ^{99m}Tc-sestamibi scan (**c**) and ^{99m}Tc-sestamibi/^{99m}Tc-pertechnetate subtraction scan images (**d**)

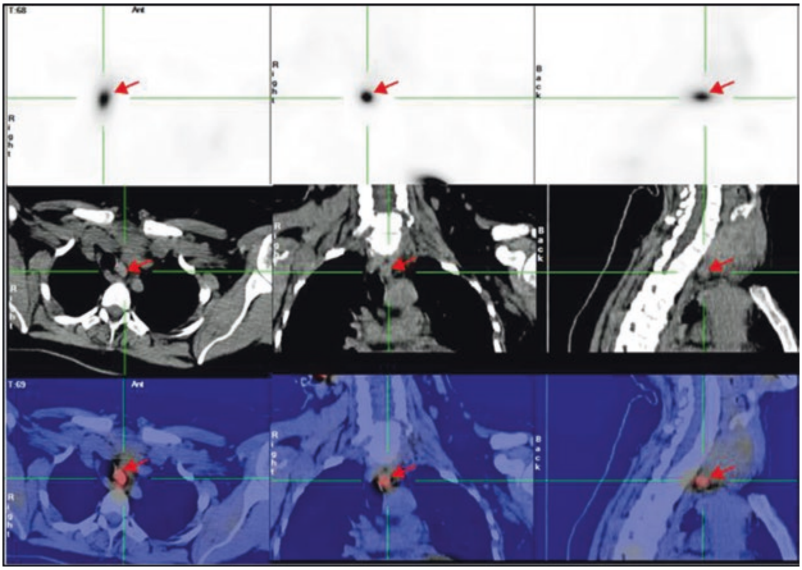

Fig. 7.93 ^{99m}Tc-sestamibi SPECT/CT scan images with SPECT scan images (top row), CT images (middle row) and fused SPECT/CT images (bottom row) in the transaxial (left column), coronal (middle column) and sagittal (right column) planes

scan images showed multiple residual foci of activity within the thyroid bed (Fig. 7.92d). The ^{99m}Tc-sestamibi SPECT/CT scan (Fig. 7.93) showed tracheal deviation to the right caused by the enlarged left thyroid lobe and a clear-cut focus of uptake in the superior mediastinum located on the left side of the trachea at C7/T1 vertebral level, which corresponded to the left lower pole nodule seen on the planar image. The lesion measured 13.6 × 11.5 × 10 mm in size on the CT image (Fig. 7.94).

7.36.4 Conclusion

Findings consistent with multinodular goitre with a left lower parathyroid adenoma as the cause of primary hyperparathyroidism.

The patient underwent total thyroidectomy with solid and cystic nodules seen in both the lobes. The ectopic parathyroid nodule measuring 2.5 × 1.5 × 1.2 cm was also removed and was confirmed as a parathyroid adenoma on histopathology. The PTH and the serum calcium levels normalised postsurgery.

7.36.5 Comments and Teaching Points

- This case with a coexisting multinodular goitre and a parathyroid adenoma showed the unsuitability of planar parathyroid scintigraphy for the diagnosis of a hyperactive parathyroid lesion.

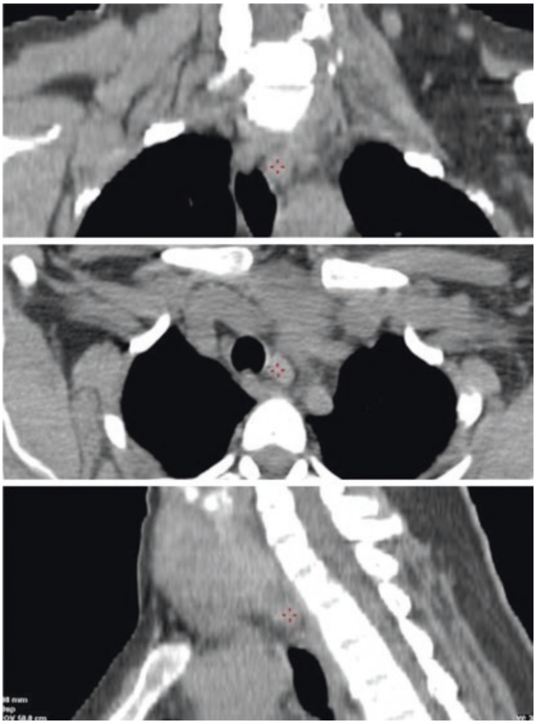

Fig. 7.94 CT component of the SPECT/CT scan in coronal (top) transaxial (middle) and sagittal (bottom) axes showing a multinodular thyroid gland with a small left lower parathyroid adenoma (cross) measuring 13.6 × 11.5 × 10 mm in size

- Parathyroid SPECT/CT was crucial to the diagnosis of the parathyroid adenoma through precise localisation of the hyperactive parathyroid lesion.
- Variable uptake and retention in the hyperactive parathyroid lesions in the presence of multinodular goitre hampers lesion detection and image subtraction as seen in this case causing both false-positive and false-negative results.

7.37 Case 7.37. Resected Parathyroid Adenoma with Possible Recurrence

7.37.1 Background

A 59-year-old male with diabetes mellitus and hypertension presented with leg and foot pain and biochemical evidence of hyperparathyroidism with raised serum PTH and calcium. Serum PTH was 104.74 pmol/L (normal 1.3–9.3), corrected calcium 3.08 mmol/L (normal 2.2–2.6), phosphorus 0.63 mmol/L (normal 0.84–1.45), alkaline phosphatase 467 IU/L (normal 42–98), magnesium 0.78 mmol/L (normal 0.73–1.06), urea 3.1 mmol/L (normal range 2.5–6.4) and creatinine 34 μmol/L (normal range 53–97).

7.37.2 Procedure

The patient was injected with 58 MBq of ^{99m}Tc-pertechnetate, and a thyroid scan acquired for 5 min at 20 min postinjection. Next, 820 MBq of ^{99m}Tc-sestamibi was injected without moving the patient and a 10-min duration planar scan performed after 10 min. ^{99m}Tc-sestamibi SPECT/CT scan was performed at 2 h followed by a late planar ^{99m}Tc-sestamibi scan at 3 h.

7.37.3 Findings

The pertechnetate thyroid scan showed uniform radiotracer uptake in the thyroid gland (Fig. 7.95a) with the early planar ^{99m}Tc-sestamibi scan showing a similar pattern of uptake (Fig. 7.95b) but the 3-h late ^{99m}Tc-sestamibi scan showing focal retention of activity at the lower pole of the right thyroid lobe (Fig. 7.95c) and the ^{99m}Tc-sestamibi/^{99m}Tc-pertechnetate subtraction scan image showed a small residual focus of activity at the right lower pole region of the thyroid bed (Fig. 7.95d). The ^{99m}Tc-sestamibi SPECT/CT scan (Fig. 7.96a) showed a clear-cut focus of activity corresponding to a 12 × 11 × 7.4 mm size nodule on the right side of trachea above the level of the sternum (Fig. 7.96).

7.37.4 Conclusion

Findings consistent with a right lower parathyroid adenoma as the cause of primary hyperparathyroidism.

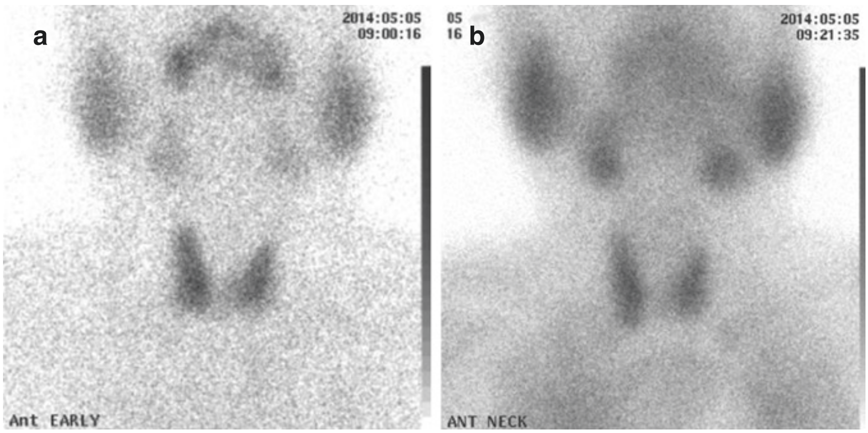

Fig. 7.95 ^{99m}Tc-pertechnetate thyroid scan (**a**), early planar ^{99m}Tc-sestamibi scan (**b**), late planar ^{99m}Tc-sestamibi scan (**c**) and ^{99m}Tc-sestamibi/^{99m}Tc-pertechnetate subtraction scan images (**d**)

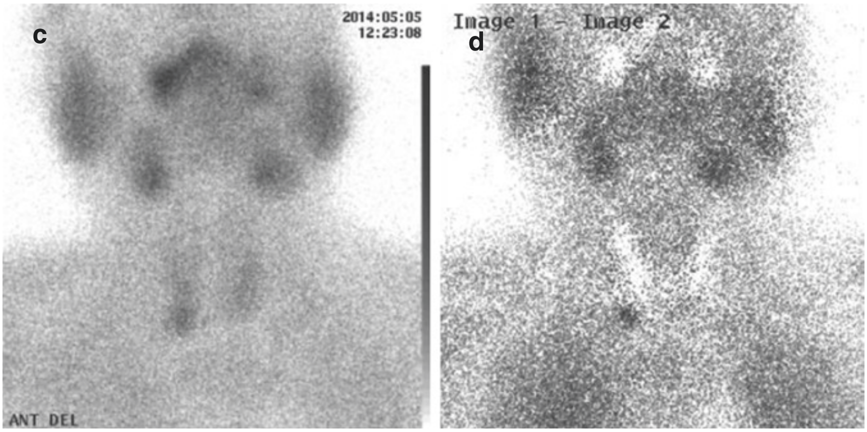

Fig. 7.95 (continued)

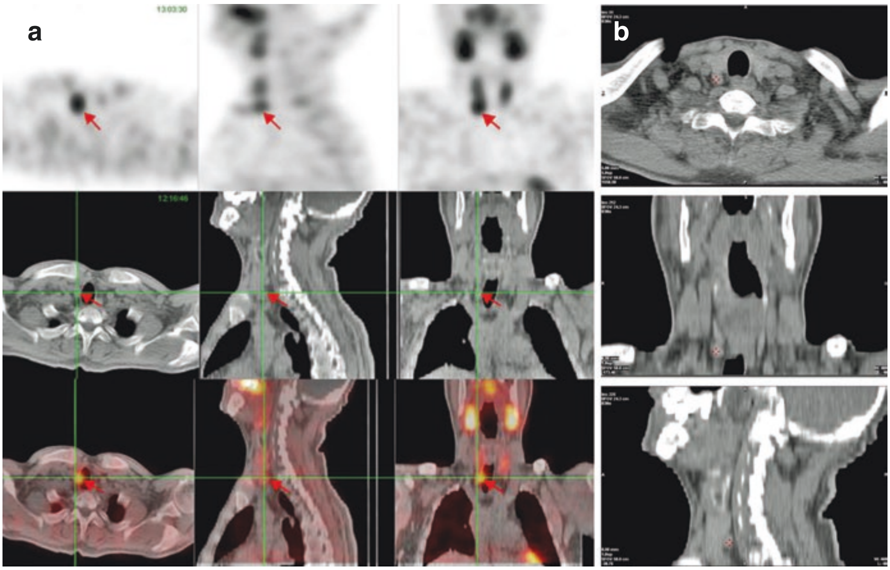

Fig. 7.96 ^{99m}Tc-sestamibi SPECT/CT scan images (**a**) with SPECT scan images (top row), CT images (middle row) and fused SPECT/CT images (bottom row) in the transaxial (left column), coronal (middle column) and sagittal (right column) planes, showing a right lower parathyroid adenoma (arrows) measuring 12 × 11 × 7.4 mm on the CT scan (**b**)

Surgical excision of the right lower parathyroid gland was performed and a 1 × 1 × 0.5 cm nodule removed with the histopathology confirming a parathyroid adenoma.

The PTH and the serum calcium levels normalised post-surgery, with the serum PTH level falling to 1.08 pmol/L and calcium to 2.32 mmol/L. The patient remained asymptomatic for the next year after which period his calcium and PTH levels have again risen and a second parathyroid scan is being scheduled to establish the cause of recurrent hyperparathyroidism.

7.37.5 Comments and Teaching Points

- This likely represents a case of recurrent PHPT presumably due to a second parathyroid adenoma following successful resection of the first adenoma. Parathyroid surgery is deemed successful when serum calcium level is normal at 6 months after surgery.
- When calcium levels are initially normal after parathyroid surgery but after 6 months again become abnormal, it is considered as "recurrent primary hyperparathyroidism". Recurrent hyperparathyroidism usually results from one or more of the remaining glands becoming hyperactive [50].
- Reoperative parathyroid surgery may be required in patients who have persistent primary hyperparathyroidism after an unsuccessful operation and in patients who had an initially successful exploration but develop recurrent disease at an interval greater than 6 months postoperatively.

7.38 Case 7.38. Papillary Thyroid Carcinoma Masquerading as an Intrathyroidal Parathyroid Adenoma

7.38.1 Background

A 46-year-old female presented with hypercalcaemia and mildly raised PTH levels. Her serum PTH was 10.52 pmol/L (normal 1.3–9.3), corrected calcium 2.78 mmol/L (normal 2.2–2.6), phosphorus 1.83 mmol/L (normal 0.84–1.45), alkaline phosphatase 61 IU/L (normal 42–98), magnesium 0.66 mmol/L (normal 0.73–1.06), urea 1.9 mmol/L (normal range 2.5–6.4) and creatinine 32 μmol/L (normal range 53–97).

7.38.2 Procedure

The patient was injected with 59 MBq of ^{99m}Tc-pertechnetate, and a thyroid scan was acquired for 5 min at 20 min postinjection. Next, 820 MBq of ^{99m}Tc-sestamibi was injected without moving the patient and a 10-min duration planar scan performed after 10 min. ^{99m}Tc-sestamibi SPECT/CT scan was performed at 2 h followed by a late planar ^{99m}Tc-sestamibi scan at 3 h.

7.38.3 Findings

The pertechnetate thyroid scan showed uniform radiotracer uptake in a normal-sized thyroid gland (Fig. 7.97a) with the early planar ^{99m}Tc-sestamibi scan showing a focus of relatively increased uptake in the lower left lobe of the thyroid (Fig. 7.97b), which region showed mild relative decreased uptake on the pertechnetate thyroid

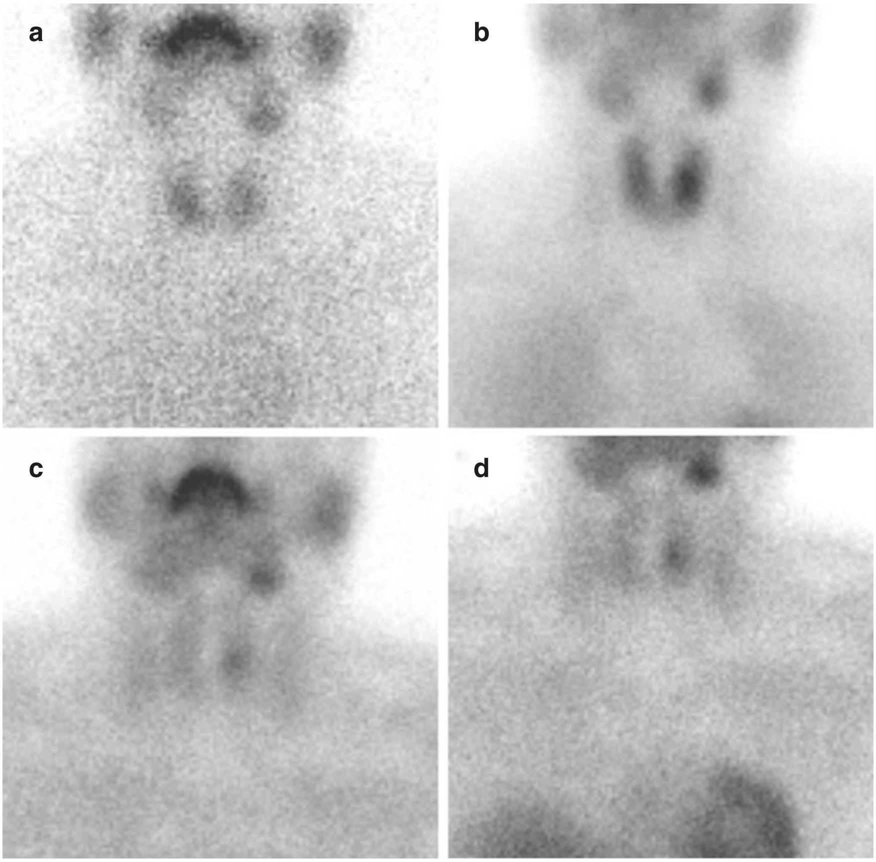

Fig. 7.97 ^{99m}Tc-pertechnetate thyroid scan (**a**), early planar ^{99m}Tc-sestamibi scan (**b**), late planar ^{99m}Tc-sestamibi scan (**c**) and unzoomed neck and chest late planar ^{99m}Tc-sestamibi scan images (**d**)

scan. The delayed 3-h ^{99m}Tc-sestamibi scans showed focal retention of activity here (Fig. 7.97c, d). The ^{99m}Tc-sestamibi SPECT/CT scan (Fig. 7.98) showed a clear-cut focus of activity in the left thyroid lobe located posteriorly measuring 17 × 16.4 mm on the CT component (Fig. 7.98).

7.38.4 Conclusion

The scan findings were consistent with a left lower intrathyroidal parathyroid adenoma as the cause of primary hyperparathyroidism.

At surgery, partial excision of the left thyroid lobe was performed along with an enlarged local lymph node. Histopathology of the nodule showed papillary carcinoma (follicular type) with a section of the lymph node showing metastatic deposit from the thyroid carcinoma. The thyroid tissue showed lymphocytic thyroiditis.

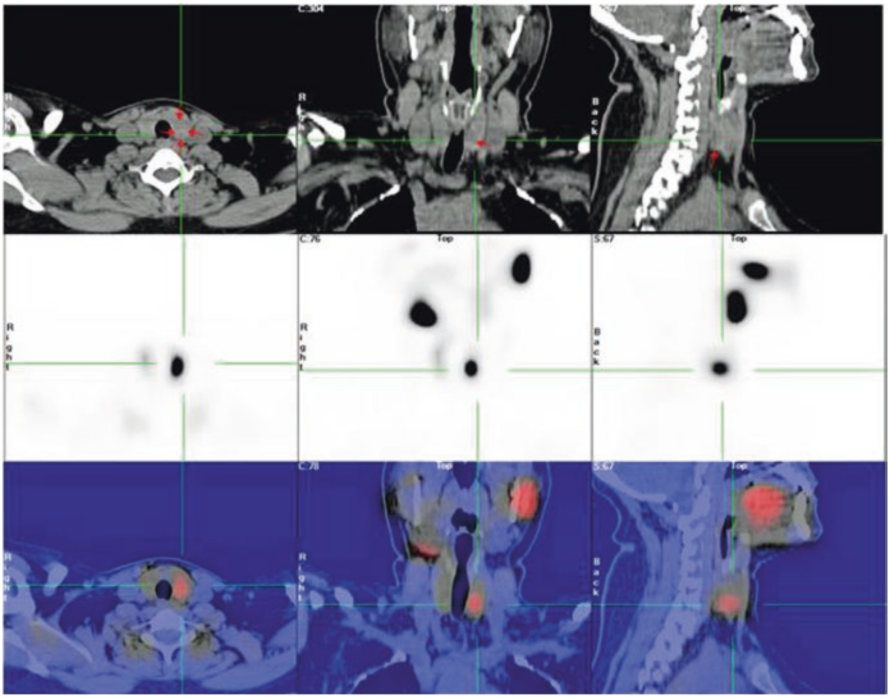

Fig. 7.98 ^{99m}Tc-sestamibi SPECT/CT scan images with CT scan images (top row), SPECT images (middle row) and fused SPECT/CT images (bottom row) in the transaxial (left column), coronal (middle column) and sagittal (right column) planes, showing a left lower thyroid lobe nodule presumed an intrathyroidal parathyroid adenoma measuring 17 × 16.4 mm on the CT component (arrows)

The PTH and the serum calcium levels normalised postsurgery, with the serum PTH level falling to below normal at 0.09 (previously 10.52 pmol/L) and calcium to 2.2 (previously 2.78 mmol/L).

The final diagnosis was a false-positive parathyroid adenoma due to sestamibi-positive papillary thyroid carcinoma.

7.38.5 Comments and Teaching Points

- Abnormal intrathyroidal parathyroid glands are indistinguishable from thyroid adenomas or thyroid cancer. False-positive parathyroid scan secondary to a thyroid follicular cancer has been reported [51].
- Papillary thyroid carcinoma is the most common cancer of the thyroid with a female preponderance and constitutes more than 70% of thyroid malignancies and can present either as a single nodule or can be multifocal.
- In patients with hypercalcaemia detected unexpectedly on a biochemical profile, the most important cause of the hypercalcaemia to exclude is hypercalcaemia associated with malignancy.

- Few cases exist in which the production and secretion of PTH by malignant non-parathyroid tumours have been authenticated [52].

7.39 Case 7.39. Synchronous Parathyroid Adenoma and Papillary Thyroid Carcinoma (Oncocytic Variant)

7.39.1 Background

A 39-year-old female presented with neck swelling and biochemical evidence of primary hyperparathyroidism. Her serum PTH was 43.29 pmol/L (normal 1.3–9.3), corrected calcium 3.08 mmol/L (normal 2.2–2.6), phosphorus 0.83 mmol/L (normal 0.84–1.45), alkaline phosphatase 169 IU/L (normal 42–98), magnesium 0.82 mmol/L (normal 0.73–1.06), urea 3.3 mmol/L (normal range 2.5–6.4) and creatinine 48 μmol/L (normal range 53–97).

7.39.2 Procedure

The patient was injected with 87 MBq of ^{99m}Tc-pertechnetate, and a thyroid scan was acquired for 5 min at 20 min postinjection. Next, 825 MBq of ^{99m}Tc-sestamibi was injected without moving the patient and a 10-min duration planar scan performed after 10 min. ^{99m}Tc-sestamibi SPECT/CT scan was performed at 2 h followed by a late planar ^{99m}Tc-sestamibi scan at 3 h.

7.39.3 Findings

The pertechnetate thyroid scan (Fig. 7.99a) showed an enlarged right lobe of the thyroid with a large area of reduced uptake occupying the lower two-thirds of the lobe surrounded by a rim of activity (arrows), with the early planar ^{99m}Tc-sestamibi scan (Fig. 7.99b) showing no uptake in this area (arrows); however, there was an oval-shaped focal area of uptake seen occupying lower half of the left lobe of the thyroid which appeared cold on the pertechnetate thyroid scan (arrowheads). The delayed 3-h ^{99m}Tc-sestamibi scans showed retention of activity here (Fig. 7.99c, d). The ^{99m}Tc-sestamibi SPECT/CT scan (Fig. 7.100a) showed a large nodule with intense uptake located posterior to the left lower thyroid lobe region, measuring 31 × 21 × 25 mm in size on the CT component. The cold nodule in the left thyroid lobe with absent sestamibi uptake is seen to measure 27 × 15.5 × 18.3 mm in size (Fig. 7.100b).

7.39.4 Conclusion

Findings consistent with a large left lower parathyroid adenoma as the cause of primary hyperparathyroidism together with a dominant cold (non-functional) right thyroid lobe nodule which needed further investigation to rule out thyroid malignancy.

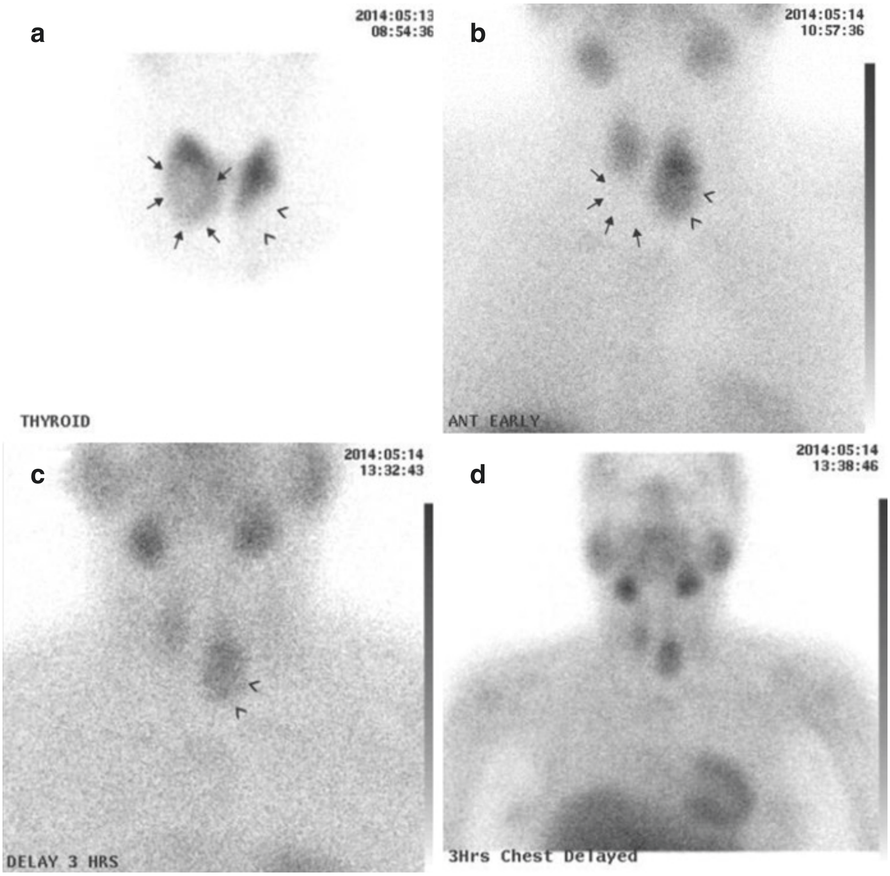

Fig. 7.99 ^{99m}Tc-pertechnetate thyroid scan (**a**), early planar ^{99m}Tc-sestamibi scan (**b**), late planar ^{99m}Tc-sestamibi scan (**c**) and unzoomed neck and chest late planar ^{99m}Tc-sestamibi scan images (**d**)

Total thyroidectomy was performed, and histopathology confirmed a 10 g left lower parathyroid adenoma together with 21 g right thyroid lobe containing a unifocal tumour with microscopic features of an oncocytic variant of papillary thyroid carcinoma. The PTH and the serum calcium levels normalised postsurgery.

7.39.5 Comments and Teaching Points

- Concurrent presence of papillary thyroid carcinoma and parathyroid adenoma is rare [53, 54].
- The association of thyroid disease and primary hyperparathyroidism is well described, with thyroid carcinoma being reported in 2–15% of cases. There are several reports of an increased occurrence of non-parathyroid cancers in patients with PHPT [55, 56].

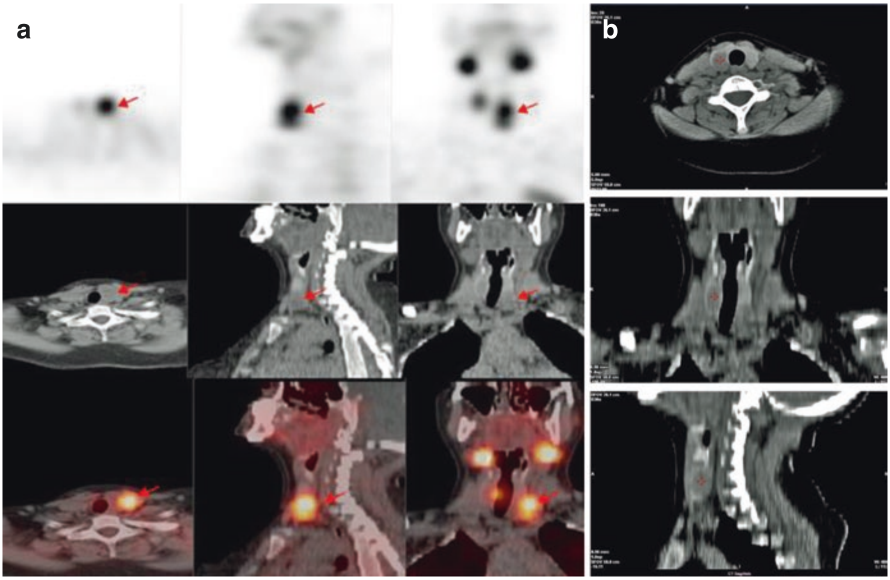

Fig. 7.100 ^{99m}Tc-sestamibi SPECT/CT scan images (**a**) with SPECT scan images (top row), CT images (middle row) and fused SPECT/CT images (bottom row) in the transaxial (left column), sagittal (middle column) and coronal (right column) planes, showing a large left lower parathyroid adenoma (arrows) measuring 31 × 21 × 25 mm and a dominant cold (non-functional) right thyroid lobe nodule (cross) measuring 27 × 15.5 × 18.3 mm in size on the CT component (**b**)

7.40 Case 7.40. Single Parathyroid Adenoma with Reversible Renal Damage

7.40.1 Background

A 41-year-old male presented with elevated serum parathormone with his neck US showing a left parathyroid adenoma (Fig. 7.101). His serum PTH was 18.34 pmol/L (normal 1.3–9.3), corrected calcium 3.22 mmol/L (normal 2.2–2.6), phosphorus 0.46 mmol/L (normal 0.84–1.45), alkaline phosphatase 179 IU/L (normal 42–98), magnesium 0.66 mmol/L (normal 0.73–1.06), urea 4.5 mmol/L (normal range 2.5–6.4) and creatinine 153 μmol/L (normal range 74–115).

7.40.2 Procedure

The patient was injected with 55 MBq of ^{99m}Tc-pertechnetate, and a thyroid scan was acquired for 5 min at 20 min postinjection. Next, 800 MBq of ^{99m}Tc-sestamibi was injected without moving the patient and a 10-min duration planar scan performed after 10 min. ^{99m}Tc-sestamibi SPECT/CT scan was performed at 2 h followed by a late planar ^{99m}Tc-sestamibi scan at 3 h.

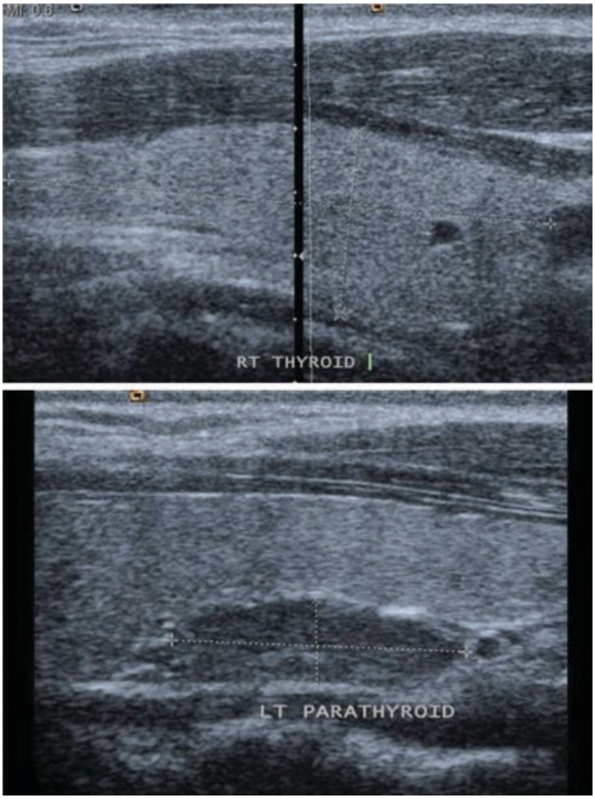

Fig. 7.101 Thyroid ultrasound showing a normal right lobe (top) and a parathyroid adenoma at the posterior aspect of the left thyroid (bottom)

7.40.3 Findings

The pertechnetate thyroid scan (Fig. 7.102a) showed a normal-sized image of the gland with homogenous distribution of activity, with the early planar ^{99m}Tc-sestamibi scan (Fig. 7.102b) showing a focus of mild increased uptake in the mid part of the left thyroid lobe, with the delayed 3-h ^{99m}Tc-sestamibi scan (Fig. 7.102c) showing focal retention of activity here and the ^{99m}Tc-sestamibi/^{99m}Tc-pertechnetate subtraction scan (Fig. 7.102d) showing a residual focus of activity here. The ^{99m}Tc-sestamibi SPECT/CT scan (Fig. 7.103) showed a focus of intense uptake located posterior to the left lower thyroid lobe region, measuring 24 × 9.6 × 9.4 mm in size on the CT component (Figs. 7.103 and 7.104).

7.40.4 Conclusion

Findings consistent with a left parathyroid adenoma as the cause of primary hyperparathyroidism.

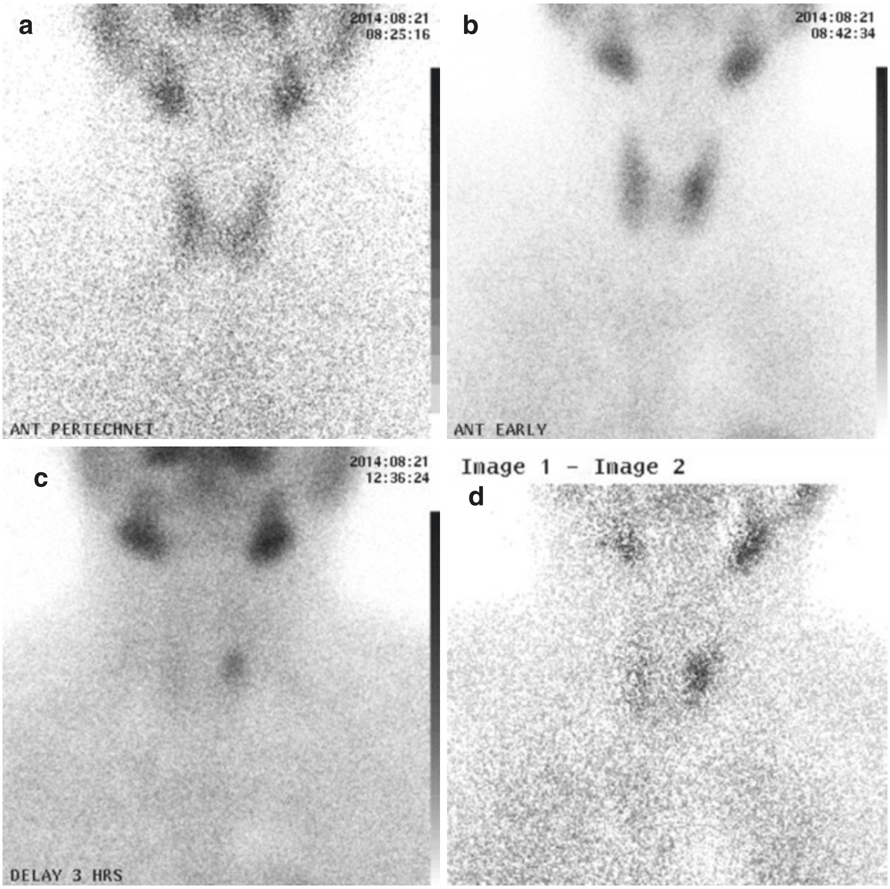

Fig. 7.102 ^{99m}Tc-pertechnetate thyroid scan (**a**), early planar ^{99m}Tc-sestamibi scan (**b**), late planar ^{99m}Tc-sestamibi scan (**c**) and ^{99m}Tc-sestamibi/^{99m}Tc-pertechnetate subtraction scan image (**d**)

Surgical excision of the nodule was undertaken with histopathology consistent with a parathyroid adenoma. Following surgery, the PTH and the serum calcium levels normalised, and serum creatinine fell from 153 to 105 μmol/L (normal range 74–115).

7.40.5 Comments and Teaching Points

- PTH oversecretion in PHPT causes hypercalcaemia due to increased dietary calcium absorption and calcium mobilisation from the bone. Hypercalcaemia, in turn, damages the healthy kidneys with a fall in renal function. However, the removal of the culprit lesion, i.e. parathyroid adenoma, can reverse the process as seen in this case.

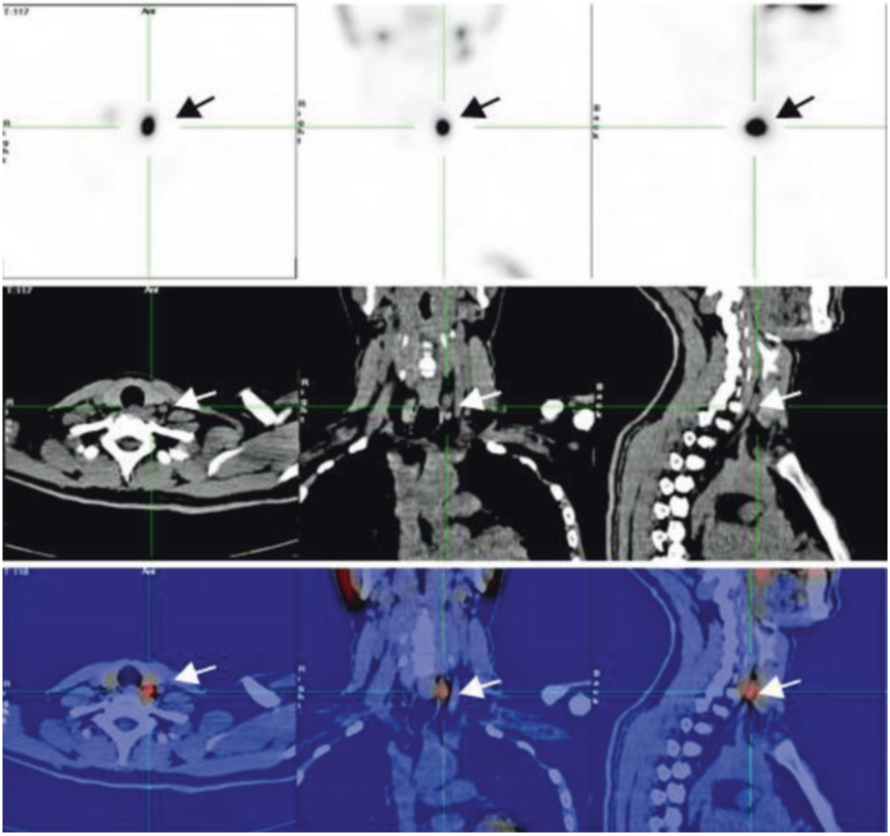

Fig. 7.103 ^{99m}Tc-sestamibi SPECT/CT scan images with SPECT scan images (top row), CT images (middle row) and fused SPECT/CT images (bottom row) in the transaxial (left column), coronal (middle column) and sagittal (right column) planes, showing a left parathyroid adenoma (arrows)

Fig. 7.104 The CT component in the transverse (top), coronal (middle) and sagittal (bottom) axes showing a left upper parathyroid adenoma (arrows) measuring 24 × 9.6 × 9.4 mm in size

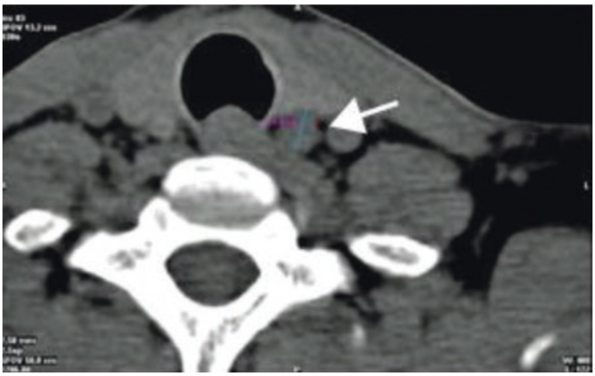

Fig. 7.104 (continued)

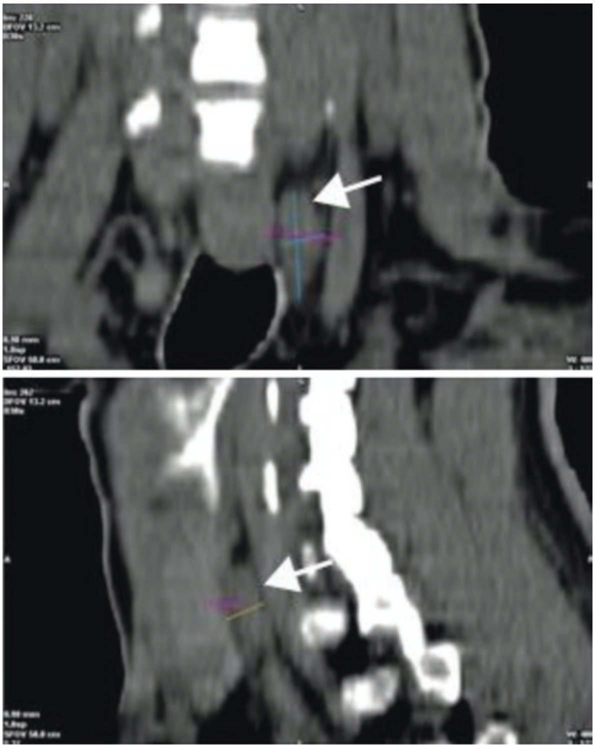

7.41 Case 7.41. Ectopic Non-oncocytic Cell Parathyroid Adenoma

7.41.1 Background

A 40-year-old male with osteoporosis and a multinodular goitre developed biochemical hyperparathyroidism with a very high serum PTH level of 120 pmol/L. The patient was found to have a low vitamin D level and was treated with oral vitamin D following which his serum PTH levels fell to normal. At the time of the scan, his serum PTH was 4.90 pmol/L (normal 1.3–9.3), corrected calcium 2.33 mmol/L (normal 2.2–2.6), phosphorus 1.02 mmol/L (normal 0.84–1.45), alkaline phosphatase 91 IU/L (normal 42–98), urea 4.0 mmol/L (normal range 2.5–6.4) and creatinine 90 μmol/L (normal range 74–115).

7.41.2 Procedure

The patient was injected with 87 MBq of ^{99m}Tc-pertechnetate, and a thyroid scan was acquired for 10 min at 20 min postinjection. Next, 767 MBq of ^{99m}Tc-sestamibi was injected without moving the patient and a 10-min duration planar scan performed after 10 min. ^{99m}Tc-sestamibi SPECT/CT scan was performed at 2 h followed by a late planar ^{99m}Tc-sestamibi scan at 3 h.

7.41.3 Findings

The pertechnetate thyroid scan (Fig. 7.105a) showed an enlarged image of the gland with a larger right lobe and homogenous distribution of activity within the gland with a focus of mildly reduced uptake at the right lower pole (arrow). The early planar ^{99m}Tc-sestamibi scan (Fig. 7.105b) showed a pattern of uptake similar to that seen in the thyroid with a faint focus of activity adjacent to the right lower pole (arrow). There was no focal retention seen here on the delayed 3-h ^{99m}Tc-sestamibi washout scan image (Fig. 7.105c), but the ^{99m}Tc-sestamibi/^{99m}Tc-pertechnetate subtraction scan (Fig. 7.105d) showed residual activity below and at the lower pole of the right thyroid lobe. The ^{99m}Tc-sestamibi SPECT/CT scan (Fig. 7.106a) showed a large ectopic focus of mild uptake (lower than the activity in the thyroid) below the right

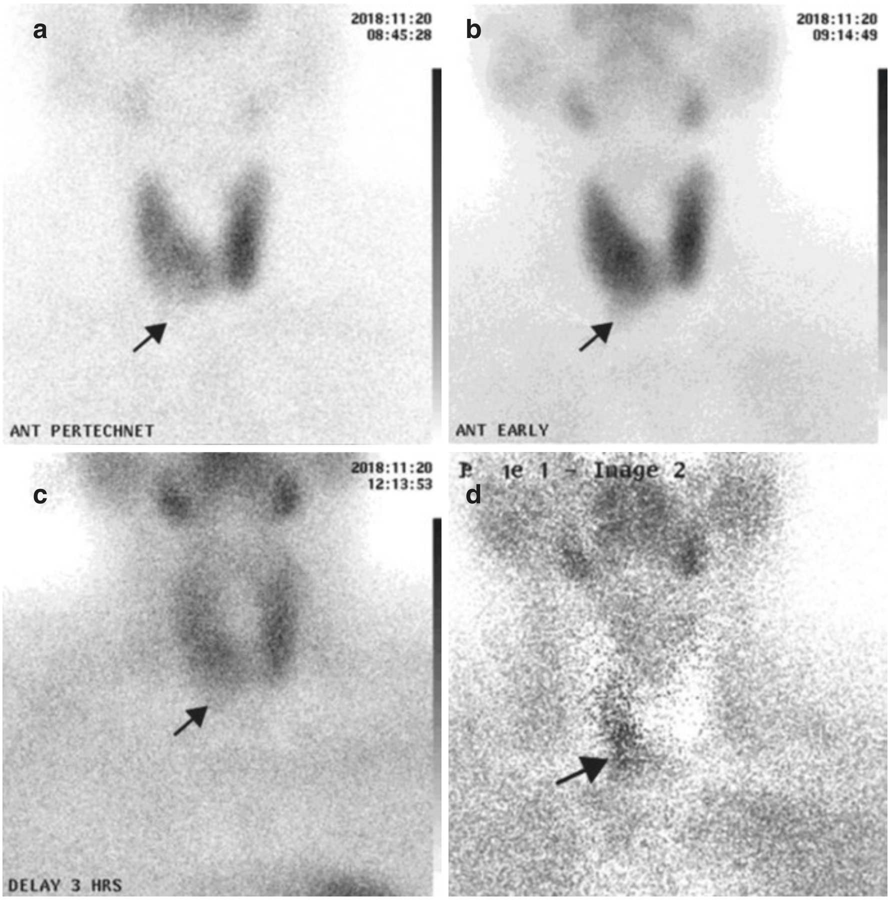

Fig. 7.105 ^{99m}Tc-pertechnetate thyroid scan (**a**), early planar ^{99m}Tc-sestamibi scan (**b**), late planar ^{99m}Tc-sestamibi scan (**c**) and ^{99m}Tc-sestamibi/^{99m}Tc-pertechnetate subtraction scan image (**d**).

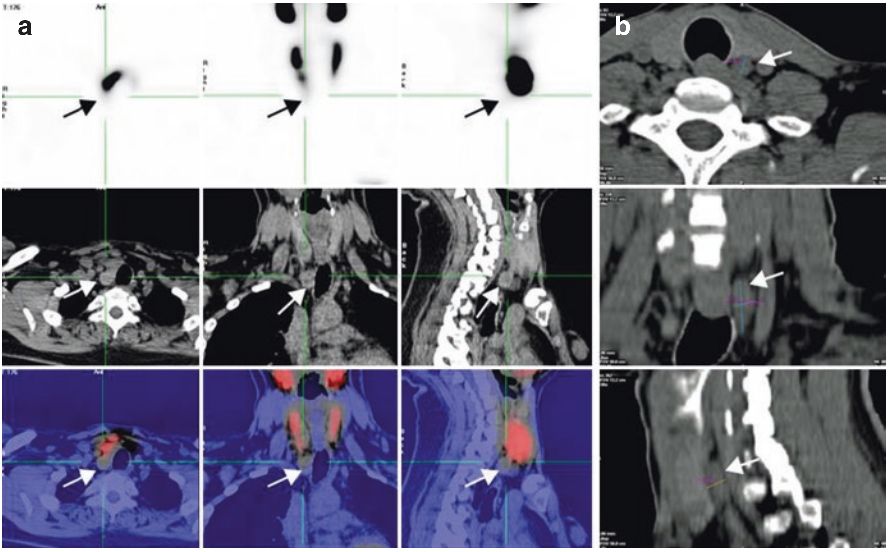

Fig. 7.106 ^{99m}Tc-sestamibi SPECT/CT scan images (**a**) with SPECT scan images (top row), CT images (middle row) and fused SPECT/CT images (bottom row) in the transaxial (left column), coronal (middle column) and sagittal (right column) planes, showing a right lower parathyroid adenoma measuring 24 × 9.6 × 9.4 mm on the CT component (**b**) located lateral to the trachea at the level of D1/D2 intervertebral space

lower pole measuring 21 × 21 × 16.6 mm in size on the CT component (Fig. 7.106b) at the level of D1/D2 intervertebral disk along the lateral wall of trachea.

7.41.4 Conclusion

Findings consistent with primary hyperparathyroidism due to a poorly sestamibi-avid large ectopic right lower parathyroid adenoma, which is presumably non-oncocytic cell in nature.

7.41.5 Comments and Teaching Points

- The adenoma was diagnosed on the CT component of the SPECT/CT scan and did not show any sestamibi uptake on the SPECT though there was a suggestion of a hyperactive lesion with early washout as it was detected on the ^{99m}Tc-sestamibi/^{99m}Tc-pertechnetate subtraction scan which subtracts the pertechnetate image from the early planar sestamibi image.
- Sestamibi scan results are affected by the cellular composition of the enlarged parathyroid glands. The chief cells are responsible for parathyroid hormone production, whereas the oxyphil cells are mainly involved in the proliferative activity. Therefore, it appears that sestamibi only indirectly images hyperactive parathyroid glands by localising in the mitochondria-rich oxyphil cells.

- Normally, 1,25-dihydroxy vitamin D inhibits PTH synthesis and secretion. The parathyroid responds to changes in serum 1,25(OH) 2 vitamin D (1,25D) which decreases PTH levels as seen in this case where vitamin D treatment immediately produced a fall of PTH level from a very high pretreatment value of 120 pmol/L to 4.90 pmol/L.
- Vitamin D deficiency may also be a potential causal factor for the development of parathyroid adenomas [57] since parathyroid cells are regulated by active vitamin D, which transcriptionally inhibits PTH secretion and cell proliferation. To date, however, there is no definitive evidence that vitamin D nutrition is associated with the development of PHPT [58].

7.42 Case 7.42. Three-Gland Parathyroid Hyperplasia with Incidental Unsuspected Dilated Cardiomyopathy

7.42.1 Background

A 61-year-old male with end-stage renal disease presented with biochemical hyperparathyroidism. His serum PTH was very high at 260.9 pmol/L (normal 1.3–9.3), adjusted calcium 2.26 mmol/L (normal 2.2–2.6), phosphorus high at 3.04 mmol/L (normal 0.84–1.45), urea high at 33.5 mmol/L (normal range 2.5–6.4), creatinine very high at 1086 μmol/L (normal range 74–115) and 25(OH) vitamin D insufficient at 66 nmol/L.

7.42.2 Procedure

The patient was injected with 76 MBq of ^{99m}Tc-pertechnetate and a thyroid scan was acquired for 10 min at 15 min postinjection. Next, 839 MBq of ^{99m}Tc-sestamibi was injected without moving the patient and a 10-min duration planar scan performed after 10 min. ^{99m}Tc-sestamibi SPECT/CT scan was performed at 2 h followed by a late planar ^{99m}Tc-sestamibi scan at 3 h.

7.42.3 Findings

The pertechnetate thyroid scan (Fig. 7.107a) showed a normal-sized image of the gland with homogenous distribution of activity. The early planar ^{99m}Tc-sestamibi scan (Fig. 7.107b) showed foci of increased activity in both the upper and the lower poles of the left lobe of the thyroid and in the right lower pole, with the 3-h ^{99m}Tc-sestamibi washout scans (Fig. 7.107c, d) showing residual focal retention of activity here. The ^{99m}Tc-sestamibi SPECT/CT scan (Fig. 7.108) showed focal uptake posterior to both lower poles of the thyroid, with the lesion at the right lower pole appearing larger (18 × 13 × 12 mm) compared with that seen in the left lower pole (13.5 × 9.3 × 6.3 mm), and an intermediate-sized lesion (17 × 8.3 × 6.5 mm) behind

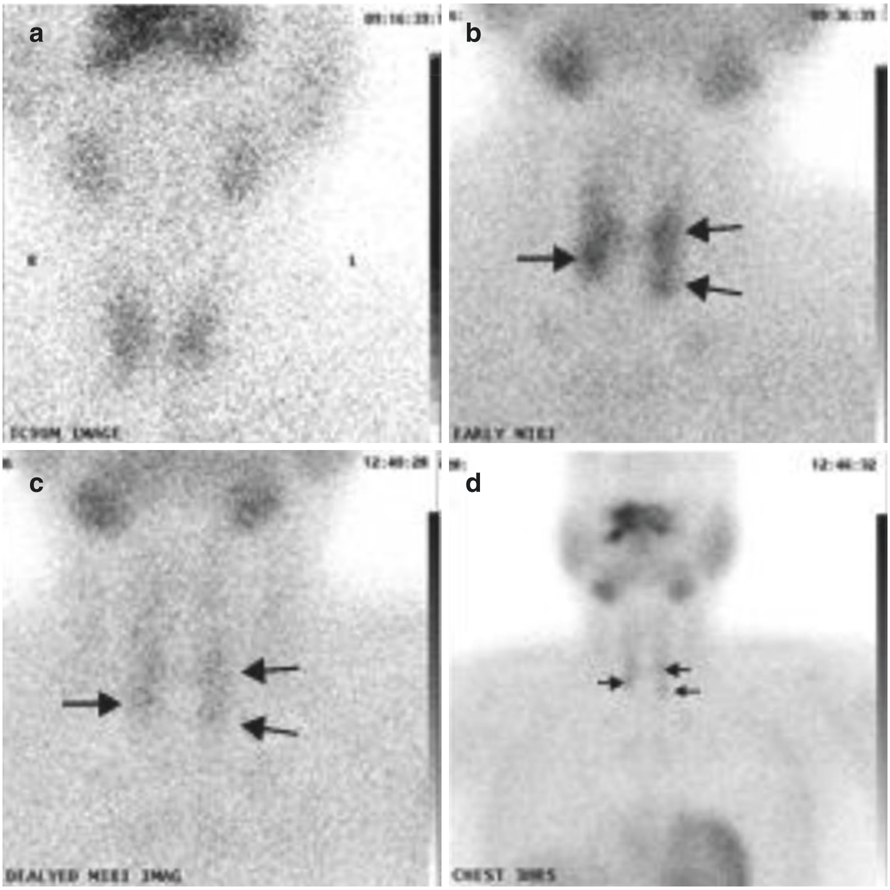

Fig. 7.107 ^{99m}Tc-pertechnetate thyroid scan (**a**), early planar ^{99m}Tc-sestamibi scan (**b**), late planar ^{99m}Tc-sestamibi scan (**c**) and unzoomed planar ^{99m}Tc-sestamibi image of the neck and chest (**d**). Arrows point to the foci of increased uptake in the right lower and the left upper and lower lobes

the middle one-third of the left thyroid lobe. The SPECT/CT images also showed a dilated left ventricular cavity (Fig. 7.109) which was further investigated by ^{99m}Tc-tetrofosmin myocardial perfusion stress and rest scans (Fig. 7.110) before renal transplantation. The scan showed a dilated left ventricle with normal perfusion, reduced left ventricular ejection fraction at 37% and global hypokinesia, which findings were consistent with dilated non-ischaemic cardiomyopathy.

7.42.4 Conclusion

Findings consistent with three-gland parathyroid hyperplasia associated with secondary hyperparathyroidism with incidental diagnosis of non-ischaemic dilated cardiomyopathy and associated impairment of left ventricular function.

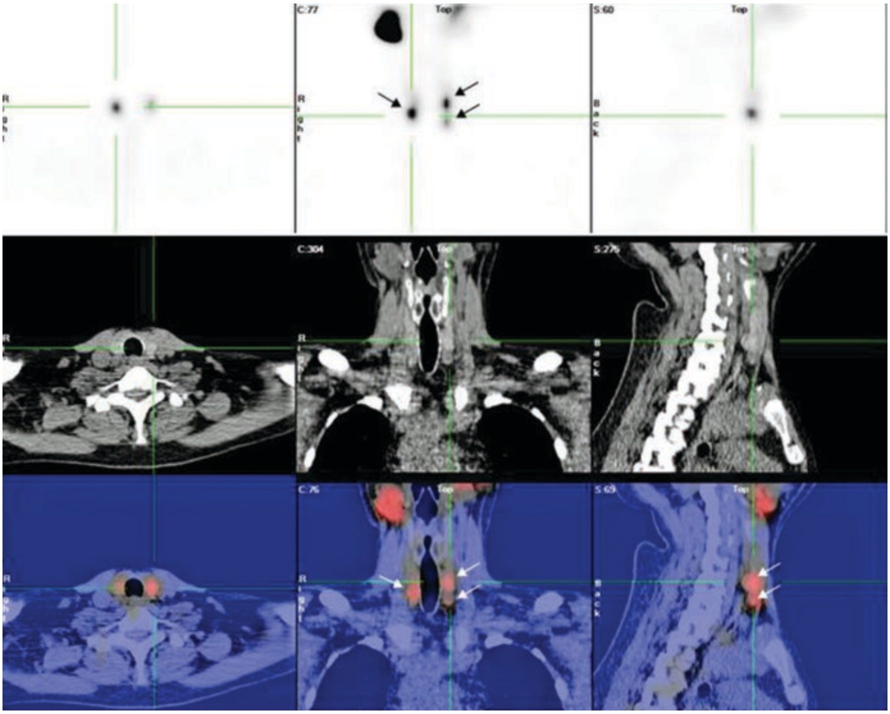

Fig. 7.108 [99m]Tc-sestamibi SPECT/CT scan images with SPECT scan images (top row), CT images (middle row) and fused SPECT/CT images (bottom row) in the transaxial (left column), coronal (middle column) and sagittal (right column) planes, showing a focus of increased uptake in the right lower pole and foci of increased uptake in the left upper and lower poles (arrows), with the sizes of the lesions measuring 18 × 13 × 12 mm, 13.5 × 9.3 × 6.3 mm and 17 × 8.3 × 6.5 mm, respectively

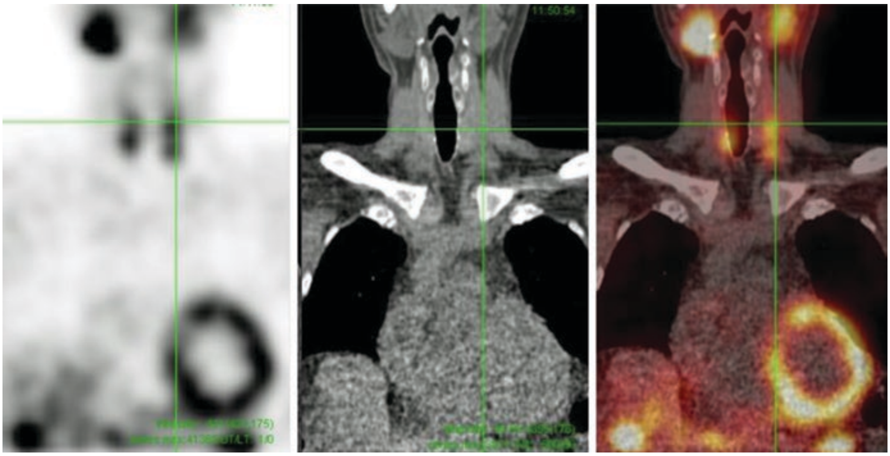

Fig. 7.109 [99m]Tc-sestamibi SPECT/CT scan images in the coronal axis with SPECT scan image (left), CT image (middle) and fused SPECT/CT image (right) showing a dilated left ventricular cavity

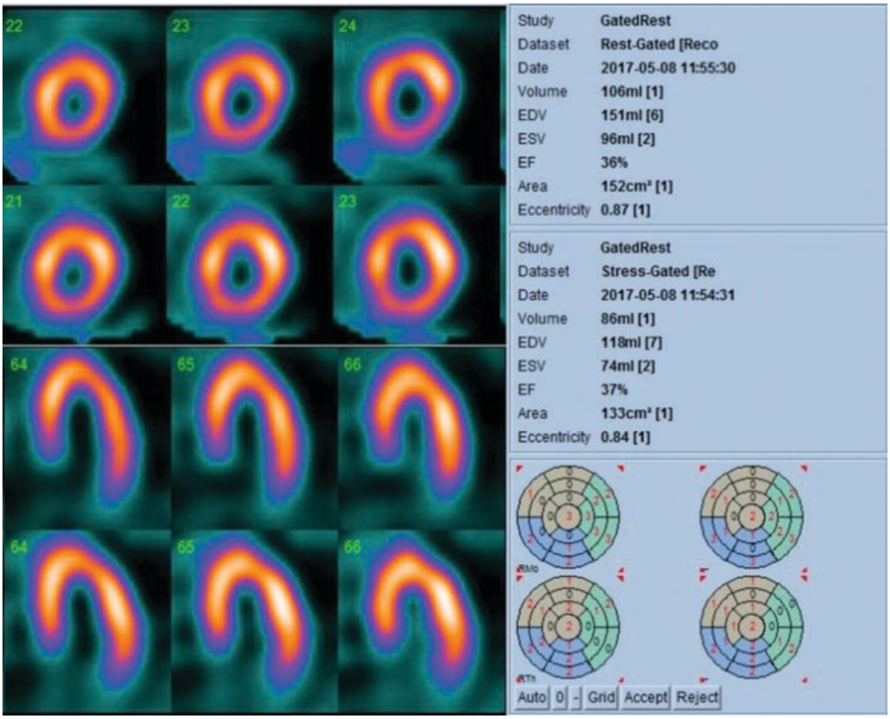

Fig. 7.110 ^{99m}Tc-tetrofosmin stress (upper rows) and rest (lower rows) images in the short and horizontal long axes show normal myocardial perfusion, left ventricular dilatation, global hypokinesia and reduced resting left ventricular ejection fraction at 37% (normal >55%)

7.42.5 Comments and Teaching Points

- ^{99m}Tc-sestamibi is a myocardial perfusion and parathyroid imaging agent, and occasionally the scans may show unsuspected cardiac abnormalities as seen in this case. It is, therefore, a good practice to visually evaluate the heart on the SPECT images to rule out unsuspected myocardial perfusion and other cardiac abnormalities.
- Falling levels of 1,25-dihydroxy vitamin D in chronic kidney disease lead to disproportionately increased PTH levels as seen in this case.
- Hyperplasia of a single parathyroid gland is rare and accounts for only 3.3% of all PHPT cases. Multiple hyperplasia is observed in 15–20% of patients [59].
- In chronic renal failure, PTH hypersecretion and parathyroid hyperplasia is initiated by some combination of hypocalcaemia, hyperphosphataemia and vitamin D deficiency, each alone able to stimulate parathyroid cell proliferation [60, 61].
- Secondary hyperparathyroidism is usually due to multiglandular parathyroid hyperplasia, although parathyroid adenomas may develop in rare instances.

7.43 Case 7.43. Six-Gland Parathyroid Hyperplasia

7.43.1 Background

A 50-year-old hypertensive male with polycystic kidneys (on haemodialysis for end-stage renal disease) and biochemical hyperparathyroidism was evaluated prior to renal transplantation. His serum PTH was 75.4 pmol/L (normal 1.3–9.3), adjusted calcium 2.26 mmol/L (normal 2.2–2.6), phosphorus 2.46 mmol/L (normal 0.84–1.45), urea 31.3 mmol/L (normal range 2.5–6.4) and creatinine 1291 μmol/L (normal range 74–115).

7.43.2 Procedure

The patient was injected with 78 MBq of ^{99m}Tc-pertechnetate, and a thyroid scan acquired for 10 min at 15 min postinjection. Next, 782 MBq of ^{99m}Tc-sestamibi was injected without moving the patient and a 10-min duration planar scan performed after 10 min. ^{99m}Tc-sestamibi SPECT/CT scan was performed at 2 h followed by a late planar ^{99m}Tc-sestamibi scan at 3 h.

7.43.3 Findings

The pertechnetate thyroid scan (Fig. 7.111a) showed a normal-sized image of the thyroid gland with homogenous distribution of activity within the gland. The early planar ^{99m}Tc-sestamibi scan (Fig. 7.111b) showed a pattern of uptake similar to that

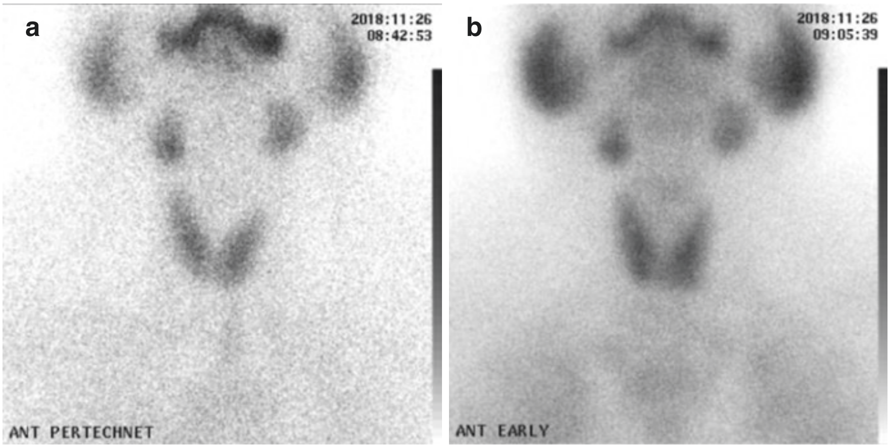

Fig. 7.111 ^{99m}Tc-pertechnetate thyroid scan (**a**), early planar ^{99m}Tc-sestamibi scan (**b**), late planar ^{99m}Tc-sestamibi scan (**c**) and ^{99m}Tc-sestamibi/^{99m}Tc-pertechnetate subtraction image (**d**). Arrows point to the foci of increased uptake in the right lower and the left upper and lower lobes on the subtraction image

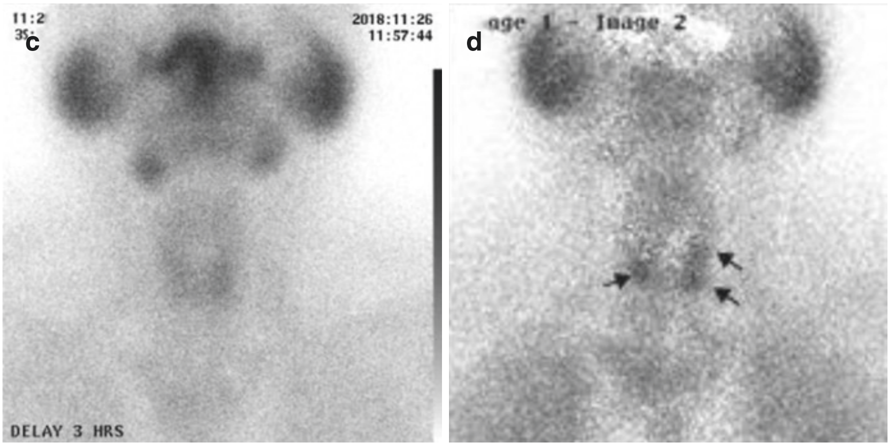

Fig. 7.111 (continued)

seen on the pertechnetate thyroid scan image. The 3-h ^{99m}Tc-sestamibi washout scan (Fig. 7.111c) showed mild residual focal retention of activity at the left lower pole. The ^{99m}Tc-sestamibi/^{99m}Tc-pertechnetate subtraction image (Fig. 7.111d) showed foci of residual uptake in the right lower pole and the left upper and lower lobes.

The ^{99m}Tc-sestamibi SPECT/CT scan (Figs. 7.112 and 7.113) showed three distinct lesions located on the right, with the CT component showing a 7.8 × 4.9-mm-sized nodule below and separate from the right lower pole, a 12.9 × 8.6-mm-sized nodule located behind the right lower pole and a 13 × 8.3-mm-sized nodule behind the right upper pole. On the left, the SPECT/CT scan (Figs. 7.114 and 7.115) showed three distinct nodules including a 10 × 7.5-mm nodule below the left lower pole, a 10 × 6.8-mm-sized nodule behind the left lower pole and a 7.9 × 4.9-mm-sized nodule behind the left upper pole.

7.43.4 Conclusion

Findings consistent with six-gland parathyroid hyperplasia associated with secondary hyperparathyroidism.

7.43.5 Comments and Teaching Points

- This is the first reported case of six-gland parathyroid hyperplasia in a patient with two supernumerary parathyroid glands.
- Most individuals have four parathyroid glands, but the percentage of individuals with supernumerary glands varies from 2.5% to 13% [62].
- The case underscores the importance of ^{99m}Tc-sestamibi/^{99m}Tc-pertechnetate subtraction image which showed three distinct lesions as compared to one or possibly two suspected on the early and late planar ^{99m}Tc-sestamibi scans.

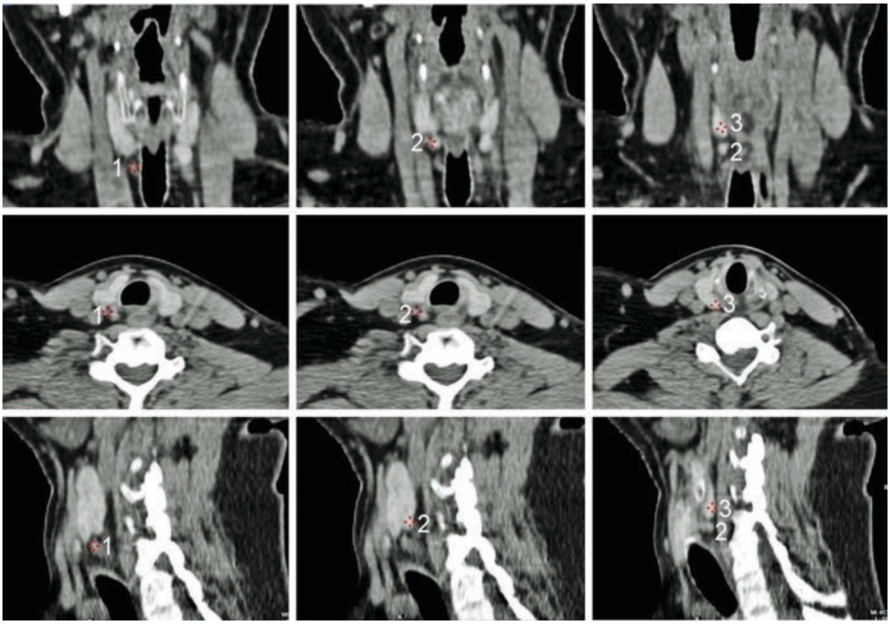

Fig. 7.112 CT component of the SPECT/CT scan images in the coronal (top row), transaxial (middle row) and sagittal (bottom row) showing three enlarged parathyroid glands on the right side including a 7.8 × 4.9-mm-sized gland below and separate from the right lower pole (1), a 12.9 × 8.6-mm-sized gland behind the right lower pole (2) and a 13 × 8.3-mm-sized gland behind the right upper pole (3). Note the leaf-like shape of the topmost gland

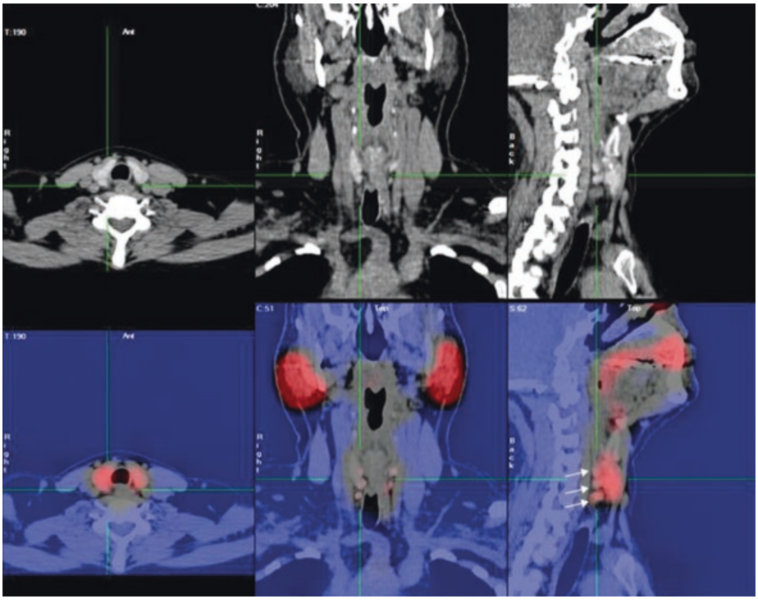

Fig. 7.113 ^{99m}Tc-sestamibi SPECT/CT scan with CT (top row) and fused SPECT/CT (bottom row) in the transaxial (left), coronal (middle) and sagittal (right) axes. The arrows point to the three hyperplastic parathyroid glands on the right

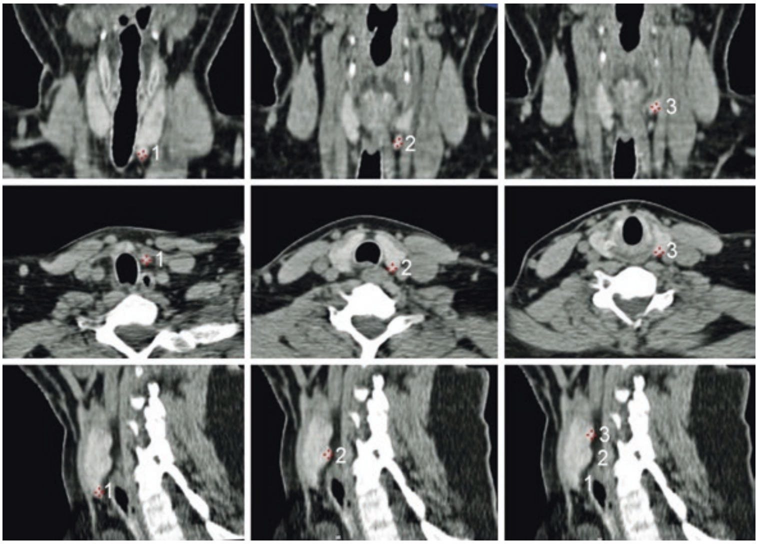

Fig. 7.114 CT component of the SPECT/CT scan images in the coronal (top row), transaxial (middle row) and sagittal (bottom row) showing three enlarged parathyroid glands on the left side including a 10 × 7.5-mm-sized gland abutting the left lower pole (1), a 10 × 6.8-mm-sized gland behind the mid left lobe (2) and a 7.9 × 4.9-mm-sized gland behind the left upper pole (3). Note the leaf-like shape of the top gland

- The SPECT/CT was crucial to comprehensive diagnosis as it detected double the number of lesions than suspected on the planar and subtraction images.
- Even on SPECT alone, it was not possible to discriminate between the individual lesions due to their small size and proximity with the activity in one overlapping with the activity in the nearby lesion with the result that the lesions appeared as a single oblong focus of uptake. However, the CT clearly localised the six hyperplastic parathyroids which showed a variable uptake presumably related to the size of the lesions, the metabolic activity of the individual lesions and the resolution limits associated with single-photon SPECT imaging.
- Enlarged parathyroid glands in the majority of cases exhibit stretched, flattened shapes. This especially refers to superior parathyroid glands typically located near the posterior thyroid surface.
- Most of the parathyroid glands are oval shaped. However, leaf-like, spherical-, teardrop-, rod-, sausage-, pancake- and bean-shaped parathyroid glands have also been found [62–66].

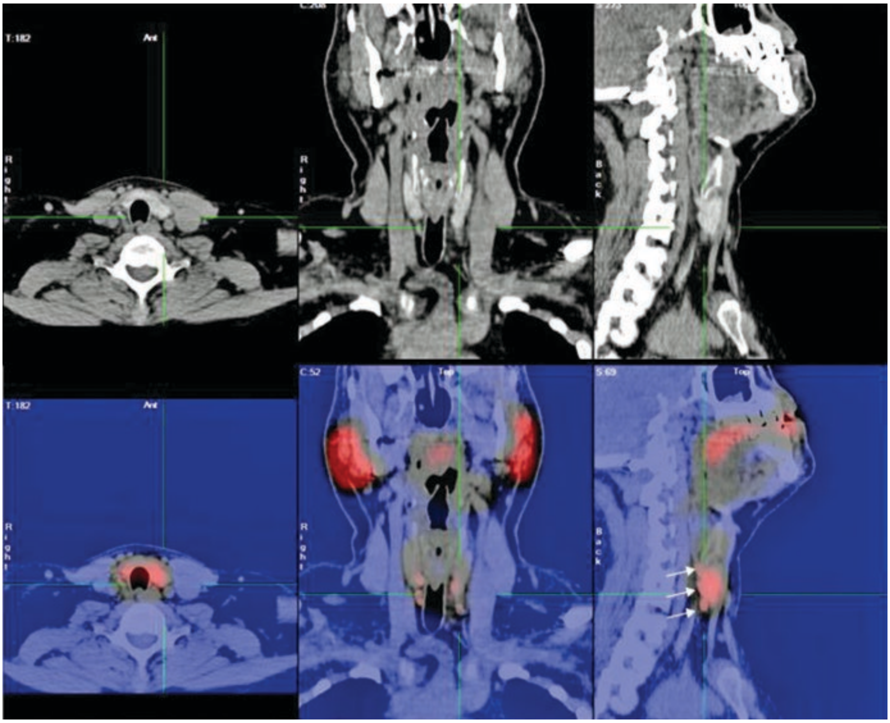

Fig. 7.115 ^{99m}Tc-sestamibi SPECT/CT scan with CT (top row) and fused SPECT/CT (bottom row) in the transaxial (left), coronal (middle) and sagittal (right) axes. The arrows point to the three hyperplastic parathyroid glands on the left side

7.44 Case 7.44. Concurrent Hyperthyroidism Due to Graves' Disease and Vitamin D Deficiency-Induced Normocalcaemic Primary Hyperparathyroidism with a Sestamibi-Negative but Thallium-Positive Parathyroid Adenoma

7.44.1 Background

A 46-year-old female presented with a history of weight loss, diarrhoea, palpitations, restlessness and fatigue. Thyroid biochemistry revealed a fT4 of 54.8 pmol/L (normal 7.86–14.4) and TSH at 0.1 µIU/mL (normal 0.27–4.2). Thyroid ultrasound showed an enlarged image of the thyroid gland with a small isthmal nodule only (Fig. 7.116). Thyroid scintigraphy was consistent with Graves' disease (Fig. 7.117a). Subsequent biochemical examination revealed a low total 25(OH) vitamin D level at 32 nmol/L (deficient <50 nmol/L), mildly elevated serum PTH at 13.1 pmol/L (normal 1.3–9.3), corrected calcium normal at 2.25 mmol/L (normal 2.2–2.6), phosphorus low at 0.66 mg/dL (normal 0.84–1.45), alkaline phosphate at 86 IU/L (normal 42–98), urea normal at 2.2 mmol/L (normal range 2.5–6.4) and creatinine normal at 48 µmol/L (normal range 53–97).

Fig. 7.116 Thyroid ultrasound showing small indistinct thyroid nodules with no evidence of a parathyroid adenoma seen

7.44.2 Procedure (^{99m}Tc-Pertechnetate Thyroid Scan + ^{99m}Tc-Sestamibi Parathyroid Scan)

The patient was injected with 75 MBq of ^{99m}Tc-pertechnetate and a thyroid scan acquired for 10 min at 15 min postinjection. Next, 839 MBq of ^{99m}Tc-sestamibi was injected without moving the patient and a 10-min duration planar scan performed after 10 min. ^{99m}Tc-sestamibi SPECT/CT scan was performed at 2 h followed by a late planar ^{99m}Tc-sestamibi scan at 3 h. Radioiodine uptake was later performed at 4 and 24 h after administration of 0.28 MBq of ^{131}I sodium iodide orally.

7.44.3 Procedure (^{201}Tl-Thallous Chloride Parathyroid Scan)

^{201}Tl-thallous chloride (120 MBq) was administered intravenously, and a planar thallium scan was acquired for 10 min at 10 min postinjection followed by a thallium-201 SPECT/CT scan.

7.44.4 Findings

The pertechnetate thyroid scan (Fig. 7.117a) showed a markedly enlarged image of the gland with fairly homogenous distribution of activity in the gland with 20-min uptake for pertechnetate high at 64% (normal <3.5%), with 4-h ^{131}I uptake high at 34% (normal 10–15%) and 24-h ^{131}I uptake at 34% (normal 15–35%) indicating a high radioiodine turnover rate. The early planar ^{99m}Tc-sestamibi scan (Fig. 7.117b) showed a pattern of uptake similar to that seen on the pertechnetate thyroid scan, with the delayed washout sestamibi images appearing normal (Fig. 7.117b, c). The ^{99m}Tc-sestamibi/^{99m}Tc-pertechnetate subtraction image (Fig. 7.117d) was normal as well. The ^{99m}Tc-sestamibi SPECT/CT scan (Fig. 7.118) showed no focal abnormality in the thyroid bed to indicate the presence of a hyperactive parathyroid lesion. The planar thallium-201 scan (Fig. 7.118a) showed homogenous distribution of activity in the thyroid gland with the ^{201}Tl/^{99m}Tc subtraction image (Fig. 7.118c)

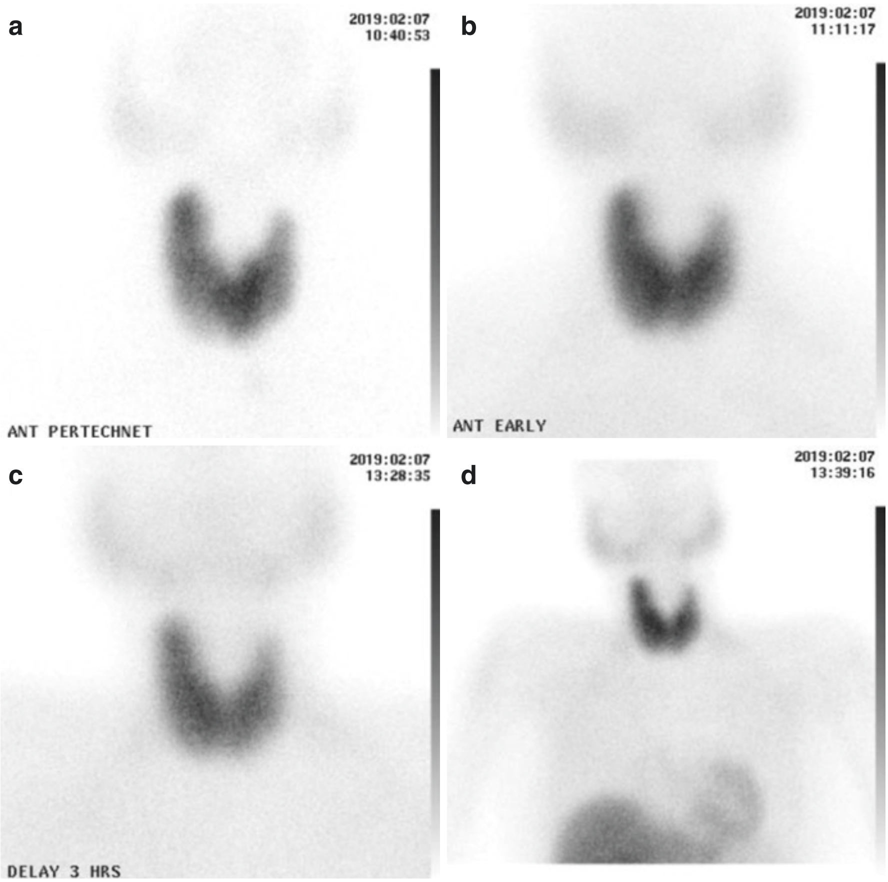

Fig. 7.117 ^{99m}Tc-pertechnetate thyroid scan (**a**), early planar ^{99m}Tc-sestamibi scan (**b**), late planar ^{99m}Tc-sestamibi scan (**c**) and late unzoomed neck and chest scan (**d**) showing no evidence of a parathyroid adenoma

showing a focus of uptake in the thyroid bed at the right lower pole of the thyroid. The thallium-201 SPECT/CT scan (Fig. 7.119) showed a clear-cut focus of intense uptake at the lower pole of the right lobe of the thyroid corresponding to an 18 × 13.8 × 16-mm-sized nodule at the posterior aspect of the right lower pole of the thyroid on the CT component (Figs. 7.120 and 7.121).

7.44.5 Conclusion

The ^{99m}Tc-pertechnetate thyroid scan and ^{131}I uptake results were in keeping with a diffuse toxic goitre (Graves' disease). The sestamibi parathyroid planar and SPECT/CT scans were false-negative, but the thallium planar and SPECT/CT scans were true-positive for a parathyroid adenoma. The scintigraphic and biochemical

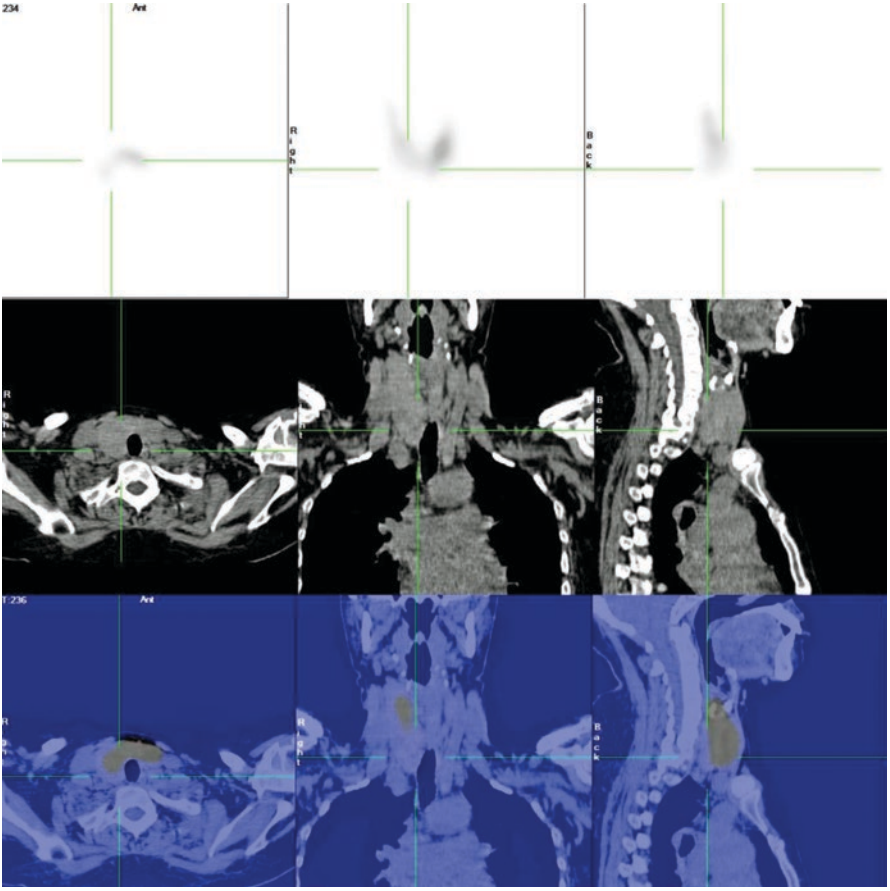

Fig. 7.118 ^{99m}Tc-sestamibi SPECT scan images (top row), CT scan images (middle row) and fused SPECT/CT images (bottom row) in the transaxial (left column), coronal (middle column) and sagittal (right column) planes, showing no evidence of a hyperactive parathyroid lesion

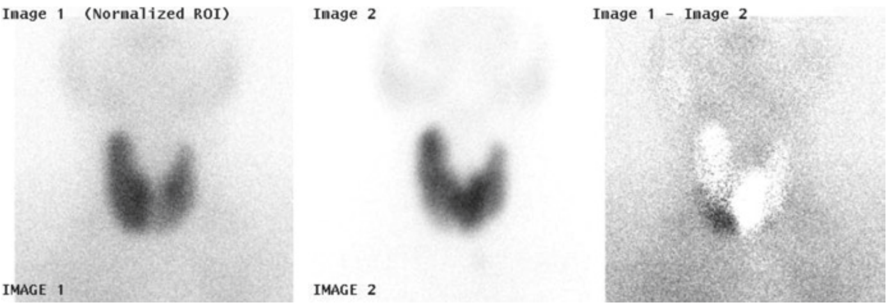

Fig. 7.119 ^{99m}Tl-thallous chloride planar scan (left), ^{99m}Tc-pertechnetate thyroid scan (middle), and thallium-201/technetium-99m subtraction scan image(right) showing a residual focus of activity at the right lower pole of the thyroid

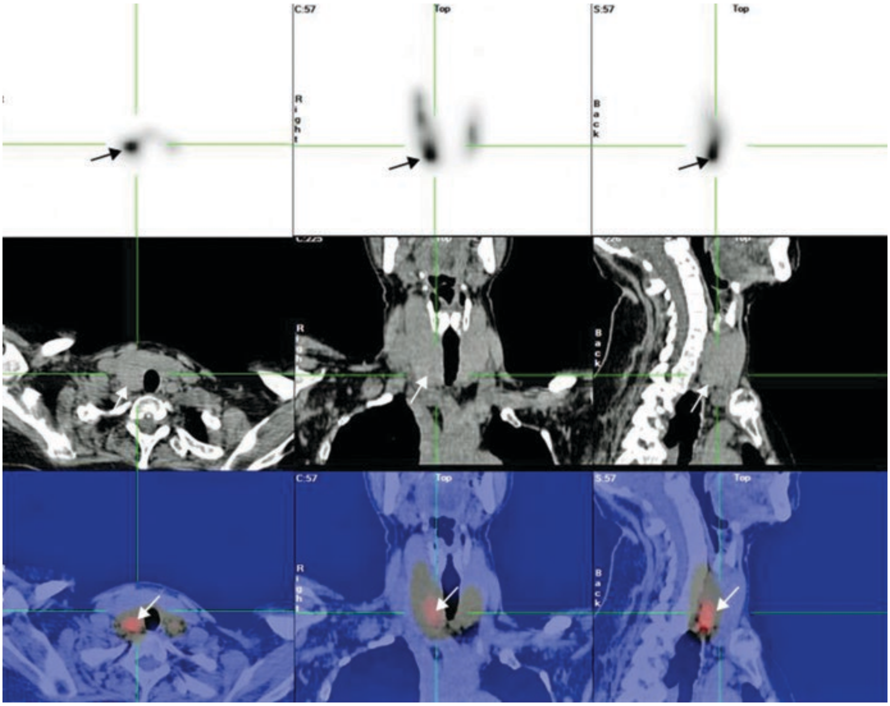

Fig. 7.120 ^{201}Tl-thallous chloride SPECT scan images (top row), CT scan images (middle row) and fused SPECT/CT images (bottom row) in the transaxial (left column), coronal (middle column) and sagittal (right column) planes, showing a thallium-avid right lower parathyroid adenoma (arrows) which appeared negative on the ^{99m}Tc-sestamibi scan

findings were consistent with concurrent hyperthyroidism due to Graves' disease and vitamin D deficiency-related normocalcaemic primary hyperparathyroidism with a sestamibi-negative but thallium-positive (non-oncogenic cell) parathyroid adenoma. Following oral administration of 50,000 UI of vitamin D, the PTH levels fell from 13.1 to 1.10 pmol/L and then gradually started rising again.

7.44.6 Comments and Teaching Points

- This is a unique case of a combination of Graves' disease, vitamin D deficiency-related normocalcaemic primary hyperparathyroidism with a sestamibi-negative but thallium-positive parathyroid adenoma. The patient had biochemical hyperthyroidism, phosphate deficiency, raised serum PTH, normal serum calcium and low $1,25(OH)_2D_3$. Normocalcaemic PHPT has been increasingly recognised over the past decade [40].
- The simultaneous occurrence of primary hyperparathyroidism and hyperthyroidism due to Graves' disease in the same patient is quite rare, but preoperative

Fig. 7.121 CT scan images in the coronal (top), transaxial (middle) and right sagittal (bottom) showing a right lower parathyroid adenoma (arrows) measuring 18 × 13.8 × 16 mm in size

localisation of a parathyroid adenoma may help direct treatment such as a combination of partial thyroidectomy and parathyroidectomy.

- It is presumed that parathyroid adenoma associated with early or normocalcaemic PHPT mainly induces non-oncogenic cellular proliferation and that sustained PHPT and hypercalcaemia may be associated with a proliferation of oxyphil cells, which may account for the sestamibi-negative but thallium-positive adenoma as seen in this case.
- The impact of simple nutritional vitamin D deficiency and the decreased production of 1,25(OH)2D3 in chronic renal insufficiency differ because of pathophysi-

ological differences in the two situations, namely, phosphate deficiency in the former and phosphate retention in the latter [67]. Vitamin D deficiency is frequently associated with a high serum PTH level and normal serum calcium [68].

- Patients with vitamin D deficiency are more likely to have positive parathyroid scans. In a study of 421 consecutive patients with PHPT, those with cholecalciferol levels <25 ng/mL had PTH levels and adenoma weight higher than those with normal vitamin D and were eight times more likely to have a positive scan after adjusting for age and sex [69].
- Normal serum calcium along with elevated PTH levels can be seen in a patient with coexisting PHPT and vitamin D deficiency. Despite their PHPT, the low vitamin D state could have a calcium-lowering effect, pushing levels into the normal range [70] as in this case.
- PTH decreases quite linearly during vitamin D supplementation at any given baseline 1,25(OH)2D3 D level [71] as seen in this case.

7.45 Case 7.45. Double Parathyroid Adenomas: (1) One Thallium-Avid but Sestamibi-Non-avid and (2) Other Both Sestamibi- and Thallium-Avid

7.45.1 Background

A 61-year-old female presented with hypercalcaemia and hyperparathyroidism. Her PTH was 20.20 pmol/L (normal 1.3–9.3), corrected calcium 2.72 mmol/L (normal 2.2–2.6), phosphorus 1.03 mmol/L (normal 0.84–1.45), alkaline phosphate 71 IU/L (normal 42–98), urea 3.8 mmol/L (normal range 2.5–6.4) and creatinine 36 μmol/L (normal range 53–97).

7.45.2 Procedure (^{99m}Tc-Sestamibi Parathyroid Scan)

The patient was injected with 83 MBq of ^{99m}Tc-pertechnetate and a thyroid scan acquired for 10 min at 15 min postinjection. Next, 759 MBq of ^{99m}Tc-sestamibi was injected without moving the patient and a 10-min duration planar scan performed after 10 min. ^{99m}Tc-sestamibi SPECT/CT scan was performed at 2 h followed by a late planar ^{99m}Tc-sestamibi scan at 3 h.

7.45.3 Procedure (^{201}Tl-Thallous Chloride Parathyroid Scan)

The patient was injected with 79 MBq of ^{99m}Tc-pertechnetate, and a thyroid scan was acquired for 10 min at 15 min postinjection. Next 110 MBq of ^{201}Tl-thallous chloride was injected without moving the patient and 10-min duration planar scan performed after 10 min followed by a thallium-201 SPECT/CT scan.

7.45.4 Findings

The pertechnetate thyroid scan showed a moderately enlarged image of the thyroid with a relatively prominent right lobe with relatively increased uptake compared with the left lobe but with a generally homogenous distribution of activity in the gland (Fig. 7.122a). The early planar ^{99m}Tc-sestamibi scan (Fig. 7.122b) showed a pattern of uptake similar to that seen on the pertechnetate thyroid scan, with the delayed washout sestamibi images (Fig. 7.122c) showing a proportionate distribution of activity within the gland without any focal retention seen. The ^{99m}Tc-sestamibi/^{99m}Tc-pertechnetate subtraction image (Fig. 7.122d) was normal as well. The ^{99m}Tc-sestamibi SPECT/CT scan showed a smaller partly intrathyroidal nodule at the posterior aspect of the right upper lobe of the thyroid with increased ^{99m}Tc-sestamibi uptake (Figs. 7.123 and 7.124) and a larger paratracheal nodule located

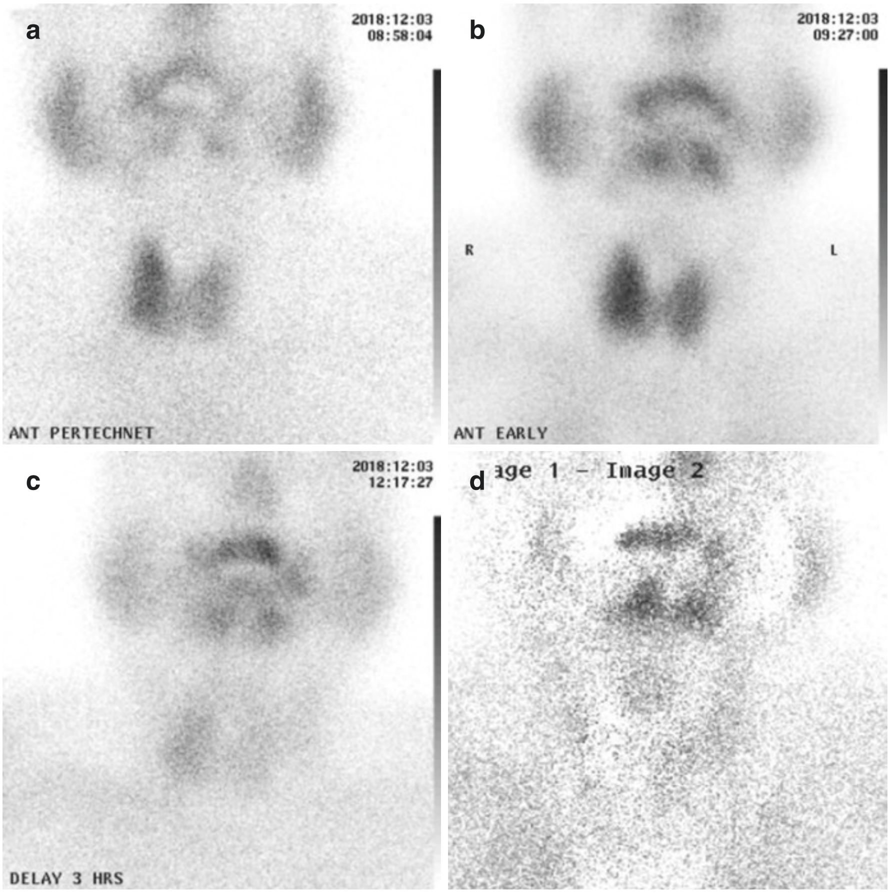

Fig. 7.122 ^{99m}Tc-pertechnetate thyroid scan (**a**), early planar ^{99m}Tc-sestamibi scan (**b**), late planar ^{99m}Tc-sestamibi scan (**c**) and ^{99m}Tc-sestamibi/^{99m}Tc-pertechnetate subtraction scan image (**d**)

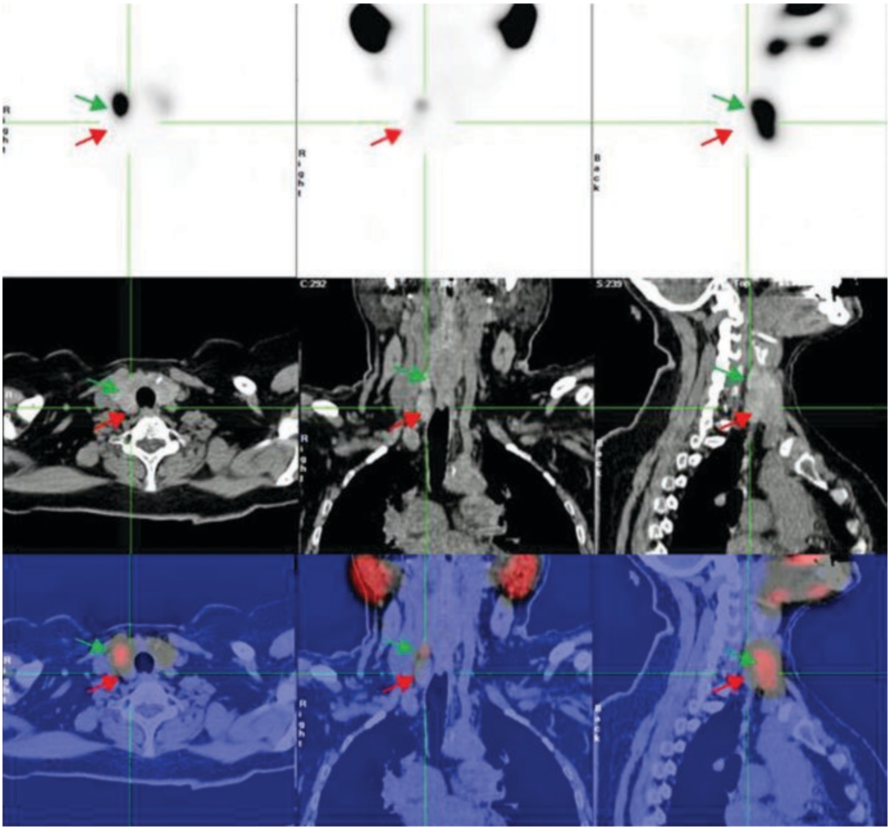

Fig. 7.123 ^{99m}Tc-sestamibi SPECT scan images (top row), CT scan images (middle row) and fused SPECT/CT images (bottom row) in the transaxial (left column), coronal (middle column) and sagittal (right column) planes, showing a smaller partly intrathyroidal nodule at the posterior aspect of the right upper lobe of the thyroid with increased ^{99m}Tc-sestamibi uptake (green arrows) and a larger nodule located behind the lower part of the right lobe of the thyroid with absent ^{99m}Tc-sestamibi uptake (red arrows)

behind the lower part of the right lobe of the thyroid with absent ^{99m}Tc-sestamibi uptake. The CT component of the SPECT/CT showed right lower parathyroid nodule measuring 23 × 15.9 × 16.9 mm in size and the right upper parathyroid nodule measuring 17 × 9.1 × 8.7 mm in size (Fig. 7.124).

The scan was repeated with thallium-201 to establish/rule out a false-negative right lower parathyroid adenoma due to possible non-oncocytic cell composition of the lower nodule. The planar thallium-201 scan showed a pattern of uptake similar to that seen in the planar technetium-99m pertechnetate thyroid scan with higher uptake in the right compared with the left lobe without any residual uptake seen on the thallium-201/technetium-99m subtraction scan image (Fig. 7.125). The thallium-201 SPECT/CT scan showed moderately increased thallium uptake in the smaller partly intrathyroidal nodule at the posterior aspect of the right

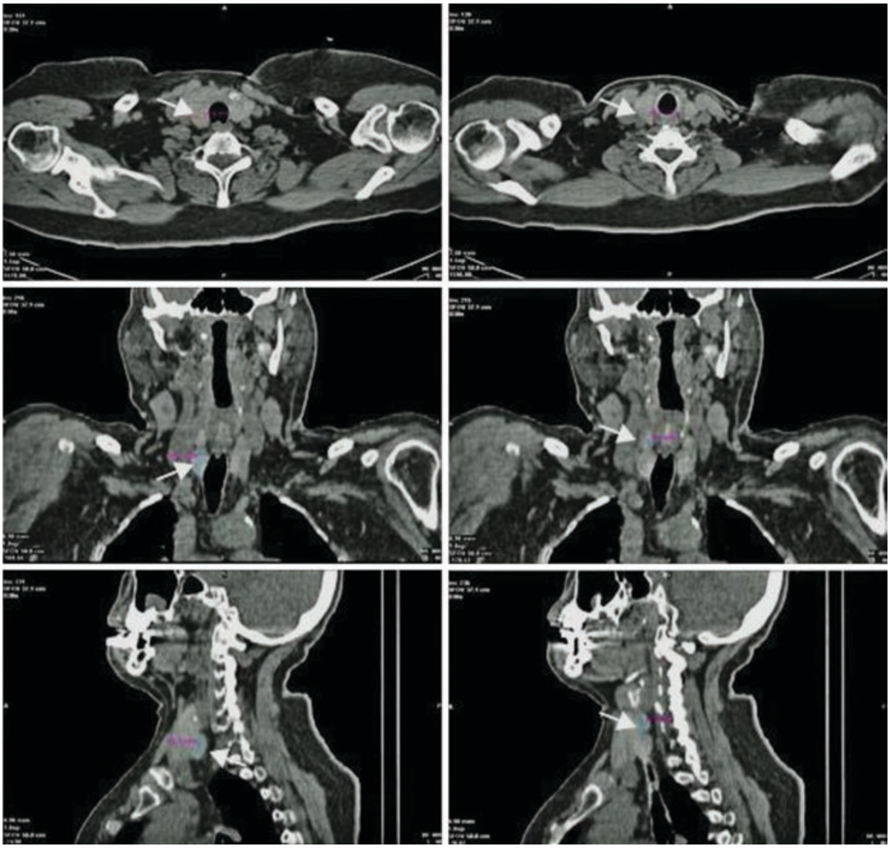

Fig. 7.124 CT scan images in the transaxial (top row), coronal (middle row) and sagittal (bottom row) axes with the white arrows showing a right lower parathyroid nodule (left column) measuring 23 × 15.9 × 16.9 mm in size and a right upper parathyroid nodule (right column) measuring 17 × 9.1 × 8.7 mm in size

upper lobe of the thyroid, but the larger right lower parathyroid nodule which appeared negative on the ^{99m}Tc-sestamibi scan showed intensely increased thallium uptake (Fig. 7.126).

7.45.5 Conclusion

Findings consistent with two parathyroid adenomas on the right with a smaller right upper parathyroid adenoma showing equal avidity for ^{99m}Tc-sestamibi and thallium-201 but the larger sestamibi-non-avid (false-negative) right lower parathyroid adenoma showing intense thallium-201 uptake presumably representing a non-oncogenic cell parathyroid adenoma.

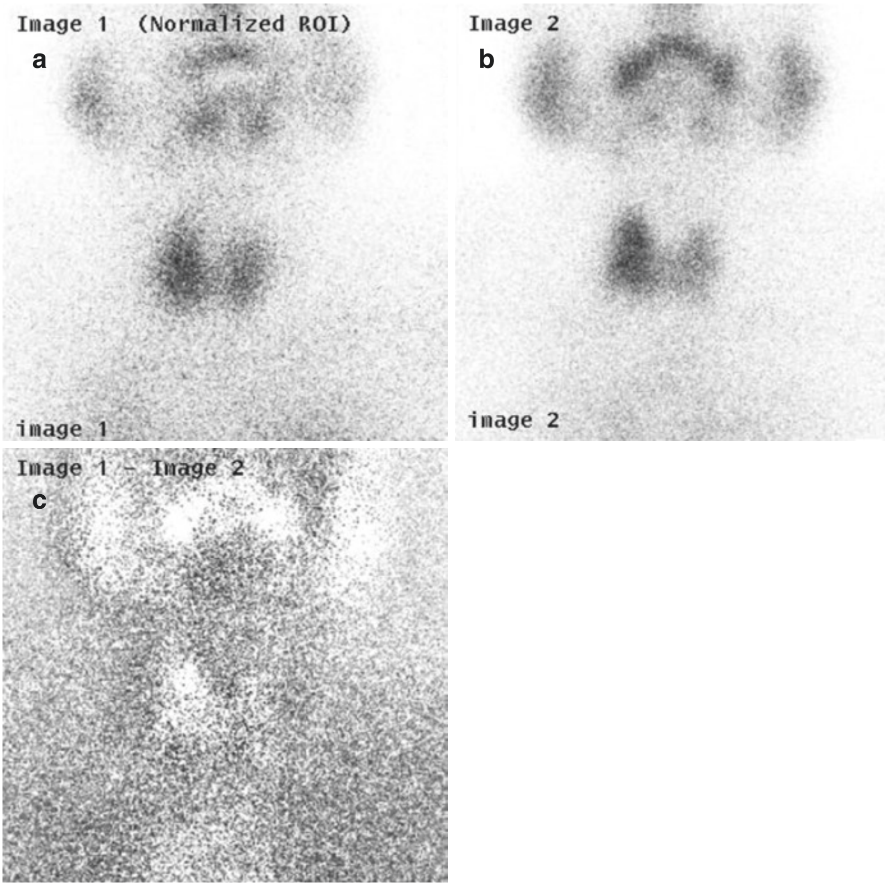

Fig. 7.125 ^{99m}Tl-thallous chloride planar scan (**a**), ^{99m}Tc-pertechnetate thyroid scan (**b**) and thallium-201/technetium-99m subtraction scan image (**c**)

7.45.6 Comments and Teaching Points

- This is a unique first-time report of a case of double parathyroid adenomas in one lobe of the thyroid where sestamibi parathyroid scintigraphy was false-negative and failed to detect the larger of the two adenomatous parathyroid glands, but thallium SPECT was true-positive and successfully detected both parathyroid adenomas.
- Mitochondria-rich oxyphil cells account for sestamibi uptake in parathyroid lesions. Fewer oxyphil cells, and hence fewer mitochondria, may explain both lower uptake and rapid washout of sestamibi from some parathyroid adenomatous lesions, and it is logical to assume that parathyroid adenomas composed mostly of chief or water-clear cells would appear false-negative on a ^{99m}Tc-sesta-

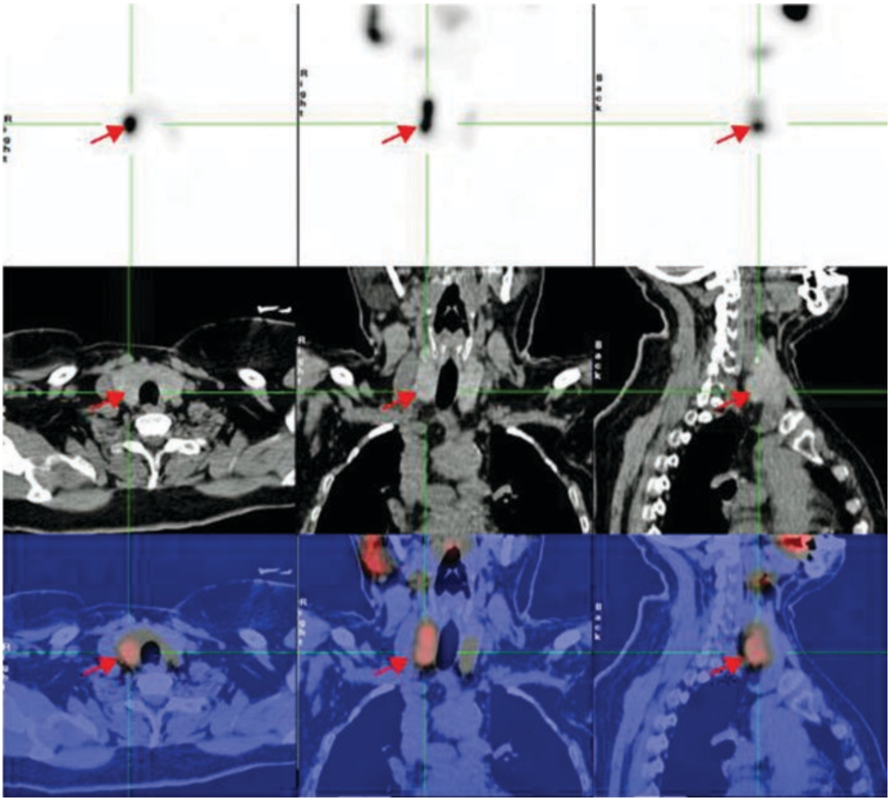

Fig. 7.126 ^{201}Tl-thallous chloride SPECT scan images (top row), CT scan images (middle row) and fused SPECT/CT images (bottom row) in the transaxial (left column), coronal (middle column) and sagittal (right column) planes, showing the smaller partly intrathyroidal nodule at the posterior aspect of the right upper lobe of the thyroid with moderately increased thallium uptake but the larger right lower parathyroid nodule which appeared negative on the ^{99m}Tc-sestamibi scan showing intense increased thallium uptake (red arrows)

mibi parathyroid scan as seen in this case where the smaller of the two adenomas was sestamibi-positive but the other larger adenoma showed no sestamibi uptake but was found to be intensely thallium-avid.

- It has been reported that an adenoma with an oxyphil cell content >20% and adenoma weight >600 mg, increased the rate of obtaining a positive sestamibi scan result by four- and ten-fold, respectively [72].
- The thallium/pertechnetate subtraction scintigraphy was the only available parathyroid imaging modality in the 1980s, but with the introduction of dual-phase sestamibi imaging in the 1990s, thallium subtraction scintigraphy was abandoned. This, however, preceded SPECT imaging which could have improved the diagnostic yield of thallium scintigraphy as can be appreciated in this case where the planar thallium/technetium subtraction scan was normal but the SPECT

showed intense uptake in the adenoma indicating the better diagnostic yield of thallium SPECT over planar thallium scan.

- This case also indicates an important role for thallium SPECT or SPECT/CT imaging in sestamibi-equivocal or sestamibi-negative parathyroid adenomas. The combination of two functional hybrid imaging techniques increases the sensitivity, accuracy and diagnostic yield of parathyroid scintigraphy.

7.46 Case 7.46. Four-Gland Parathyroid Hyperplasia

7.46.1 Background

A 45-year-old female with end-stage renal disease (on dialysis) presented with hyperparathyroidism. Serum PTH was high at 145.20 pmol/L (normal 1.3–9.3), corrected calcium low at 2.17 mmol/L (normal 2.2–2.6), phosphorus high at 1.93 mmol/L (normal 0.84–1.45), alkaline phosphate high at 550 IU/L (normal 42–98), urea high at 22 mmol/L (normal range 2.5–6.4) and creatinine also high at 702 µmol/L (normal range 53–97).

7.46.2 Procedure

The patient was injected with 79 MBq of ^{99m}Tc-pertechnetate, and a thyroid scan was acquired for 10 min at 15 min postinjection. Next, 906 MBq of ^{99m}Tc-sestamibi was injected without moving the patient and a 10-min duration planar scan performed after 10 min. ^{99m}Tc-sestamibi SPECT/CT scan was performed at 2 h followed by a late planar ^{99m}Tc-sestamibi scan at 3 h.

7.46.3 Findings

The pertechnetate thyroid scan (Fig. 7.127a) showed asymmetry of the right lobe but with uniform uptake of the tracer in both lobes of the thyroid gland. The early planar ^{99m}Tc-sestamibi scan (Fig. 7.127b) showed focal uptake in the upper and the lower poles of both lobes of the thyroid gland with the delayed washout images showing focal retention of tracer here (Fig. 7.127b, c). The ^{99m}Tc-sestamibi/^{99m}Tc-pertechnetate subtraction image, however, showed only a single residual focus of activity at the left lower pole of the thyroid (Fig. 7.127d).

The SPECT/CT scan showed four clear-cut foci of uptake at the upper and lower poles of both thyroid lobes (Fig. 7.128). The sizes of the four enlarged parathyroid glands measured on the CT component (Fig. 7.129) were 22.3 × 8.5 × 8.4 mm (upper right), 16.2 × 8 × 6.3 mm (lower right), 15.4 × 4 × 6 mm (upper left) and 18.7 × 10.8 × 10 mm (lower left).

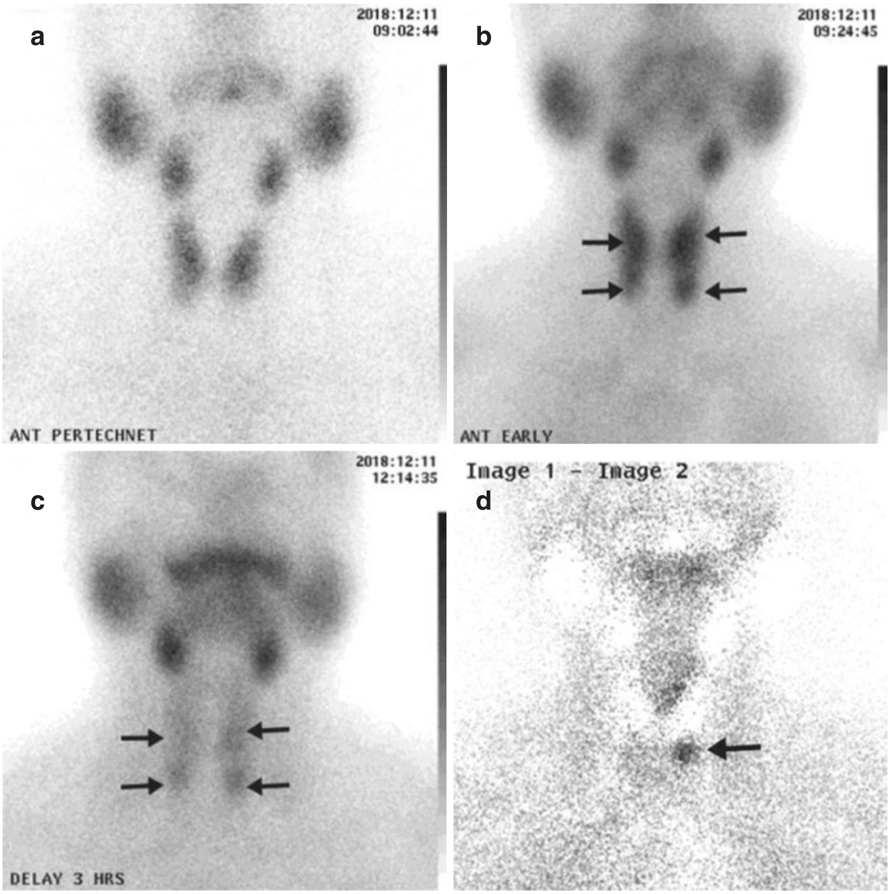

Fig. 7.127 ^{99m}Tc-pertechnetate thyroid scan (**a**), early planar ^{99m}Tc-sestamibi scan (**b**), late planar ^{99m}Tc-sestamibi scan (**c**) and ^{99m}Tc-sestamibi/^{99m}Tc-pertechnetate subtraction scan image (**d**). The arrows point to the suspect hyperplastic parathyroid glands

7.46.4 Conclusion

Findings consistent with four-gland parathyroid hyperplasia associated with secondary hyperparathyroidism.

7.46.5 Comments and Teaching Points

- The planar sestamibi scans were suggestive of 4-gland hyperplasia, but the SPECT/CT, however, was unequivocally diagnostic of four-gland hyperplasia with the hyperplastic parathyroid glands visualised both on the SPECT and the CT components.

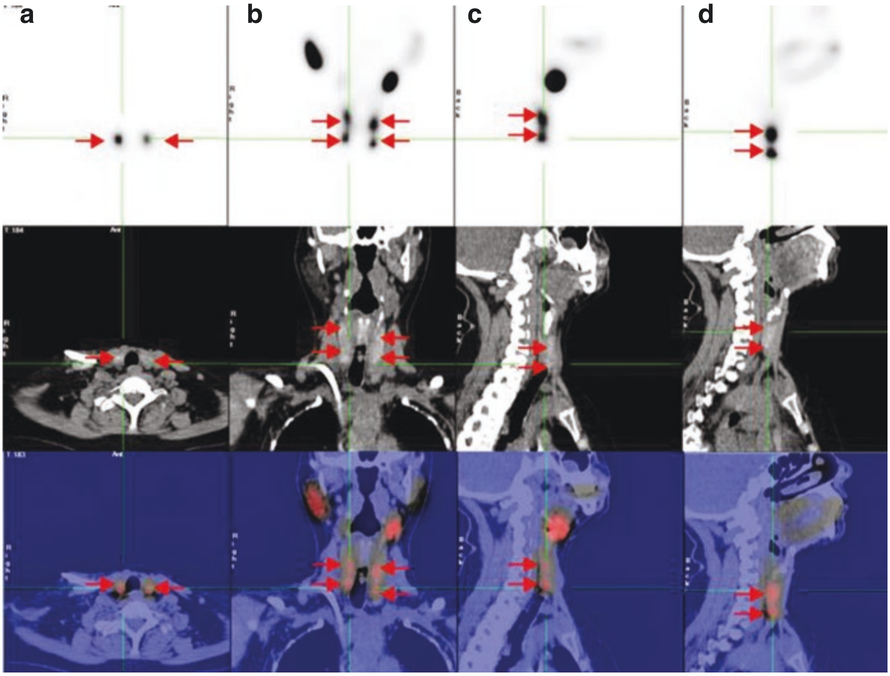

Fig. 7.128 ^{99m}Tc-sestamibi SPECT scan images (top row), CT scan images (middle row) and fused SPECT/CT images (bottom row) in the transaxial (**a**), coronal (**b**), right sagittal (**c**) and left sagittal (**d**) planes, showing bilateral upper and lower hyperplastic parathyroid glands (arrows)

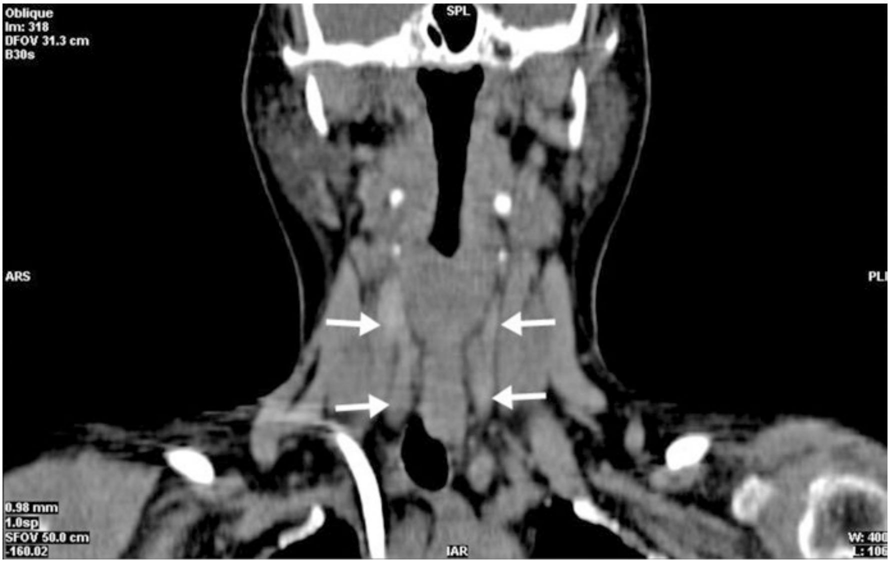

Fig. 7.129 Coronal CT image component of the SPECT scan showing four hyperplastic parathyroid glands (arrows) measuring 22.3 × 8.5 × 8.4 mm (upper right), 16.2 × 8 × 6.3 mm (lower right), 15.4 × 4 × 6 mm (upper left) and 18.7 × 10.8 × 10 mm (lower left)

- Diffuse or nodular hyperplasia of the parathyroid gland in patients with chronic renal failure may affect a different number of parathyroid glands to include all of them as seen in this case.
- Secondary hyperparathyroidism is a serious complication of chronic renal failure. Hypocalcaemia, hyperphosphataemia, deficiency of 1,25-dihydroxy vitamin D3, decreased expression of both calcium-sensing receptors and vitamin D receptors and resistance to PTH play an important role in its development.

7.47 Case 7.47. Brown Tumour Associated with Parathyroid Adenocarcinoma Mimicking a Mediastinal Parathyroid Adenoma

A 39-year-old male presented with complaints of backache and progressive loss of hearing for 3 months. Biochemical tests revealed serum calcium high at 17.7 mg/dL (normal 8.5–10.3 m/dL), blood urea raised at 129 mg/dL (normal 7–30 mg/dL), serum creatinine raised at 2.4 (normal 0.7–1.4 mg/dL) and serum parathyroid hormone (PTH) high at 882 pg/mL (normal 11–54 pg/mL). The patient was referred to the nuclear medicine department for parathyroid and skeletal scintigraphy.

7.47.1 Procedure

Whole-body skeletal scintigraphy was performed with ^{99m}Tc-methylene diphosphonate (Fig. 7.130), and dual-phase (early and late) ^{99m}Tc-sestamibi planar scan was performed after injection of 800 MBq of ^{99m}Tc-sestamibi at 20 min and 2 h postinjection. A SPECT scan was also performed at 150 min postinjection.

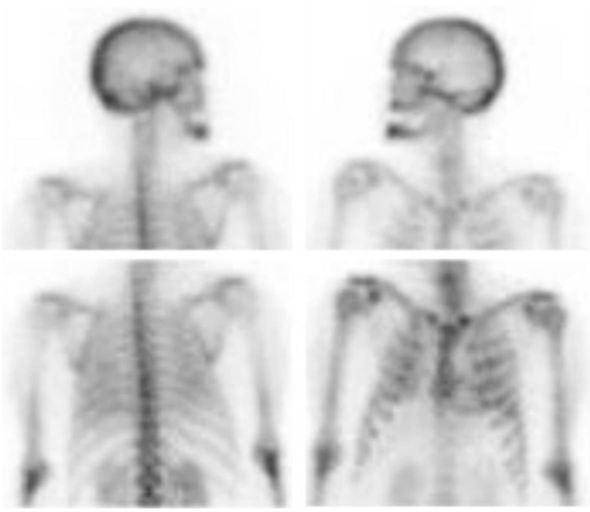

Fig. 7.130 ^{99m}Tc-methylene diphosphonate bone scan is essentially normal

7.47.2 Findings

The whole-body bone scan revealed diffuse calvarial uptake with no focal pathology documented. Both the early and the late planar sestamibi scans showed a focal area of intensely increased uptake in the chest. Also, there was faint focal uptake adjacent to the lower pole of the left lobe of the thyroid on both the early and late planar ^{99m}Tc-sestamibi scans (Fig. 7.131a). There was no abnormality noted at this site on the SPECT scan, which only showed the abnormal focus of uptake in the anterior mediastinum (Fig. 7.131b).

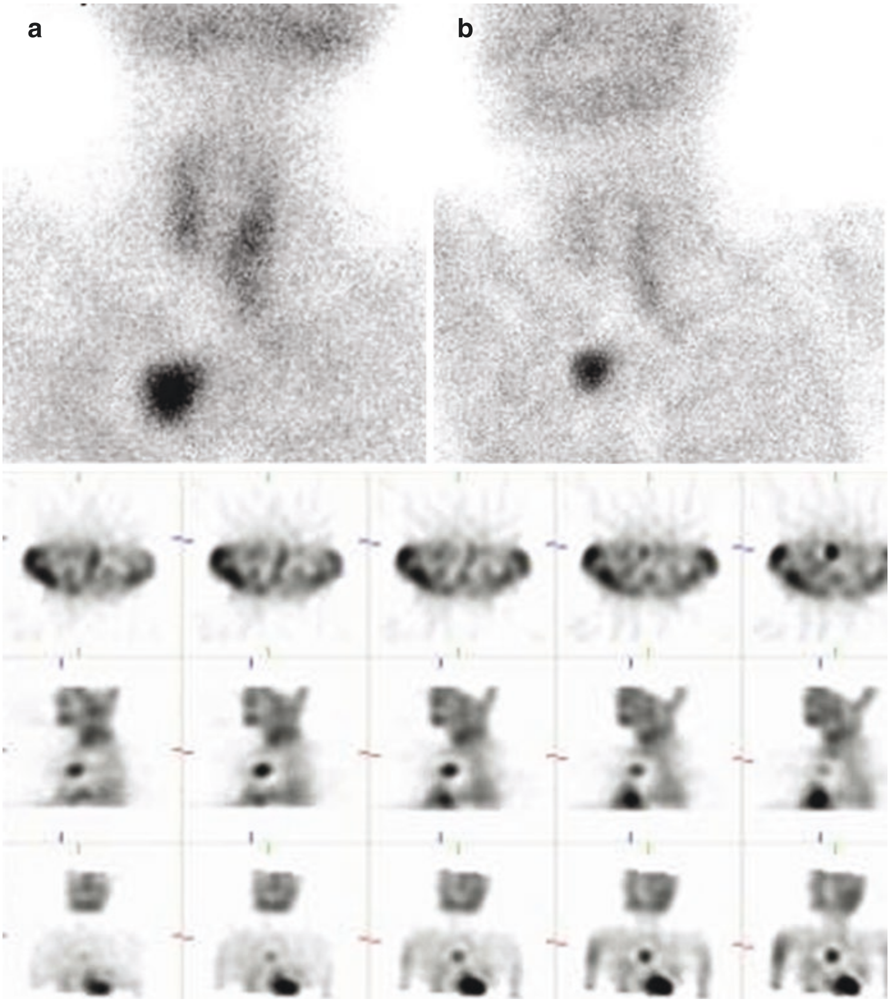

Fig. 7.131 ^{99m}Tc-sestamibi dual-phase planar scans (top row) at 20 min (**a**) and 120 min (**b**) and SPECT scan (**c**) acquired at 150 min postinjection (bottom row)

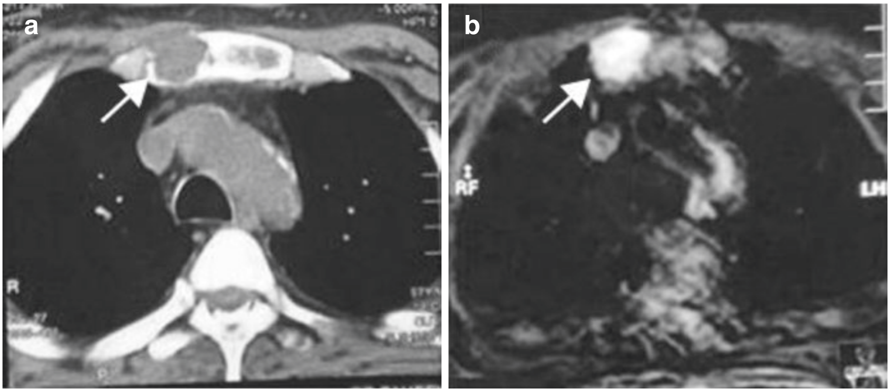

Fig. 7.132 CT scan viewed on the bone window (**a**) and MRI chest (**b**). Arrows point to the brown tumour in the sternum

7.47.3 Conclusion

The chest lesion was thought to represent an ectopic parathyroid adenoma. However, MRI images of the chest (Fig. 7.132b) revealed an expansile abnormal signal lesion over the right side of the manubrium sternum without any evidence of a mediastinal lesion seen. CT scan (Fig. 7.132a) viewed on the bone window confirmed the MRI finding of a lytic lesion with anterior cortical break involving the right side of the manubrium sternum. The CT findings were suggestive of brown tumour.

Parathyroidectomy was performed given the left lower parathyroid lobe abnormality suggestive of a possible left lower parathyroid adenoma, and a brown firm parathyroid nodule (2.4 × 1.9 × 1.5 cm) adjacent to the lower pole of the left lobe of the thyroid was resected. Histopathology of the parathyroid gland showed a nodular and cellular tumour with evidence of cellular and capsular invasion. Most of the cells were chief cells with some pleomorphism and calcification. The appearances were those of an active and cellular parathyroid adenocarcinoma.

7.47.4 Comments and Teaching Points

- Parathyroid carcinoma is a very cause of PTH-dependent hypercalcaemia, accounting for less than 1% of all cases of hyperparathyroidism [73].
- In primary hyperparathyroidism, brown tumour is an uncommon bone disease [74], and sternal involvement has been reported previously [75–77].
- The present case demonstrates intense focal ^{99m}Tc-sestamibi uptake in a brown tumour associated with parathyroid cancer [77] mimicking an ectopic parathyroid adenoma giving a false-positive diagnosis and thus leading to diagnostic pitfall.

7.48 Case 7.48. Normocalcaemic Primary Hyperparathyroidism and Bilateral Upper Parathyroid Gland Hyperplasia

7.48.1 Background

A 51-year-old female complaining of bone pains was found to be biochemically hyperparathyroid. Her serum PTH was high at 76.57 pmol/L (normal 1.3–9.3), calcium 2.53 mmol/L (normal 2.2–2.6), phosphorus 1.21 mmol/L (normal 0.84–1.45), alkaline phosphate 83 IU/L (normal 42–98), urea 5.6 mmol/L (normal range 2.5–6.4) and creatinine 99 µmol/L (normal range 53–97).

7.48.2 Procedure

The patient was injected with 76 MBq of ^{99m}Tc-pertechnetate, and a thyroid scan was acquired for 10 min at 15 min postinjection. Next, 754 MBq of ^{99m}Tc-sestamibi was injected without moving the patient and a 10-min duration planar scan performed after 10 min. ^{99m}Tc-sestamibi SPECT/CT scan was performed at 2 h followed by a late planar ^{99m}Tc-sestamibi scan at 3 h.

7.48.3 Findings

The ^{99m}Tc-pertechnetate thyroid scan (Fig. 7.133a) showed a normal-sized image of the thyroid with a larger left lobe and fairly normal uptake. The early planar ^{99m}Tc-sestamibi scan (Fig. 7.133b) showed faint focal uptake in the upper part of the right and the left thyroid lobes with marginal retention of activity seen here on the washout images (Fig. 7.133c). The ^{99m}Tc-sestamibi/^{99m}Tc-pertechnetate subtraction image did not show any residual focal activity in the thyroid bed (Fig. 7.133d).

The SPECT/CT scan (Fig. 7.134) showed bilateral foci of activity behind the middle one-third of both thyroid lobes corresponding to the bilateral elongated enlarged upper parathyroid glands on the CT component, with the right gland measuring 19.9 × 5.5 × 12 mm and the left 19.2 × 6 × 11 mm in size (Fig. 7.135).

7.48.4 Conclusion

Findings consistent with bilateral upper parathyroid gland hyperplasia associated with primary hyperparathyroidism.

7.48.5 Comments and Teaching Points

- 15% of the cases of PHPT are due to parathyroid gland hyperplasia.

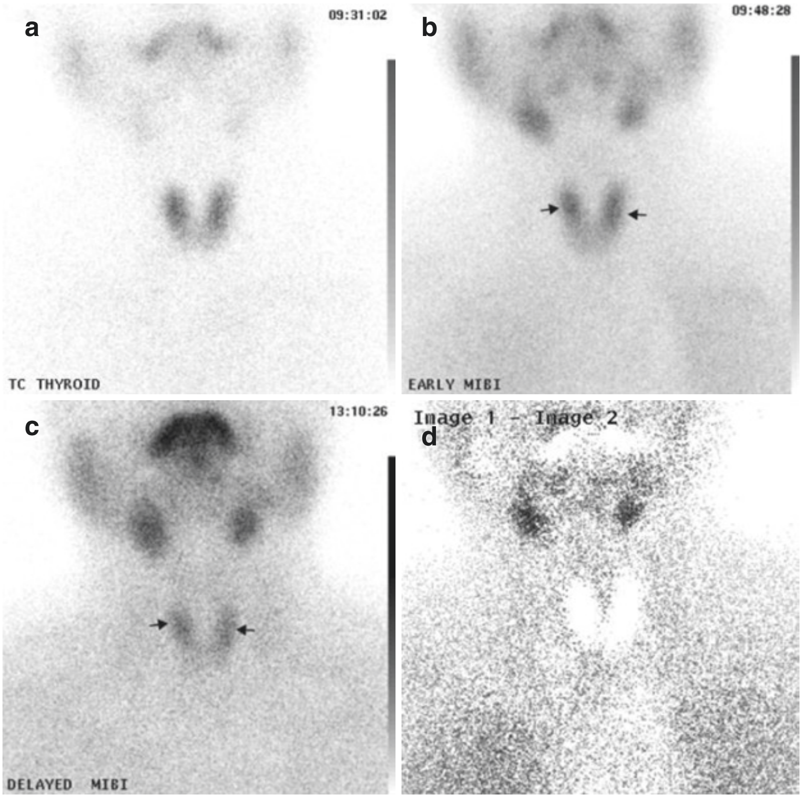

Fig. 7.133 ^{99m}Tc-pertechnetate thyroid scan (**a**), early planar ^{99m}Tc-sestamibi scan (**b**), late planar ^{99m}Tc-sestamibi scan (**c**) and ^{99m}Tc-sestamibi/^{99m}Tc-pertechnetate subtraction scan image (**d**). The arrows point to the foci of increased uptake in both upper thyroid lobes with a negative subtraction image

- The planar images were equivocal for parathyroid hyperplasia, and the ^{99m}Tc-sestamibi/^{99m}Tc-pertechnetate subtraction scan image was negative. Hyperplastic parathyroid glands are usually not detected on a subtraction image except for a large-sized hyperplastic parathyroid gland.
- The SPECT/CT images were not only diagnostic but accurate as the hyperplastic lesions were independently detected of both of the hybrid modalities.
- The upper parathyroid glands are generally thin or flat and leaf-like in shape as seen in this case, and expertise in parathyroid CT is important for their correct identification and localisation because the glands are often located very close to the thyroid and may exhibit an enhancement pattern similar to that of the thyroid parenchyma and because of their thin, elongated shape may easily be mistaken for a lobulation of the thyroid parenchyma.
- In our experience, the hyperplastic parathyroid glands are generally slightly brighter than the thyroid or less frequently have an equivalent density as compared to the thyroid parenchyma, whereas in contrast, the adenomatous parathyroid glands generally tend to be darker than the thyroid parenchyma.

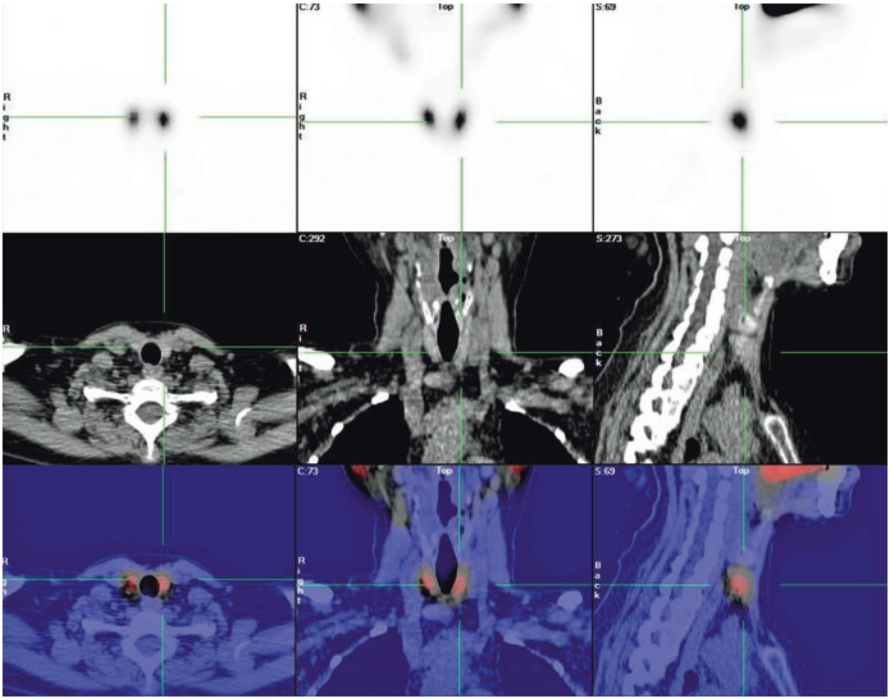

Fig. 7.134 ^{99m}Tc-sestamibi SPECT scan images (top row), CT scan images (middle row) and fused SPECT/CT images (bottom row) in the transaxial (left column), coronal (middle column) and sagittal (right column) planes, showing bilateral upper parathyroid gland hyperplasia

Fig. 7.135 Coronal (top) and transaxial (bottom) CT scan images showing bilateral hyperplastic parathyroid glands (arrows) with the right gland measuring 19.9 × 5.5 × 12 mm and the left 19.2 × 6 × 11 mm. Note the leafy oblong shape of the upper parathyroid glands

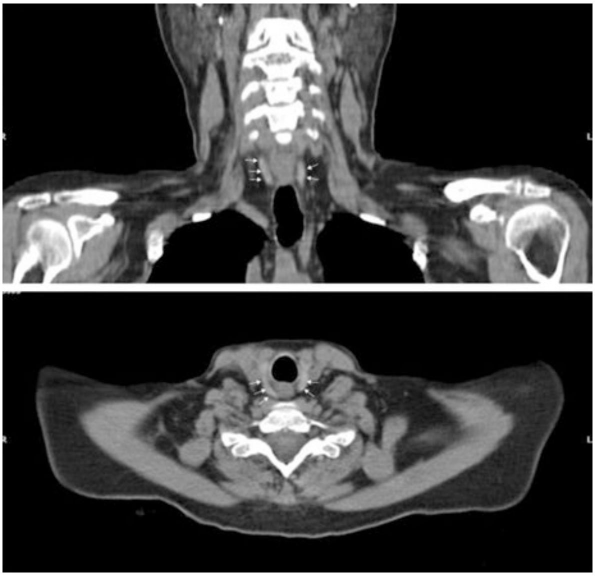

7.49 Case 7.49. Normocalcaemic Primary Hyperparathyroidism and Five-Gland Hyperplasia

7.49.1 Background

A 14-year-old boy with spastic paraparesis was found to have increased PTH without any renal disease. Serum PTH was 15.3 pmol/L (normal 1.3–9.3), calcium 2.36 mmol/L (normal 2.2–2.6), phosphorus 1.4 mmol/L (normal 0.84–1.45), alkaline phosphate 313 IU/L (normal 53–390), urea 4.9 mmol/L (normal range 1.8–6.4) and creatinine 54 µmol/L (normal range 53–106).

7.49.2 Procedure

The patient was injected with 65 MBq of ^{99m}Tc-pertechnetate, and a thyroid scan was acquired for 10 min at 15 min postinjection. Next, 760 MBq of ^{99m}Tc-sestamibi was injected without moving the patient and a 10-min duration planar scan performed after 10 min. ^{99m}Tc-sestamibi SPECT/CT scan was performed at 2 h followed by a late planar ^{99m}Tc-sestamibi scan at 3 h.

7.49.3 Findings

The ^{99m}Tc-pertechnetate thyroid scan (Fig. 7.136a) showed a larger right lobe and a smaller left lobe with slight non-homogeneity of uptake. The early planar

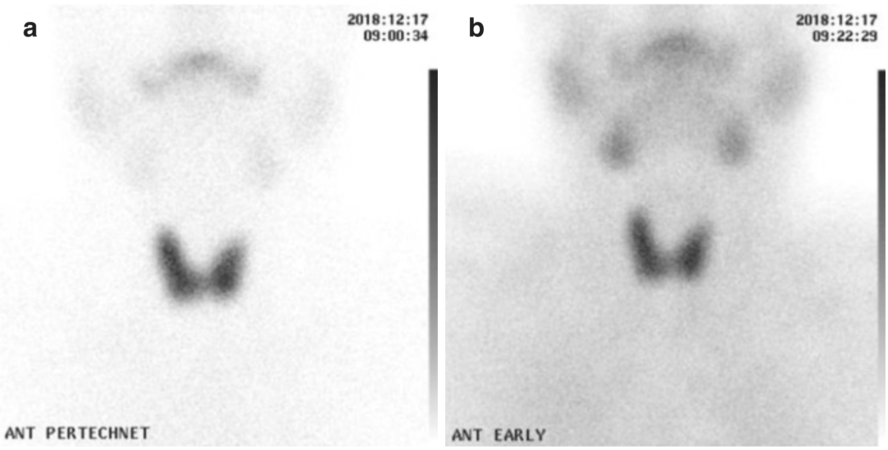

Fig. 7.136 ^{99m}Tc-pertechnetate thyroid scan (**a**), early planar ^{99m}Tc-sestamibi scan (**b**), late planar ^{99m}Tc-sestamibi scan (**c**) and ^{99m}Tc-sestamibi/^{99m}Tc-pertechnetate subtraction scan image (**d**). All images are normal

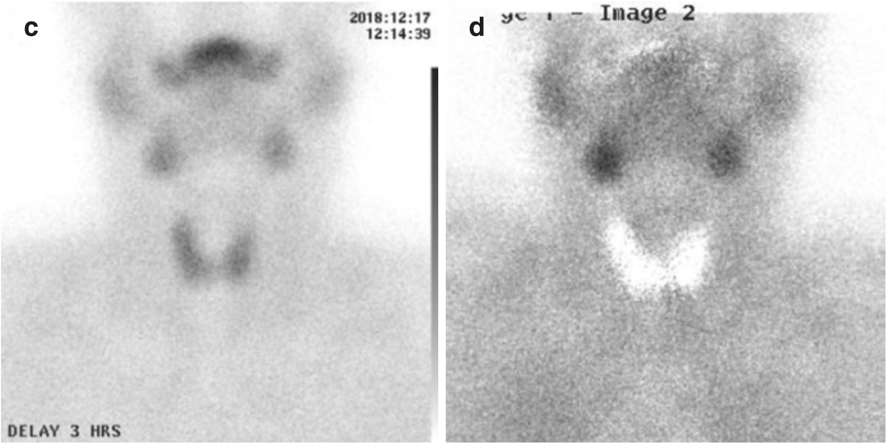

Fig. 7.136 (continued)

^{99m}Tc-sestamibi scan (Fig. 7.136b) showed a pattern of uptake similar to that seen in the pertechnetate thyroid scan with no focal retention seen in the thyroid bed on the washout images (Fig. 7.136c). The ^{99m}Tc-sestamibi/^{99m}Tc-pertechnetate subtraction image did not show any residual focal activity in the thyroid bed (Fig. 7.136d).

The CT component of the SPECT/CT scan (Fig. 7.137) showed five enlarged parathyroid glands including a left upper measuring 9.4 × 5.5 × 10.5 mm, a left lower measuring 8.4 × 6.3 × 5.2 mm, a right lower measuring 6.8 × 5.8 × 10 mm, an upper right measuring 12.2 × 6.2 × 7.7 mm and a top upper right measuring 17.8 × 9.8 × 7.7 mm in size. The SPECT scan (Fig. 7.138) showed moderately increased uptake in the superior right upper gland and mildly increased uptake in the left lower gland.

7.49.4 Conclusion

Findings consistent with five-gland parathyroid hyperplasia associated with normocalcaemic primary hyperparathyroidism.

7.49.5 Comments and Teaching Points

- This is a novel case of normocalcaemic primary hyperparathyroidism due to five-gland parathyroid hyperplasia.
- Due to improvement in PTH assays and early diagnosis, cases with elevation of PTH but consistently normal serum calcium (normocalcaemic primary hyperparathyroidism) are increasingly being detected [78, 79].
- Normocalcaemic primary hyperparathyroidism is postulated to be due to a resistance to target tissues [78] with another concept based upon the evolution of the

Fig. 7.137 Coronal CT scan image slices showing five hyperplastic parathyroid glands including left upper measuring 9.4 × 5.5 × 10.5 mm (#1), left lower measuring 8.4 × 6.3 × 5.2 mm (#2), right lower measuring 6.8 × 5.8 × 10 mm (#3), second upper right measuring 12.2 × 6.2 × 7.7 mm (#4) and first upper right 17.8 × 9.8 × 7.7 mm (#5)

hypercalcaemic form, with the first detectable abnormality being an increase in the circulating PTH with a certain proportion of patients showing a gradual rise in calcium over time [80].

- The sestamibi uptake in the glands is directly in proportion to the size of the glands with no uptake seen in the smaller three glands, which were false-negative on SPECT, but the larger two of the five glands showed sestamibi uptake and were true-positive.
- All five glands were detected on the diagnostic-quality CT scan without contrast.

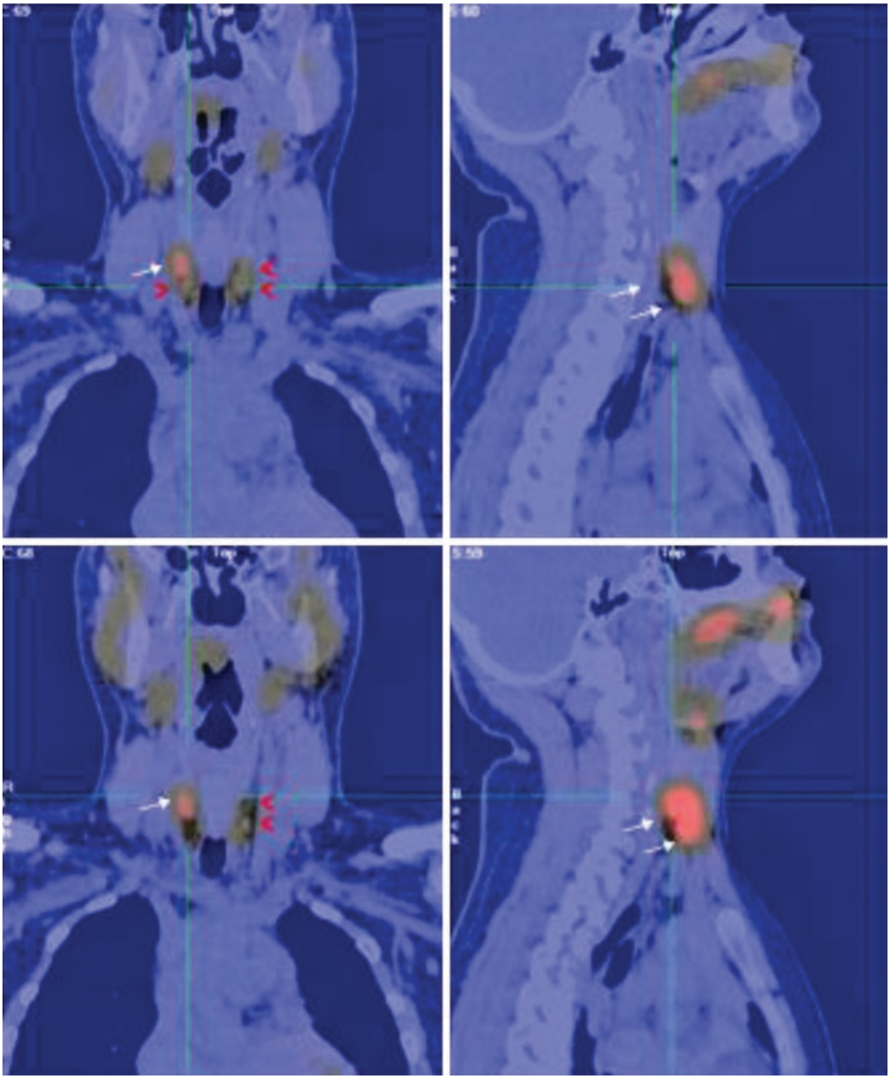

Fig. 7.138 Fused SPECT/CT scan images in the coronal (left) and sagittal (right) axes showing no uptake in the small upper and lower left and the lower right parathyroid glands (red arrowheads) with ^{99m}Tc-sestamibi uptake seen in the larger right upper two parathyroid glands (white arrows)

- SPECT/CT is the best modality for the diagnosis of parathyroid gland hyperplasia due to the incremental value of CT which can detect very-small-sized glands that are difficult to detect on the SPECT alone.
- Progressive spastic paraparesis has been reported in a patient with undiagnosed primary hyperparathyroidism [81] but not in a patient with normocalcaemic primary hyperparathyroidism. It is however not clear if this is incidental.

7.50 Case 7.50. Right Upper Parathyroid Adenoma Pre- and Post-surgery

7.50.1 Background

A 38-year-old female presented in October 2011 with generalised bone pains, elevated serum parathormone levels and hypercalcaemia and slightly elevated serum parathormone level at 11.41 pmol/L (normal 1.3–9.3). Corrected calcium was 2.76 mmol/L (normal 2.2–2.6), phosphorus 1.09 mmol/L (normal 0.84–1.45), alkaline phosphate 93 IU/L (normal 53–97), urea 4.4 mmol/L (normal range 2.5–6.4) and creatinine 66 μmol/L (normal range 53–97).

7.50.2 Procedure

The patient was injected with 65 MBq of ^{99m}Tc-pertechnetate and a thyroid scan was acquired for 5 min at 20 min postinjection. Next, 845 MBq of ^{99m}Tc-sestamibi was injected without moving the patient and a planar scan performed after 10 min. ^{99m}Tc-sestamibi SPECT/CT scan was performed at 2 h followed by a late planar ^{99m}Tc-sestamibi scan at 3 h. The scans were repeated with similar imaging parameters 7 months later after successful excision of a right upper parathyroid adenoma.

7.50.3 Findings

The pertechnetate thyroid scan showed a normal-sized image of the thyroid with homogenous distribution of activity in the gland (Fig. 7.139a). The early planar ^{99m}Tc-sestamibi scan (Fig. 7.139b) showed a pattern of uptake similar to that seen on the pertechnetate thyroid scan but with a suggestion of a suspicious focus of very faint uptake in the mid right lobe, which showed marginal focal retention on the delayed washout sestamibi images (Fig. 7.139c). The ^{99m}Tc-sestamibi/^{99m}Tc-pertechnetate subtraction image however showed a residual focus of activity in the middle of the right thyroid bed (Fig. 7.139d). The SPECT/CT scan (Fig. 7.140) showed a focus of uptake on the SPECT scan located behind the middle one-third of the right thyroid lobe with the CT component (Fig. 7.141) showing the focus of activity to correspond to a hypodense lesion measuring 17.8 × 14.5 × 10 mm in size. The patient underwent parathyroidectomy and a cystic right upper parathyroid gland was removed. The postsurgical parathyroid scans were normal with no evidence of a hyperactive parathyroid lesion seen (Figs. 7.142 and 7.143).

7.50.4 Conclusion

Findings consistent with a right upper parathyroid adenoma as the cause of primary hyperparathyroidism.

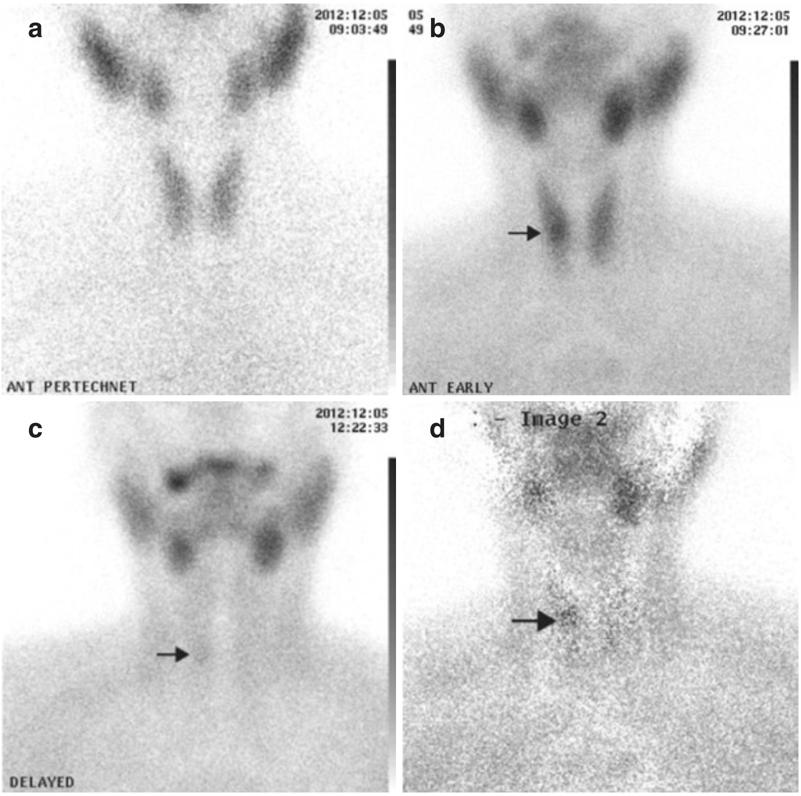

Fig. 7.139 Baseline ^{99m}Tc-pertechnetate thyroid scan (**a**), early planar ^{99m}Tc-sestamibi scan (**b**), late planar ^{99m}Tc-sestamibi scan (**c**) and ^{99m}Tc-sestamibi/^{99m}Tc-pertechnetate subtraction scan images (**d**) with the arrow pointing to the focus of mildly increased uptake in the right thyroid lobe

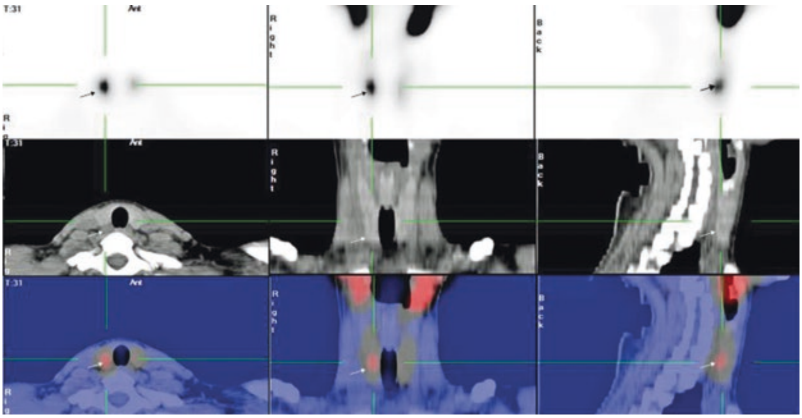

Fig. 7.140 Baseline ^{99m}Tc-sestamibi SPECT scan images (top row), CT scan images (middle row) and fused SPECT/CT images (bottom row) in the transaxial (left column), coronal (middle column) and sagittal (right column) planes, showing a right parathyroid adenoma (arrows)

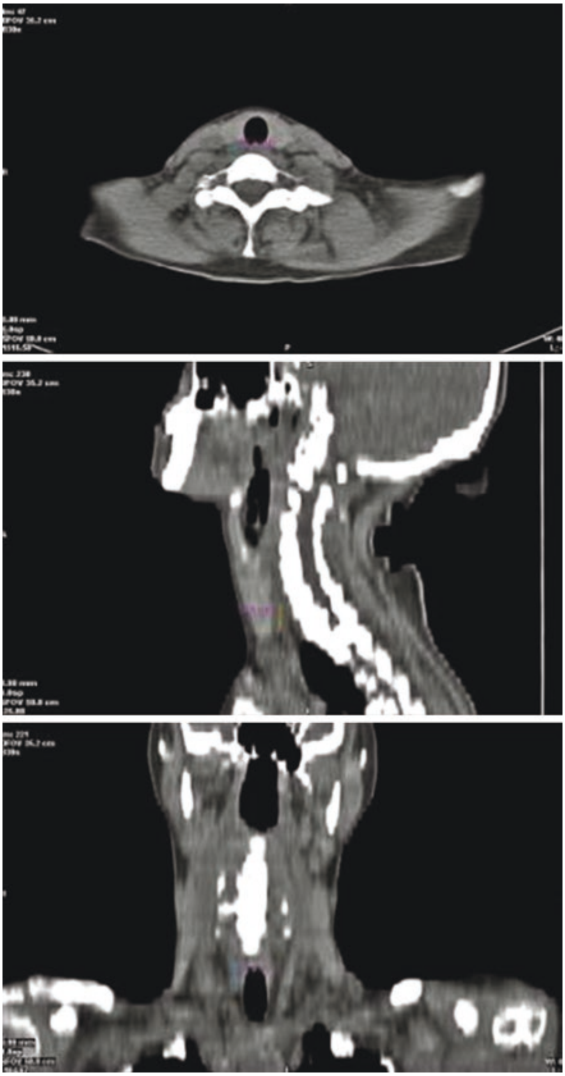

Fig. 7.141 Baseline CT scan images in transaxial (top), sagittal (middle) and coronal axes (bottom) showing a right parathyroid adenoma (arrows) measuring 17.8 × 14.5 × 10 mm in size

Following resection of the right parathyroid adenoma, the patient's serum PTH levels fell from a preoperative value of 11.41 to 4.92 pmol/L (normal 1.3–9.3), and serum calcium level normalised to 2.38 mmol/L (normal 2.2–2.6).

7.50.5 Comments and Teaching Points

- Present-day routine biochemical analysis with multichannel autoanalysers has allowed the diagnosis of hyperparathyroidism mostly before the development of symptoms by the patients.

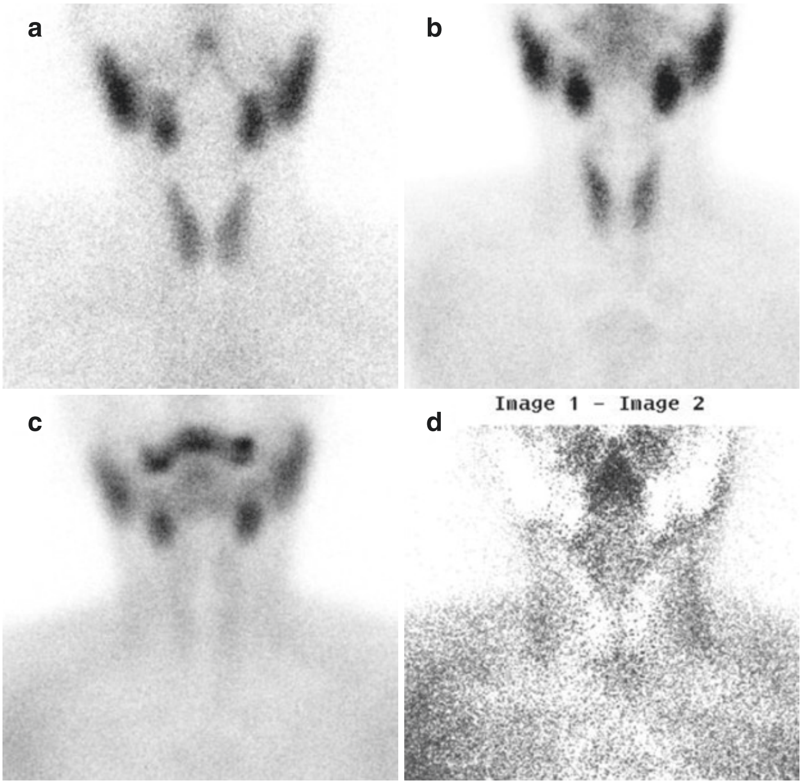

Fig. 7.142 Postsurgery ^{99m}Tc-pertechnetate thyroid scan (**a**), early planar ^{99m}Tc-sestamibi scan (**b**), late planar ^{99m}Tc-sestamibi scan (**c**) and ^{99m}Tc-sestamibi/^{99m}Tc-pertechnetate subtraction scan images (**d**) all appear normal consistent with successful removal of the right upper parathyroid adenoma

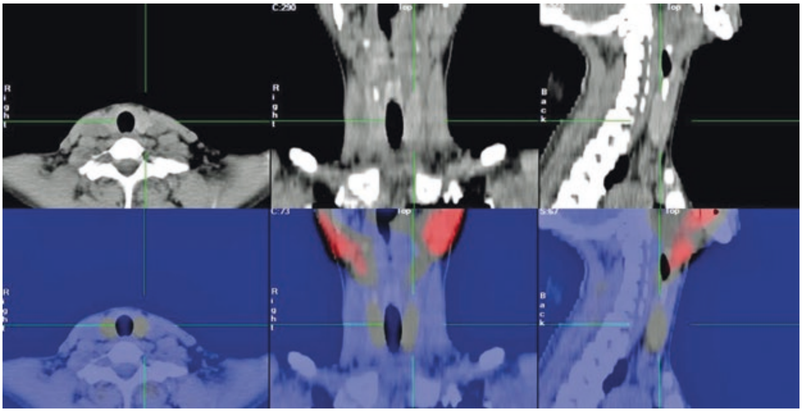

Fig. 7.143 Postsurgery ^{99m}Tc-sestamibi SPECT scan with CT scan images (top) and fused SPECT/CT images (bottom) in the transaxial (left column), coronal (middle column) and sagittal (right column) planes all appearing normal following successful removal of the right upper parathyroid adenoma

- The most common clinical presentation today is that of asymptomatic mild hypercalcaemia discovered incidentally on a blood chemistry panel as seen in this case.
- Approximately 10% of patients with primary hyperparathyroidism will have elevated calcium levels with relatively normal PTH levels [82].
- Hypercalcaemia is said to be PTH-mediated if serum calcium is elevated and the PTH level is high or inappropriately normal as in this case.

7.51 Case 7.51. Probable Non-oncogenic Cell Parathyroid Adenoma

7.51.1 Background

A 37-year-old male presented with hypercalcaemia and hyperparathyroidism. The patient had kidney stones and was a stone passer. Serum PTH was 33.90 pmol/L (normal 1.3–9.3), corrected calcium 2.96 mmol/L (normal 2.2–2.6), phosphorus 0.82 mmol/L (normal 0.84–1.45), alkaline phosphate 109 IU/L (normal 53–97), urea 5.1 mmol/L (normal range 2.5–6.4) and creatinine 51 µmol/L (normal range 53–97).

7.51.2 Procedure

The patient was injected with 72 MBq of ^{99m}Tc-pertechnetate and a thyroid scan was acquired for 10 min at 15 min postinjection. Next, 763 MBq of ^{99m}Tc-sestamibi was injected without moving the patient and a 10-min duration planar scan acquired after 10 min. ^{99m}Tc-sestamibi SPECT/CT scan was performed at 2 h followed by a late planar ^{99m}Tc-sestamibi scan at 3 h.

7.51.3 Findings

The pertechnetate thyroid scan (Fig. 7.144a) showed an enlarged image of the gland with a larger right lobe and multiple warm (functional) nodules in the gland. The early ^{99m}Tc-sestamibi scan (Fig. 7.144b) showed a pattern of uptake similar to that seen on the pertechnetate thyroid scan but the lower pole of the right lobe seemingly extended further downwards than on the pertechnetate thyroid scan. There was no significant focal retention seen in the thyroid bed on the delayed washout sestamibi images (Fig. 7.144c). The ^{99m}Tc-sestamibi/^{99m}Tc-pertechnetate subtraction image showed irregular patchy activity in the thyroid bed presumably related to the multiple thyroid nodules (Fig. 7.144d). The CT component of the SPECT/CT scan (Fig. 7.145) showed an oval-shaped nodule below the lower pole of the right lobe of the thyroid measuring 28.1 × 12.6 × 17.5 mm in size. The SPECT/CT scan (Fig. 7.146) showed only faint sestamibi uptake in the nodule.

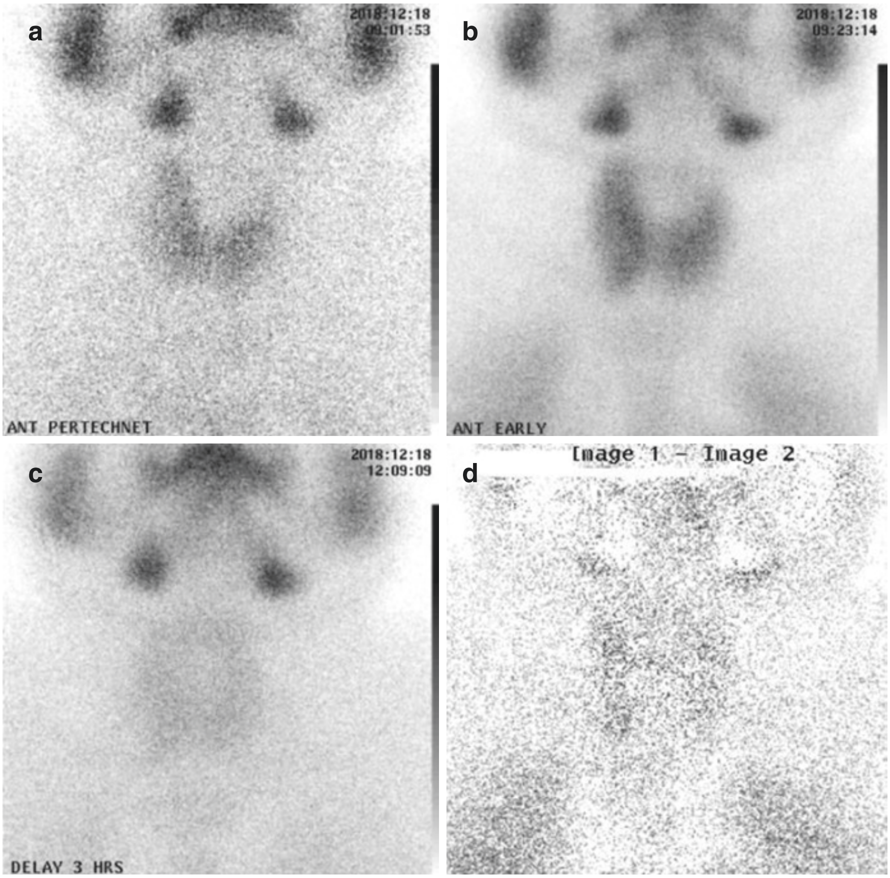

Fig. 7.144 ^{99m}Tc-pertechnetate thyroid scan (**a**), early planar ^{99m}Tc-sestamibi scan (**b**), late planar ^{99m}Tc-sestamibi scan (**c**) and ^{99m}Tc-sestamibi/^{99m}Tc-pertechnetate subtraction scan images (**d**) showing residual areas of mildly increased uptake in the right thyroid bed

7.51.4 Conclusion

Findings consistent with a presumed predominantly non-oncogenic cell right lower parathyroid adenoma as the cause of primary hyperparathyroidism.

7.51.5 Comments and Teaching Points

- A thallium-201 scan can be performed for confirmation if necessary because of the higher likelihood of thallium uptake in sizeable non-oncocytic cell adenomas than sestamibi which is better concentrated by mitochondria-rich adenomas. This premise has proven correct in other such cases in this chapter.

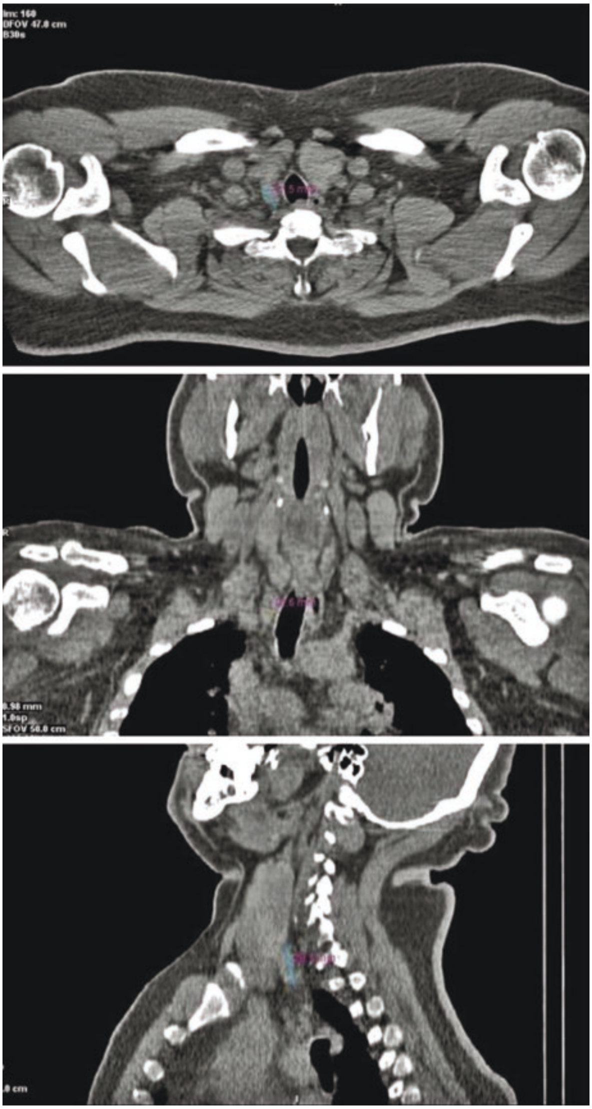

Fig. 7.145 Baseline CT scan images in transaxial (top), sagittal (middle) and coronal axes (bottom) showing a right parathyroid adenoma (arrows) measuring 17.8 × 14.5 × 10 mm in size

- The sensitivity of detection of parathyroid adenomas in the presence of multinodular goitre is relatively low.
- Thyroid nodules often mask parathyroid pathology, and multinodular goitres are associated with an increased rate of both false-positive and false-negative parathyroid scans.

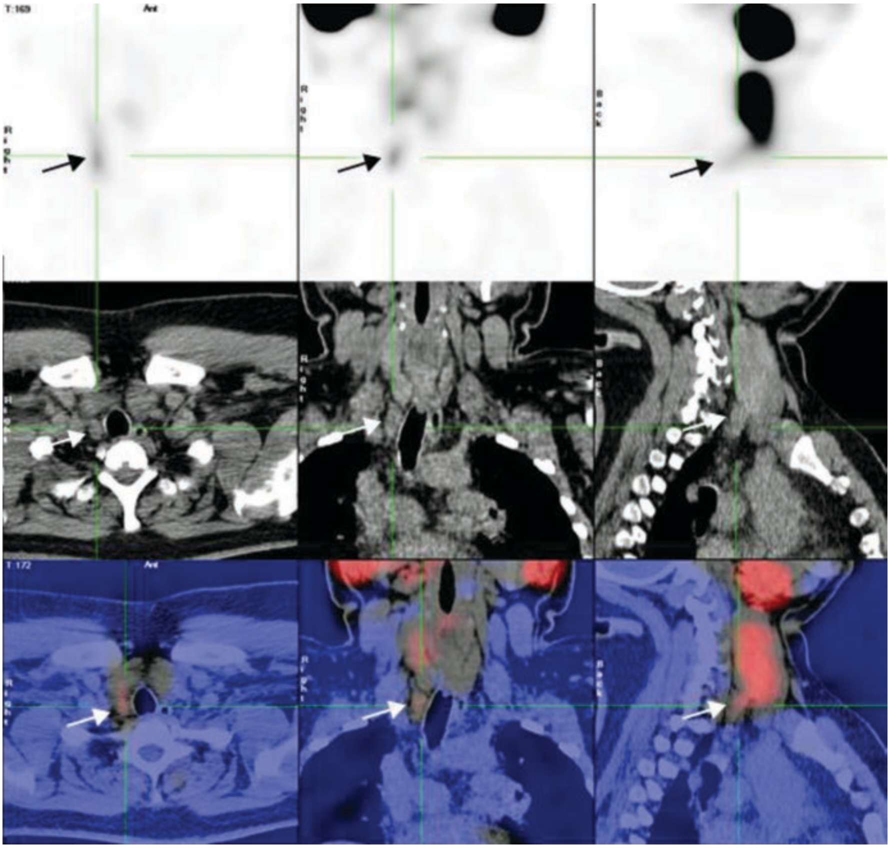

Fig. 7.146 Baseline ^{99m}Tc-sestamibi SPECT scan images (top row), CT scan images (middle row) and fused SPECT/CT images (bottom row) in the transaxial (left column), coronal (middle column) and sagittal (right column) planes, showing a right parathyroid adenoma (arrows)

7.52 Case 7.52. Pertechnetate- and Sestamibi-Avid Intrathyroidal Parathyroid Adenoma

7.52.1 Background

A 70-year-old female with increased serum parathormone and hypercalcaemia was referred for a parathyroid scan. Her serum PTH level was 20.3 pmol/L (normal 0.8–5.7), corrected calcium 2.87 mmol/L (normal 2.2–2.6), phosphorus 0.86 mmol/L (normal 0.84–1.45), urea 3.5 mmol/L (normal range 2.5–6.4) and creatinine 71 μmol/L (normal range 53–97). Ultrasound showed multiple thyroid nodules in both lobes of the gland.

7.52.2 Procedure

The patient was injected with 82 MBq of ^{99m}Tc-pertechnetate, and a thyroid scan was acquired for 10 min at 15 min postinjection. Next, 782 MBq of ^{99m}Tc-sestamibi was injected without moving the patient and a planar scan performed after 10 min. ^{99m}Tc-sestamibi SPECT/CT scan was performed at 2 h followed by a late planar ^{99m}Tc-sestamibi scan at 3 h.

7.52.3 Findings

The ^{99m}Tc-pertechnetate thyroid scan (Fig. 7.147a) showed a "hot" nodule in the right lobe with apparent partial suppression of uptake elsewhere in the gland. The

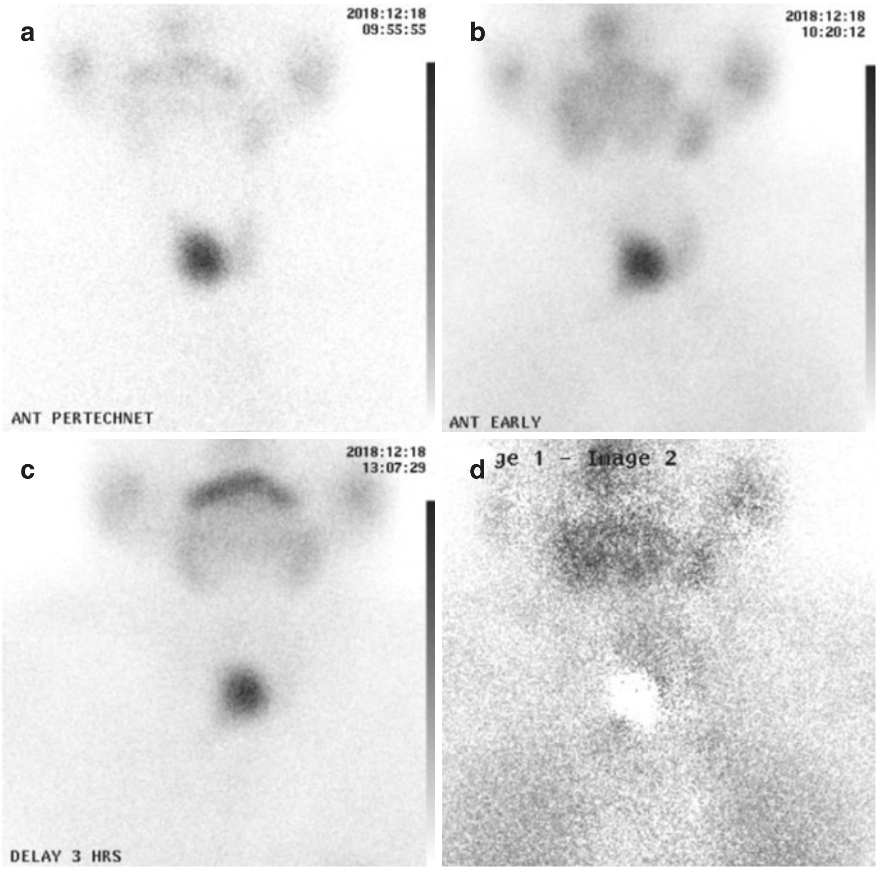

Fig. 7.147 ^{99m}Tc-pertechnetate thyroid scan (**a**), early planar ^{99m}Tc-sestamibi scan (**b**), late planar ^{99m}Tc-sestamibi scan (**c**) and ^{99m}Tc-sestamibi/^{99m}Tc-pertechnetate subtraction scan (**d**)

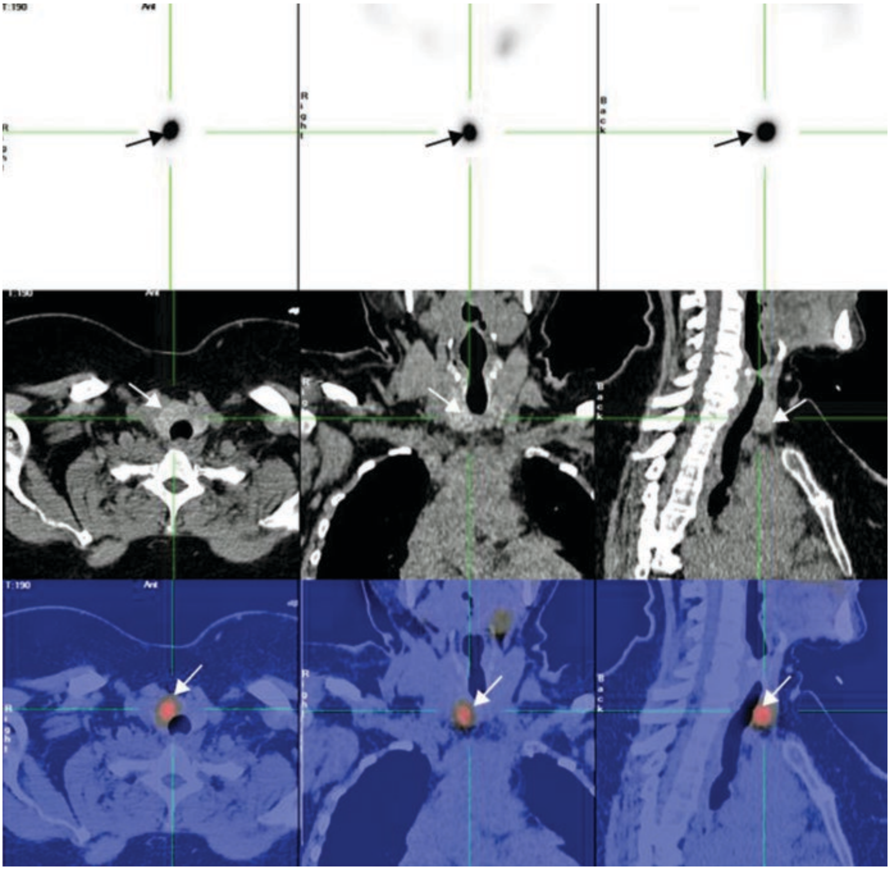

Fig. 7.148 ^{99m}Tc-sestamibi SPECT scan images (top row), CT scan images (middle row) and fused SPECT/CT images (bottom row) in the transaxial (left column), coronal (middle column) and sagittal (right column) planes, showing a right intrathyroidal parathyroid adenoma (arrows)

early planar ^{99m}Tc-sestamibi scan (Fig. 7.147b) showed a pattern of uptake similar to that seen on the pertechnetate thyroid scan, with the delayed washout sestamibi scan (Fig. 7.147c) showing marked retention of activity in the nodule and washout of uptake from the surrounding thyroid parenchyma. The ^{99m}Tc-sestamibi/^{99m}Tc-pertechnetate subtraction image did not however show any residual focus of activity in the thyroid bed (Fig. 7.147d). The SPECT/CT scan (Fig. 7.148) showed a large focus of intense uptake in the lower part of the right lobe anteriorly located within the thyroid gland. The nodule was seen to measure 28.8 × 22.5 × 13.6 mm on the CT component (Fig. 7.149).

7.52.4 Conclusion

Findings consistent with a pertechnetate- and sestamibi-avid right intrathyroidal parathyroid adenoma as the cause of primary hyperparathyroidism.

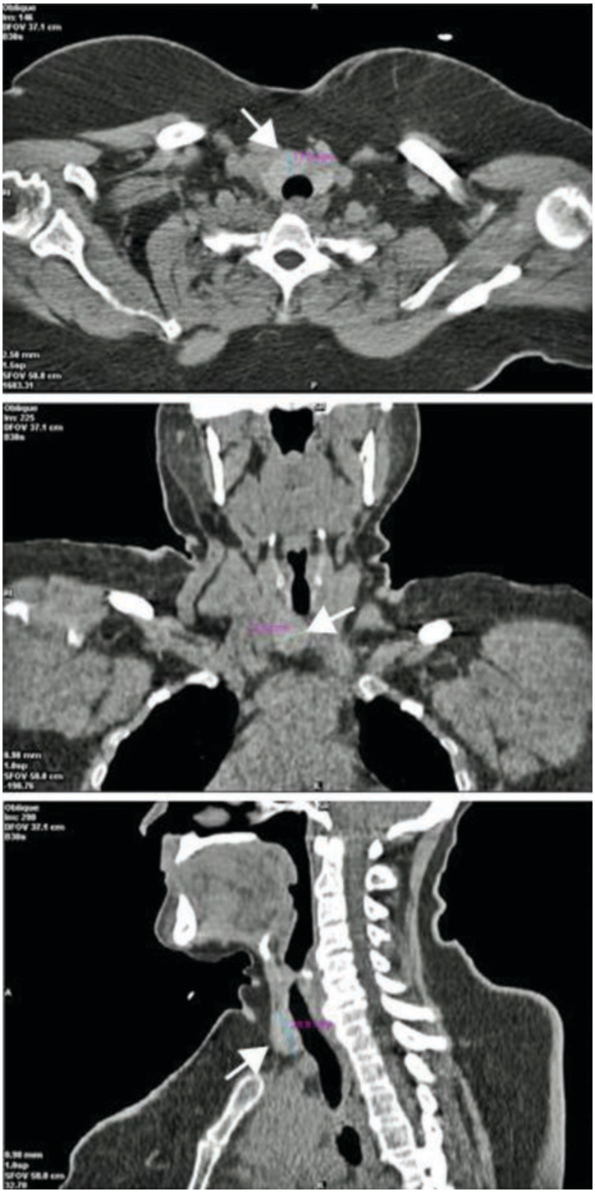

Fig. 7.149 CT scan images in transaxial (top), sagittal (middle) and coronal axes (bottom) showing an intrathyroidal right parathyroid adenoma (arrows) measuring 28.8 × 22.5 × 13.6 mm in size

7.52.5 Comments and Teaching Points

- This is a rare case of a pertechnetate- and sestamibi-avid ectopic intrathyroidal parathyroid adenoma.
- Parathyroid adenoma avid for both ^{99m}Tc-sestamibi and ^{123}I has been previously reported [83], and we have included several cases of pertechnetate- and sestamibi-avid parathyroid adenomas in this book. This is also true for thyroid

adenomas which may demonstrate both pertechnetate and sestamibi uptake. A combination of SPECT/CT and biochemical analysis helps differentiate between thyroid and parathyroid adenomas.

- ^{99m}Tc-pertechnetate uptake by intrathyroidal parathyroid adenoma has been reported in intrathyroidal parathyroid adenomas and has been attributed to the hypervascularity of the lesion [84].
- The shape of a lesion serves as a criterion for differential diagnosis between thyroid and parathyroid tumours. Thyroid lesions are characterised by a roundish shape, but as seen in this case, inferior parathyroid gland adenomas are often seen as spherical or elliptical lesions which can be mistaken for thyroid lesions.

7.53 Case 7.53. Bilateral Lower Parathyroid Gland Hyperplasia

7.53.1 Background

A 37-year-old male with hypertension and diabetes mellitus with bilateral diabetic retinopathy and end-stage renal disease developed biochemical hyperparathyroidism. His serum parathormone level was 72 pmol/L (normal 1.3–9.3), corrected calcium 2.33 mmol/L (normal 2.2–2.6), magnesium 1.20 mmol/L (normal 0.73–1.06), phosphorus 2.16 mmol/L (normal 0.84–1.45), alkaline phosphate 103 IU/L (normal 53–97), urea 20 mmol/L (normal range 2.5–6.4) and creatinine 718 μmol/L (normal range 53–97).

7.53.2 Procedure

The patient was injected with 75 MBq of ^{99m}Tc-pertechnetate, and a thyroid scan was acquired for 10 min at 15 min postinjection. Next, 765 MBq of ^{99m}Tc-sestamibi was injected without moving the patient and a planar scan performed after 10 min. ^{99m}Tc-sestamibi SPECT/CT scan was performed at 2 h followed by a late planar ^{99m}Tc-sestamibi scan at 3 h.

7.53.3 Findings

The pertechnetate thyroid scan showed a normal-sized image of the thyroid with homogenous distribution of activity in the gland (Fig. 7.150a). The early planar and the delayed washout ^{99m}Tc-sestamibi scans (Fig. 7.150b, c) were all essentially normal and similar in appearance to the pertechnetate scan. The ^{99m}Tc-sestamibi/^{99m}Tc-pertechnetate subtraction image was normal as well (Fig. 7.150d). The SPECT/CT scan (Fig. 7.151) showed focal increased uptake at the posterior aspect of the lower poles of both lobes of the thyroid corresponding to the bilaterally enlarged lower parathyroid glands, with the CT component showing a right gland measuring 16.5 × 10 × 10.9 mm and the left measuring 17.9 × 8.6 × 14.6 mm in size.

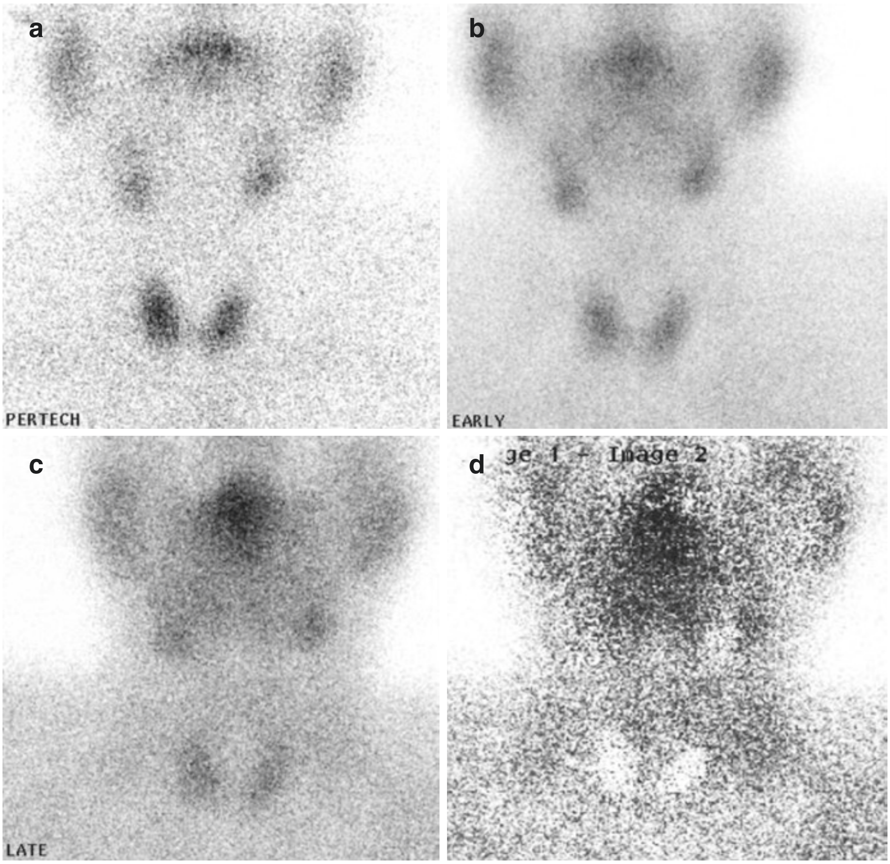

Fig. 7.150 ^{99m}Tc-pertechnetate thyroid scan (**a**), early planar ^{99m}Tc-sestamibi scan (**b**), late planar ^{99m}Tc-sestamibi scan (**c**) and ^{99m}Tc-sestamibi/^{99m}Tc-pertechnetate subtraction scan (**d**) images all appearing normal

7.53.4 Conclusion

Findings consistent with bilateral lower parathyroid gland hyperplasia associated with secondary hyperparathyroidism.

7.53.5 Comments and Teaching Points

- The planar early and late ^{99m}Tc-sestamibi scans and the ^{99m}Tc-sestamibi/^{99m}Tc-pertechnetate subtraction image were false-negative presumably due to the small size of the hyperplastic glands, but the hyperplastic parathyroid glands could be detected on both of the hybrid modalities of the SPECT/CT scan.

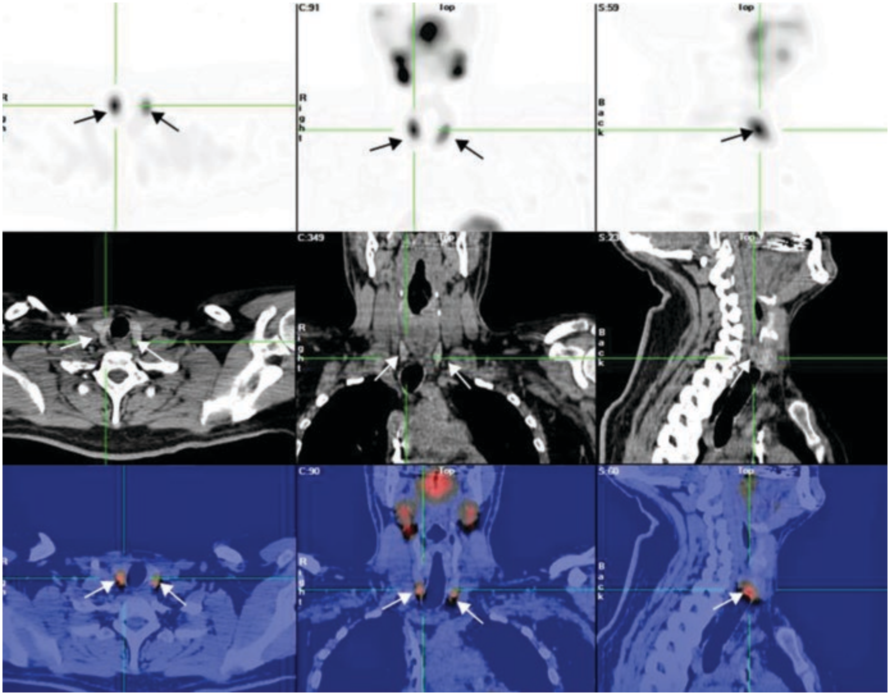

Fig. 7.151 ^{99m}Tc-sestamibi SPECT scan images (top row), CT scan images (middle row) and fused SPECT/CT images (bottom row) in the transaxial (left column), coronal (middle column) and sagittal (right column) planes, showing bilateral lower parathyroid gland hyperplasia (arrows)

7.54 Case 7.54. Double Parathyroid Adenomas

7.54.1 Background

A 60-year-old female with of osteoporosis and long standing history of fatigue presented with raised PTH and hypercalcaemia. MRI showed a well-defined solid-cystic lesion in the left infra-thyroid location. Serum parathormone level was 72.5 pmol/L (normal 1.3–9.3), calcium 3.04 mmol/L (normal 2.2–2.6), phosphorus 0.68 mmol/L (normal 0.84–1.45), urea 4 mmol/L (normal range 2.5–6.4) and creatinine 60 μmol/L (normal range 44–80).

7.54.2 Procedure

The patient was injected with 67 MBq of ^{99m}Tc-pertechnetate and a thyroid scan was acquired for 5 min at 20 min postinjection. Next, 855 MBq of ^{99m}Tc-sestamibi was injected without moving the patient and a planar scan performed after 10 min. ^{99m}Tc-sestamibi SPECT/CT scan was performed at 2 h followed by a late planar ^{99m}Tc-sestamibi scan at 3 h.

7.54.3 Findings

The pertechnetate thyroid scan (Fig. 7.152a) showed a normal-sized thyroid gland with uniform uptake with a focus of activity seen located below the thyroid. The early planar ^{99m}Tc-sestamibi scan (Fig. 7.152b) showed a pattern of uptake in the right lobe similar to that seen on the pertechnetate thyroid scan; however, there was a large oblong area of increased uptake occupying the lower left lobe and extending downwards, which area appeared to show no uptake on the pertechnetate scan and covered the region between the lower pole of the left lobe and the detached focus of activity seen on the pertechnetate scan thus indicating a filling-in of a large cold defect on the pertechnetate scan. On the late planar

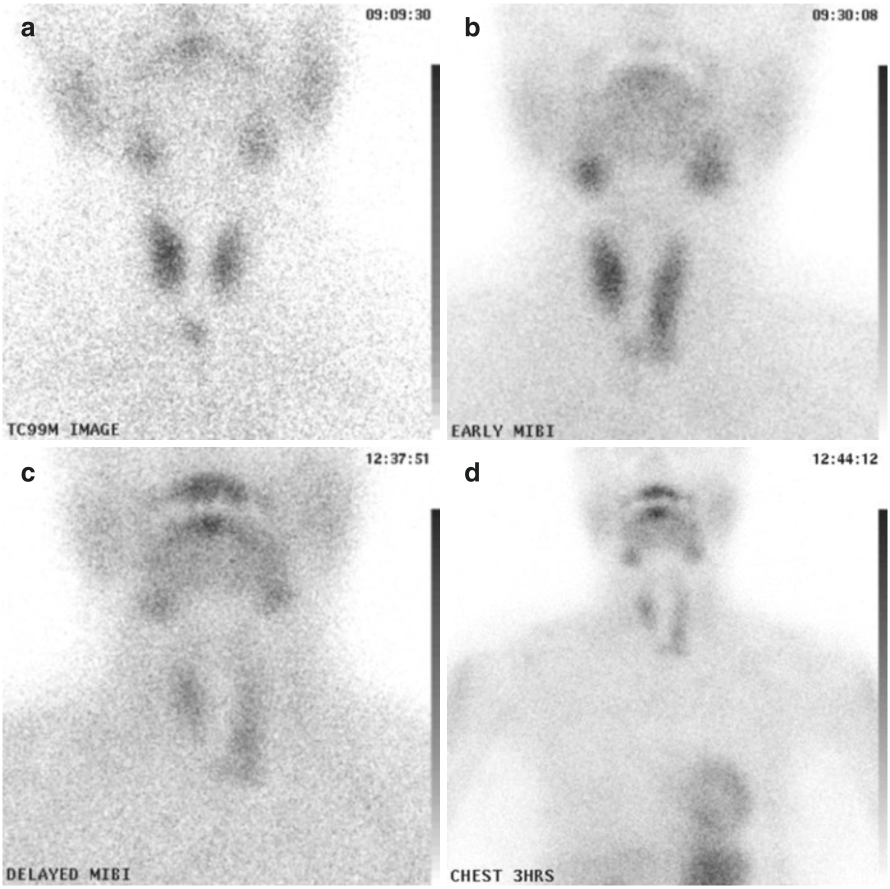

Fig. 7.152 ^{99m}Tc-pertechnetate thyroid scan (**a**), early planar ^{99m}Tc-sestamibi scan (**b**), late planar ^{99m}Tc-sestamibi scan (**c**) and (**d**) unzoomed neck and chest delayed sestamibi scan

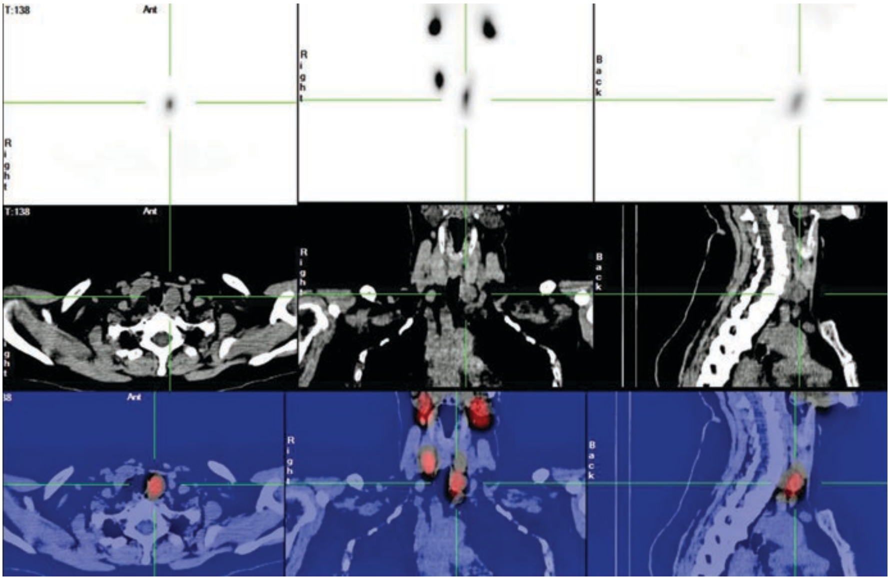

Fig. 7.153 ^{99m}Tc-sestamibi SPECT/CT scan images with CT scan images (rows a, c) and fused SPECT/CT images (rows b, d) in the transaxial (left column), coronal (middle column) and sagittal (right column) planes showing the right (rows a, b and the left (rows c, d) parathyroid adenomas (crosshairs)

^{99m}Tc-sestamibi scan washout image (Fig. 7.152c, d) there was retention of tracer uptake in the left lower thyroid lesion together with focal retention in the right thyroid lobe region.

The ^{99m}Tc-sestamibi SPECT/CT scan (Fig. 7.153) showed a large, well-defined hypodense solid nodule (measuring 23 × 16 × 28 mm) located infero-posteriorly to the left thyroid lobe at the level of C6–C7 vertebrae. There was a faint line of separation between the nodule and the thyroid. Also, a smaller ill-defined isodense-to-thyroid gland nodule (measuring 6 × 4 mm) with a faint thin border was seen located posterior to the upper part of the right lobe at the level of C6 vertebra.

7.54.4 Conclusion

Findings consistent with two large parathyroid adenomas (left adenoma larger than the right) in a patient with primary hyperparathyroidism.

7.54.5 Comments and Teaching Points

- Double parathyroid adenomas are reported to occur in 3–12% of cases of primary hyperparathyroidism [11].
- In the past there was considerable debate about whether double parathyroid adenomas are a discrete entity or represent hyperplasia with parathyroid glands of varying sizes, but it is now established that double adenomas are a discrete entity [85] occurring more often in older patients (>60 years) than in younger patients (<60 years) [86].
- Patients with double adenomas can be successfully treated by removal of the two abnormal glands.

7.55 Case 7.55. Double Parathyroid Hyperplasia: One with Early Sestamibi Washout and One with Sestamibi Retention

7.55.1 Background

A 44-year-old female with hypertension, hyperparathyroidism and end-stage renal disease (on dialysis) awaiting renal transplantation was referred for a parathyroid scan. Her serum parathormone level was 171.1 pmol/L (normal 1.3–9.3), calcium 2.59 mmol/L (normal 2.2–2.6), phosphorus 1.93 mmol/L (normal 0.84–1.45), alkaline phosphate 42 IU/L (normal 53–97), urea 4.3 mmol/L (normal range 2.5–6.4) and creatinine 108 μmol/L (normal range 53–97).

7.55.2 Procedure

The patient was injected with 79 MBq of ^{99m}Tc-pertechnetate and a thyroid scan was acquired for 10 min at 15 min postinjection. Next, 753 MBq of ^{99m}Tc-sestamibi was injected without moving the patient and a planar scan performed after 10 min. ^{99m}Tc-sestamibi SPECT/CT scan was performed at 2 h followed by a late planar ^{99m}Tc-sestamibi scan at 3 h.

7.55.3 Findings

The pertechnetate thyroid scan showed a normal-sized image of the thyroid gland with a comparatively slightly larger right lobe with homogenous distribution of activity in the gland (Fig. 7.154a). The early planar ^{99m}Tc-sestamibi scan (Fig. 7.154b) showed a pattern of uptake similar to that seen on the pertechnetate thyroid scan but with a focus of increased activity below and separate from the lower pole of the left lobe of the thyroid with the degree of uptake in the nodule lower than the activity in the thyroid gland. There was minimal focal retention of activity seen in this

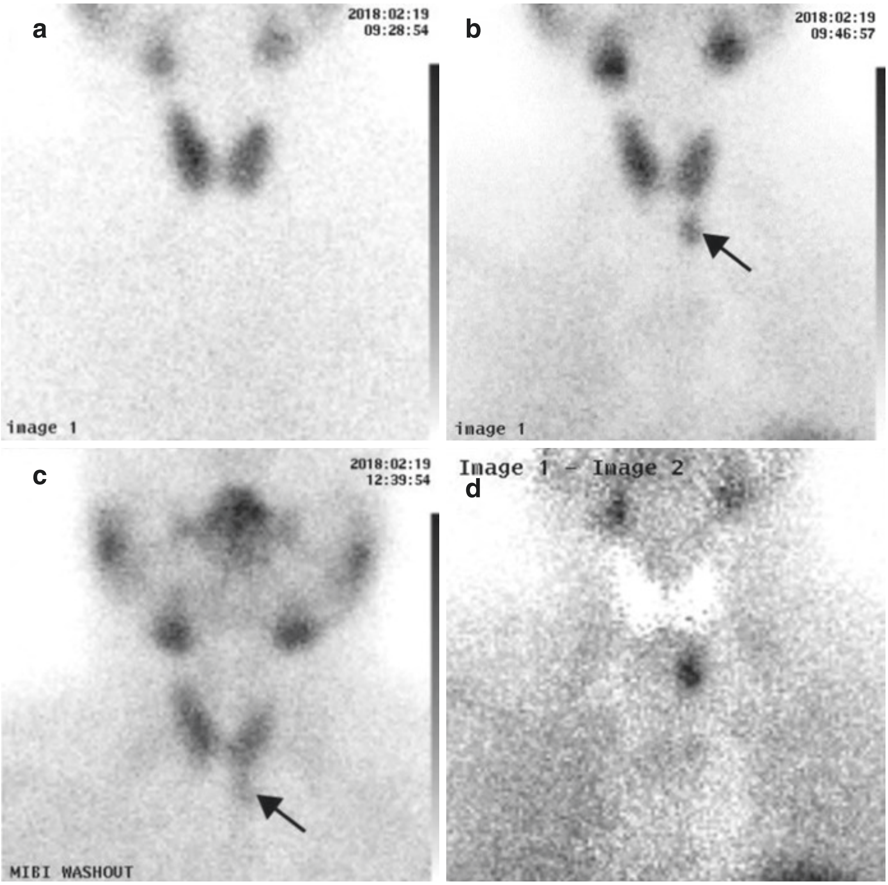

Fig. 7.154 ^{99m}Tc-pertechnetate thyroid scan (**a**), early planar 99mTc-sestamibi scan (**b**), late planar ^{99m}Tc-sestamibi scan (**c**) and ^{99m}Tc-sestamibi/^{99m}Tc-pertechnetate subtraction scan (**d**) images with the arrow pointing to the focus of mildly increased uptake below the left thyroid lobe. The nodule is better seen on the early planar image with partial washout of activity from the nodule on the delayed washout image

nodule on the delayed washout sestamibi images (Fig. 7.154c) with the activity in the nodule lower than the activity retained in the thyroid gland on the delayed images. The ^{99m}Tc-sestamibi/^{99m}Tc-pertechnetate subtraction image (Fig. 7.154d) however showed a residual focus of intense activity below the lower pole of the left lobe of the thyroid. The SPECT/CT scan (Fig. 7.155) showed the nodule below the left lower lobe showing reduced uptake compared with the thyroid gland because of higher uptake on the earlier images and relatively rapid washout of tracer from the nodule as compared with the thyroid gland. The inverse logarithmic greyscale display clearly showed poor uptake in the left lower nodule with intense increased uptake seen in the nodule in the right lobe. The CT component (Fig. 7.156) of the SPECT/CT showed the nodule on the left measuring 26 × 13.2 × 11.3 mm in size and that on the right measuring 20.8 × 13.3 × 12 mm in size.

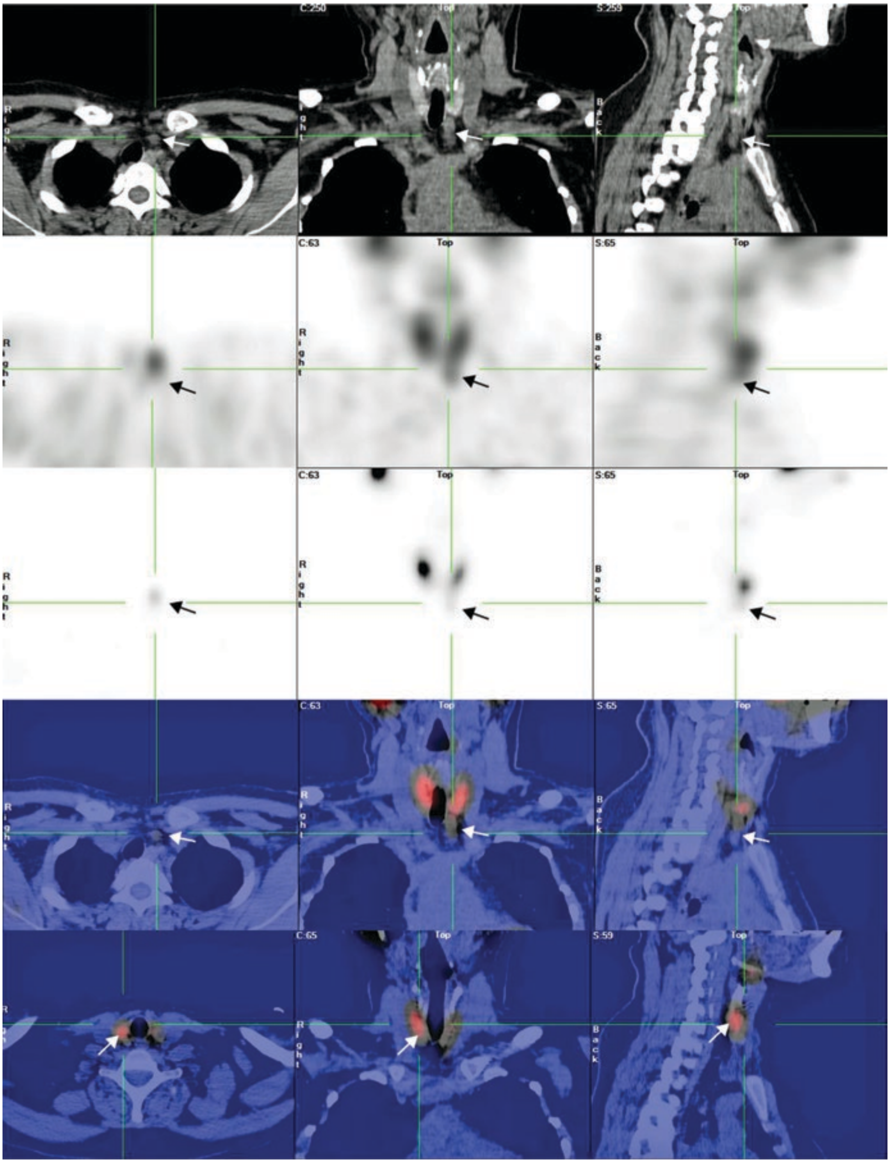

Fig. 7.155 ^{99m}Tc-sestamibi SPECT scan with CT scan images (top row), SPECT scan images in inverse linear greyscale display (second row), SPECT scan images in inverse logarithmic greyscale display (third row), and fused SPECT/CT images (bottom two rows) showing the poorly sestamibi-avid nodule below the left lower lobe (fourth row) and fused SPECT/CT images showing a sestamibi-avid nodule behind the right lobe of the thyroid (bottom row) in the transaxial (left column), coronal (middle column) and sagittal (right column) axes. Note the poor retention in the ectopic nodule below the left lower pole with a degree of uptake much lower than that in the thyroid gland and better intensity discrimination on the inverse logarithmic greyscale display compared with the linear display. The inverse logarithmic inverse greyscale display also shows a right lobe nodule with intense uptake which couldn't be discerned on the linear greyscale display

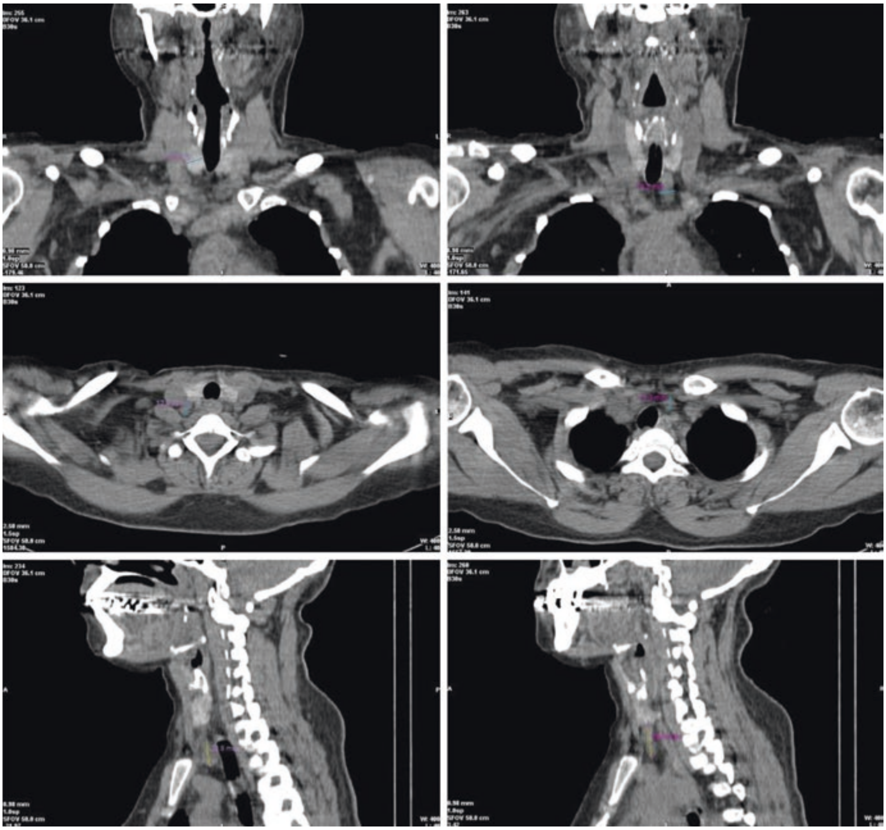

Fig. 7.156 CT scan images in coronal (top), transaxial (middle) and sagittal axes (bottom) showing the right parathyroid adenoma (left column) measuring 20.8 × 13.3 × 12 mm in size, and the left parathyroid adenoma (right column) measuring 26 × 13.2 × 11.3 mm in size

7.55.4 Conclusion

Findings consistent with double parathyroid hyperplasia/adenoma associated with secondary hyperparathyroidism with the gland on the right being sestamibi-avid and an ectopic left lower parathyroid gland which is presumably predominantly non-oncogenic cell in composition showing early washout of sestamibi.

7.55.5 Comments and Teaching Points

- In patients with long standing end-stage renal disease on dialysis, the continuous stimulation of parathyroid tissue causes parathyroid cell hyperplasia resulting in secondary hyperparathyroidism and over time results in progression to an autonomous state. This transition from compensatory to autonomous PTH secretion results in calcium levels from low to normal, moving through the normal range and then moving eventually to hypercalcaemia. Since this patient's calcium levels are at the upper limit of normal and the glands are quite large in size, the patient is now biochemically borderline hypercalcaemic and on the verge of tertiary hyperparathyroidism.

- Hyperplastic parathyroid glands can be quite large in size with a length of 10–50 mm and a weight of 500–6000 mg [35].
- In addition to their congenital ectopia, the parathyroid glands can leave their usual locations under the weight of the growing tissue of an adenomatous or hyperplastic gland. This phenomenon is referred to as "acquired parathyroid ectopia". Upward movements of the larynx and pharynx in swallowing, and negative intrathoracic pressure, promote migration of the parathyroids [87].

7.56 Case 7.56. Unsuspected Primary Hyperparathyroidism Diagnosed on FDG Scan Confirmed by Sestamibi Scan

7.56.1 Background

A 50-year-old female with known breast cancer had an ^{18}F-fluorodeoxyglucose (^{18}F-FDG) positron emission tomography (PET) scan for restaging and screening for breast metastases. The scan showed an incidental focus of increased uptake in the paravertebral region on the right at the level of C7/D1 posterior to the lower right pole of the thyroid. Given the possibility of a hyperfunctioning parathyroid gland, a ^{99m}Tc-sestamibi parathyroid scan was undertaken. Biochemical analysis revealed a serum PTH at 17.1 pmol/L (normal 1.3–9.3), corrected calcium 2.69 mmol/L (normal 2.2–2.6), magnesium 1.22 mmol/L (normal 0.73–1.06), phosphorus 1.08 mmol/L (normal 0.84–1.45), alkaline phosphate 92 IU/L (normal 53–97), urea 4.4 mmol/L (normal range 2.5–6.4) and creatinine 66 µmol/L (normal range 53–97).

7.56.2 Procedure

For the ^{18}F-FDG-PET/CT scan, the patient was injected with 170 MBq of ^{18}F-FDG and imaging performed after a 70-min uptake period. A CT scan without contrast or breath holding at low mA level was acquired for attenuation correction and localisation purposes only. Images were reconstructed in the standard transaxial, sagittal and coronal axes (Figs. 7.157 and 7.158).

For the parathyroid scan, the patient was injected with 777 MBq of ^{99m}Tc-sestamibi with early and late anterior neck and chest images acquired at 10, 60 and 120 min postinjection. SPECT/CT of the neck and chest was acquired at 60 and 120 min postinjection using a low-dose diagnostic CT for anatomical localisation and attenuation purposes only.

7.56.3 Findings

The ^{18}F-FDG-PET scan (Fig. 7.157) showed a focus of intense uptake posterior to the lower pole of the right lobe of the thyroid gland corresponding to a soft-tissue

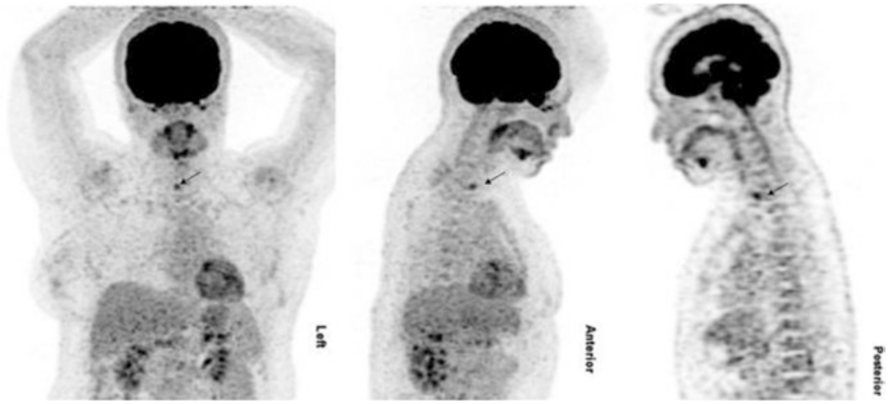

Fig. 7.157 Maximum intensity projection ^{18}F-FDG-PET scan images in the anterior (left), right lateral (middle) and left lateral (right) projections showing a small FDG-avid focus of activity (arrows) in the lower neck on the right side of the midline

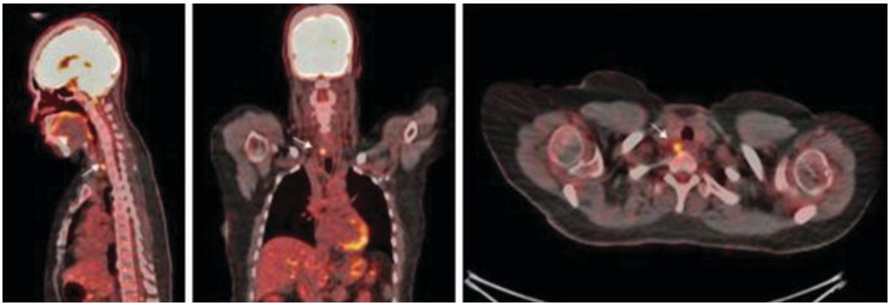

Fig. 7.158 Fused ^{18}F-FDG-PET/CT scan images in the sagittal (left), coronal (middle) and trans-axial (right) axes showing an FDG-avid lesion (arrows) posterior to the right lower pole of the thyroid. The SUV_{max} of the hypermetabolic lesion was measured at 6.9

density lesion on the CT. The maximum standard uptake value (SUV_{max}) of the lesion was measured at 6.9. The lesion was thought to represent a metabolically active lymph node, or a hyperfunctional exophytic thyroid nodule, or perhaps a hyperfunctioning right parathyroid gland. A ^{99m}Tc-sestamibi multiphase planar and SPECT/CT scan was subsequently performed to investigate the possibility of a parathyroid adenoma.

The planar ^{99m}Tc-sestamibi scans at 10, 60 and 120 min postinjection (Fig. 7.159) showed focus of uptake in the lower right thyroid lobe of the thyroid gland with otherwise uniform uptake in the gland, with the delayed washout images at 60 and 120 min showing washout of activity from the thyroid gland and focal retention of tracer in the lower right thyroid lobe nodule. The ^{99m}Tc-sestamibi SPECT/CT scan

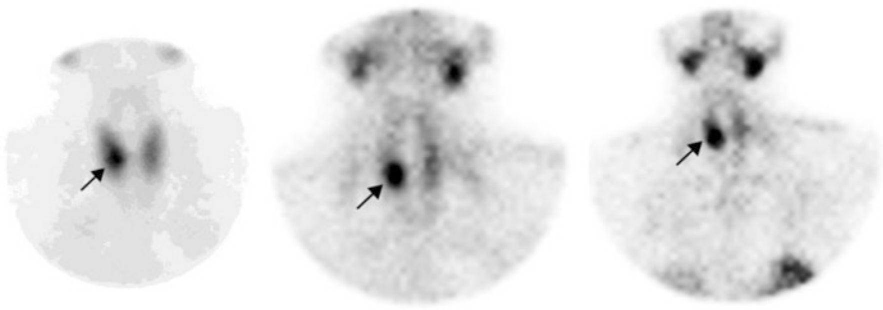

Fig. 7.159 The early planar ^{99m}Tc-sestamibi scan at 10 min (left) showing a focus of uptake in the lower right thyroid lobe with otherwise uniform uptake in the gland, with delayed washout images at 60 min (middle) and 120 min (right) showing washout of activity from the thyroid gland and focal retention of tracer in the right lower lobe nodule (arrows)

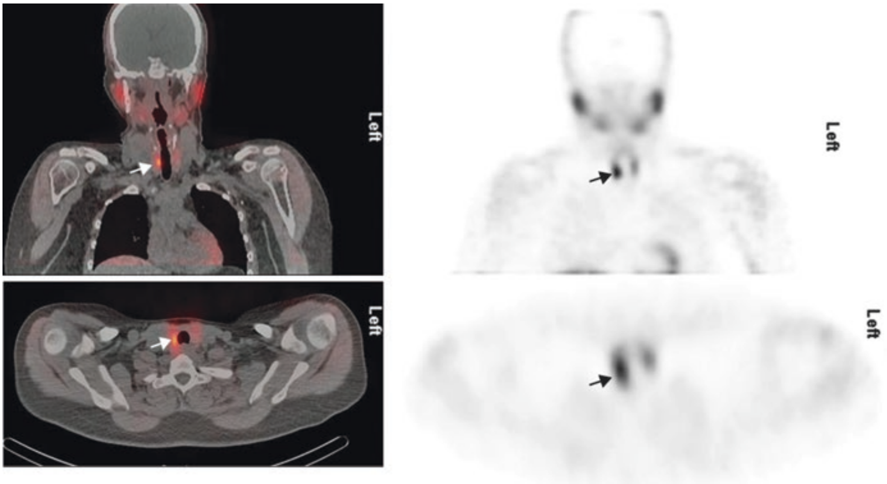

Fig. 7.160 ^{99m}Tc-sestamibi fused SPECT/CT scan (left column) and SPECT scan images (right column) in the coronal (top row) and transaxial (bottom row) axes showing a focus of intense uptake posterior to the lower pole of the right lobe of the thyroid consistent with a right lower parathyroid adenoma (arrows)

showed the lesion to be located behind the lower one-third of the right thyroid lobe posterolateral to the trachea at C6–C7 vertebral body level (Fig. 7.160).

7.56.4 Conclusion

Findings of a metabolically active ^{18}F-FDG-avid lesion in the right thyroid bed confirmed as a right lower parathyroid adenoma on ^{99m}Tc-sestamibi dual-phase planar and SPECT/CT scans as the cause of unsuspected primary hyperparathyroidism.

7.56.5 Comments and Teaching Points

- ^{18}F-FDG is the most commonly used PET radiopharmaceutical and is widely available. Incidental detection of parathyroid adenomas on FDG-PET scan has been reported in patients with unsuspected primary hyperparathyroidism [88].
- FDG-PET has been reported to be useful for the detection of parathyroid adenoma with some reporting a relatively higher sensitivity than sestamibi SPECT in the preoperative localisation of parathyroid adenomas in patients with primary hyperparathyroidism [89]. However, a meta-analysis noted highly discrepant findings with a varying sensitivity of 0–94% and a wide range of PPV from 62% to 100% [90]. Due to these highly discrepant findings, FDG appears to be a less useful tracer for the detection of pathological parathyroids.

7.57 Case 7.57. Cystic and Non-cystic Parathyroid Adenomas

7.57.1 Background

A 52-year-old female with biochemical hyperparathyroidism was referred for preoperative localisation of the overactive parathyroid glands. Prior to surgery, the patient's serum PTH level was 14.0 pmol/L (normal 1.3–9.3), corrected calcium 2.82 mmol/L (normal 2.2–2.6), magnesium 0.78 mmol/L (normal 0.73–1.06), phosphorus 0.84 mmol/L (normal 0.84–1.45), alkaline phosphate 74 IU/L (normal 53–97), urea 2.5 mmol/L (normal range 2.5–6.4) and creatinine 55 μmol/L (normal range 53–97).

7.57.2 Procedure

The patient was injected with 69 MBq of ^{99m}Tc-pertechnetate, and a thyroid scan was acquired for 10 min at 15 min postinjection. Next, 848 MBq of ^{99m}Tc-sestamibi was injected without moving the patient and a planar scan performed after 10 min. ^{99m}Tc-sestamibi SPECT/CT scan was performed at 2 h followed by a late planar ^{99m}Tc-sestamibi scan at 3 h.

7.57.3 Findings

The ^{99m}Tc-pertechnetate thyroid scan (Fig. 7.161a) showed a larger right lobe and a photopenic focus indenting the lateral border of the mid part of the right lobe. The left lobe appeared normal. The early planar ^{99m}Tc-sestamibi scans (Fig. 7.161b) showed a pattern of uptake similar to that seen on the pertechnetate thyroid scan.

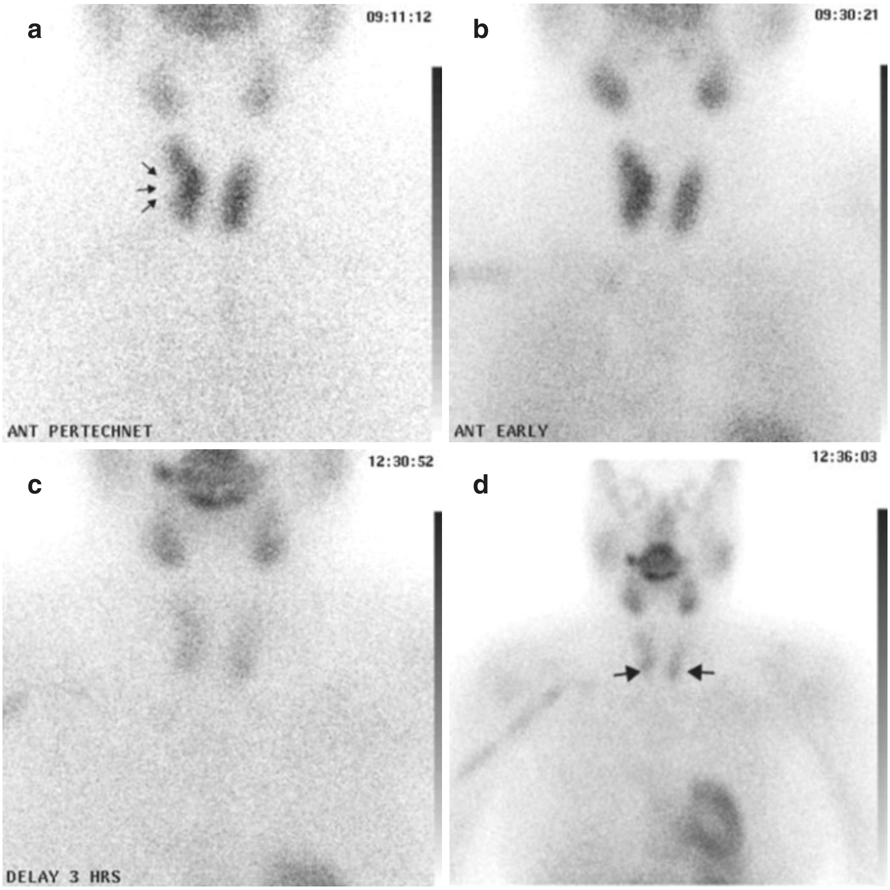

Fig. 7.161 ^{99m}Tc-pertechnetate thyroid scan (**a**) showing a larger right lobe with a small cold nodule (arrows) in its mid part laterally, the early planar ^{99m}Tc-sestamibi scan (**b**) showing a pattern of uptake similar to the pertechnetate thyroid scan (**c**), and the delayed planar ^{99m}Tc-sestamibi washout scan (**d**) image showing faint focal retention at the lower poles of the two thyroid lobes (arrows)

The delayed sestamibi washout images suggested possible faint focal retention of tracer around the lower poles of both thyroid lobes (Fig. 7.161d). The ^{99m}Tc-sestamibi/^{99m}Tc-pertechnetate subtraction image however showed a residual focus of activity in the middle of the right thyroid bed (Fig. 7.162).

The SPECT/CT scan (Fig. 7.163) greyscale and colour scale thresholding showed a larger focus of uptake extending from the right lower pole to the upper pole with cystic changes in its mid part laterally. There is also another focus of uptake seen in the left lower pole. The CT component (Fig. 7.164) of the SPECT/CT showed the cystic right parathyroid adenoma measuring 31.8 × 20.6 × 18 mm in size and the left parathyroid adenoma measuring 28.6 × 10.2 × 12.9 mm in size.

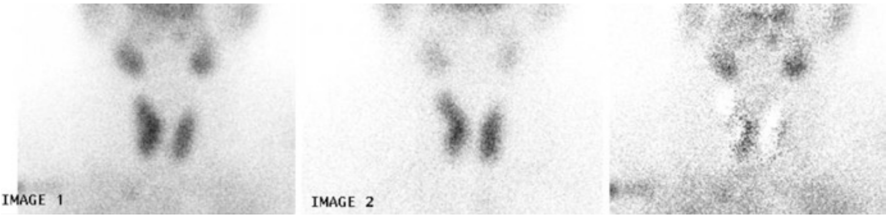

Fig. 7.162 ^{99m}Tc-sestamibi/^{99m}Tc-pertechnetate subtraction scan images showing residual focal uptake in the region of the right thyroid lobe

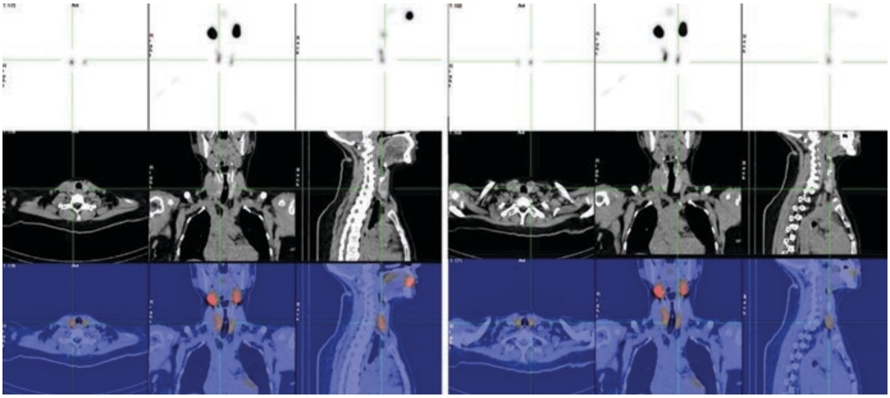

Fig. 7.163 ^{99m}Tc-sestamibi SPECT scan images (top row), CT scan images (middle row) and fused SPECT/CT images (bottom row) in the transaxial (left column), coronal (middle column) and sagittal (right column) planes, showing (crosshairs) the cystic right parathyroid adenoma (left panel) and the left lower parathyroid adenoma (right panel)

7.57.4 Conclusion

Findings consistent with bilateral parathyroid adenomas as the cause of primary hyperparathyroidism with a cystic right upper parathyroid adenoma and a left lower parathyroid adenoma.

The patient subsequently underwent parathyroidectomy, and the adenomatous parathyroid glands were resected with histopathology confirming the scan diagnosis.

The serum PTH levels fell from a preoperative value of 14 pmol/L to 0.50 pmol/L (normal 1.3–9.3), and serum calcium level normalised to 2.16 mmol/L (normal 2.2–2.6).

7.57.5 Comments and Teaching Points

- The majority of parathyroid cysts are non-functional, and are the true parathyroid cysts. These non-functional parathyroid cysts are not associated with

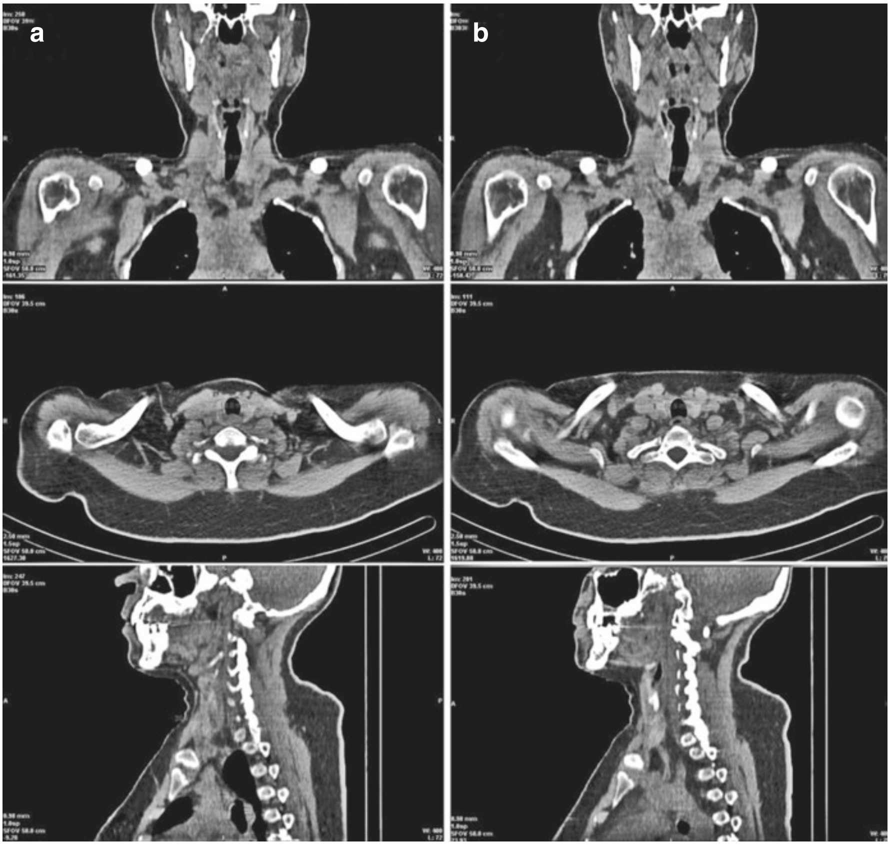

Fig. 7.164 CT scan images in the coronal (top), transaxial (middle) and sagittal (bottom) axes showing the cystic right parathyroid adenoma (**a**) measuring 31.8 × 20.6 × 18 mm in size and the left parathyroid adenoma (**b**) measuring 28.6 × 10.2 × 12.9 mm in size

increased serum calcium and PTH levels but are identified by a raised level of PTH in the cystic fluid [91]. There are only a few published case reports on this entity in the radiology literature [92, 93]. Functional cysts are pseudocysts caused by cystic degeneration of the parathyroid adenoma [94].

- Functional parathyroid cysts can be either "silent" or associated with a wide range of clinical symptoms. Only about 10% of the parathyroid cysts are reported to be functional and associated with hypercalcaemia and primary hyperparathyroidism which can manifest as fatigue, weakness, polydipsia, polyuria, depression, nephrolithiasis, osteoporosis, peptic ulcer disease and abdominal pain, and in some cases resulting in parathyroid crisis [92, 93].
- The heterogeneous clinical presentation of parathyroid cysts is determined by their hormonal activity, size and location.

- Complete surgical removal of the cyst is the treatment of choice, and therefore pre-surgical localisation of the functional parathyroid cysts by dual-phase sestamibi scan can be extremely helpful to the surgeon.

7.58 Case 7.58. Cystic Ectopic Parathyroid Adenoma

7.58.1 Background

A 46-year-old lady presented in the emergency department with severe abdominal pain associated with vomiting and fever. A diagnosis of acute pancreatitis was established, and the patient managed conservatively. Her routine laboratory results in addition to raised WBC counts and raised CRP also showed serum calcium raised at 4.14 (normal range 2.2–2.6 mmol/L) and a high parathormone (PTH) level of 25.1 (normal range 1–7.5 pmol/L). Chest x-ray demonstrated a mass in the right mediastinum (Fig. 7.165), and contrast-enhanced CT (Fig. 7.166) showed a fairly well-defined mediastinal cystic lesion in the right paratracheal region, measuring 5.5 × 4.0 × 3.7 cm, with marginal enhancement and fine internal septations. Bilateral pleural effusions were also visible. The patient was referred for a ^{99m}Tc-sestamibi parathyroid scan.

7.58.2 Procedure

The patient was injected with 805 MBq of ^{99m}Tc-sestamibi, and dual-phase planar imaging was performed at 10 min and 3 h. The scan was repeated again after surgery (see below) using similar acquisition parameters.

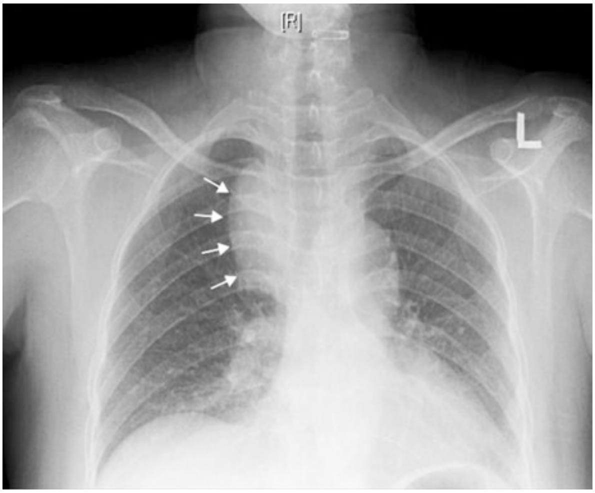

Fig. 7.165 Chest x-ray showing a soft-tissue mass (arrow) in the right mediastinum

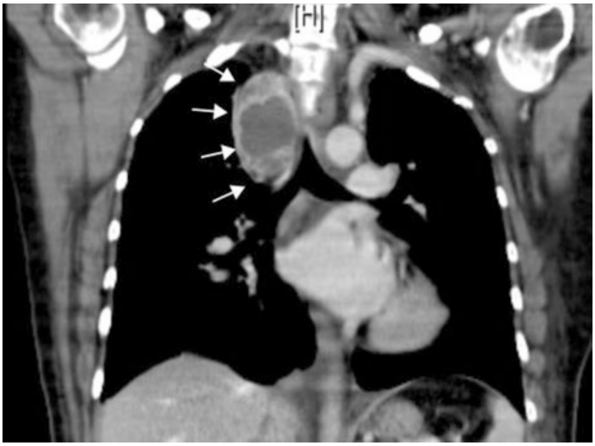

Fig. 7.166 Contrast-enhanced CT showing a fairly well-defined mediastinal cystic lesion in the right paratracheal region measuring 5.5 × 4.0 × 3.7 cm, with marginal enhancement and fine internal septations

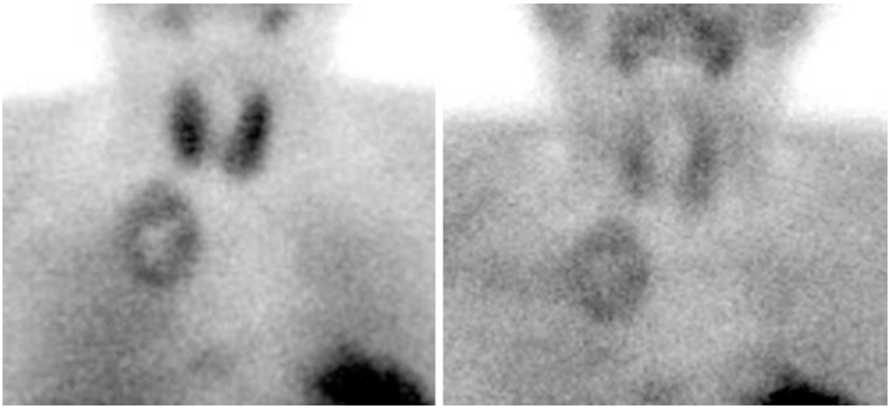

Fig. 7.167 Baseline scan with early (left) and delayed washout (right) images showing uniform thyroid bed uptake together with a doughnut lesion in the right superior mediastinum

7.58.3 Findings

The patient's early planar ^{99m}Tc-sestamibi parathyroid scan showed homogenous distribution of activity in the thyroid with the late sestamibi planar scan showing washout of activity from the thyroid gland (Fig. 7.167). Both the early and the late planar scans showed a large doughnut-shaped lesion in the right upper mediastinum characterised by increased uptake at the periphery, which was seen to correspond to the lesion seen on CT (Fig. 7.166).

7.58.4 Conclusion

Findings consistent with a large ectopic cystic mediastinal parathyroid adenoma as the cause of primary hyperparathyroidism.

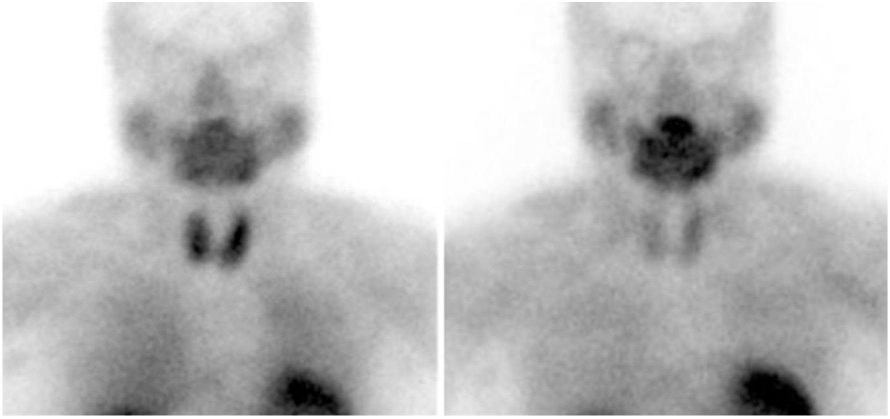

Fig. 7.168 Postoperative parathyroid scan with early (left) and delayed washout (right) images normal physiological distribution of the radiotracer with activity in the thyroid

Pre-surgical serial PTH levels showed a rising pattern with the highest value of 125.40 pmol/L. A diagnosis of a bronchogenic cyst was made and video-assisted thoracoscopic surgery performed. Excision biopsy of the lesion confirmed parathyroid adenoma. PTH level fell to 38.3 following surgery and subsequently normalised. A repeat dual-phase ^{99m}Tc-sestamibi scan was negative (Fig. 7.168).

7.58.5 Comments and Teaching Points

- About 10% of the parathyroid adenomas are ectopic in location. Cystic degeneration in parathyroid adenomas is seen in 4% of the cases and represents 1–2% of the cases with primary hyperparathyroidism. Hence, the combination of parathyroid cysts, which are both ectopic and functional, is extremely rare [94].
- The clinical manifestation of disease, in this case, was acute pancreatitis. Acute pancreatitis secondary to hypercalcaemia is an uncommon presentation of primary hyperparathyroidism and has been reported in 1–8% of cases [95, 96].
- The relationship between acute pancreatitis induced and primary hyperparathyroidism is not incidental [97, 98].
- Hypercalcaemia induces pancreatic injury via a secretory block, accumulation of secretory proteins and possibly activation of proteases [99].
- Increased levels of serum calcium documented in a patient presenting with an episode of acute pancreatitis should raise the suspicion of primary hyperparathyroidism [100, 101].

7.59 Case 7.59. Ectopic Parathyroid Adenoma + an Apparent Ectopic Cystic Mediastinal Parathyroid Adenoma (Thymic Neoplasm with Functional Parathyroid Tissue)

7.59.1 Background

A 16-year-old male was found to be hypercalcaemic with a corrected serum calcium of 4.14 mmol/L (normal range 2.2–2.6). Serum parathormone (PTH) level was subsequently also found to be raised at 50 pmol/L (normal range 1–7.5). Routing chest x-ray showed mediastinal widening and a right-sided shadow suggesting a tumour (Fig. 7.169). The patient was referred for parathyroid scintigraphy for preoperative localisation of hyperfunctional parathyroid pathology.

7.59.2 Procedure

The patient was injected with 55 MBq of ^{99m}Tc-pertechnetate, and a thyroid scan was acquired for 5 min at 20 min postinjection. Next, 829 MBq of ^{99m}Tc-sestamibi was injected without moving the patient and a planar scan performed after 10 min. ^{99m}Tc-sestamibi SPECT/CT scan was performed at 2 h followed by a late planar ^{99m}Tc-sestamibi scan at 3 h.

7.59.3 Findings

The pertechnetate thyroid scan showed a larger right lobe and a smaller left lobe with fairly homogenous distribution of activity in the gland (Fig. 7.170a). The early

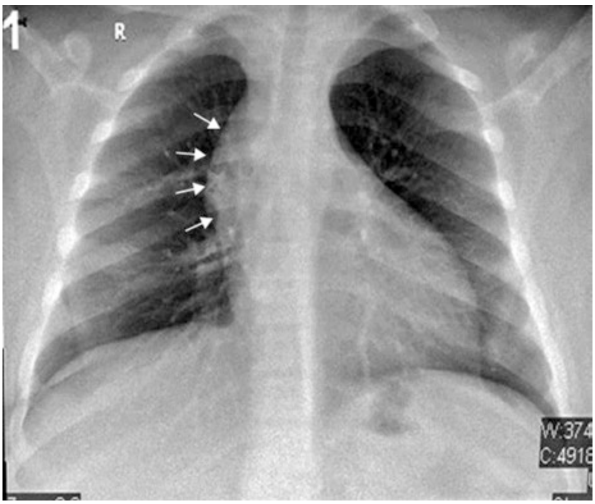

Fig. 7.169 Chest x-ray showing mediastinal widening and a right-sided shadow (arrows)

and late planar ^{99m}Tc-sestamibi scans (Fig. 7.170b, c) showed a pattern of uptake similar to that seen on the pertechnetate thyroid scan, but the late unzoomed neck and chest view additionally showed a large eccentric mass in the mediastinum on the right of the midline with an irregular crescentic rim of increased uptake (Fig. 7.170d). The planar parathyroid scan findings were clearly those of a cystic ectopic parathyroid adenoma in the chest.

The SPECT/CT scan (Fig. 7.171) showed an incomplete doughnut-shaped lesion with increased uptake in the periphery and central photopenia corresponding to a multicystic mass on the CT component. Additionally, the SPECT/CT scan showed a focus of uptake in the right thyroid lobe posteriorly measuring 23 × 8.9 × 8.1 mm on the CT component of the SPECT/CT.

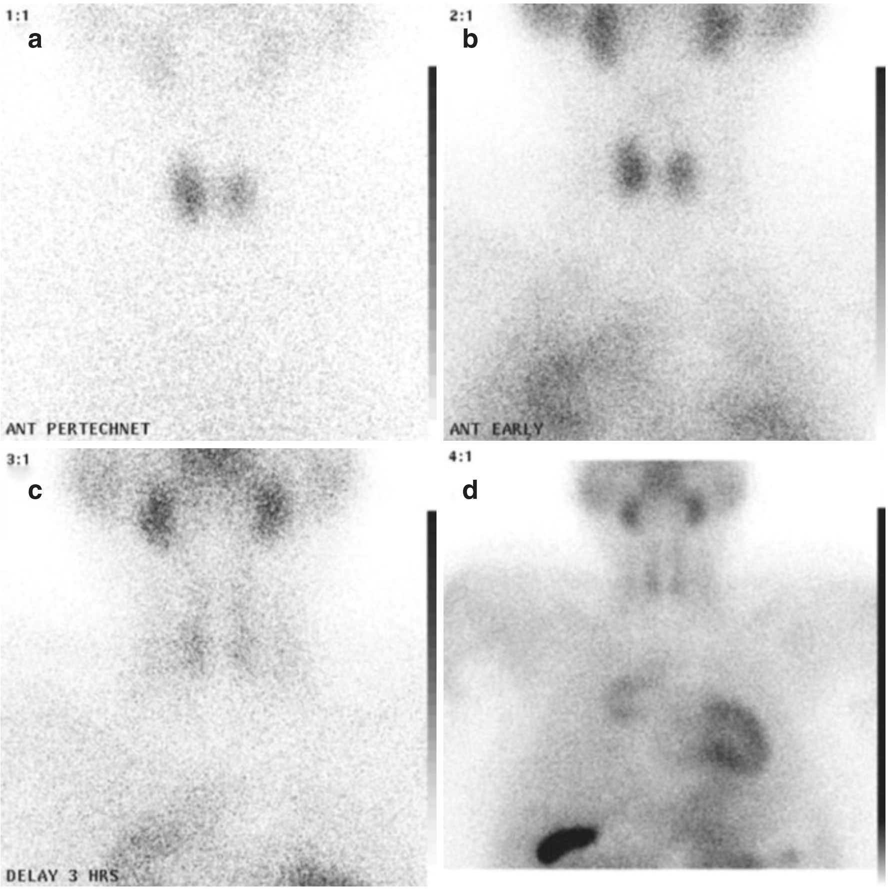

Fig. 7.170 ^{99m}Tc-pertechnetate thyroid scan (**a**), early planar ^{99m}Tc-sestamibi scan (**b**), late planar ^{99m}Tc-sestamibi scan (**c**) and late unzoomed neck and chest image (**d**)

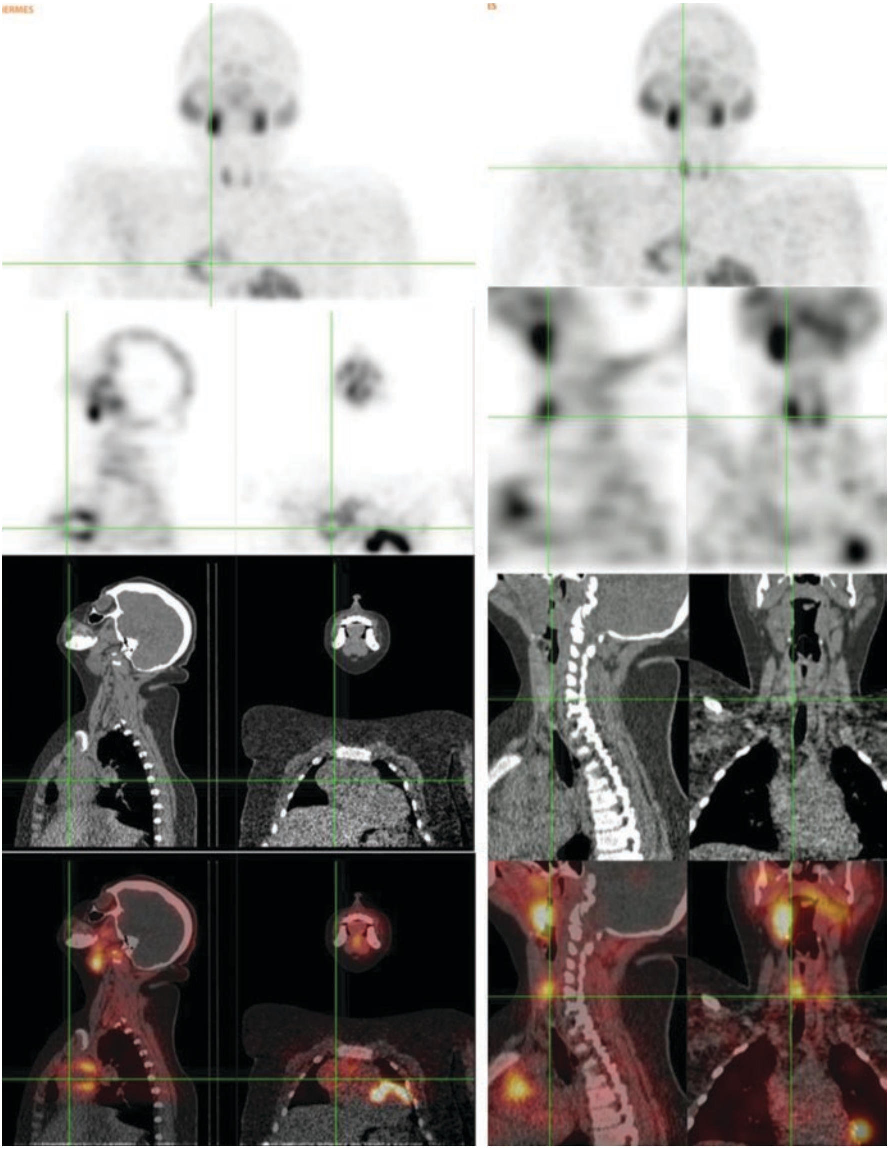

Fig. 7.171 ^{99m}Tc-sestamibi SPECT scan images with the MIP image (top row), SPECT scan images (second row), CT images (third row) and fused SPECT/CT images (bottom row) in the sagittal (left column) and coronal (right column) with crosshairs showing a right parathyroid adenoma (right panel) and a cystic sestamibi-avid mediastinal mass (left panel)

7.59.4 Conclusion

The findings of primary biochemical hyperparathyroidism with a sestamibi-avid cystic mass in the mediastinum and a hyperactive right parathyroid lesion are suggestive of a right upper parathyroid adenoma and a possible ectopic cystic parathyroid adenoma in the chest. This was further investigated by contrast CT which showed a multicystic mass lesion in the mediastinum measuring 6 × 5 × 7 cm located between the sternum and the great vessels, with well-defined low-attenuation fluid density areas and tiny foci of fat density suggesting a thymic neoplasm (Fig. 7.172). This coincidental detection of a thymic neoplasm with sestamibi uptake was attributed to the presence of functional parathyroid tissue in the neoplasm due to common migration pathway of these two organs.

7.59.5 Comments and Teaching Points

- Parathyroid cysts can be found anywhere between the neck and the mediastinum. The inferior parathyroid glands are the most common sites for the cysts, which are usually located in the lower part of the neck.
- The presence of parathyroid and thymic tissue in the same locations may be explained on the embryological basis as thymus and inferior parathyroids both usually develop from the third pharyngeal pouch with the inferior parathyroids separating from the thymic tissue but remaining close to the lower pole of the thyroid, whereas the thymus descends into the mediastinum. During thymic migration, small fragments of thymus may separate and attach themselves to any site along this route, with the parathyroid tissue either close to or embedded within the thymus as a result of their common origin and path of descent [102].

Fig. 7.172 Contrast-enhanced CT scan showing a mediastinal mass measuring 6 × 5 × 7 cm in size

Fig. 7.172 (continued)

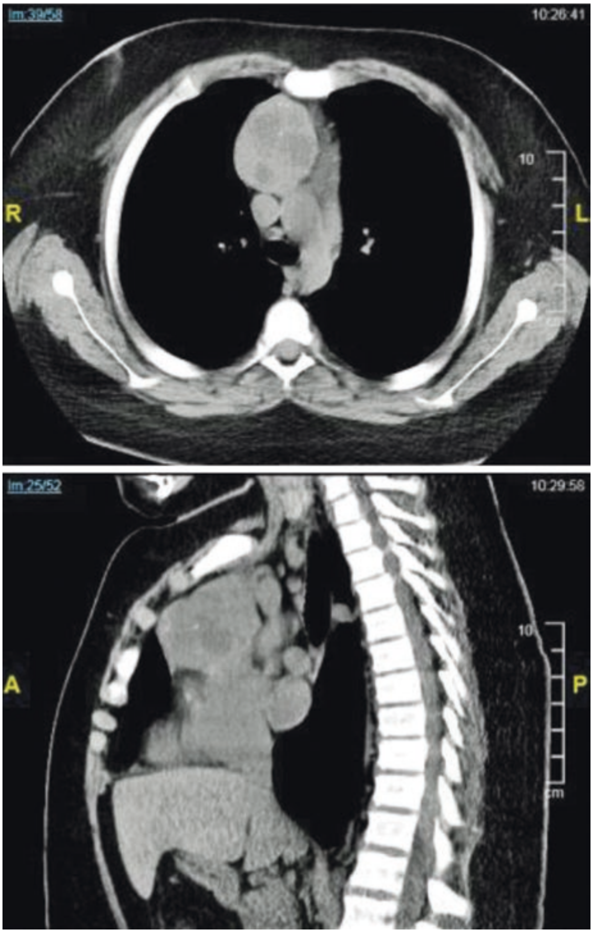

7.60 Case 7.60. Tertiary Hyperparathyroidism with Five Adenomatous Parathyroid Glands

7.60.1 Background

A 74-year-old male with diabetes mellitus, hypertension and ischaemic heart disease and end-stage renal failure (on dialysis) presented with hyperparathyroidism and hypercalcaemia. Serum PTH level was 189 pmol/L (normal 1.3–9.3), corrected calcium 2.71 mmol/L (normal 2.2–2.6), magnesium 0.82 mmol/L (normal 0.73–1.06), phosphorus 1.95 mmol/L (normal 0.84–1.45), urea 24.4 mmol/L (normal range 2.5–6.4) and creatinine 592 μmol/L (normal range 53–97).

7.60.2 Procedure

The patient was injected with 59 MBq of ^{99m}Tc-pertechnetate, and a thyroid scan was acquired for 5 min at 20 min postinjection. Next, 741 MBq of ^{99m}Tc-sestamibi

was injected without moving the patient and a planar scan performed after 10 min. ^{99m}Tc-sestamibi SPECT/CT scan was performed at 2 h followed by a late planar ^{99m}Tc-sestamibi scan at 3 h.

7.60.3 Findings

The ^{99m}Tc-pertechnetate thyroid scan (Fig. 7.173a) showed poor uptake in the thyroid bed. The early planar ^{99m}Tc-sestamibi scan (Fig. 7.173b) showed three distinct areas of increased uptake in the thyroid bed. The late planar ^{99m}Tc-sestamibi scan (Fig. 7.173c) suggested five indistinct foci of retention of tracer in the upper and

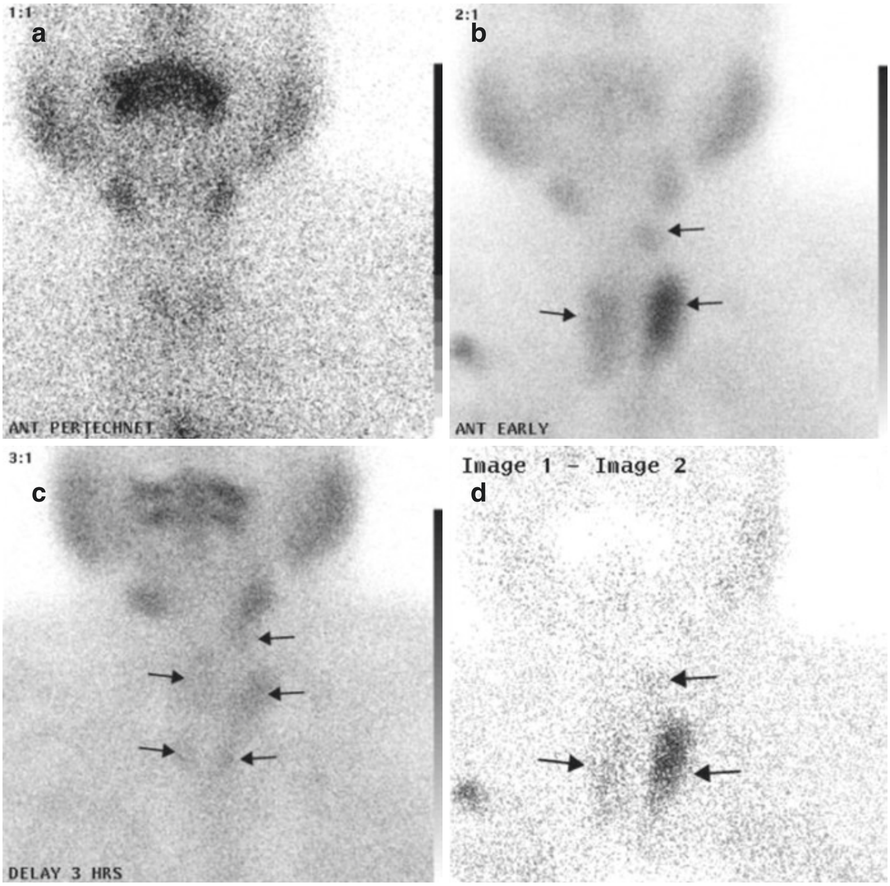

Fig. 7.173 ^{99m}Tc-pertechnetate thyroid scan (**a**) showing poor uptake in the thyroid bed, early planar ^{99m}Tc-sestamibi scan (**b**) showing three distinct areas of increased uptake in the thyroid bed, with the late planar ^{99m}Tc-sestamibi scan (**c**) suggesting five indistinct foci of retention of tracer in the upper and lower poles of both thyroid lobes and one below the left submandibular gland (arrows) and the ^{99m}Tc-sestamibi/^{99m}Tc-pertechnetate subtraction scan (**d**) image with the arrow pointing to three foci of residual uptake in the thyroid bed

lower poles of both thyroid lobes and one below the left submandibular gland, with the ^{99m}Tc-sestamibi/^{99m}Tc-pertechnetate subtraction image (Fig. 7.173d) showing three foci of residual uptake in the thyroid bed.

The SPECT/CT scan (Fig. 7.174) showed a multinodular goitre and five enlarged parathyroid glands including one left submandibular parathyroid gland and bilateral upper and lower parathyroid glands. The CT component of the SPECT/CT (Fig. 7.175) showed corresponding hypodense nodules of various sizes.

7.60.4 Conclusion

Findings consistent with five adenomatous parathyroid glands associated with tertiary hyperparathyroidism.

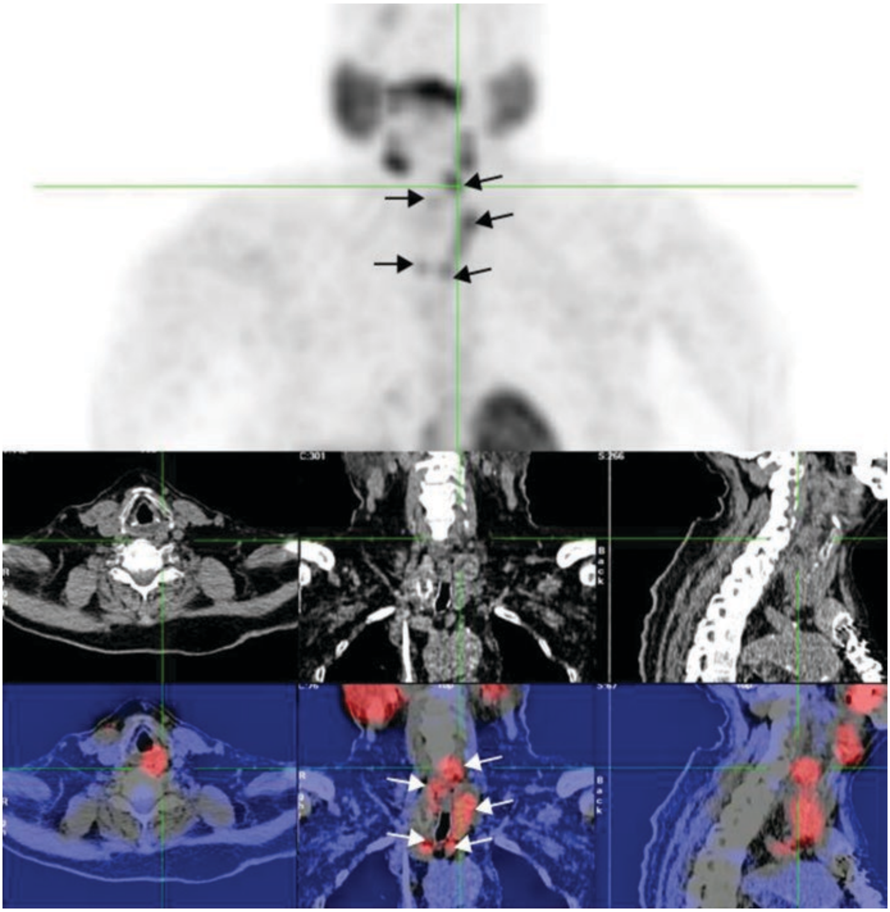

Fig. 7.174 ^{99m}Tc-sestamibi SPECT scan with top row showing MIP image, middle row showing CT images and the bottom row showing fused SPECT/CT images in the transaxial (left), coronal (middle) and sagittal (right) axes. The arrows point to the five adenomatous parathyroid glands

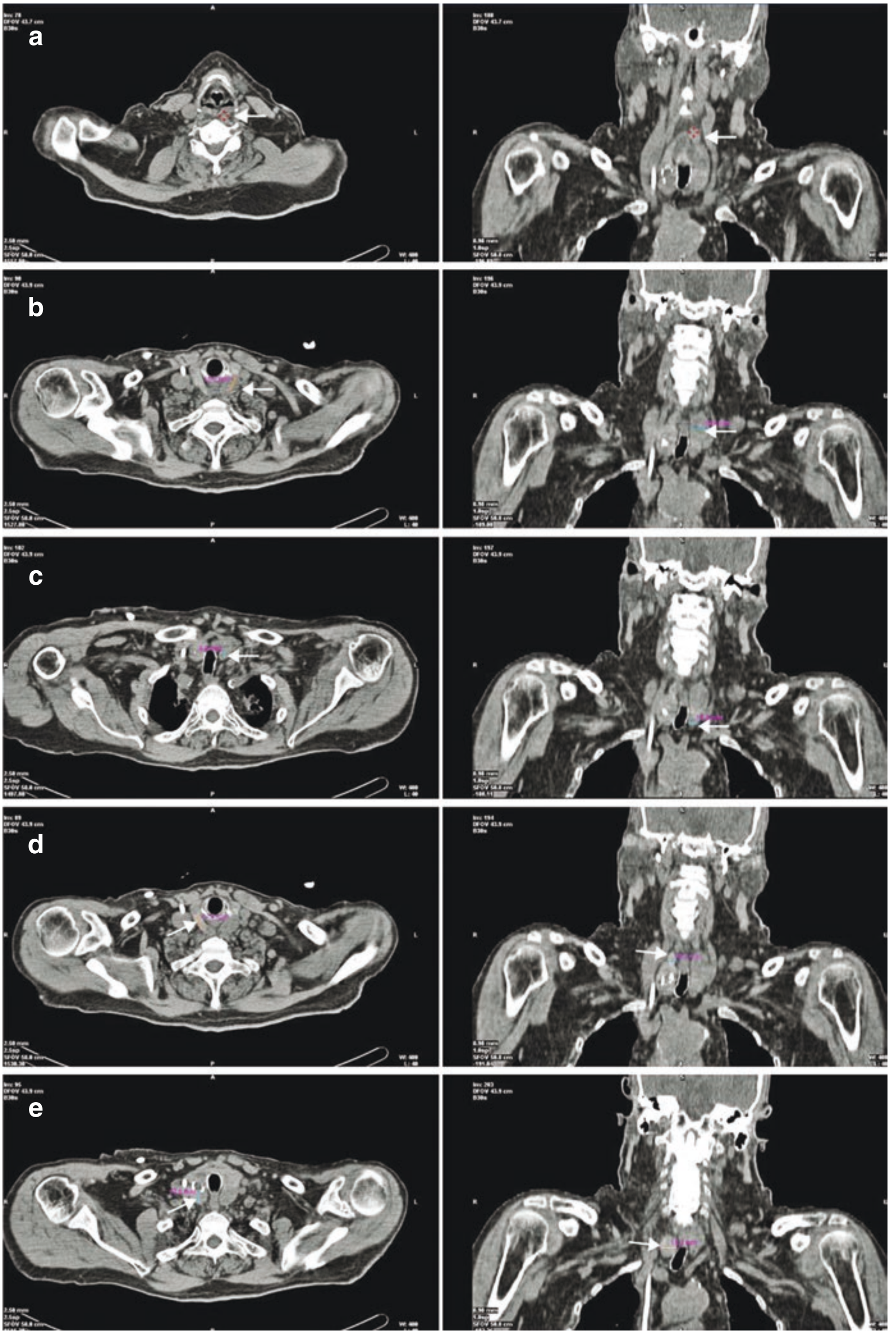

Fig. 7.175 CT scan images in transaxial (left column) and coronal (right column) axes showing the left submandibular parathyroid gland measuring 15.6 × 10.6 × 6.7 mm (**a**), the top left gland measuring 24.3 × 10.6 × 16.6 mm (**b**), the left lower gland measuring 12.3 × 12.0 × 8.0 mm (**c**), the right upper gland measuring 20.3 × 10.2 × 17.8 mm (**d**) and the right lower gland measuring 16.8 × 18.2 × 12.0 mm in size (**e**)

7.60.5 Comments and Teaching Points

- A high PTH level associated with a normal level of calcium usually defines SHPT, but when the calcium levels rise above normal, it implies biochemical progression from secondary to tertiary form of SHPT as seen in this case with five adenomatous parathyroid glands.
- Tertiary hyperparathyroidism refers to autonomous parathyroid hyperfunction in patients who have a history of prior secondary hyperparathyroidism [103]. Secondary hyperparathyroidism usually results from low vitamin D levels or renal failure, while the tertiary form of the disease occurs when there is autonomous hypersecretion from one or more affected glands, despite resolution of secondary hyperparathyroidism [104].
- The term “tertiary hyperparathyroidism” is often misapplied to patients with “hypercalcaemic secondary hyperparathyroidism” but should be more accurately reserved for the disorder that combines in its aetiology the hyperplasia of secondary hyperparathyroidism with the monoclonality of primary hyperparathyroidism [105, 106]. Since in this patient, both the SPECT and the CT scan appearances are in keeping with adenomatous parathyroid gland disease, it is more likely that this is a genuine case of tertiary rather than the hypercalcaemic secondary hyperparathyroidism.

7.61 Case 7.61. Sestamibi-Avid Cold Thyroid Nodule Suggesting Thyroid Neoplasm + Ectopic Parathyroid Adenoma

7.61.1 Background

A 40-year-old female presented with elevated serum parathormone levels and hypercalcaemia. Serum PTH was 12.40 pmol/L (normal 1.3–9.3), corrected calcium 3.05 mmol/L (normal 2.2–2.6), magnesium 0.77 mmol/L (normal 0.77–1.03), phosphorus 1.23 mmol/L (normal 0.84–1.45), alkaline phosphate 117 IU/L (normal 53–97), urea 8.2 mmol/L (normal range 2.5–6.4), uric acid 559 μmol/L (normal 137–393) and creatinine 93 μmol/L (normal range 53–97).

7.61.2 Procedure

The patient was injected with 50 MBq of ^{99m}Tc-pertechnetate, and a thyroid scan was acquired for 5 min at 20 min postinjection. Next, 800 MBq of ^{99m}Tc-sestamibi was injected without moving the patient and a planar scan performed after 10 min. ^{99m}Tc-sestamibi SPECT/CT scan was performed at 2 h followed by a late planar ^{99m}Tc-sestamibi scan at 3 h.

7.61.3 Findings

The pertechnetate thyroid scan showed an apparently normal-sized image of the thyroid (Fig. 7.176a). The early planar ^{99m}Tc-sestamibi scan (Fig. 7.176b) showed a large focus of intense increased uptake in the region of the upper part of the right lobe of the thyroid which however appeared "cold" on the pertechnetate thyroid scan. The early sestamibi scan also showed a small focus of uptake below the lower

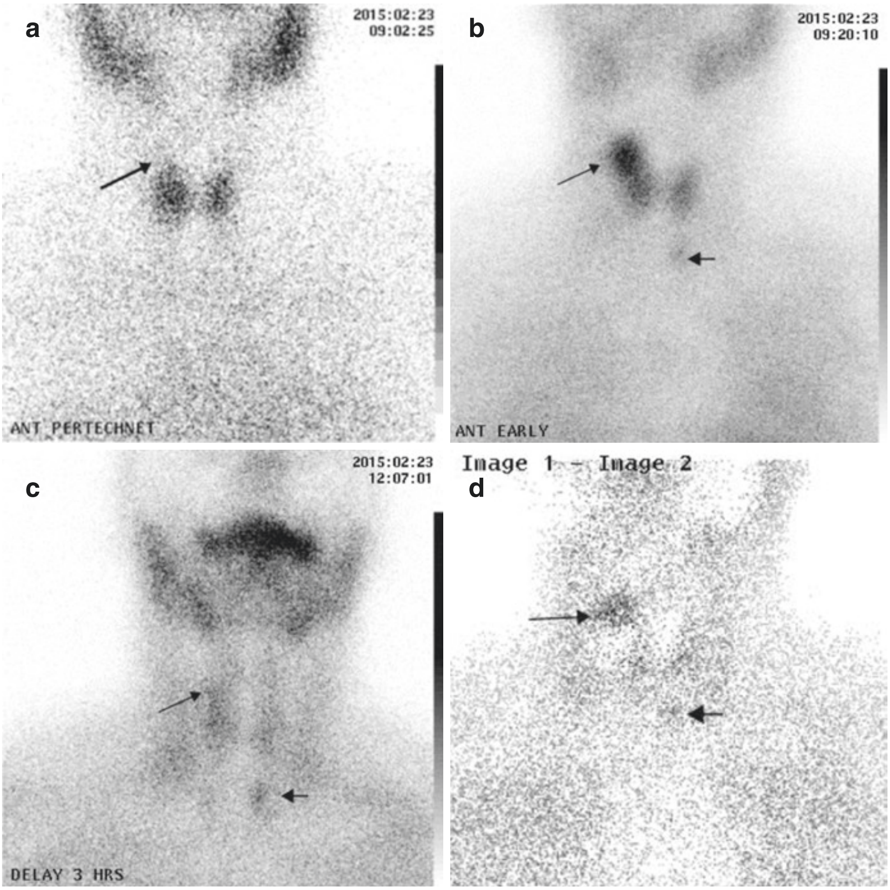

Fig. 7.176 ^{99m}Tc-pertechnetate thyroid scan (**a**), early planar ^{99m}Tc-sestamibi scan (**b**), late planar ^{99m}Tc-sestamibi scan (**c**) and ^{99m}Tc-sestamibi/^{99m}Tc-pertechnetate subtraction scan image (**d**) with the long arrow pointing to the "cold" right upper pole nodule on the thyroid scan with intense sestamibi uptake on the early image with the delayed sestamibi image showing washout of tracer from the nodule. The short arrow pointing to the left lower ectopic parathyroid gland showing relative retention of the radiotracer

pole of the left lobe of the thyroid. The delayed washout sestamibi scan image (Fig. 7.176c) showed complete washout of tracer from the right upper pole nodule with retention of activity in the ectopic nodule below the lower pole of the left lobe of the thyroid. The ^{99m}Tc-sestamibi/^{99m}Tc-pertechnetate subtraction image (Fig. 7.176d) showed a residual focus of activity above the right upper pole of the thyroid as well as a focus of activity corresponding to the nodule below the left lower pole.

The SPECT/CT scan (Fig. 7.177a, b) showed the focus of increased uptake in the upper pole of the right lobe of the thyroid appearing relatively less intense than on the early planar scan due to partial washout of activity from this lesion at the time of the SPECT/CT imaging (120 min postinjection). The CT component of the SPECT/CT (Fig. 7.177c) showed a corresponding hypodense lesion measuring 21.6 × 16.1 × 16.9 mm in size in the upper half of the right lobe of the thyroid gland together with significant ipsilateral lymphadenopathy. The SPECT/CT also showed a smaller focus of activity below the lower pole of the left lobe of the thyroid measuring 10.5 × 5.8 × 8.7 mm in size at the level C7 vertebra located lateral to the trachea (Fig. 7.177c, d).

7.61.4 Conclusion

Findings consistent with a sestamibi-avid ectopic left lower parathyroid adenoma showing characteristic delayed sestamibi washout as the cause of primary hyperparathyroidism. The sestamibi-avid non-functional thyroid nodule raises the possibility of thyroid malignancy.

7.61.5 Comments and Teaching Points

- The nodule in the right upper lobe of the thyroid appeared cold (non-functional) on the pertechnetate thyroid scan but showed intense sestamibi uptake on both the early planar sestamibi scan and on the sestamibi SPECT scan and could easily have been mistaken for a parathyroid adenoma on the nuclear medicine imaging modalities alone. However, the diagnostic-quality non-contrast CT showed the nodule to be located in the thyroid and thus avoided a false-positive diagnosis for a parathyroid adenoma. However, an intrathyroidal parathyroid adenoma can be included in the differential diagnosis along with thyroid malignancy.
- Non-functional or cold thyroid nodules which show intense sestamibi uptake have a significant likelihood of harbouring thyroid cancer [107], whereas a negative sestamibi scan in a cold nodule accurately excludes malignancy [108].
- Primary hyperparathyroidism can cause renal failure secondarily, which can be reversed after adenoma resection. In this case with high serum uric acid and raised urea with normal creatinine, it appears that there is early impairment of

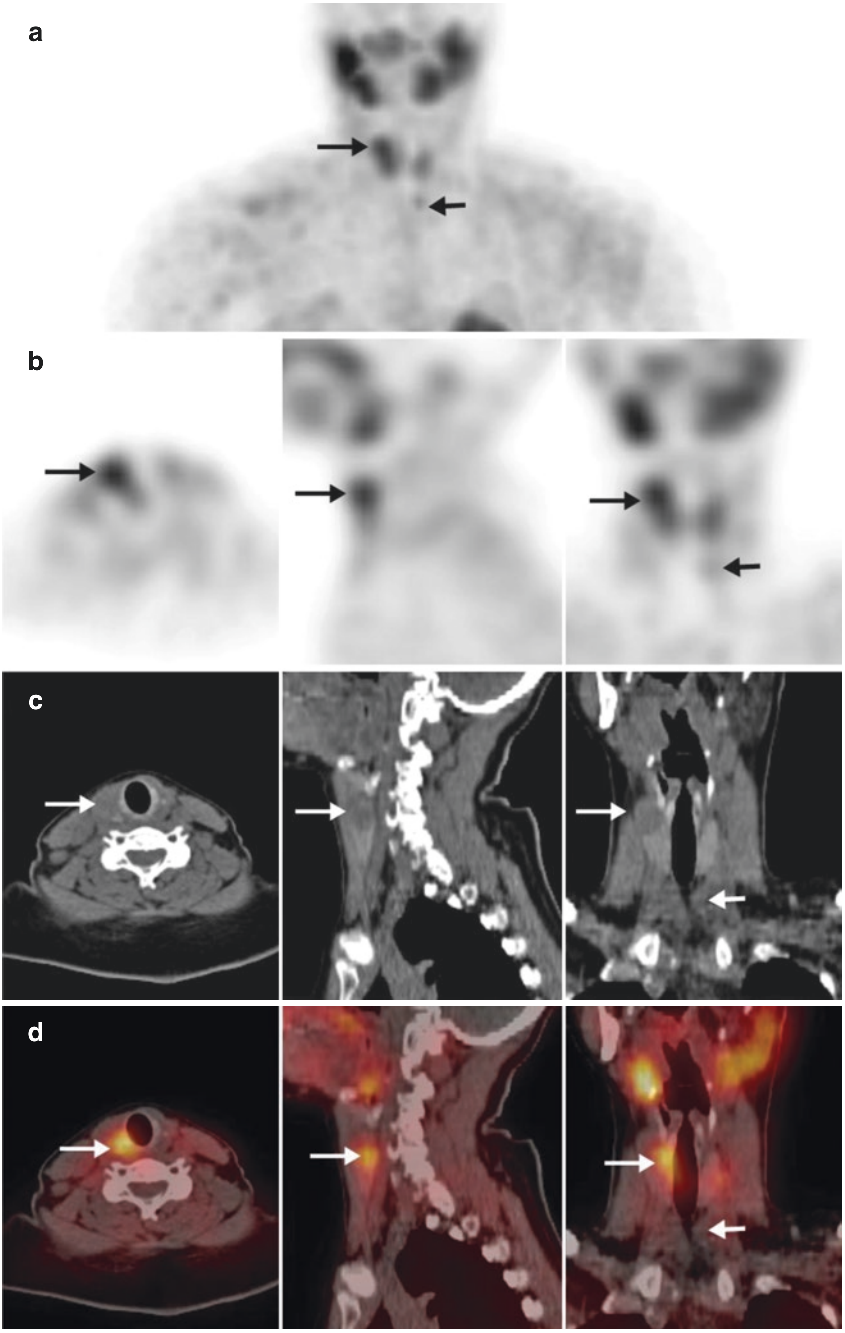

Fig. 7.177 ^{99m}Tc-sestamibi SPECT/CT scan with MIP image (**a**) and SPECT (**b**), CT (**c**) and fused SPECT/CT (**d**) in the transaxial (left column), sagittal (middle column) and coronal (right column) axes. The large arrow on images (**a**) and (**b**) points to the "cold" thyroid nodule on the pertechnetate scan which shows early sestamibi avidity. The small arrow points to the ectopic small left lower parathyroid adenoma

renal function as serum uric acid is reportedly raised in patients with impaired renal function.

- The permeability of the kidney is lowered in conditions of renal insufficiency; this becomes evident in the blood, first by a retention of uric acid, later by that of urea and lastly by that of creatinine, indicating that creatinine is the most readily eliminated of these three nitrogenous waste products and uric acid the most difficulty eliminated, with urea standing in an intermediate position. This is well substantiated in this case.

7.62 Case 7.62. Autonomous Thyroid Nodule + Bilateral Lower Parathyroid Gland Hyperplasia/Adenoma with Primary Hyperparathyroidism

7.62.1 Background

A 73-year-old female with a history of an ischaemic stroke and a non-ST elevation MI presented with hypercalcaemia and hyperparathyroidism. Serum PTH was 14.43 pmol/L (normal 1.3–9.3), corrected calcium 2.69 mmol/L (normal 2.2–2.6), phosphorus 0.51 mmol/L (normal 0.84–1.45), alkaline phosphate 57 IU/L (normal 53–141), urea 6.3 mmol/L (normal range 2.9–7.5) and creatinine 97 μmol/L (normal range 53–106).

7.62.2 Procedure

The patient was injected with 59 MBq of ^{99m}Tc-pertechnetate, and a thyroid scan was acquired for 5 min at 20 min postinjection. Next, 816 MBq of ^{99m}Tc-sestamibi was injected without moving the patient and a 10-min duration planar scan performed after 10 min. ^{99m}Tc-sestamibi SPECT/CT scan was performed at 2 h followed by a late planar ^{99m}Tc-sestamibi scan at 3 h.

7.62.3 Findings

The pertechnetate thyroid scan (Fig. 7.178a) showed a “hot” nodule in the right lobe of the thyroid suppressing uptake in the remainder of the gland. The early planar ^{99m}Tc-sestamibi scan (Fig. 7.178b) showed a mildly enlarged thyroid with homogenous distribution of activity in the gland. The delayed washout sestamibi image (Fig. 7.178c, d) showed focal retention of tracer in the lower poles of both lobes of the thyroid. The SPECT/CT scan (Fig. 7.179) however showed intense focal increased uptake at the lower poles of both lobes of the thyroid corresponding to enlarged parathyroid glands on the CT component (Figs. 7.179 and 7.180).

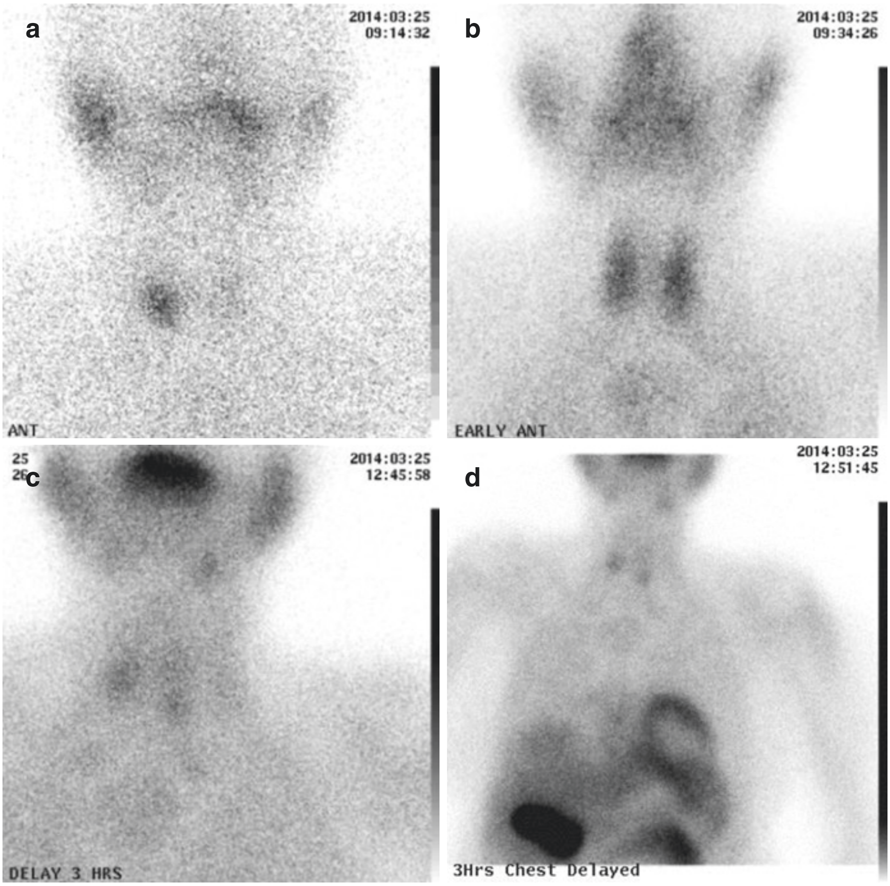

Fig. 7.178 ^{99m}Tc-pertechnetate thyroid scan (**a**), early planar ^{99m}Tc-sestamibi scan (**b**), late planar ^{99m}Tc-sestamibi scan (**c**) and unzoomed delayed neck and chest planar sestamibi scan (**d**)

7.62.4 Conclusion

Findings consistent with an autonomous thyroid nodule and bilateral hyperplastic or adenomatous lower parathyroid glands associated with primary hyperparathyroidism.

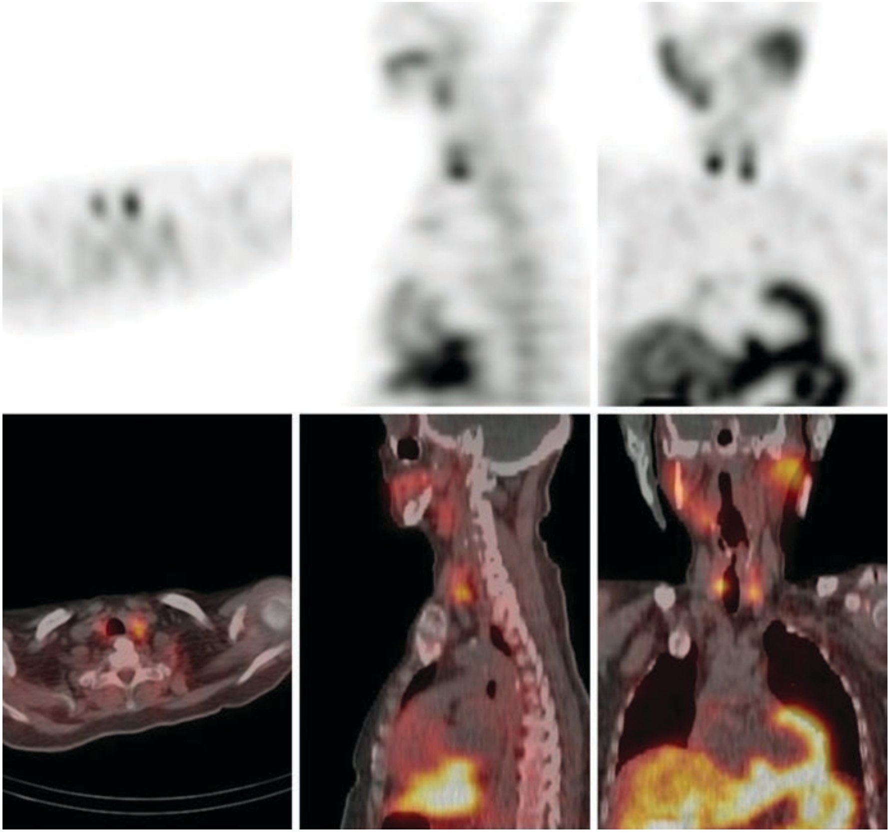

Fig. 7.179 ^{99m}Tc-sestamibi SPECT scan in inverse log scale (top row), CT scan (middle row) and fused SPECT/CT scan images (bottom row) in the transaxial (left column), coronal (middle column) and sagittal (right column) planes, showing bilateral adenomatous lower parathyroid glands (arrows)

7.62.5 Comments and Teaching Points

- It is not possible to comment if the overactive enlarged lower parathyroid glands are due to parathyroid hyperplasia or adenoma, but the symmetrical lower parathyroid gland involvement and the CT texture are more in keeping with hyperplastic rather than the adenomatous parathyroid disease.

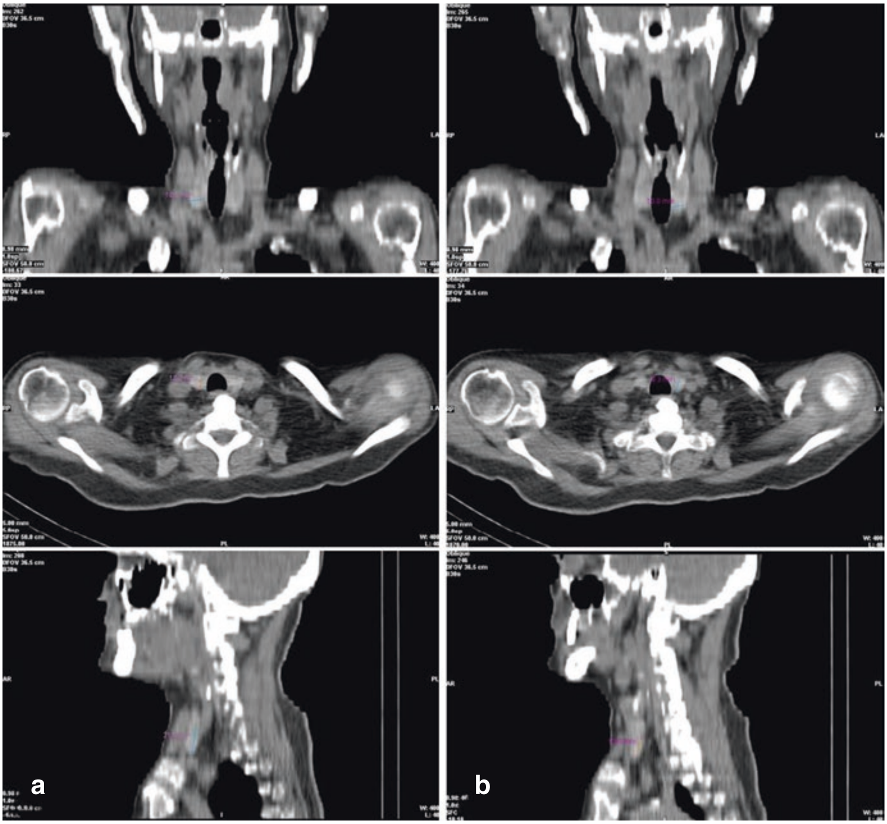

Fig. 7.180 Coronal (top row), transaxial (middle row), and sagittal (bottom row) images of the CT component of the SPECT/CT scan showing bilateral adenomatous lower parathyroid glands with the right gland (**a**) measuring 21.1 × 10.1 × 10 mm and the left gland (**b**) measuring 13.6 × 10 × 9.3 mm in size

7.63 Case 7.63. Ectopic Midline Retrosternal Parathyroid Adenoma

7.63.1 Background

A 43-year-old female with bilateral renal stones with elevated serum parathormone levels and hypercalcaemia was referred for a parathyroid scan. Her serum parathormone level was 40.80 pmol/L (normal 1.3–9.3), corrected calcium 2.98 mmol/L (normal 2.2–2.6), magnesium 0.77 mmol/L (normal 0.77–1.03), phosphorus 0.97 mmol/L (normal 0.84–1.45), alkaline phosphate 97 IU/L (normal 53–97), urea 3.7 mmol/L (normal range 2.5–6.4) and creatinine 60 μmol/L (normal range 53–97).

7.63.2 Procedure

The patient was injected with 58 MBq of ^{99m}Tc-pertechnetate, and a thyroid scan was acquired for 5 min duration at 20 min postinjection. Next, 845 MBq of ^{99m}Tc-sestamibi was injected without moving the patient and a planar scan performed after 10 min. ^{99m}Tc-sestamibi SPECT/CT scan was performed at 2 h followed by a late planar ^{99m}Tc-sestamibi scan at 3 h.

7.63.3 Findings

The pertechnetate thyroid scan showed a relatively larger right lobe and a normal-sized left lobe with homogenous distribution of activity in the gland (Fig. 7.181a).

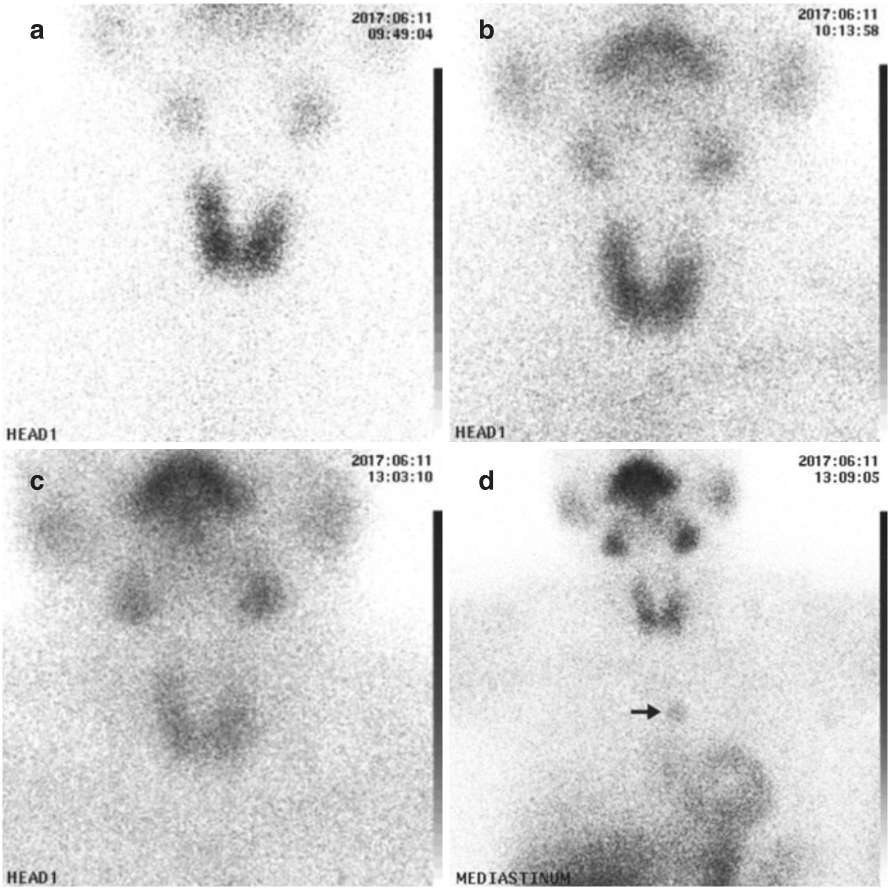

Fig. 7.181 ^{99m}Tc-pertechnetate thyroid scan (**a**), early planar ^{99m}Tc-sestamibi scan (**b**), late planar ^{99m}Tc-sestamibi scan (**c**) and unzoomed late sestamibi neck and chest scan image (**d**), with the arrow pointing to the small focus of increased uptake in the mediastinum

The early planar ^{99m}Tc-sestamibi scan (Fig. 7.181b) showed a pattern of uptake similar to that seen on the pertechnetate thyroid scan with partial washout of tracer from the thyroid seen on the delayed sestamibi image (Fig. 7.181c) without any focal retention seen in the thyroid bed. However, there is a tiny focus of uptake in the mediastinum seen on the delayed sestamibi unzoomed chest image (Fig. 7.181d). The SPECT/CT scan (Fig. 7.182) showed a focus of uptake on the SPECT scan located behind the middle one-third of the right thyroid lobe with the CT component showing the focus of activity to correspond to a hypodense lesion measuring 17.8 × 14.5 × 10 mm in size.

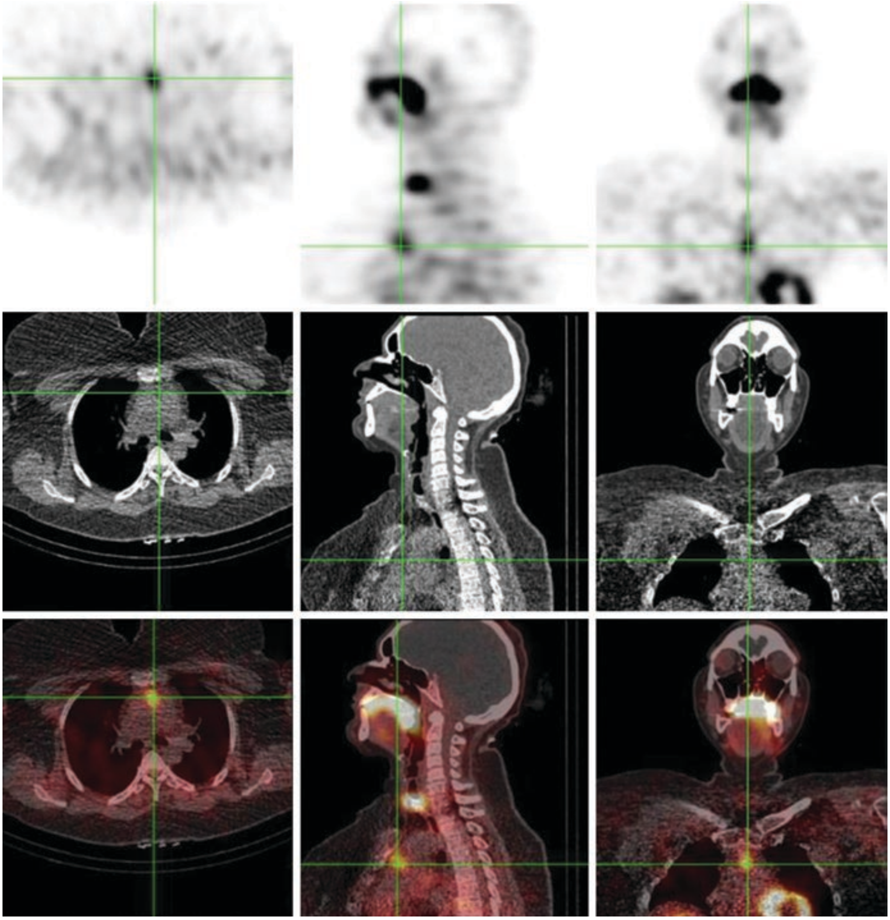

Fig. 7.182 ^{99m}Tc-sestamibi SPECT scan images (top row), CT scan images (middle row) and fused SPECT/CT images (bottom row) in the transaxial (left column), sagittal (middle column) and coronal (right column) planes, showing an ectopic midline adenoma in the mediastinum (crosshair)

7.63.4 Conclusion

Findings consistent with an ectopic midline retrosternal parathyroid adenoma in the anterior mediastinum associated with primary hyperparathyroidism.

Surgical resection of the retrosternal nodule was undertaken, and histopathological examination showed an enlarged cellular parathyroid gland in keeping with a parathyroid adenoma.

The serum PTH levels fell from a preoperative value of 40.80 pmol/L to 3.8 pmol/L (normal 1.3–9.3), and serum calcium level normalised to 2.41 mmol/L (normal 2.2–2.6).

7.63.5 Comments and Teaching Points

- Mediastinal parathyroid is defined as a parathyroid gland found completely below the level of the clavicle. The actual prevalence of mediastinal parathyroid adenomas is unknown but has been reported to be 6–30% [109].
- Ectopic inferior parathyroids are most frequently found in the anterior mediastinum usually embedded in the thymus gland, while superior parathyroids are generally found in the posterosuperior mediastinum.
- Mediastinal parathyroid adenomas have been reported to be associated with more severe clinical manifestations of primary hyperparathyroidism, presenting with higher calcium levels and more frequently with bone disease [110].

7.64 Case 7.64. Right Lower Parathyroid Adenoma Pre- and Post-surgery

7.64.1 Background

A 53-year-old female with a history of hypothyroidism (on thyroxine) presented with primary hyperparathyroidism and severe hypercalcaemia. Serum parathormone level was 80.5 pmol/L (normal 1.3–9.3), corrected calcium 4.94 mmol/L (normal 2.2–2.6), magnesium 0.86 mmol/L (normal 0.77–1.03), phosphorus 1.80 mmol/L (normal 0.84–1.45), uric acid 422 µmol/L (normal 138–393), urea 10.1 mmol/L (normal range 2.5–6.4) and creatinine 270 µmol/L (normal range 53–97).

7.64.2 Procedure

The patient was injected with 50 MBq of ^{99m}Tc-pertechnetate, and a thyroid scan was acquired for 10 min at 15 min postinjection. 800 MBq of ^{99m}Tc-sestamibi was then injected without moving the patient and a planar scan performed after 10 min. ^{99m}Tc-sestamibi SPECT/CT scan was performed at 2 h followed by a late planar ^{99m}Tc-sestamibi scan at 3 h. The scan was repeated 7 weeks later after surgery using a similar dose and acquisition parameters.

7.64.3 Findings

The baseline pertechnetate thyroid scan showed a normal-sized image of the thyroid with mildly reduced and patchy uptake due to thyroxine suppression (Fig. 7.183a). The early planar ^{99m}Tc-sestamibi scan (Fig. 7.183b) showed a large oval focus on intense increased uptake at the lower pole of the right lobe of the thyroid, with the delayed sestamibi scan showing moderate retention of tracer here (Fig. 7.183c). The ^{99m}Tc-sestamibi/^{99m}Tc-pertechnetate subtraction image showed a residual focus of activity at the lower pole of the right thyroid lobe (Fig. 7.183d). The SPECT/CT scan (Fig. 7.184) showed a clear-cut posteriorly

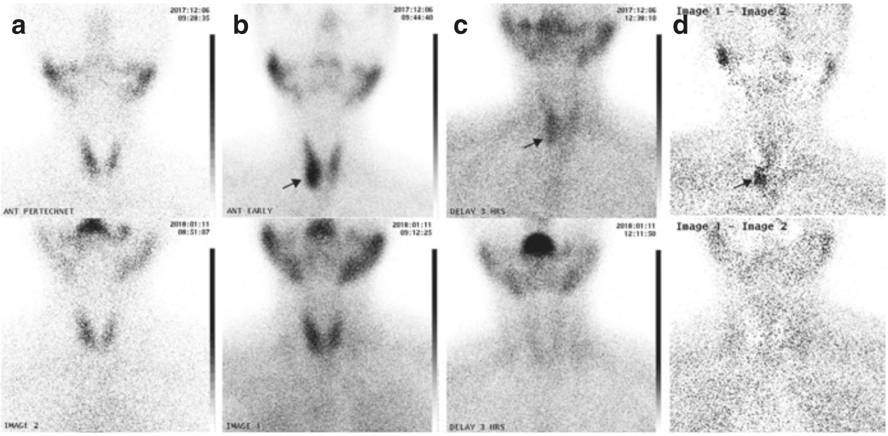

Fig. 7.183 Baseline (top row) and postsurgery (bottom row) scans with ^{99m}Tc-pertechnetate thyroid scan (**a**), early planar ^{99m}Tc-sestamibi scan (**b**), late planar ^{99m}Tc-sestamibi scan (**c**) and ^{99m}Tc-sestamibi/^{99m}Tc-pertechnetate subtraction scan (**d**) images with the arrow pointing to an oval focus of intense increased uptake at the lower pole of the right thyroid lobe on the baseline scans with a normal postsurgery scan

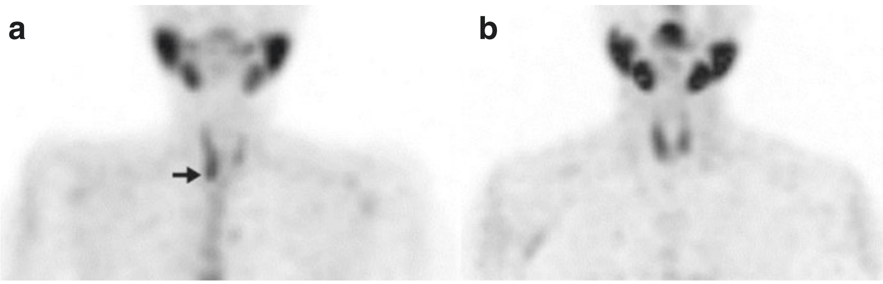

Fig. 7.184 Maximum intensity projection (MIP) ^{99m}Tc-sestamibi SPECT scan images showing the right parathyroid adenoma (arrow) before (**a**) and after surgery (**b**)

located focus of uptake at the right lower pole, which was seen to correspond to a hypodense nodule on the CT component (Fig. 7.185) of the SPECT/CT measuring 26.3 × 14.8 × 14.3 mm in size. The planar and SPECT images postsurgery were normal (Figs 7.183 and 7.184).

Fig. 7.185 CT scan images in the coronal (top), transaxial (middle) and sagittal axes (bottom) showing a right parathyroid adenoma (cross) measuring 26.3 × 14.8 × 14.3 mm in size

7.64.4 Conclusion

Findings consistent with a large right lower parathyroid adenoma as the cause of primary hyperparathyroidism and associated mild renal failure.

At surgery, a large lower parathyroid adenoma was removed and confirmed on histopathology.

The serum PTH levels fell from a preoperative value of 80.5 pmol/L to –8.70 pmol/L (normal 1.3–9.3), and serum calcium level normalised to 2.39 mmol/L (normal 2.2–2.6). The renal function improved postoperatively: phosphorus fell from 1.80 to 1.17 mmol/L (normal 0.84–1.45), uric acid from 422 to 235 μmol/L (normal 138–393), urea from 10.1 to 9.1 mmol/L (normal range 2.5–6.4) and creatinine from 270 to 88 μmol/L (normal range 53–97).

7.64.5 Comments and Teaching Points

- Primary hyperparathyroidism is associated with mild renal failure which is benefited from surgical removal of the adenoma as seen in this case.
- Renal failure and primary hyperparathyroidism can independently coexist. PHPT has been recognised as a risk factor for impaired renal function, though the specific relationship between PHPT and this condition is not completely understood. Prolonged hypercalcaemia has been considered to impair kidney function, and a reduced glomerular filtration rate is common in advanced severe PHPT [111, 112].
- Monitoring and management of PHPT patients with established chronic kidney disease (CKD) can be a challenge as CKD-related biochemical and clinical alterations alter the classic clinical presentation of PHPT.

7.65 Case 7.65. Tertiary Hyperparathyroidism with Four Adenomatous Parathyroid Glands

7.65.1 Background

A 52-year-old female with diabetes mellitus, hypertension and a past history of renal cell carcinoma was admitted with pathological fracture of the right neck of the femur. The patient was on haemodialysis for chronic kidney disease (CKD) and had biochemical hyperparathyroidism and hypercalcaemia. Serum parathormone level was 254.15 pmol/L (normal 1.3–9.3), corrected calcium 2.75 mmol/L (normal 2.2–2.6), magnesium 0.75 mmol/L (normal 0.77–1.03), phosphorus 1.75 mmol/L (normal 0.84–1.45), alkaline phosphate 505 IU/L (normal 42–98), urea 10.9 mmol/L (normal range 2.5–6.4) and creatinine 617 μmol/L (normal range 53–97). The patient was vitamin D insufficient.

7.65.2 Procedures

A whole-body bone scan with SPECT/CT of the pelvis was performed 3 h after intravenous injection of 930 MBq of ^{99m}Tc-methylene diphosphonate. Planar dual-phase parathyroid scintigraphy was performed 10 min and 3 h after intravenous injection of 799 MBq of ^{99m}Tc-sestamibi with additional spot views of the whole body also acquired.

7.65.3 Findings

The whole-body bone scan (Fig. 7.186a) showed generalised increased uptake in the skeleton with a high bone/soft-tissue ratio and non-visualisation of the kidneys consistent with "super scan" of metabolic bone disease. There was intense increased

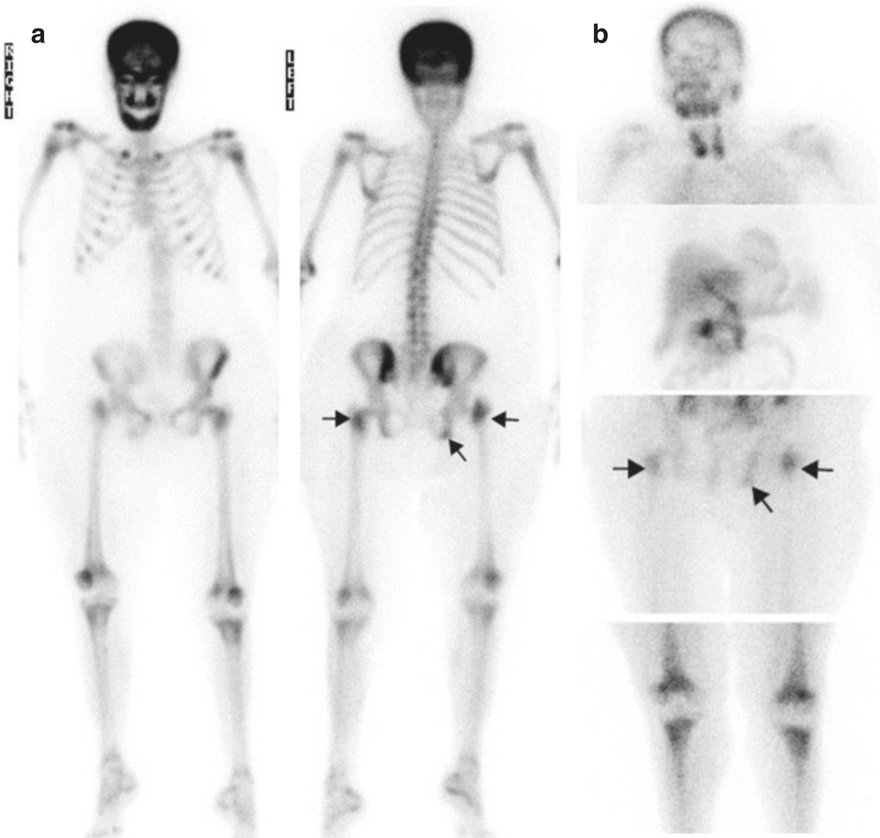

Fig. 7.186 ^{99m}Tc-methylene diphosphonate bone scan (**a**) and spot views of the ^{99m}Tc-sestamibi scan (**b**). Arrows point to the brown tumours

uptake in the calvarium and facial bones including the mandible. Bilateral costochondral calcification was noted together with a widening of the costal angle. There was linear increased uptake seen in the sacroiliac joints bilaterally consistent with insufficiency fractures. There was increased uptake in the shafts of the long bones typical tramline appearance. There was localised increased uptake seen on the whole-body bone (Fig. 7.186a) and sestamibi scans (Fig. 7.186b) in the femoral trochanters and in the left ischium associated with fibrous osteitis (brown tumours). The bone scan findings were in keeping with renal osteodystrophy. There was increased uptake seen at the fracture site in the right neck of the femur with SPECT/CT showing photopenia in the fracture line. The bone scan findings were consistent with renal osteodystrophy and atrophic non-union of the pathological fracture of the right neck of femur and bilateral sacroiliac joint insufficiency fractures.

The early ^{99m}Tc-sestamibi scan neck image (Fig. 7.187a) showed focal uptake corresponding to four parathyroid glands including both the upper and the lower

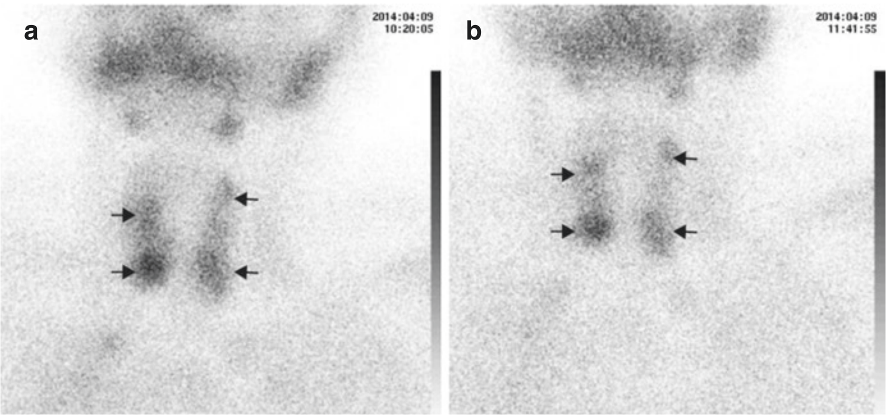

Fig. 7.187 ^{99m}Tc-sestamibi early (**a**) and late planar scans (**b**) with arrows pointing to bilateral upper and lower parathyroid adenomas

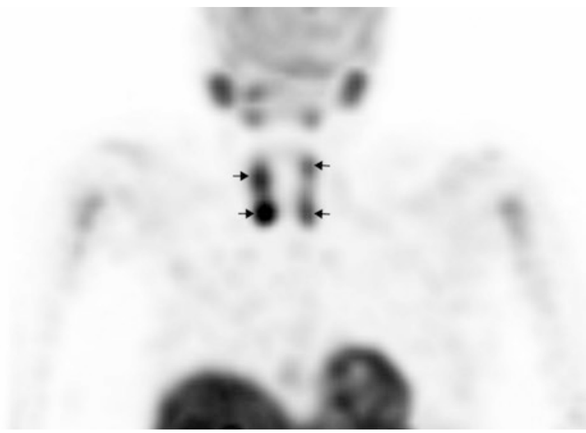

Fig. 7.188 ^{99m}Tc-sestamibi SPECT scan MIP image showing four adenomatous parathyroid glands (arrows)

pair of parathyroid glands, with the delayed neck view (Fig. 7.187b) showing retention of tracer in these four glands. The SPECT scan (Fig. 7.188) clearly demarcated these glands. The sizes of the four glands measured on the CT component were 17 × 10.7 × 11 mm (right upper), 18 × 17 × 12 mm (left upper), 24.5 × 20.2 × 18.9 mm (right lower) and 28.2 × 19.8 × 12.7 mm (left lower).

The multiple ^{99m}Tc-sestamibi scan spot views (Fig. 7.186b) covering the body additionally showed rounded areas of uptake in the mandible, the trochanter of both femora and the left ischium corresponding to the active lesions seen on the bone scans with CT features consistent with brown tumours.

7.65.4 Conclusion

The bone scan findings were consistent with renal osteodystrophy and atrophic nonunion of the pathological fracture of the right neck of femur and bilateral sacroiliac joint insufficiency fractures.

The parathyroid scan and biochemical findings were consistent with tertiary hyperparathyroidism (THPT) due to four-gland adenomatous disease. At surgery, the four enlarged glands were resected, and histopathology confirmed these as parathyroid adenomas. The serum PTH levels fell from a preoperative value of 254.15 pmol/L to 2.4 pmol/L (normal 1.3–9.3), and serum calcium level normalised to 2.27 mmol/L (normal 2.2–2.6).

Hyperphosphataemia associated with hyperparathyroidism resolved with phosphorus falling from 1.75 to 1.15 mmol/L (normal 0.84–1.45) and alkaline phosphate also falling from a preoperative value of 505 to 325 IU/L (normal 42–98).

Uric acid, urea and creatinine continued to rise as resection of glands in secondary hyperparathyroidism will not benefit the kidney function which is the cause rather than the result of hyperparathyroidism.

7.65.5 Comments and Teaching Points

- The patient had low magnesium status which is commonly associated with vitamin D inadequacy and osteoporosis.
- Phosphorus retention and hyperphosphataemia indirectly promote the secretion of PTH and are also important factors in the pathogenesis of secondary hyperparathyroidism but only in the late stages of chronic kidney disease.
- Hypertension and hypercalcaemia usually go hand in hand as calcium increases peripheral resistance arteriole smooth muscle cell contraction.
- In the most advanced cases of PHPT, generalised bone loss, localised brown tumours (osteitis fibrosa cystica), bone cysts and subperiosteal resorption of phalanges and the distal clavicle may occur associated with significantly enhanced bone remodelling. Also, the risk of fractures may increase in the more severe forms of PHPT as seen in this case [113].
- The biochemical hypercalcaemia and the appearances of the four glands are in keeping with adenomatous rather than hyperplastic parathyroid disease associated with tertiary hyperparathyroidism.

- Enhanced proliferative activity of parathyroid cells has a polyclonal character in the initial stages. Later, foci of nodular hyperplasia develop with transformation into monoclonal neoplasia. The parathyroid gland loses its capability to regulate PTH synthesis depending on the level of extracellular calcium. Thus, a THPT may develop against the background of persisting SHPT. This condition is associated with autonomous parathyroid adenoma.

7.66 Case 7.66. Thyroiditis + Ectopic Left Lower Parathyroid Adenoma

7.66.1 Background

A 40-year-old female with a history of multiple urinary tract infections, hypertension and hypothyroidism secondary to thyroiditis was referred with a raised serum parathyroid hormone. Her PTH was 39.99 pmol/L (normal 1.3–9.3), corrected calcium 2.85 mmol/L (normal 2.2–2.6), phosphorus 0.92 mmol/L (normal 0.84–1.45), alkaline phosphate 231 IU/L (normal 53–128), urea 1.6 mmol/L (normal range 2.5–6.4) and creatinine 35 μmol/L (normal range 74–115). Thyroid function tests revealed a fT4 of 7.39 pmol/L (normal 7.86–14.4) and TSH at 2.52 μIU/mL (normal 0.27–4.2) with the patient on levothyroxine replacement.

7.66.2 Procedure

The patient was injected with 52 MBq of ^{99m}Tc-pertechnetate, and a thyroid scan was acquired for 5 min at 20 min postinjection. Next, 844 MBq of ^{99m}Tc-sestamibi was injected without moving the patient and a planar scan performed after 10 min. ^{99m}Tc-sestamibi SPECT/CT scan was performed at 2 h followed by a late planar ^{99m}Tc-sestamibi scan at 3 h.

7.66.3 Findings

The pertechnetate thyroid scan (Fig. 7.189a) showed very poor uptake in the thyroid bed due to a combination of thyroiditis and thyroxine replacement with a small nodule at the right upper pole. The early planar ^{99m}Tc-sestamibi scan (Fig. 7.189b) showed moderate uptake in the thyroid gland with an oblong focus of increased uptake below the lower pole of the left lobe of the thyroid. The delayed washout sestamibi image (Fig. 7.189c) showed almost complete washout of activity from the thyroid gland with marked focal retention of tracer in the lesion below the left lower pole of the thyroid, with the ^{99m}Tc-sestamibi/^{99m}Tc-pertechnetate subtraction image (Fig. 7.189d) showing a residual focus of activity here. The SPECT/CT scan (Fig. 7.190) showed a large elongated hypodense lesion with increased activity seen located on the left side of the trachea inferior to the left thyroid lobe above the manubrium sternum at D2 vertebral level. The size of the lesion on the CT component was measured at 24.3 × 14.6 × 15.3 mm.

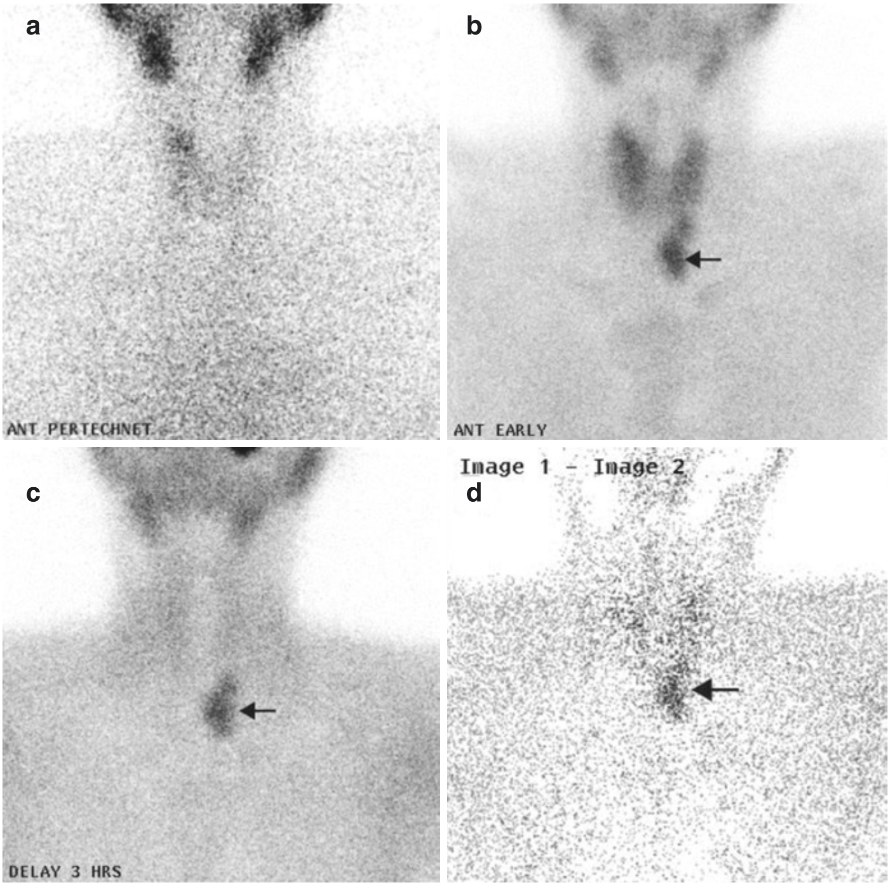

Fig. 7.189 ^{99m}Tc-pertechnetate thyroid scan (**a**), early planar ^{99m}Tc-sestamibi scan (**b**), late planar ^{99m}Tc-sestamibi scan (**c**) and ^{99m}Tc-sestamibi/^{99m}Tc-pertechnetate subtraction scan (**d**) images with the arrow pointing to the left ectopic parathyroid adenoma

7.66.4 Conclusion

Findings consistent with a large left lower ectopic parathyroid adenoma as the cause of primary hyperparathyroidism in a patient with hypothyroidism secondary to thyroiditis.

7.66.5 Comments and Teaching Points

- The parathyroid glands, in addition to their congenital ectopia, can leave their usual locations under the weight of the growing adenomatous or hyperplastic glands. This phenomenon is referred to as “acquired parathyroid ectopia”. Upward movements of the larynx and pharynx in swallowing, and negative intrathoracic pressure, promote migration of the parathyroids [87].

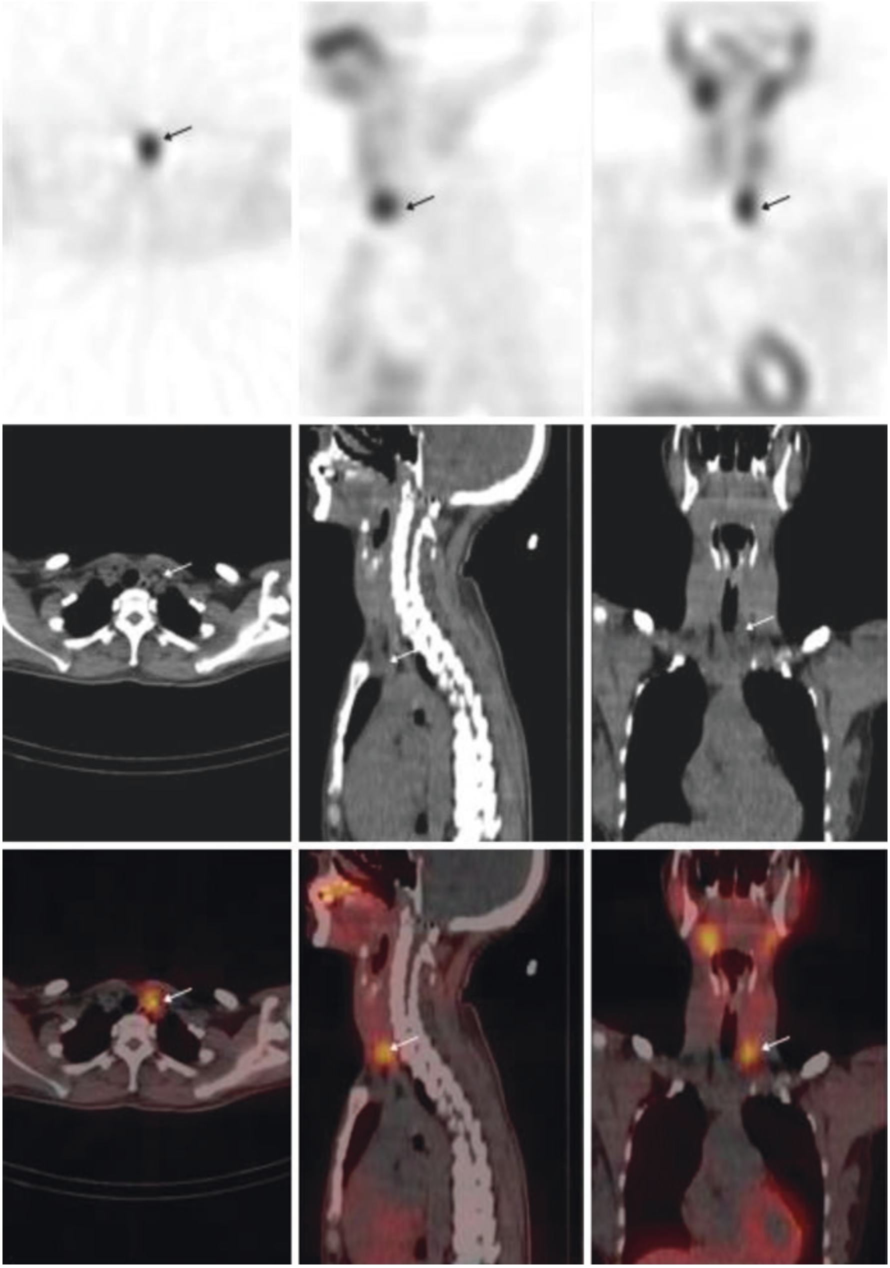

Fig. 7.190 ^{99m}Tc-sestamibi SPECT scan images (top row), CT scan images (middle row) and fused SPECT/CT images (bottom row) in the transaxial (left column), sagittal (middle column) and coronal (right column) planes, showing the ectopic left lower parathyroid adenoma (arrows)

7.67 Case 7.67. Triple Modality (Scintigraphy, contrast CT and US) Imaging of a Solitary Parathyroid Adenoma

7.67.1 Background

A 67-year-old female with a history of a brain tumour presented with complaints of bone pains. Laboratory tests revealed raised serum parathormone and hypercalcaemia. Her serum PTH level was 12.33 pmol/L (normal 1.3–9.3), corrected calcium 2.82 mmol/L (normal 2.2–2.6), phosphorus 1.07 mmol/L (normal 0.84–1.45), alkaline phosphate 76 IU/L (normal 42–98), uric acid 277 μmol/L (normal 137–393), urea 3.2 mmol/L (normal 2.5–6.4) and creatinine 71 μmol/L (normal range 53–97).

7.67.2 Procedure

The patient was injected with 53 MBq of ^{99m}Tc-pertechnetate, and a 5-min duration thyroid scan was acquired after 20 min. Next, 845 MBq of ^{99m}Tc-sestamibi was injected without moving the patient and a planar scan performed after 10 min. ^{99m}Tc-sestamibi SPECT/CT scan was performed at 2 h followed by a late planar ^{99m}Tc-sestamibi scan at 3 h.

7.67.3 Findings

The pertechnetate thyroid scan (Fig. 7.191a) showed a normal-sized image of the thyroid with homogenous distribution of activity in the gland. The early planar ^{99m}Tc-sestamibi scan (Fig. 7.191b) showed an oblong focus of activity extending upwards from the upper pole of the left lobe of the thyroid with marginally increased uptake compared with the thyroid gland. The delayed sestamibi washout (Fig. 7.191c) scan image showed symmetrical clearance of activity from the

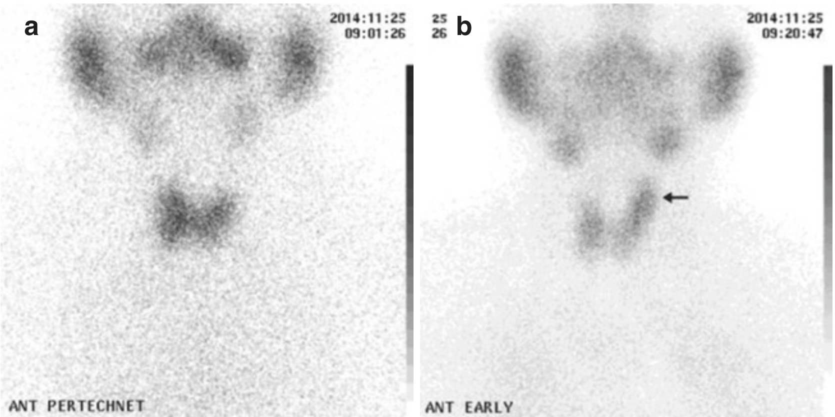

Fig. 7.191 ^{99m}Tc-pertechnetate thyroid scan (**a**), early planar ^{99m}Tc-sestamibi scan (**b**), late planar ^{99m}Tc-sestamibi scan (**c**) and ^{99m}Tc-sestamibi/^{99m}Tc-pertechnetate subtraction scan (**d**) images with the arrow pointing to the left upper parathyroid adenoma

thyroid gland and the left upper pole nodule. The ^{99m}Tc-sestamibi/^{99m}Tc-pertechnetate subtraction image (Fig. 7.191d) however showed a clear-cut residual focus of activity abutting the upper pole of the left lobe of the thyroid. The SPECT/CT scan (Fig. 7.192) showed an oblong focus of intense uptake corresponding to a

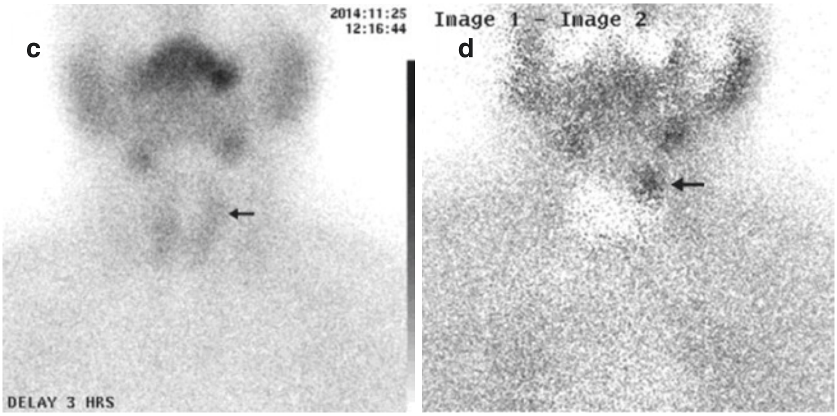

Fig. 7.191 (continued)

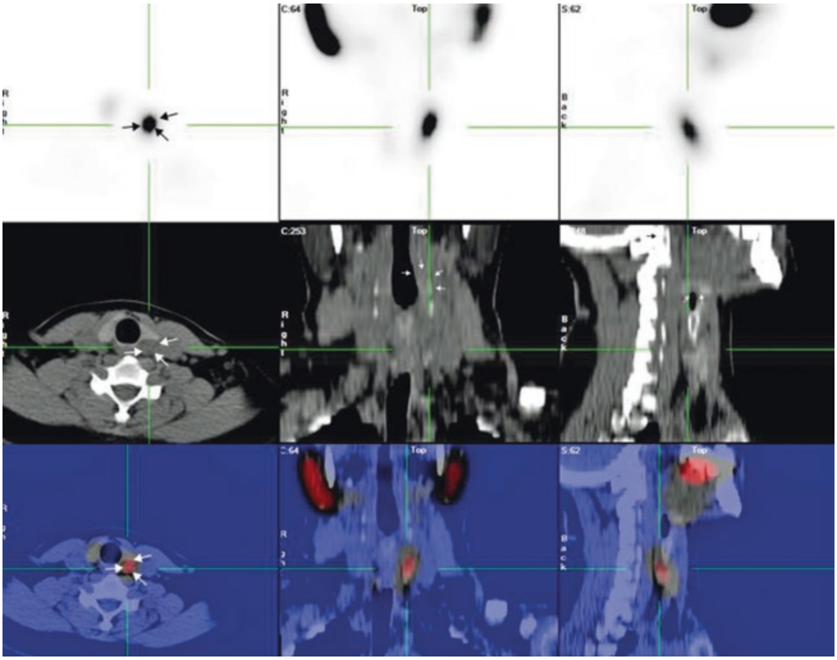

Fig. 7.192 ^{99m}Tc-sestamibi SPECT scan images (top row), CT scan images (middle row) and fused SPECT/CT images (bottom row) in the transaxial (left column), coronal (middle column) and sagittal (right column) planes, showing an oblong focus of intense uptake corresponding to a hypodense lesion on the CT extending upwards from behind the left upper pole of the thyroid

hypodense lesion on the CT extending upwards from behind the left upper pole of the thyroid.

The patient next had a thyroid ultrasound which showed a well-defined hypoechoic oval-shaped lesion posterior to the upper pole of the left lobe of the thyroid with the colour Doppler study showing vascularity in the lesion (Fig. 7.193).

Pre- and post-contrast CT of the neck (Fig. 7.194) was next performed, which showed a well-defined soft-tissue density lesion at the posterosuperior aspect of the left thyroid lobe. In the non-contrast scan, the lesion appeared hypodense but showed intense contrast enhancement with a small hypodense

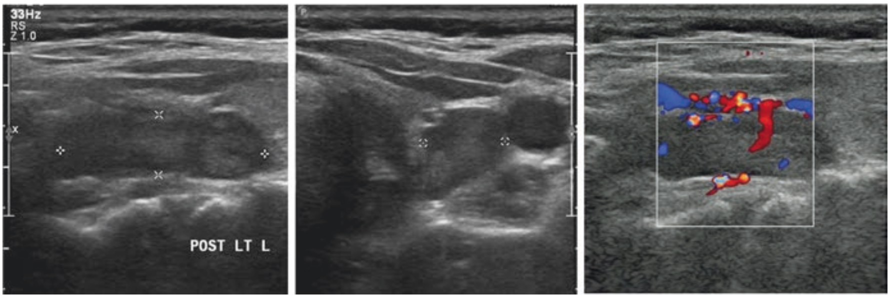

Fig. 7.193 Thyroid ultrasound showing a well-defined hypoechoic oval-shaped lesion measuring 2.5 × 1.0 × 0.8 cm in size located posterior to the upper pole of the left lobe of the thyroid. The colour Doppler study shows vascularity in the lesion

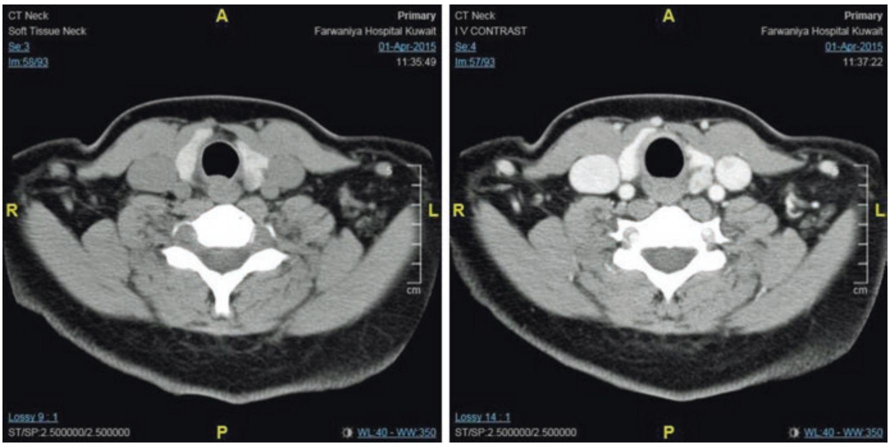

Fig. 7.194 Transaxial pre- and post-contrast CT scan images showed a hypodense lesion (arrows) with intense contrast enhancement with a small hypodense non-enhancing area likely to be a small cystic component

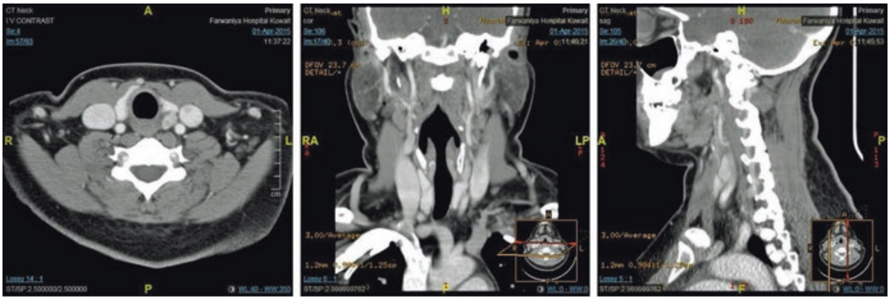

Fig. 7.195 Postcontrast CT delayed phase image in the transaxial, transaxial (left), coronal (middle) and sagittal (right) axes (bottom) showing the at the posterosuperior aspect of the left thyroid lobe medial to the carotid sheath, lateral to the trachea and oesophagus.measuring 1.5 × 1 × 2 cm in maximum axial, transverse and cranio-caudal dimensions respectively. There is a partial washout of the contrast from the lesion which appears hypodense compared with the adjacent thyroid gland

non-enhancing area likely to be a small cystic component. On the delayed phase, the lesion washed out and became hypodense compared with the adjacent thyroid gland (Fig. 7.195).

7.67.4 Conclusion

Findings consistent with a left upper parathyroid adenoma as the cause of primary hyperparathyroidism.

7.67.5 Comments and Teaching Points

- This case demonstrates the utility and role of current imaging modalities in the diagnosis of parathyroid adenomatous disease as the adenoma was diagnosed on all three of the recommended diagnostic modalities including radionuclide imaging, ultrasound and contrast CT.
- Normal parathyroid glands are usually not detected by ultrasound. Parathyroid adenomas are usually seen as round or oval, hypoechogenic structures, contrasting the hyperechogenic thyroid tissue, and are most useful in identifying adenomas close to the thyroid gland [114] as seen in this case.
- CT is useful in localising ectopic mediastinal parathyroid glands with a sensitivity of approximately 46–87%. Another technique that is being used recently with high sensitivity is the 4D-CT, with time being the fourth dimension. CT allows rapid assessment of the glands but has a higher cost and exposure to radiation and requires iodinated contrast agents [114].

7.68 Case 7.68. Water-Clear Cell Right Lower Adenoma

7.68.1 Background

A 40-year-old male with long standing biochemical hyperparathyroidism was referred for preoperative localisation of a suspect parathyroid adenoma. Serum parathormone level was 30.17 pmol/L (normal 1.3–9.3), corrected calcium 2.85 mmol/L (normal 2.2–2.6), phosphorus 0.95 mmol/L (normal 0.84–1.45), alkaline phosphate 118 IU/L (normal 53–128), urea 2.7 mmol/L (normal range 2.5–6.4) and creatinine 63 µmol/L (normal range 74–115).

7.68.2 Procedure

The patient was injected with 42 MBq of ^{99m}Tc-pertechnetate, and a thyroid scan was acquired for 5 min at 20 min postinjection. Next, 800 MBq of ^{99m}Tc-sestamibi was injected without moving the patient and a planar scan performed after 10 min. ^{99m}Tc-sestamibi SPECT/CT scan was performed at 2 h followed by a late planar ^{99m}Tc-sestamibi scan at 3 h.

7.68.3 Findings

The pertechnetate thyroid scan showed a normal-sized image of the thyroid with homogenous distribution of activity in the gland (Fig. 7.196a). The early planar ^{99m}Tc-sestamibi scan (Fig. 7.196b) showed a pattern of uptake similar to that seen on the pertechnetate thyroid scan with a focus of faint uptake seen below the lower

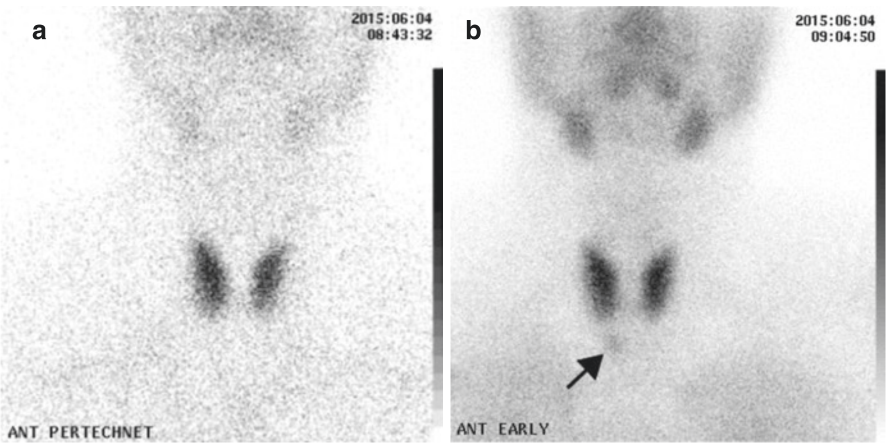

Fig. 7.196 ^{99m}Tc-pertechnetate thyroid scan (**a**), early planar ^{99m}Tc-sestamibi scan (**b**), late planar ^{99m}Tc-sestamibi scan (**c**) and ^{99m}Tc-sestamibi/^{99m}Tc-pertechnetate subtraction scan (**d**) images with the arrow pointing to the focus of faint increased uptake below the lower pole of the right thyroid lobe

pole of the right lobe of the thyroid, which showed marginal focal retention seen in the lesion on the delayed washout sestamibi image (Fig. 7.196c). The ^{99m}Tc-sestamibi/^{99m}Tc-pertechnetate subtraction image however showed a faint residual focus of activity below the right lower pole of the thyroid (Fig. 7.196d). The SPECT/CT scan (Fig. 7.197) showed very faint uptake in the nodule in the right lower with equivocal uptake only.

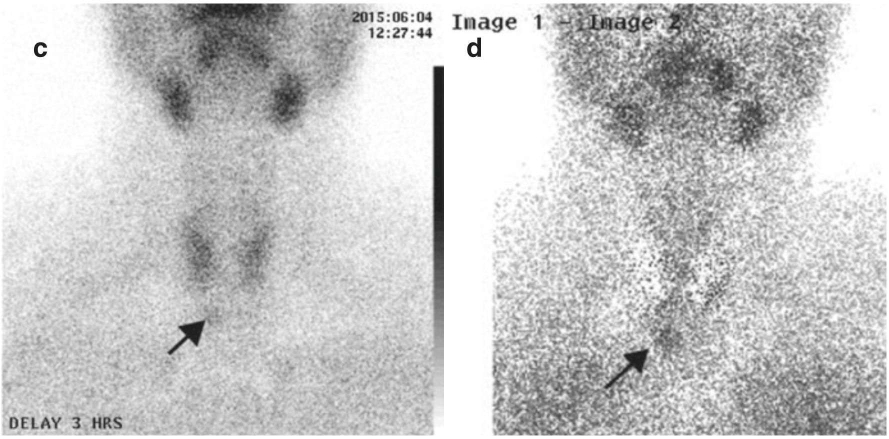

Fig. 7.196 (continued)

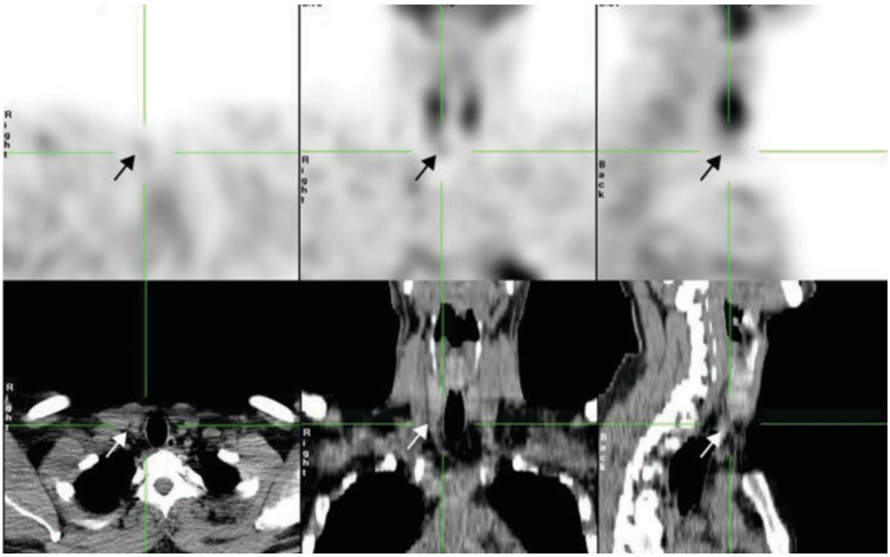

Fig. 7.197 ^{99m}Tc-sestamibi SPECT scan images (top row) and CT scan images (bottom row) in the transverse (left column), coronal (middle column) and sagittal (right column) axes showing a right parathyroid adenoma (arrows) with very faint uptake which is much less than the activity in the thyroid and only marginally higher than the surrounding background

7.68.4 Conclusion

Findings suggestive of a non-oncogenic cell right lower parathyroid adenoma as the cause of primary hyperparathyroidism.

At surgery, a right lower parathyroid gland measuring 2.3 × 1.0 × 0.8 cm was removed. Histopathology showed an encapsulated cellular lesion with a rim of normal parathyroid tissue. The lesion was seen to consist of water-clear cells, lymphocytic aggregates and adipose tissue.

The serum PTH levels fell from a preoperative value of 30.17 pmol/L to 1.6 pmol/L (normal 1.3–9.3), and serum calcium level normalised to 2.48 mmol/L (normal 2.2–2.6).

7.68.5 Comments and Teaching Points

- This is the second rare case of water-clear cell adenoma reported in this book. So far there have been 21 cases reported worldwide [1, 5, 115].
- Water-clear cell hyperplasia is a very rare condition with marked enlargement of all four glands. The upper glands can be 5–10 times larger than the lower pair of glands. The water-clear cell hyperplastic glands commonly contain large cysts with haemorrhagic areas. Histologically, the gland contains large (20 μm) water-clear cells with peripherally located nuclei [116]. Water-clear cell adenomas consist of nests and acini of water-clear cells containing abundant foamy, granular cytoplasm, and mild nuclear pleomorphism.
- Non-oncogenic cell adenomas including water-clear cell adenoma are false-negative on sestamibi parathyroid scan and can be better visualised by thallium parathyroid SPECT/CT scan as shown in several other cases in this book.

7.69 Case 7.69. Giant Right Lower Parathyroid Gland Cancer

7.69.1 Background

A 42-year-old female complaining of generalised bone pains and orthopnoea with biochemical hyperparathyroidism and hypercalcaemia. Serum parathormone level was 86.72 pmol/L (normal 1.3–9.3), corrected calcium 3.19 mmol/L (normal 2.2–2.6), phosphorus 0.65 mmol/L (normal 0.84–1.45), alkaline phosphate 272 IU/L (normal 42–98), urea 4.9 mmol/L (normal range 2.5–6.4) and creatinine 46 μmol/L (normal range 53–97).

7.69.2 Procedure

The patient was injected with 65 MBq of ^{99m}Tc-pertechnetate, and a thyroid scan was acquired for 5 min at 20 min postinjection. Next, 849 MBq of ^{99m}Tc-sestamibi

was injected without moving the patient and a planar scan performed after 10 min. ^{99m}Tc-sestamibi SPECT/CT scan was performed at 2 h followed by a late planar ^{99m}Tc-sestamibi scan at 3 h.

7.69.3 Findings

The pertechnetate thyroid scan showed a normal-sized image of the thyroid with homogenous distribution of activity in the gland (Fig. 7.198a). The early planar ^{99m}Tc-sestamibi scan (Fig. 7.198b) showed a very large diamond-shaped lesion with intense sestamibi uptake extending downwards from the lower pole of the right lobe of the thyroid. The delayed sestamibi scan (Fig. 7.198c) image showed marked retention of tracer in the lesion. The ^{99m}Tc-sestamibi/^{99m}Tc-pertechnetate

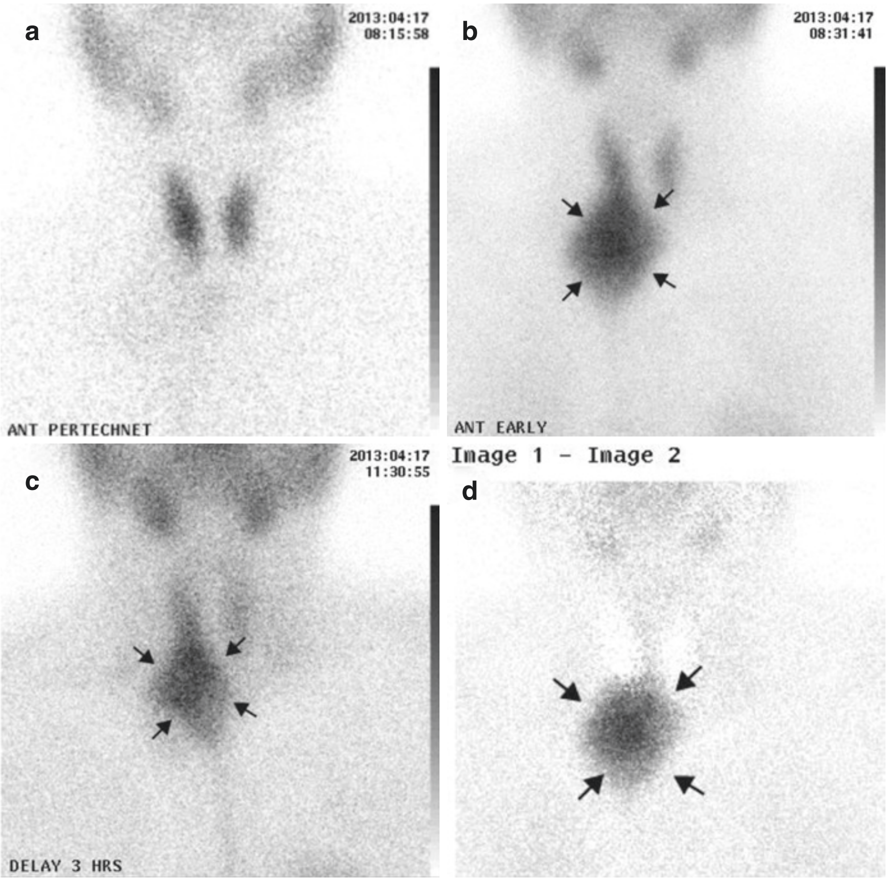

Fig. 7.198 ^{99m}Tc-pertechnetate thyroid scan (**a**), early planar ^{99m}Tc-sestamibi scan (**b**), late planar ^{99m}Tc-sestamibi scan (**c**) and ^{99m}Tc-sestamibi/^{99m}Tc-pertechnetate subtraction scan (**d**) images, with the arrows pointing to the large diamond-shaped sestamibi-avid mass extending downwards from the lower pole of the right lobe of the thyroid with intense increased uptake on the early scan and marked sestamibi retention on the delayed scan images

subtraction image (Fig. 7.198d) showed a large residual focus of activity corresponding to the lesion below the lower pole of the right lobe on the thyroid. The SPECT/CT scan (Fig. 7.199) showed a large hypodense mass with intense sestamibi uptake on the right side of the trachea causing marked deviation of the trachea to the left and extending retrosternally downwards into the thoracic inlet.

Ultrasound of the neck (Fig. 7.200) was performed, which showed a grossly enlarged right thyroid lobe with a large nodular lesion of mixed echogenicity with soft-tissue and cystic components. The mass was seen to extend into the right thoracic inlet retrosternally and was located posterior to the major neck vessels in the lower neck and medial to the right neck vessels in the mid-neck region.

CT scan images of the neck and chest (Fig. 7.201) showed a large soft-tissue mass lesion with a lobulated outline measuring 4.1 × 5 × 7.8 cm in size which appeared inseparable from the posterior aspect of the right lobe of the thyroid and was seen indenting and displacing the cervical trachea and oesophagus to the left.

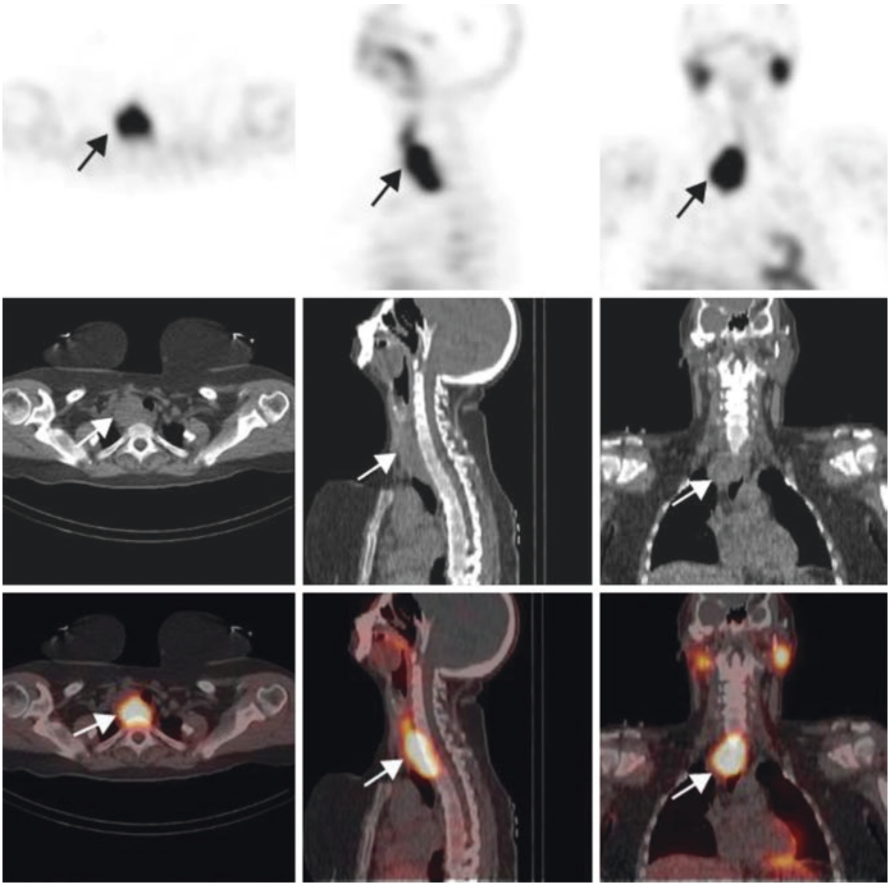

Fig. 7.199 ^{99m}Tc-sestamibi SPECT scan images (top row), CT scan images (middle row) and fused SPECT/CT images (bottom row) in the transaxial (left column), coronal (middle column) and sagittal (right column) planes, showing a right hypodense mass with intense uptake (arrows) extending retrosternally downwards into the thoracic inlet

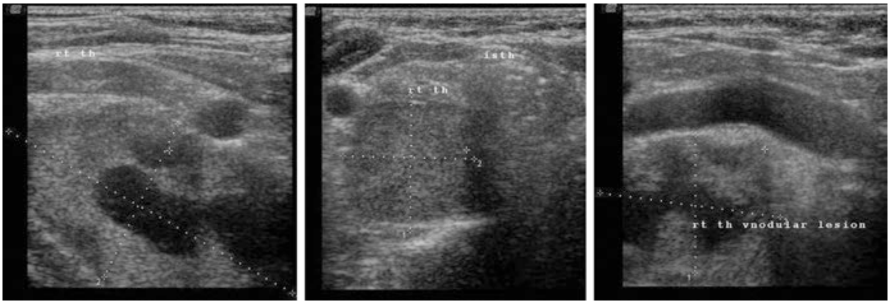

Fig. 7.200 Ultrasound of the neck shows a grossly enlarged right thyroid lobe with a large nodular lesion of mixed echogenicity with soft-tissue and cystic components, extending to the right thoracic inlet retrosternally, posterior to the major neck vessels in the lower neck and medial to the right neck vessels in the mid-neck region

Fig. 7.201 CT scan images of the neck and chest in the coronal (left), sagittal (middle) and trans-axial (right) planes showing a large soft-tissue mass lesion inseparable from the posterior aspect of the right lobe of the thyroid measuring 4.1 × 5 × 7.8 cm along its maximum anteroposterior, transverse and cranio-caudal diameters. The mass has a lobulated outline and is seen indenting and displacing the cervical trachea and oesophagus to the left

7.69.4 Conclusion

Findings consistent with a huge right lower hyperactive parathyroid mass, presumably an adenoma or perhaps parathyroid carcinoma as the cause of primary hyperparathyroidism.

On surgery, a parathyroid tumour was removed. Histopathology confirmed parathyroid cancer: the tumour had invasive borders and was covered by a thick fibrous capsule which extended into the parenchyma to form thick fibrous septa, with the tumour composed of chief-like, oncocytic and clear cells and immunohistochemical stains demonstrating positive expression of cyclin D1, bcl-2 and Ki-67.

7.69.5 Comments and Teaching Points

- A large palpable neck or a large ectopic mass lesion with marked biochemical hyperparathyroidism is suggestive of parathyroid carcinoma.

- Parathyroid carcinoma affects fewer than 1/1,000,000 population per year and develops in all ages, although more frequently in older adults (mean sixth decade) and up to a decade earlier than adenoma.
- The nonspecific symptoms (weakness, fatigue, anorexia, weight loss, nausea, polyuria, polydipsia, etc.) overlap with adenoma, but concurrent bone disease with bone pains is more common in patients with carcinoma than adenoma as seen in this case.
- Although parathyroid cancer predominantly affects older patients, but compared with parathyroid adenomas, the patients are younger by ~10 years—the average age of patients with parathyroid cancer being 50 years [117].

7.70 Case 7.70. Dual-Tracer (^{99m}Tc-Sestamibi and ^{201}Tl-Thallous Chloride) Avid Parathyroid Adenoma

7.70.1 Background

A 53-year-old female with hypertension and diabetes mellitus was found to be biochemically hypercalcaemic with mildly elevated parathormone level. Her PTH was 13.10 pmol/L (normal 1.3–9.3), corrected calcium 2.77 mmol/L (normal 2.2–2.6), magnesium 0.72 mmol/L (normal 0.77–1.03), phosphorus 0.92 mmol/L (normal 0.84–1.45), alkaline phosphate 88 IU/L (normal 42–98), urea 3.5 mmol/L (normal range 2.5–6.4) and creatinine 40 μmol/L (normal range 53–97).

7.70.2 Procedure

The patient was injected with 80 MBq of ^{99m}Tc-pertechnetate, and a thyroid scan was acquired for 10 min at 15 min postinjection. Next, 788 MBq of ^{99m}Tc-sestamibi was injected without moving the patient and a planar scan performed after 10 min. ^{99m}Tc-sestamibi SPECT/CT scan was performed at 2 h followed by a late planar ^{99m}Tc-sestamibi scan at 3 h.

For the thallium-201 parathyroid scan, the patient was injected with 110 MBq of ^{201}Tl-thallous chloride intravenously and a 10-min duration static image acquired after 10 min postinjection followed by a SPECT/CT scan.

7.70.3 Findings

The pertechnetate thyroid scan (Fig. 7.202a) showed a normal-sized image of the thyroid with homogenous distribution of activity in the gland but with a dominant right lobe showing higher uptake compared with the left lobe. The early planar ^{99m}Tc-sestamibi scan (Fig. 7.202b) showed a pattern of uptake similar to that seen on the pertechnetate thyroid scan, with the delayed washout sestamibi scan images (Fig. 7.202c) showing no focal retention in the thyroid bed. The

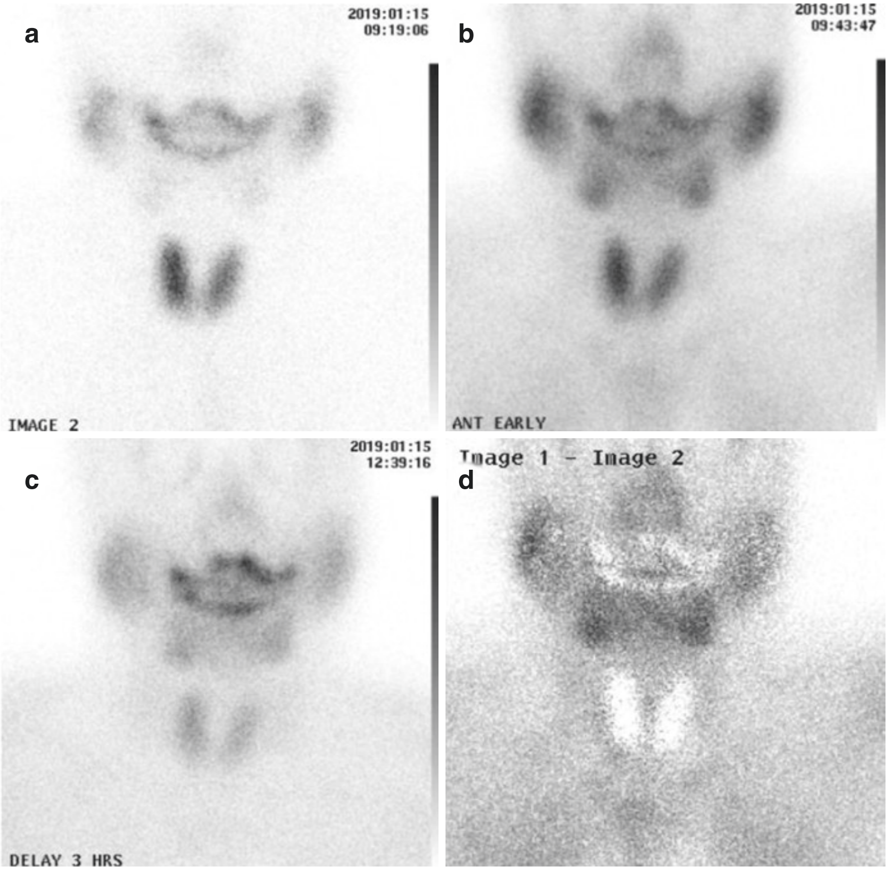

Fig. 7.202 ^{99m}Tc-pertechnetate thyroid scan (**a**), early planar ^{99m}Tc-sestamibi scan (**b**), late planar ^{99m}Tc-sestamibi scan (**c**) and ^{99m}Tc-sestamibi/^{99m}Tc-pertechnetate subtraction scan images (**d**)

^{99m}Tc-sestamibi/^{99m}Tc-pertechnetate subtraction image (Fig. 7.202d) also did not show any residual activity in the thyroid bed. The SPECT/CT scan (Fig. 7.203) showed a focus of uptake on the SPECT scan located at the right lower pole of the thyroid posteriorly with moderately increased uptake.

The ^{201}Tl/^{99m}Tc subtraction scan (Fig. 7.204) showed no residual focus of activity in the thyroid bed. The thallium-201 SPECT/CT (Fig. 7.205), however, showed a clear-cut focus of activity at the right lower pole of the thyroid posteriorly with intense uptake with the CT component (Figs. 7.203, 7.205, and 7.206) showing the focus of activity to correspond to a hypodense nodule measuring 16.7 × 10.4 × 11.2 mm in size.

7.70.4 Conclusion

Findings consistent with a sestamibi- and thallium-avid right lower parathyroid adenoma.

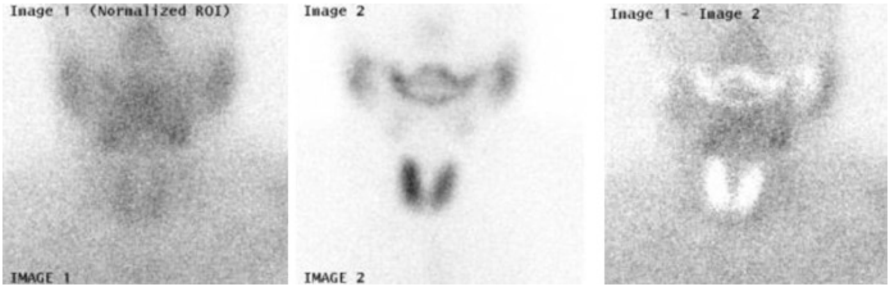

Fig. 7.203 $^{201}Tl/^{99m}Tc$ subtraction scan showing no residual focus of activity in the thyroid bed

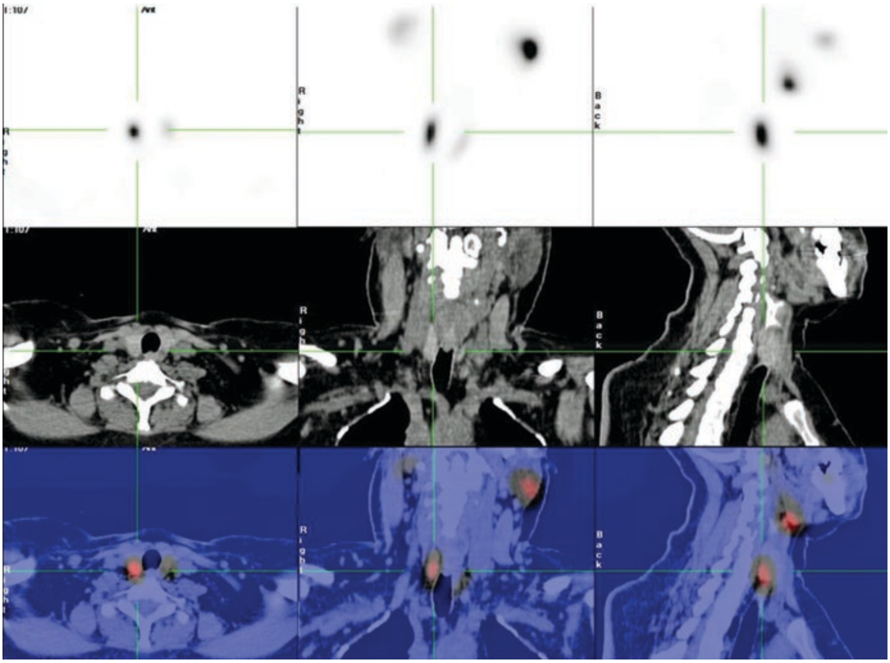

Fig. 7.204 ^{99m}Tc-sestamibi SPECT scan images (top row), CT scan images (middle row) and fused SPECT/CT images (bottom row) in the transaxial (left column), coronal (middle column) and sagittal (right column) planes, showing a right parathyroid adenoma (crosshair)

7.70.5 Comments and Teaching Points

- As seen in this case, the planar and subtraction scan images, for both sestamibi and thallium, were negative presumably due to the small size of the adenoma.
- Both components of the SPECT/CT however accurately identified the adenoma with the thallium scan showing relatively more intense uptake, presumably due to the cellular composition and biological properties of the adenoma as shown in other cases.

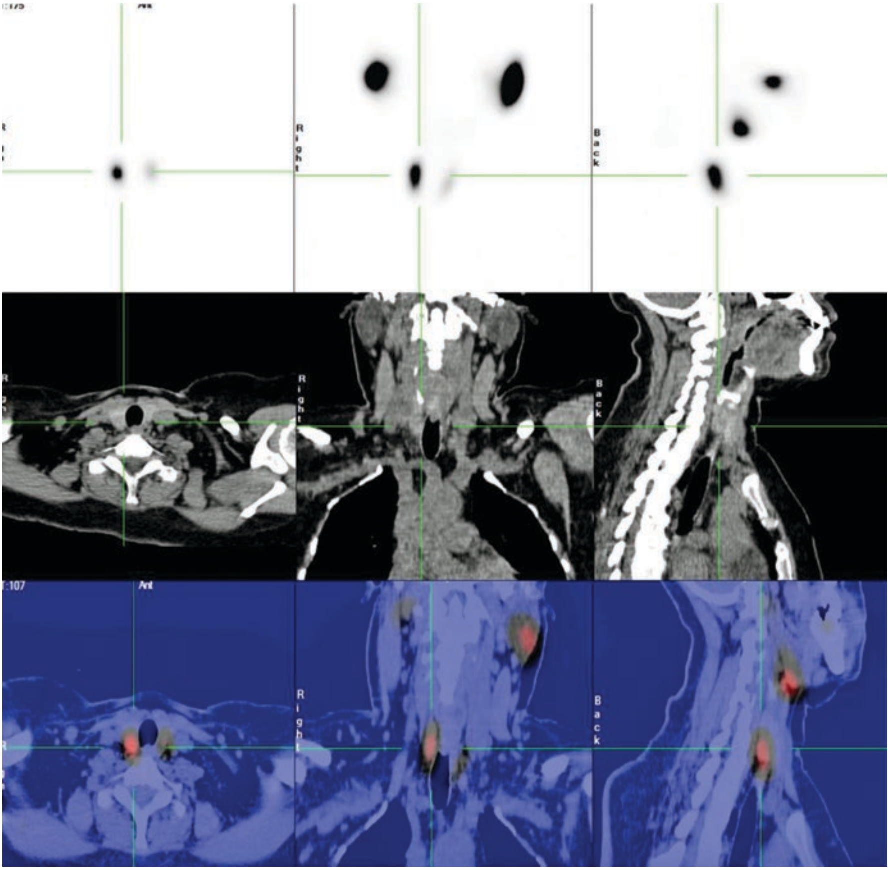

Fig. 7.205 Thallium-201 SPECT/CT scan with SPECT scan images (top), CT images (middle) and fused SPECT/CT images (bottom) in the transaxial (left column), coronal (middle column) and sagittal (right column) planes showing a right lower parathyroid adenoma (crosshair)

- The classical thallium-201/technetium-99m subtraction scan was abandoned in favour of sestamibi imaging due to the better physical characteristics of technetium and due to dual-phase imaging with sestamibi with the parathyroid lesions showing retention of tracer compared with the thyroid gland.
- However, as seen in this case, thallium SPECT shows similar accuracy, if not better, to sestamibi SPECT, presumably due to higher thallium uptake per gramme of tissue compared with sestamibi though there is also higher uptake in the surrounding thyroid gland with thallium. SPECT imaging, however, removes the background activity, and hence equivalent quality images can, therefore, be obtained with thallium SPECT.
- Another advantage of thallium SPECT is that unlike sestamibi it is positive in both oncocytic and non-oncocytic hyperactive parathyroid glands.

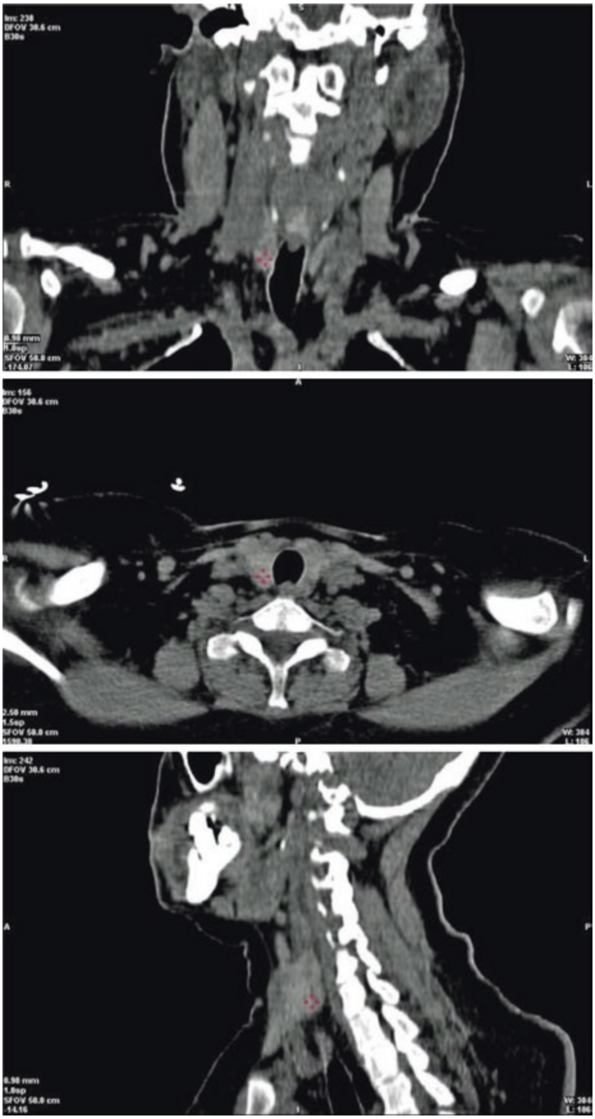

Fig. 7.206 CT scan images in transaxial (top), sagittal (middle) and coronal axes (bottom) showing a right lower parathyroid adenoma (arrows) measuring 16.7 × 10.4 × 11.2 mm in size

- Parathyroid adenoma cell content affects the scintigraphic outcome with sestamibi more than that with thallium parathyroid imaging. As oxyphil cells have a higher mitochondrial content compared with the chief cells, they are more likely to uptake technetium isotopes. The presence of oxyphil cells within the parathyroid adenomas is associated with a positive ^{99m}Tc-sestamibi scan [118].

7.71 Case 7.71. Four-Gland Parathyroid Hyperplasia: Two Sestamibi-Avid Glands and all Four Thallium-Avid Glands

7.71.1 Background

A 56-year-old female with hypertension, diabetes mellitus and ischaemic heart disease was found to be biochemically hypercalcaemic with elevated parathormone level. Her corrected serum calcium was 2.84 mmol/L (normal 2.2–2.6), PTH 14.90 pmol/L (normal 1.3–9.3), magnesium 0.48 mmol/L (normal 0.77–1.03), phosphorus 1.03 mmol/L (normal 0.84–1.45), alkaline phosphate 95 IU/L (normal 42–98), urea 2.9 mmol/L (normal range 2.5–6.4) and creatinine 50 μmol/L (normal range 53–97).

7.71.2 Procedure

The patient was injected with 83 MBq of ^{99m}Tc-pertechnetate, and a thyroid scan was acquired for 10 min at 15 min postinjection. Next, 751 MBq of ^{99m}Tc-sestamibi was injected without moving the patient and a planar scan performed after 10 min. ^{99m}Tc-sestamibi SPECT/CT scan was performed at 2 h followed by a late planar ^{99m}Tc-sestamibi scan at 3 h.

For the thallium-201 parathyroid scan, the patient was injected with 114 MBq of ^{201}Tl-thallous chloride intravenously and a 10-min duration static image acquired after 10 min postinjection followed by a SPECT/CT scan.

7.71.3 Findings

The pertechnetate thyroid scan (Fig. 7.207a) showed an enlarged image of the thyroid with a relatively larger right lobe and homogenous distribution of activity in the gland. The early planar ^{99m}Tc-sestamibi scan (Fig. 7.207b) showed a pattern of uptake similar to that seen on the pertechnetate thyroid scan, with the delayed washout sestamibi scan images (Fig. 7.207c, d) however showing focal retention of activity at both lower poles of the thyroid.

The SPECT/CT scan (Fig. 7.208) showed clear-cut focal increased uptake at both lower poles of the thyroid seen corresponding to posteriorly located lesions on the CT component. These lesions were consistent with bilateral enlargement of both lower parathyroid glands with the left larger than the right. However, the CT component also showed large-sized lesions without any sestamibi uptake at both upper poles of the thyroid, which was investigated further by a thallium-201 planar and SPECT/CT scans.

The thallium-201 planar SPECT scan (Fig. 7.209a) showed a similar pattern of uptake as seen in the ^{99m}Tc-pertechnetate thyroid scan (Fig. 7.209b), but the thallium SPECT maximum intensity projection image (Fig. 7.209c) showed four hyperplastic parathyroid glands with the upper two glands larger with more intense uptake

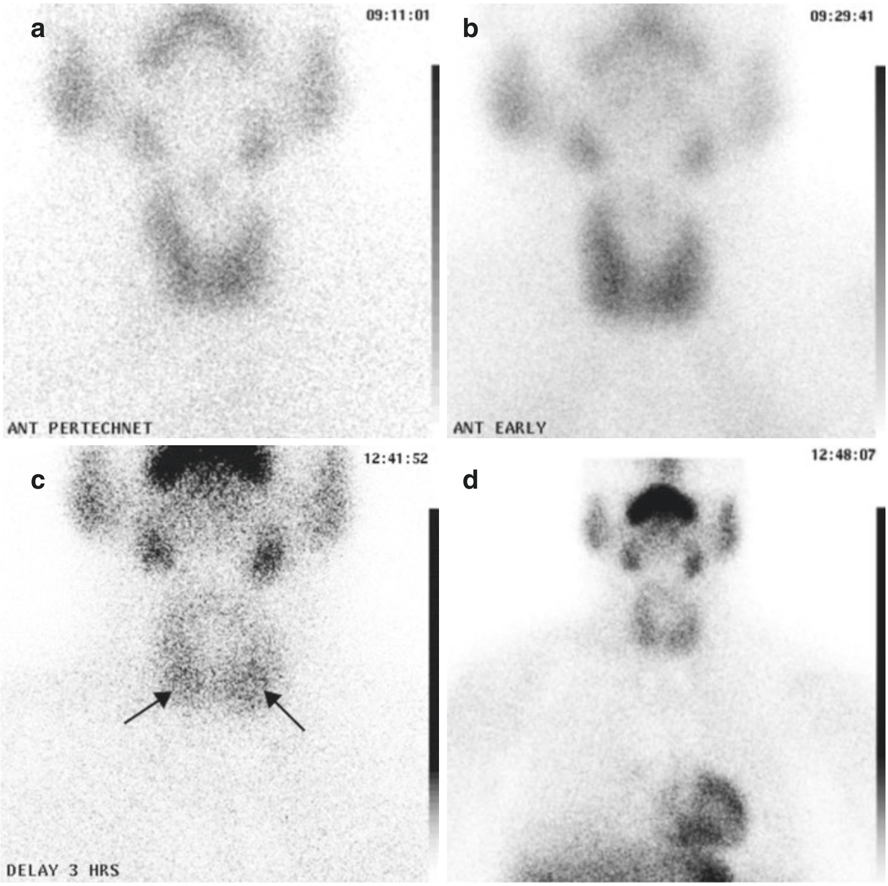

Fig. 7.207 ^{99m}Tc-pertechnetate thyroid scan (**a**), early planar ^{99m}Tc-sestamibi scan (**b**), late planar ^{99m}Tc-sestamibi scan (**c**) and unzoomed late sestamibi neck and chest scan image (**d**). Note the retention of activity at both lower poles of the thyroid on the delayed washout image (arrows)

than the lower two parathyroid glands. The thallium-201 SPECT/CT scan (Fig. 7.210) not only showed uptake in the bilateral lower parathyroid gland similar to that seen on the ^{99m}Tc-sestamibi SPECT/CT scan but also showed intense increased uptake in the larger bilaterally enlarged upper parathyroid glands which showed no uptake on the sestamibi scans. The sizes of the glands measured on the CT component (Fig. 7.211) were 19 × 19 × 12 mm (right lower), 25 × 17 × 18 mm (left lower), 20 × 20 × 17 mm (right upper) and 23.5 × 16.5 × 16.1 mm (left upper).

7.71.4 Conclusion

Findings consistent with four markedly enlarged and hyperplastic parathyroid glands as the cause of primary hyperparathyroidism. Only the lower two parathyroid glands were true-positive on the sestamibi SPECT/CT scan with the larger

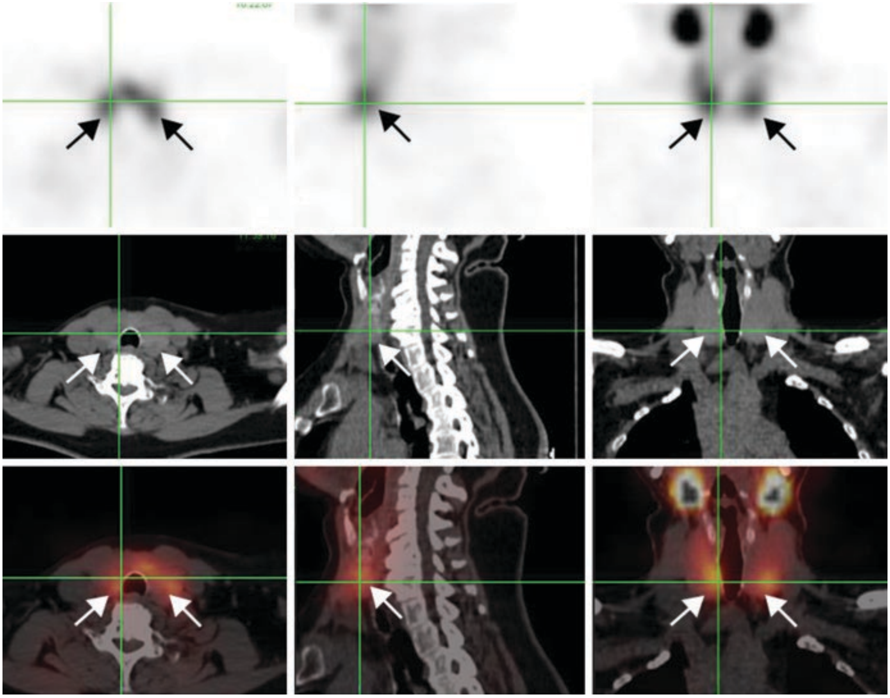

Fig. 7.208 ^{99m}Tc-sestamibi SPECT scan images (top row), CT scan images (middle row) and fused SPECT/CT images (bottom row) in the transaxial (left column), sagittal (middle column) and coronal (right column) planes, showing bilateral enlargement of the lower parathyroid glands (arrows)

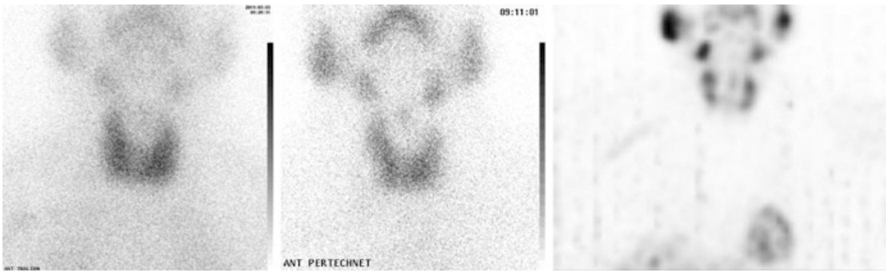

Fig. 7.209 ^{201}Tl planar scan (left) and ^{99m}Tc-pertechnetate planar scan (middle) showing symmetrical uptake of the tracer in the thyroid gland. The thallium MIP image (right) however shows 4 hyperplastic parathyroid glands with the upper two glands showing relatively more intense uptake

upper two parathyroid glands false-negative on the sestamibi scan showing no sestamibi avidity, which are presumably predominantly composed of non-oncocytic cells. All four parathyroid glands show intense uptake on the thallium SPECT/CT scan.

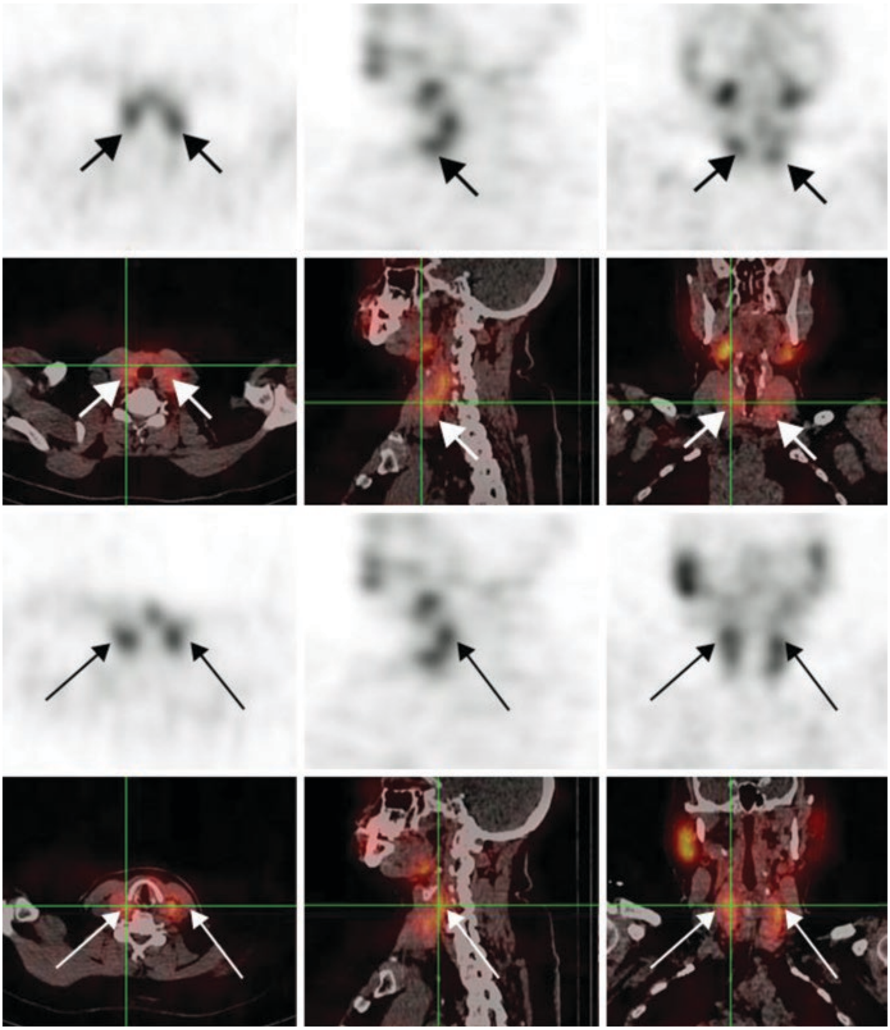

Fig. 7.210 Thallium-201 SPECT (top row) and fused SPECT/CT scan (second row) showing the bilaterally enlarged lower parathyroid glands (short arrows), with the SPECT scan (third row) and the fused SPECT/CT scans (fourth row) showing bilaterally enlarged upper parathyroid glands (long arrows) with intense thallium uptake

7.71.5 Comments and Teaching Points

- This is a novel case of four markedly hyperplastic and enlarged parathyroid glands causing primary hyperparathyroidism.
- On the basis of sestamibi uptake in the lower two parathyroid glands only, as seen in this case, a false diagnosis of double parathyroid adenomas would have been made, and targeted surgery would therefore have failed as the larger upper two parathyroid glands were false-negative on the sestamibi SPECT.

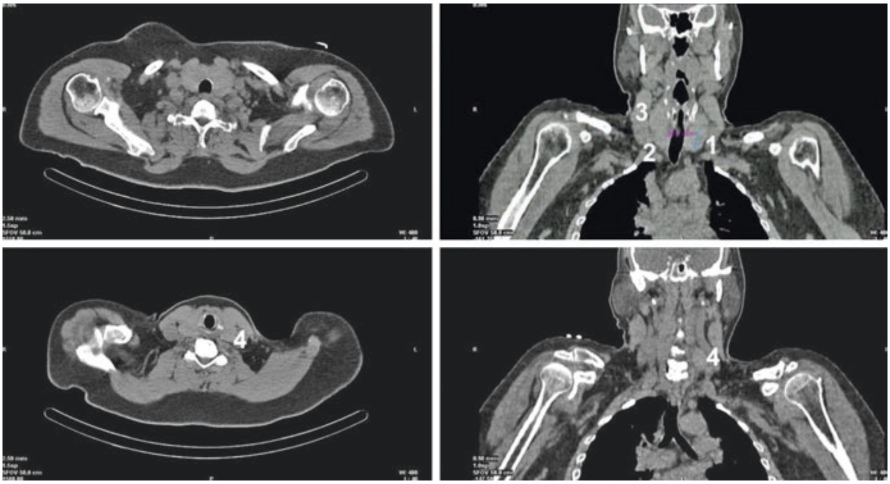

Fig. 7.211 CT scan images in transaxial (left) and coronal axes (right) showing the four markedly enlarged hyperplastic parathyroid glands with the lower two (numbered 1 and 2) smaller than the upper two (numbered 3 and 4) parathyroid glands

- Thallium SPECT correctly identified all the four large hyperplastic parathyroid glands confirming four-gland parathyroid hyperplasia as the underlying cause of primary hyperparathyroidism.
- Thallium-201 SPECT has proven superior to sestamibi SPECT due to its superior biological characteristics and a high true-positive and lower false-negative result with a higher accuracy of detection of parathyroid adenomas, but this case proves thallium is also superior to sestamibi in the diagnosis of sizeable hyperplastic parathyroid glands.
- Another advantage of thallium SPECT/CT scan is the short duration of the procedure (~30 min) compared to the 3–4 h for the dual-phase sestamibi planar and SPECT scans, not to mention the overall imaging time which is considerably less for the thallium scan.

7.72 Case 7.72. Sestamibi-Negative Thallium-Positive 3-Gland Parathyroid Hyperplasia

7.72.1 Background

A 25-year-old female with Sagliker syndrome (sister of patient in Case 7.27) was referred for parathyroid scintigraphy. She had stage IV chronic kidney disease with eGFR of 14 mL/min. Her corrected serum calcium was 2.47 mmol/L (normal 2.2–2.6), PTH 68.9 pmol/L (normal 1.3–9.3), phosphorus 1.57 mmol/L (normal 0.84–1.45), urea 12.6 mmol/L (normal range 2.5–6.4), and creatinine 306 μmol/L (normal range 53–97).

7.72.2 Procedure

The patient was injected with 79 MBq of ^{99m}Tc-pertechnetate, and a thyroid scan was acquired for 10 min at 15 min postinjection. Next, 832 MBq of ^{99m}Tc-sestamibi was injected without moving the patient and a planar scan performed after 10 min. ^{99m}Tc-sestamibi SPECT/CT scan was performed at 2 h followed by a late planar ^{99m}Tc-sestamibi scan at 3 h.

A week later, a thallium-201 parathyroid scintigraphy was performed. The patient was injected with 110 MBq of ^{201}Tl-thallous chloride intravenously with a 10-min duration static image acquired 10 min postinjection followed by a SPECT/CT scan.

7.72.3 Findings

The pertechnetate thyroid scan (Fig. 7.212a) showed a normal-sized image of the gland with a prominent/dominant right lobe and uniform distribution of activity in the gland. The early planar ^{99m}Tc-sestamibi scan (Fig. 7.212b) showed faint uniform uptake in the thyroid gland without any evidence of focal uptake seen, with the delayed washout sestamibi scan images (Fig. 7.212c, d) showing no focal retention of activity in the thyroid bed. The ^{99m}Tc-sestamibi SPECT/CT scan (Fig. 7.213) showed no focal uptake in the thyroid bed to indicate the presence of a hyperactive parathyroid lesion.

The thallium-201 planar scan showed a similar pattern of uptake as seen in the ^{99m}Tc-pertechnetate thyroid scan, and the ^{201}Tl/^{99m}Tc subtraction image was normal (Fig. 7.214). The thallium-201 SPECT/CT scan (Fig. 7.215) showed clear-cut posteriorly located focal increased uptake at the lower pole of the right lobe of the

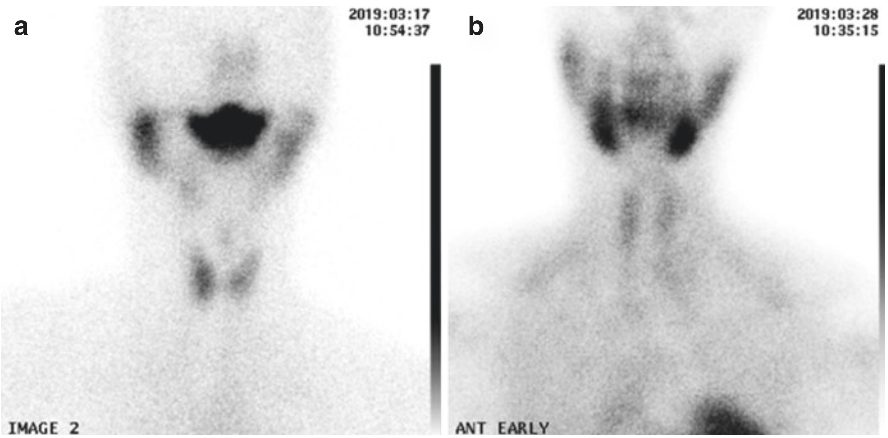

Fig. 7.212 ^{99m}Tc-pertechnetate thyroid scan (**a**), early planar ^{99m}Tc-sestamibi scan (**b**), late planar ^{99m}Tc-sestamibi scan (**c**), and unzoomed late sestamibi neck and chest scan image (**d**)

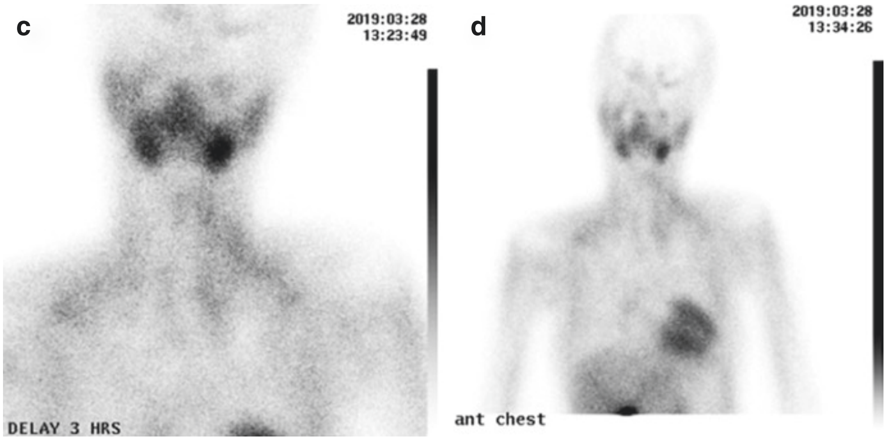

Fig. 7.212 (continued)

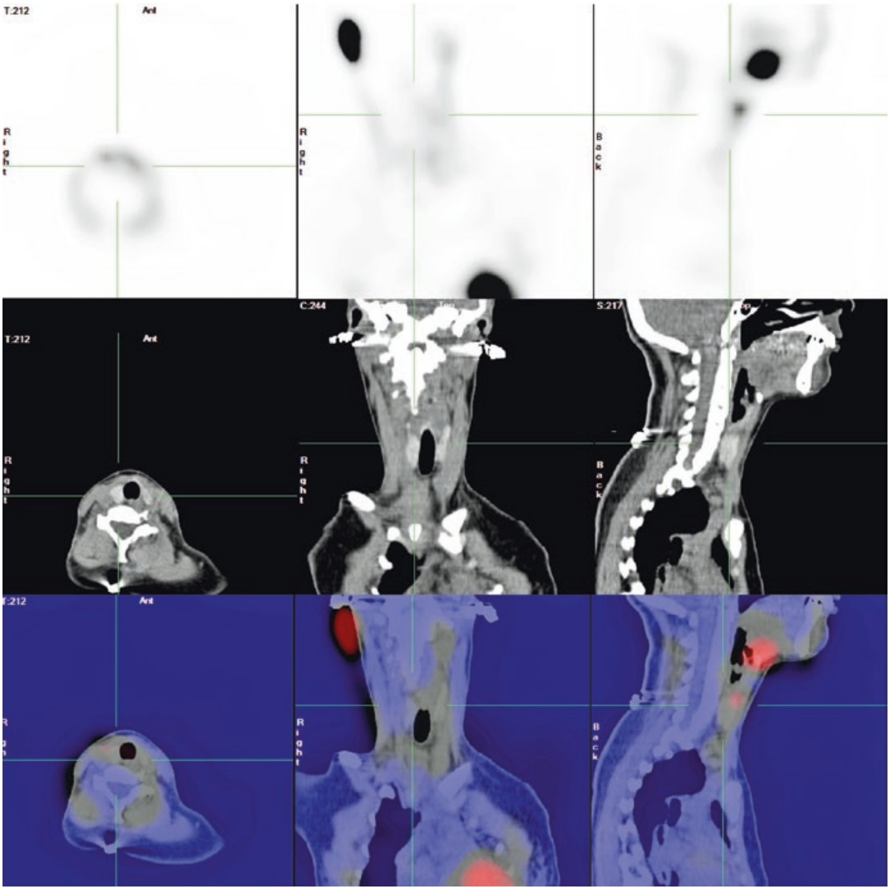

Fig. 7.213 ^{99m}Tc-sestamibi SPECT scan images (top row), CT scan images (middle row), and fused SPECT/CT images (bottom row) in the transaxial (left column), coronal (middle column), and sagittal (right column) planes, showing normal uptake in the thyroid bed with no evidence of a sestamibi-avid lesion seen

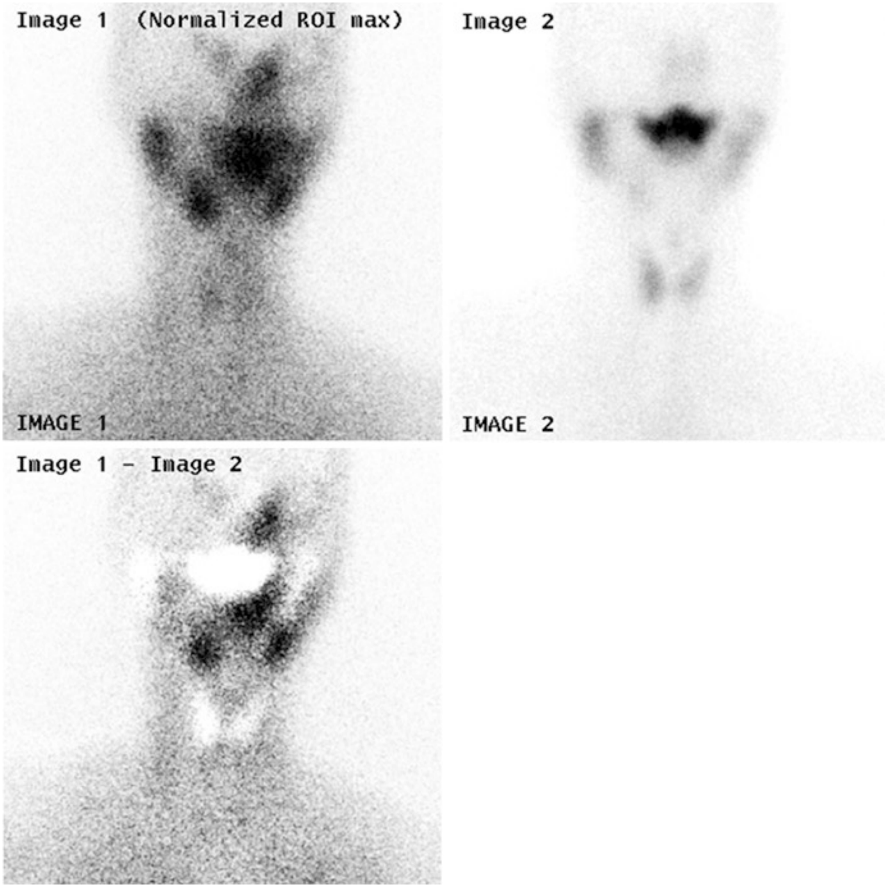

Fig. 7.214 ^{201}Tl planar scan (left) and ^{99m}Tc-pertechnetate planar scan (middle) showing symmetrical uptake of the tracer in the thyroid gland. The ^{201}Tl/^{99m}Tc subtraction image (right) is normal

thyroid and at the upper and lower poles of the left lobe of the thyroid corresponding to enlarged parathyroid glands on the CT component.

7.72.4 Conclusion

Findings consistent with sestamibi-negative thallium-positive 3-gland parathyroid hyperplasia associated with secondary hyperparathyroidism.

7.72.5 Comments and Teaching Points

- This is the first reported case of sestamibi-negative thallium-positive 3-gland parathyroid hyperplasia.

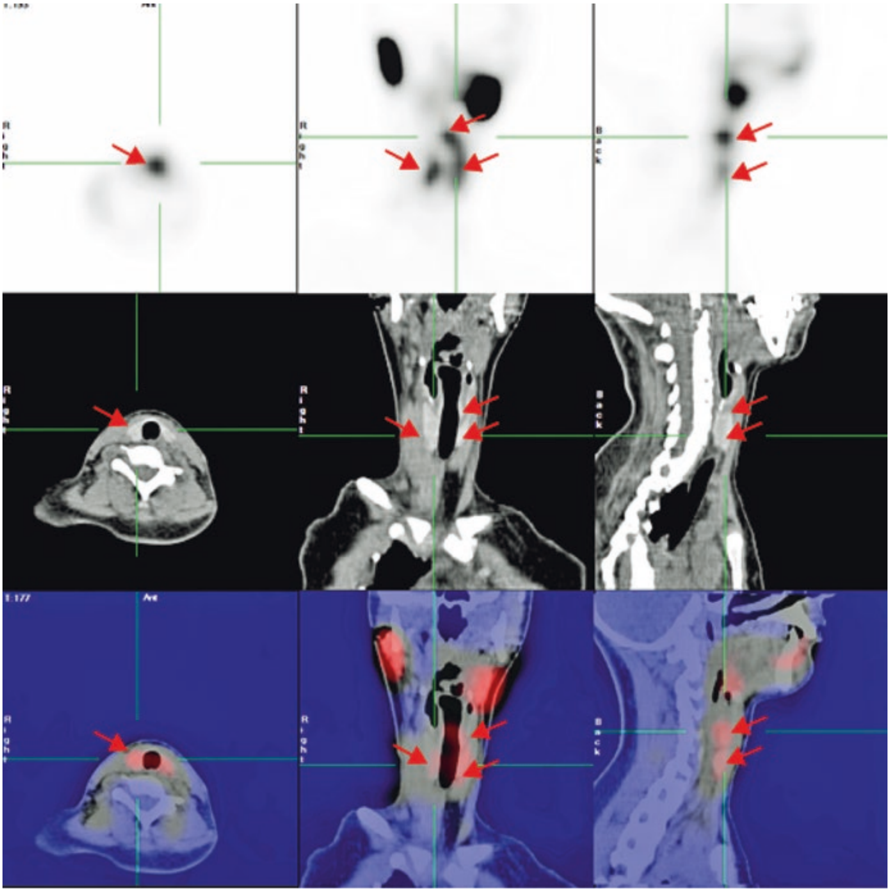

Fig. 7.215 Thallium-201 SPECT (top row), CT scan (middle row), and the fused SPECT/CT scan (bottom row) in the transverse (left columns), coronal (middle column) and sagittal (right column) axes showing three hyperplastic parathyroid glands (red arrows)

- The lack of sestamibi avidity by the hyperplastic parathyroid glands is presumably due to the non-oncogenic cellular predominance of parathyroid hyperplasia in this case.
- Several cases in this atlas section have demonstrated the value of thallium-201 SPECT/CT scanning in patients with sestamibi-negative parathyroid adenomas, but this case as well as the case before shows a role for thallium SPECT/CT scanning in sestamibi-negative hyperplastic parathyroid glands.

References

1. Prasad KK, Agarwal G, Krishnani N. Water-clear cell adenoma of the parathyroid gland: a rare entity. Indian J Pathol Microbiol. 2004;47(1):39–40.
2. Weymouth MD, Serpell JW, Chambers D. Palpable parathyroid adenomas presenting as clinical solitary thyroid nodules and cytologically as follicular thyroid neoplasms. ANZ J Surg. 2003;73:36–9.

3. Arnstein AR, Rosenberg IK, Belamaric J, et al. Palpable calcified parathyroid gland in primary chief-cell hyperplasia. N Engl J Med. 1971;285:1365–6.
4. Woolfson AM, Fleming JA, Stewart JS. A palpable parathyroid tumour in a patient with osteogenesis imperfecta. Proc R Soc Med. 1975;68:61–2.
5. Bégueret H, Belleannée G, Dubrez J, Trouette H, Parrens M, Velly JF, de Mascarel A. Clear cell adenoma of the parathyroid gland: a rare and misleading lesion. Ann Pathol. 1999;19(4):316–9.
6. Kanda K, Okada Y, Tanikawa T, Morita E, Tsurudome Y, Konishi T, et al. A rare case of primary hyperparathyroidism with clear cell adenoma. Endocr J. 2004;51(2):207–12.
7. Henry J-F, Lacobone M. Ectopic parathyroid glands. In: Licata AA, Lerma EV, editors. Diseases of the parathyroid glands. New York, NY: Springer Science+Business Media; 2012.
8. Akerstrom G, Malmaeus J, Bergstrom R. Surgical anatomy of human parathyroid glands. Surgery. 1984;95:14–21.
9. Roses DF, Karp NS, Sudarsky LA, et al. Primary hyperparathyroidism associated with two enlarged parathyroid glands. Arch Surg. 1989;124:1261–5.
10. Attie JN, Bock G, Auguste LJ. Multiple parathyroid adenomas: report of thirty-three cases. Surgery. 1990;108:1014–20.
11. Tezelman S, Shen W, Shaver JK, Siperstein AE, Duh Q-Y, Klein H, Clark OH. Double Parathyroid adenomas clinical and biochemical characteristics before and after parathyroidectomy. Ann Surg. 1993;218(3):300–9.
12. Taillefer R, Boucher Y, Potvin C, et al. Detection and localization of parathyroid adenomas in patients with hyperparathyroidism using a single radionuclide imaging procedure with technetium-99m-sestamibi (double-phase study). J Nucl Med. 1992;33:1801.
13. Osmanagouglu K, Schelstraete K, Lippens M, et al. Visualization of a parathyroid adenoma with Tc-99m MIBI in a case with iodine saturation and impaired thallium uptake. Clin Nucl Med. 1993;18:214.
14. Wheeler MH. Clinical anatomy, developmental aberrations and endocrinology. In: Arora A, Tolley N, Tuttle M, editors. A practical manual of thyroid and parathyroid disease. London: Wiley-Blackwell; 2010. p. 184–5.
15. Gupta Y, Ahmed R, Happerfield L, Pinder SE, Balan KK, Wishart GC. P-glycoprotein expression is associated with sestamibi washout in primary hyperparathyroidism. Br J Surg. 2007;94(12):1491–5.
16. Sun SS, Shiau YC, Lin CC, et al. Correlation between P-glycoprotein (P-gp) expression in parathyroid and Tc-99m MIBI parathyroid image findings. Nucl Med Biol. 2001;28:929–33.
17. Seki K, Hashimoto K, Hisada T, Maeda M, Satoh T, Uehara Y, et al. A patient with classic severe primary hyperparathyroidism in whom both Tc-99m MIBI scintigraphy and FDG-PET failed to detect the parathyroid tumor. Intern Med. 2004;43:816–23.
18. Mehta NY, Ruda JM, Kapadia S, Boyer PJ, Hollenbeak CS, StackJr BC. Relationship of technetium Tc99m sestamibi scans to histopathological features of hyperfunctioning parathyroid tissue. Arch Otolaryngol Head Neck Surg. 2005;131:493–8.
19. Philippon M, Guerin C, Taieb D, Vaillant J, Morange I, Brue T, Conte-Devolx B, Henry JF, Slotema E, Sebag F, Castinetti F. Bilateral neck exploration in patients with primary hyperparathyroidism and discordant imaging results: a single-centre study. Eur J Endocrinol. 2014;170:719–25.
20. Mahoney EJ, Monchik JM, Donatini G, De Lellis R. Life-threatening hypercalcemia from a hepatocellular carcinoma secreting intact parathyroid hormone: localization by sestamibi single-photon emission computed tomographic imaging. Endocr Pract. 2006;12(3):302–6.
21. Ohi S, Niimi S, Okada N, Yamada K, Tachibana T, Hashimoto H, Nakajima M, Yasuda M, Tanaka T, Sato K, Ishikawa H. Establishment and characterization of a human ovarian small cell carcinoma, hypercalcemic type, cell line (OS-1) secreting PTH, PthrP and ACTH--special reference to the susceptibility of anti-cancer drugs. Hum Cell. 2004;17(4):203–9.
22. Kar P, Meeking D. A probable PTH- secreting metastatic breast carcinoma. 197th Meeting of the Society for Endocrinology, London, UK. Endoc Abs. 2006;12:64.
23. Thompson NW, Eckhauser FE, Harness JK. The anatomy of primary hyperparathyroidism. Surgery. 1982;92:814–21.

24. Levin KE, Clark OH. The reasons for failure in parathyroid operations. Arch Surg. 1989;124:911–4.
25. Summers GW. Parathyroid update: a review of 220 cases. Ear Nose Throat J. 1996;75:434–9.
26. Mariani G, Mazzeo S, Rubello D, Bartolozzi C. Preoperative localization of abnormal parathyroid glands. In: Bilezikian JP, Marcus R, Levine MA, Marcocci C, Silverberg SJ, Potts JT, editors. The parathyroids: basic and clinical concepts. 3rd ed. London: Academic Press; 2014.
27. Wheeler MH, Williams ED, Wade JSH. The hyperfunctioning intrathyroidal parathyroid gland: a potential pitfall in parathyroid surgery. World J Surg. 1987;11:110–4.
28. Sheffield EA. An approach to common pathological conditions in the parathyroid glands. CPD Cell Pathol. 2002;4:135–8.
29. Rink T, Schroth HJ, Holle LH, Garth H. Limited sensitivity of parathyroid imaging with (99m) Tc-sestamibi (123)I subtraction in an endemic goiter area. J Nucl Med. 2002;43(9):1175–80.
30. Goljan EF. Rapid review of pathology. 4th ed. Philadelphia, PA: Saunders; 2014.
31. Mallet E, Castanet M. Primary hyperparathyroidism in neonates and children [1]. In: Licata AA, Lerma EV, editors. Diseases of the parathyroid glands. New York, NY: Springer Science+Business Media; 2012.
32. Sagliker Y, Acharya V, Ling Z, et al. International study on Sagliker syndrome and uglifying human face appearance in severe and late secondary hyperparathyroidism in chronic kidney disease patients. J Ren Nutr. 2008;18(1):114–7.
33. Wittenberg A. The Rugger Jersey spine sign. Radiology. 2004;230(2):491–2.
34. Ming-Che C, Shih-Chuan C, Wan-YuLin T. Dual-phase ^{99m}Tc-MIBI parathyroid imaging reveals synchronous parathyroid adenoma and papillary thyroid carcinoma: a case report. Kaohsiung J Med Sci. 2008;24(10):542–7.
35. Kalinin AP, Pavlov AV, Alexandrov YK, Kotova IV, Patrunov YN, Pamputis SN. The parathyroid glands imaging and surgery. Berlin: Springer; 2013.
36. Mezosi E, Bajnok L, Gyory F, Varga J, Sztojka I, Szabo J, Galuska L, Leovey A, Kakuk G, Nagy. The role of technetium-99m methoxyisobutylisonitrile scintigraphy in the differential diagnosis of cold thyroid nodules. Eur J Nucl Med. 1999;26(8):798–803.
37. Rubello D, Toniato A, Pelizzo MR, Casara D. Papillary thyroid carcinoma associated with parathyroid adenoma detected by pertechnetate-MIBI subtraction scintigraphy. Clin Nucl Med. 2000;25(11):898–900.
38. Sekine O, Hozumi Y, Takemoto N, Kiyozaki H, Yamada S, Konishi F. Parathyroid adenoma without hyperparathyroidism. Jpn J Clin Oncol. 2004;34(3):155–8.
39. Akerstrom G, Rudberg C, Grimelius L, Bergstrom R, Johansson H, Ljunghall S, et al. Histologic parathyroid abnormalities in an autopsy series. Hum Pathol. 1986;17:520–7.
40. Silverberg SJ, Clarke BL, Peacock M, Bandeira F, Boutroy S, Cusano NE, Dempster D, Lewiecki EM, Liu JM, Minisola S, Rejnmark L, Silva BC, Walker MD, Bilezikian JP. Current issues in the presentation of asymptomatic primary hyperparathyroidism: proceedings of the Fourth International Workshop. J Clin Endocrinol Metab. 2014;99:3580–94.
41. Anne-Sophie P, Salima B, Bruno K, Simona B, Marie-Cécile N, Luc M, Julian D, Thierry VB. Unusual parathyroid adenoma avid for both Tc-99m sestamibi and I-123 iodine. Clin Nucl Med. 2010;35(11):888–90.
42. Kiratli PO, Peksoy I, Erbaş B, Gedikoğlu G, Karabulut N. Technetium-99m pertechnetate uptake in ectopic parathyroid adenoma. Ann Nucl Med. 1999;13(2):113–5.
43. Palestro CJ, Tomas MB, Tronco GG. Radionuclide imaging of the parathyroid glands. Semin Nucl Med. 2005;35(4):266–76.
44. Bronner M, Li VV. Oxyphilic (Askanazy/Hürthle cell) tumors of the thyroid: microscopic features predict biological behaviour. Surg Pathol. 1988;1:137–50.
45. Carcangiu ML, Bianchi S, Savino D, Voynick IM, Rosai J. Follicular Hürthle cell tumors of the thyroid gland. Cancer. 1991;68:1944–53.
46. McIvor NP, Freeman JL, Rosen, Bedard YC. Value of fine-needle aspiration in the diagnosis of Hurthle cell neoplasms. Head Neck. 1993;15:335–41.
47. Boi F, Lai ML, Deias C, Piga M, Serra A, Uccheddu A, Faa G, Mariotti S. The usefulness of ^{99m}Tc-SestaMIBI scan in the diagnostic evaluation of thyroid nodules with oncocytic cytology. Eur J Endocrinol. 2003;149:493–8.

48. Wermers RA, Khosla S, Atkinson EJ, et al. The rise and fall of primary hyperparathyroidism: a population-based study in Rochester, Minnesota, 1965–1992. Ann Intern Med. 1997;126:433.
49. Khan A, Bilezikian J. Primary hyperparathyroidism: pathophysiology and impact on bone. Can Med Assoc J. 2000;163:184.
50. Cannon J, Lew JI, Solorzano CC. Parathyroidectomy for hyperparathyroid crisis: 40 years experience and long term outcomes. Surgery. 2010;148:807–13.
51. Koss WGM, Brown MR, Balfour JF. A False-positive localization of a parathyroid adenoma with technetium Tc 99m sestamibi scan secondary to a thyroid follicular carcinoma. Arch Surg. 1996;131(2):216–7.
52. Strewler GJ, Budayr AA, Clark OH, Nissenson RA. Production of parathyroid hormone by a malignant nonparathyroid tumor in a hypercalcemic patient. J Clin Endocrinol Metab. 1993;76:1373–5.
53. Lehwald N, Cupisti K, Krausch M, Ahrazoglu M, Raffel A, Knoefel WT. Coincidence of primary hyperparathyroidism and nonmedullary thyroid carcinoma. Horm Metab Res. 2013;45(9):660–3.
54. Vysetti S, Sridhar P, Theckedath B, Gilden JL, Morawiecki P. Synchronous papillary thyroid carcinoma and primary hyperparathyroidism: diagnosis and management issues. Hosp Pract. 2012;40(4):16–9.
55. Palmer M, Adami HO, Krusemo UB, Ljunghall S. Increased risk of malignant diseases after surgery for primary hyperparathyroidism - a nationwide cohort study. Am J Epidemiol. 1988;127:1031–40.
56. Ogard CG, Engholm G, Almdal TP, Vestergaard H. Increased mortality in patients hospitalised with primary hyperparathyroidism during the period 1977–1993 in Denmark. World J Surg. 2004;28:108–11.
57. Arnold A, Brown MF, Urena P, Gaz RD, Sarfati E, Drueke TB. Monoclonality of parathyroid tumors in chronic renal failure and in primary parathyroid hyperplasia. J Clin Invest. 1995;95:2047–53.
58. Nygren P, Larsson R, Johansson H, Ljunghall S, Rastad J, Akerstrom G. 1,25(OH)2D3 inhibits hormone secretion and proliferation but not functional dedifferentiation of cultured bovine parathyroid cells. Calcif Tissue Int. 1988;43:213–8.
59. Kalinin AP, Pavlov AV, Alexandrov YK, Kotova IV, et al. The parathyroid glands. Imaging and surgery. Berlin: Springer; 2013.
60. Parfitt AM. The hyperparathyroidism of chronic renal failure: a disorder of growth. Kidney Int. 1997;52:3–9.
61. Slatopolsky E, Delmez JA. Pathogenesis of secondary hyperparathyroidism. Am J Kidney Dis. 1994;23:229–36.
62. Huppert BJ, Reading CC. Parathyroid sonography: imaging and intervention. J Clin Ultrasound. 2007;35:144–55.
63. Gartner LP, Hiatt JL. Color textbook of histology. 3rd ed. Philadelphia, PA: W.B. Saunders; 2006. p. 314–6.
64. Berkovitz BK. Neck and upper aero-digestive tract. In: Standring S, Ellis H, Healy JC, Johnson D, Williams A, Collins P, et al., editors. Gray's anatomy: the anatomical basis of clinical practice. 39th ed. London: Elsevier Churchill Livingstone; 2005. p. 564–5.
65. Mahbub S, Ara S, Alim A, Nurunnabi ASM, Ahmed R, Begum M. Different shapes of the human parathyroid glands – a postmortem study. J Dhaka Med Coll. 2009;18(1):44–6.
66. Akerström G, Malmaeus J, Bergström R. Surgical anatomy of human parathyroid glands. Surgery. 1984;95:14–21.
67. Brown EM. Control of parathyroid hormone secretion by its key physiological regulators. In: Bilezikian JP, Marcus R, Levine MA, Marcocci C, Silverberg SJ, Potts JT, editors. The parathyroids: basic and clinical concepts. 3rd ed. London: Elsevier; 2014.
68. Licata AA, Lerma EV, editors. Diseases of the parathyroid glands. New York, NY: Springer Science+Business Media; 2012.
69. Kandil E, Tufaro AP, Carson KA, Lin F, Somervell H, Farrag T, et al. Correlation of plasma 25-hydroxyvitamin D levels with severity of primary hyperparathyroidism and likelihood

of parathyroid adenoma localization on sestamibi scan. Arch Otolaryngol Head Neck Surg. 2008;134(10):1071–5.
70. Silverberg SJ, Bilezikian JP. Asymptomatic primary hyperparathyroidism. In: Bilezikian JP, Marcus R, Levine MA, Marcocci C, Silverberg SJ, Potts JT, editors. The parathyroids: basic and clinical concepts. 3rd ed. London: Elsevier; 2014.
71. Björkman M, Sorva A, Tilvis R. Responses of parathyroid hormone to vitamin D supplementation: a systematic review of clinical trials. Arch Gerontol Geriatr. 2009;48:160–6.
72. Erbil Y, Kapran Y, Issever H, Barbaros U, Adalet I, Dizdaroglu F, et al. The positive effect of adenoma weight and oxyphil cell content on preoperative localization with 99mTc-sestamibi scanning for primary hyperparathyroidism. Am J Surg. 2008;195(1):34–9.
73. Hundahl SA, Fleming ID, Fremgen AM, Menck HR. Two hundred eighty-six cases of parathyroid carcinoma treated in the U.S. between 1985–1995: a National Cancer Data Base Report. Cancer. 1999;86:538–44.
74. Parisien M, Silverberg SJ, Shane E, Dempster DW, Bilezikian JP. Bone disease in primary hyperparathyroidism. Endocrinol Metab Clin North Am. 1990;19:19–34.
75. Kao CL, Chang JP, Lin JW, Lin CC. Brown tumor of the sternum. Ann Thorac Surg. 2002;73:1651–3.
76. Ozkan E, Arslan N, Arslanoglu A, Karacalioglu AO. Decreased Tc-99m sestamibi uptake in a sternal brown tumor indicating response to anti metabolic therapy for secondary hyperparathyroidism. Clin Nucl Med. 2007;32(8):661–2.
77. Niyaz K, Ahmed A, Mehboob J, Hussain W, UzZaman M, Hameed A. False-positive mediastinal parathyroid adenoma on ^{99m}Tc-MIBI scanning in a patient with parathyroid carcinoma. Pak J Nucl Med. 2011;1:24–5.
78. Maruani G, Hertig A, Paillard M, Houillier P. Normocalcemic primary hyperparathyroidism: evidence for a generalized target-tissue resistance to parathyroid hormone. J Clin Endocrinol Metab. 2003;88:4641–8.
79. Silverberg SJ, Bilezikian JP. “Incipient” primary hyperparathyroidism: a “forme fruste” of an old disease. J Clin Endocrinol Metab. 2003;88:5348–52.
80. Rao DS, Wilson RJ, Kleerekoper M, Parfitt AM. Lack of biochemical progression or continuation of accelerated bone loss in mild asymptomatic primary hyperparathyroidism: evidence for biphasic disease course. J Clin Endocrinol Metab. 1988;67:1294–8.
81. Thomas P, Lebrun C. Progressive spastic paraparesis revealing primary hyperparathyroidism. Neurology. 1994;44(1):18–9.
82. Mallet E, Castanet M. Primary hyperparathyroidism in neonates and children. In: Licata AA, Lerma EV, editors. Diseases of the parathyroid glands. New York, NY: Springer Science+Business Media; 2012.
83. Pirson A-S, Bouazza S, Krug B, Bostan S, Nollevaux M-C, Michel L, Donckier J, Vander Borght T. Unusual parathyroid adenoma avid for both Tc-99m sestamibi and I-123 iodine. Clin Nucl Med. 2010;35(11):888–90.
84. Leslie WD, Riese KT, Guzman R, Dupont JO, Peterdy AE. Technetium-99m-pertechnetate uptake by intrathyroidal parathyroid adenoma. J Nucl Med. 1996;37:861–2.
85. Bergson EJ, Heller KS. The clinical significance and anatomic distribution of parathyroid double adenomas. J Am Coll Surg. 2004;198(2):185–9.
86. Uden P, Chan A, Duh QY, et al. Primary hyperparathyroidism in younger and older patients: symptoms and outcome of surgery. World J Surg. 1992;16:791–8.
87. Henry JF, Sebag F. Applied embryology of the parathyroid glands. Vestn Khir Im I I Grek. 2006;165(5):41–4.
88. Evangelista L, Cervino AR, Gregianin M, Saladini G. FDG-PET/CT visualizes a case of primary hyperparathyroidism in a patient with gastrointestinal stromal tumor. Thyroid Sci. 2010;5(4):1–4.
89. Neumann DR, Esselstyn CB, Maclntyre WJ, Go RT, Obuchowski NA, Chen EQ, Licata AA. Comparison of FDG-PET and sestamibi-SPECT in primary hyperparathyroidism. J Nucl Med. 1996;37:1809–15.

90. Kluijfhout WP, Pasternak JD, Drake FT, Beninato T, Gosnell JE, Shen WT, Duh Q-Y, Allen IE, et al. Use of PET tracers for parathyroid localization: a systematic review and meta-analysis. Langenbecks Arch Surg. 2016;401:925–35.
91. Pontikides N, Karras S, et al. Diagnostic and therapeutic review of cystic parathyroid lesions. Hormones (Athens). 2012;11(4):410–8.
92. Krishnasamy S, Moulik P, Macleod A. Ectopic parathyroid cyst presenting with parathyroid crisis. Endoc Abs. 2012;28:82.
93. Shields TW, Immerman SC. Mediastinal parathyroid cysts revisited. Ann Thorac Surg. 1999;67(2):581–90.
94. da Silva DA, Machado MC, Brito LL, Renato A, et al. Parathyroid cysts: diagnosis and treatment. Rev Bras Otorrinolaringol. 2004;70(6):840–4.
95. Agarwal A, George RK, Gupta SK, Mishra SK. Pancreatitis in patients with primary hyperparathyroidism. Indian J Gastroenterol. 2003;22:224–5.
96. Koppelberg T, Bartsch D, Printz H, Hasse C, Rothmund M. Pancreatitis in primary hyperparathyroidism (pHPT) is a complication of advanced pHPT. Dtsch Med Wochenschr. 1994;119:719–24.
97. Husova L, Senkyrik M, Lata J, Hrbkova V, Husa P, Dolina J, Podral M, Ourednicek P. Acute pancreatitis as the road to diagnosis of primary hyperparathyroidism. Vnitr Lek. 2000;46:724–7.
98. Abdullah M. Pancreatitis in primary hyperparathyroidism. Med J Malaysia. 2003;58:600–3.
99. Frick TW, Mithöfer K, Fernández-del CC. Hypercalcemia causes acute pancreatitis by pancreatic secretory block, intracellular zymogen accumulation, and acinar cell injury. Am J Surg. 1995;169(1):167–72.
100. Foroulis CN, Rousogiannis S, Lioupis C, et al. Ectopic paraesophageal mediastinal parathyroid adenoma, a rare cause of acute pancreatitis. World J Surg Oncol. 2004;2:41.
101. Rasulova N, Siraj QH, Javaid A, Al-Banna A. Functional ectopic cystic parathyroid adenomas: case reports and literature review. Pak J Nucl Med. 2016;6:63–8.
102. Gayatri P, Sanjay D, Ajay N, Amrut A. Mixed multilocular ectopic thymic cyst with parathyroid element presenting as neck mass. Ann Acad Med Singapore. 2012;41(6):271–2.
103. Rivkees SA, el-Hajj-Fuleihan G, Brown EM, Crawford JD. Tertiary hyperparathyroidism during high phosphate therapy of familial hypophosphatemic rickets. J Clin Endocrinol Metab. 1992;75:1514–8.
104. Rahbari R, Holloway AK, He M, Khanafshar E, Clark OH, Kebebew E. Identification of differentially expressed microRNA in parathyroid tumors. Ann Surg Oncol. 2011;18:1158–65.
105. Parfitt AM. Osteomalacia and related disorders. In: Avioli LV, Krane SM, editors. Metabolic bone disease and clinically related disorders. 3rd ed. Philadelphia, PA: Saunders; 1998. p. 328–86.
106. Williams ED. Pathology of the parathyroid glands. Clin Endocrinol Metab. 1974;3:285–303.
107. Sathekge MM, Mageza RB, Muthuphei MN, Modiba MC, Clauss RC. Evaluation of thyroid nodules with technetium-99m MIBI and technetium-99m pertechnetate. Head Neck. 2001;23(4):305–10.
108. Giovanella L, Suriano S, Maffioli M, Ceriani L, Spriano G. 99mTc-sestamibi scanning in thyroid nodules with non-diagnostic cytology. Head Neck. 2009;32(5):607–11.
109. Mendoza V, Ramírez C, Espinoza AE, et al. Characteristics of ectopic parathyroid glands in 145 cases of primary hyperparathyroidism. Endocr Pract. 2010;6:977–81.
110. Moran CA, Suster S. Primary parathyroid tumors of the mediastinum. Am J Clin Pathol. 2005;124:749–54.
111. Jones DB, Jones JH, Lloyd HJ, Lucas PA, Wilkins WE, Walker DA. Changes in blood pressure and renal function after parathyroidectomy in primary hyperparathyroidism. Postgrad Med J. 1983;59:350–3.
112. Kristoffersson A, Backman C, Granqvist K, Järhult J. Pre- and postoperative evaluation of renal function with five different tests in patients with primary hyperparathyroidism. J Intern Med. 1990;227:317–24.

113. Goltzman D. PTH action on the skeleton. In: Bilezikian JP, Marcus R, Levine MA, Marcocci C, Silverberg SJ, Potts JT, editors. The parathyroids: basic and clinical concepts. 3rd ed. London: Academic Press; 2014.
114. Khan A, Hanley D, Rizzoli R, Bollerslev J, Young J, Rejnmark L, Thakker R, D'Amour P, Paul T, Van Uum S. Primary hyperparathyroidism: review and recommendations on evaluation, diagnosis, and management. A Canadian and International Consensus. Osteoporos Int. 2017;28:1–19.
115. Ioannis P, Stavros P, Nektarios K, Chrysa S, Kalliopi P, et al. Water-clear cell adenoma of parathyroid gland: a case report and concerns on differential diagnosis. J Endocrinol Diabetes Obes. 2018;6(1):1117.
116. Lynn J, Lewis P. Pathological spectrum of parathyroid disease. In: Arora A, Tolley NS, Tuttle RM, editors. A practical manual of thyroid and parathyroid disease. Chichester: Wiley-Blackwell; 2010. p. 164–73.
117. Cetani F, Marcocci C. Parathyroid carcinoma. In: Bilezikian JP, Marcus R, Levine MA, Marcocci C, Silverberg SJ, Potts JT, editors. The parathyroids: basic and clinical concepts. 3rd ed. London: Elsevier; 2014.
118. Mehta NY, Ruda JM, Kapadia S, Boyer PJ, Hollenbeak CS, Stack BC Jr. Relationship of technetium Tc-99m sestamibi scans to histopathological features of hyperfunctioning parathyroid tissue. Arch Otolaryngol Head Neck Surg. 2005;131(6):493–8.

PET/CT Cases

8

Luka Lezaic and Marko Grmek

8.1 Case 8.1. ^{18}F-Choline PET/CT Scan: Normal Physiological Distribution

8.1.1 Background

A 76-year-old man with prostate cancer underwent an ^{18}F-choline PET/CT scan for detecting the presence of possible metastatic disease. The patient had normal serum parathormone (PTH) level with normal serum calcium and biochemistry.

8.1.2 Procedure

The patient received an intravenous injection of 201 MBq (2.4 MBq/kg of body weight) of ^{18}F-choline. Whole-body PET/CT scanning (2 min per bed position) was performed 1 h after tracer administration.

8.1.3 Findings

^{18}F-choline accumulation in the lower part of the head, neck and thorax is shown in Fig. 8.1. Usually high uptake of tracer is present in salivary glands (green arrows). Normally there are no structures with distinctively increased tracer accumulation in the neck and thorax. The focus of mildly increased uptake seen on the image (marked with orange arrow) most probably indicates a small lymph node located in left hilum of the lung. Mildly elevated activity (pink arrow) is seen in the thyroid gland (Fig. 8.2). Mildly elevated ^{18}F-choline uptake is often seen in the thyroid and represents physiological uptake.

L. Lezaic (✉) · M. Grmek
Department of Nuclear Medicine, University Medical Centre Ljubljana, Ljubljana, Slovenia
e-mail: luka.lezaic@kclj.si; marko.grmek@kclj.si

© Springer Nature Switzerland AG 2019
Q. Siraj (ed.), *Radionuclide Parathyroid Imaging*,
https://doi.org/10.1007/978-3-030-17351-7_8

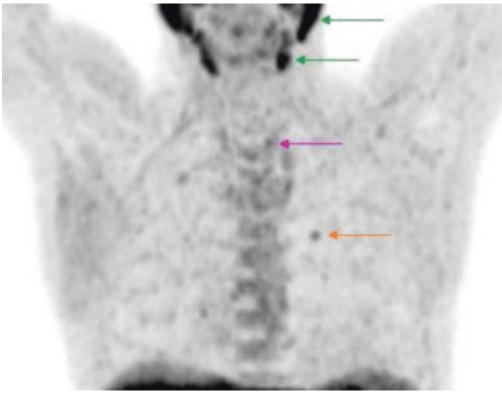

Fig. 8.1 MIP images of the ^{18}F-choline PET/CT performed 1 h after tracer administration. Increased tracer accumulation (marked with green arrows) is seen in salivary glands—normal finding. Focal structure with mildly elevated activity (marked with orange arrow) indicates most probably small inflammatory-reactive lymph node located in the hilum of the left lung. Mildly increased activity in the neck (marked with pink arrow) most probably represents the thyroid

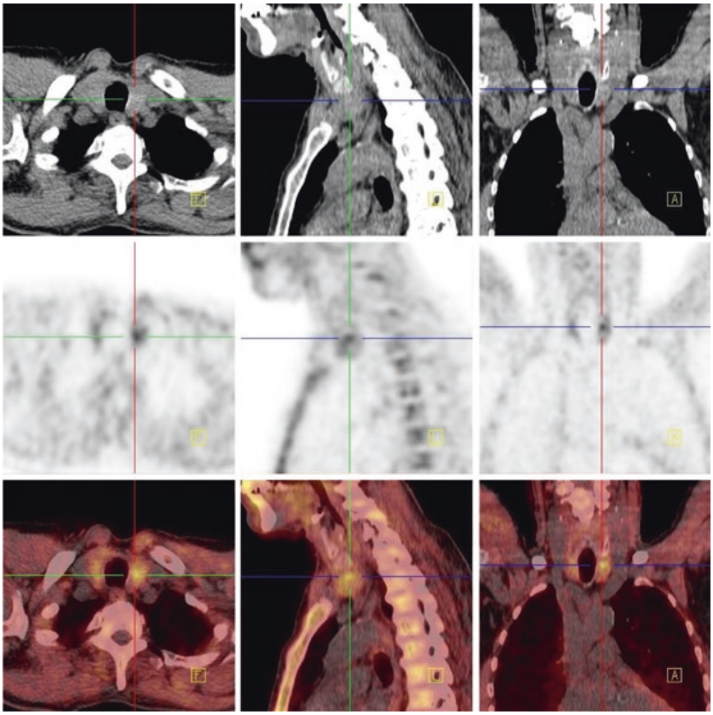

Fig. 8.2 ^{18}F-choline PET/CT scan performed 1 h after tracer administration. Top row showing transversal (left), sagittal (middle) and coronal (right) CT scan imaging of the neck and upper thorax. The middle row shoving corresponding PET scan images and the bottom row corresponding fused PET/CT images. Mildly increased focal activity (SUV_{max} 4.04) is present in the left thyroid lobe

8.1.4 Conclusion

Normal physiological distribution is seen on the ^{18}F-choline PET/CT scan.

8.1.5 Comments and Teaching Points

- Minimally to mildly elevated ^{18}F-choline is often present in the thyroid gland.
- Inflammatory-reactive lymph nodes with mildly elevated ^{18}F-choline are occasionally seen in the mediastinum and lung hila.

8.2 Case 8.2. ^{18}F-Choline PET/CT Scan: Left Lower Parathyroid Adenoma

8.2.1 Background

A 47-year-old male presented with urolithiasis. His ionized serum calcium was 1.48 mmol/L (normal range: 1.12–1.35 mmol/L), and the serum PTH level was high at 186 ng/L (normal range: 12–65 ng/L). Neck US showed a hypoechoic lesion located behind the lower part of the left thyroid lobe measuring 17 × 11 mm in the transverse plane. ^{18}F-choline PET/CT was performed to investigate the cause of primary hyperparathyroidism (Figs. 8.3 and 8.4).

8.2.2 Procedure

The patient received 100 MBq of ^{18}F-choline intravenously with PET/CT scanning (4 min per bed position) performed at three time intervals including 5 min after tracer administration (Fig. 8.3a), 1 h after tracer administration (Fig. 8.3b) and 2 h after tracer administration (Fig. 8.3c). Acquisition of neck and total thorax was performed on the first scan, but after 1 and 2 h, only the neck and the upper mediastinum were scanned.

8.2.3 Findings

A lesion with increased ^{18}F-choline accumulation was detected behind the left lower thyroid lobe. Dimensions of the lesion measured on low-dose CT were 16 × 9 × 22 mm. Contrast between lesion (enlarged hyperactive parathyroid gland) and thyroid gland was high in all three phases. SUV_{max} values of the lesion after ^{18}F-choline administration at 5 min, 1 h and 2 h were 11.00, 12.09 and 10.56,

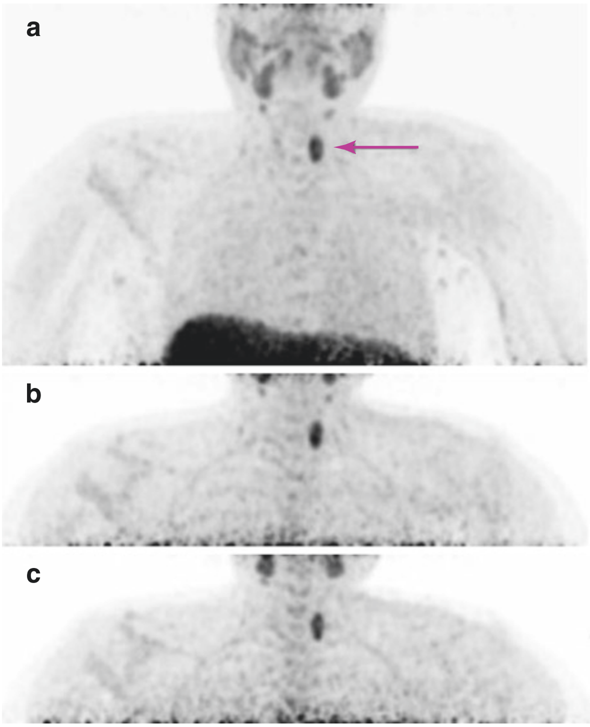

Fig. 8.3 MIP images of the ^{18}F-choline scans performed 5 min (**a**), 1 h (**b**) and 2 h (**c**) after tracer administration. Intense focal uptake and retention of ^{18}F-choline in the lesion—enlarged hyperactive parathyroid gland (parathyroid adenoma) is seen (marked with pink arrow). Uptake and retention of the tracer in the thyroid are low

respectively. At the same time points, the SUV_{max} values of the thyroid gland were 3.34, 2.84 and 3.40. The activity in the other structures in the neck and upper mediastinum was even lower.

8.2.4 Conclusion

Findings of high ^{18}F-choline uptake and retention in the lesion are consistent with a left lower parathyroid adenoma. Excision biopsy of the lesion confirmed parathyroid adenoma. After surgical removal of adenoma, PTH level fell to normal value.

8.2.5 Comments and Teaching Points

- The contrast between lesion representing enlarged hyperactive parathyroid gland and surrounding structures is in most cases the highest 1 h after ^{18}F-choline administration.
- ^{18}F-choline uptake and retention in parathyroid tissue (parathyroid adenoma or enlarged parathyroid gland) are not organ specific.

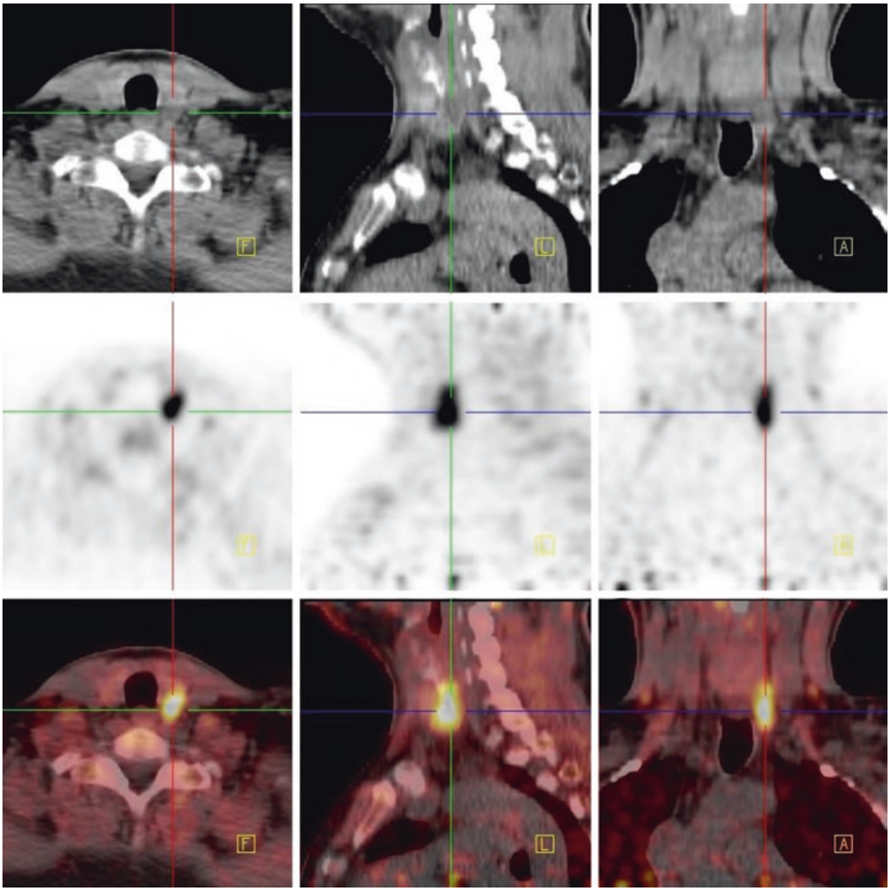

Fig. 8.4 ^{18}F-choline PET/CT scan performed 1 h after tracer administration. Top row showing transverse (left), sagittal (middle) and coronal (right) CT scan images. The middle row shows the corresponding PET scan images and the bottom row corresponding fused PET/CT images. Enlarged parathyroid gland (measuring 16 × 9 × 22 mm), a parathyroid adenoma with increased ^{18}F-choline uptake is seen behind the lower left thyroid lobe

8.3 Case 8.3. ^{18}F-Choline PET/CT Scan: Ectopic Right Lower Parathyroid Adenoma

8.3.1 Background

A 54-year-old woman with history of primary hyperparathyroidism was referred for ^{18}F-choline PET/CT parathyroid scintigraphy. Serum PTH and calcium levels were raised with PTH level at 125 ng/L (normal range: 12–65 ng/L) and calcium at 2.65 mmol/L (normal range: 2.10–2.60 mmol/L). Serum phosphate level was normal at 0.94 mmol/L (normal range: 0.80–1.40 mmol/L).

8.3.2 Procedure

The patient received 103 MBq of ^{18}F-choline intravenously with PET/CT scanning of neck and upper mediastinum (4 min per bed position) performed at 5-min (Fig. 8.5a), 1-h (Fig. 8.5b) and 2-h (Fig. 8.5c) post tracer administration.

8.3.3 Findings

The PET/CT scan showed an enlarged parathyroid gland (measuring 9 × 8 × 18 mm) in the right posterior superior mediastinum, lateral to the oesophagus. Contrast between the enlarged hyperactive parathyroid gland and thyroid gland was the highest 5 min after tracer administration (Figs. 8.5 and 8.6). SUV_{max} of the enlarged

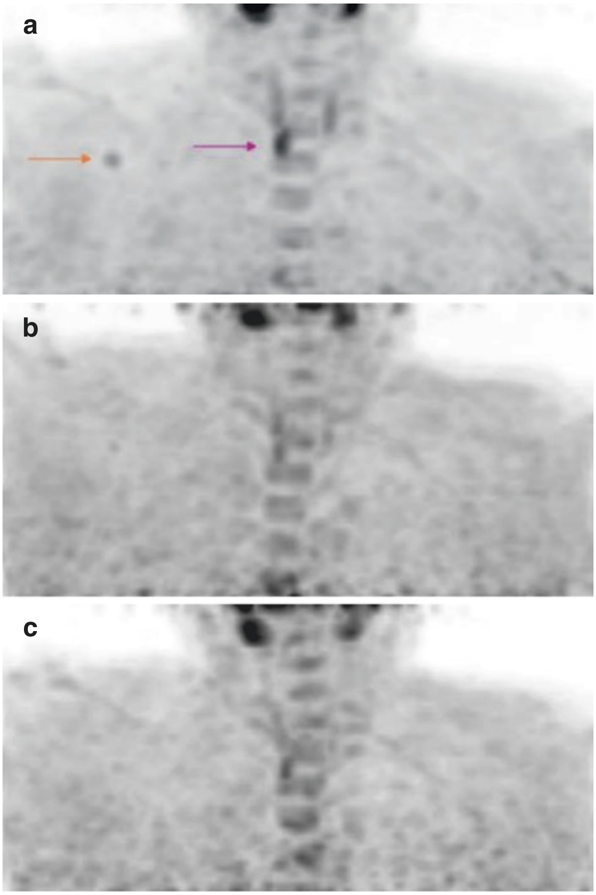

Fig. 8.5 MIP images of the ^{18}F-choline scans performed 5 min (**a**), 1 h (**b**) and 2 h (**c**) after tracer administration. Intense focal uptake of ^{18}F-choline in enlarged parathyroid gland (parathyroid adenoma) is seen most prominent on the top scan (purple arrow). Focal increased activity (marked with orange arrow) most probably represents small inflammatory-reactive lymph node

parathyroid gland after ^{18}F-choline administration at 5 min, 1 h and 2 h was 5.78, 3.60 and 3.68, respectively; the SUV_{max} of the thyroid gland at these three time points was 3.87, 3.42 and 3.15. Activity in the other structures in the neck and upper mediastinum was lower.

The enlarged parathyroid gland was surgically removed. The PTH level fell to 47.1 ng/L (normal). Histology confirmed the parathyroid adenoma which was seen to be predominantly composed of chief cells.

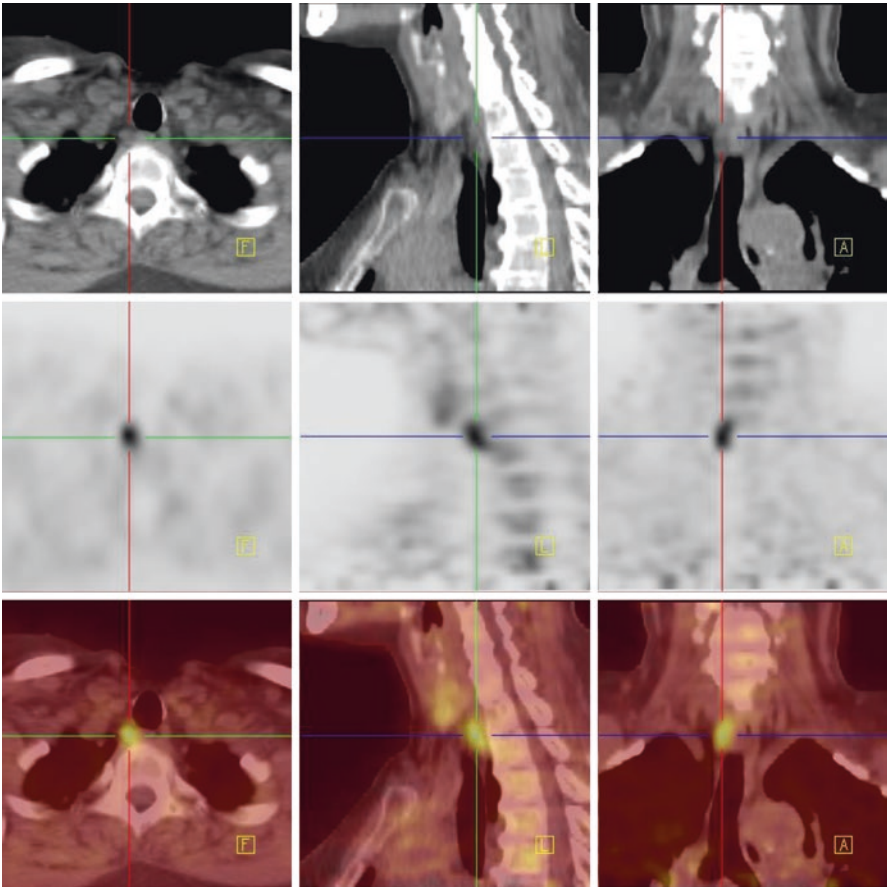

Fig. 8.6 ^{18}F-choline PET/CT scan performed 5 min after tracer administration. Top row showing transversal (left), coronal (middle) and sagittal (right) CT scan imaging. The middle row shoving corresponding PET scan images and the bottom row corresponding fused PET/CT images. Enlarged parathyroid gland measuring 9 × 8 × 18 mm (parathyroid adenoma) with increased ^{18}F-choline uptake is seen in the right posterior superior mediastinum, lateral to the oesophagus

8.3.4 Conclusion

Findings of high ^{18}F-choline uptake and retention in the lesion are consistent with an ectopic right lower parathyroid adenoma.

8.3.5 Comments and Teaching Points

- The contrast between enlarged hyperactive parathyroid gland (parathyroid adenoma), thyroid and other surrounding structures is in some patients the highest few minutes after ^{18}F-choline administration.
- Scanning few minutes and 1 h after ^{18}F-cloline administration is recommended.

8.4 Case 8.4. ^{18}F-Choline PET/CT Scan: Ectopic Retrosternal Parathyroid Adenoma

8.4.1 Background

A 43-year-old female with history of loss of appetite, abdominal pain, muscle weakness and malaise. Serum PT and calcium levels were raised with PTH level at 748 ng/L (normal range: 12–65 ng/L) and calcium at 4.0 mmol/L (normal range: 2.10–2.60 mmol/L). This patient with primary hyperparathyroidism was referred for ^{18}F-choline PET/CT parathyroid scintigraphy to elucidate the underlying cause.

8.4.2 Procedure

The patient received 98 MBq of ^{18}F-choline intravenously. PET/CT scanning of neck and upper mediastinum (4 min per bed position) was performed at 5 min and 1 h (Figs. 8.7 and 8.8) after tracer administration.

8.4.3 Findings

A lesion with increased ^{18}F-choline accumulation was seen behind the sternum in front of ascending aorta (Fig. 8.8). The lesion dimensions measured on low-dose CT were 26 × 11 × 32 mm. SUV_{max} of the lesion was 16.82. Activity in the surrounding structures was low. Comparison of the 5-min and 1-h image showed a higher contrast between lesion and surroundings after 1 h (Figs. 8.7 and 8.8).

After 14 days of pretreatment, the patient was operated. Video-assisted thoracoscopic surgery (VATS) was performed. Excision biopsy of the lesion confirmed parathyroid adenoma. After surgical removal of the lesion, PTH level fell to 47 ng/L (normal value).

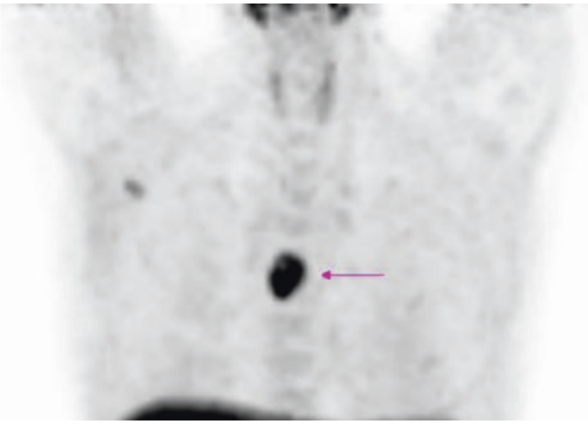

Fig. 8.7 MIP image of the ^{18}F-choline PET/CT scan performed 1 h after tracer administration in a patient with pronounced hyperparathyroidism. Intense focal activity in an ectopic parathyroid adenoma is seen in the thorax (marked with arrow). The small focus of uptake in the right axilla most probably represents a reactive inflammatory lymph node

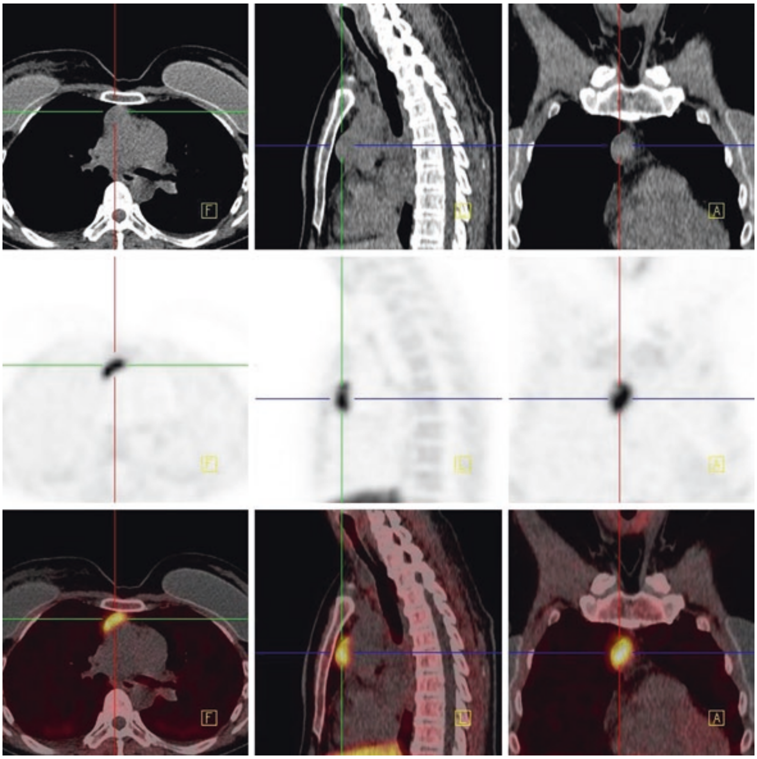

Fig. 8.8 ^{18}F-choline PET/CT scan performed 1 h after tracer administration. An ectopic parathyroid adenoma measuring 26 × 11 × 32 mm with intense increased ^{18}F-choline uptake is seen behind the sternum in front of ascending aorta

8.4.4 Conclusion

Findings of high ^{18}F-choline uptake and retention in the mediastinal lesion are consistent with an ectopic parathyroid adenoma.

8.4.5 Comments and Teaching Points

- Usually at least one lesion with increased ^{18}F-choline accumulation is seen in the neck and mediastinum in patients with hyperparathyroidism.

8.5 Case 8.5. ^{18}F-Choline PET/CT Scan + ^{99m}Tc-Sestamibi SPECT/CT: Cystic and Non-cystic Parathyroid Adenomas (Oncogenic Type)

8.5.1 Background

A 28-year-old female with a palpable nodule on the right side of the neck had a high serum calcium level of 3.77 mmol/L (normal range: 2.10–2.60 mmol/L), high PTH level of 250 ng/L (normal range: 12–65 ng/L) and normal phosphate level. ^{99m}Tc-sestamibi SPECT/CT and ^{18}F-choline PET/CT were preformed to investigate the cause of hyperparathyroidism.

8.5.2 Procedure

The patient received 612 MBq of ^{99m}Tc-sestamibi for SPECT/CT imaging. SPECT/CT imaging of the neck and mediastinum (20 min acquisition time) was performed 1 h after tracer administration. ^{18}F-choline (105 MBq) was administered intravenously and PET/CT scanning of neck and upper mediastinum performed (4 min per bed position) at 5 min and 1 h after tracer administration.

8.5.3 Findings

Two lesions with increased ^{99m}Tc-sestamibi and ^{18}F-choline accumulation were detected on the right side of the neck (Fig. 8.9). Behind upper right thyroid lobe was a nodule measuring 10 × 13 × 17 mm, and under the right thyroid lobe was a nodule measuring 19 × 33 × 41 mm with nonhomogeneous tracer accumulation (Fig. 8.10). Contrast between lesions and thyroid gland on ^{18}F-choline PET/CT was higher after 5 min than after 1 h. The upper lesion had a SUV_{max} of 8.06, the lower lesion had an SUV_{max} of 14.06, and the SUV_{max} of the thyroid gland was 5.20.

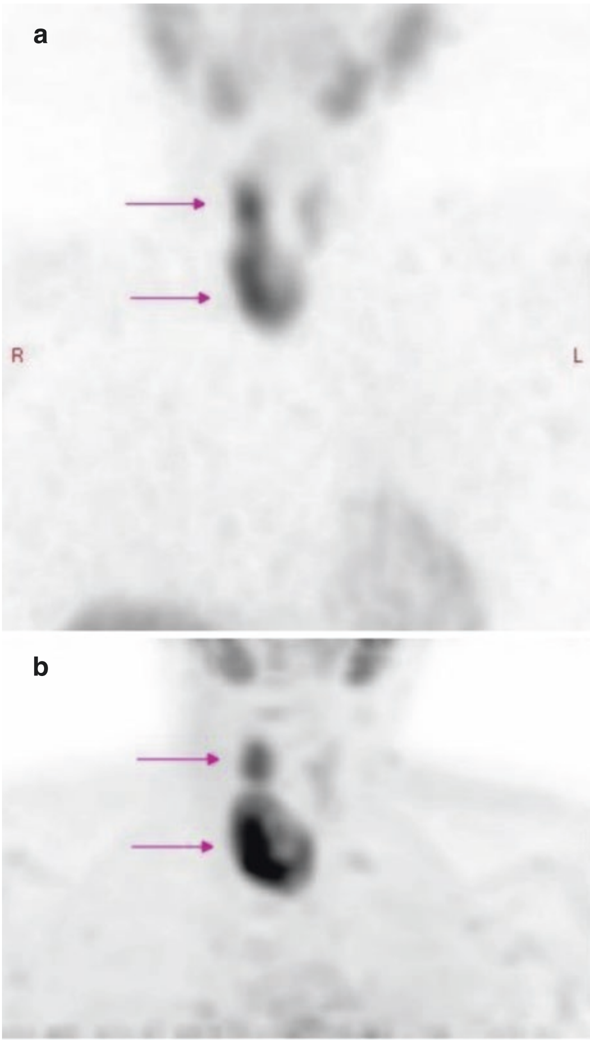

Fig. 8.9 (**a**) MIP images of the ^{99m}Tc-sestamibi SPECT/CT (performed 1 h after tracer administration) and (**b**) ^{18}F-choline PET/CT (performed 5 min after tracer administration). Two lesions with increased tracer accumulation are seen in both images (marked with arrows)

8.5.4 Conclusion

Findings are consistent with two right parathyroid adenomas. The lesions were surgically removed. The mass of the upper lesion was 1.6 g and that of the lower lesion 24.1 g. Result of excision biopsy of both lesions was oncocytic adenoma. After surgery, the PTH and calcium levels fell to normal.

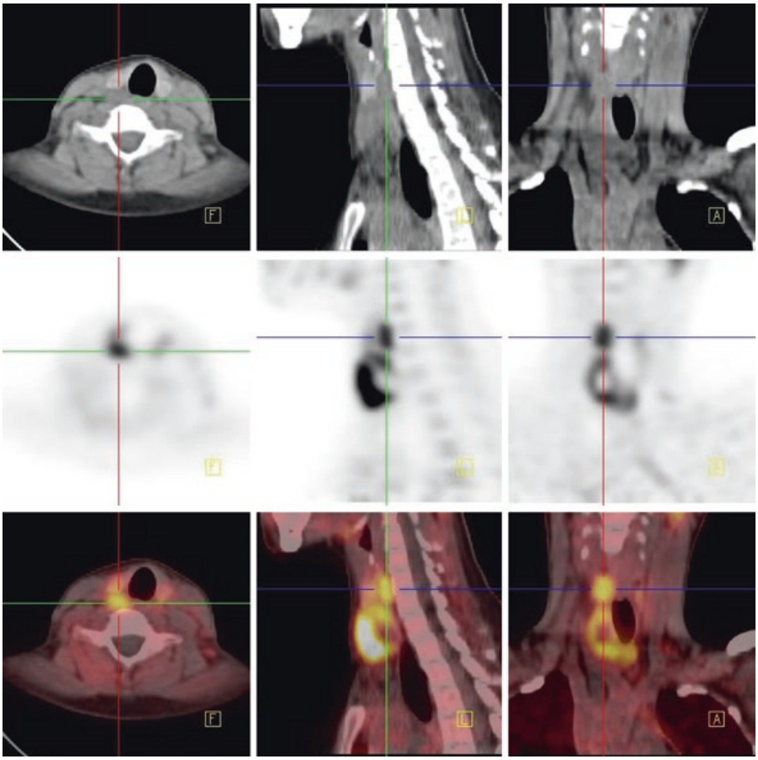

Fig. 8.10 ^{18}F-choline PET/CT scan performed 5 min after tracer administration. Top row showing transversal (left), sagittal (middle) and coronal (right) CT scan imaging. The middle row shows the corresponding PET scan images and the bottom row the corresponding fused PET/CT images. Two enlarged lesions (measuring 10 × 13 × 17 mm and 19 × 33 × 41 mm) with increased ^{18}F-choline uptake are seen behind and below the right thyroid lobe. The lower lesion appears to have a central cystic area—a cystic parathyroid adenoma

8.5.5 Comments and Teaching Points

- Increased ^{99m}Tc MIBI and ^{18}F-choline uptake is present in oncocytic parathyroid adenomas.

8.6 Case 8.6. ^{18}F-Choline PET/CT Scan + ^{99m}Tc-Sestamibi SPECT/CT: Four Glands Parathyroid Hyperplasia on Choline, Two Positive on Sestamibi

8.6.1 Background

A 54-year-old man with end-stage renal disease (on haemodialysis for the last 10 years) presented with hyperparathyroidism. At the time of investigations, serum parathormone (PTH) level was 952 ng/L (normal range: 12–65 ng/L).

8.6.2 Procedure

^{99m}Tc-sestamibI SPECT/CT and ^{18}F-choline PET/CT scans were performed. SPECT/CT of the neck and mediastinum was performed 1 h after administration of 633 MBq ^{99m}Tc-sestamibi intravenously (Fig. 8.11a). PET/CT scan covering the neck and chest region was performed a few days later (Fig. 8.11b). Following intravenous injection of 101 MBq ^{18}F-choline, PET/CT scan was performed 1 h post tracer administration. The scanning time for ^{99m}Tc-sestamibi SPECT/CT was 20 and 12 min (3 × 4 min) for ^{18}F-choline PET/CT.

8.6.3 Findings

The ^{99m}Tc-sestamibi SPECT/CT scan showed two lesions corresponding to the upper and lower poles of the left lobe of the thyroid. The ^{18}F-choline PET/CT scan however showed two additional smaller lesions at the corresponding sites in the right thyroid lobe region. The sizes of the parathyroid lesions measured on the low-dose CT component were 10 × 10 × 15 mm (upper left), 6 × 7 × 9 mm (lower left), 8 × 7 × 7 mm (upper right) and 5 × 6 × 6 mm (lower right). See Fig. 8.12.

8.6.4 Conclusion

Findings consistent with four-gland parathyroid hyperplasia associated with secondary hyperparathyroidism.

8.6.5 Comments and Teaching Points

- The resolution of PET is superior to SPECT and allows detection of smaller sized lesion that those which can be seen on the SPECT scan.
- ^{18}F-choline PET/CT is more sensitive than ^{99m}Tc-sestamibi SPECT/CT for detecting enlarged hyperactive parathyroid glands.
- ^{18}F-choline PET/CT is able to detect enlarged parathyroid gland with a mass over 0.1 g.

8.7 Case 8.7. ^{18}F-Choline PET/CT Scan + ^{18}F-FDGC PET/CT Scan + ^{99m}Tc-Sestamibi SPECT/CT: Tertiary Hyperparathyroidism Due to Three-Gland Parathyroid Adenomas with Brown Tumours

8.7.1 Background

A 29-year-old male on haemodialysis for the last 7 years reported with markedly increased serum PTH value for several months with the highest PTH value of 1452 ng/L (normal range: 12–65 ng/L).

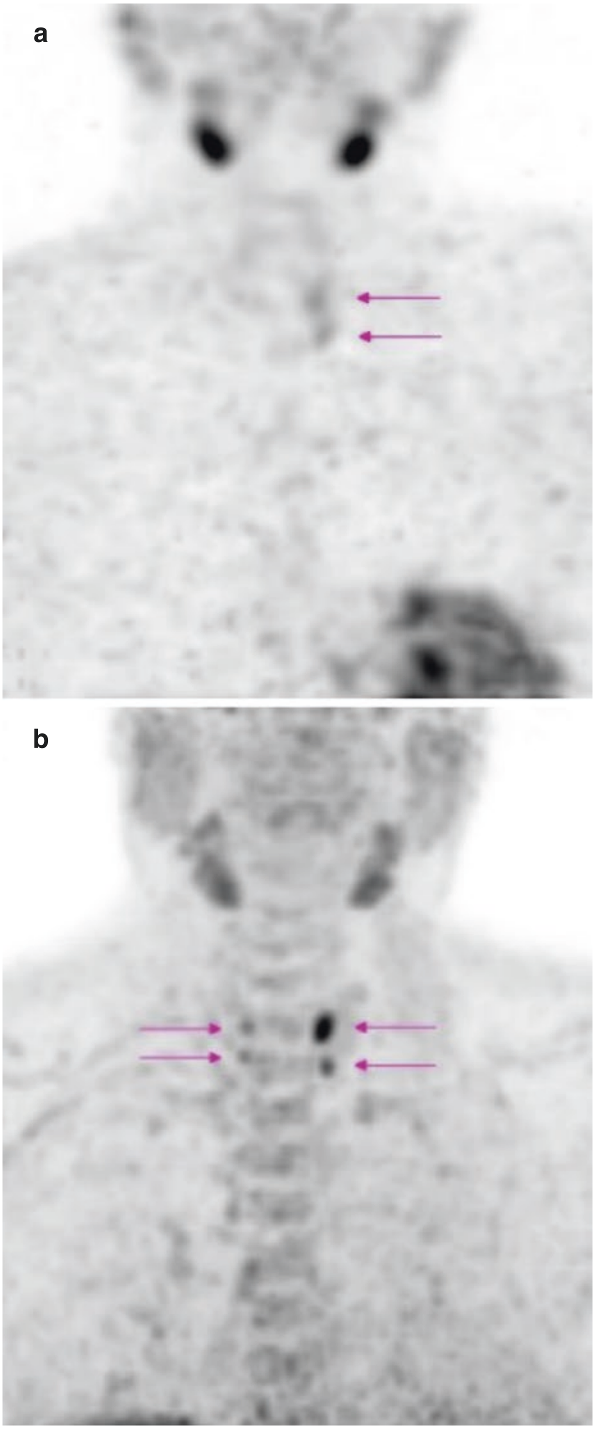

Fig. 8.11 (**a**) MIP images of the ^{99m}Tc-sestamibi SPECT/CT and (**b**) ^{18}F-choline PET/CT. Two enlarged parathyroid glands are seen on the ^{99m}Tc-sestamibi SPECT/CT and four on the ^{18}F-choline PET/CT (marked with arrows)

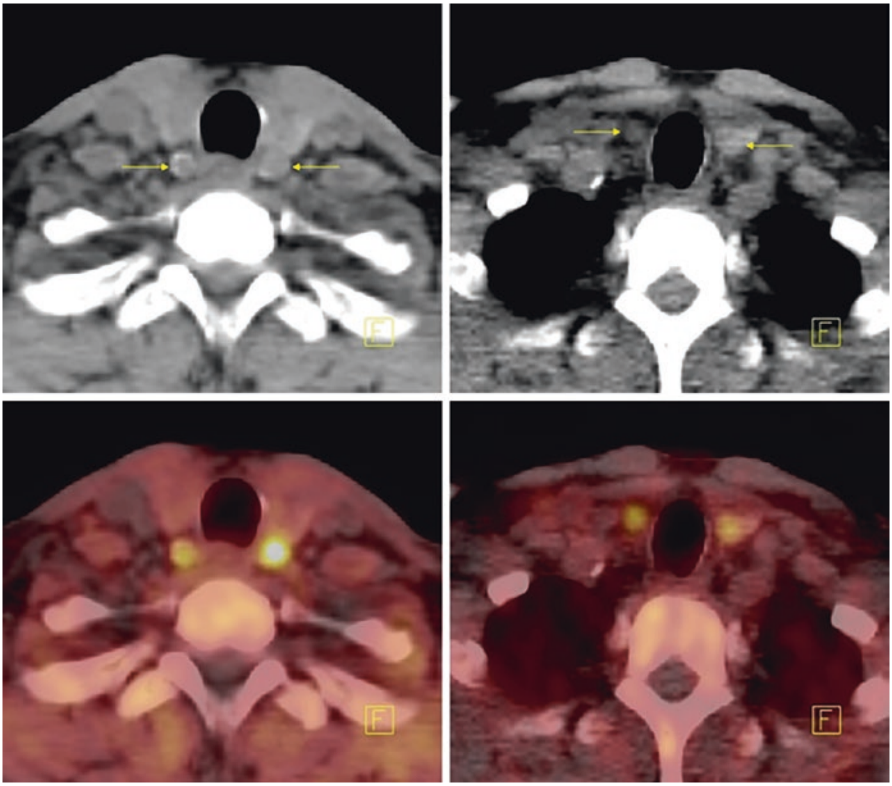

Fig. 8.12 ^{18}F-choline PET/CT scan performed 1 h after tracer administration. Four enlarged parathyroid glands (marked with yellow arrows) are seen on transverse CT scan (top row). Fused PET/CT images are presented in the bottom row. The size of the lesions was upper right 8 × 7 × 7 mm, upper left 10 × 10 × 15 mm, lower right 5 × 6 × 6 mm and lower left 6 × 7 × 9 mm

^{99m}Tc-sestamibi SPECT/CT ^{18}F-choline PET/CT scans were performed to localize hyperactive parathyroid gland lesions. An ^{18}F-FDG PET/CT scan was also requested to investigate possible malignant disease because of the skeletal changes.

8.7.2 Procedure

^{18}F-choline (dose 88 MBq) was injected intravenously and PET/CT scan of the neck and mediastinum performed 5 min and 1 h after tracer administration (Figs. 8.13 and 8.14). The scanning time for the bed position was 4 min. ^{99m}Tc-sestamibi SPECT/CT (Fig. 8.15) of the same region was performed 1 h after intravenous radiopharmaceutical (dose 654 MBq) administration. The scanning time for SPECT/CT was 20 min. For ^{18}F-FDG PET/CT, the patient was injected with 250 MBq of ^{18}F-FDG (4 MBq/kg body weight) with scan acquisition starting 1-h post tracer administration, with 2 min per bed position (see Fig. 8.16).

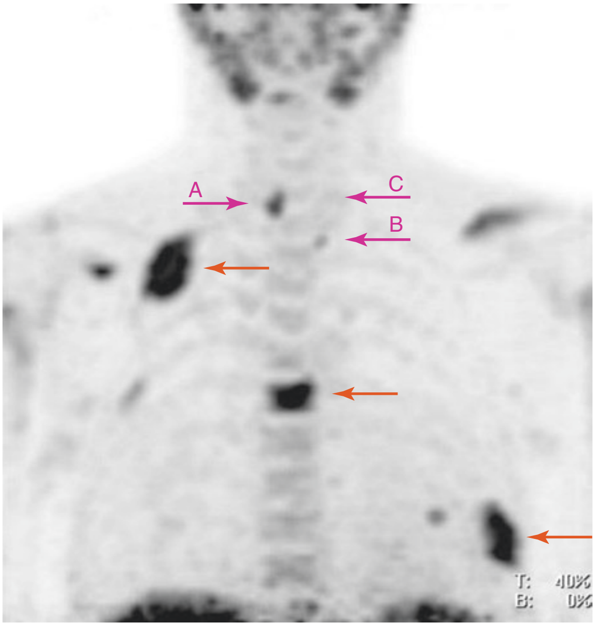

Fig. 8.13 MIP images of the ^{18}F-choline PET/CT. Two parathyroid lesions are seen (A, B) with the larger lesion in the upper right lobe and a small lesion in the lower left lobe, together with a possible lesion in the upper left pole region (C)—marked with pink arrows. Several lesions representing brown tumours (the biggest three lesions are marked with orange arrows) are seen in the skeleton

8.7.3 Findings

Two to three lesions with increased tracer activity were detected in the neck on the ^{18}F-choline PET/CT scan and only two on ^{99m}Tc-MIBI SPECT/CT (Figs. 8.13, 8.14, and 8.15). The biggest lesion measuring 7 × 10 × 12 mm located behind the lower pole of the right thyroid lobe and the smaller lesion measuring 5 × 7 × 7 mm located below the lower pole of the left thyroid lobe were seen on both the SPECT and the PET scans. The smallest lesion measuring 4 × 6 × 7 mm located behind the upper left thyroid lobe was only detected on the ^{18}F-choline PET/CT scan. The ^{18}F-choline PET/CT additionally showed intense uptake is several bone lesions (brown tumours).

On ^{18}F-FDG PET/CT, several bone lesions with increased tracer accumulation were detected in the skeleton (Fig. 8.16). The biggest lesion located in second right rib was 42 mm in diameter. There was increased ^{18}F-FDG accumulation seen in the parathyroid lesions.

The three parathyroid lesions that were seen on ^{18}F-choline PET/CT (Fig. 8.14) were surgically removed. Excision biopsy proved tertiary hyperparathyroidism. The patient subsequently developed hypoparathyroidism after surgery with the serum PTH level falling to 21 ng/L (normal range: 12–65 ng/L).

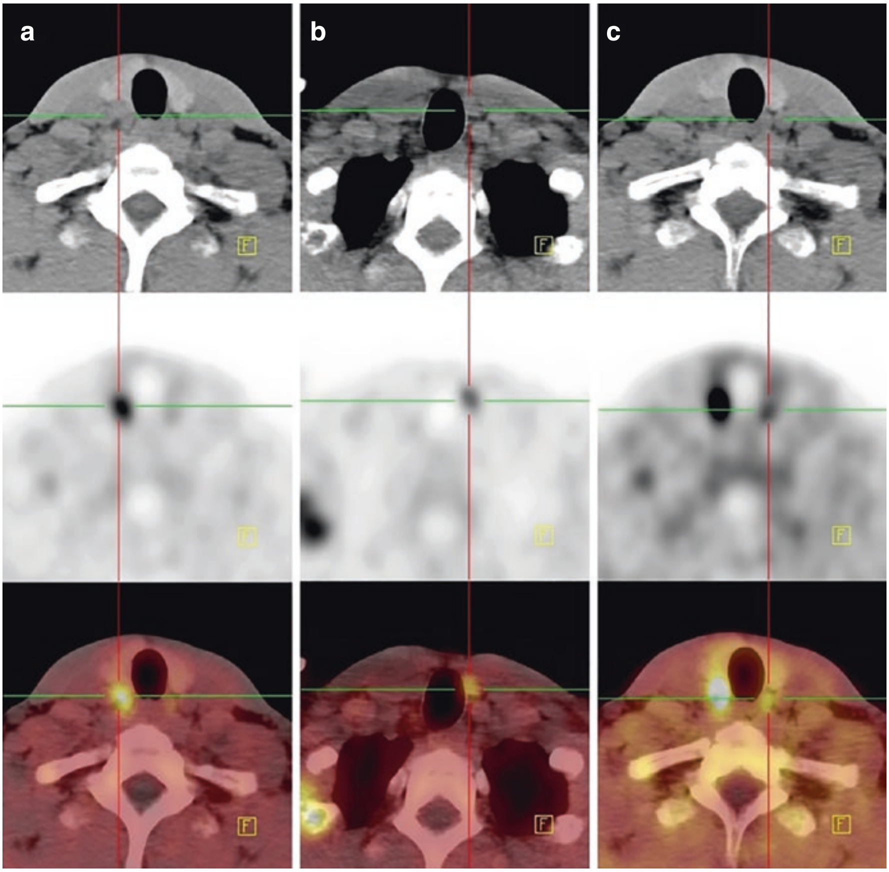

Fig. 8.14 ^{18}F-choline PET/CT scan performed 1 h after tracer administration. Two enlarged and one borderline enlarged parathyroid glands are seen on transverse CT scan (top row), PET scans (middle row) and PET/CT (bottom row). The right upper parathyroid gland is largest in size measuring 7 × 10 × 12 mm (**a**), followed by the left lower parathyroid measuring 5 × 7 × 7 mm (**b**), with the left upper parathyroid borderline enlarged at 4 × 6 × 7 mm (**c**) at the lower limit of the detectability of ^{18}F-choline PET/CT

Histology of the bone lesions with increased ^{18}F-choline and ^{18}F-FDG uptake confirmed brown tumours.

8.7.4 Conclusion

Findings are consistent with tertiary hyperparathyroidism due to three-gland parathyroid disease.

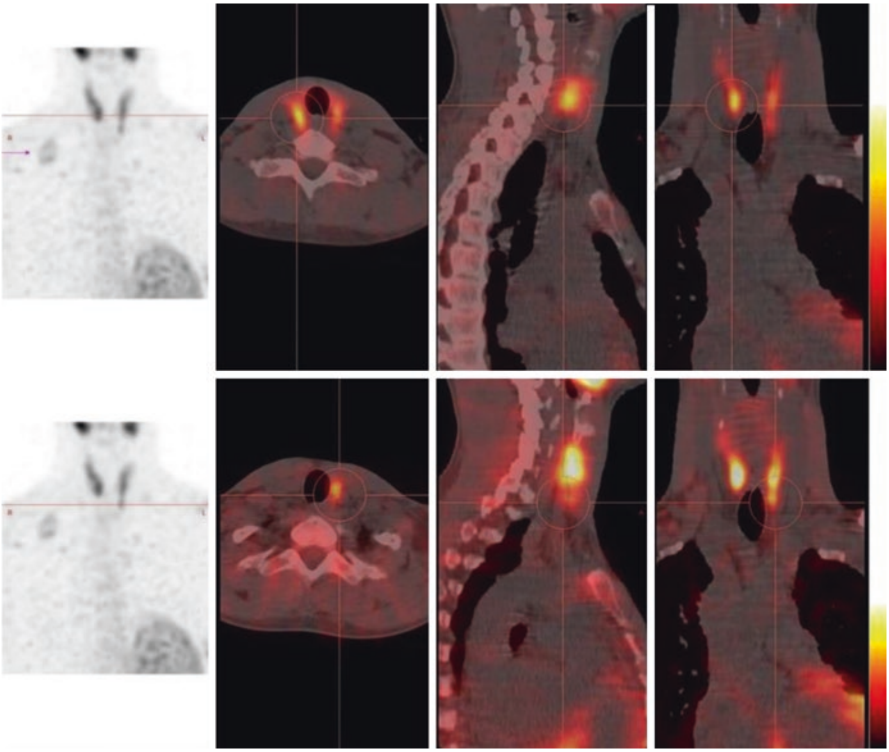

Fig. 8.15 ^{99m}Tc-sestamibi SPECT/CT scan performed 1 h after tracer administration. The height of the cut is indicated by a line on MIP images (on the left). Two enlarged parathyroid glands (parathyroid adenomas) are seen on scans

8.7.5 Comments and Teaching Points

- Small parathyroid adenomas can also cause a pronounced hyperparathyroidism.
- Brown tumours have a higher accumulation of ^{18}F-FDG and ^{18}F-choline compared with ^{99m}Tc-sestamibi.

8.8 Case 8.8. ^{18}F-Choline PET/CT Scan: Left Lower Parathyroid Adenoma – Incidental Finding

8.8.1 Background

^{18}F-choline PET/CT was performed in a 73-year-old man for prostate cancer staging. Based on the changes found in the neck, the patient was advised to visit the endocrinologist. At that time, he had a serum calcium of 2.68 mmol/L (normal range: 2.10–2.60 mmol/L), ionized serum calcium 1.32 mmol/L (normal range: 1.15–1.35 mmol/L), serum phosphate 0.89 mmol/L (normal range: 0.80–1.40 mmol/L)

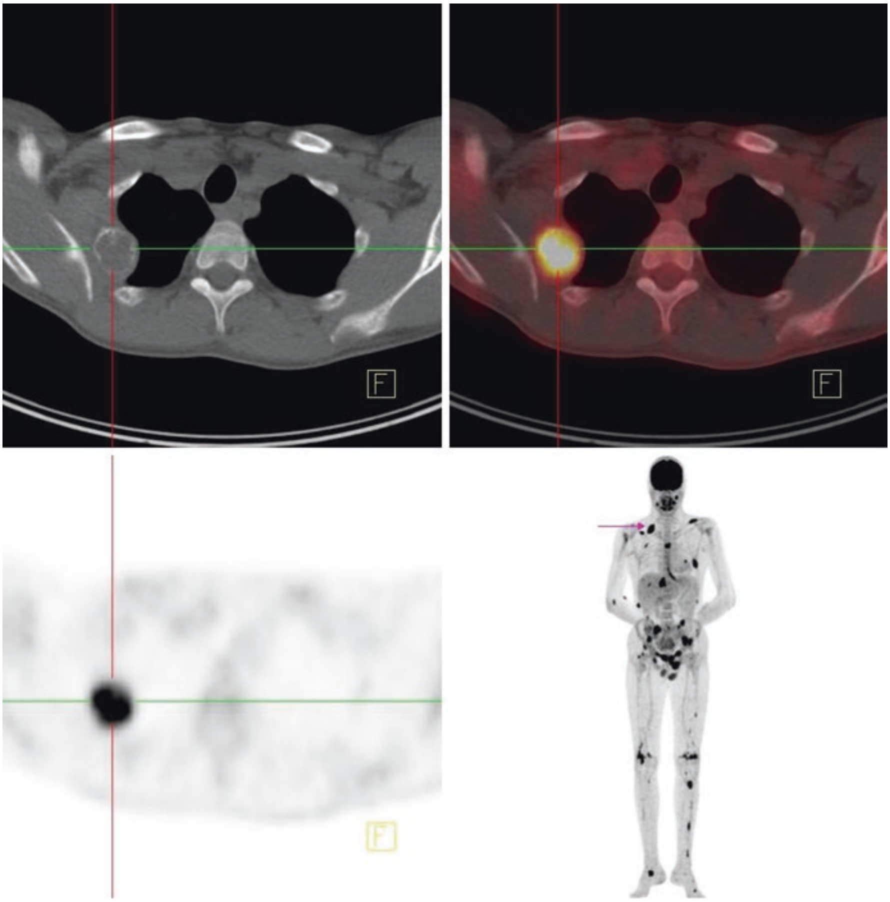

Fig. 8.16 ^{18}F-FDG PET/CT scan performed 1 h after tracer administration. The MIP image shows several lesions (brown tumours) with increased ^{18}F-FDG uptake. The crosshair marks the lesion in the right second rib seen on the transverse CT, PET and fused PET/CT scan which is 42 mm in diameter (marked also with an arrow on MIP image). There are no FDG-avid soft-tissue lesions seen

and serum PTH at 109 ng/L (normal range: 12–65 ng/L). Conservative treatment was recommended. The ^{18}F-choline PET/CT was repeated 23 months later for prostate cancer follow-up.

8.8.2 Procedure

The patient received 210 MBq of intravenous ^{18}F-choline for both the initial and the follow-up scans. Whole-body PET/CT scanning (2 min per bed position) was performed 1 h after tracer administration (Fig. 8.17) on both occasions.

Fig. 8.17 MIP image of the ^{18}F-choline scan performed 1 h after tracer administration for staging the prostate cancer. Intense focal uptake is seen in a moderately enlarged hyperactive parathyroid gland (marked with an arrow)

8.8.3 Findings

A lesion with increased tracer activity (SUV_{max} 7.20) was detected behind the left lower thyroid lobe (Fig. 8.18). SUV_{max} in the thyroid gland was 3.19. Dimensions of the lesion (enlarged hyperactive parathyroid gland) measured on low-dose CT were 6 × 5 × 8 mm.

The size and SUV_{max} of the lesion were practically the same on the repeated investigation 23 months later, and the PTH remained high. Given the scintigraphic and biochemical findings, a diagnosis of primary hyperparathyroidism due to the parathyroid adenoma was established.

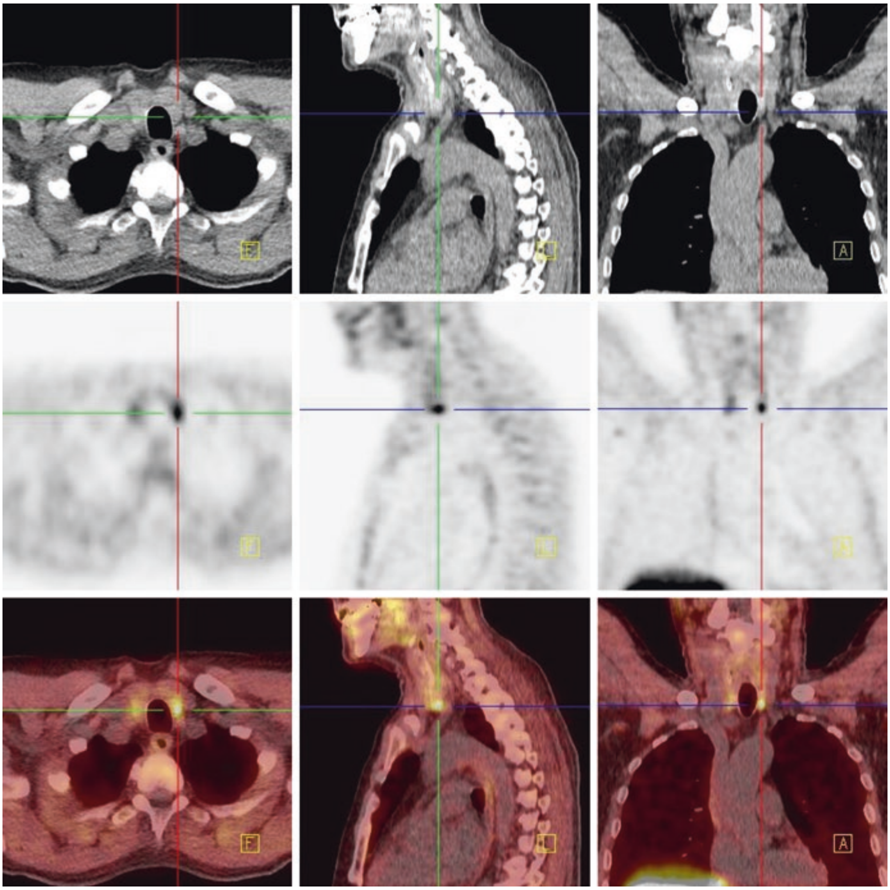

Fig. 8.18 ^{18}F-choline PET/CT scan performed 1 h after tracer administration in a patient with prostate cancer. Top row showing transaxial (left), sagittal (middle) and coronal (right) CT scan images, with the middle row showing corresponding PET scan images and the bottom row the corresponding fused PET/CT images. A moderately enlarged (size 6 × 5 × 8 mm) parathyroid gland with increased ^{18}F-choline uptake (SUV_{max} 7.20) is seen behind the left lower thyroid lobe

8.8.4 Conclusion

Findings are consistent with primary hyperparathyroidism due to a single left lower parathyroid gland adenoma.

8.8.5 Comments and Teaching Points

- An incidentally found lesion with increased ^{18}F-choline uptake on PET/CT in the neck region or upper mediastinum may represent a parathyroid adenoma.
- The serum PTH values should be estimated in such cases.

Further Readings

1. Albright F, Reifenstein EC Jr. The parathyroid glands and metabolic bone disease. Baltimore, MD: Williams & Wilkins; 1948.
2. Mundy GR, Cove DH, Fisken R. Primary hyperparathyroidism: changes in the pattern of clinical presentation. Lancet. 1980;1:1317–20.